IVANE JAVAKHISHVILI TBILISI STATE UNIVERSIT

MIKHEIL NODIA INSTITUTE OF GEOPHYSICS

TECHNICAL UNIVERSITY OF GEORGIA

INSTITUTE OF HYDROMETEOROLOGY

GEORGIAN GEOPHYSICAL ASSOCIATION

1st INTERNATIONAL SCIENTIFIC CONFERENCE

„MODERN PROBLEMS IN GEOPHYSICS”

Tbilisi, Georgia, November 6-8, 2025

PROCEEDINGS

2025 – Tbilisi

Ivane Javakhishvili Tbilisi State University

Mikheil Nodia Institute of Geophysics

Technical University of Georgia

Institute of Hydrometeorology

Georgian Geophysical Association

1st INTERNATIONAL SCIENTIFIC CONFERENCE

"Modern problems in Geophysics"

Tbilisi, Georgia, November 6-8, 2025

PROCEEDINGS

უნივერსიტეტის გამომცემლობა
Tsu Press

ISBN 978-9941-36-434-1

ISSN 3088-4349

1st International Scientific Conference "Modern problems in Geophysics", Proceedings,
ISBN 978-9941-36-434-1, ISSN 3088-4349, Tbilisi, Georgia, November 6-8, 2025

ARCHITECTURAL HISTORY OF THE TBILISI GEOPHYSICAL OBSERVATORY

Mania M.

Giorgi Chubinashvili National Research Centre for Georgian Art History and Heritage Preservation, Tbilisi, Georgia
maia_mania@hotmail.com

Abstract. *The article deals with the history of the foundation and development of the 19th century Tbilisi Magnetic-Meteorological Observatories, with a focus on the so-called Kukia observatory. Built between 1859 and 1861, it was the first building to be designed as an observatory not only in Tbilisi but also in the Caucasus. The article also traces the history of the successors of Tbilisi Magnetic-Meteorological Observatory: Karsani and Dusheti.*
The paper pays tribute to the medieval observatory of Tbilisi: Shahistakhti.

Key words: *Magnetic-Meteorological Observatories, architectural history, buildings.*

The 19th century was an era of the beginning of uninterrupted absolute observations. It is when terrestrial magnetism, meteorology and other earth sciences began to be studied on a large scale.

As is well known the idea of establishing a chain of magnetic observatories worldwide was proposed by the prominent German scientist and naturalist Alexander von Humboldt (1769-1859). He argued that magnetic measurements were to be made simultaneously in the observatories, or 'magnetic houses' as he referred to them, which were located at quite a distance from each other [5, p. 291].

The history of observatories in Georgia in general and in Tbilisi in particular has its roots in medieval centuries. Tradition has it that the first observatory in Tbilisi was established towards the end of the 8th century, under the rule of the Arabs. It has been presumed that it was located in Shahistakhti (Shaistakhti) part of the Narikhala Fortress. The ruins of Shahistakhti, built from old brick and stone, can still be seen at approximately half a kilometer from Fort Narikhala, in what is now Sololaki Alley. The exact age of the multilayered Shahistakhti remains unknown.

The tradition and findings of scientific studies show that Tbilisi born scientist and doctor Fakhr ad-Din al-Khilati (1191-1282) presumably set up the ancient observatory of Tbilisi. Later he was invited by the famous Persian scholar, Nasir ad-Din at-Tusi, to the Marageh observatory [8, pp. 99-110]. As is well known, the Marageh observatory played an instrumental role in the history of medieval Muslim observatories (Fig. 1).

Fig. 1. Shahistakhti and the first Magnetic Observatory on its top. Early 20th century.

When organizing the observatories in the Russian Empire, Adolph Theodor von Kupffer (1799-1865) was instructed to apply to the Caucasian Viceroy (Commander in Chief), General Adjutant Baron Rosen (Georg Andreas von Rosen, 1781-1841) with a letter asking to assign the implementation of preparatory works for establishing an observatory in Tbilisi [1, p.59; 6, p. 56].

Though founded in the mid 1830s, the Tbilisi observatory was engaged in the common system of terrestrial studies only in 1844 when it was integrated into an international net of observatories together with the launch of regular absolute magnetic and meteorological observations.

Like many other observatories across the world, the Tbilisi observatory covered a huge space encompassing the southern areas of the Russian Empire, the entire Caucasus and the adjacent Caspian, Black Sea and Azov aquatoria.

Before moving into Tiflisser Kolonie, the Tbilisi observatory had changed its premises four times. The reason for this frequent relocation was that magnetic observations which are impossible to be conducted even under a slight distortion of a magnetic field, especially when it is caused by the high density of settlement and electrification of transport [6, p. 57].

The first magnetic and meteorological observations in the Transcaucasus, by demand of the Commander-in Chief Baron Rosen, were organized and launched by Major General Ober- Quartermeister of the separate Caucasian Corps Baron von der Hoven. For this very reason, during 1836 and 1837, he specially constructed an observatory on Mount Sololaki on the ruins of Shakhistakhti. 'This was the first 'magnetic house' erected on the site of the former observatory, which is strongly associated with a senior teacher of mathematics and physics at the Tbilisi gymnasium, the collegiate assessor Ivan Shestakov (born 1815). On 1 May 1844 (14 May old style), the date on which magnetic and meteorological observations were launched in Georgia, marked a new stage in the history of the observatory. It is thanks to the uninterrupted observations that this date has been accepted as the official opening date of the observatory. It is associated with the teacher of mathematics of the senior pupils of the gymnasium and a director of the Tbilisi observatory, Andrei Tymofeevitch Filadelfin (born 1815) who conducted observations until 14 August 1847: 'I started my observations on 1 May (old style) 1844 and continued up to 14 August, 1847', noted Filadelfin. Shestakov and Filadelfin must therefore be considered to be founders of the meteorological and magnetic study of Tbilisi. This very observatory was built on the slopes of Mount Mtatsminda and the design was commissioned to Jacob Ivanov, chief architect of Tbilisi from 1841 to 1846 [11, pp. 99,101,103]. The Mtatsminda observatory was the second of its kind established in Tbilisi in the 19th century.

To build the third magnetic observatory one of the elevations of the left bank of the River Mtkvari was chosen. Though altered, the three-storey building of Tbilisi Magnetic-Meteorological Observatory, still stands at the intersection of Martkopi and Observatory streets in the district of Avlabari. It was constructed under the direct supervision of Arnold Moritz (1821-1902) famous astronomer between 1850 and 1851. Hourly observations were launched on 1 December, 1851 (new style) and lasted until 5 pm, 13 April, 1860 (Fig. 2).

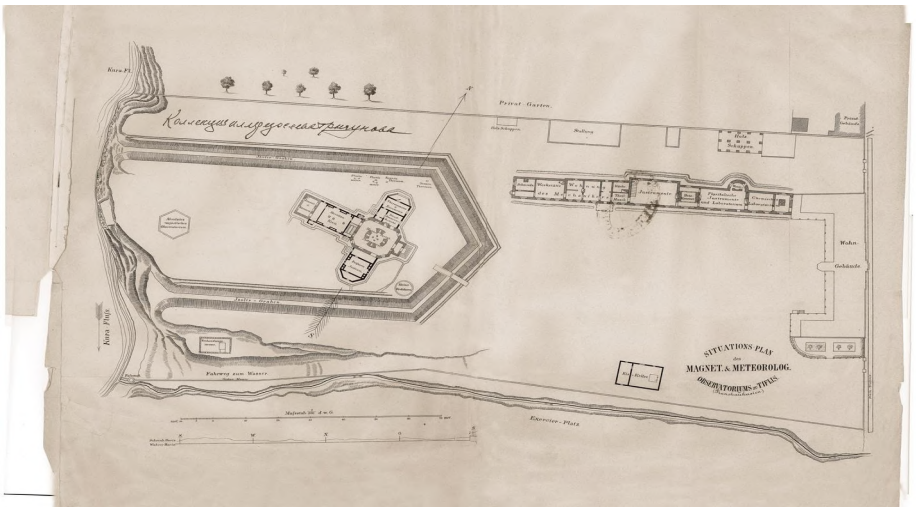

Fig. 2. Layout plan of the Kukia observatory instrumentally surveyed and drawn by Heinrich Kiefer, 1866.

According to scientific sources, Otto Wilhelm Hermann von Abich (1806-1886) preceded Arnold Moritz to the position of director of the observatory [11, pp. 53,55,57,59].

It was Arnold Moritz who, together with his companions, laid a firm foundation for the undertaking of geophysical studies in Georgia and later, from the early 1850s, the advancement of this branch of science.

Moritz in the middle of the 19th century was responsible for the construction of a magnetic-meteorological observatory which was the first building designed as an observatory in the cultural and administrative hub of the Caucasus. It is the history of this building, distinctive in many respects.

The land taken up by what was then the district of Kukia, in Tiflisser Kolonie, was selected for the building of the complex of Tbilisi Magnetic-Meteorological Observatory (Fig. 3- Fig. 5).

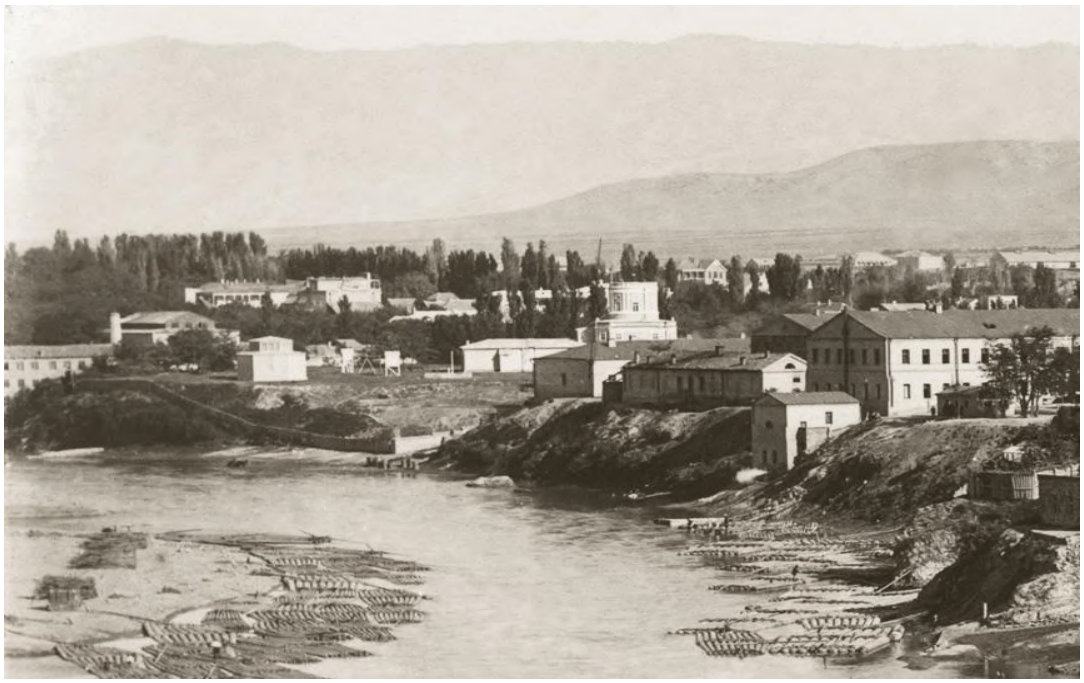

Fig. 3. General view of Tiflisser Kolonie from the river Mtkvari. Tbilisi Physical Observatory with its absolute building. Photo by D.Yermakov. End of the 19th century.

Fig. 4. Main building of the Kukia observatory. 1860 s.

Fig. 5. Main building of the former Tbilisi Geophysical Observatory as it stands today. General view. 2024.

The design for the observatory was made in 1859, while the construction was carried out between 1860 and 1861. It started functioning in a newly constructed building at 0 o'clock astronomical time, 1 May, 1862 [6, p. 57].

The chief of the Caucasian Triangulation Ioseph Khodzko was entrusted with the writing of a charter of the main observatory of the Caucasus. It was he who named the observatory as the Main Observatory of the Caucasus, defined its goals and objectives and set up physical and astronomical departments within the observatory assigning respective functions to each [11, pp. 35, 37, 39,41].

According to a layout plan dating from the time when Moritz was active (Situations Plan des Magnet. & Meteorolog. Observatoriums zu Tiflis (Transkaukasien), the dominant of the complex, was the main building of the observatory provided with a tall wooden tower rotating around the axis in the centre and with widely extended arms. The main building of the observatory (Hauptgebaude) still stands in the eastern half of a narrow strip of land between former Michael Street and the Mtkvari. It was designed by the engineer Ferdinand Lehmkul and architect Otto Jakob Simonson (1829-1914). The main building dominated the entire complex and served to organize the extremely spacious observatory grounds. The building was enclosed by a deep ditch (Isolir. Graben). The observatory was designed in Neo Classical style. The Tbilisi Observatory ranked as one of the most remarkable public buildings in Tbilisi. Having been home to the earliest scientific center

in the Caucasus and having been the first geophysical institution in Georgia, is remarkable for its architectural merit. Unique in the Caucasus, the building was characterized by its unusual typology, which, in turn, was conditioned by the unique function it was designed to serve [11, p.14-42].

The main building of the observatory was the first building designed as an observatory not only in Tbilisi but also in the Caucasus, which accounts for its distinction among scientific buildings in the Caucasus. It is this building that should be considered as the main point of reference in the history of the architecture of the Tbilisi observatories.

The participation of the Tbilisi observatory in the first International Polar Year held between 1882 and 1883, which involved fifteen countries, was initiated by the then director of the Tbilisi observatory Johann Mielberg (1841-1894) [6, p.58]. The reconstruction was done by the architect Leopold Bielfeld (1838-1922) who removed the moveable timber tower of the main building and replaced it by the brick one. Giving a tribute to Lehmkul-Simonson's Classicistic style the tower was designed in Classicistic manner [11, p. 123].

In terms of the architectural decoration, the main building bears all the features of the classicist style and retains the simplicity, austerity and monumentality typical of public buildings erected in Tbilisi in the first half and middle of the 19th century [11 p. 133].

The electrification of streets in Tbilisi in 1904 affected the normal magnetic field thus impeding magnetic observations, hence the decision to move the observatory with its belongings to Karsani, near Mtskheta, while the construction of the Zahes power station and the electrification of the Tbilisi-Khashuri railway section required its transfer from Karsani to the town of Dusheti [7, pp.13, 13', 14].

The Karsani observatory was initiated by Stephan Hlasek, director of the Tbilisi observatory. He is associated with the launching of a seismic station in Tbilisi Physical Observatory in December 1899. He had organised a reconnaissance expedition to the surroundings of Mount Karsani near Mtskheta in 1910 before launching the construction of an observatory on steep terrain. The building work was completed in 1913, while the installation of magnetic instruments by Hlasek and the magnetologist Sitnov finished in 1914. Worth noting is that Ernst Rudolph Assaffrey (1846-1925) of Estonian origin also took part in building the Karsani observatory and in the observations made there [3, pp. 7-9; 6, p.58]. The complex was designed by the civil engineer Hermann Otto Barth (1873-1937). The main building at Karsani is distinguished by Art Nouveau features and is of high artistic merit. Faced with an alteration of rough blocks of stone and brick with architectural decorative elements (a projection and a pilaster), the façades feature mullions and a wavy cornice on the tower-like structure, all inspired by Art Nouveau. The interior of the building also reveals the influence of Art Nouveau. The main building of the Karsani observatory demonstrates the extent of the influence of this movement in Georgia. Barth was also responsible for other structures of the Karsani observatory, including a residential building for the staff and a large magnetic pavilion [12, pp. 227, 229, 233] (Fig. 6, Fig. 7).

Fig. 6. Main building of the former Karsani observatory. 2004.

Fig. 7. Main building of the former Karsani observatory. 2024.

In 1918, Andria Benashvili (1868-1941), the well-known astronomer and geodesist, was appointed director of the Tbilisi observatory. During his tenure (1918-1922) a seismic bulletin was launched and meteorological and seismic stations expanded. Abandoned by foreign scientists, the Tbilisi observatory and the Karsani Magnetic Department remained non-functional during the First World War. Rudolf Assaffrey was among those few scientists who stayed in Tbilisi. The further advance of Tbilisi Physical Observatory and the restoration of Karsani Magnetic Department was largely due to Ernst Rudolph Assaffrey together with former directors of the Tbilisi Observatory Alexander Didebulize (1882-1951), Razhden Khutsishvili (1887-1942), Micheil Nodia. The mechanics of precise instruments, Florentin Weiss and Arnold Weiss also played an important role in this undertaking. Other figures who contributed to the revival of the observatory include the magnetologist Nikoloz Intskirveli (1900-1943), Shalva Pavlenishvili (1898-1938), weather forecaster S. Pantskhava who died in the Second World War and assistant at the Karsani observatory, Shalva Khuchua (Fig. 8).

a.

Fig. 8. Large pavilion for absolute observations of the Karsani observatory. 1910 s. Large pavilion for absolute observations. Dusheti. 2007.

b.

As early as 1932, Professor Micheil Nodia (1891-1975) organized and led a preliminary reconnaissance survey of some of the sites of the Dusheti district with absolute instruments and the so-called Schmidt scales, which confirmed the acceptability of the magnetic field of the town of Dusheti and its surrounding areas [4, pp. 7-14, 15-2, 7-14, 15-25].

It was at that time that the foundation was laid of the temporary magnetic observatory. Like the Tbilisi observatory and then its successor Karsani Magnetic Department, it was to serve the entire Caucasus and the vast water areas surrounding it. Hence Dusheti Observatory has a history of one hundred and eighty years.

Thanks to its scientific importance the Dusheti observatory ranked among the world's leading observatories. It should also be noted that among the edifices of Dusheti Magnetic Complex the so-called Old Variation Pavilion built in 1935 [10, p. 57] and the Pavilion of Absolute Observations was an exact copy of the one at Karsani. It was built in 1953 of material originally used for the Karsani magnetic pavilion [5, p. 297; 9, p.7-12; 11, pp.175, 177].

References

1. Pismo akademika Kupfera k Baronu Rosenu, ot 20 dekabrja 1834 goda. // akti sobrannie kavkazskoju arxeologicheskoju kommisieju, tom VIII, 1881, (in Russian).
2. Moritz Arnold, Schreiben des Herrn Staatsraths Moritz. Direktors des magnetisch-meteorologischen Observatoriums in Tiflis an den Herausgeber. // Astronomische Nachrichten, Altona, Deutschland, 1867 (Russian translation of Arnold Moritz's text done by Alexander (Sandro) Didebulidze is kept in the archives of the Institute of Hydrometeorology of Georgia).
3. Nodia M. Geophysikalisches Observatorium Georgiens in Tiflis, Magnetische Abteilung in Karsani (bei Mzcheta). // Tiflis, 1926, (in Georgian, Russian and German).
4. Nodia M., Didebulidze A. Reports in: SAHES und das Magnetische Observatorium in Karssani. // Tiflis, 1927, (in Georgian, Russian and German).
5. Nodia M. tbilisis magnituri observatoria – magnitur observatoriata msoflio kselshi. // tbilisi 1500, saiubileo krebuli, tbilisi, 1958, (in Georgian).
6. Nodia M. Tbilisi ert-erti uzvelesi fundamenturi geopizikuri centria ssrk-sa da msoplioshi. // bunebismetkvelebisa da teknikis istorikosta sabchos shromebis krebuli 1-2, Tbilisi, 1970, (in Georgian).
7. Nodia M. Authobiography. // Manuscript, Tbilisi, 10.03.1966.
8. Japaridze G. XIII saukunis tbileli mecnieri mararis observatoriashi. // "macne", istoriis, etnograpiis da xelovnebis istoriis seria, # 2, Tbilisi, 1984, (in Georgian).
9. Kaciashvili N.A. Magnitnie nabljudenia v Gruzii // (in Russian, Hard copy is kept in the library of the Institute of Hydrometeorology).
10. Gogua R. dushetis (Tbilisis) magnituri observatoria 175 wlisaa. // micheil nodias sax. geopizikis institutis sromebi, ISSN 151-1135, v. LXX, 2019, (in Georgian).
11. Mania M. Tbilisi Geophysical Observatory. History and Architecture. // Goethe-Institut Georgien, Tbilisi, 2010, (in Georgian and English).
12. Mania M. German Architects in Tbilisi. // Goethe-Institut Georgien, Tbilisi, 2018, (in Georgian and English).

Photos featured in the article are from the following sources:

Museum of the History of Geophysic Science of Georgia; Amiranashvili State Museum of Georgia (Georgian National Museum); Grishashvili Museum of Tbilisi History (Carvasla, Georgian National Museum); M. Nodia, Geophysikalisches Observatorium Georgiens in Tiflis, Magnetische Abteilung in Karsani (bei Mzcheta), Tiflis, 1926.

The contemporary photos of Tbilisi and Karsani Geophysical Observatory main buildings as well as Dusheti Large Pavilion for Absolute Observations are by the author.

1st International Scientific Conference "Modern problems in Geophysics", Proceedings,
ISBN 978-9941-36-434-1, ISSN 3088-4349, Tbilisi, Georgia, November 6-8, 2025

DYNAMICS OF THE AFTERSHOCK ZONE OF THE 1988 SPITAK EARTHQUAKE BASED ON 35 YEARS OF DATA.

***Nazaretyan S.N., **Mirzoyan L.B., ***Kazarian A. A., *Mazmanyan L.V.**

**Territorial Survey for Seismic Protection of MIA, Yerevan, Armenia.*
*** Yerevan State University, Yerevan, Armenia.*
**** Institute of Geological Sciences of the National Academy of Sciences of the Republic of Armenia, Yerevan, Armenia.*
snaznssp@mail.ru

Abstract*. The features of aftershock manifestations of the 1988 Spitak earthquake have been studied in sufficient detail, but based on data for the first 2-3 years. The aftershock process is divided into highly active (1988-1991) and weakly active (1992 – present) periods. The overwhelming majority of 14,000 aftershocks (95%) and the predominant part of their energy (98%) were released during the active period. During the weakly active period, relative activation is observed in all the identified segments. Against the general background of attenuation of the number and strength of aftershocks, no patterns in their manifestation are observed.*

Key words: *earthquake, aftershock, segments dynamics.*

Introduction

The 1988 Spitak earthquake (φ = 40.90; λ = 44.20, M = 7.0, I = 9-10 unit by EMS-98, depth – 10 km, main shock duration – 35-40 sec) is one of the most multilaterally and detailed studied earthquakes in the world [6]. The processes of aftershock activity have also been studied in detail: their spatio-temporal distribution, connection with tectonic structures, internal structure of the aftershock zone, periods of activity, etc. However, all this was considered for 07.12.1988-01.01.1992 [1-3, 5]. Little attention was paid to the events after 1992. The **main objective** of this paper is to identify the features of the internal structure and dynamics of the aftershock zone of the 1988 Spitak earthquake over a long period of time (35 years) depending on individual shocks of the main event and the structure of the aftershock zone. To achieve this goal, it is necessary to solve the following main tasks: a) identification of the structural features of the aftershock zone and allocation of the main segments based on the characteristics of the main event, distribution of aftershock epicenters, parameters of the aftershock focal mechanism; b) connection of segments with geological structures formed on the earth's surface as a result of the earthquake; c) presentation of the main features of the dynamics of the aftershock zone development during the weakly active period of development; d) features of the attenuation of the aftershock process in individual segments; e) identification of patterns of occurrence of strong aftershocks, etc.

Main results

As many researchers, as well as the authors of this article, believe that the spatial-temporal distribution of aftershocks is closely related to the main event, more specifically to the parameters of 3 separate shocks of the main event and large structures formed on the day surface – regional faults and seismogravitational structures [6,7]. As will be shown below, the dynamics of aftershock development also depend on these features.

Location of the three shocks of the main event of the 1988 Spitak earthquake

The 1988 Spitak earthquake began under the city of Spitak, at a depth of about 10 km. The population felt a strong vertical shock. Almost all apartment buildings and private 1-2 story stone houses immediately collapsed. The majority of victims were at that moment. The main material and social losses were in the city of Vanadzor as a result of this shock. In the city of Gyumri, as a result of this shock, the losses, in comparison

with the total losses of the Spitak earthquake, were relatively small. On the outskirts of the city of Spitak, a fault 11 km long was formed. According to all calculations, this first shock had a magnitude of about 7.0.

5 seconds after the first shock, the second, weakest, and most superficial (depth about 5 km) shock of all three main events occurred near the village of Alavar. A fault 10 km long was formed. This shock caused minor destruction in the city of Vanadzor. Experts assume that this second shock did not cause any significant damage in Gyumri.

The third, the strongest and deepest (10-15 km) shock of the main event of the 1988 Spitak earthquake, occurred 14 s. after the second, near the village of Dzorashen. As a result of this shock, a continuous, long fault did not form on the earth's surface, but two large seismogravitational dislocations did. Rock masses weighing 2 million tons or more moved along the slope at an angle of about 20^0, forming a 7 m high "wall" in front and a 25 m deep ravine in the rear. The villages located nearby were completely destroyed. The main destruction of buildings and human casualties in Gyumri were precisely due to this third shock, since its epicenter was 20 km from the city. After the first shock of the main event, the population of Gyumri, who were in high-rise buildings, had about 30 seconds to leave the buildings [7]. Quite a few people, during this time, managed to get out from the 3rd floor into the open space and save themselves.

Segmentation of the aftershock zone

The segmentation (division into subzones) of the aftershock zone was based on: a) three separate shocks of the main event of the 1988 Spitak earthquake, occurring within 35-40 seconds; b) the main tectonic structures formed on the earth's surface as a consequence of these shocks. Analysis of the main parameters of the aftershocks showed that different fragments of the aftershock zone have almost the same parameters and focal mechanism, which coincide with similar parameters of a specific shock of the main event. Thus, such a genetic connection can serve as an argument for identifying individual segments of the aftershock zone [6].

In Fig. 1. the aftershock zone is divided into 4 segments, which differ from each other in important aftershock parameters. The 3 segments (No 1, 2 and 3) correspond to the three shocks of the main event, and the 4th segment is a consequence of the influence of the fault junction. If there were no fault node (the intersection of the Sarikamish and Pambak-Sevan regional faults), then this segment probably would not exist. Despite the fact that the 3 separate shocks of the main event are elements of a single fault formation process (upthrust-slip), their consequences, i.e. aftershocks and their segments, differ from each other. Segmentation of the aftershock zone is important for considering the features of the aftershock process development.

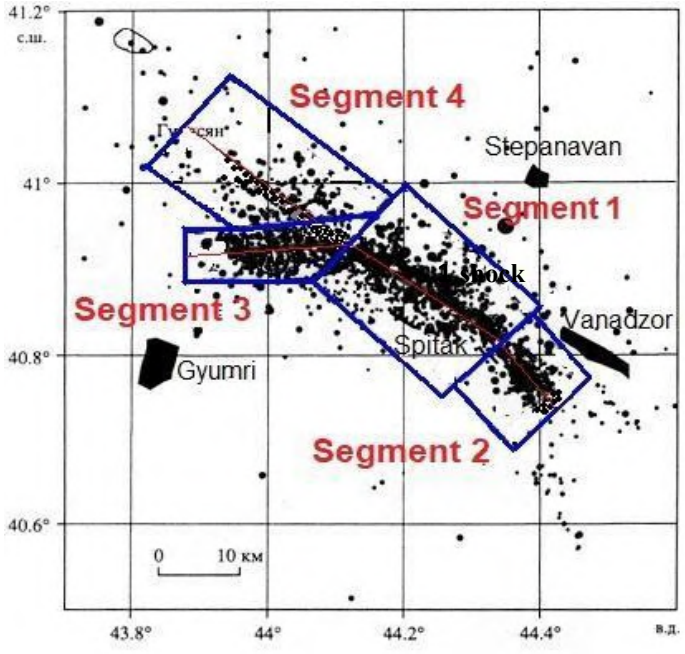

Fig. 1. Map of the aftershock zone segments of the 1988 Spitak earthquake and the distribution of about 14,000 aftershock epicenters for 09.12.1988-01.01.2025 with M≥1.0 [5,6].

Periods of the aftershock process

Usually, experts divide the aftershock process into two periods: highly active and weakly active. For the 1988 Spitak earthquake, the active period ends in early 1992, when the number of aftershocks sharply decreases (Fig. 2 and Fig. 3). The processes of this period have been studied by experts in sufficient detail and from many sides based on a rich database. The vast majority of the 14,000 aftershocks (95%) and the bulk of the total energy released by them (98%) occurred during the highly active period [1,2,6].

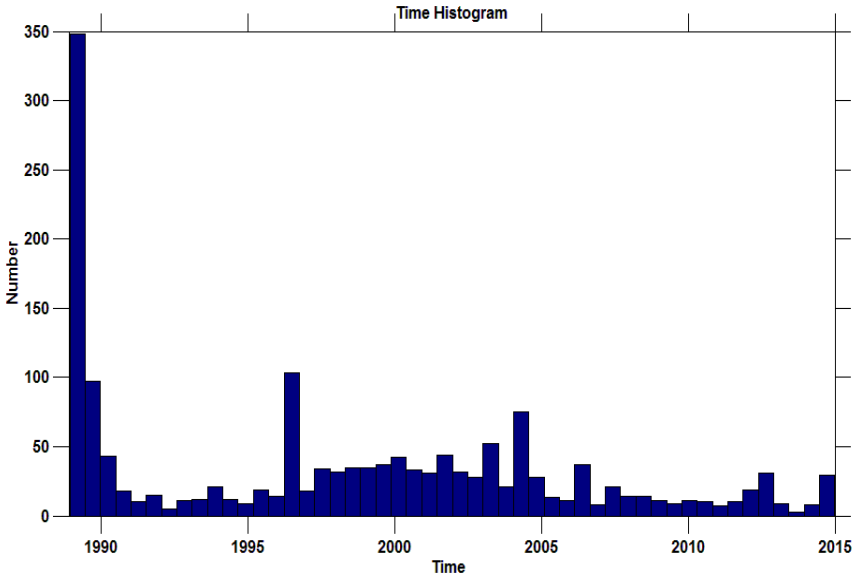

Fig. 2. Distribution of aftershocks of the 1988 Spitak earthquake from 1988 to 2016 [5].
It is obvious that most of the aftershocks occurred in the first three years after the earthquake, in 1988-1991. Aftershocks with magnitude 1.0≤M≤5.0 continue to this day.

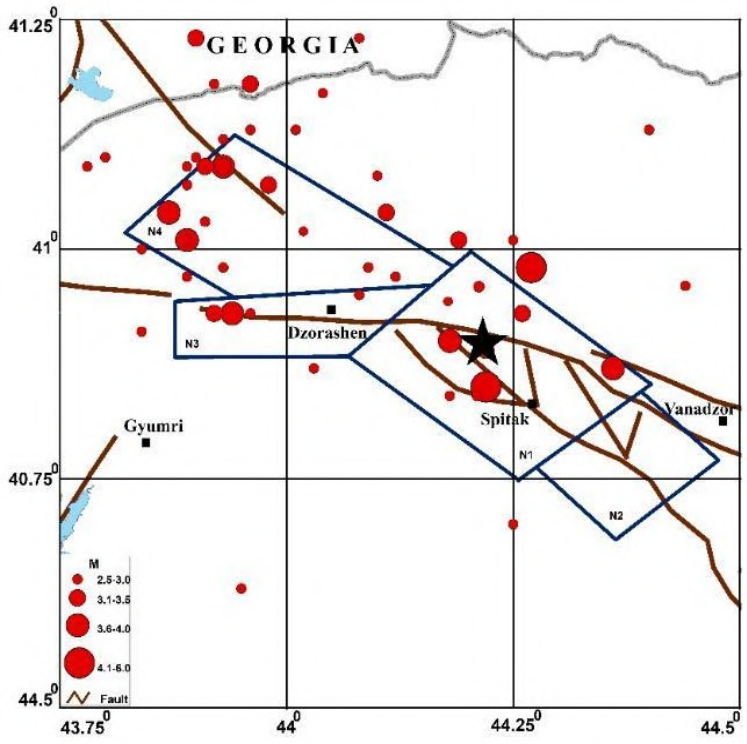

Fig. 3. Map of regional faults [4, 8], 4 segments of aftershock zone of 1988 Spitak earthquake, and epicenters of earthquakes with M≥2.5 for 01.01.2018-01.01.2025. The map shows the epicenter of the Spitak earthquake of 12/07/1988 as a star.

Conclusion

During the weakly active period, i.e. from 01.01.1992 to 01.01.2025, the following patterns of aftershock dynamics are observed:

- The activity of the aftershock process is still observed.
- The number and released energy of aftershocks during the weakly active period in the aftershock zone is significantly higher than in the adjacent areas.
- In the period 1995-2005, a certain activation (in terms of the number and energy of aftershocks) was observed in all 4 segments of the zone (Fig. 3).
- It is assumed that the 2nd segment, which corresponds to the weakest and most superficial shock of the main event of 07.12.1988, has already ceased to show aftershock activity in 2018 (Fig. 3).
- Against the general background of the attenuation of the number of aftershocks and their strength, no pattern in the manifestation of strong aftershocks is observed.

References

1. Cisternas A., Philip H., Arefiev S.S., Bousquet J.C., The Spitak (Armenia) earthquake of 7 December 1988: Field observations, seismology and tectonics. // Nature, vol. 339, N 6227, 1989, pp. 675-679. DOI:10.1038/339675a0
2. Dorbath L., Dorbath C., Rivera L., Fuenzalida A., Cisternas A., Tatevossian R., Aptekman J., Arefev S., Geometry, segmentation and stress regime of the Spitak (Armenia) earthquake from the analysis of the aftershock sequence. // Geophys. J. Intern, vol.108, 1992 pp. 309-328. https://hal.science/hal-03186267/document
3. Haessler H., Deschamps A., Dufumier H., Fuenzalida H. and Cisternas A**.,** The rupture process of the Armenian earthquake from broad-band teleseismic body wave records. // Geophys. 1. Int. 109, 1992, pp. 151-161. https://academic.oup.com/gji/article/109/1/151/573691
4. Karakhanyan A., Arakelyan A., Avagyan A., Sadoyan T., Aspects of the seismotectonics of Armenia: New data and reanalysis. Tectonic Evolution, Collision, and Seismicity of Southwest Asia: In Honor of Manuel Berberian's Forty Years of Research Contributions. Geological Society of America, 2017, pp. 445–477. https://doi.org/10.1130/2016.2525(14)
5. Mirzoyan L.B., Nazaretyan S.N., Features of the structure and dynamics of the development of the aftershock zone of the Spitak earthquake of 1988. // Bulletin of the NAS RA. Earth Sciences. LXI, №1, 2008, pp. 32-38 (in Russian). https://arar.sci.am/Content/119524/file_0.pdf
6. Nazaretyan S.N., The Seismic Hazard and Risk of territories of cities located in the zone of 1988 Spitak earthquake. (Editor- Dr., Prof. Darbinyan S.). // Publ. house Gitutiun- Sciences of National Academy of Sciences of Armenia, Yerevan: 2013, 205 p. (in Russian), ISBN: 978-5-8080-0999-8
7. Nazaretyan S.N., Durgaryan R.R., Shakhbekyan T.A., Mirzoyan L.B., Grigoryan A.G., Regional faults of the territory of the Republic of Armenia according to geophysical data and their seismicity. // "Gitutyun" National Academy of Science. Yerevan, 2015, 198 p. (in Russian). https://www.geokniga.org/books/20055
8. Nazaretyan S.N., Igityan G.A., Assessment of the maximum seismic risk for the territory of Armenia. // Issues of engineering seismology, Vol. 52, No. 2, 2025, pp. 38–54 (in Russian). DOI: https://doi.org/10.21455/VIS2025.2-3

1st International Scientific Conference "Modern problems in Geophysics", Proceedings,
ISBN 978-9941-36-434-1, ISSN 3088-4349, Tbilisi, Georgia, November 6-8, 2025

ASSESSMENT OF THE CONSEQUENCES OF A DESTRUCTIVE EARTHQUAKE AND THE NEEDS FOR RAPID RESPONSE FORCES (BY THE EXAMPLE OF ARMENIA)

***Nazaretyan S.N., **Igityan H.A., **Hakobyan H.P., **Bakunts S.H.**

**Territorial Survey for Seismic Protection of the Ministry of Internal Affairs of the Republic of Armenia, Yerevan, Armenia.*
***National Polytechnic University of Armenia, Yerevan, Armenia.*
snaznssp@mail.ru

Abstract. *In case of a seismic disaster occurring in a developing country, it is very important to determine promptly the number of possible victims and need for rescue forces to estimate the scope of required international assistance and to plan operations of rapid response forces. Rates of the seismic vulnerability of buildings, readiness of the rapid response forces, and other factors, differ from country to country and determine each country's individual capacities and effectiveness in responding to a disaster. Using the example of Armenia, general approaches are proposed for assessing losses and needs for rescue forces.*

Key words: *earthquake, losses, disaster response, needs*

Introduction

For rapid planning and organization of rescue operations and for requesting external rescue assistance, some, albeit approximate, data are needed to assess the scale of the disaster, the number of people and areas affected, the required response forces, etc. The purpose of this article is to help make an initial prompt (in a few hours) assessment of the earthquake effects and the needs for rapid response, especially rescue forces (specialists and equipment) in the event of a devastating earthquake ($7.5 \geq M \geq 7.0$).
The **main purpose** of the article is to propose an approach, which helps to determine the numbers of victims and patients subject to hospitalization approximately and to estimate the need for rescue forces within about 3 hours after a devastating earthquake.

Main results

The main outcome is related to the method of determining the consequences of an earthquake and the required rapid reaction forces, as well as the reference data for their calculation.

1.1. Important tasks and supporting indicators of the calculation

Values and objects to be determined include the following:

1. Parameters of the earthquake using seismograms to establish the time, coordinates, magnitude, depth of the hypocenter, and duration of the main event;
2. Intensity on the EMS-98 scale and based on the statistical isoseismal models of earthquake intensity distribution in the territory of the Republic of Armenia;
3. Cities located in the 8-point intensity zone, and all settlements located in the zone of intensity 9 and higher;
4. Number of possible victims and serious injuries for cities falling in the 8-point intensity zone based on the seismic risk maps, and considering the affected seismically vulnerable multi-apartment, educational and healthcare institutions;
5. Possible damage caused to infrastructure lines (transport, life support, and power supply communications) located in the 9-10-point earthquake intensity zone;
6. The required scope of rescue forces and medical staff (specialists, equipment, medical supplies and medicines) based on a tentative calculation;

7. List of medical institutions that could have become not operational, especially surgical ones, by affected settlements.

2.2. Time available for effective response.

In the territory of the Republic of Armenia, the approximate relationship between earthquake magnitude (*M*) and intensity (*Io*) is as follows: $I_0 = {}^{M}/_{2.5} + MI_0 = {}^{M}/_{2.5} + M$, or $I_0 = 1.4MI_0 = 1.4M$

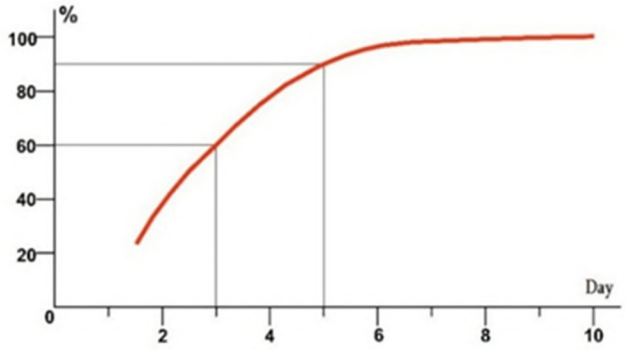

Fig. 1. Graph of the change in the percentage of irreversible losses of people trapped in the rubble during the first 10 days after a devastating earthquake [1].

2.3. Indicators to support calculation of possible casualties and serious injuries.

Depending on specific location or type of building affected [6], expected numbers of victims are estimated as follows:

A. Destroyed apartment of a residential building:

- 1.5-2.0 during the daytime, and
- 3 at night.

B. Potential random locations (shops, restaurants, markets, clubs, streets, bus stations, etc.) in the 9-point intensity zone:

- 0.5% of the total population in the daytime;
- Much smaller rates at night.

C. Private 1 or 2 story-high stone houses:

- About 0.3% and 1.0% of the total number of residents during the daytime and at night, respectively (in the case of a 9-point intensity earthquake),

D. The ratio of the number of hospitalized patients to the number of victims is 2.0-3.0.

2.4. Dependence of the average damage rate values on the earthquake intensity for different types of residential buildings

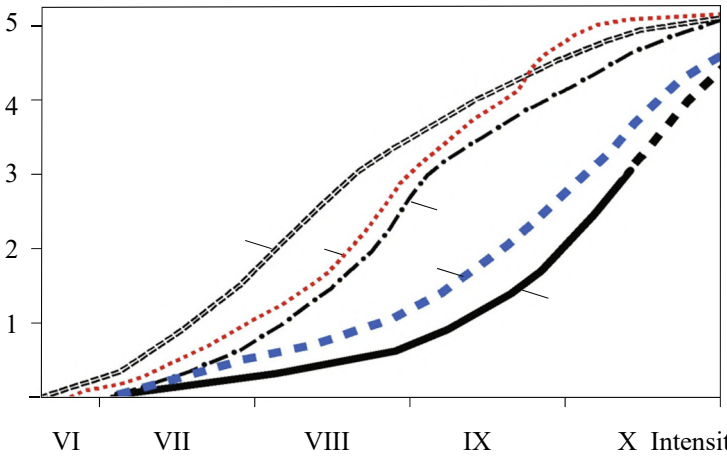

Fig. 2. Dependence of the average rates of damage suffered by different types of residential buildings based on the intensity of the 1988 Spitak earthquake [2]. Types of buildings: (1) private one to two story-high stone houses of the midis system with sand–clay or lime mortar without use of metal elements; (2) private one or two story-high stone houses of the midis system with cement mortar and use of metal structures (antiseismic belts, reinforced concrete lintels and ceilings, etc.); (3) frame-type apartment buildings of Series 111, 4–12 floors; (4) stone buildings of Series IA-450 or I-451, with 4 or 5 floors; and (5) large-panel apartment buildings with 4 to 9 floors.

Table1. The main structural types of multi-apartment buildings in Armenia, their brief description [7], the level of seismic vulnerability of buildings located in a seismic zone with an intensity of 9 points for Category 2 soils [5].

N_o.	Structural type of buildings	Number of floors	Construction period	Brief Description of the Design	Rates of Seismic vulnerability
1	Stone, built by individual project	3–6, (4 floors)	Before 1958	Masonry of the *midis* type (stones laid on both sides of wall and lime mortar with crushed stone filled in between). Walls were 60 cm thick; wooden floors, concrete stairs	Medium
2	Stone, Series I-451	4–5	1958–1970	Midis-type walls were used, wall thickness corresponded to 50cm, cement mortar. Factory-made (precast) hollow panels of concrete. Antiseismic belts were built between the floors and around the ceilings.	Medium
3	Stone, Series IA-450	4–5	From early in 1970 to early in 1988	Midis-type walls 50 cm thick with cement mortar. Factory-made (precast) concrete hollow panels. Antiseismic belts were built between the floors and around the ceilings. The walls were reinforced with vertical reinforced concrete elements.	High
4	Frame-panel, Series111	9	1975–1988	The bearing reinforced-concrete frame was applied in the longitudinal direction. Columns and structural panels (wall) were built in the transverse direction. The columns were sized 40×40 cm. Factory-made hollow panels were used.	High
5	Built by the method of floor lifting	12 or 16	1970–1988	Solid-core walls and factory-made columns with solid floor panels. Floor panels were lifted into the correct position up along the columns.	High
6	Frame-bonded types of design by Badalyan and Manukyan	Badalyan type had 12 (10) or 14 (18) floors; Manukyan type had (10) floors	1960–1988	Factory-made (precast) reinforced-concrete frames were applied for both types. The columns were sized 50×50cm. It was estimated that buildings of this type were more resistant than those of the frame-panel type, taking into account the position of the reinforcement joints. The Manukyan-type column had the size of 40×40 cm. Note: There were no buildings of these types in the area of the Spitak earthquake in1988.	Medium
7	Large-panel, Series 1-451КП	9 or 5	1970–the present	Factory-made (precast) walls, reinforced-concrete structure	Low
8	Monolithic, reinforced-concrete Bearing frame	4 floors or higher	1989 and after 1994	The load-bearing frame is made of monolithic reinforced concrete, including the walls. The design was based on the 1994 RA seismic standards. Non-bearing walls are built of light-weight concrete blocks..	Low

Note: Low-vulnerability buildings have damage degrees of 1-2 and, according to the current RA building codes, can be operated. Buildings with **medium** rate of vulnerability suffer 3rd degree damage mainly, and their safe operation will no longer be guaranteed; hence, these buildings are subject to reinforcement. **Highly** vulnerable buildings are damaged at the rate of 4-5 degrees, and if they are not important as historical and architectural monuments, it is more economical to demolish them.

Table 2. Estimates of potential damage caused to the RA infrastructure lines (life support, transport, communication) falling within earthquake intensity zones of 8-10 points [1,4].

Infrastructure	Rates of Damage by Earthquake Intensity		
	8 points	9 points	9–10 points
Water supply lines	Low	Medium	Strong
High-voltage power supply lines	Low	Medium	Strong
High-pressure gas supply lines	Low	Strong	Strong
Cable telecommunication lines	Low	Strong	Strong
Railways	Low	Weak	Strong
Highways	Low	Weak	Strong

Indicators to support calculation of the required rescue forces

Some estimates of the rescue efforts are provided below.

3.1. Required fire-rescue forces.

For the territory of the Republic of Armenia, it is necessary to use the following data for the 1988 Spitak earthquake [1,3]:

- The scope of rescue forces is estimated at about 38,000 rescuers and 3,150 units of heavy rescue equipment. The required staff of professional rescuers is estimated at 900. This scope would be sufficient number for a destruction zone with a population of about 1,000,000;
- Firefighters carried out about 1,500 missions during the first 10 days.

3.2. Required medical care.

- The number of medical workers who provided timely medical care to 40,000 seriously ill patients was estimated at 5,000.
- During the first 5 days after the earthquake, they performed about 60,000 operations. Each surgeon performed up to 5-8 operations per day.
- The amount of drugs and medical supplies used for 5,000 hospitalized patients is provided in [6].

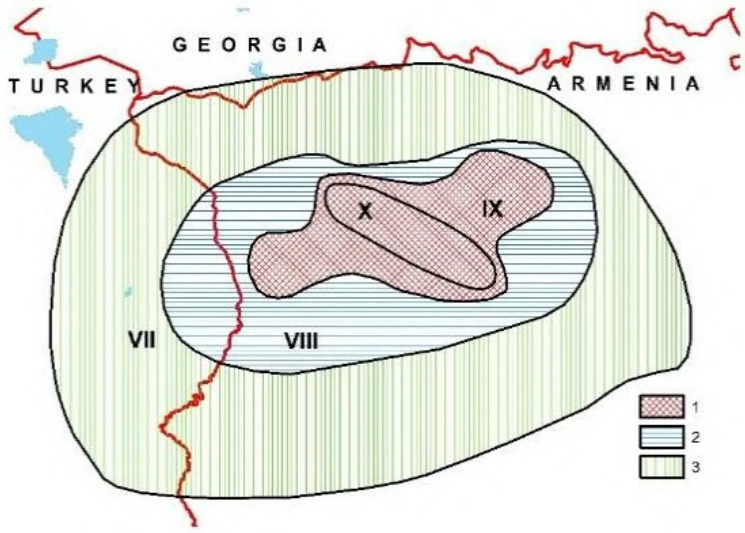

Fig. 2. Schematic map demonstrating the zones of potential damage of buildings and the factors of the impact on human health as a result of the 1988 Spitak earthquake [5]: 1 – the main zone of building damage related to the 4th and 5th degrees (earthquake intensity of IX–X points) and possible victims and heavy injuries; 2 – the zone of building damage related to the 3rd degree (intensity of VIII points) and wounded patients with minor injuries; 3 – the zone of minor building damage (intensity of VII points) and deterioration of living conditions of the population.

Conclusion

This article presents general approaches and some indicators to support preliminary calculations of possible losses and required rapid response forces as soon as 2-3 hours after a devastating earthquake (7.5≥M≥7.0) occurs in Armenia or in adjacent areas. They are extremely important for: a) planning and organizing rescue and medical assistance to the victims; b) determining the need to request international assistance. The approach can serve as an example for carrying out similar work in different countries.

Acknowledgments

The work was financed from the state budget of the RA within the framework of a comprehensive program to reduce seismic risk in the territory of the Republic of Armenia and the Higher Education and Science Committee of MESCS RA (Research project № 25RG-1E115).

References

1. Nazaretyan S.N., The Seismic Hazard and Risk of territories of cities located in the zone of 1988 Spitak earthquake. (Editor- Dr., Prof. Darbinyan S.). // Publ. house Gitutiun- Sciences of National Academy of Sciences of Armenia, Yerevan, 2013, 205 p. (in Russian), ISBN: 978-5-8080-0999-8
2. Nazaretyan S.N. ,Main features of the new methodology for seismic risk assessment of Armenian cities//Seismic Instruments, USA, vol. 56,2020: 317-331. https://doi.org/10.3103/S0747923920030093
3. Nazaretyan S.N., Nazaretyan S.S., Assessment of the Need for Rescue Forces during Destructive Earthquakes (a Case Study of Armenia) // Seismic Instruments, USA, Vol.57, N 2, 2021:150-162, Doi.org/10.3103/S0747923921020298
4. Nazaretyan S.N. and Igityan H.A., Possible Environmental Impact of a Destructive Earthquake // Izvestiya, Atmospheric and Oceanic Physics, Vol. 58, Suppl. 1, 2022: S79-S92. Doi: 10.1134/S0001433822130072
5. Nazaretyan S.N., Gevorgyan M.R., Igityan H.A., Mirziyan L.B., Mughnetsyan E.A., Dynamics of Time Changes in the Seismic Risk of a Big City Due to the Vulnerability of Apartment Buildings(a Case Study of Yerevan) // Izvestiya, Atmospheric and Oceanic Physics, v. 58, No. 8, 2022: 867–880. DOI:10.1134/S0001433822080023
6. Nazaretyan S.N., Haroutiunian R.A., Impact of a Destructive Earthquake on People's Life and Health // Seismic Instruments, USA, Vol. 60, No. 4–6, 2024: 80–92. 2024. DOI:10.3103/S0747923925700136
7. The project for seismic risk assessment and risk management planning in the Republic of Armenia: Final Report JICA, 2012, p. 245. https://openjicareport.jica.go.jp/pdf/12086054_01.pdf.

FROM INITIAL DESIGN TO PRESENT STANDARDS: SEISMIC SOURCES AND CATALOGUES FOR THE ENGURI DAM

Tsereteli N., Varazanashvili O., Khvedelidze I., Kupradze M.

M. Nodia Institute of Geophysics of the I. Javakhishvili Tbilisi State University, Tbilisi, Georgia
nino_tsereteli@tsu.ge

Abstract*. The Enguri High Dam, the highest arch dam in Europe and one of the tallest worldwide (271.5 m), was originally designed in the 20th century for a seismic input corresponding to PGA up to 0.56 g. However, recent probabilistic seismic hazard models developed within the GEM–EMME frameworks suggest higher ground motions, with PGA values approaching 0.9 g. This discrepancy raises critical questions regarding the robustness of the existing hazard assessments and the seismic safety of the dam.*

To address this issue, we initiated a comprehensive investigation combining local and regional seismic data. Spatial clustering of microseismicity allowed us to identify active faults. At the regional scale, we compiled a new unified Georgian earthquake catalogue by merging and harmonizing recently published datasets. For consistency, we also evaluated the completeness and derived Gutenberg–Richter parameters for three independent catalogues: new national catalogue, the EMME dataset, and the GEM-ISC compilation. The comparison highlights both commonalities and discrepancies in seismicity rates and recurrence characteristics, which are crucial for subsequent hazard modeling.While the current study focuses on catalogue development, source characterization, and preliminary seismotectonic insights, the next step will be a probabilistic seismic hazard assessment that integrates the refined catalogues and updated source models.

Key words: *Earthquake catalog, microseismisity, seismic hazard.*

References

1. Sesetyan K., Danciu L., Demircioglu M. B., Giardini D., Erdik M., Akkar S., Gulen L., Zare, M., Adamia Sh., Ansari A., Arakelyan A., Askan A., Avanesyan M., Babayan H., Chelidze T., Durgaryan R., Elias A., Hamzehloo H., Hessami Kh., Kalafat D., Kale O., Karakhanyan A., Khan M. A., Mamadli T., Al-Qaryouti M., Sayab M., Tsereteli N., Utkucu M., Varazanashvili O., Waseem M., Yalcin H., Yılmaz M.T., The 2014 Seismic hazard model of the Middle East: overview and results. // Bulletin of Earthquake Engineering. 16(8), 2018, pp. 3465-3496. **DOI:** 10.1007/s10518-017-0096-8
2. Tsereteli, N., Danciu, L., Varazanashvili, O., Sesetyan, K., Qajaia, L., Sharia, T., Svanadze, D., Khvedelidze, I., The 2020 national seismic hazard model for Georgia (Sakartvelo). NATO Science for Peace and Security Series C: Environmental Security: Building Knowledge for Geohazard Assessment and Management in the Caucasus and other Orogenic Regions, 2021, pp. 131–168.
3. Basili R., Danciu L., Beauval C., Sesetyan K. et. al., The European Fault-Source Model 2020 (EFSM20): geologic input data for the European Seismic Hazard Model 2020. // *Natural Hazards and Earth System Sciences.* 2024, 24(11), 2024, pp. 3945–3976. DOI 10.5194/nhess-24-3945-2024
4. Tsereteli N., Ghomidze L., Tugushi N., Temporal Evolution of Microseismicity in Response to Reservoir Operation at the Enguri Dam (Georgia). // Journal of the Georgian Geophysical Society, e-ISSN: 2667-9973, p-ISSN: 1512-1127. Physics of Solid Earth, Atmosphere, Ocean and Space Plasma, v. 28(1), 2025, pp. 5 – 20.
5. Bondár I., Godoladze T., Cowgill E., Yetirmishli G., Myers S. C., Gunia I., Buzaladze A., Czecze B., Onur T., Gök R. et al., Relocation of the seismicity of the Caucasus region. // Bull. Seismol. Soc. Am., 2023. doi: 10.1785/0120230155
6. Godoladze T., Gök R., Onur T., Gunia I., Dzmanashvili M., Boichenko G., Buzaladze A., Bondár I., Ratiani L., Rostomashvili T., Nabelek J., Javakhishvili Z., Yetirmishli G., Sandvol E., Kadirioğlu F.T., Chiang A., *Compilation of a Comprehensive Earthquake Catalog and Relocations in the Caucasus Region. //* Seismological Research Letters 95(2), 2024. DOI:10.1785/0220230206

1st International Scientific Conference "Modern problems in Geophysics", Proceedings,
ISBN 978-9941-36-434-1, ISSN 3088-4349, Tbilisi, Georgia, November 6-8, 2025

THE RESULTS OF FIFTY YEARS MONITORING OF THE STRAIN DYNAMICS OF THE FAULT CROSSING THE LARGE ENGURY DAM FOUNDATION

****Chelidze T., *Dovgal N., *Kiria J., Tsaguria T., *Davitashvili L.**

**Mikheil Nodia Institute of Geophysics of Ivane Javakhishvili Tbilisi State University, Tbilisi, Georgia*
***Academy Member, Georgian National Academy of Sciences, Tbilisi, Georgia*
tamaz.chelidze@gmail.com

Abstract. *The high Enguri arch dam (271 m) was erected in the 1970s in the canyon of the river Enguri. The dam area is a zone of high seismicity with the moment magnitude Mw = 8. It is close (several hundred meters) to the large Ingirishi active fault (Figure 1). The high seismic and geodynamical activities together with the dense population downstream of the dam made the Enguri dam with its one billion cubic meters water reservoir a potential source of a major catastrophe in Georgia. In turn, this means that the dam should be under permanent monitoring. Accordingly, this problem is the object of research of the M. Nodia Institute of Geophysics and European Specialized Centre "Geodynamical Hazards of High Dam" of the European-Mediterranean Open Partial Agreement on Major Disasters, organized in 1996 by the Council of Europe.*

Key words: *Enguri Dam, fault crossing dam foundation, fault strain dynamics*

Introduction

In this paper we consider the results of half-century permanent monitoring of deformation of the fault zone, which is crossing the dam foundation. This leads to understanding complicated dynamics of the fault zone deformation, reflecting a joint influence of local tectonics, man-made engineering stresses and environmental factors. The strain-rate on the fault in the period 1974 – 2019 varied between 250-150 μm/year, but in the last years, 2019-2024 the strain rate abruptly fell to zero. The change of the strain regime in the last years can be connected either with the final stabilization of the fault or with a temporary braking of fault motion by a strong asperity on the fault interface, which can lead to dynamical discharge of accumulated strain.

Study area,material and methods

The permanent multi-disciplinary geodynamical/geophysical monitoring network was organized in the dam area [1, 2, 3] in order to control the stress–strain state in the foundation of the dam according to existing standards [4]. Monitoring of the fault zone (FZ) strain and local seismicity began several years before the start of reservoir filling in April 1978. The monitoring system of Enguri Dam and its foundation (Figs. 1 ,2, 3) includes a network of tiltmeters, strain-meters and reverse plumblines in the dam body, meteo-station, water level gauge for monitoring water level in the lake. After the organization of the European Specialized Centre "Geodynamical Hazards of High Dam", the monitoring network improved significantly. Automation of monitoring data retrieval and their telemetric transfer using Internet connection, ensure obtaining information on the strains in dam foundation and its body in a close to the real time regime. This is important for operative detection of strain dynamics' deviations from the background (design) pattern and finding possible sources of anomalous behavior. The M. Nodia Institute of Geophysics and European Centre "Geodynamical Hazards of High Dams" developed the real-time geotechnical telemetric monitoring system of large dams (DAM-WATCH). This low-cost early warning system consists of tilt sensors (tiltmeters, APPLIED GEOMECHANICS Model 701-2) and quartz strainmeter with optical registration (Laser model R-39568, Green HeNe Laser, 633 nm and Laser Position Sensor OBPA-9L), which are connected to terminals and central controllers and by a GSM/GPRS modem transmits the data to the diagnostic center in Tbilisi (Fig.1, 2, 3). The fixed and free

parts of the strainmeter are located on the intact rocks on the opposite sides of the fault zone (FZ); the full length of the strainmeters' quartz tube is 22.5 m. This means that the device records displacement of the intact blocks, divided by the fault zone in the normal to the fault plane direction, so it records the fault zone's extension/contraction.

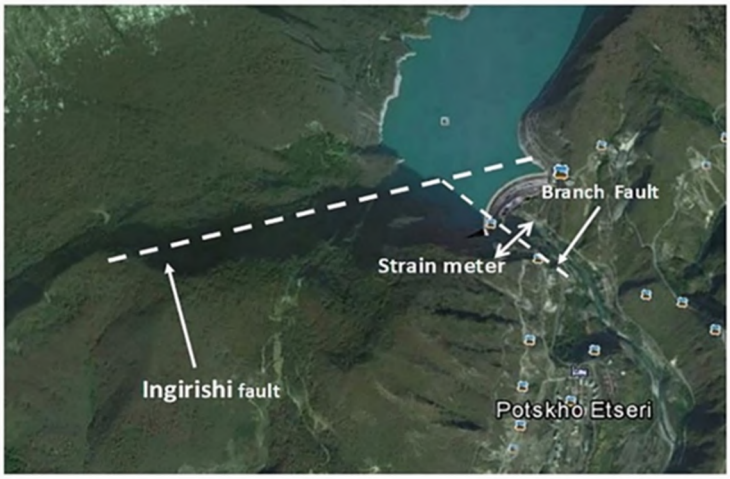

Fig.1. Google image of Enguri Dam area. The main tectonic units of the area are Ingirishi fault and its branch, which is crossing the foundation of Enguri dam as well as the tunnel 3413, where the strainmeter is installed (see also scheme 2).

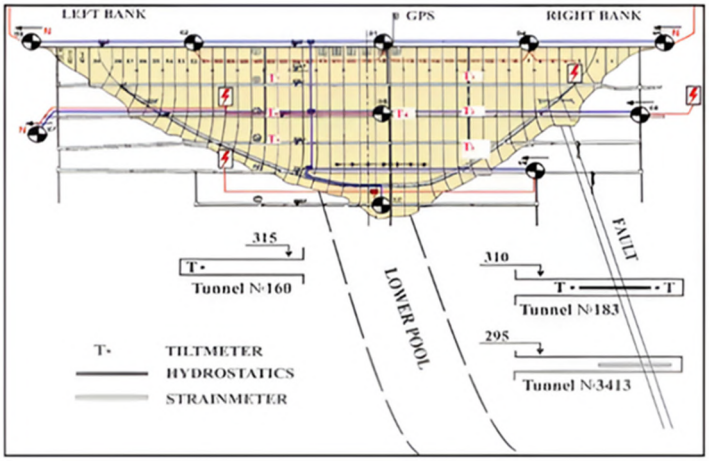

Fig. 2. The monitoring system at Enguri High Dam. The strainmeter is installed on the fault crossing the dam, in the tunnel N3414, at the distance 120 m from the dam foundation.

Transmission system, connected sensors installed at Enguri Dam area are carried out by the group of German Geophysicists from Karlsruhe of Technology.

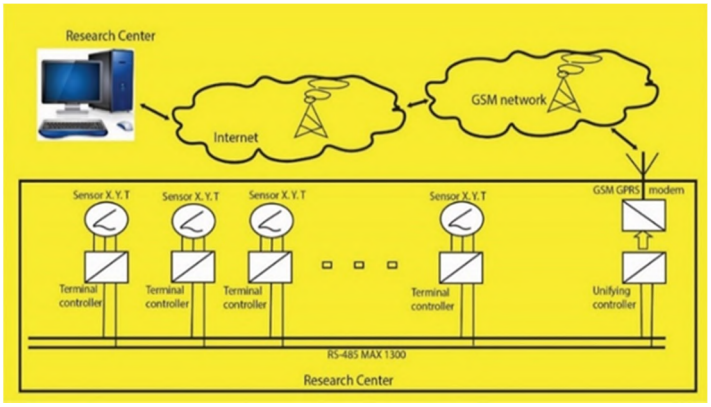

Fig 3. Transmission system, connecting sensors installed at Enguri dam with monitoring centre in the Institute of Geophysics

Results

The strain rate history of the branch fault crossing the Enguri Dam is complicated: it reflects the strong variations in the slip velocity [5]. The initial strain rate (SR) values for 1974-1985 reflect the natural (tectonic) component dynamics of the fault strain rate: V1= 250 μm/year; this SR characterizes the mechanical properties of the natural system of force chains in the fault gorge under the natural strain rate. In the following 1985-2004 period velocity decreased to V2 = 160 μm /year, which can be due to the damage of the initial system of force chains in the fault volume by water load cycles as a result of the reversed–stress fatigue effect. In the following epoch (2004-2013) the strain rate V3 increases to almost initial value V3 = 233 μm /year, which can be interpreted as the result of temporary healing of disrupted force chains. In the following period V4 the strain rate decreased again to 150 μm /year, i.e. it almost returns to V2, which again can be explained by the repeated weakening of force chains in the fault gorge. This repeated pattern of slip from 1974 to 2013 can be explained by the quasiperiodic slip process with alternating velocity of slip, due to varying fault surface roughness.

In the last years, 2019-2024 the strain rate abruptly fell to zero: V5 = 0 μm. The change of the strain regime in the last years can be connected either with the final stabilization of the fault or with a temporary full braking of the fault motion by a strong asperity/asperities on the fault interface. In the last case, the stress on the fault will build up, till attaining the critical stress value, necessary for overcoming the resistance of asperity/asperities in a dynamical manner. The dynamical discharge of the accumulated energy can generate an earthquake. Taking into consideration the length of the dam-crossing fault (2-3 km) the magnitude of EQ can be of the order of M3-4 [6,7], which should not be dangerous the dam structure, as according to previous engineering assessment [8], the Enguri Dam should withstand the impact of the maximal expected earthquake of magnitude M8.

Table 1. Periods with different strain rates of trend, from the data, presented in Fig. 4.

Number of periods	Periods: month, years	Strain rate α in the period, microns/year
1	May 1974-Feb. 1985	250
2	Feb. 1985-May 2004	160
3	May 2004-May 2013	233
4	May 2013-Apr. 2019	150
5	Apr. 2019-Aug.2024	0

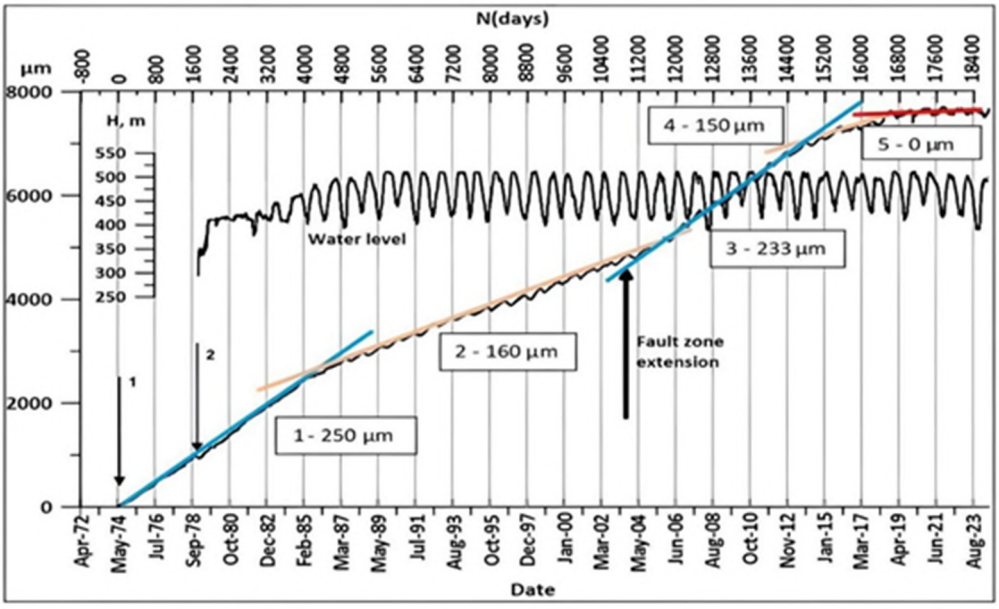

Fig. 4. WL in the Enguri lake from 1978 (upper curve) to 2023 and the data of the extension/compaction of the branch of the large Ingirishi fault, crossing the foundation of the dam (lower curve). Arrow 1 corresponds to the start of strainmeter monitoring and arrow 2 – to fault compaction by approximately 90 μm at WL, rising to 100 m in 1978. The upper horizontal axis shows the number of days from the zero day (1 May 1974) to August 2024. Note different strain rates during 50 years of the observation period.

Conclusion

It cannot be excluded that strain on the dam-crossing fault is governed by the deformation of the main Ingirishi fault of which the dam-crossing fault is a side fault. In this case, the leading seismogenic factor will be the main Ingirishi fault, which is characterized by much larger seismic potential, than the small side fault. As the existing strain observation system of Enguri Dam does not cover the main Ingirishi fault, the problem should be studied in detail by installation of strainmeter and seismic station on the Ingirishi fault and analysis of its dynamics.

References

1. Abashidze V., Geophysical monitoring of geodynamical processes at Enguri Dam. // Publishing House Metsniereba, Tbilisi, 2001. (in Russian).
2. Savich A. (ed)., Complex engineering-geophysical Investigations in construction of hydropower objects. // Nedra, Moscow, 2002. (in Russian)
3. Chelidze T., Matcharashvili T., Abashidze V., Kalabegashvili M., Zhukova N., Real time monitoring for analysis of dam stability: potential of nonlinear elasticity and nonlinear dynamics approaches. // Front Struct Civ Eng 7, 2013, pp. 188–205. https://doi.org/10.1007/s11709-013-0199-5
4. Automated Dam Monitoring Systems. Bulletin of International Committee of Large Dams, N 118. Paris, 2000. https:// www.academia.edu/4094909/Automated_dam_ monitoring_systems. Guidelines_and_case_histories.
5. Chelidze, T., Matcharashvili, T., Abashidze, V. et al., Complex dynamics of fault zone deformation under large dam at various time scales. // Geomechanics and Geophysics for Geo-Energy and Geo-Resources, 2019. https://doi.org/10.1007/s40948-019-00122-3
6. Westwood R., et al., Horizontal respect distance for hydraulic fracturing in the vicinity of existing faults. // Geomechanics and Geophysics for Geo-Energy and Geo-Resources, 2017. . DOI: 10.1007/540948-017-0065-3.
7. Madariaga R., Ruiz, S., Earthquake dynamics on circular faults: a review. // Journal of Seismology, 2016. DOI: 10.1007/510950-016-9590-8.
8. Emukhvari N, Bronshtein V., Enguri HPP-system of allowable and limiting parameters of arch dam state for operative control of its safety during exploitation. Ministry of Energy USSR, Moscow, 1991. (In Russian).

1st International Scientific Conference "Modern problems in Geophysics", Proceedings,
ISBN 978-9941-36-434-1, ISSN 3088-4349, Tbilisi, Georgia, November 6-8, 2025

USING SEISMIC SURVEY METHODS TO SOLVE ENGINEERING (HYDROTECHNICAL) PROBLEMS

Gigiberia M., Kiria J.

[*]Mikheil Nodia Institute of Geophysics of Ivane Javakhishvili Tbilisi State University, Tbilisi, Georgia
kiria51@yahoo.com

Abstract. *The development of hydroelectric construction has necessitated a comprehensive study of the rock masses forming the foundations of hydraulic structures. This issue becomes particularly relevant in the case of high dams, which are often accompanied by large reservoirs and are frequently located in areas of high seismic activity. The paper focuses on the role of engineering geophysics – specifically, seismics – in the construction of major structures. As an example, we present a specific project and the methods used for its implementation, namely the studies conducted by the Institute of Geophysics in the design area of the Nenskra Hydropower Plant.*

Key words: *Seismic Survey, Hydropower, Elastic Parameters.*

Introduction

According to the construction and operational project of the hydroelectric power plant (HPP), it is planned to build and operate a 280 MW high-pressure, seasonally regulated HPP in the Samegrelo-Zemo Svaneti region, specifically within the Mestia Municipality [1-5]. The construction is planned in the Nenskra River valley, utilizing the runoff from both the Nenskra and Nakra rivers.

It should be noted that the research was preceded by extensive exploratory work carried out over many years by various design and construction organizations from different countries. The goal of these studies was to select suitable locations for the intake structures and powerhouse of the future hydropower complex. A significant volume of geological and geophysical work was performed for this purpose.

Unfortunately, the results of these works did not allow for the selection of an optimal location for the intake structure. One of the main reasons was that the obtained data did not provide a clear, convincing image of the cross-section for the potential foundation of the future dam. This issue was further complicated by the fact that, based on borehole data from the study area, the thickness of alluvial gravel deposits above the bedrock in some places exceeds 70–80 meters. Under such local conditions, standard impact sources for elastic wave generation (e.g., hammer strikes) become ineffective for seismic investigations.

As a result, a new task was set: to conduct investigations in the designated areas using such methodology and equipment that would allow us to obtain reliable results and gain information about the subsurface structure down to the required depths.

Fieldwork was conducted using a 24-channel seismograph of the GEODE brand, produced by the American company GEOMETRICS, along with a full set of accessories. This equipment fully meets the requirements of the task at hand and is capable of operating with various seismic methods, including the refraction wave method and the common depth point (CDP) method.

Regarding the methodology, both the **refraction wave method** and the **common depth point method** were used.

The **refraction wave method** allows for determining the thickness of both shallow and deeper layers, as well as the velocities of elastic wave propagation through them. The method is based on determining the first arrival times of elastic waves from a source to geophones arranged in a straight line. Therefore, the research objective was to determine the structure of the rock formations [6-11].

Seismic profiling using the refraction wave method was carried out at the study site, providing information to depths of 45–120 meters. In addition to velocities, the density of each layer was also determined from the seismic profiles. Six seismic profiles, each 230 meters in length (totaling 1380 meters), were carried out. Fig. 1 shows the study area and the layout of the seismic profiles.

Fieldwork was conducted in collaboration with the geodesy service and explosives specialists.

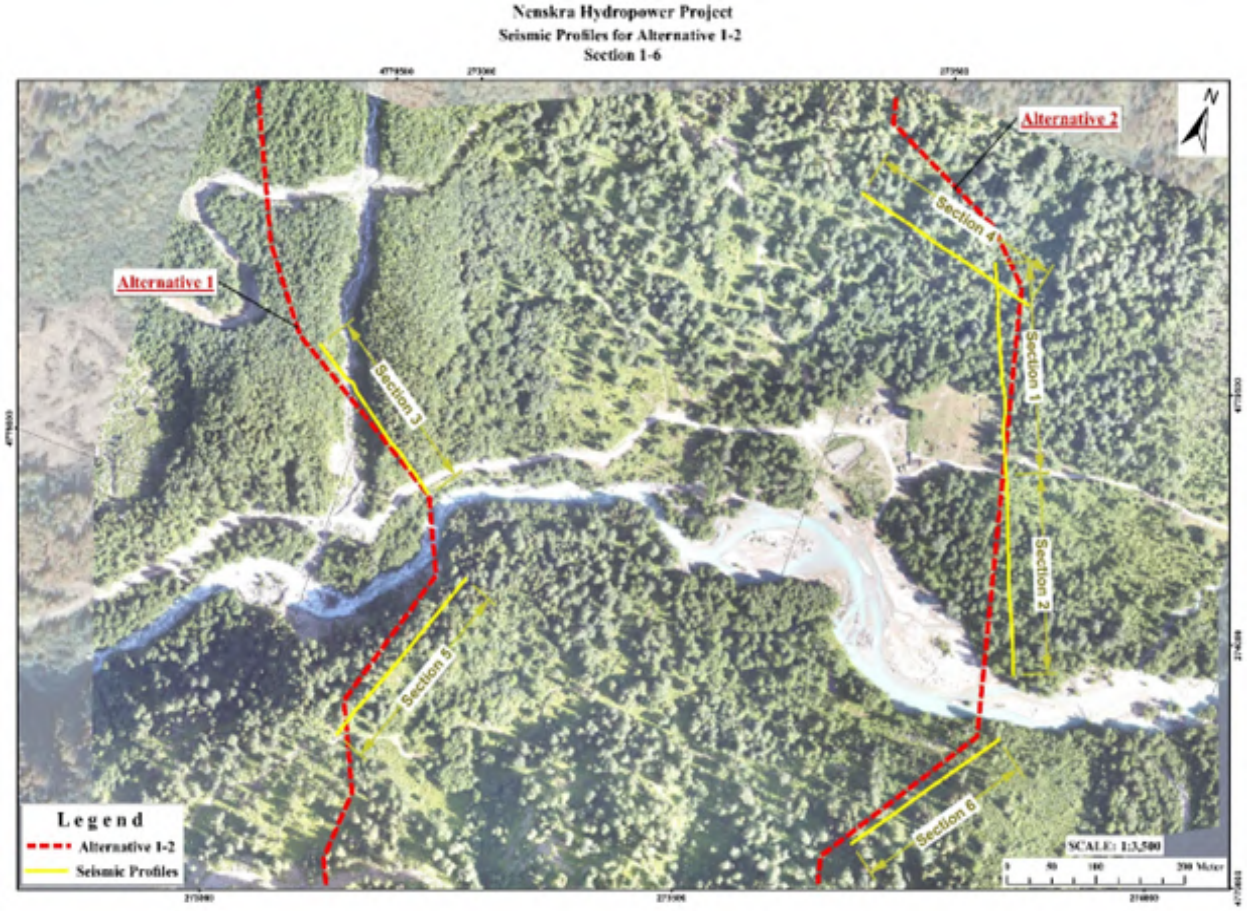

Fig. 1.

Results of Geophysical Surveys in the Nenskra River Valley

In our case, the survey area was quite limited, which posed certain challenges when selecting the survey geometry.

For each profile, 47 seismic impulses were generated – 23 within the profile itself, and 24 from points offset at the beginning and end of the profile. The spacing between both geophones and impulses was 10 meters.

The survey employed 10 Hz geophones, and the seismic waves were induced by small explosive charges (up to 300 grams) in compliance with Georgian safety standards, ensuring the acquisition of clear records. The coordinates for the geophones and shot points were determined by a geodetic team.

Wave registration in both methods was carried out using a 24-channel engineering seismograph of the GEODE brand by the American company GEOMETRICS. Interpretation of the refraction wave method was performed using the licensed **SeisImager** software by the same company, while the **Common Depth Point (CDP)** method used licensed **RadexPro** software.

The acquired seismograms were analyzed, cross-sections constructed, and corresponding density values estimated.

Seismic Profile No. 1

The first superficial layer (Layer 1) extends from the surface to a depth of 3–20 meters, with an average compressional wave velocity of Vp = 1445 m/s and an average density of $\rho = 1.99$ g/cm³. It is followed by **Layer 3**, which is in a water-saturated state, with a thickness ranging from 1 to 45 meters, an average compressional wave velocity of Vp = 2023 m/s, and an average density of $\rho = 2.16$ g/cm³. Next is **Layer 4**, observed at depths ranging from 55 to 75 meters, with an average compressional wave velocity of Vp = 2868 m/s and an average density of $\rho = 2.36$ g/cm³.

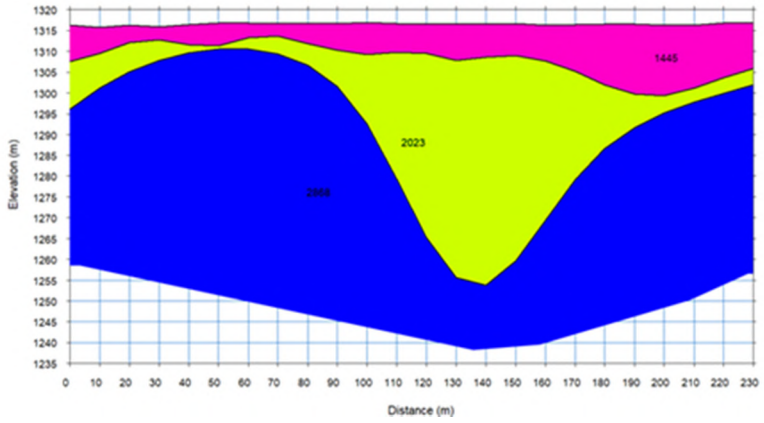

Layer №	V m/s	ρ g/cm³)
1	1445	1.99
3	2023	2.16
4	2868	2.36

Seismic Profile No. 2

The first near-surface layer (Layer 1) extends from the surface down to a depth of 10–17 meters, with an average compressional wave velocity Vp = 1449 m/s and an average density ρ = 1.99 g/cm³.

It is followed by Layer 3, in a water-saturated state, with a thickness of 2.5–15 meters, an average compressional wave velocity Vp = 2291 m/s, and an average density ρ = 2.23 g/cm³.

Next is Layer 4, observed at depths from 45 to 54 meters, with an average compressional wave velocity Vp = 3107 m/s and an average density ρ = 2.40 g/cm³.

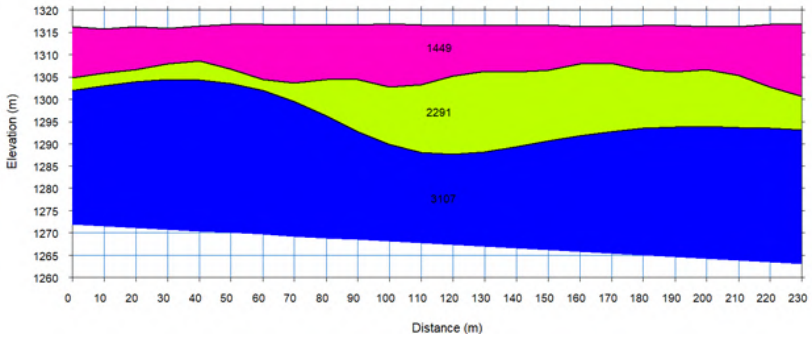

Layer №	V m/s	ρ g/cm³)
1	1449	1.99
3	2291	2.23
4	3107	2.40

Seismic profiling was conducted using the Common Depth Point (CDP) method. Corresponding seismic-geological cross-sections were constructed, and compressional wave velocities were determined. The report includes cross-sections from two seismic profiles, each 230 meters in length. Fig. 1 shows the study area and the layout of the seismic profiles.

The resulting seismic sections are presented in Fig. 2 and Fig. 3. On these sections, the presumed reflective surfaces observed during the investigation are marked with black contours, based on our interpretation.

Seismic Profiles No. 1 and 2:

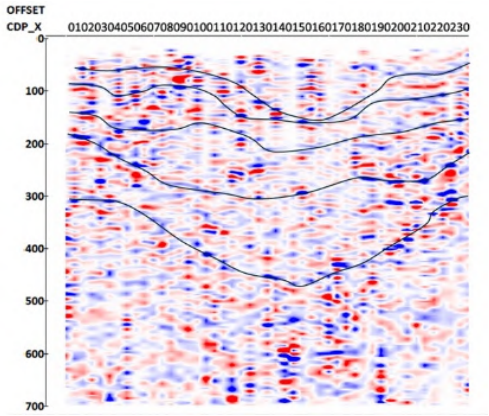

Fig. 2

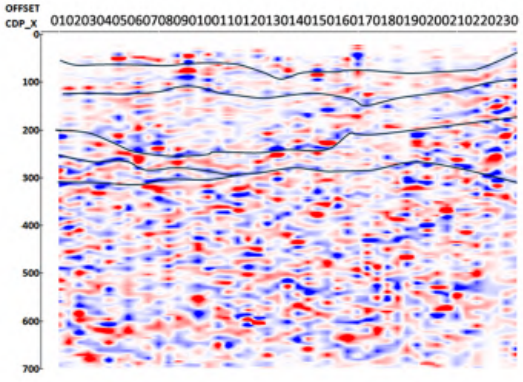

Fig. 3

Conclusion

Based on geophysical parameters, various engineering-geological elements (layers) have been identified, and the distribution of velocity values within them has been determined.

According to the geophysical data, the resulting cross-sections mainly reveal four distinct layers with different physical properties (identification was guided by engineering-geological information):

Layer 1 – Soil layer, loose fill;

Layer 2 – Boulder with clay filler;

Layer 3 – River alluvium, gravel and pebbles;

Layer 4 – Magmatic bedrock, presumably granite, with varying degrees of weathering and fracturing.

Seismic profiling was conducted using the Common Depth Point (CDP) method. Seismic-geological cross-sections were created, and compressional wave velocities were determined. The report includes cross-sections of two seismic profiles, each 230 meters long.

The presumed reflective surfaces observed during the survey are marked on the sections with black contours, based on our interpretation.

The results obtained through the refracted wave method and the Common Depth Point (CDP) method are in good agreement with each other, considering the observed depths.

References

1. Dortman N.B., Physical properties of rocks and minerals, 1984.
2. Goryainov N.N., Seismic Methods in Engineering Geology. // Nedra, 1979, p. 150.
3. Kobayashi Y., Horike M., Analysis of seismic exploration data using ray method. // J. Phys. Earth 35, 1987, p.127-141.
4. Majan A.K., Slob S., Ranjan R., Sporry R.J., Champati P.K. van Westen C.J., Seismic microzonation of Dehradun City using geophysical and geotechnical characteristics in the upper 30 m of soil column. // Journal of Seismology, vol11, n. 4, pp. 355-370.
5. Laster S., Backus M., Schell R., Analog model studies of the simple refraction problem. // Seismic refraction prospecting, Tilsa, 1967, pp.15-66.
6. Nikitin V.N., Fundamentals of Engineering Seismics. Moscow State University, 1981, p. 175.
7. Media T., Hammer refraction seismic in engineering geophysics. // “Geophysics”, v.34, № 3, 1969, pp.383-395.
8. Savich A.I., Kuiyndjich B.D., Complex-ingineering research in building hydraulic facilities, 1990.
9. Sheriff R., Geldart L., Exploration Seismology. // Mir, Moscow, v.1 and 2, 1987, p. 900.
10. Earthquake motion and ground conditions, The Archtectural Institute of Japan (AIJ), 1993, p. 595.
11. International Building code, International code council, INC, USA, 2006, P. 680.

1st International Scientific Conference "Modern problems in Geophysics", Proceedings,
ISBN 978-9941-36-434-1, ISSN 3088-4349, Tbilisi, Georgia, November 6-8, 2025

INVESTIGATION OF DYNAMIC BEHAVIOR VARIATIONS OF THE ENGURI ARCH DAM

***Matcharashvili T., *,**Sborshchikovi A., *Mepharidze E., *Chelidze T., *Zhukova N., *Tepnadze D., *Laliashvili L.**

** Mikheil Nodia Institute of Geophysics of Ivane Javakhishvili Tbilisi State University, Tbilisi, Georgia*
*** Business and Technology University, Tbilisi, Georgia*
a.sborshchikov@gmail.com

Abstract. *The primary objective of this study is to investigate the dynamic variations in the displacement of the Enguri Arch Dam foundation in relation to periodic fluctuations in the reservoir's water level. The analysis is based on a comprehensive dataset spanning the period from 1974 to 2021. In this work, we applied several modern nonlinear analytical techniques to examine these dynamical changes, with a focus on the highly effective* ***Multifractal Detrended Fluctuation Analysis (MF-DFA)*** *method. Our findings indicate a clear connection between the displacement dynamics of the dam foundation and the overall behavior of the structure. Notably, one of the key factors influencing these dynamics is the variation in the water level of the reservoir behind the Enguri high dam.*

Key words*: Dynamical changes, nonlinear analyses, datasets.*

Introduction

The initial phase of our research involved an in-depth review of existing literature relevant to our topic. This review revealed numerous references highlighting the significant environmental impact of constructing and operating large water reservoirs. Among the documented effects are increased local seismic activity, alterations in regional climate patterns, and the triggering of landslides. These findings underscore the importance of addressing the issue through a multidisciplinary approach, warranting further and more detailed investigation.

Our study focuses on the Enguri Dam area due to its prominence as one of the tallest arch dams in the world, with a height of 271 meters. Located in western Georgia, the Enguri Arch Dam is an integral part of the Enguri Hydropower Plant (HPP), situated within the Enguri River Gorge. Since the commencement of its construction, a comprehensive geodynamical and geophysical monitoring system – advanced for its time – was established in the area to track various physical and structural processes [1–3].

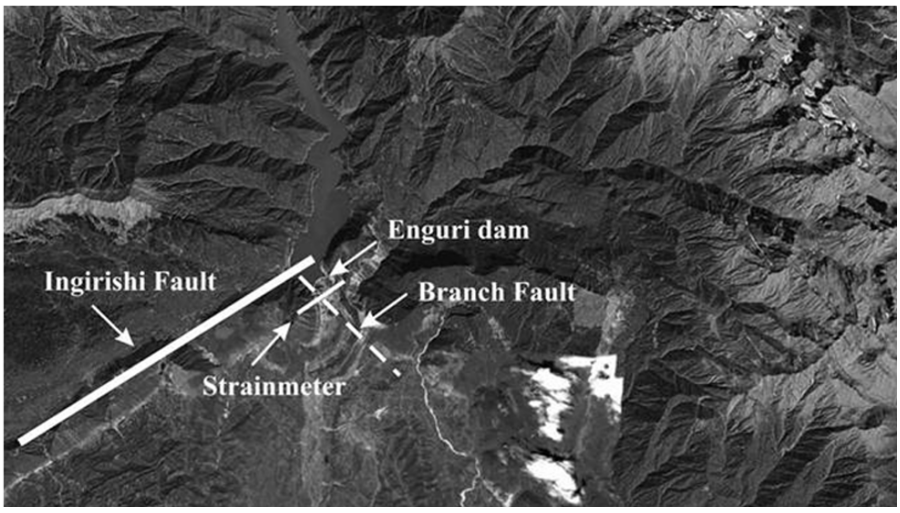

Fig. 1. Enguri dam and reservoir area with locations of the main Ingirishi fault and the branch fault.

Geological surveys have revealed that a branch of the major active Ingirishi Fault intersects the right abutment of the Enguri Dam foundation. The presence of an active or potentially active fault beneath a large dam represents a serious risk to its structural integrity and overall safety [1,4,5]. Given this risk, continuous monitoring of the fault zone began well before the construction of the dam and the subsequent filling of the reservoir.

The branch of the Ingirishi Fault (Fig. 1) that crosses the dam foundation is a significant geotechnical concern, making this site particularly valuable for studying the interaction between tectonic processes and anthropogenic influences. In fact, the Enguri Dam region serves as a natural large-scale laboratory for investigating the deformation behavior of fault zones under the combined effects of tectonic forces, human activity, and environmental factors.

Two key influences on the fault zone behavior were identified. The first, **tectonic strain**, results in a piecewise linear displacement, which we interpret as the **trend component** of the deformation. The second influence is associated with **quasiperiodic oscillations**, which modulate this trend and are likely linked to cyclic environmental or operational factors.

The dataset used in our research covers the period from **1974 to 2021** and is particularly valuable due to its inclusion of critical parameters such as high weir foundation and body tilt measurements, foundation deformation data, internal temperature of the dam body, and water level variations in the reservoir. Portions of this dataset have already been published in peer-reviewed journals [2–6]. In this study, we focus specifically on the **displacement of the dam foundation** recorded over the full observational period (Fig. 2).

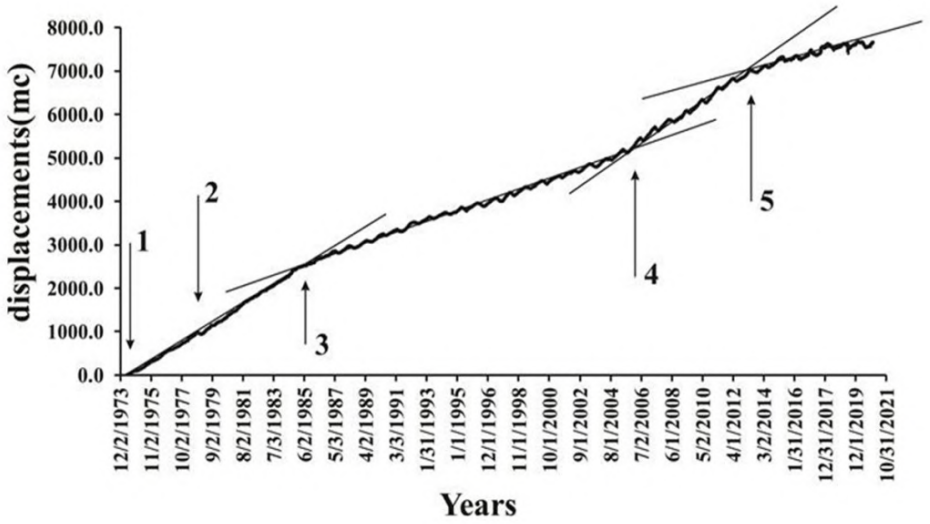

Fig. 2. Dam foundation displacement data sets around Enguri in period from 1974 to 2021. Arrows 1, 2, 3, correspond to the initial periods of fault zone extension.

To enable continuous monitoring of fault zone behavior, a **quartz strainmeter** was installed in 1974 – four years prior to the initial filling of the Enguri reservoir. Positioned across the fault zone, this instrument measures relative displacement of the blocks separated by the fault (approximately 10 meters in width), specifically in the direction normal to the fault plane. As such, the strainmeter captures fault zone **extension and contraction**. The total length of the quartz tube is **22.5 meters**, and the system's **free end** is equipped with a **photo-optical recording device**, now operating in parallel with a **laser-based system**. The strainmeter is designed with its fixed and free ends anchored on opposite sides of the fault, each several meters away from the fault plane. Measurements were recorded daily at the same time, with a system sensitivity of approximately **0.18 micrometers per millimeter**.

The **stepwise filling** of the Enguri reservoir commenced on **April 15, 1978**, and from **1987 onwards**, the water level has exhibited **regular seasonal fluctuations**. Seismic data were collected from a network of monitoring stations installed throughout the Enguri area, with a **magnitude threshold** of **M2.2** for inclusion in the local earthquake events catalogue spanning **1974 to 2021**.

In our study, we utilize the **strainmeter data** to analyze displacement in the **foundation of the high Enguri Arch Dam**. As previously noted, fluctuations in the reservoir's water level appear to influence **local seismic activity**, which in turn may affect the deformation dynamics of the dam foundation.

To examine the **nonlinear dynamics** of foundation displacement, we applied the **Multifractal Detrended Fluctuation Analysis (MF-DFA)** technique. The analytical software used was developed by specialists at the **M. Nodia Institute of Geophysics, Ivane Javakhishvili Tbilisi State University**. MF-DFA is a powerful method capable of revealing **hidden multifractal structures** within non-stationary time series and is an extension of the traditional **Detrended Fluctuation Analysis (DFA)** introduced by Kantelhardt et al. [7].

Our analysis explores the **multifractal scaling behavior** of the displacement time series. We examine three key metrics:

- the **generalized Hurst exponent** H(q),
- the **multifractal spectrum dimension** D(q)
- the **fluctuation functions** F(q).

The **Hurst exponent**, originally proposed by Hurst (1951), provides insight into the correlation structure of the time series. If H(q) lies between 0.5 and 1, the data exhibits **long-range correlations**; values between 0 and 0.5 indicate **anti-correlated** behavior, and H(q)=0.5H(q) signifies **uncorrelated or short-memory** processes. Values above 1 are characteristic of **random-walk-like** dynamics.

It is important to note that while MF-DFA accurately determines **positive generalized Hurst exponents**, it may lose precision in the presence of **strong anti-correlations**, where h(q) approaches zero [9,10]. Nevertheless, MF-DFA remains one of the most effective tools for analyzing **multifractal properties of non-stationary geophysical time series**.

The displacement data spanning **1974 to 2021** were affected by various external influences – including **reservoir filling**, **meteorological variability**, and **seismic activity** – necessitating **detrending** prior to analysis. For this purpose, we divided the overall dataset into several distinct sub-periods: **1974–1978**, **1978–1985**, **1985–2006**, **2006–2013**, **2013–2017**, and **2017–2021**, – each representing a phase with noticeably different displacement behaviors. MF-DFA was then applied using **polynomial detrending** of various orders, such as **p = 2** and **p = 5**, to capture both local and global trends (Fig. 3a, 3b).

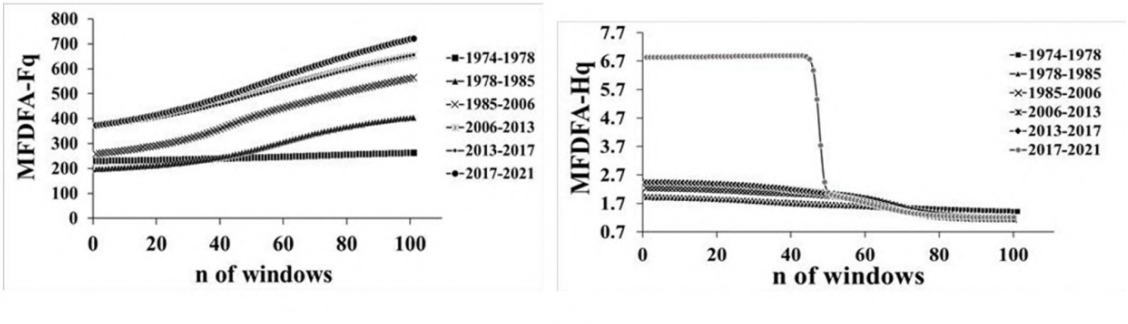

a.

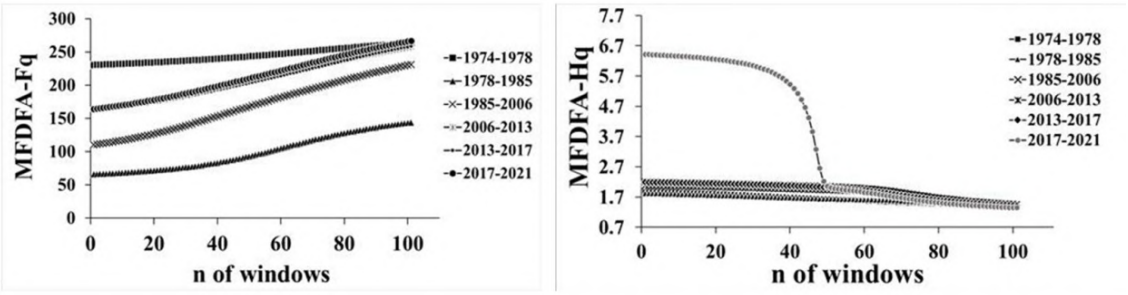

b.

Fig. 3. MF-DFA (Fq, Hq) analysis of displacements of Enguri Arc Dam foundation (a. polynomial degree =p2; b. polynomial degree =p5).

The results obtained from the MF-DFA analysis reveal the evolution of the three principal characteristics – **Hurst exponent H(q)** and **fluctuation function F(q) –** over the observation period, with particularly pronounced activity during **2017–2021**. The analysis shows that **increasing the polynomial order used in detrending leads to a reduction in F(q)**, indicating a decrease in fluctuation amplitude.

The values of the **Hurst exponent H(q)** were generally found to be in the range **0.5 to above 1**, which signifies a **long-range dependence** or **positive correlation** in the time series of dam foundation displacements.

Our results suggest that **increasing the polynomial degree in the MF-DFA method alters the underlying dynamic structure**, effectively smoothing the series and reducing fluctuations. This behavior points to a strong influence of external factors – such as structural and environmental conditions – on the temporal variability of the displacement data.

Conclusion

In this study, we investigated the **dynamic characteristics of the Enguri Arch Dam foundation displacements** using long-term monitoring data collected between **1974 and 2021**. We employed the **Multifractal Detrended Fluctuation Analysis (MF-DFA)** method, which enabled a detailed examination of the nonlinear and multifractal properties of the displacement time series.

Our findings demonstrate that the dynamics of foundation displacement are significantly affected by both the **construction process** of the arch dam and, more importantly, by **fluctuations in the reservoir water level**. The MF-DFA results provided a clear and quantitative understanding of the system's dynamic behavior, allowing us to assess the **degree and nature of structural changes** over time. These insights are crucial for ensuring the **ongoing safety and stability** of the Enguri high dam, especially in the context of long-term geophysical and environmental influences.

Reference

1. Chelidze T., Matcharashvili T., Abashidze V., Kalabegashvili M. and Zhukova N., Real-time monitoring for analysis of dam stability: Potential of nonlinear elasticity and nonlinear dynamics approaches // Frontiers in Structural and Civil Engineering, 7, 2013, pp. 188–205.
2. Chelidze T., Tepnadze D., Mepharidze E., Sborshchikovi A., Laliashvili L. and Matcharashvili T. Scaling features of earthquake occurrences in the equally distributed non-overlapping time windows // Bulletin of the Georgian National Academy of Sciences 14(4), 2020, pp. 40–45.
3. Chelidze, T., Matcharashvili T., Abashidze V., Dovgal N., Mepharidze E., and Chelidze L., Time series analysis of fault strain accumulation around large dam: the case of enguri dam, greater Caucasus, building knowledge for geohazard assessment and management in the Caucasus and other orogenic regions. In: Bonali, F. L., Mariotto, F. P, Tsereteli, N. (eds). Building Knowledge for Geohazard Assessment and Management in the Caucasus and other Orogenic Regions. Dordrecht: Springer, 2021, pp. 185–204.
4. Matcharashvili T., Hatano T., Chelidze T. and Zhukova N., Simple statistics for complex earthquake time distributions/ / Nonlinear Processes in Geophysics 25, 2018, pp. 497–510.
5. Matcharashvili,T., Chelidze T., Zhukov, N., Mepharidze E., Sborshchikovi A., Tephnadze D. and Laliashvili, L., Dynamical Changes of Foundation Displacements and Local Seismic Activity Occurred During Construction of Enguri Arch Dam // 25th European Meeting of Environmental and Engineering Geophysics The Hague, Netherlands: European Association of Geoscientists & Engineers, vol. 1, 2019, pp. 1–5.
6. Peinke J., Matcharashvili T., Chelidze T., Gogiashvili J., Nawroth A., Lursmanashvili O. and Javakhishvili Z., Influence of periodic variations in water level on the regional seismic activity around a large reservoir: field data and laboratory model // Physics of the Earth and Planetary Interiors 156, 2006, pp. 130–142.
7. Kantelhardt J.W., Zschiegner S.A., Koscielny-Bunde E., Havlin S., Bunde A. and Stanley H.E., Multifractal detrended fluctuation analysis of nonstationary time series // Physica A: Statistical Mechanics and its Applications 316, 2002, pp. 87–114.
8. Espen, I.A.F. Introduction to multifractal detrended fluctuation analysis in Matlab // Frontiers in Physiology 3(141), 2012, pp. 1–18.
9. Gao K., Hu J., Tung W.-W., Cao Y., Sarshar N. and Roychowdhury V. P., Assessment of long-range correlation in time series: how to avoid pitfalls // Phys. Rev. E, Stat. Nonlin. Soft Matter Phys., 73, 2006, 016117.
10. Sborshchikovi A., Chelidze T., Mepharidze E., Tepnadze D., Zhukova N., Matcharashvili T. and LaliashviliL., The Analysis of Dynamical Changes and Local Seismic Activity of the Enguri Arch Dam, In: Dinesh C. S. Bisht, Mangey Ram, Computational Intelligence-based Time Series Analysis, River Publishers, Denmark, 2022, pp. 53–63.

1st International Scientific Conference "Modern problems in Geophysics", Proceedings,
ISBN 978-9941-36-434-1, ISSN 3088-4349, Tbilisi, Georgia, November 6-8, 2025

TEMPORAL ANALYSIS OF EARTHQUAKE AND QUANTILE FUNCTION ESTIMATION

***,**Sborshchikovi A., *Mepharidze E., *Chelidze T.**

**Mikheil Nodia Institute of Geophysics of Ivane Javakhishvili Tbilisi State University, Tbilisi, Georgia **Business and Technology University, Tbilisi, Georgia*
a.sborshchikov@gmail.com

Abstract. *This study explores a novel method for estimating and approximating quantile and quantile density functions based on known moments. In this context, the moments are represented by time intervals (waiting times) between earthquakes recorded in seismic catalogs. The research utilizes global seismic data on earthquake waiting times and evaluates three different approximation models: frequency moments, conventional moments, and transposition moments. While multiple approaches exist for estimating quantile functions, the key advantage of our method lies in its reliance solely on moment information.*

Key Words: *Earthquake, waiting time, quantile function*

Introduction

Among the notable outcomes of previous research are well-established insights into the temporal characteristics of seismicity, which align with contemporary perspectives on the fractal nature of tectonic structures, fault systems, and hypocenter distributions. These findings support the understanding of seismic processes as inherently complex and dynamic, where earthquake occurrences exhibit "switching" or "shifting" behavior – alternating between phases of heightened and diminished seismic activity. Despite this progress, many core aspects of how time intervals between earthquakes are distributed remain insufficiently understood, and in some cases, have yet to be thoroughly investigated [1–3].

Currently, the moment problem holds a significant place in statistics and finds applications in fields such as mathematics, financial mathematics, economics, and insurance. Over the past three centuries, it has been extensively explored in numerous publications, yet it remains a subject of great mathematical interest to this day [4–6].

In this study, we focus on the approximation and estimation of the quantile function, assuming that the moments are known [7].

We can say that the moment problem has the only solution when the system of equations $\int x^j dF(x) = \int x^j dG(x); j = 0,1,..$, has one solution, *F=G*.

Methods

There exist various nonparametric approaches for estimating the quantile function. For instance, Harrell and Davis [8] examine the use of statistical order statistics, while Bolancé et al. [9] and Brewer [10] explore quantile estimation based on Bernstein polynomials.

The innovative aspect of this research lies in its applicability in cases where limited information about the underlying distribution function is available – specifically, when only the moments are known. This advantage allows for more flexible modeling in data-sparse scenarios.

In this study, we aim to combine the analysis of time intervals (waiting times) between earthquakes with the approximation of results using the quantile function, supported by modern computational techniques. Our approach incorporates both classical linear and nonlinear methods for studying time distribution patterns.

By analyzing waiting time series originating from various sources, we seek to uncover key characteristics in the temporal dynamics of seismic activity. This project aligns closely with fundamental challenges in Earth sciences and involves the integration of advanced data analysis techniques within a custom-developed software platform.

For the estimation, we consider three distinct models. The first utilizes frequency moments, the second relies on conventional moments, and the third is based on transposition moments.

Results and discussion.

For the analysis of time intervals (waiting times), data from the Southern California Seismic Catalog were used. Specifically, we utilized records from the Southern California Local Earthquake Catalog, accessible at http://www.data.scec.org/ftp/catalogs/. The dataset spans the period from 1932 to 2013.

This catalog is considered highly reliable due to its near-continuous data collection throughout the entire period.

Subsequently, using software developed at the M. Nodia Institute of Geophysics, Ivane Javakhishvili Tbilisi State University, we processed the dataset to extract waiting times between earthquake events.

Based on these waiting time sequences, we computed an approximate estimate of the quantile function using the first model. This result will be compared with the well-known Harrell-Davis estimator. The analysis employs the following formulas:

$$\widehat{Q_{HD}} = \sum_{i=1}^{n} X_{(i)} \int_{\frac{i-1}{n}}^{\frac{i}{n}} \beta(y, \lfloor \alpha x \rfloor + 1, \alpha - \lfloor \alpha x \rfloor + 1) dy$$

$$\widehat{Q_{\alpha}}(x) = \sum_{i=1}^{n+1} \Delta X_{(i)} B_{\alpha}\left(\frac{i-1}{n}, x\right) = \sum_{i=1}^{n} \Delta X_{(i)} [B_{\alpha}\left(\frac{i-1}{n}, x\right) - B_{\alpha}\left(\frac{i}{n}, x\right)]$$

The behavior for different parameters for first model will be as follows (Fig.1- Fig.3).

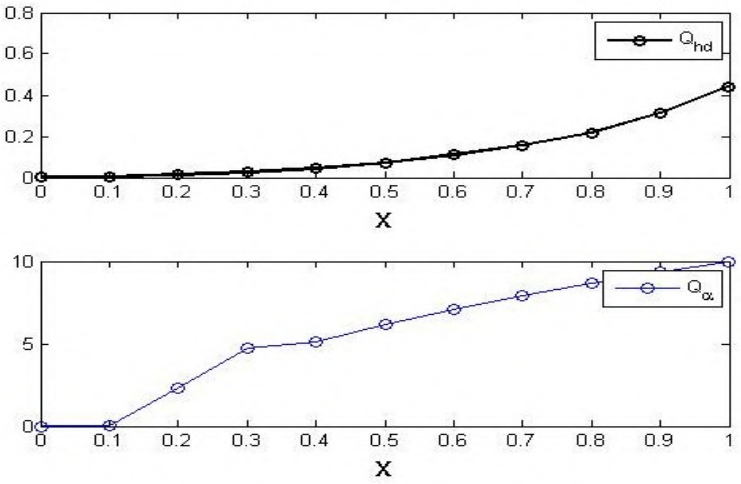

Fig. 1. Comparison of estimates of Harrell Davis and the first model (frequency moments) for the waiting time when.α =20, *n=100*

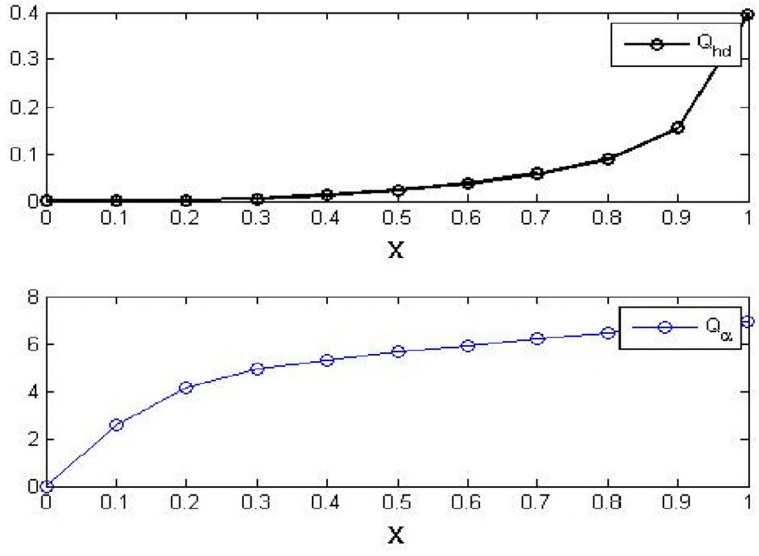

Fig. 2. Comparison of the estimates of Harrell Davis and the first model (frequency moments), for the waiting time when α =50, *n=100*

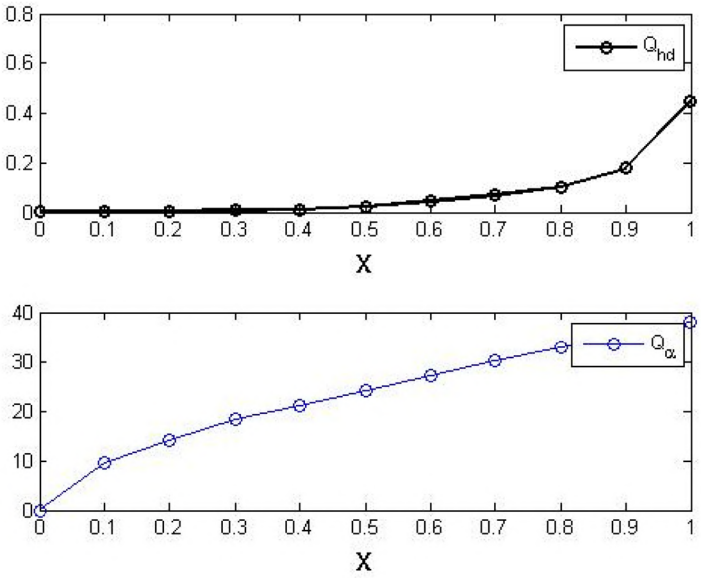

Fig. 3. Comparison of the estimates of Harrell Davis and the first model (frequency moments), for the waiting time when α =100,*n=100*

The results of the research will help to understand the nature of seismic processes and what most important it will contribute in the future to solving the problem of understanding the nature of strong earthquakes.

Conclusion

Our study focuses on analyzing the time intervals between earthquake events and employs specific datasets to approximate and estimate the quantile function. This approach has broad applicability in fields such as financial mathematics, economics, and insurance. The project takes on a global scope, addressing significant challenges across multiple scientific disciplines. It holds both theoretical and practical value, as understanding the temporal distribution of earthquakes is essential for assessing seismic hazards and making meaningful advancements in comprehending the underlying mechanisms of earthquakes.

References

1. Telesca L., Matcharashvili T., Chelidze T., Investigation of the temporal fluctuations of the 1960–2010 seismicity of Caucasus. // Nat. Hazards Earth Syst. Sci., Göttingen Germany, 12, 2012, pp. 1905–1909.
2. Talbi A., Yamazaki F., Sensitivity analysis of the parameters of earthquake recurrence time power law scaling. // J. Seismol, Springer, Netherlands, 13, 2009, pp. 53−72.
3. Molchan G., Interevent time distribution in seismicity: a theoretical approach. // Pure Appl Geophys., Springer, Netherlands, 162, 2005, pp. 1135−1150.
4. Mnatsakanov R., Sborshchikovi A., Recovery of a Quantile Function from Moments. // Journal of Computational and Applied Mathematics, Elsevier, Netherlands, 315, 2017, pp. 354-364.
5. Mnatsakanov R., Sborshchikovi A., Recovery of quantile and quantile density function using the frequency moments. // Journal of Statistics and Probability Letters, Elsevier, Netherlands, 140, 2018, pp. 53-62.
6. Sborshchikovi A., On Nonparametric Quantile Function Estimation Using Transformed Moments. // Bulletin of the Georgian National Academy of Sciences, Tbilisi, Georgia, 11(3), 2017, pp. 22-27.
7. Cheng C., Parzen E., Unified estimators of smooth quantile and quantile density functions. // J. Statist. Plann. Inference, Elsevier, Netherlands, 59, 1997, pp. 291–307.
8. Harrell F.E., Davis C.E., A new distribution-free quantile estimator. // Biometrika, Oxford University Press, 69, 1982, pp. 635–640.
9. Bolance C., Guillen M., Nielsen, J., Transformation kernel estimation of insurance claim cost distributions. in: M. Corazza, et al. (Eds.), Mathematical and Statistical Methods for Actuarial Sciences and Finance, Springer-Verlag, Italy, 2010, pp. 43–51.
10. Brewer K.R.W., Likelihood Based Estimation of Quantiles and Density Estimation, 1986.

1st International Scientific Conference "Modern problems in Geophysics", Proceedings,
ISBN 978-9941-36-434-1, ISSN 3088-4349, Tbilisi, Georgia, November 6-8, 2025

STATISTICAL ANALYSIS OF THE ANNUAL NUMBER OF REGISTERED LANDSLIDES AND MUDFLOWS IN GEORGIA IN 1995-2024

[*]Amiranashvili A., [**]Brocca L., [*]Chelidze T., [*]Svanadze D., [***]Tsamalashvili T., [*]Varamashvili N.

[*]M. Nodia Institute of Geophysics of I. Javakhishvili Tbilisi State University, Tbilisi, Georgia
[**]Research Institute for Geo-Hydrological Protection, Perugia, Italy
[***]A. Janelidze Geological Institute of I. Javakhishvili Tbilisi State University, Tbilisi, Georgia
avtandilamiranashvili@gmail.com

Abstract. *The results of statistical analysis of data from the Geological Department of the Environment Agency of Georgia on the annual number of re-activated and newly formed landslides (LS) and mudflows (MF) in Georgia for the period from 1995 to 2024 are presented. In particular, the following results were obtained. The number of landslides varies in the range from 56 to 1360 with an average annual value of 581, and mudflows – from 23 to 355 with an average annual value of 141. There is a high linear correlation between the studied parameters (the correlation coefficient is 0.81). The trends of the LS and MF values have the form of a polynomial of the seventh degree.*

Key Words: *landslide, debris flow, natural disaster, risk assessment, statistical analysis.*

Introduction

Landslides and mudflows are a type of natural disaster that are common almost everywhere [1-4], including in Georgia [5-8]. Landslides and mudflows damage roads and bridges, destroy residential buildings and structures, lead to power line shutdowns, pose a threat to human health and life, cause significant material damage, etc. [9-11].

The activation of landslides and mudflows depends on many factors – slope steepness, lithology, vegetation, precipitation, etc. Accordingly, a large number of studies have been and are being conducted to study the relationships between these processes and these factors [3,12].

Given the importance of the problem in Georgia, in recent years, work has begun to systematize data on landslides and mudflows [10,11], which will improve the quality of scientific research. This paper presents the results of statistical analysis of thirty-year time series of annual landslide and mudflow events in Georgia, published in the bulletins of the Geological Department of the Environment Agency of Georgia [10]

Study area, material and methods

Study area – Georgia. The data of the Department of Geology at Georgian National Environmental Agency about registered re-activated and new landslides and mudflows number per year are used [10]. Period of observation: 1995-2024 (30 years).

In the proposed work the analysis of data is carried out with the use of the standard statistical analysis methods of random events and methods of mathematical statistics for the non-accidental time series of observations [13, 14].

The following designations will be used below: Mean – average values; Min – minimal values; Max – maximal values; Range = Max – Min; St Dev – standard deviation; C_v – coefficient of variation, %; R^2 – coefficient of determination; R – coefficient of linear correlation; K_{DW} – Durbin-Watson statistic; α – level of signification; x – number of year, 1-1995, … 30 – 2024; LS – landslides number per year; MF – mudflows number per year.

The curve of trend is an equation of the regression of the connection of the investigated parameter with the time at the significant value of the determination coefficient and such values of K_{DW}, where the residual values (Res) are accidental.

Results

Results in Fig. 1-3 and Tables 1-2 are presented.

In Fig. 1 data about the annual number of landslides and mudflows in Georgia from 1995 to 2024 and in Table 1 statistical characteristics of these parameters are presented.

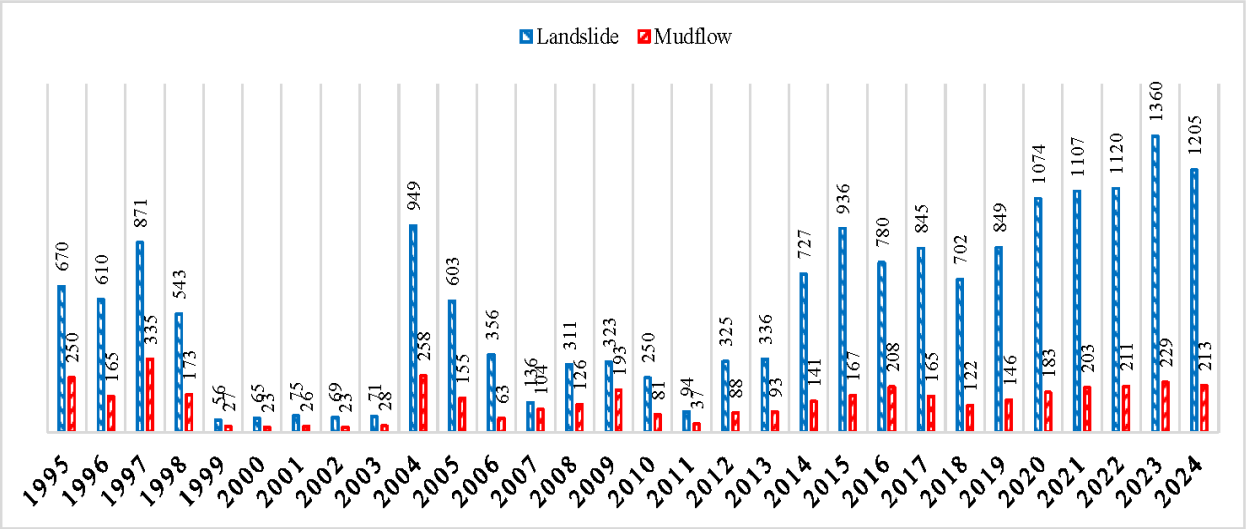

Fig. 1. Number of landslides and mudflows per year in Georgia from 1995 to 2024 [10].

Table 1. Statistical characteristics of LS and MF numbers in Georgia from 1995 to 2024

Variable	LS	MF
Max	1360	335
Min	56	23
Range	1304	312
Mean	581	141
St Dev	397	81
C_v, %	68.3	57.5
	Correlation Matrix	
LS	1	0.81
MF	0.81	1

As follows from Fig. 1 and Table 1 the number of landslides varies in the range from 56 to 1360 with an average annual value of 581, and the mudflows – from 23 to 355 with an average annual value of 141. The variation coefficient for LS and MF, respectively, is 68.3 % and 57.8 %. Between the studied parameters there is a high linear correlation connection (R = 0.81).

Trends of time series of LS and MF values have the form of a polynomial of the seventh degree (Table 1, Fig. 2 and 3). In Table 2 data on coefficients of the regression equation of the time series of the landslides and mudflows numbers per year in Georgia in 1995-2024 are presented.

Fig. 2 and 3 show graphs of real values, trends and random components of the time-series under study.

Table 2. Coefficients of the regression equation of the time series of the landslides and mudflows numbers per year in Georgia in 1995-2024.

$Y = a \cdot x^7 + b \cdot x^6 + c \cdot x^5 + d \cdot x^4 + e \cdot x^3 + f \cdot x^2 + g \cdot x + h$

Variable	LS	MF
a	4.67E-05	1.50E-05
b	-0.00503	-0.00167
c	0.214609	0.073752
d	-4.57933	-1.64238
e	50.91851	19.16392

f	-273.141	-108.763
g	517.521	226.481
h	423.2351	104.5595
R^2	0.73	0.493
K_{DW}	1.51	1.91
α	0.05	0.05

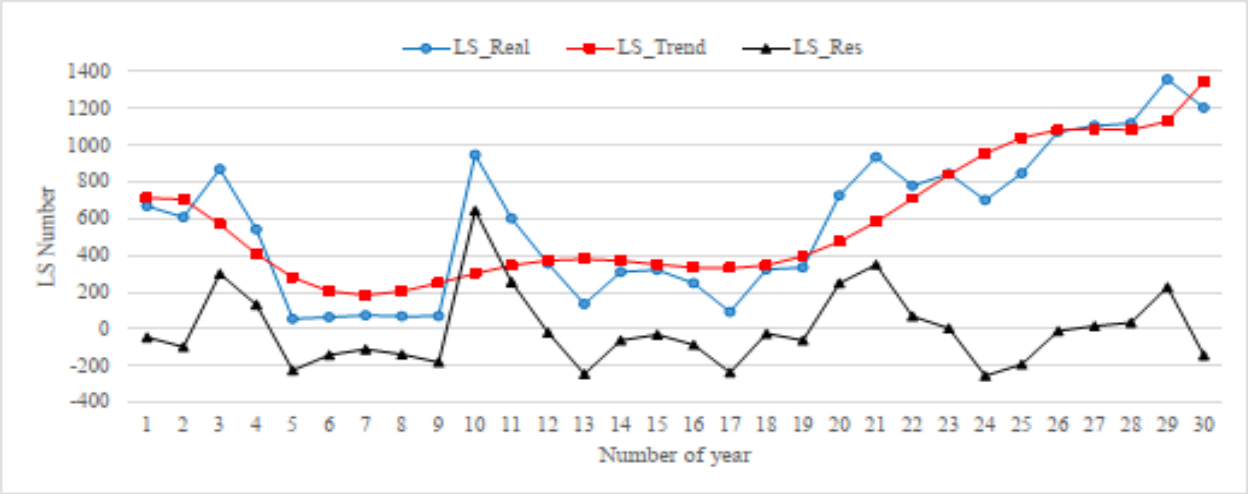

Fig. 2. Trend of the landslides number per year in Georgia in 1995-2024.

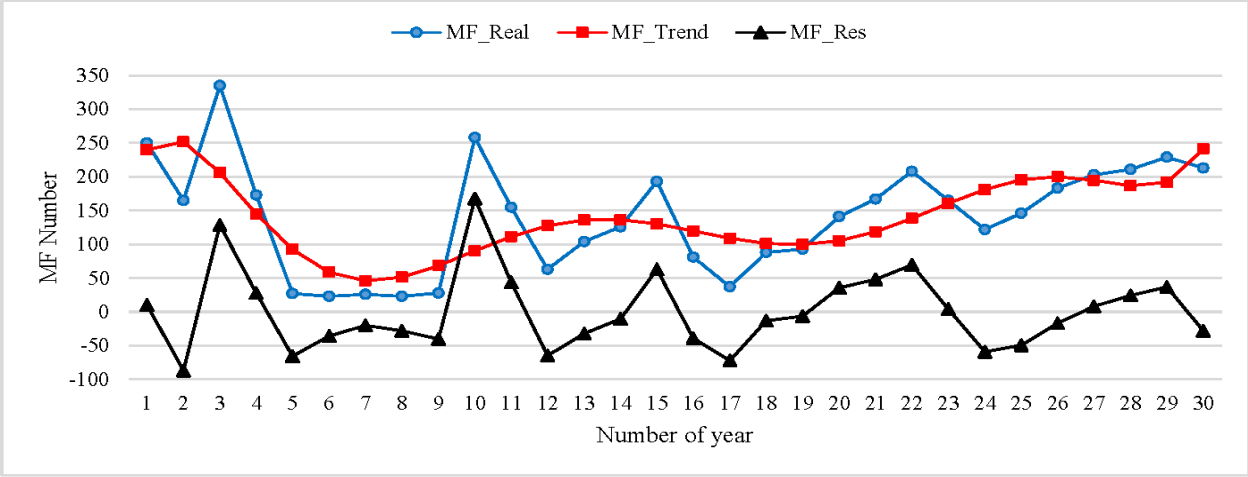

Fig. 3. Trend of the mudflows number per year in Georgia in 1995-2024.

Note that between the random components of the time-series of LS and MF, the linear correlation coefficient is 0.87.

Conclusion

In the near future, we plan to study the periodicity of landslide and mudflow time series with the aim of using these data to forecast these time series for several years. We also plan to compare different methods for long-term and short-term landslide and mudflow forecasting, including machine learning methods.

Acknowledgments

This work was supported by Shota Rustaveli National Science Foundation of Georgia (SRNSFG), Grant number FR-23-5466, “Machine Learning Approach to the Landslide Activation Prediction in Georgia”.

References

1. Aleotti P., Chowdhury R. Landslide Hazard Assessment: Summary. Rev N Perspect. // Bull Eng. Geol. Env. 58, 1999, pp. 21–44.
2. Li H., Samsudin N. A. A Systematic Review of Landslide Research in Urban Planning Worldwide. // Nat Hazards, 121, 2025, pp. 6391–6411. https://doi.org/10.1007/s11069-024-07064-4
3. Alcántara-Ayala I. Landslides in a Changing World. // Landslides, 2025. https://doi.org/10.1007/s10346-024-02451-1
4. Dalğıç S., Karimov E. Investigation of Landslide Mechanism in the Balaban Landslide Area using 3D Numerical Modelling. // Int. Journal of Sustainability and Risk Control, Vol.1, No 2(2), Baku, Azerbaijan, September 2025, pp. 31-35.
5. Varazanashvili O., Tsereteli N., Amiranashvili A., Tsereteli E., Elizbarashvili E., Dolidze J., Qaldani L., Saluqvadze M., Adamia Sh., Arevadze N., Gventcadze A. Vulnerability, Hazards and Multiple Risk Assessment for Georgia. // Natural Hazards, Vol. 64, Number 3, 2012, pp. 2021-2056. DOI: 10.1007/s11069-012-0374-3, http://www.springerlink.com/content/9311p18582143662/fulltext.pdf.
6. Fourth National Communication of Georgia Under the United Nations Framework Convention on Climate Change. // Chapter 4.9 Geological Hazards in Georgia, Tbilisi, 2021, pp. 278-286.
7. Gaprindashvili M., Tsereteli E., Gaprindashvili G., Kurtsikidze O. Landslide and Mudflow Hazard Assessment in Georgia. // In: Bonali F.L., Pasquaré Mariotto F., Tsereteli N. (eds) Building Knowledge for Geohazard Assessment and Management in the Caucasus and other Orogenic Regions. NATO Science for Peace and Security Series C: Environmental Security. Springer, Dordrecht, 2021. https://doi.org/10.1007/978-94-024-2046-3_14
8. Amiranashvili A., Elizbarashvili E., Gaprindashvili G., Varazanashvili O., Fuchs S. Statistical Analysis of Parameterized Landslide Data in Georgia from 1900 to 2022. // Reliability: Theory and Applications, ISSN 1932-2321, Special Issue № 6 (81), Part-2, Vol. 19, 2024, pp. 812 – 818. https://doi.org/10.24412/1932-2321-2024-681-812-818
9. Froude M., Petley D., Global Fatal Landslide Occurrence from 2004 to 2016. // Nat. Hazards Earth Syst. Sci., 18, 2018, pp. 2161–2181.
10. Geological Bulletins. 2016-2025, (in Georgian). https://nea.gov.ge/c/Departments/Geology
11. Varazanashvili O., Gaprindashvili G., Elizbarashvili E., Basilashvili Ts., Amiranashvili A., Fuchs S. The First Natural Hazard Event Database for the Republic of Georgia (GeNHs). // Catalog, 2023, 270 p. http://dspace.gela.org.ge/handle/123456789/10369; DOI: 10.13140/RG.2.2.12474.57286
12. Amiranashvili A., Chelidze T., Svanadze D., Tsamalashvili T., Tvauri G., Study of the Relationship Between the Mean Annual Sum of Atmospheric Precipitation and Re-Activated and New Mudflow Cases in Georgia. // Journal of the Georgian Geophysical Society, e-ISSN: 2667-9973, p-ISSN: 1512-1127, // Physics of Solid Earth, Atmosphere, Ocean and Space Plasma, v. 26(1), 2023, pp. 19–29.
https://ggs.openjournals.ge/index.php/GGS/article/view/6958; DOI: https://doi.org/10.48614/ggs2620236958
13. Kendall M.G., Time-series. // Moscow, 1981, 200 p., (in Russian).
14. Hinkle D. E., Wiersma W., Jurs S. G., Applied Statistics for the Behavioral Sciences. // Boston, MA, Houghton Mifflin Company, ISBN: 0618124055; 9780618124053, 2003, 756 p.
15. Aliyev V., Pkhovelishvili M., Archvadze N., Gasitashvili Z., Hybrid Risk Review. // Int. Journal of Sustainability and Risk Control, Vol.1, No 1(1), Baku, Azerbaijan, June 2025, pp. 12-23.

1st International Scientific Conference "Modern problems in Geophysics", Proceedings,
ISBN 978-9941-36-434-1, ISSN 3088-4349, Tbilisi, Georgia, November 6-8, 2025

THE RESPONSE OF GEORGIAN WELLS TO KAMCHATKA EARTHQUAKES

Kobzev G., Melikadze G., Jimsheladze T., Chelidze T., Tchankvetadze A., Goguadze N.

M. Nodia Institute of Geophysics of the I. Javakhishvili Tbilisi State University, Tbilisi, Georgia
jimsheladzetamuna@gmail.com

Abstract. *A consistent water level response to earthquakes occurring 7,800 km from Georgia was observed. Typically, the Oni well responds 2-2.5 times more than other wells. However, to the M8.8 earthquake, the Oni well's response was six times greater than that of other wells.*

Key Words: *Earthquake, water response in wells of Georgia.*

Introduction

Water level monitoring is made at the following deep boreholes of Georgia: Kobuleti, Nakalakevi, Gori and Oni.

The article contains information about several hydrodynamic anomalies that were observed during the earthquake (2025, Mag ≥7.4) in Georgia on the multiparametric monitoring network of M. Nodia Institute of Geophysics. Study area, material and methods

A water level recording system is in operation in Georgia. It records water level, atmospheric pressure, and air temperature. The XR5-SE-M data logger records this data every minute. Data transmission is accomplished via an MC-35i modem. Data processing and figures creation is realized by program StationsMany. These programs are written in MatLab-language.

Information on magnitude, depth and distance about earthquakes was extracted from www.msc-csem.org. Additional information for these earthquakes: the value of the vertical component of the surface wave velocity, received from www.iris.edu/app/station_monitor (GNI station, Armenia).

Results

In July and September 2025, earthquakes with magnitudes of M=7.4, 8.8, 7.4 and 7.8 occurred in Kamchatka. They were detected by a water level recording system in Georgia, located 7800 km away from the event site.

Table 1. Earthquakes and water reaction in Georgian wells

Time	Magnitude	Depth, km	Distance, km	Water reaction, cm
20 July 2025, 06:49	7.4	25	7810	Oni: 6.3 cm
29 July 2025, 23:24	8.8	20	7817	Oni: 61 cm; Gori: 9.3 cm; Nakalakevi: 9.2 cm; Kobuleti: 2.1 cm
13 September 2025, 02:37	7.4	46	7778	Oni: 6.8 cm
18 September 2025, 18:58	7.8	30	7819	Oni: 16.2 cm; Gori: 2 cm; Nakalakevi: 4.3 cm;

For these earthquakes, the value of the vertical component of the surface wave velocity reached, respectively: 168 μms/sec; 1195 μms/sec; 141 μms/sec, 381 μms/sec.

For earthquakes with M=7.4, the P-wave arrived at a speed of 12.1-12.3 km/sec. The surface wave arrived at a speed of 3.8-3.9 km/sec. For earthquakes with M8.8 speeds are 12.87 km/sec and 4.03 km/sec. For M7.8 speeds are 12.54 km/sec and 3.89 km/sec.

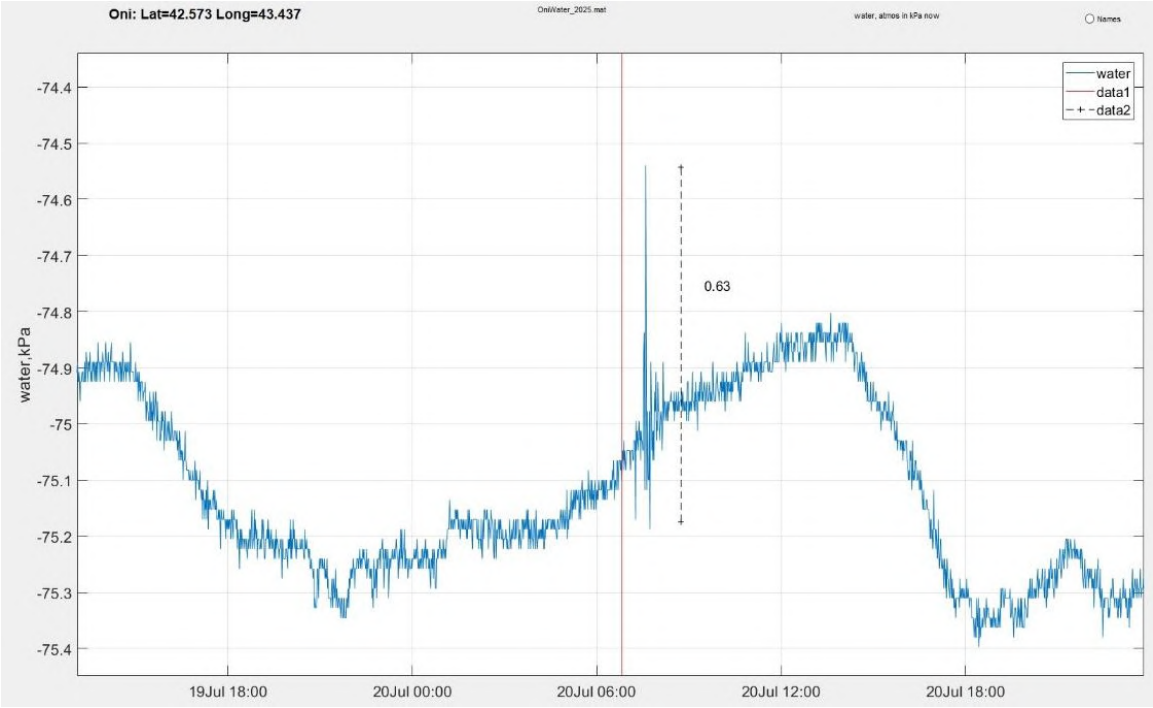

Fig. 1. Water level response to the M=7.4 earthquake in Oni Station

In all cases, the Oni station produced the most consistent results. For the M8.8 earthquake, four stations responded. Fig. 2 shows the response to a wave arriving along the shortest path of 7800 km. A slight response is also noticeable to a wave traveling from the opposite direction, a distance of 32200 km.

Long-term observations have shown that the Oni borehole is more sensitive to earthquakes than other stations. Typically, its response amplitude is 2-2.5 times greater than that of any other well [1,2]. However, to an M8.8 earthquake, its response was 6.6 times greater, significantly exceeding normal.

Possible reasons for this behaviour: a) The value of the vertical component of the surface wave velocity M8.8 is 7.1 bigger. b) Depth of Oni well is small, resonance period 32 sec. c) Phase shift is positive and equal +15°+24° [3].

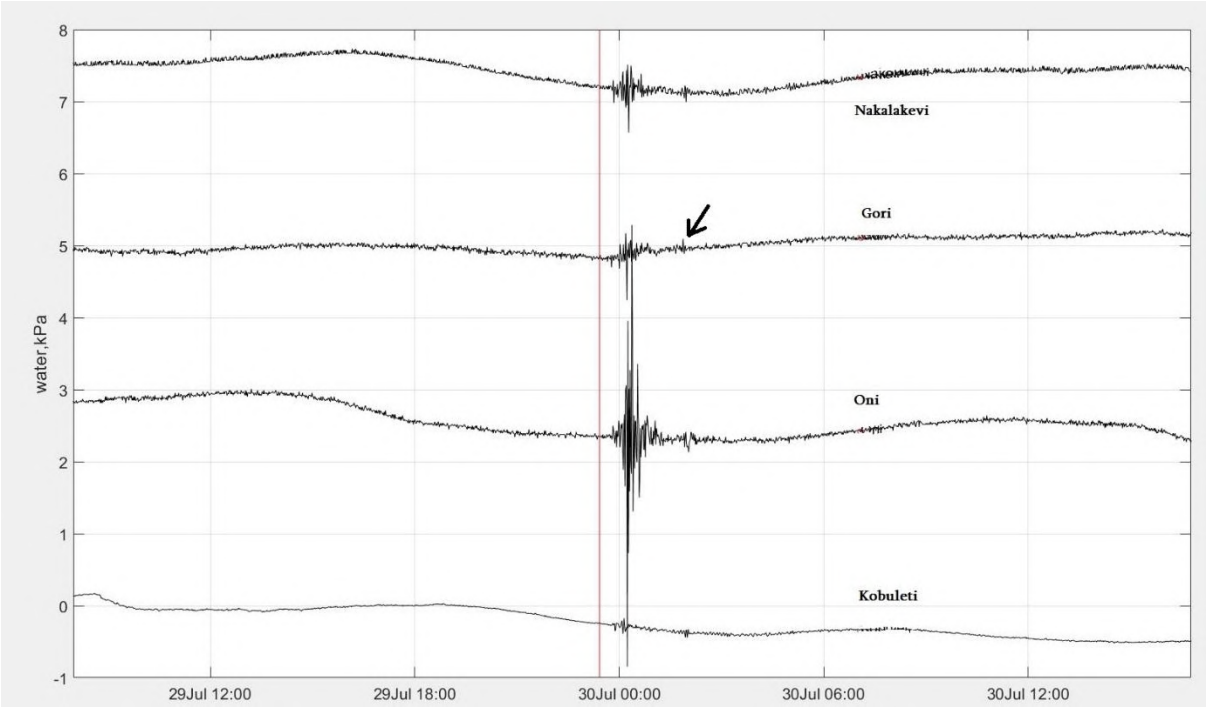

Fig. 2. Water level response to the M=8.8 earthquake in Nakalakevi, Gori, Oni and Kobuleti

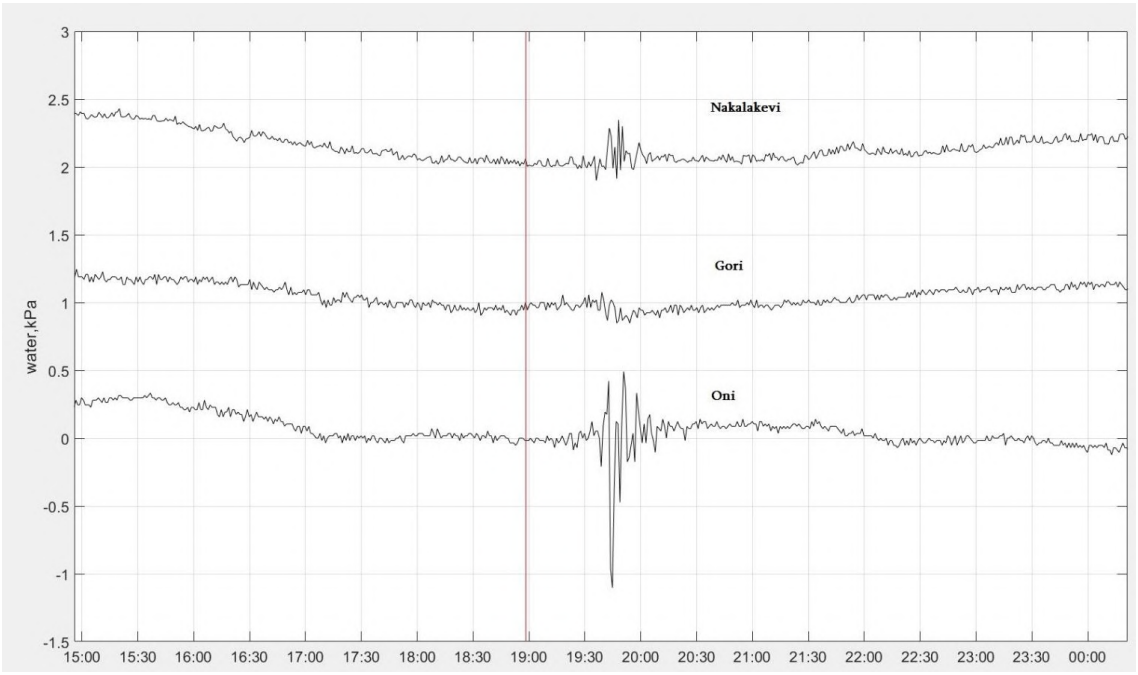

Fig.3. Water level response to the M=7.8 earthquake in Nakalakevi, Gori, Oni.

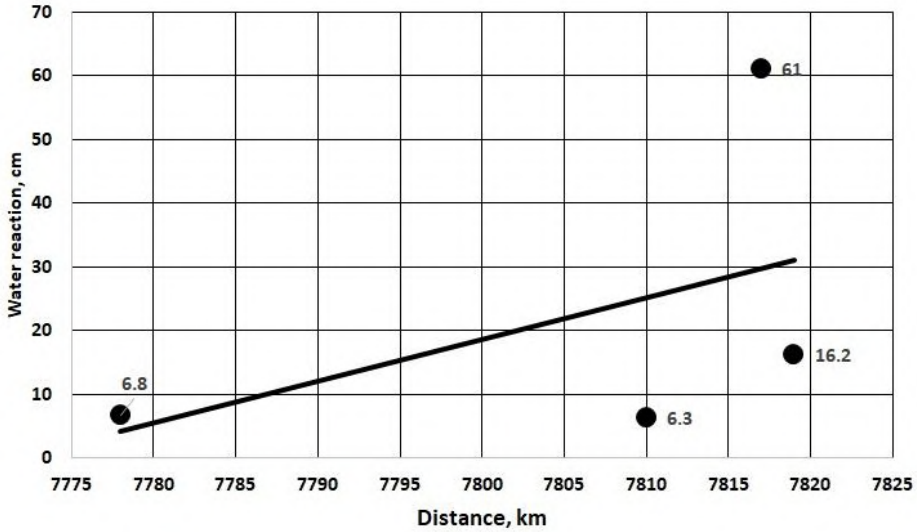

Fig. 4. Water reaction vs Distance in Oni Station

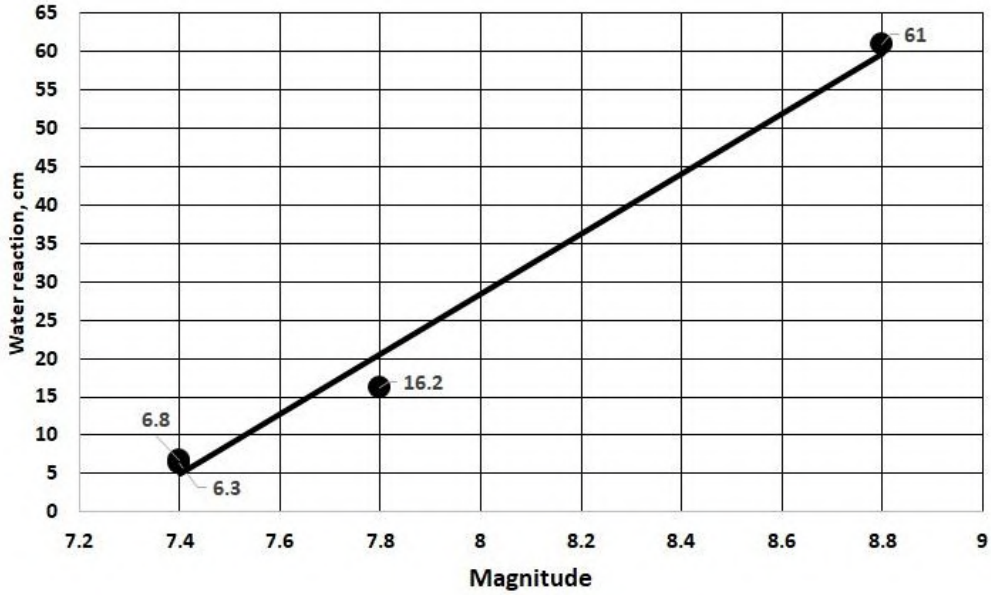

Fig.5. Water reaction vs Magnitude in Oni Station

It is important to answer the question: What properties should a sensitive well have? Let us recall the properties of our wells. Possible cause is the following properties or a combination of them.

Depth: Oni=255 m; Nakalakevi=600 m; Gori=1500 m; Kobuleti=2000 m.

Resonance period: Oni=32 sec; Nakalakevi=49 sec; Gori=77 sec; Kobuleti=89 sec.

Phase shift (M2): Oni:+15° ÷ +24°; Nakalakevi:+0.1° ÷ +1°; Gori:+9° ÷ +10°; Kobuleti: -26° ÷ -28°.

Conclusion

In some cases, the well in Oni begins to react radically more strongly to earthquakes than other wells.

Acknowledgement

This work was supported by the Shota Rustaveli National Science Foundation of Georgia (SRNSFG), Grant number FR24-17839.

References

1. Chelidze T., Melikadze G., Kobzev G., Jimsheladze T. and Dovgal N., Geophysical Reactions to Remote 2022 Tonga Eruption and to Türkiye Earthquakes in Georgia (Caucasus): Hydrogeology, Geomagnetics and Seismicity. // Open Journal of Earthquake Research, 12, 2023, pp. 223-237. https://doi.org/10.4236/ojer.2023.124009
2. Kobzev G., Melikadze G., Jimsheladze T., Reaction of Georgian Wells to Remote and Nearby Earthquakes. Similarities and Differences. // Physics of Solid Earth, Atmosphere, Ocean and Space Plasma, v. 24(2), 2021, pp. 35-37.
3. Kobzev G., Chelidze T., Melikadze G., Jimsheladze T., Kiria T., Tchankvetadze A., Maghradze Z., Goguadze N. Water Level Phase Shift relative to Gravity into Georgian wells. // Physics of Solid Earth, Atmosphere, Ocean and Space Plasma, v. 28(1), 2025, pp. 36-39.

1st International Scientific Conference "Modern problems in Geophysics", Proceedings,
ISBN 978-9941-36-434-1, ISSN 3088-4349, Tbilisi, Georgia, November 6-8, 2025

GEOLOGICAL CONDITIONS AND FACTORS OF KARST FORMATION (ON THE EXAMPLE OF GEORGIA)

Lezhava Z. I., Tsikarishvili K. D., Tolordava T. A.

Ivane Javakhishvili Tbilisi State University, Vakhushti Bagrationi Institute of Geography
zazalezhava@gmail.com

Abstract*. This paper discusses the role of geological conditions and factors (stratigraphy, lithology, chemistry of karstified rocks, structural-textural characteristics, the nature of the cementing substances of the mineral particles making up the rock, issues of general and fracture tectonics, stratification of karst waters and the nature of their bedding) in karst development in the karst belt of Georgia.*

Key words*: karst, syncline, anticline, orogen*

Introduction

Georgia is one of the outstanding countries in the world for the diversity of karst processes. Limestone rocks occupy more than 10% of the territory of Georgia, where various surface and underground karst landscapes are represented. Karst is especially well developed in Western Georgia, where it stretches as a continuous belt for 325 km in length and from 2-3 km to 30-35 km in width, from the Psou River to the area of Lake Ertso. It includes the northern hilly part of the Colchis lowland and the adjacent southern slopes of the Western Caucasus. The vertical spread of karst begins at sea level (Gagra) and reaches up to 2757.6 m absolute height (Speleologists' Peak, Arabika massif) (Fig. 1).

Study area, material and methods

The belt of carbonate sediments on the southern slope of the Caucasus, where karst phenomena are developed, is characterized by rather complex stratigraphic, lithological and tectonic conditions. Based on materials and knowledge accumulated over years by previous researchers of Georgian karst and ourselves, as well as the analysis of geological maps of different scales, the work presents the significant role of the geological factor in karst formation. The paper uses field, experimental and laboratory research methods. The chemical composition of the carbonate sediments was studied in the laboratory. The data of boreholes and geological sections, electrometric prospecting methods, and tracing experiments of underground waters were used.

Results

According to Petre Gamkrelidze's tectonic scheme, the limestone belt of Georgia is situated between the fold system of the southern slope of the Caucasus and the Georgian belt, as a result, both orogenic and platform karsts are presented here, which are characterized by different karst formation conditions and features [1].

In tectonic terms, the common Caucasian strike linear anticline and syncline folds predominate in the Georgian karst belt, while disjunctive dislocations play a subordinate role [2]. This fact is linked to the comparatively weak openness of vertical fractures in the mountainous limestone regions of Georgia. Nevertheless, a number of karst massifs (Bzipi Ridge, Arabika, Migaria, Askhi, Kudaro-Buba, Racha Ridge, Migaria) are distinguished by significant break-fault tectonic dislocations, which accounts for the extensive development of karst shafts and abysses. A completely different picture is found on the Zemo Imereti Plateau, which is the only platform-structural karst in the Caucasus. Here, karst voids are represented mainly by sub-horizontal caves and are related to widely spread stratification fractures and other break-fault dislocations in thin (on average 230-240 m) bedded Upper Cretaceous limestones lying quietly on the Dzirula crystalline basement, which were revealed by structural interpretation of aerial photographs of the Zemo Imereti structural plateau and by field studies (Fig. 2) [3, 4, 5, 6].

Fig.1. Map of the karst of Georgia

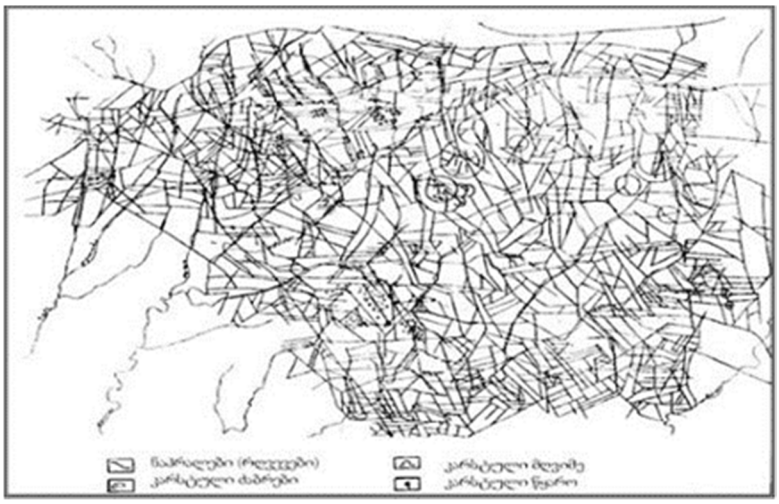

Fig. 2. Scheme of break-fault dislocations of the Zemo Imereti structural plateau.

Karst formations of rocks of various ages create a certain lithological-facies, structural and textural variability, which affects the intensity of karstification of different horizons, and the morphogenesis of underground and surface forms.

Here, karstification affects Upper Jurassic (Lias), Lower and Upper Cretaceous and Paleogene age carbonate sediments. The Cretaceous system is especially widely represented, all stages of which reach major thicknesses (1200-2600). Such significant thicknesses of carbonate rocks, along with other contributing factors, determine the geomorphological, hydrogeological and speleological complexity and diversity of several massifs (Arabika, Bzipi Ridge, Okhchakhue, Askhi, Migaria, and others), whereas regions composed of karstifiable rocks of relatively small thickness (Zemo Imereti, Kudaro-Buba, Central Samegrelo, Sataplia-Tskaltubo, etc.) are characterized by karst phenomena of relatively smaller scale. In the first case, complex systems of vertical and horizontal voids are formed, and meteoric waters appear after migration from absorption areas through quite complicated routes after prolonged flow; in the second case, mainly horizontal cave systems are formed, and due to the minor thickness of karstifiable rocks, precipitation quickly passes into horizontal channels via fractures.

One of the hydrogeological features of high-mountain massifs composed of thick karstifiable rocks is that they not only allow significant dynamic reserves of underground waters to accumulate, but also to be stored and discharged gradually, which cannot be said about massifs composed of thin karstifiable rocks [7].

The bedded or massive nature of limestones and the bedding characteristics, together with other contributing conditions, determine several essential points in the morphology of both surface and deep karst forms. For example, karst voids initiated in bedded, inclined limestones are characterized by distinctly stepped floors (bottoms) and frequent change in the direction of the cave's main channel (e.g., Kelasuri, Tkibula-Dzevrula, Mtiskalta and other caves), which is caused by alternation of easily and poorly soluble bedded fractured limestones. By contrast, voids developed in massive limestones are distinguished by high vertical and sometimes

cascade-like steps, unlike regions composed of thin-bedded limestones. For example, the Asazkhitsri karst shaft located in the Bzipi Ridge is represented by a single 85 m deep vertical step, while "Snowy Abyss" is with a 165 m deep shaft. A similar situation is observed in the Kudaro-Buba, Rikhva and other massifs, which are related not only to the textural characteristics of rocks but also to the nature of fracturing. Sometimes horizontal and inclined karst voids with balanced longitudinal profiles develop even in massive limestones, linked mainly to the corresponding fracturing.

Areas built of massive and bedded limestones are characterized by different morphological peculiarities of surface karst forms. Karst surfaces in massive limestones are distinguished by deep, severely dissected grooves and sharp crests forming intricate meandering labyrinths. In contrast, karst developed in thin-bedded limestones are characterized by frequent but shallow (0.3-0.7 m) dissection and comparatively smoothed crests. Karstic dolines in massive or poorly bedded limestones predominantly have rounded outlines and straight conical shapes, while in inclined bedded limestones, they are mainly asymmetric in form.

The rate of solubility and, therefore, the intensity of karst processes largely depends on the chemistry of rocks, structural-textural features, and the nature of the cementing substance of the mineral particles forming the rock.

The study of the chemical composition of Georgia's carbonate rocks confirms the known fact that, in the presence of other favorable conditions, karst formation is more intensive in rocks with a negligible percentage of insoluble residues. Mainly, this explains the concurrence of rather intensely karstified surfaces of Georgian karst regions (certain areas of the Arabika massif, Rikhva, Bzipi Ridge, Gumista-Pskritskha, certain areas of the Askhi Ridge, etc.) with the distribution areas of relatively pure lower and upper Cretaceous carbonate rocks [8].

Coarse-grained rocks are destroyed more quickly than fine-grained rocks, although their solubility is conversely lower. Also, calcitic cement is more easily soluble than clayey or siliceous cement.

Conclusion

Karst formations of rocks of various ages create certain lithological-facies, structural and textural variability, which affects the intensity of karstification of different horizons, and the morphogenesis of underground and surface forms. The bedded or massive nature of limestones and the bedding characteristics, together with other contributing conditions, determine several essential points in the morphology of both surface and deep karst forms. The rate of solubility and, therefore, the intensity of karst processes largely depends on the chemistry of rocks, structural-textural features, and the nature of the cementing substance of the mineral particles forming the rock. The available factual material and our research confirm the immense role of break-fault tectonics in the migration of waters and, accordingly, in the formation of karst voids in the karst massifs of Georgia.

References

1. Gamkrelidze P. D., Deep Faults in the Tectonic Structure of Georgia. In: Himalayan and Alpine Orogenesis, Moscow, 1964, pp. 85-87.
2. Tintilozov Z. K., Karst Caves of Georgia (Morphological Analysis). // Tbilisi, Metsniereba, 1976, 276 p.
3. Jashi G., Lezhava Z., Amilakhvari Z., Giginashvili G., Zardalishvili T., Tavartkiladze SH., Tabidze D., Tatashidze Z., For the Study of Karst-hydrogeological and Geophysical Peculiarities of Grudos Underground Basin. // Works of the M. Nodia Institute of Geophysics, GCI, Tbilisi, 1997, pp. 5-13.
4. Lezhava Z. Karst of Zemo Imereti Plateau and Adjacent Areas. // Tbilisi, Universali, 2015, 290 p.
5. Lezhava Z., Bolashvili N., Tsikarishvili K., Asanidze L., Chikhradze N. Hydrological and Hydrogeological Characteristics of the Platform Karst (Zemo Imereti Plateau, Georgia). 14th Multidisciplinary Conference on Sinkholes and the Engineering and Environmental Impacts of Karst. 2015, pp. 93-100. Rochester, USA.
6. Lezhava Z., Tsikarishvili K., Asanidze L., Chikhradze N., Karalashvili T., Odilavadze D., Tarkhnishvili A., The results of a complex study of the Turchu limestone hollow (polje). Western Georgia, Caucasus. // European Journal Of Geography; Volume 12, Issue 3, 2021, pp. 006 – 020. DOI:https://doi.org/10.48088/ejg.lez.12.3.006.020.
7. Lezhava Z., Tsikarishvili K., Bolashvili N., Asanidze L., Fichkhaia, I., Karst and caves of Migaria limestone massif. Tbilisi, Universali, 2022, 240 p.
8. Supatashvili G. D., Lezhava Z.I., Tintilozov Z. K., Shioshvili L SH., Hydrochemical Characteristics of Karst Regions of Upper Imereti. // Reports of the Academy of Sciences of Georgia, 140, No. 2, Tbilisi, 1990. pp. 345-348.

1st International Scientific Conference "Modern problems in Geophysics", Proceedings,
ISBN 978-9941-36-434-1, ISSN 3088-4349, Tbilisi, Georgia, November 6-8, 2025

PHYSICAL-GEOGRAPHICAL FACTORS OF THE GEODYNAMICAL PROCESSES ACTIVATION (THE REGION RACHA-LECHKHUMI)

Salukvadze E., Chaladze T.

Vakhushti Bagrationi Institute of Geography of the Ivane Javakhishvili Tbilisi State University,Tbilisi, Georgia
elene.salukvadze@tsu.ge

Abstract*. Racha and Lechkhumi is a mountainous regions characterized with complex relief and geological structure. Here, nearly all kinds of hazardous geodynamical processes such as landslides, mudflows, erosion, rock flows, avalanches, karst and suffosive phenomena are observed, though the most frequent are landslides, mudflows and erosive processes and washing-off of river banks. The activation of the geodynamical process, hazard of large-scale development of gravitational phenomena are extremely increased by the fact that the whole region territory is prone to earthquakes of intensity 7-9. Among the factors taking part in geodynamical processes the most noteworthy are geological, geomorphological, climatic and anthropogenic factors. The large-scale map (1:50 000) of distribution of geodynamical processes in the Racha – Lechkhumi region, has been compiled on GIS.*

Key words: *Erosion, landslide, mudflow, Racha -Lechkhumi*

Introduction

The territory of Racha and Lechkhumi is one of the mountainous regions of Georgia, where erosive and other hazardous geodynamical processes (landslides, mudflows, avalanches, rock flows, etc.) take place in different degrees.

The economic damage caused by them is enormous and dangerous for the environment. Among all the well-known geodynamical processes in Racha – erosion (with different types), landslides and mudflows are the most hazardous phenomena.

Study area, material and methods

Regions Racha (Ambrolauri and Oni Municipalityes) and Lechkhumi (Tsageri Municipality) are located in the northeastern part of Western Georgia on the southern slopes of the Caucasus. The hypsometric levels of the territory vary from 320 m (Tvishi Cliff) to 4462 m (Mount Chanchakhi, Great Caucasus Ridge).

The research is based on a complex physical-geographic, field, cartographic and GIS methods. The research was based on the existing published literary and foundation material about Racha -Lechkhumi region. Namely, Transcaucasus Medium-Sized Landscape Map [1], also Topographic Maps Racha -Lechkhumi region (scale: 1: 50 000, 1: 100 000) and statistical data [2, 3]. The important component was the field expedition research conducted in 2019- 2022.

Results

Among the factors, which have a unique role in generating geodynamical hazardous processes, the main ones are the lithological structure, history of the relief development and age, morphologic characteristics of the mountain region, hydrologic conditions, behaviour of soil and vegetation cover and also anthropogenic factors.

Its complex geological structure distinguishes the relief of Racha – Lechkhumi. The top of the Caucasus Ridge has a horst-anticline structure. Its crystalline core reaches 4000-4500 m above sea level and is outcropped because of erosive processes; it is composed of pre-Palaeozoic and Palaeozoic granite, gneiss and schist [4].

Characteristically the complex, segmented relief, 22% of the territory is occupied with lowlands, 78% is covered with mountains and foothills with high-mountainous. In the relief's development, together with tectonic and erosive-accumulative, karst, gravity and other processes, the modern and old glaciations have an active role.

In the development of geodynamic processes the orographic properties of the territory, hypsometric disposition and exposition, sloping of the relief surface, fragmentation degree and etc. are of great significance.

The moderately sloped relief (15-20%, 20-25%) occupies most of the area, totalling 30.4%, extremely sloped relief (25-30%) covers 14.5%, steep slopes (30-35%) make up 19.2% and sheer cliffs cover 2.8% of the territory.

In Racha – Lechkhumi, the modern erosive processes are widely distributed in flysch, terrigenous and volcanic sediments, there are two kinds of erosion: vertical and lateral. Surface washing-off (with soil erosion) is widely distributed here. In most of the territory, vertical erosion is observed. It is observed in the areas of nearly all tributaries of the rivers Rioni, Tskhenistskali, Lajanuri and Jejori because of the great thickness of the deluvium cover, an abundance of atmospheric precipitations and flow of underground waters at little depths [2,3]. Vertical erosion is extreme during summer rains and snow melting periods. At the same time, vertical erosion becomes more severe because of ploughing activities on slopes, which are highly slanted. It is hazardous regarding the development of liquid impact erosion. Lateral erosion is observed almost everywhere, and hundreds of hectares of fertile soil are degraded for this reason. Terraces are intensively washed down in town Ambrolauri, Tsageri, villages of Chrebalo, Shardometi, Sori, Gvirishi, Chalistavi, Orbeli, Tsiperchi, etc.

Erosion, potential hazards of landslides and mudflows are influenced by precipitation quantity. On the one hand, precipitation distribution during a whole year is more significant for the generation of erosion.

Seasonal distribution of atmospheric precipitations over the whole territory of Racha – Lechkhumi is as follows: in Racha there are two peaks of precipitation fall: maximum – in May (105-215 mm) and in October (99-202 mm), minimum – in August (79-163 mm) and in January (79-162 mm). In Lechkhumi precipitation falls: maximum – in June (114 mm) and in October (122 mm), minimum – in August (87 mm) and in January (106 mm). On the territory of Racha the most quantity of atmospheric precipitation is observed in Kharistvala (2178 mm annually) that is mainly conditioned by its orographic conditions, On the territory of Lechkhumi 1292 mm annually [5, 6].

The precipitation quantity during one rainfall is also significant. Flow formation and erosion development is highly influenced by precipitation intensity, i.e., the quantity (mm) of water that falls in a unit of time. During heavy rains, when water falls on the surface so rapidly that the soil cannot absorb it, a surface flow is formed and it washes the soil off. The more persistent and long-lasting the torrential rain is, the more dramatic is the effect of the erosive processes. During drizzling rains, even in case of high quantities of precipitations, soil washing-off is not observed or it is quite inconsiderable.

Erosive processes are highly influenced by considerable variation of daily air temperature. In Racha, average annual air temperature varies from 11.4° to -2.4°. The coldest month is January (-0.2°,-12°) and the hottest month is August (23.8°). In the most part of the territory (at 500-1600 m above sea level) the annual temperature amplitude is 22°-23°, whereas in the high-mountainous zone it is 19°. In spring low temperature at night causes soil freezing. During daytime the surface of a thin soil layer thaws, becomes saturated with water and is easily washed off.

While studying erosive processes it is essential to take into consideration the structure of the soil cover, also the water permeability of the soil, on which the value of the surface runoff depends greatly and which is the major reason for soil washing-off.

In the study region, when the daily quantity of the atmospheric precipitation is 100-120 mm and more during torrential rains and there is a significant slanting of slopes, then liquid impact erosion takes place. In the zone of forest dark grey and humus-carbonate soil, on the 10-15° slopes, where hoeing cultures are grown, after one torrential rain (0.5 mm/min) 20-25 t/ha soil is washed off (table 1).

Table 1. Washing soil off arable lands Racha-Lechkhumi

Municipality	**Arable lands completely (Thousand ha)**	**Relief inclination**	**Washing soil off arable lands in year t/ha**	**Degree of soil erosion Metric t/ha**		
				Low	Medium	High
Ambrolauri	2.7	$15\text{-}20^0$	5-10;	1.0.	0.8	0.3
Oni	1.4	$25^0>$	5-10; 20-25	0.7	0.5	0.1
Tsageri	1.5	$25^0>$	5-10; 15-20	0.6	0.5	0.2

On the territory of Racha, in Ambrolauri Municipality, from moderately slanting slopes (15-20°) 5-10 t/ha soil is washed off annually, while in Oni Municipality 20-25 t/ha soil is washed off on extremely slanting (more than 25°) slopes, Tsageri Municipality 15-20 t/ha soil, from more than 25° slanting slopes [7,8].

Erosion is in tight relation with vegetation cover. Vegetation cover always decreases the development of erosion or completely stops it. Erosive processes, especially lateral erosion, are one reason for landslide formation. The main factor that causes generation and activation of landslide processes are complex geologic structure, distribution of rocks with low physical properties on large areas, deep fragmentation of relief and excess of extremely slanted surfaces, a large number of tectonic clefts, high seismic activity, variation of climate conditions and contrasting meteorological elements. Activation of landslide processes highly depends also on anthropogenic economic activities.

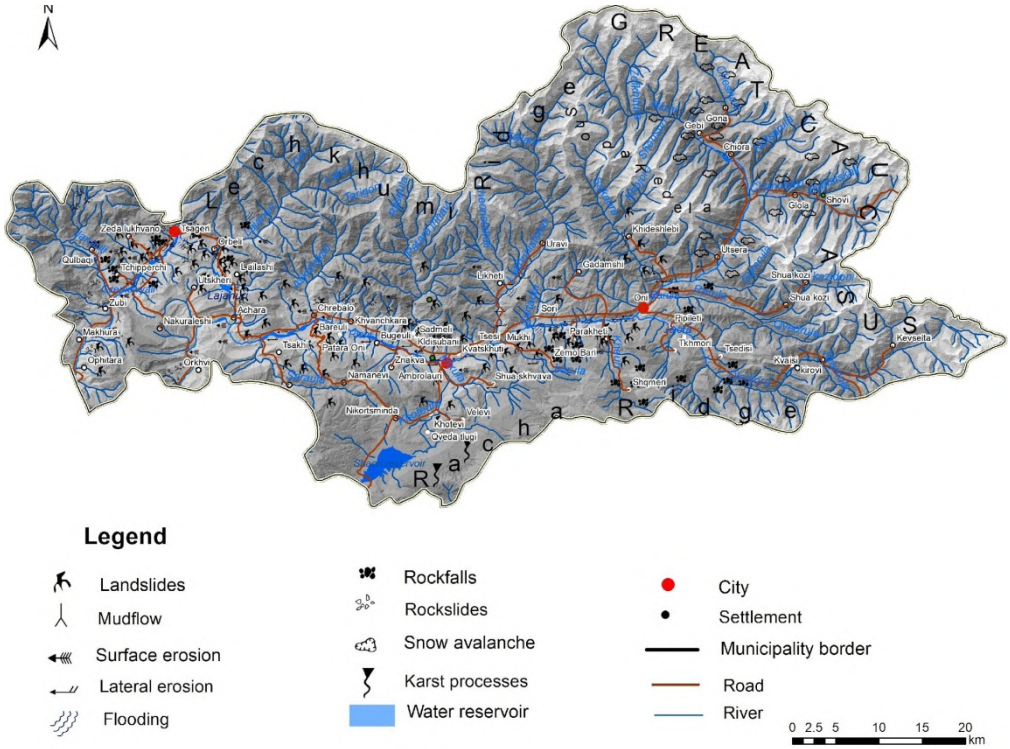

Distribution of geodynamical processes in the Racha – Lechkhumi

In Oni Municipality, the area of the Somitso Landslide is 550 ha, the Zhashkva Landslide area is 1500 ha, the volumes of which vary from several thousand m^3 to tens and hundreds of millions of cubic meters. The volume of the Chorda Landslide is 150 mln m^3, and the Zhashkva Landslide volume is 200 mln m^3 (in Oni Municipality), in Tsageri Municipality, landslides: Sairme, Lukhvano, Orbeli, Lajana, Lailashi, Ckhuteli, Gveso, Surmushi, Gagulechi, Spatagora, Leshkedi, Okureshi, Larchvali, Chalistavi, Zaragula etc.

The most active landslides are observed in Parakheti, Shardometi, Tsedisi and Ghebi. The 1991Racha Earthquake with magnitude 7.2 and intensity IX, which along with the 1988 Spitak Earthquake (Armenia), is the strongest among the earthquakes recorded in the Caucasus so far, in village Chorda triggered a massive landslide (volume 150 mln m^3) that destroyed the village of 70 households. Landslides with volumes of 170-200 mln m^3 were formed on the territories of Zhashkva and Bajikhevi.

According to the landslide damage and hazard risk zoning of the territory of Georgia, Racha belongs to extremely high (0.9-0.7) and high (0.7-0.5) risk categories [3].

According to the risk of damage caused by mudflow processes on the territory of Georgia, the region of Racha „includes an extremely “great hazard” (0.8-0.6) area, which covers the middle mountain and high mountain belts of Racha, the zones of Jurassic slates and terrigene-carbonate flysch. It mainly covers the territory of Oni and Tsageri Municipalities. The “considerable” mudflow area covers the middle mountain and low mountain belts in Ambrolauri Municipality and the low mountain belt in Oni Municipality.

The area of “weak” (less than 0.01) mudflows covers the foothill zone, the part of the Racha Ridge built of carbonate rocks. Mudflows are most characteristic of the rivers originating from the Shoda-Kedela Ridge

(the head river Rioni): Sakhrikilo, Gizhura, Shodura, Lagora, Sakaura. In summer 2020, as a result of the flood and mudflow caused by overflowing of the rivers Sakaura (the right tributary of the river Rioni) and Rioni, the Tbilisi-Oni main highway was substantially damaged, a bridge collapsed, village Lagvanta and several other villages were left entirely isolated from the regional centre and were enormously damaged. Mudflows are common in the basins of the rivers Kondarula, Tchioriskhevi, Shkhiroruli, Dagoruli, Rubodzali, Sasvanostskali, Barula, Shardometiskhvi, Tcheshora, Seva, Parakheti, Tskhenistskali, Jonouli, lajanuri.

Based on the studies of the properties of geomorphologic and composing rocks there are certain regularities in the formation of mudflow foci. Foci transformed by erosion and erosion-landslide processes dominate in the foothills and low mountain zones; gravitational-landslide processes are observed in the middle mountain zone; in high mountain zones there are gravitational processes formed due to solifluction and snow avalanches. Mudflows are formed in the alpine-nival belt and so called “glacial mudflows” are observed in Quaternary glaciation sediments and moraine sediments of the modern glaciers.

On August 3, 2023, a catastrophic glacial mudflow developed in the Bubistskali River Gorge, which was caused by the coincidence of hydrometeorological (intensive melting of the glacier and residual snow cover, atmospheric precipitation in the form of rain, high atmospheric air temperature) and geological events (rockfall at the headwaters of the gorge; landslide-erosion processes). The mudflow of the Bubistskali, a right tributary of the Chanchakhi River, first became a mudflow and then a flowing landslide. The total volume of this mass is 1 million m^3 and still covers the resort area [9]. As a result of the disaster, buildings were destroyed in the Shovi resort area, 33 people died.

The quantity of mudflows is increased due to exceeding the average long-term precipitation norm and also anthropogenic load, especially forest clearance.

Conclusion

The analysis of the physical-geographical factors of Racha-Lechkhumi enables us to make the following conclusions: the mountainous, extremely fragmented relief, the climatic conditions, often unreasonable economic activities (clearance of soil-conserving forests, wrong land farming activities on mountain slopes, washing-off of pastures) contributes to the rapid development of liquid impact erosion that later causes washing-off processes in the upper layers of arable lands.The vegetation cover plays a significant role regarding soil-conserving, especially the forests of timber trees [10].These are oak-oriental hornbeam and oak-hornbeam forests, which can be assigned to the category of forest non-prone to erosion.

References

1. Ukleba D.,Budagov B., Museibov M., Sokhadze E., Bagdasarov A., Landscape map of the South Caucasus, (1: 600 000)], Main Department of Geodesy and Cartography // Russia, Moscow: 1983 (in Russian)
2. Goishvili B., Geoecology of Racha, Geology, Hazards processes and geochemical phenomena: In Racha Past, Present, Future.Tbilisi, 2012, pp. 94-96; (in Georgian).
3. Tatashidze Z., Tsereteli E., Khazaradze R., Elemental natural processes: In Geography of Georgia, Part I, Physical Geography of Georgia; Tbilisi: Metsniereba, 2000, pp. 69-83; (in Georgian).
4. Gobejishvili R., Racha-Lechkhumi//In: Geography of Georgia, Part I, [Physical Geography of Georgia], Tbilisi: Metsniereba, 2000, pp. 256-258; (in Georgian).
5. Scientific and applied reference book of climate in Georgia, Part I.,Tbilisi: Bakur Sulakauri Publishing, 2004, pp. 55-82; (in Georgian).
6. Meladze G., Meladze M., Racha-Lechkhumi-Kvemo Svaneti: In Agroclimatic resources of Western regions of Georgia, Tbilisi: Universali, 2012, pp. 404-406; (in Georgian).
7. Gogichaishvili G., Washing soil off arable lands: In National atlas of Georgia, Tbilisi, 2012, p. 74; (in Georgian).
8. Salukvadze E., Chaladze T**.,** The Natural resource Potential of landscapes in the Lechkhumi Region (Tsageri Municipality). Georgian Geographical journal 2024, Vol.4 (1) 64-74 https://doi.org/10.52340/ggj.2024.04.01.08
9. Assessment report on the natural disasters that occurred in the Bubistskali River Gorge on August 3, 2023, Tbilisi, 2024, pp. 64 – 65; (in Georgian).
10. Kharaishvili G., Water protection and soil protection role of mountain forests, in: The role of forests in nature protection/ Georgia. // Tbilisi:Tsodna, 1988, pp.14 -18, (in Georgian).

1st International Scientific Conference "Modern problems in Geophysics", Proceedings,
ISBN 978-9941-36-434-1, ISSN 3088-4349, Tbilisi, Georgia, November 6-8, 2025

THREE-DIMENSIONAL REPRESENTATION OF THE INITIAL SURVEY OF THE NARIKALA CITADEL

Odilavadze D.T., Chelidze T.L., Yavolovskaya O.V.

Ivane Javakhishvili Tbilisi State University, Mikheil Nodia Institute of Geophysics
odildavit@gmail.com

Abstract. *Due to the construction and rehabilitation works in the territory of "Old Tbilisi", one of the historically ancient and archaeologically very important places in the capital of Georgia, Tbilisi, there was a need to carry out a preliminary reconnaissance archaeogeoradiolocation survey. The pre-marked area for the archaeogeoradiolocation survey was intended as a place for the operation of construction equipment. During the construction process, it was possible to damage multi-ton construction equipment and cause accidents as a result of underground voids, as well as destroy possible archaeological monuments.*

It turned out that the study area is loaded with objects containing cavities of various shapes and contents. The continentality of the soil is disturbed by numerous cavities. Their depth ranges from 0.5 m to 5 m and their length is 1-5 m. A boundary between geological layers has been identified, on which a radio image of a man-made object could be located, such as a foundation, tunnel, culvert, or other cylindrical object located above the foundation and with a width of 1–1.5 m. A radio 3D image of a possible partially collapsed underground passage or partially disintegrated foundation remains is presented.

***Keywords*:** *archaeogeoradiolocation survey, georadar works, radio image.*

Introduction

The paper presents radar images of geo-radiolocation profiles of one of the historically ancient and archaeologically very important sites in the capital of Georgia, Tbilisi. Due to the construction and rehabilitation works in the territory of "Old Tbilisi", there was a need to carry out a preliminary reconnaissance archaeogeoradiolocation survey. The pre-marked area of the archaeogeoradiolocation [1, 2, 3] survey was intended as a place for the operation of construction equipment, where it was possible to destroy archaeological monuments.

The survey revealed a number of voids, signs of the existence of possible archaeological monuments and mapped their locations. The archaeo-geo-radiolocation works were carried out [4, 5, 6, 7, 8] using the Zond 12e ground penetrating radar, the data were collected, processed, and interpreted using the software Prizm 2.6.

Since a significant two-dimensional band structure was revealed [8], it was decided to investigate it using a specific three-dimensional methodology, which yielded positive results.

Task/Objective

The purpose of the task was to conduct a geo-radiolocation survey to detect voids in the underground near-subsurface arrangement [4, 5, 6, 7, 8] and their three-dimensional representation in order to clarify the nature of the revealed object.

Environment and Instrumentation

On the territory, adjacent to the "Old Tbilisi" citadel, "Narikala", in conditions of geographically difficult terrain, in a pre-marked area, the geo-radiolocation survey was conducted using Georadar Zond 12e, with its standard 150MHz dipole antenna and Prizm-2.6 software, to detect voids in the underground near-subsurface arrangement.

To obtain a three-dimensional representation, Prizm-2.6 and its compatible software, Voxler 4 were additionally used.

For clarity, old engravings of the study area from the book “European Engravings of Old Tbilisi” are included (Engraving 1, 2).

We present a schematic drawing of the placement of a number of profiles (Scheme 1). The schematic drawing (Scheme 1) shows the conditional placement of geo-radiolocation profiles and their directions.

Engraving 1. Narikala Fortress, from the first panoramic sketch of Tbilisi. Jean Chardin's Travels, 1673. Artist Guillaume Joseph Grelot. Published by Moses Pitt, London, 1686 [9].

Engraving 2. Tbilisi, unknown German edition. 19th century.[9]

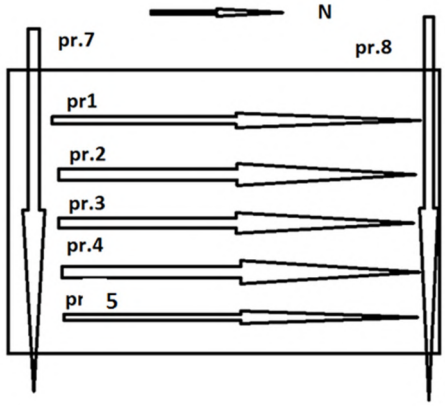

Scheme 1.

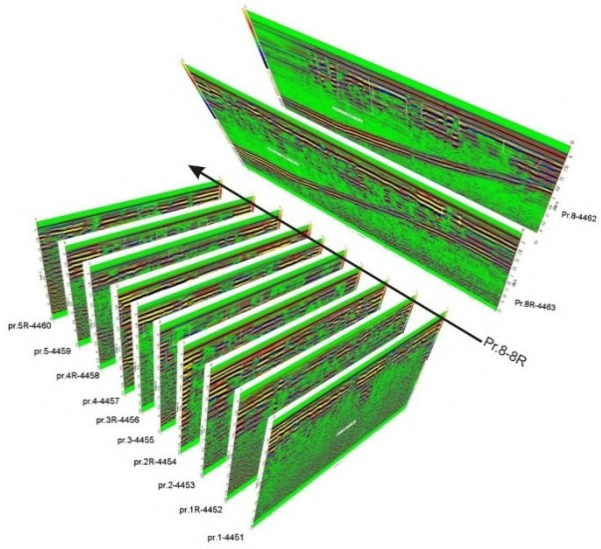

Fig. 1

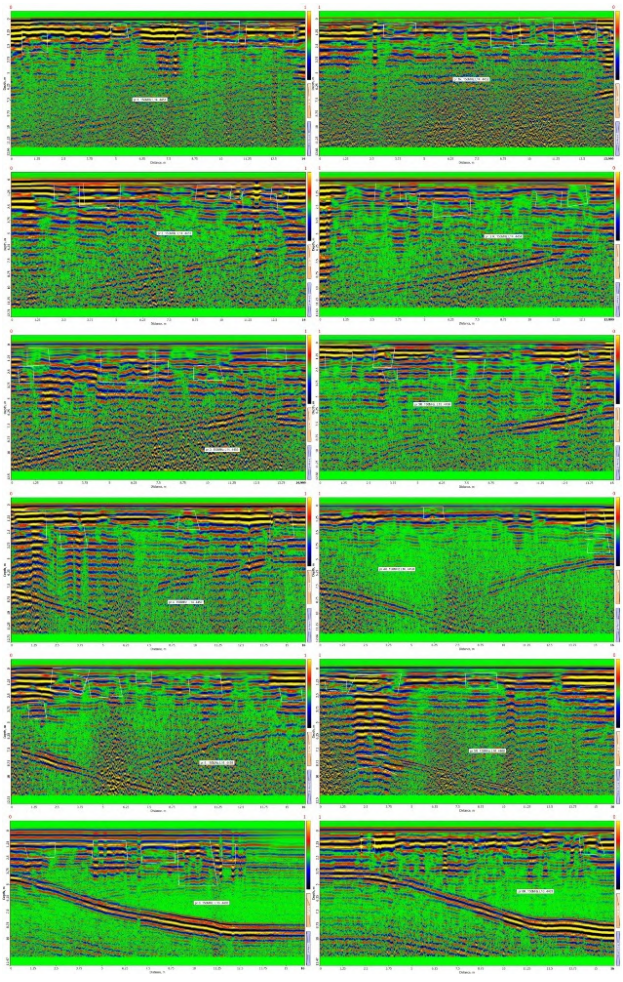

Fig. 2 Sequence of radar profiles

From the profiles presented in Fig. 1, the R-indexed profiles are separated from the corresponding parallel profiles by a distance of approximately 1-1.5 m. Layout of radarograms from profile 1 to profile 8 is presented in Scheme 1. In Fig.1 are shown 2 longitudinal (Pr-8-4462 and Pr 8R-4463) as well as 10 crossing sections of the territory. On profiles Pr.. 8-8R, the sequential subsidence of the banded object is visible, which was reflected both in Fig. 1 in the direction of Pr-5R, and in most radarograms in Fig. 2 (some of them are incompletely visible in profile 8-8R (due to the difficult terrain).

The intersections are indicated by the inhomogeneities observed at the edges of the profile-1-5R. On the radar profiles, the strip passing through the foundation of the tower, Pr.5R, while on the radar profile, the radio image of the tower is no longer visible, since the profiles are 1-1.5m apart and the radio image of the tower obtained by diffracted waves did not appear. However, the dip of the strip is clearly visible (Fig. 2).

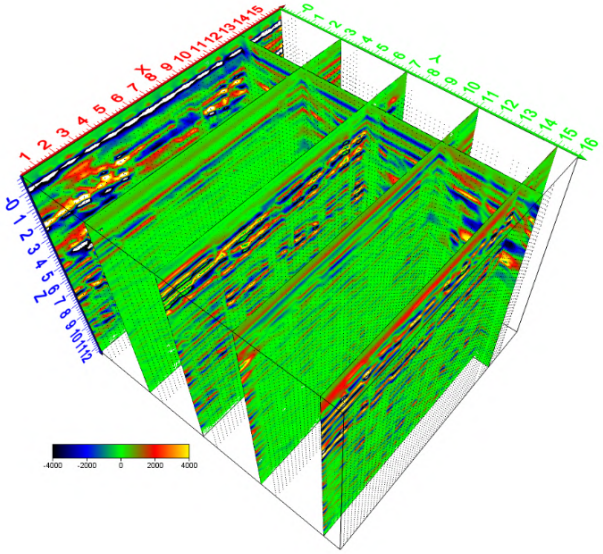

Fig. 3. The intersections of the profiles 1R-5R and 8R

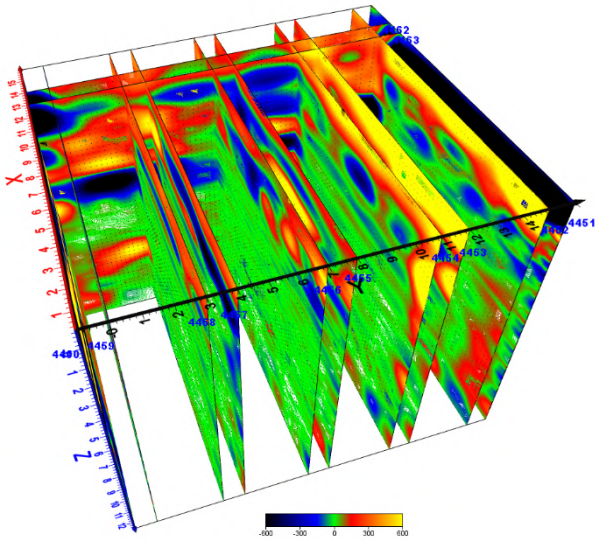

Fig. 4. Gaussian variant. The continuity of the radio image representation at the intersection of the profiles are determined

Reversal profiles 1R-5R and 8R. Clear spots appear at the intersections of the profiles, which indicates the detection of common continuous radio image (Fig. 3).

Voxler-4 uses a Gaussian variant (Fig. 4), which minimizes weak signals. The location of strong signals and the continuity of the synphasic axes of their radio image representation at the intersection of the profiles are determined/

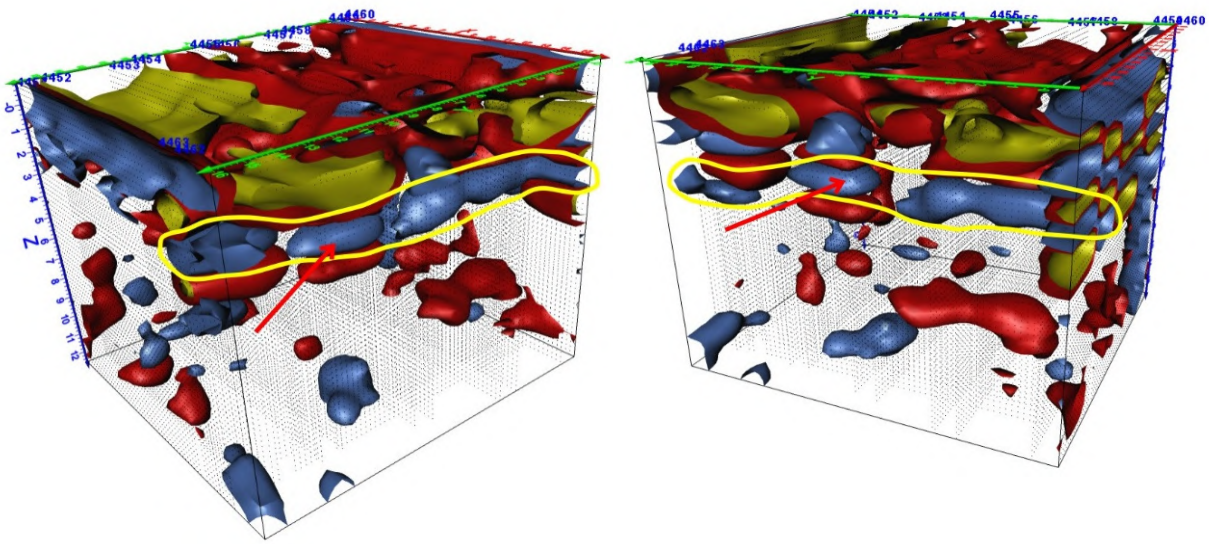

Fig. 5 The three-dimensional representation from two different angles clearly shows the location of the longitudinal body, which is marked with red lines at the location indicated by the arrow.w

Fig. 5 presents a radio image of a possible partially collapsed underground passage or partially disintegrated foundation remnant. It coincides in length with profile 8. With a height of 1-5m. The coordinates of the cut-off points are read from the 3D spatial location of the profiles.

Conclusion

The study area is loaded with objects containing cavities of many shapes and contents, [8] the continentality of the soil is violated by multiple cavities. Their depth ranges from 0.5 m to 5m and their length is 1-5m.

Using the 3D method, 2D georadiolocation profiles were investigated and, according to the interpretation of the obtained results, a corresponding radio image of a banded continuous object was observed, from which it follows that the object is a body containing hollow spaces of anthropogenic origin at an average depth of 5 m, with a length of 16 m. A radio 3D image of a possible partially collapsed underground passage or partially disintegrated foundation remains is presented

References

1. Odilavadze D., Kiria J., Ghlonti N., Yavolovskaya O., The Results of Archaeogeoradiolocation Investigations of the Territory Inside the Rampart of St. Sophia Church of Khobi. // „Moambe" Bulletin of the Georgian National Academy of Sciences, V.14, n.4, 2020, pp. 51-56.
2. Chelidze T., Odilavadze D., Pitskhelauri K., Archaeogeophysics in Georgia-New Results, New Prospects. Journal of Georgian Geophysical Society. // Proceedings OF THE GEORGIAN NATIONAL ACADEMY OF SCIENCES. Series of History, Archeology, Ethnology and Art History, №.15, 2013, pp. 24-34.
3. Odilavadze D. T., Chelidze T.L., A Preliminary GPR investigation of Metekhi Cathedral and the surrounding area. // Journal of Georgian Geophysical Society, № 14, 2011.
4. Kofman L., Ronen A., Frydman S., Detection of model voids by identifying reverberation phenomena in GPR records. // Journal of Applied Geophysics. (59), 2006, pp. 284-299.
5. Odilavadze D., Chelidze T., Yavolovskaya O., Some georadiolocation images of cylindrical bodies built with different dielectric fillers, placed in a dielectric environment. Mikheil Nodia Institute of Geophysics of Ivane Javakhishvili Tbilisi State University, Tbilisi, Georgia, International Scientific Conference "Geophysical Processes in the Earth and its Envelopes". // Proceedings, ISBN 978-9941-36-147-0, Tbilisi, Georgia, November 16-17, 2023, pp.217-220.
6. Odilavadze D. T., Chelidze T. L., Ghlonti N. Y., Yavolovskaya O.V., Determining the Presence and Structure of a Subsurface Radioactive Burial when Interpreting the Results of the GPR Method by Analyzing a Three-Dimensional Rotating Radio Image. // Journal of the Georgian Geophysical Society, e-ISSN: 2667-9973, p-ISSN: 1512-1127. Physics of Solid Earth, Atmosphere, Ocean and Space Plasma, v. 25(1), 2022, pp.21-28.
7. Odilavadze D. T., Chelidze T. L., Yavolovskaya O. Y., THE RADIO IMAGE OF AN OBJECT WITH AN ELONGATED, FACE-FRAGMENTED, DIELECTRICALLY COMPLEX STRUCTURE WAS STUDIED USING THE METHOD OF GEORADAR PHYSICAL MODELING. // Journal of the Georgian Geophysical Society, e-ISSN: 2667-9973, p-ISSN: 1512-1127, Physics of Solid Earth, Atmosphere, Ocean and Space Plasma, v. 27(2), 2024, pp.15 – 28.
8. Odilavadze D. T., Chelidze T. L., Yavolovskaya O. Y., Preliminary archaeogeophysical survey of the construction site in the vicinity of the Narikala Citadel. // Journal of the Georgian Geophysical Society, e-ISSN: 2667-9973, p-ISSN: 1512-1127, Physics of Solid Earth, Atmosphere, Ocean and Space Plasma, v. 28(1), 2025, pp.27-35
9. European gravures of old Tbilisi ISBN 978-9941-487-96-5 /Artanuji Publishing www.artanuji.ge, Author-compiler Sulkhan Saladze, 2020, pp.197.

1st International Scientific Conference "Modern problems in Geophysics", Proceedings,
ISBN 978-9941-36-434-1, ISSN 3088-4349, Tbilisi, Georgia, November 6-8, 2025

RECONNAISSANCE ARCHAEOGEORADIOLOCATION STUDY OF THE TERRITORY OF THE NINOTSMINDA MONASTERY COMPLEX

Odilavadze D. T., Chelidze T. L., Ghlonti N. Y., Kiria J. K., Yavolovskaya O. V.

Ivane Javakhishvili Tbilisi State University, Mikheil Nodia Institute of Geophysics
odildavit@gmail.com

Abstract. *Georgia, Kakheti, Sagarejo, Ninotsminda Monastery Complex. Ninotsminda Cathedral is a notable monument dating back to the 6th century. It was built on an old idol site [1, 2] during the time of Saint Nino. Within the framework of the Ninotsminda Complex Geophysical Expedition, archaeogeoradiolocation work was carried out using the Zond-12e georadar, 500MHz screened and 150MHz dipole staff antennas [3, 4, 5, 6]. Georadiolocation data were collected, processed and interpreted using the Prizm 6 staff software. Georadiolocation profiles/GPR-sections were conducted in the inner courtyard of the monastery and on the territory of the monastery itself. This paper presents the results GPR-section obtained and interpreted by the 500 MHz antenna conducted in the inner courtyard of the monastery complex.*

Keywords: *georadiolocation, georadar Zond-12e, radar images, Ninotsminda Monastery Complex.*

Introduction

Fig. 1. Remains of the walls and surroundings of the Ninotsminda Cathedral in the territory of the complex

Fig. 2. Remains of the walls and interior of the Ninotsminda Cathedral

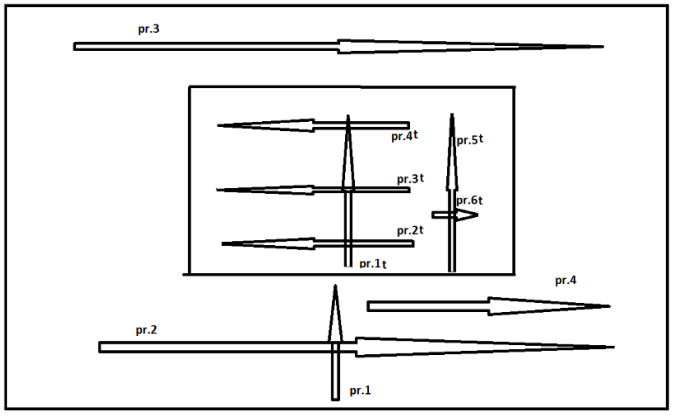

Fig. 3. Schematic drawing 1.

To create a large dome space, an additional small stall was inserted on the diagonal axes between the four apses in the corners of the central square. From the outside, the temple was a star-shaped building in plan, with semicircular apses arranged alternately according to size. Only the altar apse in the middle, where the windows are cut, has a pointed shape (Fig. 1- Fig. 3). The building was a developed form of the tetra-conch and a direct predecessor of the cross-type monuments. The temple was extensively renovated many times (XI-XII centuries, XVI centuries). It was destroyed during the earthquakes of 1824 and 1848.

Environment and Instrumentation

A schematic drawing 1 of shows the location of the archaeo-geo-radiolocation profiles/GPR-section conducted on the territory of the Ninotsminda complex.

The small rectangle corresponds to the territory of the temple, and the large rectangle corresponds to the temple courtyard. The arrows show the approximate directions of the conducted geo-radiolocation cuts.

The Zond-12e georadar and the Prizm-2.6 software used.

The geo-radiolocation profiles were conducted with 500 MHz shielded and dipole 150 MHz antennas, three areas were allocated on the outer and inner territories of the temple.

We present radargrams of geo-radiolocation cuts conducted on the territory of the Ninotsminda temple courtyard, area-1, for 7-8 meter penetration using a 500 MHz antenna. In addition, Prof-1 and Prof-2 intersect each other at a distance of approximately 10m for Prof-1 and 17m for Prof-2.

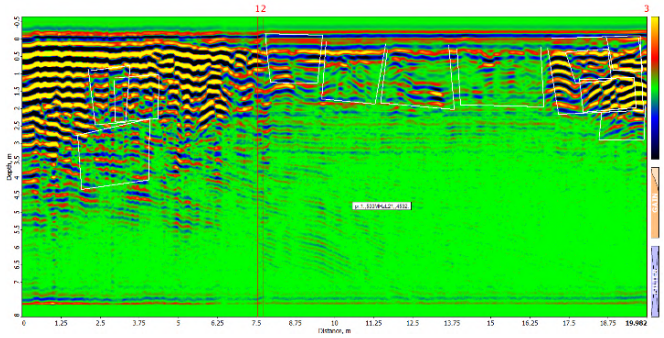

Fig. 4. Profile-1 was performed with a 500 MHz shielded GPR antenna. Profile length -21 m.

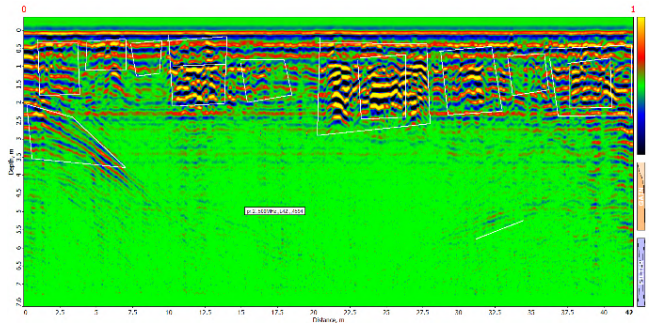

Fig. 5. Profile-2 was performed with a 500 MHz shielded staff GPR antenna. Profile length -42 m.

On the presented radargram (Fig. 4) the radio faces of objects containing vertical, mutually parallel surfaces containing a cavity are marked with white lines [7, 8, 9, 10], presumably of anthropogenic origin, e.g., a burial ground, an underground storage room, etc. The radio faces of objects, including those with a structurally complex structure, are located on the radargram at distances: 2-5m, 6-9m, 9-16m. At distances of 17-20m, a cavity containing a complex structure (17-18.75m) built of a strongly reflective material was marked. The radio face of this object also rests on the radio face of the object containing the cavity on its right side. Three meters below, at distances of 1.25-6.5m, a deformed radio image of an object, presumably of anthropogenic origin, was also noted.

On the presented radargram (Fig. 5) the radio faces of objects containing vertical, mutually parallel surfaces containing a cavity are marked by white lines, presumably the cavities are of anthropogenic origin, e.g., a burial ground, an underground storage room, etc. The radio faces of objects, including those of structurally

complex construction, are located on the radargram at distances: 10-15m, 21-27m. Also, a 38-40m cavity containing a complex, arched structure built of a strong reflective material. At a depth of 2 m, at distances of 0-5m, the radio image of the object of the foundation part was also marked.

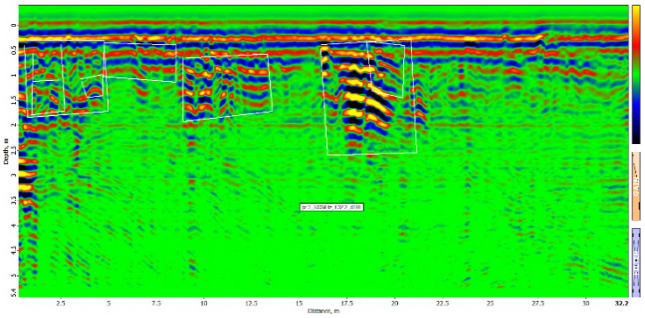

Fig. 6. Profile-3 was performed with a 500 MHz shielded staff georadar antenna. Profile length -32m.

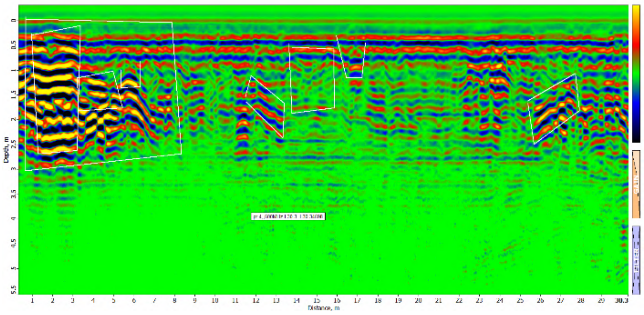

Fig. 7. Prof-4 was performed with a 500 MHz shielded georadar antenna. Profile length-30m.

On the presented radargram (Fig. 6) the radio faces of objects containing vertical and deformed, mutually parallel surfaces containing cavities are marked with white lines, presumably of anthropogenic origin, located on the top of each other, for example, burials, radio faces of objects, including those of structurally complex construction, are located on the radargram at distances: 1-5 m, 10-12 m. At distances of 17-20m, a complex cavity built of a strong reflective material, with an overlap, containing a structure (17-18m) cavity was marked. The radio face of this object is shifted and deformed on the right side. Three meters below, at distances of 0-1m, a radio image of the remnant part of the foundation was also marked.

On the presented radargram (Fig. 7), the radio faces of objects, including those of structurally complex construction, Prof-4, are located at distances: 0-9m. At distances 11-13m, 26-27m, oblique planes containing a complex recess structure were marked. The radio face of this object rests with its right side on the radio face of an object containing a recess oval-like cavity at 28-39m.

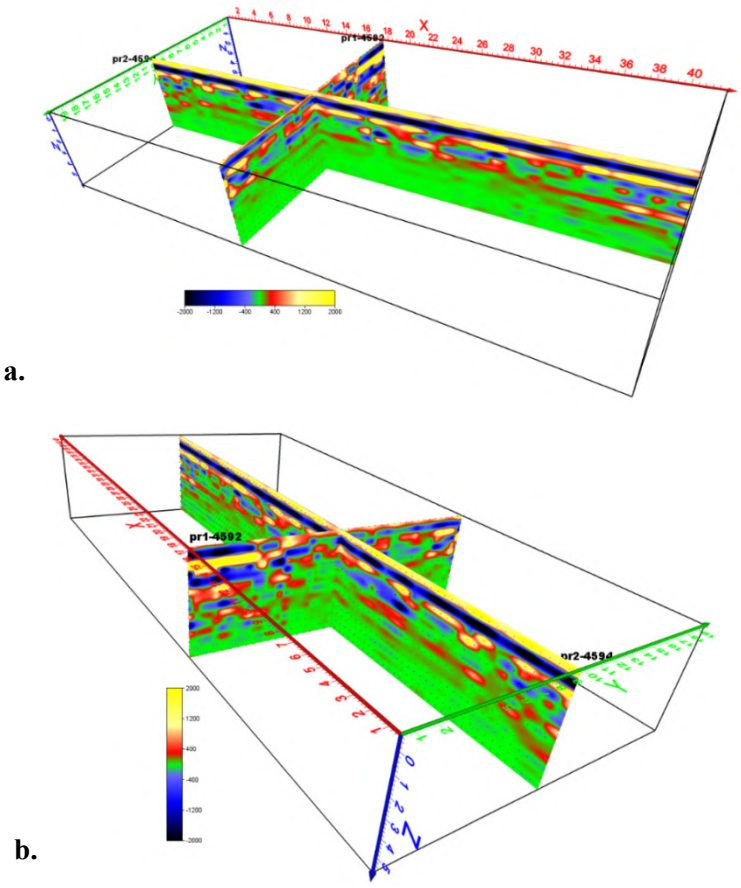

Fig. 8. Intersecting profile-1 and profile-2.

Fig. 8(a,b) shows the intersecting profile-1 and profile-2. It follows from the joint interpretation that the intersection point will clearly show the dimensions of the 3D spatial object, which is well confirmed by presenting the intersection from two different perspectives, according to the radio images.

Area-1. Conclusion

At the intersection of Prof-1 and Prof-2, a common radio feature is recorded, which probably corresponds to an anthropogenic cavity with dimensions of 2x2m, at a distance of 10.5m for Prof-1 and 17.5m for Prof-2. When cross-sectioning profiles 1 and 2, the presence of a three-dimensional underground object was revealed at the intersection, which is well confirmed by presenting the intersection from two different perspectives.

The georadar Zond-12e with its 500MHz shielded antenna revealed multiple georadiolocation radio features representing various types of cavities, which correspond to anthropogenic objects. Their location Prof-1, 2, 3, 4, 5, and depth are determined by the corresponding coordinates at the distances and depths indicated by the radar images.

References

1. Ioseliani P., Description of the antiquities of the city Tiflis. 1866, pp. 132-133 (in Russian).
2. Georgian Soviet Encyclopedia, T. 7, Tbilisi., 1984, P. 440, (in Georgian).
3. Odilavadze D., Kiria J., Ghlonti N., Yavolovskaya O., The Results of Archaeogeoradiolocation Investigations of the Territory Inside the Rampart of St. Sophia Church of Khobi. // „Moambe" Bulletin of the Georgian National Academy of Sciences, V.14, n.4, 2020, pp. 51-56.
4. Chelidze T., Odilavadze D., Pitskhelauri K., Archaeogeophysics in Georgia-New Results, New Prospects. Journal of Georgian Geophysical Society. // Proceedings OF THE GEORGIAN NATIONAL ACADEMY OF SCIENCES. Series of History, Archeology, Ethnology and Art History, №.15, 2013, pp. 24-34.
5. Odilavadze D. T., Chelidze T.L., A Preliminary GPR investigation of Metekhi Cathedral and the surrounding area. // Journal of Georgian Geophysical Society, 2010, № 14, pp.32-38.
6. Kofman L., Ronen A., Sam Frydman. Detection of model voids by identifying reverberation phenomena in GPR records. // Journal of Applied Geophysics. (59), 2006, pp.284-299.
7. Odilavadze D., Chelidze T., Yavolovskaya O., Some georadiolocation images of cylindrical bodies built with different dielectric fillers, placed in a dielectric environment. // M. Nodia Institute of Geophysics of I. Javakhishvili Tbilisi State University, Tbilisi, Georgia, International Scientific Conference "Geophysical Processes in the Earth and its Envelopes". Proceedings, ISBN 978-9941-36-147-0, Tbilisi, Georgia, November 16-17, 2023, pp.217-220.
8. Odilavadze D. T., Chelidze T. L., Ghlonti N.Y., Yavolovskaya O. V., Determining the Presence and Structure of a Subsurface Radioactive Burial when Interpreting the Results of the GPR Method by Analyzing a Three-Dimensional Rotating Radio Image. // Journal of the Georgian Geophysical Society, e-ISSN: 2667-9973, p-ISSN: 1512-1127. Physics of Solid Earth, Atmosphere, Ocean and Space Plasma, v. 25(1), 2022, pp.21-28.
9. Odilavadze D. T., Chelidze T. L., Yavolovskaya O. V., THE RADIO IMAGE OF AN OBJECT WITH AN ELONGATED, FACE-FRAGMENTED, DIELECTRICALLY COMPLEX STRUCTURE WAS STUDIED USING THE METHOD OF GEORADAR PHYSICAL MODELING. // Journal of the Georgian Geophysical Society, e-ISSN: 2667-9973, p-ISSN: 1512-1127, Physics of Solid Earth, Atmosphere, Ocean and Space Plasma, v. 27(2), 2024, pp.15–28.
10. Odilavadze D. T., Chelidze T. L., Yavolovskaya O. V., Preliminary archaeogeophysical survey of the construction site in the vicinity of the Narikala Citadel. // Journal of the Georgian Geophysical Society, e-ISSN: 2667-9973, p-ISSN: 1512-1127. Physics of Solid Earth, Atmosphere, Ocean and Space Plasma, v. 28(1), 2025, pp. 27-35.

1st International Scientific Conference "Modern problems in Geophysics", Proceedings,
ISBN 978-9941-36-434-1, ISSN 3088-4349, Tbilisi, Georgia, November 6-8, 2025

MODELING OF MESOSCALE CIRCULATION AND OIL POLLUTION SPREADING IN THE GEORGIAN COASTAL AREA OF THE BLACK SEA UNDER REAL ATMOSPHERIC FORCING

[*,**] **Demetrashvili D.,** [*] **Kukhalashvili V.,** [*]**Kvaratskhelia D.**

[*] *M. Nodia Institute of Geophysics, I. Javakhishvili Tbilisi State University*
[**]*Institute of Hydrometeorology, Georgian Technical University*
demetr_48@yahoo.com

Abstract. *The paper presents some results of numerical experiments on modeling mesoscale circulation and oil spill propagation in the coastal zone of Georgia and adjacent waters. Calculations of circulation and thermohaline fields are performed using a regional numerical model of the Black Sea dynamics based on solving the full system of ocean hydrothermodynamics equations using the method of splitting into physical processes, coordinate planes and lines. A 2-D advection–diffusion equation of impurity is applied to simulate and forecast oil slick transport. Numerical experiments conducted under conditions of real non-stationary atmospheric forcing with a horizontal resolution of 1km have shown that circulation in the southeastern region is characterized by the generation of cyclonic and anticyclonic eddies with diameters from about 5-8 km to 200 km. Mesoscale eddies make a significant contribution to the spread of oil pollution.*

Key words: *modeling system, Atmospheric forcing, splitting method, circulation.*

Introduction

The Black Sea, which is a nearly enclosed body of water and is connected to the World Ocean only through the narrow Bosphorus Strait, is a very vulnerable marine environment and faces increasing pressure from human activity. The coastal/shelf zone, including the coastal zone of Georgia, is under particular pressure. The Black Sea coastal zone of Georgia has been characterized in recent years by the intensification of human economic activity: the flow of tourists is increasing, coastal infrastructure is developing, the creation of a system of artificial islands and peninsulas in the waters of Batumi is planned, etc. In this regard, the threat of pollution of coastal waters with oil products and other impurities is significantly increasing. The study and forecast of hydrothermodynamic processes occurring in the coastal zone is very important, since they have a significant impact on the marine ecosystem [1] and the features of the distribution of various pollutants in the marine environment.

Currently, mathematical modeling is widely used to study and predict hydrophysical processes in various regions of the oceans and seas, including the Black Sea. Numerical models of the Black Sea dynamics are successfully used both at the basin scale and at the regional scale [2-4].

This paper presents some results of numerical experiments on modeling hydrophysical processes and transport of oil slick under real atmospheric forcing in the southeastern Black Sea, including the Georgian Black Sea coastal zone and the surrounding water area. This region is separated from the open part of the Black Sea by a liquid boundary coinciding with meridian 39.08^0E.

Materials and methods

Numerical experiments on modeling hydrophysical fields were carried out based on the regional model of hydrothermodynamics of the Black Sea developed at M. Nodia Institute of Geophysics of I. Javakhishvili Tbilisi State University. The model is based on a full system of equations of ocean hydrothermodynamics, written in z-coordinates, based on solving the full system of ocean hydrothermodynamics equations using the method of splitting into physical processes, coordinate planes and lines. The regional model with a spatial resolution of 1km was nested in the basin-scale model of the Marine Hydrophysical Institute (Sevastopol,

Ukraine) with a spatial resolution of 5 km. The regional model and the solution algorithm based on the splitting method are described in [5-7].

The surface circulation field calculated using the regional model is used to simulate the spread of oil pollution on the sea surface using a 2-D advection-diffusion equation

$$\frac{\partial C}{\partial t}+\frac{\partial uC}{\partial x}+\frac{\partial vC}{\partial y}+\sigma C=\frac{\partial}{\partial x}\mu_c\frac{\partial C}{\partial x}+\frac{\partial}{\partial y}\mu_c\frac{\partial C}{\partial y}+f(x,y,t) \quad (1)$$

with the following boundary and initial conditions

$$\frac{\partial C}{\partial n}=\beta C \qquad \text{on S} \quad (2)$$

$$\mathbf{C}=\mathbf{C^0} \qquad \text{at t = 0.} \quad (3)$$

Here C is the volume concentration of the pollutant; u and v are the components of the current velocity vector along the horizontal axes x and y, respectively. μ_c is the turbulent diffusion coefficient, n is the outer normal vector to the lateral boundary S. β is a parameter characterizing the interaction of the pollutant with the coastline. σ is a parameter taking into account the change in the pollutant concentration due to some non-hydrodynamic factors (evaporation, sedimentation, etc.). *f* describes the pollutant source, which is a function of time and coordinates.

To solve the problem (1) – (3) the two-cycle splitting method with respect to spatial coordinates is used [8].

Research results

The regional model was applied to simulate and forecast 3-D hydrophysical fields – the current, temperate and salinity with a resolution of 1 km in the southeastern part of the Black Sea, which is separated from the open part of the Black Sea by a liquid boundary coinciding with meridian 39.08^{0}E. The 3-D solution domain was covered by a grid having non-uniform vertical step from 2 m to 100 m with 30 calculated levels. The number of grid points on each horizon was 215 x 347. The time step was equal to 0.5h.

Validation of the regional model by comparing its outputs with satellite data showed that it describes hydrophysical fields with good accuracy [6, 7, 9].

Numerical experiments conducted under conditions of real non-stationary atmospheric forcing with a horizontal resolution of 1km, have shown that circulation in the southeastern region is characterized by the generation of cyclonic and anticyclonic eddies with diameters from about 5-8 km to 200 km.

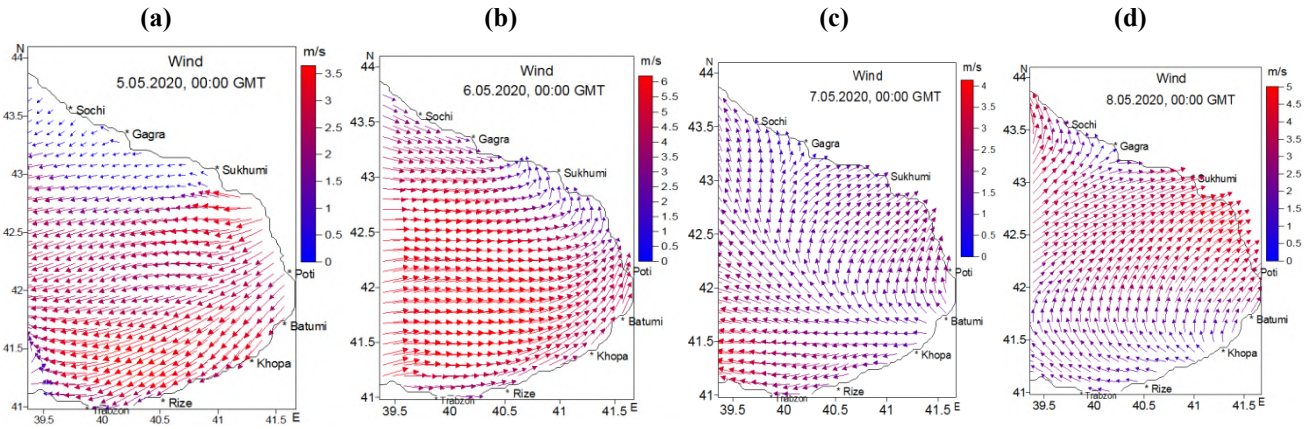

Fig. 1. Wind field over the modeling domain corresponding to 00:00 GMT, 2020:
(a) – 5 May, (b) – 6 May, (c) – 7 May, (d) – 8 May.

The present paper presents an example of forecasting hydrophysical fields corresponding to the forecast interval 00:00 GMT, 4-8 May 2020. Fig. 1 shows the wind vector field at different times over the modeling domain. The figure clearly shows that during this period of time the wind direction changed significantly, and

the wind speed practically did not exceed 6 m/s. During most of the time, the average wind speed on the horizon was 2-3 m/s.

Fig. 2 shows the calculated predicted surface circulation fields after 24, 48 and 96 hours (time is counted from the initial moment of the forecast: 00:00 GMT, 4 May, 2020). The Fig.2 shows that the circulation structure as a whole changes little, even though the wind direction is highly variable during the forecast interval. The main circulation element is an elliptical anticyclonic vortex, which covers a certain area in the southern part of the considered area.

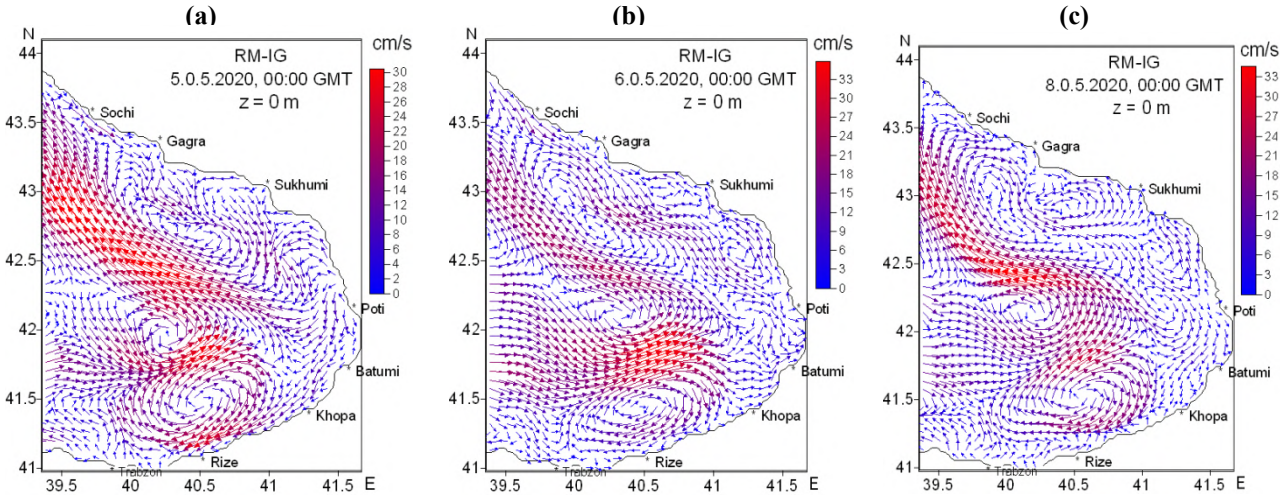

Fig. 2. The predicted surface current fields at 24 h (a), 48 h (b) and 96 h (c) (the forecasting period is 00:00 GMT, 4-8 May, 2020).

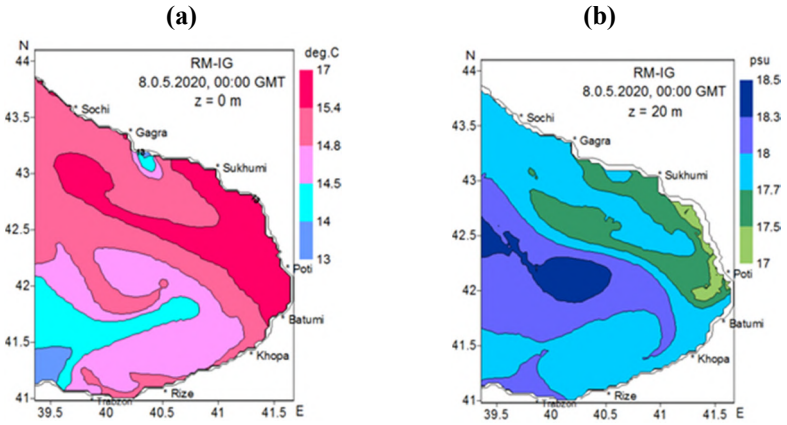

Fig. 3. Predicted sea surface temperature field (a) and salinity field at depth of 20 m corresponding to 00:00 GMT, 8 May 2020.

Fig.3 illustrates predicted sea surface temperature and salinity field at depth of 20 m corresponding to 00:00 GMT, May 8, 2020. The distribution of temperature field is typical for the coastal zone of Georgia, waters with a relatively high temperature of about 17^0C are observed near the Georgian coastline. The salinity field (Fig.3b) correlates well with the circulation. In the zones of anticyclonic movement, waters with relatively low salinity are observed and, inversely, in the zones of cyclonic movement waters with relatively high salinity are observed. This fact is in good agreement with the previous results [5-7, 9].

The circulation regime has a significant impact on the pollutants dispersion process. Numerical experiments were conducted under different real circulation modes and at different locations of the hypothetical oil spill point. The results of the calculations show that the circulation mode, characterized by various eddy structures, is one of the most important factors that essentially determines the transport of the oil slick. The turbulent diffusion factor is also important. During the spreading process of the oil slick, it changes shape, expands diffusely, and occupies more area.

Fig. 4 illustrates forecasted regional circulation in the easternmost part of the Black Sea and drifting of oil slick in case when 50 t was occurred on distance about 65 km from Poti shoreline. The forecasting interval

was: 00:00 GMT, 1-4 March, 2014. The surface circulation is essentially changeable for this forecasting period. Such circulating reorganization is essentially reflected on moving of the oil spill. In the course of migration the oil slick extends gradually and deformed. Simultaneously there is a reduction of oil pollution concentrations that is caused by diffusion expansion, evaporation and other factors.

(a) t = 4h (b) t = 24h (c) t = 72 h

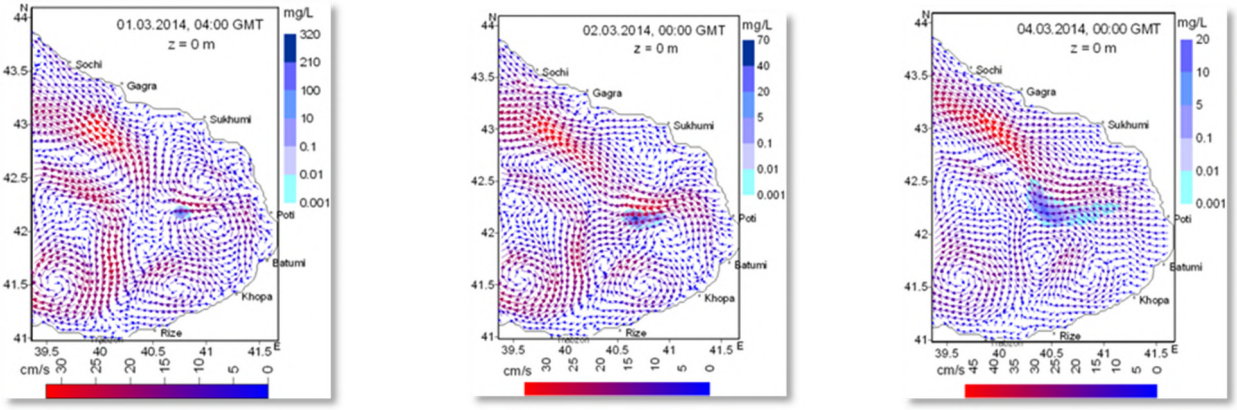

Fig. 4. Predicted surface circulation and oil slick transport at moments 4 h (a), 24 h (b), 72 h (c). (the forecasting period is 00:00 GMT, 1-4 March, 2014).

Conclusion

The regional model of the Black Sea dynamics of the M. Nodia Institute of Geophysics of I. Javakhishvili Tbilisi State University was used to model circulation and thermohaline fields with 1 km spatial resolution in the southeastern part of the Black Sea which covers the Georgian sector of the Black Sea and adjacent water area. The surface flow field is used to calculate oil pollution spreading. Numerical experiments are performed in conditions of real atmospheric forcing.

Further improvement of the modeling system is connected with the elaboration of very high resolution modeling subsystem (with horizontal grid step of 200 m) for Batumi-Poti-Anaklia water area, that undergo great anthropogenic impact.

Acknowledgments. This work was supported by Shota Rustaveli National Science Foundation of Georgia (SRNSFG) [grant number FR-22-365].

References

1. Cuthbert R. N, Sidov A, Frost K. F, Kotronaki S. G, Briski E., Emergent effects of temperature and salinity on mortality of a key herbivore. // Journal of Sea Research, 177, 2021,pp. 1-5.
2. Arthur C., Alexander B., et al., Interannual variability of Black Sea's hydrodynamics and connection to atmospheric patterns. // Deep-Sea Res. II, 2012, http://dx.doi.org/10.1016/j.dsr2.2012.04.010
3. Baltikas V., Makris C., Nagkoulis N., Karambas T., Numerical modeling of sub-mesoscale circulation processes in coastal areas of the Black Sea. International Conference on Research and Assessment for Sustainable use of Black Sea Shellfish Resources. Varna, Bolgaria, October, 2021. pp. 109-111.
4. Rusu E., Rusu L., Soares G., Prediction of extreme wave conditions in the Black Sea with numerical models. 9th International workshop on wave Hindcasting and Forecasting. September 2006.
5. Kordzadze A., Demetrashvili D., Forecast of circulation processes in the Georgian Black Sea coastal zone by the high-resolution regional model of the Black Sea dynamics. // Collected papers № 65, dedicated to the memory of academician Tsotne Mirtskhoulava. Tbilisi, 2010, pp.140-146.
6. Kordzadze A. A., Demetrashvili D. I., Operational forecast of hydrophysical fields in the Georgian Black Sea coastal zone within the ECOOP. // Ocean Science, Vol. 7, 2011, pp.793-803.
7. Demetrashvili D., Computing method applied for simulation and forecast of hydrophysical fields in the southeastern Black Sea. // WSEAS transactions on Environment and Development., vol.20, 2024, pp.662-671. DOI:10.37394/232015.2024.20.64.
8. Marchuk G. I., Methods of Numerical Mathematics. Springer-Verlag, New York, Heidelberg Berlin, 1982, 324 p.
9. Gavardashvili G., Demetrashvili D., Gavardashvili A. Clarification of hydrological regime and ecological parameters in the Georgian Black Sea coastal zone using mathematical modeling and experimental methods. // Bulletin of the Georgian National Academy of Sciences. vol.18, № 4, 2024, pp.81-87.

1st International Scientific Conference "Modern problems in Geophysics", Proceedings,
ISBN 978-9941-36-434-1, ISSN 3088-4349, Tbilisi, Georgia, November 6-8, 2025

DETERMINATION OF THE GROUNDWATER LEVEL BY THE VES METHOD IN THE CHERNORECHENSKY FOREST OF THE GROZNY

Elzhaev A.S.

Grozny State Oil Technological University named after Academician M.D. Millionshchikov
aslambek.elzhaev@mail.ru

Abstract. *This article presents the results of a VES survey conducted in the Chernorechensky forest area of Grozny. A brief description of the study site is provided, along with information on the survey methods and equipment. The study's findings, including high-quality apparent resistivity sections and geoelectrical sections, were analyzed to draw certain conclusions.*

Key words: *engineering geophysics, VES, apparent resistivity, data processing.*

Introduction

Engineering geophysical methods have recently been increasingly used to study environmental issues. This is primarily due to the fact that geophysical methods allow for a more detailed study of the study object, while maintaining the integrity of the object [1, 2, 4]. Electrical prospecting methods have become the most widely used engineering geophysical method.

At the "Chernorechye" site (Grozny), we conducted vertical electrical sounding (VES) to determine groundwater levels and study engineering and geological conditions. The site is located in the Chernorechensky forest within a water protection zone.

The trees in the study area consist of perennial stands of oak, ash, several species of maple, hornbeam, alder, and other trees. Shrub vegetation is widespread.

The main waterway in the study area is the Sunzha River, which flows from southwest to northeast through the central part of Grozny and is glacially fed. The average river depth is 1.5 meters, and the average flow velocity is 0.8 m/s.

Within the study area, the geological profile is represented by rocks of the Quaternary and Neogene systems, predominantly loams, clays, coarse-grained soils (pebbly, gravelly, or crushed rock with clay and sandy-clay aggregate), and, in places, sand, sandstone, and limestone.

Methodology and equipment

VES was conducted using a symmetrical Schlumberger array consisting of two supply electrodes (grounding electrodes) through which direct current was passed into the ground, and two measuring electrodes between which the potential difference was measured. A battery was used as a current source in the supply line. A portable electrical survey station was used to measure the potential difference and the current passing through the ground [3].

The AB/2 spacing varied from 1.5 to 150 m. At each spacing, the current in the AB line and the voltage in the MN line were measured. The measurement results were recorded in the measuring equipment's memory and in a field log.

The measuring equipment used during the study included the following: the "MERI-24" station and the "Astra-100" generator.

The MERI-24 measuring device allows for signal parameters to be measured and processing results to be obtained in real time. The Astra-100 generator is capable of depth surveys ranging from a few meters to a few hundred meters.

Sounding was conducted using a profile diagram (fig. 1). To more accurately evaluate the results, the profiles were constructed with multiple overlaps.

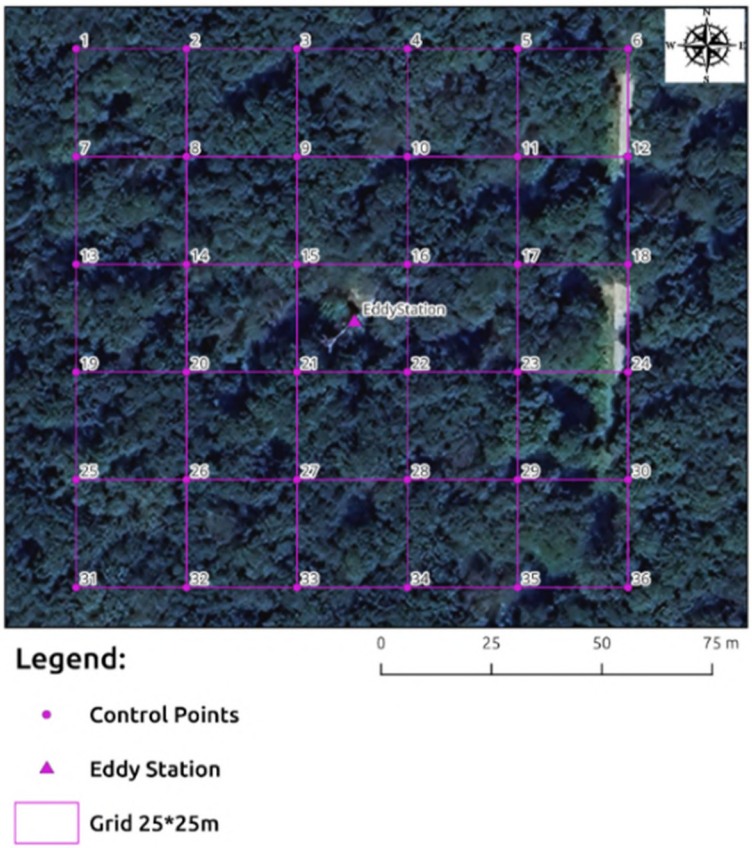

Fig. 1. Profile scheme

A 1:25000 scale topographic map was used as a reference for fieldwork. The coordinate system was WGS84. Geophysical observation points were marked on the ground with wooden pegs or painted, where possible.

The initial evaluation of the VES results was conducted in the field, with repeat measurements taken if necessary.

The initial stage of office processing was the conversion of the obtained potential difference values into apparent resistivity values using the formula:

$$\rho_A = K\,(\Delta U)/I,$$

Where: ρ_a – the apparent resistance (Ohm m); K – the installation factor; ΔU and I – are the measured potential difference (in millivolts) and current in the supply line (in milliamperes), respectively.

Field data was processed using ZOND-IP1D, a specialized program designed for one-dimensional interpretation of profile data from various VES modifications. A user-friendly interface and extensive data presentation capabilities enabled the geological task to be solved with maximum efficiency.

The VES data processing and interpretation process consisted of the following: a calculated curve is selected for the VES field curve (Fig. 2). If any point on the VES field curve significantly deviates from the calculated curve, it is adjusted. Such deviations can be caused by local inhomogeneities, underground utilities, interference, terrain features, etc.

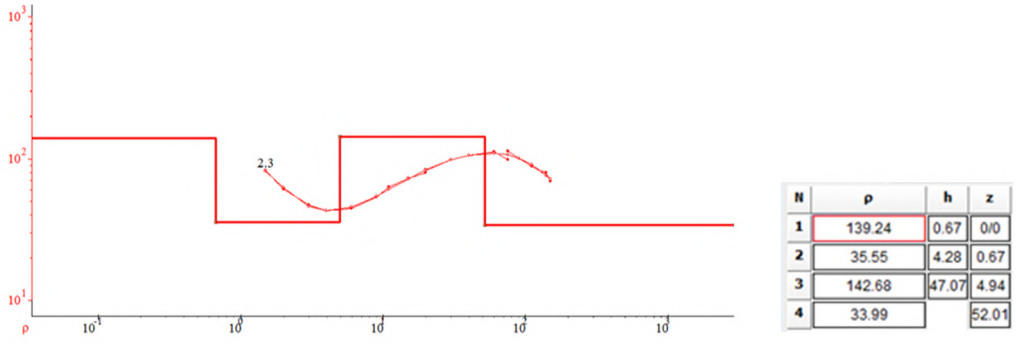

N	ρ	h	z
1	139.24	0.67	0/0
2	35.55	4.28	0.67
3	142.68	47.07	4.94
4	33.99		52.01

Fig. 2. Result of field (primary) processing of VES

Results

The geophysical surveys conducted at the “Chernorechye” site resulted in apparent resistivity (AR) and geoelectrical sections along all six profiles. As an example, Fig. 3. shows an apparent resistivity section (a) and a geoelectrical section (b) along the first profile.

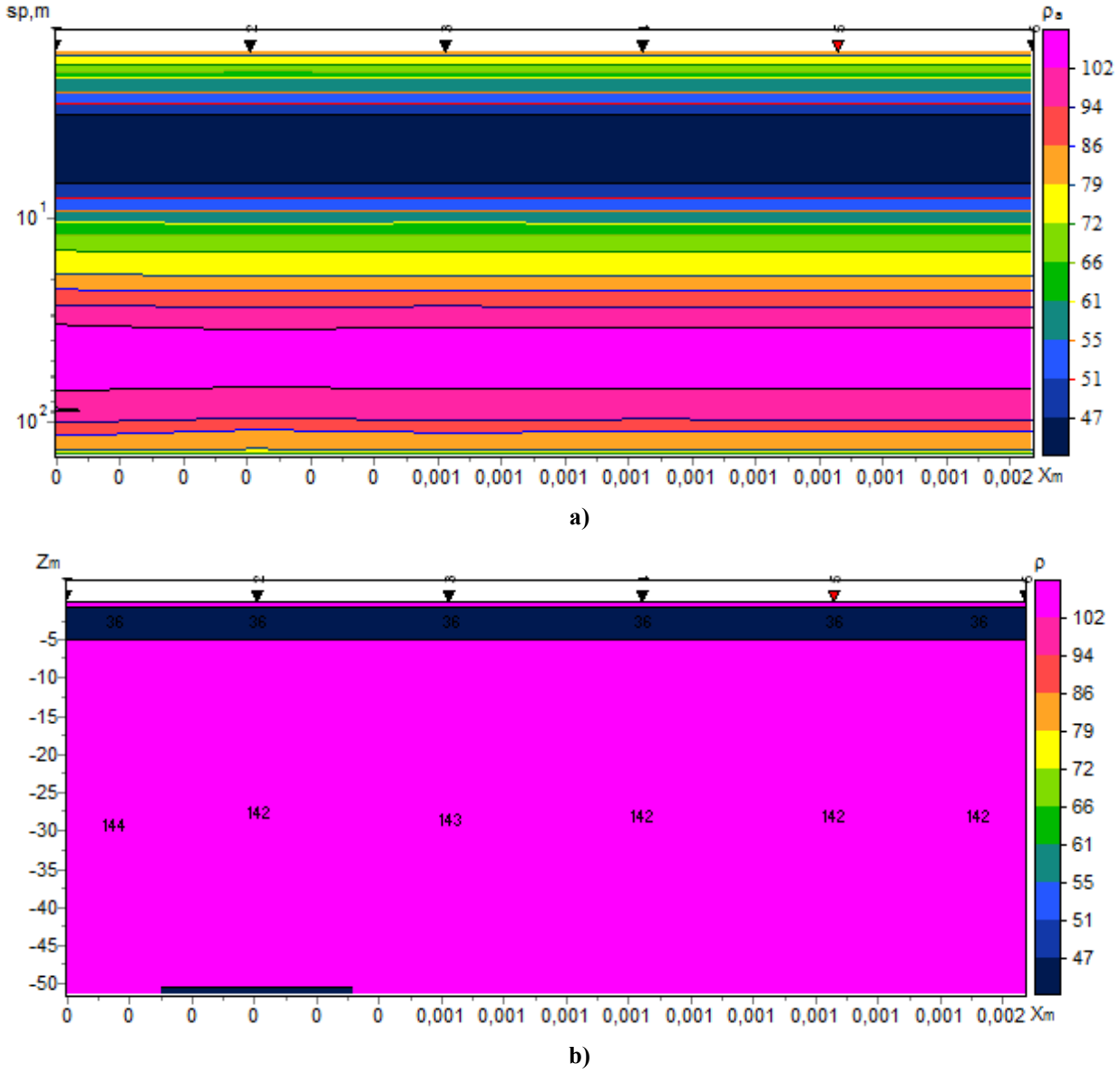

Fig. 3. Result of processing electrical sounding data along profile 1:
a – apparent resistivity section; b – geoelectric section

Conclusions

Analysis of the obtained sections showed that:
1. The study area was investigated using the VES method to a depth of 55 m;
2. Geoelectric sections constructed from the results obtained at electrical sounding points with a step of 25 m are characterized as uniform;
3. The upper layer of the section of the study area is lithologically represented by sand. This is indicated by the recorded apparent resistivity values.
4. The apparent resistivity values of the second layer are characteristic of gravel and pebble deposits.
5. The third (lower) layer, like the upper layer, is represented by sand.
6. The upper part of the section from a depth of 4.28 m is low-resistivity (35.55 Ohm m), which is typical of water-saturated soils.

Acknowledgment. The article was prepared within the framework of the state assignment for scientific research work No. FZNU-2024-0002

References

1. Zaalishvili V.B., Golik V.I., Geophysical Support for Mining Production // Geology and Geophysics of Southern Russia. 2024. Vol. 14. No. 3. pp. 85–98.
2. Kerimov I.A., Elzhaev A.S., Doduev A.A., Geophysical Surveys at the Carboniferous Test Site of the Chechen Republic // Geology and Geophysics of Southern Russia. 2023. Vol. 13. No. 3. pp. 49–62.
3. Marchenko M.N., Vertical Electrical Sounding. Textbook. Moscow, 2013.
4. Hauck C., Kneisel C., Applied geophysics in periglacial environments. Cambridge: Cambridge University Press, 2008. DOI: 10.1017/CBO9780511535628.
5. Zakaria M.T., Mohd Muztaza N., Zabidi H., Salleh A.N., Mahmud N., Rosli F.N. Integrated analysis of geophysical approaches for slope failure characterization. // Environmental Earth Sciences. 2022. Vol. 81. No. 10. pp. 1–21.

1st International Scientific Conference "Modern problems in Geophysics", Proceedings,
ISBN 978-9941-36-434-1, ISSN 3088-4349, Tbilisi, Georgia, November 6-8, 2025

RESULTS OF THE STUDY OF THE GEOECOLOGICAL STATE OF MOUNTAIN RIVER BASINS OF THE SOUTHWESTERN CASPIAN REGION IN 2024

***Kerimov I.A., **Gorbunov R.V., **Gorbunova T.Yu., *Makhmudova L.Sh., *Gagaeva Z.Sh.**

M.D. Millionshchikov Grozny State Oil Technical University, Grozny, Russia
A.O. Kovalevsky Institute of Biology of the Southern Seas of RAS, Sevastopol, Russia
ibragim_kerimov@mail.ru

Abstract. *This paper presents the results of the first phase of a major research project entitled "Dynamics of the Geoecological State of Mountain River Basins in the Northeast Caucasus, Azerbaijan, and Iran under Climate Change and Growing Anthropogenic Pressure." A methodology, concept, and methods for geoecological assessment of mountain river basins have been developed using key areas (small and medium-sized river basins in the Caspian Sea catchment area in Russia, Azerbaijan, and Iran) as examples.*

Key Words: *Mountain rivers, Caspian region, geoecology, basin, climate*

The following scientific results were obtained:

1. The types of nature management and socio-cultural processes in the mountain river basins of Caspian were characterized. It was shown that these types of nature management and socio-cultural processes form the basis for the formation of a matrix of geoecological assessment criteria. A list of criteria for the geoecological assessment of mountain river basins was proposed, based on the integration of remote sensing data and geoinformation modeling. The geoecological assessment criteria developed within the study were structured according to landscape contours.

2. The morphometric characteristics of the river basins of small and medium-sized rivers in the Northeast Caucasus, Azerbaijan, and Iran were identified and analyzed using GIS technologies. Basin boundaries were determined using DEMs and topographic maps and various geometric parameters of the basins were measured. At the current stage of scientific and technological development, the use of GIS technologies and DEMs is an effective method for identifying river drainage basins and calculating their morphometric parameters.

Although 90 m/pixel DEMs have lower accuracy, they can be used in modeling drainage basin delineation when higher resolution DEMs cannot accurately capture total runoff and build up.

The list of key morphometric parameters calculated for river basins in key areas shows minor differences, suggesting the feasibility of further use of all DEMs. The exception is the 90 m/pixel DEM, which often performs better in modeling than some 30 m/pixel DEMs. For the study area, the Copernicus 30 m DEM is optimal and, in some cases, the Copernicus 90 m DEM or SRTM 30 m DEM, where the use of the Copernicus 30 m DEM is associated with basin delineation errors.

3. Based on this data set, a matrix of criteria for geoecological assessment of the Caspian region's territory was developed as a basis for geoecological assessment of various landscape types. The matrix is based on 34 criteria describing the morphometric characteristics of the relief, seismicity, avalanche hazard, mudflow hazard, anthropogenic landscape transformation, KIZA, surface water and soil pollution, and others.

4. A methodology for geoecological assessment of the Caspian region's mountain river basins was developed. Despite the integrity of the drainage basin as a geoecological unit, its assessment criteria should vary depending on the landscape zones that make up the basin. The methodology for geoecological assessment of mountain river basins is based on two main postulates: the operational-temporal unit of study is the boundaries

of the transformation of sociocultural processes and the operational-territorial unit of study is the landscape zones.

5. A partial assessment of several geoecological assessment criteria in the Caspian region was conducted. Large-scale landscape field studies were conducted, and pollution of water, bottom sediments, soils and vegetation was assessed. The highest nitrogen dioxide and aerosol index levels were recorded in the Kheraz and Gorgan river basins. This suggests that these basins are most susceptible to atmospheric pollution among those considered. Significant concentrations of carbon monoxide were also detected in the Gorgan River basin. Maximum ozone levels were found in the Sunzha River basin.

Analysis of changes over time revealed that the COVID-19 pandemic has significantly impacted the distribution of pollutants. Correlation analysis revealed that altitude is a key factor influencing the distribution of pollutants such as carbon monoxide, ozone and the aerosol index. Population density is more strongly associated with the distribution of nitrogen dioxide. The distribution of other substances is more complex and involves different distribution mechanisms.

The study area is part of the alpine-type relief zone of the Eastern Caucasus, which encompasses early Alpine folded structures composed of Lower and Middle Jurassic shale strata. Systems of deeply dissected mountain ranges and intermontane depressions are well developed. The overall geomorphological structure is determined by the folded structures and the Alpine longitudinal faults that bound them. The formation of secondary landforms, superimposed on tectonic forms, is associated with late Quaternary glaciation and erosion-denudation processes. Modern glaciation is confined to certain of the highest mountain ranges.

Mechanical weathering of rocks and sheet denudation play a significant role in shaping the modern topography. The area is characterized by a very high degree of erosional dissection of the terrain and is highly affected by modern exogenous processes. This highly dissected terrain facilitates the formation and development of mudflows, avalanches, erosion, and landslides. Landslides are the most prevalent.

It has been established that the highest anthropogenic transformation indicators are found within the Karachay and Gorgan river basins. Low anthropogenic transformation indicators are found in the Atachay and Sulak river basins. The highest anthropogenic transformation indicators are located within the flat parts of the river basins, which have been developed for a long time and where a developed infrastructure and settlement system have been established. The lowest transformation indicators are characteristic of highlands covered by natural forest and meadow vegetation. All river basins under consideration have seen increases in average population size and population density. The most pronounced increases in population density are observed in the Gorgan and Sunzha river basins, while the most pronounced increases in population size are also observed in the Gorgan and Sunzha river basins.

6. An analysis of meteorological station data and reanalysis data in the basins of small and medium-sized rivers in the study region was conducted. Taking into account data from meteorological stations for the period from 1961 to 2023, three main time periods with their own trends in meteorological parameter changes are distinguished: Period 1 (1961-1981), Period 2 (1982-2004), and Period 3 (2005-2023). There is a very high correlation (0.99) between the reanalysis data and meteorological station data on average annual air temperature. There is a high correlation (0.77) between the reanalysis data and meteorological station data on annual precipitation. Temperatures along the Dagestan, Azerbaijan and Iranian coasts of the Caspian Sea have increased most rapidly over the past 19 years (2005-2023), with average long-term temperatures increasing by an average of 1.1°C. Precipitation along the Dagestan, Azerbaijan, and Iranian coasts of the Caspian Sea has decreased precisely during this most recent period (2005-2023), with average long-term precipitation values decreasing by an average of 35 mm. Distribution maps of average long-term values of the studied meteorological parameters were constructed within the catchment areas of the western and southern coasts of the Caspian Sea, as well as within the studied river basins.

Zones corresponding to the presence of climatic anomalies in the study areas were identified. The higher the surface level relative to sea level, the more pronounced the positive anomalies in average long-term air temperatures become. Negative anomalies of average long-term air temperatures within the study area are present in all altitudinal zones except the nival zone (above 3000 m).

Maps of anomalies of long-term average values of the studied meteorological parameters were constructed within the contours of the western and southern coasts of the Caspian Sea, taking into account altitudinal zonation, as well as within the studied river basins. The spatial distribution of long-term average temperature

anomalies is as follows: negative statistical temperature anomalies are confined to the Caucasus Mountains, while positive anomalies are confined to the Elbrus Mountains and the southeastern coast of the Caspian Sea. Positive anomalies of long-term average precipitation were identified at all levels of altitudinal zonation for all time periods. The spatial distribution of long-term average precipitation anomalies is as follows: the largest zones of positive precipitation anomalies are found on the northern slopes of the Caucasus Mountains, as well as within the southern and southwestern coasts of the Caspian Sea. Negative precipitation anomalies are found in small areas along the southern boundary of the Caspian Sea drainage basin, closer to the northern slopes of the Elbrus Mountain range.

Temperatures corresponding to these anomalous values have increased over the past 63 years: positive anomalies of mean long-term temperatures from 2005 to 2023 increased by an average of 1.6°C, while negative anomalies increased by an average of 0.9°C, compared to the first time period (1961 to 1981). Negative anomalies of mean long-term precipitation are detected only at altitudes of 2000 m and above. The volume of mean long-term precipitation values corresponding to these anomalous values has decreased over the past 63 years by an average of 18 mm for positive anomalies and by 41 mm for negative anomalies, when comparing data samples from the three time periods.

Positive temperature anomalies among the studied river basins are found only within the Gorgan River basin. Negative temperature anomalies among the studied river basins are found only within the southern part of the Sulak River basin. Positive anomalies in mean long-term precipitation are found only within the Sunzha River basin and slightly north of the Kheraz River basin.

The trend over the three time periods under consideration is a decrease in the distribution of positive temperature anomalies within the river basins. Over time, temperatures corresponding to anomalous values increased: positive anomalies in mean long-term temperatures by 1.9°C and negative anomalies by 0.7°C, when comparing data samples from the three time periods (within the river basins). Negative anomalies in mean long-term precipitation are not found for any of the time periods under consideration. By the most recent time period (2005-2023), the area covered by positive anomalies in mean long-term precipitation values within the Sunzha River basin decreased, while it increased near the Kheraz River basin. Over time, the volume of mean long-term precipitation values corresponding to positive anomalies decreased by 46 mm when comparing data samples from the three time periods (within the river basins).

7. An air pollution assessment in the study region was conducted using remote sensing data from the Sentinel-5P satellite. The Sentinel-5P satellite, with its high spatial resolution and global coverage, has become an important tool for atmospheric monitoring and analysis of pollution dynamics over large areas. The use of the GEE cloud platform made it possible to process large volumes of satellite data and conduct detailed analysis. The Google Earth Engine cloud computing platform was used for high-quality processing of large volumes of satellite imagery. Using JavaScript code, the average values were filtered and extracted, which were then analyzed and graphically presented in ArcGIS. The processing results were used to study the interannual and intraannual dynamics of the aerosol index, nitrogen dioxide, ozone, carbon monoxide, formaldehyde, sulfur dioxide and methane. Based on the obtained data, distribution maps of these pollutants for the Caspian region for 2018-2023 were compiled and correlation diagrams were constructed between pollution indicators and geographic environmental factors in the studied river basins.

8. From August to October 2024, expeditionary research was conducted in the basins of small and medium-sized mountain rivers (Sulak, Ulluchay, Sunzha, Karachay and Atachay) in Russia and Azerbaijan. This study collected samples of soil, terrestrial vegetation, water, and bottom sediments along the rivers. Laboratory analyses of soil, terrestrial vegetation, water and bottom sediment samples were conducted to determine the concentration of heavy metals and microelements, as well as soil samples for pH, total nitrogen content, petroleum products, organochlorine pesticides and microflora abundance. An electronic database of laboratory analyses was compiled.

9. The spatial structure and current state of the landscapes of small and medium-sized mountain rivers in the study region were studied. Two landscape classes are widespread in the studied area of the Northeastern and Southeastern Caucasus: 1) flat and foothill-hilly, 2) mountainous. Within the flat and foothill-hilly landscapes, three types are distinguished: flat arid, flat and hilly warm-temperate and moderate semi-arid; foothill-hilly warm-temperate and moderate semi-humid; hydromorphic and subhydromorphic. Within the mountain class of landscapes, the following types are distinguished: mountain moderate humid, mountain moderate

semi-humid, mountain moderate semi-arid, mountain cold-temperate, high-mountain meadow, high-mountain subnival, and glacial-nival. These types fully reflect the structure of altitudinal landscape zonation not only in the aforementioned regions but also on the entire northern macroslope of the Greater Caucasus.

Landscape maps of the landscape types and subtypes of the Northeastern and Southeastern Caucasus, as well as landscape maps of the basins of the small and medium-sized mountain rivers studied, have been compiled. Landscape mapping carried out in river basins will form the basis for further study of the current geoecological state of these basins in the context of dynamic climate change, the impact of exodynamic processes and the intensification of anthropogenic pressure on the mountain and lowland geosystems of the region.

10. As part of the task of developing a concept for modeling the spatiotemporal dynamics of the geoecological state of landscapes in mountain river basins of the Caspian Sea catchment using artificial intelligence (AI) methods, a review of domestic and international literature on the use of AI in geoecology was conducted and a comparative analysis of existing methods was performed. A concept for a new model of the spatial-temporal dynamics of the geoecological state of landscapes in small and medium-sized river basins was developed, aimed at identifying homogeneous regions over large territories. This methodology proposes using an artificial neural network (ANN) trained using a metric learning approach with self-supervised learning in the MoCo (momentum contrast) method to assess the differences between sample objects. This allows for a more statistically reliable and objective calculation of the measure of difference, taking into account the complex interrelations between ecosystem characteristics. To implement zoning, it is proposed to cluster the data collection, consisting of individual landscape elements that completely cover the territory subject to the region identification procedure. This clustering is proposed using a modern neural network approach based on the SPICE method, which allows for the efficient identification of homogeneous areas based on the calculated differences.

Acknowledgment. The work was carried out within the framework of the scientific project "Dynamics of the geoecological state of the mountain river basins of the Northeastern Caucasus, Azerbaijan and Iran in the context of climate change and increasing anthropogenic pressure."

References

1. Gunya A.N., Kerimov I.A., Gayrabekov U.T., Nikiforova A.A., “Landscape and geoecological framework of the Sunzha River basin”. // Sustainable development of mountain territories. 2024. Vol. 16. No. 4. pp. 1450–1459. DOI: 10.21177/1998-4502-2024-16-3-1450-1459.
2. Drygval A.V., Drygval P.V., Gorbunova T.Yu., Kerimov I.A. “Analysis of air temperature and precipitation anomalies within the southern and western coasts of the Caspian Sea in the period 1961–2023”, // Sustainable development of mountain territories. 2024. Vol. 16. No. 3. P. 1054–1070. DOI: 10.21177/1998-4502-2024-16-3-1054-1070.
3. Kerimov I.A., Elzhaev A.S., “Application of geophysical methods in the study of landslide processes”. // Geology and Geophysics of Southern Russia. 2024. Vol. 14 No. 4. P. 66–83. DOI: 10.46698/VNC.2024.77.35.009.
4. Tabunshchik V., Dzhambetova P., Gorbunov R., Gorbunova T., Nikiforova A., Drygval P**.,** Kerimov I., Kiseleva M. “Delineation and Morphometric Characterization of Small- and Medium-Sized Caspian Sea Basin River Catchments Using Remote Sensing and GISs”. // Water 2025, 17(5), 679. https://doi.org/10.3390/w17050679.
5. Tabunshchik V., Nikiforova A., Lineva N., Drygval P., Gorbunov R., Gorbunova T., Kerimov I., Pham C.N., Bratanov N., Kiseleva M. “The Dynamics of Air Pollution in the Southwestern Part of the Caspian Sea Basin (Based on the Analysis of Sentinel-5 Satellite Data Utilizing the Google Earth Engine Cloud-Computing Platform)”. // Atmosphere 2024, 15, 1371. https://doi.org/ 10.3390/atmos15111371.

1st International Scientific Conference "Modern problems in Geophysics", Proceedings,
ISBN 978-9941-36-434-1, ISSN 3088-4349, Tbilisi, Georgia, November 6-8, 2025

LANDSCAPE DIFFERENTIATION TERRITORIES OF THE SUNZHA RIVER BASIN

*,***Gunya A.N., **,***Gayrabekov U.T., ***Gelagaev A.Sh., **, ***Muzaev I.Kh.

*Institute of Geography of the Russian Academy of Sciences, Moscow, Russia
**Academy of Sciences of the Chechen Republic, Grozny, Russia
***M.D. Millionshchikov Grozny State Oil Technical University, Grozny, Russia
zsh_gagaeva@mail.ru

Abstract. *The landscape differentiation of the territory of the Sunzha River basin was carried out on the basis of landscape mapping and geoinformation analysis using data from the geological structure and vegetation cover. Classes, subclasses, types, subtypes, and groups of landscapes are highlighted. The landscapes of the mountainous and foothill parts of the Sunzha River basin differ sharply from each other, which is associated with the high-altitude zonation characteristic of the basin and long-term anthropogenic activity, which increases the stress on natural complexes.*

Key Words: *landscape mapping, anthropogenic activities, high-altitude zones.*

The basin of the Sunzha River with an area of about 12,000 km2 is located on the territory of four subjects of the Russian Federation (North Ossetia-Alania, Ingushetia, the Chechen Republic and Dagestan) and part of the adjacent territory of Georgia, in the highlands [8] This work continues the detailing of mesoscale landscape mapping, which was started earlier [1, 2, 5]. When writing the article, we used field materials and data obtained during the North Caucasian landscape expeditions (2014-2020) [6, 7], as well as the results of studying individual components and, first of all, vegetation cover in key areas [3, 4].

Landscape mapping and geoinformation analysis using data from the geological structure and vegetation cover made it possible to carry out landscape differentiation of the study area with the allocation of classes, subclasses, types, subtypes, and groups of landscapes. The division into classes corresponds to the accepted approach in landscape science of dividing mountains and plains into two large classes. There are only mountain landscapes in the study area. The foothill-plain hydromorphic complexes should be considered transitional from mountainous to lowland (Fig. 1, Table 1). In the case of landscape groups, their generalized regional variants are identified, taking into account major differences in relief and geological structure. In general, the landscape structure was formed at the intersection of two main factors of landscape differentiation.

The tectonic features and geological diversity of the region have led to the formation of various altitudinal zones in the Sunzha River basin, characterized, from south to north, by the following landscape subclasses: high-mountain, mid-mountain, low-mountain, foothill, and foothill-plain. High-mountain landscapes encompass the upper tiers of the Bokovoy and Main, or Watershed, Ranges, at elevations above 2,500 m. Slope processes are highly active here, and small areas of glaciation exist in the upper reaches of the Argun. Mid-mountain landscapes occupy the altitude range from 1,000 to 2,500 m. An important feature of the mid-mountain relief is the presence of widened valley sections in the Jurassic Depression. In these areas, the climate is relatively dry due to the formation of a rain shadow and the development of foehn processes. Low-mountain areas (up to 1,000 m), on the other hand, receive the bulk of the precipitation. Already in the foothills, characterized by a relatively monotonous flat topography, precipitation drops sharply. Hydromorphic conditions are observed in the floodplain-terrace complexes of the Sunzha River in its lower reaches, and particularly near its confluence with the Terek River.

Altitudinal and zonal differences in the ratio of heat and moisture underlie the formation of landscape types and subtypes-altitude zones and belts (subzones). The highest absolute elevations of the high-mountain subclass are occupied by nival-glacial landscapes from 3,000 to 3,500 m above sea level, represented by the rock-snow and glacial subtypes.

Mid-mountain (mountain-forest and mountain-steppe) landscapes developed primarily at elevations of up to 1800-2000 m and rise to 2400-2500 m on southern-facing slopes. Mountain-forest landscapes are further subdivided into small-leaved (combined with coniferous-small-leaved) and cultivated forest-meadow landscapes, while mountain-steppe landscapes are divided into shrub- and meadow-steppe landscapes with cultivated modifications. Mid-mountain forests predominantly occupy steep slopes and poorly accessible areas, while gentle slopes and relatively accessible areas are characterized by forest-meadow landscapes, a variant of anthropogenic modification formed as a result of long-term grazing.

Table 1. Landscape organization of the Sunzha basin

Subclasses of landscapes (high-altitude tiers)	Types of landscapes/zones (altitude-zonal ratio of heat and moisture)	Subtypes of landscapes /subzones/belts (Variations in the ratio of heat and moisture within the altitude zone)	Generalized groups of landscapes			
			Slopes composed of Jurassic sediments	Slopes composed of chalk deposits.	Slopes and foothill plains, less often, river terraces composed of Paleogene-Neogene sediments.	Slopes, intermountain depressions, and river floodplain-terrace complexes composed of Quaternary sediments
High mountain	Nival-glacial	Rock-snow and glacial	1			
	Mountain meadows	Subnival-alpine	2			
		Subalpine steppe	3			
Mid-mountain	Mountain forest	Small-leaved and coniferous-small-leaved	4			
		Forest meadow modifications	5			
	Mountain-steppe	Shrubs	6			
		Meadow-steppe cultivated modifications	7			
Lowland	Mountain forest	Broadleaf		8		
		Small-wheeled			9	
		forest-meadow-steppe cultivated modifications			10	
	Mountain forest-steppe	Cultivated modifications			11	
Foothill	Forest-steppe	Cultivated modifications			12	
		Forest modified			13	
	Steppe	Cultivated modifications				14
Foothill-plain	Hydromorphic	Floodplain-terrace modified				15
		Bayrachny				16

Within the lowlands, two types and three subtypes of landscapes are distinguished. Mountain-forest broadleaf landscapes are confined to the northern macroslope, forming a large area of forested Black Mountains. Within the Black Mountains, mountain-forest-meadow-steppe cultivated landscapes have developed on flattened areas and slopes of southern mesoexposures. Mountain-forest-steppe landscapes have developed on the slopes of the Front Ranges.

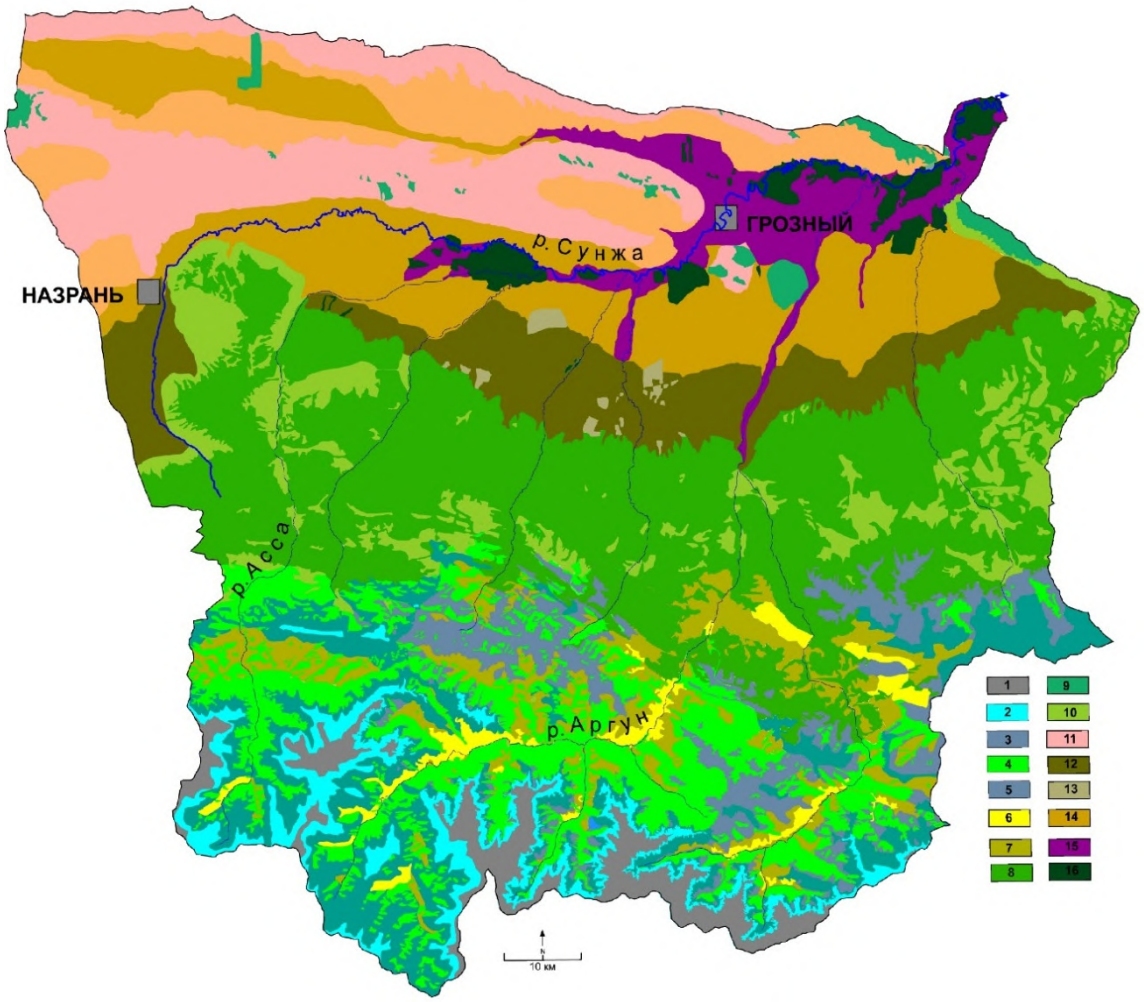

Fig. 1. Landscape structure of the Sunzha River basin.
The numbers show generalized groups of landscapes (see Table 1).

The foothill subclass includes forest-steppe and steppe landscapes, which dominate the Chechen Plain and have been largely cultivated by long-term human activity. Forested areas remain only fragmentarily, providing a glimpse into the forests that once existed here. In the foothill-plain subclass, transitional between mountains and plains, hydromorphic landscapes have developed on low terraces and in the Terek River floodplain, consisting of a complex of ravine forests with alternating meadow and wetland areas.

An analysis of the conducted studies reveals that landscape types do not always change in a strict sequence with elevation. This is due to the uneven distribution of heat and moisture ratios in the mesoclimate of the terrain. Furthermore, the rock types that compose them play a significant role in landscape differentiation. The combination of altitudinal climatic, vegetation, and geological-geomorphological conditions, coupled with anthropogenic activity, has led to the formation of 16 main landscape groups.

High-mountain nival-glacial rock-snow and glacial landscapes (1).
High-mountain mountain-meadow (subnival-alpine) landscapes (2).
High-mountain mountain-meadow (subalpine), locally steppe-like landscapes (3).
Mid-mountain mountain-forest landscapes with small-leaved and coniferous-small-leaved vegetation (4).
Mid-mountain forest-meadow landscapes (5).
Mid-mountain mountain-steppe shrub landscapes (6).
Mid-mountain mountain-steppe landscapes of cultivated meadow-steppe modification (7).
Low-mountain mountain-forest (with broad-leaved and mixed forests) landscapes (8).
Low-mountain mountain-forest (small-leaved) landscapes (9).
Low-mountain forest-meadow-steppe (residential and cultivated) landscapes (10).
Low-mountain forest-steppe landscapes of the Terek-Sunzha Upland (11).
Cultivated foothill-forest-steppe landscapes (12).

In some elevated areas of the Chechen Plain, forest patches have been preserved within the foothill-forest-steppe landscapes (13).

Cultivated foothill steppe landscapes with residential and industrial areas (14).

Foothill plain hydromorphic floodplain landscapes (15 and 16) are represented by ravine forests of floodplain terraces (16) and floodplain residential landscapes used for croplands and pastures (15).

Thus, the landscape differentiation of the river basin territory. The Sunzha basin is characterized by altitudinal-zonal and aspectual contrasts, as well as by the asymmetry of its basin structure, with the Sunzha's right tributaries predominating on the northern-facing slope. Eight altitudinal-zonal landscape types, one azonal landscape type, and sixteen main landscape groups are distinguished here.

Acknowledgments. The research was conducted within the framework of the scientific project "Dynamics of the geoecological state of the mountain river basins of the North-East Caucasus, Azerbaijan, and Iran in the context of climate change and growing anthropogenic load" supported by the Ministry of Education and Science of the Russian Federation.

References

1. Gunya A.N., Kerimov I.A., Gayrabekov U.T., Nikiforova A.A., "Landscape and geoecological framework of the Sunzha River basin". // Sustainable development of mountain territories. 2024. Vol. 16. N4. Pp. 1450-1459.
2. Gunya A.N., Kolbovsky E.Yu., Gayrabekov U.T., "Cartographic and geoinformation support for sustainable development of mountain regions". // InterCarto. InterGIS. Geoinformation support for sustainable development of territories: proceedings of the International Conference. 2019. Vol. 25. Pp. 47-65.
3. Dudagova E.Sh., Astamirova M.A.M., Taisumov M.A., Baibatyrova E.R., "Analysis of distribution of flora species by altitudinal zones of the Argun River basin". // Sustainable development of mountain territories. 2024. Vol. 16. N2 (60). P. 630-641.
4. Dudagova E.Sh., Taisumov M.A., Astamirova M.A.M., Baibatyrova E.R. "Ecological and cenotic structure of the flora of the Argun River basin", Sustainable development of mountain territories. 2024. Vol. 16. N4 (62). P. 1783-1793.
5. Purekhovsky A.Z., Gunya A.N., Kolbovsky E.Yu., "Dynamics of high-mountain landscapes of the North Caucasus according to remote sensing data in 2000-2020". // Bulletin of DSPU. Natural and exact sciences. 2022. Vol. 16. N2. P. 72-84.
6. North Caucasian Complex Expedition. Collection of Works. Issue 1 / Edited by A.N. Gunya. Grozny: ChSU. 2019. p. 156.
7. North Caucasian Complex Expedition. Collection of Works. Issue 2. Edited by A.N. Gunya, M.N. Petrushina. Grozny: ChSU. 2021. p. 166.
8. Petrushina M. N., Gunya A. N., "Semiarid Intermontane Basins of the North Caucasus: Landscapes and Land Use Transformations". // Arid Ecosystems, 2021, Vol. 11, N4, P. 343-350.

1st International Scientific Conference "Modern problems in Geophysics", Proceedings,
ISBN 978-9941-36-434-1, ISSN 3088-4349, Tbilisi, Georgia, November 6-8, 2025

CHANGES IN THE RIVER FLOW OF WESTERN GEORGIA IN THE CONTEXT OF GLOBAL CLIMATE WARMING

*** Basilashvili Ts. Z., ** Janelidze M.G., ** Basilashvili Kh. G.**

** Institute of Hydrometeorology at the Georgian Technical University,*
*** Caucasus University*
jarjinio@mail.ru

Abstract. *An analysis of long-term stationary observation data revealed that, by decade, the annual discharge of rivers in western Georgia exhibited only minor fluctuations up to 1980. Over the following two decades (1981–2000), discharge increased, particularly in glacier-fed rivers. Looking ahead, changes in air temperature and atmospheric precipitation are expected to cause a decline in river discharge, primarily due to glacier retreat. Along the coastal zone, increased evaporation will condense into torrential rains, heightening the risk of hazardous events. Further east, rising temperatures and decreasing precipitation will reduce river discharge. These findings should be taken into account in the design of various facilities, as well as in planning measures for conserving and replenishing water resources. In the coastal zone, preventive actions must be developed to mitigate the negative impacts of hazardous events.*

Key words: *formative factors, glacial waters, mean annual discharge*

Water is a natural resource of paramount importance for sustaining human, animal, and plant life, as well as for national economic development, since no sector of the economy can function without it. The water resources within Georgia's territory constitute a national asset protected by the state, which entails the rational use of all water bodies – seas, lakes, rivers, groundwater, springs, glaciers, and others – prioritizing the population's need for clean, fresh drinking water.

Unlike other water bodies, rivers provide a constant, renewable supply accessible to all. Consequently, settlements of all sizes have historically developed along riverbanks. River water is used for municipal and industrial supply, electricity generation, and crop irrigation.

In terms of hydropower potential per square kilometer, Georgia ranks among the world's leading countries. The Enguri, Rioni, Tskhenistskali, and Kodori rivers, among others, are distinguished by their high energy capacity. At present, about 60 hydroelectric power plants operate in Georgia, producing a total of 10 billion kWh annually. In total, the country could operate up to 300 medium and small hydroelectric plants, with a potential output of 40 billion kWh [1].

Given the exceptional importance of river water resources, accurate measurement and study of river discharge are essential for the efficient use of water resources and the reliable operation of hydraulic structures.

Ongoing global climate warming is transforming river runoff and altering its intra-annual distribution. In winter, when temperatures remain above freezing, precipitation falls as rain rather than snow, leading to higher river discharge instead of low-flow conditions. This change can improve water use conditions. However, increased discharge also poses environmental challenges: in summer, elevated temperatures accelerate evaporation, and the resulting condensation often manifests as torrential rain, triggering major floods, flash floods, and landslides, thereby increasing the risk of severe adverse impacts.

In recent decades, in addition to climate warming, human economic activities have had a significant impact on changes in river discharge, disrupting the natural conditions of river basins. In this regard, the effect on forest cover is noteworthy: logging alters the forest's regulatory capacity. Due to the high infiltration capacity of forest soils, the runoff volume during high-flow periods decreases, while that during low-flow periods increases. The greater the forest cover in a river basin, the more regulated the river discharge. In western Georgia, the degree of forest cover in river basins varies considerably, ranging from 95% to 40%. The forest cover of individual river basins, along with other hydrographic and hypsometric characteristics, is provided in [2].

Modern climate warming exerts a particularly strong influence on glaciers located in the headwaters of rivers along the Caucasus Range. According to the existing [3] catalog, glaciers with a total area of 466 km² were recorded within the basins of six rivers in western Georgia. In [4], the distribution of these glaciers was studied for three time periods based on satellite remote sensing data (Table 1), revealing that, by 2020, the total glacier area in the river basins had decreased by 191 km², or 41%. The greatest reduction (37%) occurred in the glaciers of the Enguri River basin.

Table 1. Glacier Areas (sq. km) in the River Basins of Western Georgia

River / Periods	Bzipi	Kelasuri	Kodori	Enguri	Khobi	Rioni	Total
Catalog, 1975	8,0	1,2	64,3	321	0,2	70,7	466
2010	4,7	0,9	50,0	229	0,2	57,2	384
2015	3,1	0,7	41,7	227	0,1	45,8	319
2020	1,7	0,6	33,3	197	0,1	41,2	275

Thus, as a result of both climate warming and anthropogenic impacts, the natural conditions previously existing in river basins have changed, and, accordingly, so has river discharge. To study this change, stationary observation data on rivers, published in reference works up to 1981 [5–8], were analyzed. It should be noted that, after 1981, observation data on river discharge in Georgia were no longer published, and until recent years, obtaining such data was prohibitively expensive for financially constrained researchers, making it impossible to conduct appropriate studies. This situation changed with the adoption of the *Law of Georgia on Water* [9], which made it possible to access observation data for 10 active gauging stations [10].

For the purposes of the study, an additional 11 previously operational stations with long-term observation records were selected. To reconstruct missing observation periods, analogous rivers were identified through correlation analysis of concurrent observation data. In cases of strong correlations, missing data were restored through graphical interpolation. As a result, a database was compiled containing annual mean discharge records for 21 gauging stations, covering 56–86 years. Using appropriate software [11], statistical analysis yielded long-term mean annual discharge values, as well as mean values for individual decades (Table 2).

The analysis shows that, for rivers fed in part by glacial waters, changes in discharge prior to 1980 were not characterized by significant fluctuations. Thereafter, over the next two decades, a marked increase in discharge occurred, associated with active glacier melting. Since 2000, the absence of observation data on rivers has prevented comparison of river discharge trends with the glacier changes presented in Table 1.

In [12], Georgian specialists used the international RCP4.5 scenario to prepare forecasts indicating that, in western Georgia, the mean annual temperature in 2041–2070 will rise by 1.8°C to 3.0°C compared to 1971–2000, and in 2071–2100 will increase by an additional 0.4°C to 1.7°C.

Atmospheric precipitation is projected to decrease during both forecast periods. The highest precipitation totals (> 2,800 mm) will occur along the Black Sea coastal zone of Adjara; to the east of this zone, annual precipitation decreases with increasing elevation above sea level. In 2041–2070, the most significant decrease in precipitation is expected in Imereti (18% in Sachkhere). In other regions, the reduction will range between 3.6% and 15%. An increase in precipitation of 8–10% is projected only for Poti and Zugdidi. During 1971–2000, the highest precipitation was recorded in Batumi (2,481 mm); in 2041–2070, it is projected to be 2,363 mm, and in 2070–2100, 2,322 mm.

Against the background of global climate warming, under such forecasts for the main formative factors of river discharge, rising temperatures are expected to reduce and ultimately eliminate glaciers in river headwaters, which will significantly diminish summer river flow. This will have a highly negative impact on power generation at hydropower plants (HPPs) located along these rivers. In this regard, the Enguri River is of particular concern, as it hosts the Enguri HPP – the largest-capacity plant in Georgia and the entire South Caucasus, with a high-arch dam. A risk of reduced water resources is also anticipated for the Rioni River and its tributaries, where both operational and planned HPPs are located.

Table 2. Multiannual and Decadal River Mean Discharges (m^3/s) in Western Georgia

River Point	Number of Years	Multi-Year Aver	1921-1930	1931-1940	1941-1950	1951-1960	1961-1970	1971-1980	1981-1990	1991-2000	2011-2020
Bzipi – Jirkva	60	97,6	—	96,9	103	96,4	95,6	93,2	108	—	—
Kodori – Lata	60	92,2	—	89,6	83,4	91,8	83,4	101	104	—	—
Enguri – Khaishi	86	122	121	111	108	119	109	118	142	131	—
Rioni – Alpana	86	104	105	102	103	94,7	99,5	97,9	107	110	—
Rioni – Namokhvani	86	147	149	133	144	128	143	149	164	159	—
Rioni – Chala-didi	86	429	410	413	388	418	408	403	475	495	—
Kvirila – Sachkhere	84	16,7	—	16,9	17,0	16,1	16,9	18,4	18,5	14,2	16,0
Kvirila – Zestaponi	84	60,0	—	65,9	62,3	58,0	58,5	54,9	66,4	68,8	53,1
Dzirula – Tse-va	84	23,1	—	28,3	28,0	26,5	20,8	27,3	26,4	21,4	23,2
Khanistsqali-Bagdati	61	15,7	—	—	15,2	17,5	14,7	14,1	18,0	14,0	—
Tskhenistsq. Luji	65	23,8	—	22,5	23,5	22,8	20,8	24,8	27,7	23,6	—
Tskhenistsq. Rtskhmeluri	65	67,0	—	67,3	61,0	63,0	60,9	65,8	75,0	68,6	—
Tskhenistsq. Khidi	65	56,9	—	87,1	76,3	72,1	38,4	38,8	48,3	39,9	—
Tekhuri – Na-kalakevi	67	33,7	—	36,1	27,6	30,1	33,5	36,5	38,7	36,6	—
Supsa – Cho-khatauri	60	13,7	—	—	15,0	12,9	12,6	13,8	14,2	13,5	—
Supsa – Khidmagala	60	48,7	—	—	44,0	47,5	45,3	46,7	56,0	48,0	—
Natanebi – Natanebi	59	25,0	—	27,2	21,7	25,8	23,7	23,4	28,6	—	—
Kintrishi – Kokhi	59	13,1	—	14,5	13,2	11,4	11,5	13,8	14,5	—	—
Chorokhi – Erge	61	274	—	304	290	255	253	269	274	—	—
Acharistsqali Khulo	56	8,06	—	—	8,20	8,50	8,50	—	9,60	—	—
Acharistsqali Keda	56	46,3	—	—	44,4	44,3	44,3	42,6	53,9	—	—

For rivers not fed by glacial waters, the decade 1981–1990 was characterized by high discharge, as this period experienced high precipitation across the entire territory. According to the compiled forecasts, however, a decline in precipitation – and correspondingly in river discharge – is expected, especially in the Qvirila River basin. In coastal areas, increased evaporation will result in greater condensation in the form of torrential rains, thereby contributing to the occurrence of hazardous events in the coastal zone, which will also be facilitated by the rising level of the world ocean.

All of the above factors must be considered in the design of projects aimed at the utilization of river water – particularly for energy production – as well as in planning measures for the conservation and replenishment of water resources. In addition, preventive measures must be implemented in coastal zones to mitigate or avert the negative consequences of hazardous events.

References

1. Svanidze G.G., Gagua V.P., Sukhishvili E.V., Renewable Energy Resources of Georgia. GIMIZ, Leningrad, 1987, 175 p.
2. Basilashvili Ts., Updated maximum flood discharges for hydrological calculations of the rivers in Western Georgia. International Scientific Conference "Complex Geophysical Monitoring in Georgia: History, Modern Problems, Promoting Sustainable Development of the Country", Tbilisi, Georgia, October 17-19, 2024, pp. 64-68. http://dspace.gela.org.ge/handle/123456789/254
3. Catalog of Glaciers of USSR, Vol. 9, Issue 3, Part 1, GIMIZ, Leningrad, 1975, 86 p.
4. Shengelia L., Kordzakhia G., Tvauri G., Guliashvili G., Beridze S., The Study of the Degradation of the Glacial Basin of Western Georgia against the background of ongoing climate change using satellite remote sensing data. Transactions IHM, GTU, Vol. 135, 2024, pp 64-68. doi.org/10.36073/1512-0902-2024-135-64-68.
5. Fundamental Characteristis of Hydrology. Vol. 9, Issued 1, GIMIZ, Leningrad, 1967, 460 p.
6. Fundamental Characteristis of Hydrology. Vol. 9, Issued 1, GIMIZ, Leningrad, 1977, 358 p.
7. Fundamental Characteristis of Hydrology. Vol. 9, Issued 1, GIMIZ, Leningrad, 1978, 300 p.
8. State Water Cadastre, Vol. VI, Georgian SSR, GIMIZ, Leningrad, 1987, 416 p.
9. Georgian Laws of the Water, № 936, 20/07/2018.
10. Department of Hydrometeorology of National Environmental Agency. Tbilisi, 2024
11. Basilashvili Ts., Statistical Analysis of Variables and Selection of Predictors for Prognostic Relationships. Annotated Index of Algorithms and Programms. World Data Center. Obninsk, 1977, p. 43
12. Kartvelishvili L., Tatishvili M., Amiranashvili A. Megrelidze L., Kutaladze N.m Weather, Climate and their Change Regularities for the Conditions of Georgia. // "Universal", Tbilisi, 2023, p. 405

1st International Scientific Conference "Modern problems in Geophysics", Proceedings,
ISBN 978-9941-36-434-1, ISSN 3088-4349, Tbilisi, Georgia, November 6-8, 2025

ASSESSMENT OF ^{222RN} DISTRIBUTION IN WATER AND SOIL GAS IN THE SHIDA KARTLI REGION, GEORGIA

[*]Kapanadze N., [*]Melikadze G., [*]Tchankvetadze A., [*]Jimsheladze T., [**]Gogichaishvili Sh., [*]Todadze M., [*]Chikviladze E., [*]Magradze Z., [**]Chelidze L.

[*]M. Nodia Institute of Geophysics of the I. Javakhishvili Tbilisi State University, Georgia,
[**]E. Andronikashvili Institute of Physics, Ivane Javakhishvili Tbilisi State University, Tbilisi, Georgia
ninokapanadze@gmail.com

Abstract. *Within the framework of the SRNSFG FN-19-22022 project "222Rn Mapping and Radon Risk Assessment in Georgia," fieldwork was carried out to quantify ^{222}Rn distribution in water and soil gas and to identify geological factors influencing ^{222}Rn concentrations in selected areas of Georgia. In Shida Kartli region, on-site ^{222}Rn measurements were performed at 78 soil gas sampling points and 90 water sources (63 springs, 27 boreholes) using the AlphaGUARD PQ2000 PRO (Saphymo GmbH) radon monitor. Measured ^{222}Rn concentrations ranged from 0.08 to 51.76 Bq/L in water and up to 46.6 kBq·m^{-3} in soil gas. Basic statistical analysis and visualization revealed that most water and soil gas values fall in the low to moderate range, with occasional localized high values. All observation sites were georeferenced using GPS. The data were digitized and integrated into a GIS to illustrate ^{222}Rn distribution in water and soil gas across Shida Kartli.*

The works [8-11] present the results of our early studies of ^{222}Rn content in soil gas and water in various regions of the country.

Key words: *radon mapping, soil gas, groundwater, GIS, Shida Kartli, Georgia*

Introduction

Radon (^{222}Rn) is a naturally occurring radioactive gas produced by the decay of uranium (^{238}U) in soils and rocks. Its presence in groundwater and soil gas poses environmental and public health concerns, particularly in areas with elevated uranium or thorium content. Mapping ^{222}Rn concentrations in both water and soil gas provides a basis for understanding local geological influences, hydrogeological pathways, and potential exposure risks.

Shida Kartli, located in central Georgia, features a complex geological setting comprising sedimentary, volcanic, and carbonate formations. Previous studies indicate that radon concentrations in both water and soil gas can vary significantly depending on lithology, structural features, and groundwater flow characteristics. However, comprehensive regional datasets integrating both media have been lacking, motivating the present study.

Geological and lithological data of the study area

Shida Kartli is characterized by a diverse geology, including Mesozoic and Cenozoic sedimentary sequences, volcanic deposits, and carbonate formations. Major lithologies include clay, siltstone, sand, limestone, and basaltic volcanics [1]. Structural features such as faults and fractures enhance groundwater circulation and can serve as preferential pathways for radon migration. This geological heterogeneity underlies the variability in measured ^{222}Rn concentrations across the region [2].

Measurement Methodology

Water

^{222}Rn in water sources was monitored at 90 points, including 63 springs and 27 boreholes, using the AlphaGUARD monitor and the AquaKIT [3-4] consisting of the AlphaGUARD monitor, degassing vessel, se-

curity vessel, and AlphaPUMP [5] (Fig. 1a). The components were connected in a closed circuit, and ^{222}Rn concentration was measured according to the manufacturer's protocol [4]. ^{222}Rn concentrations were calculated using established equations accounting for air-water partitioning and decay corrections.

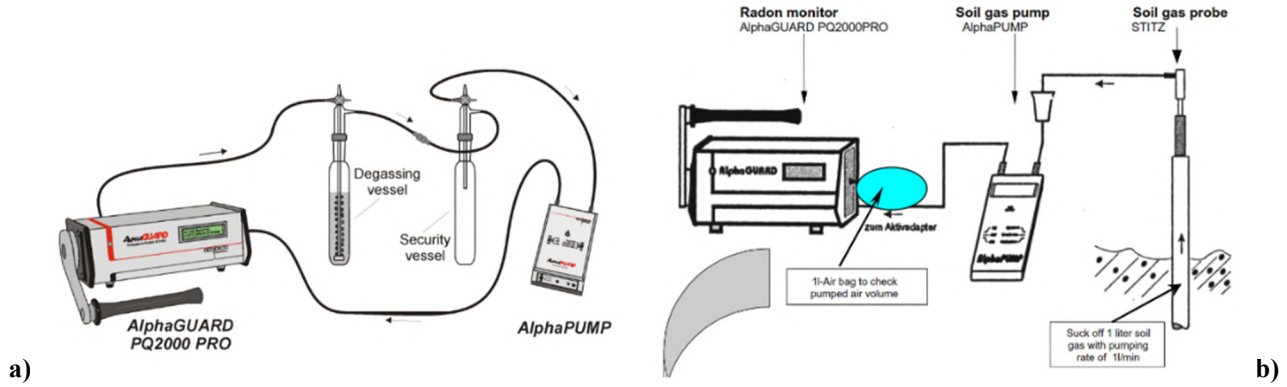

Fig. 1. Schematic views of AquaKIT, a) and soil gas, b) measurement set-ups

Soil Gas

^{222}Rn concentrations in soil gas were measured at 78 sampling points in the vicinity of water sources and additional locations to achieve dense spatial coverage. Measurements were conducted using the AlphaGUARD monitor coupled with a soil gas probe and the AlphaPUMP in a closed circuit, following the standard procedure [6] (Fig. 1b). The probe was inserted to a depth of 0.7–1.0 m, and radon concentrations were recorded after a 10-minute waiting period to allow for thoron decay. The mean values indicated on the monitor were taken as the final concentrations.

All observation sites were georeferenced, and results were analyzed to examine spatial patterns in relation to lithology and hydrogeology.

Data Calculation and Results

A total of 168 observation sites in the Shida Kartli region were georeferenced using GPS.

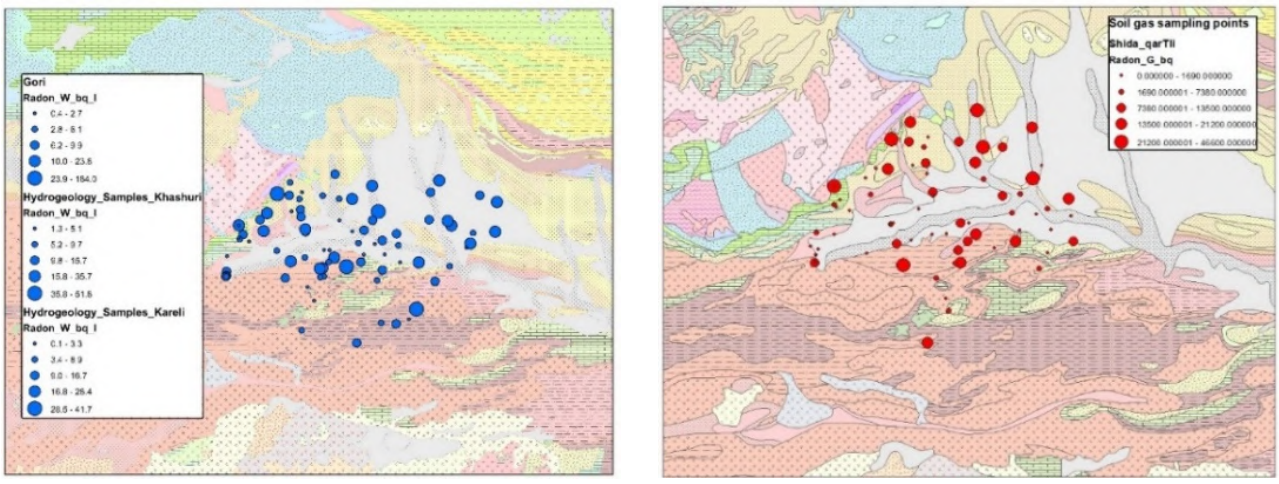

Fig. 2. Location of water and soil gas sampling points on the geological map [7]

Radon in Water

The ^{222}Rn activity concentration in the water samples was calculated using equation (1), accounting for radon transferred from water to air within the measurement setup and the fraction remaining in the aqueous phase [4]. Measurements were generally performed immediately after sampling; in cases of delayed measurement, decay correction was applied according to equation (2).

The ^{222}Rn activity in water was calculated using:

$$c_{Water} = \frac{c_{Air} \times \left(\frac{V_{System} - V_{Sample}}{V_{Sample}} + k\right) - c_0}{1000} \quad (1)$$

Where: c_Water – ^{222}Rn concentration in water sample [Bq/L], c_Air – ^{222}Rn concentration [Bq/m3] in the air of the circuit, c_0 – ^{222}Rn concentration before sampling (zero level) [Bq/m3], V_System – interior volume of the circuit [in our case 1.102 L], V_Sample – volume of the water sample [in our case 0.1 L], k – ^{222}Rn distribution coefficient [0.26, since the measurements were performed in the temperature range 10-30 ℃].

If there was a delay between sampling and measurement, decay correction was applied:

$$C_0 = C \times e^{\frac{ln2}{t_{1/2}} \Delta t} \quad (2)$$

Where C_0 is the value at the moment of sampling, C is the measured value, $t_{1/2}$ is the half-life of ^{222}Rn, Δand t is the time delay between sampling and measurement.

Basic statistical analysis for the sampled water points is presented in Table 1. Arithmetic mean (AM) ^{222}Rn concentrations were higher in springs (12.79 Bq/L) than in boreholes (9.05 Bq/L). Concentrations ranged from 1.24 to 51.76 Bq/L in springs and from 0.08 to 25.62 Bq/L in wells. These values are consistent with ranges obtained in previous studies in Georgia [8-11].

Table 1. Basic statistical analysis for the sampled water points

		^{222}Rn concentration / Bq/L						
Type	No. points	Min	Max	Median	AM	ASD	GM	GSD
Spring	63	1.24	51.76	9.97	12.79	10.47	9.62	2.19
Borehole	27	0.08	25.62	5.38	9.05	8.50	4.39	4.75

Most measured ^{222}Rn concentrations in water are in the low to moderate range, with the majority of springs and wells exhibiting values below 15 Bq/L. Approximately half of the springs show concentrations between 1 and 6 Bq/L, while about 30% fall in the 6–15 Bq/L range. A few points exhibit elevated values, with one spring reaching 51.76 Bq/L and one well at 25.62 Bq/L. The cumulative frequency distribution approximates a log-normal pattern, with a long tail caused by these high values. One of the main factors contributing to this variation is the presence of locally elevated radon, likely controlled by specific lithological features and uranium/thorium-bearing formations along groundwater flow paths. Although the dataset is limited for detailed statistical analysis, it provides valuable insights into the spatial distribution of ^{222}Rn and the underlying hydrogeological processes in the Shida Kartli region, highlighting areas where localized geological or hydrogeological conditions can lead to elevated radon concentrations in certain springs and wells.

Radon in Soil Gas

Measured soil gas ^{222}Rn concentrations ranged from 0 to 47 kBq·m^{-3}, with an arithmetic mean (AM) of 9 kBq·m^{-3} and a geometric mean (GM) of 5 kBq·m^{-3}. The standard deviation (ASD) is 8 kBq·m^{-3}, with a geometric standard deviation (GSD) of 3.5 and a log-standard deviation of 0.5. The median value is 7 kBq·m^{-3}. These values show substantial spatial variability, reflecting heterogeneity in lithology, soil properties, and shallow hydrogeological conditions. Although localized anomalies were observed, the dataset provides a reliable overview of ^{222}Rn distribution in the shallow subsurface. This information is critical for identifying radon-prone areas and supports integration with GIS-based spatial analysis of radon risk in Shida Kartli.

Table 2. Basic statistics of ^{222}Rn concentration in soil gas in volcanic rocks, Shida Kartli

	^{222}Rn concentration / kBq m^{-3}						
No	Min	Max	Median	AM	ASD	GM	GSD
78	0.09	46.60	7.40	8.79	8.43	5.12	3.49

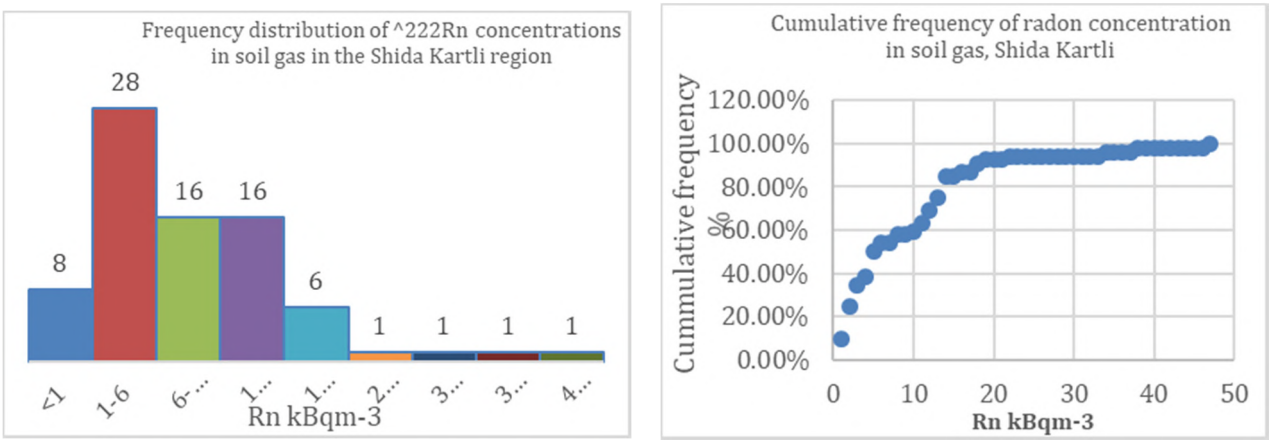

a. **b.**

Fig. 3. a) Frequency distribution of ^{222}Rn concentrations in soil gas in the Shida Kartli region; b) cumulative frequency in percent.

Most measured soil gas ^{222}Rn concentrations (28 values) fall within the 1–6 kBq·m^{-3} range, while a single measurement is observed in the 21–51 kBq·m^{-3} range, representing a localized anomaly. The cumulative frequency distribution closely follows a log-normal pattern, with a minor deviation observed in the 9–13 kBq·m^{-3} range. This distribution indicates that, although most sites exhibit low to moderate radon levels, occasional high values reflect local heterogeneities in subsurface radon sources and migration pathways.

Conclusion

This study provides the first integrated assessment of ^{222}Rn concentrations in water and soil gas in Shida Kartli, Georgia. Water measurements revealed generally low to moderate radon levels, with isolated high values in some springs (up to 51.76 Bq/L) and wells (up to 25.62 Bq/L). Soil gas measurements showed a wider range (0–47 kBq·m^{-3}), reflecting local variations in lithology, soil properties, and shallow hydrogeological pathways.

Although most concentrations are below guideline limits, localized anomalies highlight areas where radon migration is enhanced by geological or hydrogeological features. These findings provide valuable insight into radon distribution, supporting targeted monitoring and risk management strategies in the region.

Acknowledgements. The paper is a part of the research done within the SRNSFG FN-19-22022 project "^{222}Rn mapping and ^{222}Rn risk assessment in Georgia". As recipients of the Research State Grant, the authors thank the Shota Rustaveli National Science Foundation of Georgia.

References

1. Adamia S., Akhvlediani K. T., Kilasonia V. M., M. Nairn A. E., Papava D., Patton D. K., GEOLOGY OF THE REPUBLIC OF GEORGIA: A REVIEW. // International Geology Review, 34(5), 1992, pp. 447–476. https://doi.org/10.1080/00206819209465614
2. Evans J.P., Forster C.B., Goddard J.V., Permeability of fault-related rocks, and implications for hydraulic structure of fault zones. // Journal of Structural Geology, 19, 1997, pp. 1393–1404.
3. AlphaGUARD PQ2000 PRO Portable Radon Monitor, Saphymo GmbH, Frankfurt / Main – Germany; User Manual 08/2012
4. AlphaKIT Accessory for Radon in water measurement in combination with the Radon monitor AlphaGUARD. User Manual, Genitron Instruments, Frankfurt/Main, Germany, 09, 1997.
5. AlphaPUMP, Technical Description, User manual, Genitron Instruments Germany, 2001.
6. AlphaGUARD Soil Gas Measurements. Short instructions for the use of the Soil Gas Probe in combination with the Radon monitor, User Manual, Genitron Instruments, Frankfurt/Main, Germany, 2001.
7. Gudjabidze G.E., Gamkrelidze I.P. Geological map of Georgia, 2003, 1: 500 000.
8. Kapanadze N., Melikadze G., Vaupotič J., Tchankvetadze A., Todadze M., Jimsheladze T., Chikviladze E., Gogichaishvili Sh., Chelidze L., Radon-222 concentration levels in soil and water in different regions of Georgia – Radon mapping, // RAD Conf. Proc., vol. 6, 2022, pp. 60–64.

9. Kapanadze N., Melikadze G., Tchankvetadze A., Todadze M., Jimsheladze T., Gogichaishvili Sh., Chikviladze E., Chelidze L., Vaupotič J., Radon in soil gas in crystalline shales and volcanic grounds in selected regions of Georgia // 16th International workshop GARM – Geological aspects of Radon risk mapping; September 19th – 21st, 2023, Prague, Czech Republic.
10. Vaupotič J., Bezek M., Kapanadze N., Melikadze G., Makharadze T., Machaidze Z., Todadze M. Radon and thoron measurements in West Georgia, Journal of Georgian Geophysical Society. // Physics of Solid Earth, Issue (A), 15a, 2011–2012, pp. 128–137.
11. Amiranashvili A., Chelidze T., Melikadze G., Trekov I., Todadze M., Chankvetadze A., Chelidze L., Preliminary results of the analysis of Radon content in the soil and water in different regions of west Georgia. // Institute of Geophysics, ISSN 1512-1135, vol. 60, Tbilisi, 2008c, pp. 213–218 (in Russian).

1st International Scientific Conference "Modern problems in Geophysics", Proceedings,
ISBN 978-9941-36-434-1, ISSN 3088-4349, Tbilisi, Georgia, November 6-8, 2025

APPLICATION OF HYDROGEOCHEMICAL DIAGRAMS AND GEOTHERMOMETRY TO CHARACTERIZE THE SAMTSKHE-JAVAKHETI GEOTHERMAL SYSTEM, GEORGIA

[*]Kapanadze N., [*]Melikadze G., [*]Tsutskiridze E., [*]Tchankvetadze A., [*]Jimsheladze T., [*]Todadze M., [*]Chikviladze E.

[*]M. Nodia Institute of Geophysics of the I. Javakhishvili Tbilisi State University, Georgia, ninokapanadze@gmail.com

Abstract. *The Samtskhe–Javakheti region of southern Georgia hosts significant geothermal resources associated with volcanic and tectonic activity. This study applies a combined hydrogeochemical and geothermometric approach to characterize the chemical evolution and thermal regime of thermal waters in the area. Major cation and anion analyses were interpreted using Piper, Durov, diamond grid, Ludwig–Langelier, and Schoeller diagrams to classify water types, evaluate mixing processes, and assess fluid–rock interactions. Reservoir temperatures were estimated using silica geothermometers and the Giggenbach Na–K–Mg triangle, distinguishing between immature and fully equilibrated fluids.*

*Results indicate that thermal waters range from calcium–sulfate and mixed alkaline–bicarbonate types **to** sodium–potassium–chloride and alkaline–chloride–sulfate types**,** reflecting diverse geochemical evolution. Temperatures derived from silica geothermometers and the Giggenbach triangle range from 70 to 122 °C**,** consistent with medium-enthalpy geothermal reservoirs**.** The study demonstrates that Samtskhe–Javakheti thermal waters comprise a heterogeneous mixture of immature and equilibrated fluids**,** providing a comprehensive understanding of water evolution and thermal characteristics. These findings support future geothermal exploration and sustainable utilization of the region's resources.*

Key words: *Samtskhe–Javakheti, geothermal system, hydrogeochemistry, geothermometry, Piper diagram, Durov diagram, Giggenbach triangle, reservoir temperature.*

Introduction

The Samtskhe–Javakheti region of southern Georgia, part of the Lesser Caucasus volcanic arc, hosts significant geothermal resources. The area features Neogene–Quaternary volcanism, including lava plateaus, volcanic cones, and pyroclastic deposits, primarily of basaltic to andesitic composition [1-2]. Fractured volcanic rocks and interbedded sediments facilitate hydrothermal circulation, generating numerous thermal springs [3-4].

Despite its potential, systematic hydrogeochemical and geothermometric studies are limited. The application of hydrochemical diagrams (Piper, Durov, diamond grid, Ludwig–Langelier, Schoeller) and chemical geothermometers provides insights into water evolution, reservoir temperatures, and fluid–rock interaction, supporting geothermal resource assessment.

Geological setting of the study area

The Samtskhe–Javakheti region is situated within the Lesser Caucasus volcanic arc, influenced by the convergence of the Arabian and Eurasian plates. Neogene–Quaternary volcanic activity formed extensive lava plateaus, volcanic cones, and pyroclastic deposits, which are interlayered with sedimentary formations [1-2]. Tectonic fracturing and volcanic structures create hydrothermal pathways, facilitating the circulation of thermal waters. Thermal springs are mainly associated with fractured volcanic rocks, tuffs, and sedimentary interbeds, which serve as aquifers [3-4].

Methods

Water samples were collected from 10 thermal springs and wells across the study area. Major cations (Na^+, K^+, Ca^{2+}, Mg^{2+}) and anions (Cl^-, SO_4^{2-}, HCO_3^-) were analyzed following standard procedures. Hydrochemical facies were determined using Piper and Durov diagrams [5-6].

Further hydrochemical classification employed the diamond grid diagram [7-8], Ludwig–Langelier diagram [9], and semi-logarithmic Schoeller diagram [10] to evaluate water types and chemical evolution.

Reservoir temperatures were estimated using the Giggenbach Na–K–Mg triangle [11] and silica geothermometers [12]. Cation geothermometers were applied selectively for higher-temperature samples. These methods provided constraints on fluid–rock interaction, water maturation, and reservoir temperatures.

Results and Discussion

Water samples from ten thermal springs in the Samtskhe–Javakheti region (Table 1) were collected and subjected to chemical and physicochemical analyses.

Table 1. Sampled thermal water points: location, site name, temperature, and pH

ID	Location	pH	Outlet temperature ℃
JA1	Tsinubani	9.68	38.2
JA10	Corchali	8.69	25
JA11	Didi Smada	9.59	27.6
JA2	Tsinubani 2	9.94	25.2
JA27	Vardzia	7.03	41.3
JA34	Aspindza	9.24	37.5
JA71	Nakalakevi	7.43	35.5
JA72	Tmogvi	7.12	60.9
JA73	Vardzia 2	7.63	54.3
JA98	Akhaltsike	6.9	39.5

Hydrochemical Classification

The Durov diagram (Fig. 1a) reveals three zones [8]: JA71, JA72, JA73 (Zone 5): No dominant anions, indicating mixing or dilution; JA2 (Zone 6): SO_4-dominant with Na as the major cation, reflecting probable mixing influences; JA98 (Zone 9): Cl- and Na-dominated, characteristic of older, evolved waters.

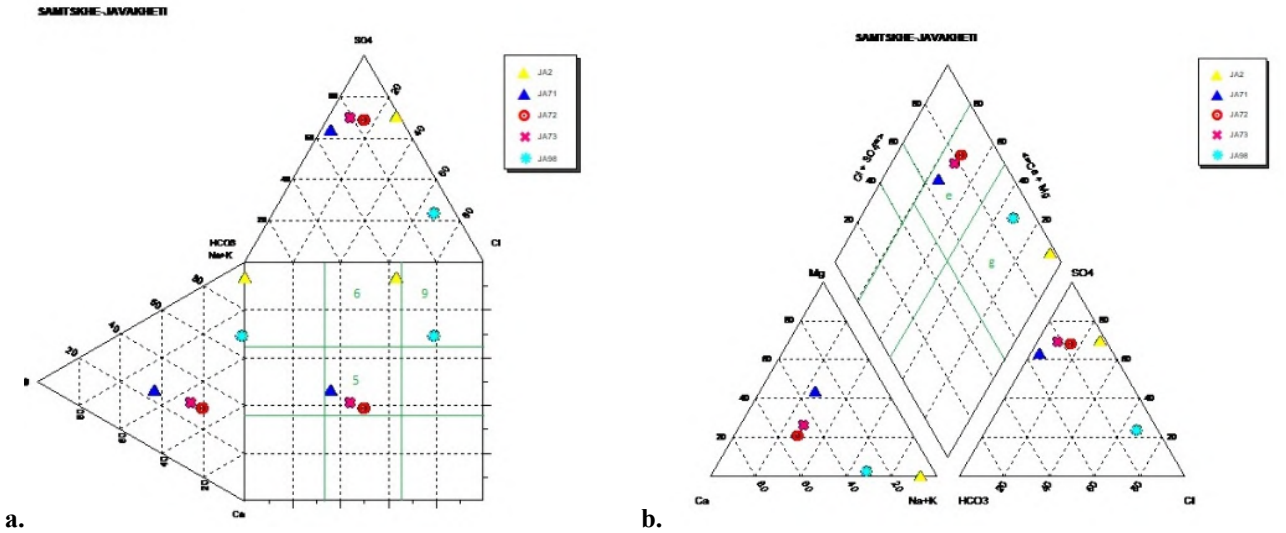

Fig. 1. Durov diagram (a) showing the hydrochemical classification of thermal water samples from the Samtskhe–Javakheti region. Piper diagram (b) illustrating the chemical facies of thermal water samples, highlighting sodium–potassium–chloride and calcium–sulfate types.

On the Piper diagram (Fig. 1b), JA2 and JA98 are classified as sodium–potassium–chloride type, while the remaining samples are calcium–sulfate type. The diamond grid diagram [7] identifies JA71, JA72, and JA73 as waters of increased alkalinity with elevated sulfate and chloride, whereas JA98 and JA2 are alkaline waters dominated by sulfate and chloride.

The Ludwig–Langelier diagram (Fig. 2a) further classifies JA71, JA72, and JA73 as mixed alkaline–bicarbonate waters (upper-left quadrant) and JA98, JA2 as alkaline–chloride–sulfate waters (upper-right quadrant).

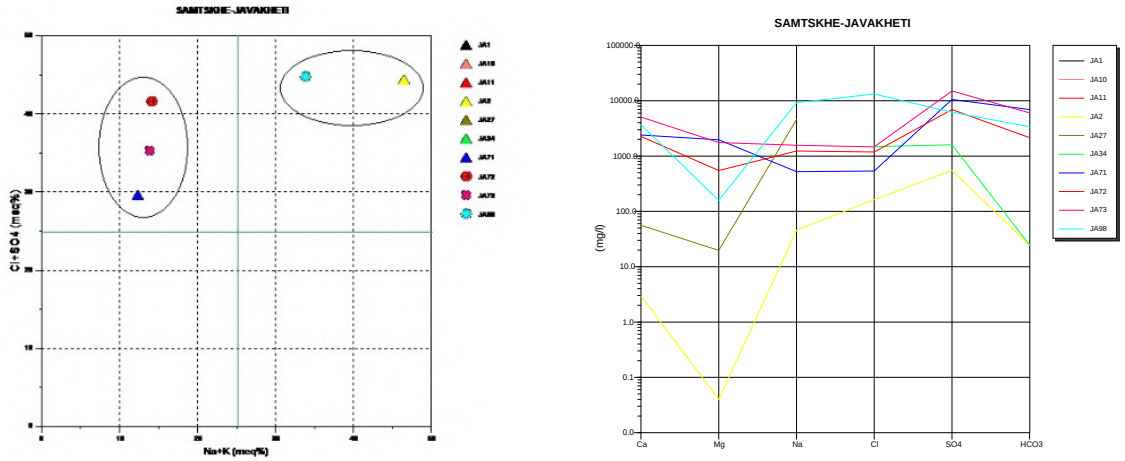

a. **b.**

Fig. 2. Ludwig–Langelier diagram (a) showing the distribution of thermal waters according to alkaline–bicarbonate and alkaline–chloride–sulfate types. Semi-logarithmic Schoeller diagram (b) displaying major cation and anion compositions of the sampled thermal waters.

The Schoeller diagram (Fig. 2b) confirms these trends: JA71, JA72, JA73: Ca > Na > Mg; SO_4 > HCO_3 > Cl ; JA2, JA27: Na > Ca > Mg; SO_4 > Cl > HCO_3 ; JA98: Na > Ca > Mg; Cl > SO_4 > HCO_3.

These results collectively indicate diverse geochemical evolution, mixing processes, and water maturity within the system.

Geothermometry

The Giggenbach Na–K–Mg triangle (Fig. 3) shows JA71, JA72, and JA73 in the "immature" water zone, indicating mixing with cold waters or conductive cooling, whereas JA2, JA27, and JA98 plot in the equilibrium zone, reflecting chemical equilibration with host rocks.

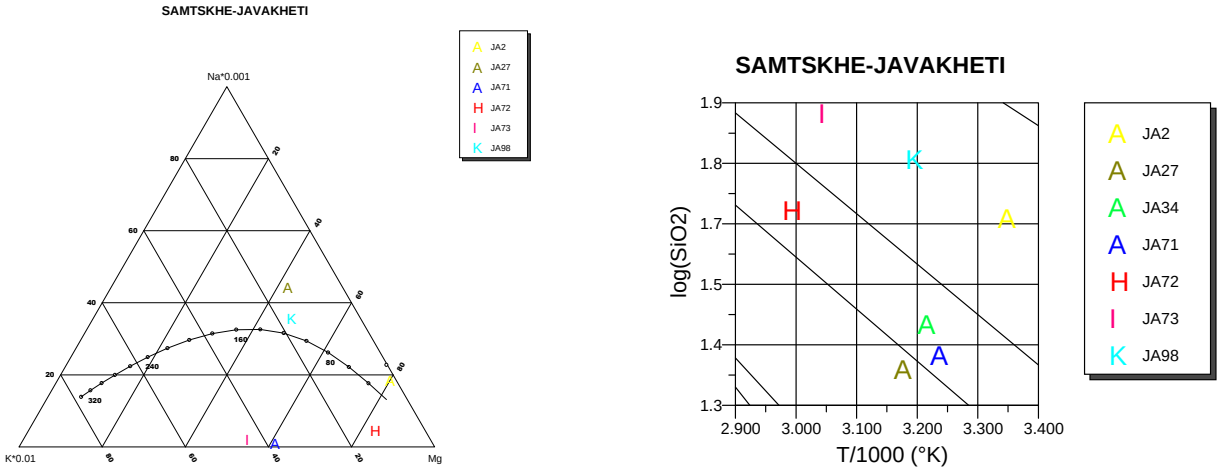

a. **b.**

Fig. 3. Giggenbach Na–K–Mg triangle (a) depicting the equilibrium status of thermal waters, distinguishing between immature and equilibrated fluids; Reservoir temperatures of Samtskhe–Javakheti thermal waters estimated using silica geothermometers (quartz and chalcedony), showing the range of thermal conditions across sampled sites (b).

Reservoir temperatures derived from the Giggenbach triangle range from 70–90°C, while silica geothermometers provide slightly higher values of 70–122°C, consistent with the triangle results. Cation geothermometers were not applied to the low-temperature immature waters due to unreliability.

These findings, combined with hydrochemical diagram results, indicate the presence of both immature and fully equilibrated fluids, highlighting the heterogeneous nature of the Samtskhe–Javakheti geothermal system.

Conclusion

The integrated hydrogeochemical and geothermometric study demonstrates that the Samtskhe–Javakheti thermal waters comprise a mixture of immature and equilibrated fluids. Water types range from calcium–sulfate and mixed alkaline–bicarbonate to sodium–potassium–chloride and alkaline–chloride–sulfate, reflecting variable water–rock interaction, mixing, and thermal maturation. Reservoir temperatures of 70–122°C indicate medium-enthalpy geothermal potential, suitable for direct-use applications. The combined use of hydrochemical diagrams and geothermometers provides a robust framework for evaluating geothermal resources and guiding sustainable utilization in the region.

Acknowledgements. The paper is a part of the research done within the SRNSFG FR-18-19173 project. As recipients of the Research State Grant, the authors thank the Shota Rustaveli National Science Foundation of Georgia.

References

1. Gamkrelidze I.P., Geology of the Caucasus. Nauka, Moscow,1986.
2. Lordkipanidze M., Volcanism of the Lesser Caucasus. Metsniereba, Tbilisi, 1991.
3. Gogichaishvili G., Geothermal resources of Georgia and perspectives on their utilization. // Proceedings of the Int. Conf. “Geology of the Caucasus”, Tbilisi, 2004.
4. Tvalchrelidze A.G., Kiziria A.G., Japaridze, L., Geothermal potential of Georgia: Current state and perspectives. // Bulletin of the Georgian National Academy of Sciences, 5(2), 2011, pp. 112–118.
5. Piper, A.M., A graphic procedure in the geochemical interpretation of water analyses. // Transactions, American Geophysical Union, 25(6), 1944, pp. 914–928.
6. Durov, S.A., Natural waters and a graphic representation of their composition. // Doklady Akademii Nauk SSSR, 59(1), 1948, pp. 87–90.
7. Furtak, K., Langguth, H. Hydrochemical classification using diamond diagrams. // Geochimica et Cosmochimica Acta, 31, 1967, pp. 139–150.
8. Lloyd, J.W., Heathcote, J.A., Natural inorganic hydrochemistry in relation to groundwater. Oxford Science Publications, 1985.
9. Langelier, W., Ludwig, H., Graphical methods for indicating the mineral character of natural waters. // J. Am. Water Ass., 34, 1942, pp. 335-352.
10. Scholler, H., Les Eaux Sutterraines, Masson et Cie. 67, 1962.
11. Giggenbach, W.F., Geothermal solute equilibria. Derivation of Na–K–Mg–Ca geoindicators. // Geochimica et Cosmochimica Acta, 52(12), 1988, pp. 2749–2765.
12. Fournier, R.O., Chemical geothermometers and mixing models for geothermal systems. // Geothermics, 5, 1977, pp. 41–50.

1st International Scientific Conference "Modern problems in Geophysics", Proceedings,
ISBN 978-9941-36-434-1, ISSN 3088-4349, Tbilisi, Georgia, November 6-8, 2025

COMPREHENSIVE ASSESSMENT OF THE ECOLOGICAL CONDITION OF SOME CONTINENTAL WATER BODIES AND ADJACENT TERRESTRIAL ECOSYSTEMS OF WESTERN GEORGIA

***Kiknadze N., *Gvarishvili N., *Gogitidze M., *Mkheidze N., *Artmeladze M., *Kharazi N., *Djibladze K., **Shavlakadze M., ***Khakhutaishvili A.,**

** Batumi Shota Rustaveli State University, Institute of Agricultural and Membrane Technologies, Batumi, Georgia*
*** Chemistry and Human Health (Non-Profit Legal Entity), Georgia*
**** Legis LLC, Testing Laboratory, Georgia*
nino.kiknadze@bsu.edu.ge

Abstract*. This study provides a comprehensive ecological assessment of selected freshwater bodies (the Pichora, Abasha, and Enguri rivers, and Lakes Paliastomi and Tsivi) and their adjacent terrestrial ecosystems in the lowland zone of Western Georgia. The findings indicate varying degrees of anthropogenic pressure across the study sites, reflected in both water quality and the structural and functional integrity of surrounding terrestrial habitats. In Lake Tsivi, organoleptic indicators were deteriorated relative to reference norms due to nearby construction activities; concentrations of phosphate (PO_4^{3-}) and nitrite (NO_2^-) exceeded regulatory limits for surface waters, while E.coli levels surpassed acceptable thresholds. In the Enguri River, maximum allowable concentrations were exceeded for Al, Fe, Si, Li, Ti, V, and Ba; in the Abasha River, for V; and in Lake Tsivi, for Al, Cu, V, As, Li, and Ba. Based on the examined parameters, the Pichora River and Lake Paliastomi exhibited the highest water quality. Terrestrial ecosystems in the study area were also subject to anthropogenic impacts of varying intensity, contributing to habitat fragmentation and a decline in biodiversity.*

Key words: *river, lake, ecological assessment, water quality, anthropogenic impact.*

Introduction

Relevance. The lowland rivers of Western Georgia represent ecologically significant systems, as their associated terrestrial habitats are distinguished by high biodiversity and unique microclimatic conditions. However, in recent decades, the intensification of anthropogenic pressures has led to the degradation of river ecosystems, soil erosion, the spread of invasive species, and a decline in local biodiversity [3, 4, 9]. In the Pichora River basin, increasing urbanization and unsustainable agricultural practices have resulted in habitat fragmentation. Around the Abasha River, land-use changes have had severe impacts on the stability of adjacent terrestrial ecosystems. In the vicinity of the Enguri Dam, hydrotechnical infrastructure has altered the structural characteristics of the surrounding landscape [5, 7]. Lakes Paliastomi and Tsivi form integral components of the unique wetland ecosystems of the Colchic Lowland, providing essential ecosystem services for the region. Their surrounding floodplain meadows, reed beds, and alluvial forests play a crucial role in maintaining habitat connectivity and landscape integrity [2, 17]. Yet, these ecosystems are increasingly affected by land-use changes, ecotone degradation, habitat fragmentation, and biodiversity loss. Under these circumstances, a comprehensive ecological assessment of local ecosystems becomes highly relevant and necessary [1, 6, 8].

Methods

The study employed a combination of field measurements [10, 11], titrimetric analyses [20], and inductively coupled plasma atomic emission spectrometry (ICP-AES) [15, 16, 19] to evaluate physicochemical parameters of surface waters. Microbiological analyses were performed to determine the presence and abundance of indicator organisms [12, 13]. In parallel, baseline surveys of terrestrial habitats adjacent to the studied rivers and lakes were conducted to document vegetation structure, land-use patterns, and habitat conditions [14, 18-23].

Results

1. Field Measurements. The pH values indicated slightly acidic conditions in the Pichora River (pH 6.0), neutral conditions in the Enguri River (pH 6.9), and slightly alkaline conditions in the Abasha River (pH 7.9). Among the studied lakes, Lake Paliastomi was slightly alkaline (pH 7.4), whereas Lake Tsivi was moderately acidic (pH 6.3). Electrical conductivity was highest in the Pichora River and lowest in the Enguri River, reflecting differences in dissolved ion content. Lake Paliastomi exhibited a conductivity of 4251 µS/cm, confirming the influence of Black Sea saline water intrusion on the lake's increasing salinity. Temperature measurements showed that the Pichora River had the lowest water temperature, while the Abasha River had the highest. Dissolved oxygen levels were greatest in the Pichora River (4.52 mg/L), whereas the Enguri River (2.01 mg/L) and Abasha River (3.65 mg/L) exhibited relatively oxygen-poor waters. Lake Tsivi also showed oxygen depletion compared to Lake Paliastomi. Transparency assessments revealed that Pichora River waters were clear, while the Abasha and Enguri rivers exhibited moderate turbidity. Floating particulate matter was abundant in the Enguri River, particularly at the surface, largely due to the accumulation of woody debris near the Enguri Dam. In contrast, Lake Paliastomi appeared transparent, while floating particles were observed on the surface of Lake Tsivi. Organoleptic analysis of odour intensity indicated no perceptible odor in the Pichora River and Lake Paliastomi (0 points), weak odor in the Enguri River (1 point), and moderate odor in the Abasha River and Lake Tsivi (2 points).

II. Assessment of Water Pollution Levels

The chemical analyses revealed detectable concentrations of phosphate (PO_4^{3-}), nitrate (NO_3^-), and nitrite (NO_2^-) in the waters of the Enguri and Abasha rivers (Table 1). In Lake Tsivi, however, the concentrations of PO_4^{3-} and NO_2^- exceeded the established regulatory standards for surface waters. The elevated phosphate levels in Lake Tsivi indicate the onset of eutrophication processes, which were also visually apparent in the form of increased algal growth and decreased water transparency.

Table 1. Concentrations of Chemical Pollutants in the Studied Waters

№	Location	pH	PO_4^{3-} (mg/L)	NO_3^-(mg/L)	NO_2^-(mg/L)
1	Pichora River (Water Transport Last Stop)	6.9	–	–	–
2	Abasha River (near Martvili township)	7.9	1.43	1.85	0.123
3	Enguri River (near Enguri Dam)	6.0	2.43	4.15	0.6
4	Lake Paliastomi (Colchic National Park)	7.4	0.95	0,14	0.08
5	Lake Tsivi (Tskaltubo Park location)	6.3	3.8	0.85	1.68
	MPC	***6.5-8.5***	***3.5***	***45***	***0.2***

Counts of total Saprotrophic bacteria and lactose-positive *Escherichia coli* (E. coli) were recorded in the waters of the Enguri and Abasha rivers. Based on these indicators, the Pichora River exhibited the highest microbiological water quality (Table 2). In Lake Tsivi, however, the *E. coli* concentration was 7.6 times higher than the established regulatory limit, indicating contamination with fecal matter and a high degree of water pollution.

Table 2. Results of Saprotrophic Bacteria and *E. coli* Determination

Parameter, Unit	Location					
	Pichora River	***Abasha River***	***Enguri River***	***Lake Paliastomi***	***Lake Tsivi***	***Standard***
Total number of Saprotrophic bacteria, Pieces/1mL	3	25	34	70	90	Not more than 100/1mL
E.coli, Piece/1L	<300	82	96	290	2300	Not more than 300/1L

III. Multi-Element Water Analysis

In the Enguri River, the concentrations of Al, Fe, Si, Li, V, and Ba exceeded the regulatory limits (MPC – Maximum Permissible Concentration) for surface waters, while in the Abasha River, elevated levels of Al and V were detected (Table 3). No detectable levels of Cr, Cu, Ni, Zn, Se, Hg, Pb, Cd, Sn, Ti, or Be were found in the waters of any of the rivers. Concentrations below the MPC were recorded as follows: B and Ba in the Pichora River; Mn, Sb, and Ba in the Abasha River; and B, Co, Mo, Sb, Be, and As in the Enguri River. In Lake Paliastomi, sodium (Na) concentration exceeded the standard by four times, and potassium (K) by three times. In Lake Tsivi, concentrations of P, Al, Cu, V, As, Li, and Ba exceeded the MPC. No Zn, Co, Be, Cd, Cr, Hg, Se, or Ti were detected in the lakes. Concentrations of Si, B, Mn, Mo, Ni, Sb, and Pb remained within Maximum Permissible Concentrations in both lakes.

Table 3. Concentrations of Micro- and Ultra-Trace Elements in Water (mg/L)

Location	Fe	Si	B	Al	Cu	Mn	Ni	V	As	Li	Ba	Sb	Mo
Pichora	-	4.62	0.005	0.437	-	-	-	-	-	-	0.003	-	-
Abasha	0.032	1.96	-	15.9	-	0.0009	-	0.002	-	-	0.005	0.002	-
Enguri	2.78	14.1	0.011	4.47	-	0.0638	-	0.001	0.01	0.04	0.268	0.001	0.004
Paliastomi	-	0.121	0.18	0.163	-	0.0017	0.008	-	-	-	0.002	0.002	0.002
Tsivi	0.054	0.230	0.218	0.546	1.24	0.0074	0.008	0.003	0.11	0.04	0.215	0.003	0.008
MPC	***0.3***	***10***	***0.5***	***0.5***	***1.0***	***0.05-0.1***	***0.01***	***0.001***	***0.05***	***<0.03***	***0.1***	***0.005***	***0.25***

IV. Assessment of the Ecological Status of Terrestrial Ecosystems Surrounding the Studied Water Bodies.

Fichora Valley represents a typical subtropical landscape characterized by Colchic forests interspersed with subtropical shrubs and riparian wild habitats. These ecosystems are partially fragmented due to anthropogenic pressures. Locally, the dominance of invasive species impedes natural ecosystem renewal processes. *Ecological risks:* habitat fragmentation and increasing tourist pressure. ***Abasha Valley*** is dominated by alluvial forests, shrubs, and cultivated agricultural plots. The river basin landscapes have been significantly transformed by human economic activities. Forest cover is fragmented due to human land use. Terrestrial ecosystems show a trend of invasive species encroachment, replacing native biocenoses. Agricultural expansion intensifies soil erosion, while widespread solid waste accumulation along riverbanks reduces the ecosystems' self-regeneration capacity. *Ecological risks:* Intensification of agricultural exploitation and deterioration of water resource quality. The ***Enguri River Basin*** and its surrounding areas are rich in Colchic-type forests, meadows, and semi-natural biodiverse zones. The expansion of the water surface upstream of the Enguri Dam and the reduced downstream flow have affected the structure of riparian habitats and reduced forested areas along the river. Changes in floristic composition have led to a decline in forest biodiversity. *Ecological risks:* Altered hydrological regimes disrupting landscape dynamics and biodiversity loss.

Conclusion

The analysis of baseline studies indicates that the landscapes of the river basins in the Colchic zone of Western Georgia are subject to both natural dynamics and strong anthropogenic pressures, resulting in habitat fragmentation, intensified soil erosion, reduction of natural vegetation, and deterioration of water quality. Elevated concentrations of PO_4^{3-}, NO_3^-, and NO_2^- were recorded in the Enguri and Abasha rivers, while in Lake Tsivi, PO_4^{3-} and NO_2^- exceeded permissible limits. The *E. coli* level in Lake Tsivi was 7.6 times above the regulatory standard. Based on elemental composition, the cleanest waters were observed in the Pichora River and Lake Paliastomi, whereas the most polluted were found in the Enguri River and Lake Tsivi.

References

1. Abramia G., Study, modeling, and preventive measures for the impact of pathogenic bacteria on the ecological state of Lake Paliastomi (PhD). Georgian Technical University. Tbilisi, 2019, p. 130 . https://dspace.nplg.gov.ge/bitstream/1234/306750/1/Disertacia.pdf
2. Iordanishvili I., Iordanishvili K., Features of the formation and use of the main natural water reserves and water resources of Western Georgia. Georgian Institute of Water Management. – Tbilisi. 2009, pp.6-142.
3. https://dspace.nplg.gov.ge/bitstream/1234/420338/1/DasavletSaqartvelosBunebriviWylisDziritadiMaragisDaWylis.pdf
4. Ministry of Environment Protection and Natural Resources of Georgia, Fourth National Communication of Georgia to the Convention on Biological Diversity, 2009, pp. 11-22. https://eiec.gov.ge/-/Documents/ViewFile/22
5. Ministry of Environment Protection and Agriculture of Georgia. Fourth National Environmental Action Program 2022–2026. Project (with the support of the United Nations Development Program and the Government of Sweden), 2022. https://mepa.gov.ge/ge/Files/ViewFile/53107
6. Government of Georgia. Samegrelo-Zemo Svaneti Region Development Strategy for 2014-2021. (Decree No. 1372 of September 18, 2013, p. 48. https://szs.gov.ge/res/docs/2014050301151521560.pdf
7. Government of Georgia. (2013, December 31). On the Technical Regulations for the Protection of Surface Waters of Georgia from Pollution: Resolution No. 425. https://www.gov.ge/files/276_39952_103569_425311213.pdf
8. Green Alternative. (2021). Georgia's Water Infrastructure – Problems and Prospects. https://greenalt.org/app/uploads/2021/05/wylis_seqtoris_mimoxilva.pdf
9. National Statistical Service of Georgia. (2013). Natural Resources and Environmental Protection of Georgia. – Tbilisi. https://www.geostat.ge/media/13595/sakartvelos-bunebrivi-resursebi-da-garemos-dacva_2012.pdf
10. Kajaia G., Ecology: Problems of Our Time., 2022, p. 226. https://rustaveli.org.ge/res/docs/89935767e06575c2c19dd121dc734daa747e9b72.pdf
11. AliExpress. (n.d.). Cloud Prime Portable pH Meter for Drinking Water with 0.01 Precision 0 to 14 pH Range. https://www.aliexpress.us/item/3256807307876552.html?gatewayAdapt=glo2usa4ite
12. AZ Instrument Corp. (n.d.). 86031 AZ EBpH/COND./SALT/TDS/DO Meter. https://www.az-instrument.com.tw/en/product-620072/pH-COND-SALT-TDS-DO-Meter-8603
13. International Organization for Standardization. (n.d.). ISO 9308: Water quality – Enumeration of Escherichia coli and coliform bacteria. https://www.iso.org/standard/55832.html
14. International Organization for Standardization. (n.d.). ISO 6107: Water quality – Vocabulary. https://www.iso.org/obp/ui/#iso:std:iso:6107:ed-1:v1:en
15. Intergovernmental Panel on Climate Change (IPCC). (2022). Sixth assessment report. https://www.ipcc.ch/report/ar6/
16. Kiknadze, N., Gvarishvili, N., Gotsiridze, R., Tavdgiridze, G., Lominadze, S., Kharazi, N., Results of chemical and ecological research of surface and waste waters in Adjara and their impact on ensuring environmental security [Monograph, electronic version]. Tallinn, 2023.
17. https://pumo.stu.cn.ua/wp-content/uploads/2023/07/19_results-of-chemical-and-ecological-research-of-surface-and-waste-waters-in-adjara-and-their-impact-on-ensuring-environmental-security-1.pdf
18. National Center for Biotechnology Information. (n.d.). Heavy metals. https://www.ncbi.nlm.nih.gov/books/NBK557806/
19. Janelidze, J., Chikhradze, N., & Janelidze, G., Assessing the impact of anthropogenic factors on the ecosystems of the Paliastomi Lake region. // Georgian Geographical Journal, 1(1), 2021, pp. 34–41. https://journals.4science.ge/index.php/GGJ/article/view/256/282
20. Releve Database. (2013). Method handbook for collecting vegetation plot data (p. 64). https://files.dnr.state.mn.us/eco/mcbs/releve/releve_singlepage.pdf
21. Shimadzu. (n.d.). Determination of elemental composition of animal feed by ICP-OES according to EN 15621.
22. https://www.shimadzu.com/an/sites/shimadzu.com.an/files/pim/pim_document_file/applications/application_note/14064/an_04-ad-0238-en.pdf
23. Thermo Fisher Scientific. (n.d.). Determination of water pollutants using photometric analysis (Application Note AN71728). https://assets.thermofisher.com/TFS-Assets/CMD/Application-Notes/AN-71728-DA-ISO-Water-Pollutants-AN71728-EN.pdf

1st International Scientific Conference "Modern problems in Geophysics", Proceedings,
ISBN 978-9941-36-434-1, ISSN 3088-4349, Tbilisi, Georgia, November 6-8, 2025

PHYSICO-CHEMICAL AND HYDROCHEMICAL STUDIES OF THE WATERS OF THE KVIRILA RIVER AND SPRING WATERS IN CHIATURA MUNICIPALITY

Shavliashvili L., *Kuchava G., *Shubladze E., **Rikadze Z.**, Kordzakhia G.* , Gavardashvili G.**

** Institute of Hydrometeorology, Georgian Technical University*
** * National Environmental Agency of the Ministry of Environment Protection and Agriculture of Georgia*
** * * Tsotne Mirtskhulava Institute of Water Management, Georgian Technical University*
gkuchava08@gmail.com

Abstract*. The paper discusses the physicochemical and hydrochemical state of the Kvirila River waters in the areas surrounding the manganese processing plants of Chiatura Municipality. Determining the purity of the Kvirila River water is necessary because the Kvirila River water is used to wash the mined ore, after which the wastewater flows into the river and pollutes it.*

Key words*: Kvirila River, bottom sediments, spring waters, manganese, pollution.*

Introduction

In terms of environmental pollution, the negative impact of the mining industry in Chiatura Municipality is very significant, especially when developing deposits using the open-pit (open-cast) method. The latter is naturally much more profitable compared to underground ore processing. At the same time, labor productivity increases by 3–5 times, and the cost of production decreases by almost the same amount. It should also be noted that the soil, natural, and cultural vegetation that have developed over centuries on the site of the open pits are destroyed, and the areas around the pits often become hotbeds of erosion, landslides, and pollution of wastewater, drinking water, as well as the atmosphere [1–3].

In Chiatura Municipality, the company "Georgian Manganese" carries out mining of manganese concentrate using the shaft method, but licenses have also been issued to small private companies. There are approximately 20 deposits in the municipality, of which 9 are shaft-type and 11 are open-careers type. Ore processing began in 1879 [https://socialjustice.org.ge].

Manganese mining in Chiatura is causing significant damage to the hydrographic network, in particular the Rgani Gorge and the Kvirila River. The Kvirila River joins the Rioni River and carries pollutants to the Black Sea, causing significant damage to the irrigation network and agricultural fields of the Zestaponi district. In Chiatura Municipality, the Kvirila River flows into a ravine, so it is not used in the irrigation system, as the location of the villages and the river makes this process difficult.

Manganese is an important element for humans and animals. The human body contains about 10 mg of manganese, which is mainly accumulated in the liver and kidneys. Manganese is also part of the composition of bones. Manganese is contained in small concentrations in almost all human organs. Manganese participates in the blood-forming functions of humans and animals, in the process of bone growth, affects the functions of the reproductive organs, and the metabolism of proteins, carbohydrates, and fats. It is one of the main components of many enzymes and endocrine glands.

Manganese does not cause acute poisoning. It is a cumulative poison and causes the following occupational diseases: manganism, coniogenic bronchitis, bronchial asthma, manganoconiosis, eczema, and allergic dermatitis [4].

Research area and methods

The paper provides a physicochemical and hydrochemical characterization of the waters of the Kvirila River in the areas surrounding the manganese processing plants of Chiatura Municipality. Determining the purity of the Kvirila River water is necessary because the Kvirila River water is used to wash mined ore, after which the wastewater flows into the river and pollutes it.

To solve the set tasks, spring waters and samples of the Kvirila River water were taken, both background and downstream of the pollution source. As well as suspended solid and bottom sediments of the Kvirila River.

The following parameters were determined in the collected water samples: physicochemical and hydrochemical parameters, namely: pH, electrical conductivity, biogenic substances – NO_2^-, NO_3^-, NH_4^+, PO_4^{3-}, main ions, mineralization, heavy metals: Cu, Zn, Pb, Cd, Ni, Co and total manganese [5] and microbiological parameters: E-coli, total coliforms, fecal streptococci [6].

The analyses were carried out using modern methods and equipment that meet and comply with European standards, namely:

1. Ion chromatograph-IC-1000; ISO100304-1:2007
2. Spectrophotometric method – SPECORD 205; ISO 7150-1: 2010;
3. Plasma emission spectrometer – ICP-OES; Epa method 200.8;
4. Field portable equipment – Hanna Combo pH/EC/TDS/PPM Tester HI98129;
5. IDEX-apparatus
6. pH-meter – Milwaukee-Mi 150.

In Table 1. Hydrochemical and microbiological data of the Kvirila River and Spring waters are shown. As can be seen from Table 1, below Kvirila-Ltd "Andro" and Kvirila-Ltd "Jruchula", a deviation of pH in the alkaline direction is observed and amounts to 7.9 – 8.1. In the river Kvirila, below the enterprises, the content of ammonium ions is increased and amounts to 0.772 (2.0 MPC) and 0.523 mg/l (1.3 MPC), respectively. The content of nitrites and nitrates is within the norm. It is noteworthy that the content of almost all ingredients is much higher below Kvirila-Ltd "Andro", compared to Kvirila-Ltd "Jruchula" and especially to the background. The sum of hydrocarbonates, sodium and potassium, calcium, and magnesium are high. The mineralization of Kvirila water at the mentioned enterprises is moderate-696.82 and average-318.15 mg/l, respectively, while the mineralization of the river Kvirila at the background point is average mineralized-241.84 mg/l [7].

Table 1. Hydrochemical and microbiological data of the Kvirila River and Spring waters, June 2025

N	Ingredients	Kvirila-below "Andro" Ltd	Kvirila-below "Jruchula" Ltd	Kvirila-background	Spring water-1	Spring water-2	MPC *	MPC **
1	pH	7.9	8.0	8.1	8.1	8.0	6-9	6.5-8.5
2	Electrical conductivity μsms/cm	860	334	233	425	975		
3	BOD_5, mg/l	3.64	3.04	1.32	3.05	2.25	6.0	6.0
4	Hardness, mg.seq./l	6.78	2.99	4.55	4.15	6.12	7-10	
5	Ammonium, mgN/l	0.772/2.0	0.523/1.3	0.383	0.235	0.222	0.39	0.39
6	Nitrites, mgN/l	0.623	0.014	0.029	0.111	0.125	0.2	3.3
7	Nitrates, mgN/l	1.552	0.361	0.269	8.55	9.15	50	45
8	Phosphates, mg/l	0.120	0.098	0.050	0.115	0.156	3.5	3.5
9	Sulfates, mg/l	337.28	44.94	14.55	80.65	450.25/1.8	250	500
10	Chlorides, mg/l	14.25	3.40	7.78	7.15	7.12	250	350
11	Bromine, mg/l	0.006	0.010	0.107	0.012	0.095		
12	Fluoride, mg/l	0.170	0.112	0.036	0.085	0.143	0.7	
13	Hydrocarbons, mg/l	161.04	163.48	159.82	212.60	214.23		
14	Potassium, mg/l	85.75	31.50	14.25	20.14	102.32		
15	Sodium, mg/l							
16	Calcium, mg/l	86.17	44.29	34.69	45.23	95.33		
17	Magnesium, mg/l	30.15	9.48	9.94	16.82	14.42		
18	Mineralization, mg/l	696.82	318.15	241.84	435.47	985.13	1000-1500	
19	E-Coli, in 250 ml				N.D	N.D	not allowed	
20	Total coliforms in 250 ml				N.D	N.D		
21	Fecal streptococci, in 300 ml				N.D	N.D		
22	Manganese, mg/l	23.800/238.0	9.892/98.9	0.0527	0.0025	0.0055	0.4	0.1
23	Copper, mg/l	0.0379	0.0355	0.0036	0.0009	0.0011	2.0	1.0
24	Zinc, mg/l	0.0454	0.0518	0.0050	0.0022	0.0042	3.0	1.0
25	Lead, mg/l	0.0082	0.0037	0.0015	0.0015	0.0027	0.01	0.03

26	Cadmium, mg/l	0.0007	0.0002	0.0001	<0.0001	<0.0001	0.003	0.001
27	Nickel, mg/l	0.0201	0.0467	0.0028	0.0008	0.0010	0.07	0.1
28	Cobalt, mg/l	0.0130	0.0097	<0.0001	0.0007	0.0005		0.1

**** – MPC** – maximum permissible concentrations according to Technical Regulations for Drinking Water (Decree №58 of the Georgian government as of 15th January 2014, Tbilisi) [10]*
***** – MPC** – maximum permissible concentrations according to Technical Regulations for Surface Water (Decree №425 of the Georgian government as of 31st December 2013, Tbilisi) [11].*

Fig.1 shows the manganese content in the surface waters of the rivers and springs of Kvirila as of June 2025.

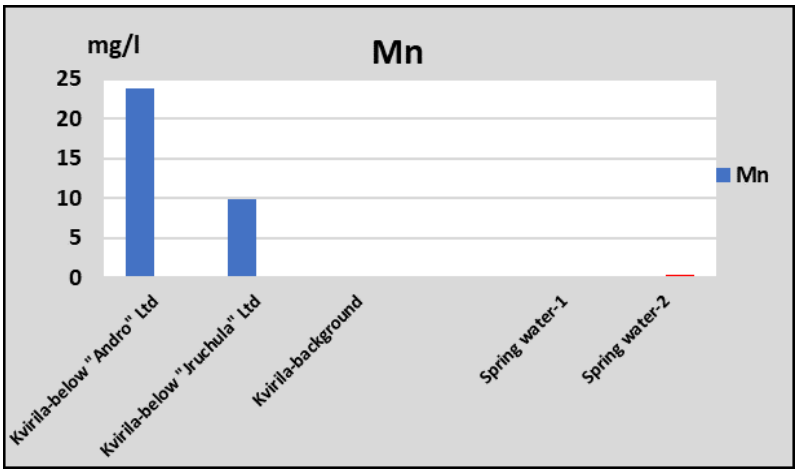

Fig. 1. Manganese content in the Kvirila rivers and spring waters, June 2025.

The situation is alarming regarding the manganese content in the Kvirila River below Ltd "Andro", where the manganese concentration reaches 23.800 mg/l, which is equivalent to 238.0 times the maximum permissible concentration (MPC). In the section of the Kvirila River near Ltd "Jruchula", the manganese concentration is 9.8920 mg/l, or 98.9 MPC. This elevated pollution level is caused by the discharge of wastewater into the Kvirila River during the washing of mined ore (Fig. 1).

The water of the second spring is notable for its high levels of certain components compared to other spring waters. The sulfate content is 450.25 mg/l, which is 1.8 times higher than the maximum permissible concentration. Its mineralization level is 985.13 mg/l, classifying it as moderately mineralized water. The manganese content in the water of both springs remains within the permissible limits.

Among the identified heavy metals, aside from manganese, none were found in concentrations exceeding the maximum permissible levels, and the spring waters showed no contamination according to the determined microbiological parameters.

According to Table 2, the manganese content in suspended particles and bottom sediments of the Kvirila River is higher downstream of Ltd "Andro" than it is below Ltd "Jruchula", at 41.5 and 19.7 mg/kg, respectively. The manganese content in the bottom sediments is higher than in the suspended particles, measuring 54.3 mg/kg below Ltd "Jruchula" and 46.1 mg/kg below Ltd "Andro". It should also be noted that the color of the Kvirila River water is black in the vicinity of the enterprises, which is due to the high content of sediments and suspended particles.

Table 2. Manganese content of suspended solids and sediments of the Kvirila River, June, 2025

N	Sampling location	Coordinates	Results	
	Suspended solid		**mg/kg**	**%**
1	Kvirila-below "Andro" Ltd	X-363027 Y-4686103	41.5	4.15
2	Kvirila-below "Jruchula" Ltd	X-363791 Y-4686878	19.7	1.97
	Sediments		**g/kg**	
1	Kvirila-below "Andro" Ltd	X-363027 Y-4686103	46.1	4.61
2	Kvirila-below "Jruchula" Ltd	X-363791 Y-4686878	54.3	5.43

Conclusion

The study of the Kvirila River and nearby spring waters reveals several key findings:

- The pH of the Kvirila River ranges from 7.9 to 8.0, while the spring waters show slightly higher values, between 8.0 and 8.1, indicating generally neutral to slightly alkaline conditions.
- The major cations and anions in the Kvirila River, both upstream and downstream of pollution sources, remain within the maximum permissible concentrations (MPC), confirming that the river water is generally medium to moderately mineralized. However, elevated ammonium ion levels were observed downstream of Ltd "Andro" and Ltd "Jruchula", with concentrations of 0.772 mg/l (2.0 MPC) and 0.523 mg/l (1.3 MPC), respectively, while nitrite and nitrate levels stayed within safe limits.
- Manganese contamination is of particular concern: its concentration in the river downstream of Ltd "Andro" reaches 23.800 mg/l (238.0 MPC) and 9.892 mg/l (98.9 MPC) below Ltd "Jruchula". This significant increase is attributed to wastewater discharge from ore washing activities.
- Additionally, the total manganese content in suspended particles and bottom sediments of the river is notably high, indicating the potential for long-term accumulation in the aquatic environment.
- Other heavy metals were detected at levels within the acceptable standards, with no exceedances of MPCs except for manganese.
- In the analyzed spring waters, sulfate concentrations are elevated in Spring 2, reaching 450.25 mg/l (1.8 MPC), classifying it as moderately mineralized. However, the manganese content in both springs remains within the permissible limits.
- The manganese content in the water of both springs is within the norm;
- Microbiological analysis of the spring waters did not reveal any signs of contamination.

Overall, the findings highlight that while the general water chemistry of the Kvirila River and springs is within acceptable ranges for most parameters, targeted measures are urgently needed to address the excessive manganese pollution and localized increases in ammonium ions, particularly downstream of mining operations. Continuous monitoring and stricter wastewater

Acknowledgements. The research was performed with the support of the Shota Rustaveli National Science Foundation of Georgia, Grant No. FR-23-6375.

References

1. "The Impact of Extractive Industries on Developing Countries", Friends of the Earth – Europe, 2007. http://www.foeeurope.org/corporates/Extractives/social.pdf.
2. Law of Georgia on the Safety of Hazardous Industrial Facilities, 10.12.1997.
3. Tsereteli E., Gobejishvili R., Bolashvili N., Gaprindashvili G., Nanobashvili T., The State of Natural Exodynamic Disasters and the Risk of Anthropogenic Load Hazards in Georgia, Actions to Optimize Their Management // V. Bagrationi Institute of Geography Collection of Works, #4 (83). Tbilisi, 2012, pp. 50-63.
4. Order of the Minister of Labor, Health, and Social Protection of Georgia N 216/n, on approval of the list of occupational diseases and the list of professional activities that are accompanied by the risk of developing an occupational disease. 13.07.2007.
5. Fomin G.S., Fomin A.G.–Water., Quality control and environmental safety according to international standards. Handbook. Moscow, 2001.
6. Guide to methods of hydrobiological analysis of surface waters and bottom sediments. // Gidrometeoizdat, Leningrad, 240 st., 1983.
7. Supatashvili G., Environmental chemistry (ecochemistry), Tbilisi, University Publishing House, 2009, p.187.

1st International Scientific Conference "Modern problems in Geophysics", Proceedings,
ISBN 978-9941-36-434-1, ISSN 3088-4349, Tbilisi, Georgia, November 6-8, 2025

THE STRATEGIC IMPORTANCE AND CHALLENGES OF THE EASTERN COAST OF THE BLACK SEA, THE WAY TO THE ECONOMIC DEVELOPMENT OF GEORGIA

Makalatia I., Tsivtsivadze N., Kereselidze D.

I. Javakhishvili Tbilisi State University, Tbilisi, Georgia
irma.makalatia@ens.tsu.edu.ge

Abstract. *Georgia is an important part of the Europe-Caucasus-Asia transport route (TRASECA). For the coastal country, it is an opportunity for economic, maritime, and other economic development. Since ancient times, our country has been connected to Asia and European countries through the Silk Road. In recent years, Georgia's role as a middle corridor connecting countries that do not have access to the Black Sea (Azerbaijan, Armenia, and Kazakhstan) has significantly increased. The construction and development of the "Anaklia Deep-Sea Port" will contribute to the development of Georgia as a transport and logistics hub.*

"The Black Sea Submarine Cable" project is a project of strategic importance and offers great opportunities for Georgia, Romania, and other neighboring countries. The project aims to export energy from the South Caucasus (SC) countries to Romania, Bulgaria, and South-Eastern Europe (SEE) via a submarine cable crossing the Black Sea. It will support the development of the renewable energy sector, increase transit opportunities between Georgia and the European Union.

The purpose of our research is to find out what economic and political benefits our country will receive in the case of the implementation of these two important projects. How attractive and profitable Georgia can become as an economy if this project is implemented. We will also assess the current situation and challenges of the eastern coast of the Black Sea.

Key words: *"Anaklia Deepwater Port". "The Black Sea Submarine Cable". "Green Energy", Black Sea, Middle Corridor.*

Introduction

The construction of the "Anaklia Deep-water Port" Project is underway in the Samegrelo Zemo-Svaneti region, where a new container terminal is planned to be built, along with the corresponding supporting port infrastructure. The construction is being carried out in several stages (phases). Before the construction, studies were conducted by the World Bank and international organizations, such as the bathymetry and geology of the seabed. It should be noted that on July 27-29, 2025, with the support and cooperation of the Rector of Ivane Javakhishvili Tbilisi State University, Mr. Jaba Samushia, the project "Introducing the Possibilities of Realizing the Anaklia Deep-water Port for TSU Geography Students" was implemented. According to this project, we visited and got acquainted with the construction process of the port. We inspected the construction progress and got acquainted with the stages of work to be carried out in the future. It is welcome that the construction is proceeding smoothly, and they expressed their desire to learn about the ongoing work and involve students in the construction process. Currently, the design and construction of Anaklia infrastructure, in particular, the deepening of the seabed of the port area and the construction of the breakwater, is being carried out by the Belgian company Jan De Nul, which specializes in marine construction works. In September 2024, the company began the geological study of the coast and the surrounding area, detailed design, and implementation of in-depth works. To ensure the safe standing and operation of the ship, the seabed is being deepened and the "molo" is being constructed with flattened mountain rocks of different sizes and weights, and will be lined with the so-called "X-" blocks, through the latter, the impenetrability of wave flows in the port's internal water will be ensured. The Anaklia Deep-water Port is of strategic importance, where the state will own 51%, and the private partner 49%. Accordingly, the state carries out the part of the works, which involves the preparation of the territories for operation, which will necessarily lead to the training/retraining of the necessary personnel [1-7]. The construction of the port will contribute to the economic strengthening of our country and attract important investments in the transport infrastructure (new railway and highway). This will be a serious incentive for the

development of production in the country, economic growth, which will increase trade relations with Asian and European countries. In the first phase, the capacity of Anaklia will be 600,000 containers, and then the port's cargo turnover will be able to handle approximately 8 million tons. In the future, the Anaklia cargo-transport hub can become an important center not only for East-West transport flows, but also for North-South cargo movement. The construction of a large-scale logistics zone is planned around the port, which will lead to the need to create additional jobs and attract investments. The port is expected to be completed by the end of 2028 and will receive its first ship by the beginning of 2029 (Fig. 1).

Fig. 1. Anaklia Deep-water Project Plan.

"The Black Sea Submarine Cable" project is also an object of strategic importance and provides a great opportunity for Georgia, Romania, and neighboring countries. The project aims to export energy from the South Caucasus (SC) countries to Romania and South-Eastern Europe (SEE) via a submarine cable crossing the Black Sea. Moreover, it will support the development of the renewable energy sector, increase transit opportunities, and trade potential with the EU countries. In Georgia and Romania, sea and coastal electrodes, transformer stations, and land and overhead power transmission lines, namely DC high-voltage power transmission system cables (ground cables) and AC high-voltage power transmission system lines (overhead power lines), will be installed. The submarine cable will connect the countries of the Black Sea and pass through the economic zones of Turkey and Bulgaria. According to the project, during the period of water abundance, Georgia will export its own electricity. This means that with the energy sold in Europe, we will be able to contribute three times more money to the Georgian budget. Saudi Arabia is also interested in the project, which will export "green" energy from Azerbaijan via Europe, which makes the implementation of this project more attractive (Fig. 2.).

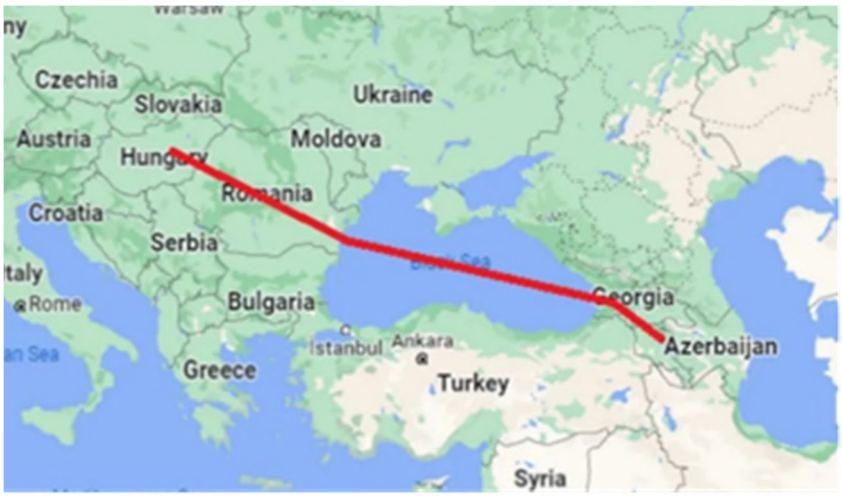

Fig. 2. The Black Sea Submarine Cable Project.

The main results

The study presents the significance of two new projects for the country. These are the construction of "Anaklia Deep Water Port" and "Black Sea Submarine Cable" and their role in the development of the Middle Corridor. It should be noted that the specifics of the wind, wave regime, geomorphological, and meteorological conditions in the Anaklia region require additional research and modeling in order to optimize the project and reduce the risks of maneuvering the operational ships. The current cycle of climate warming, which started in the 80s of the last century, is noteworthy. With independence, the country received the adjacent part of the sea water area – the so-called "Special Economic Zone", the Transcaucasian Transport Corridor of the Great Silk Road was launched with its concession sector, and the transportation of Caspian oil to the west through the Baku-Supsi oil pipeline began. The construction of the "Anaklia Deep-Water Port" and the "Black Sea Submarine Cable" can be considered the project of the century. There is a need for detailed research of the Black Sea bottom using new and modern methods. It is to be welcomed that a geological survey of the eastern coast of the Black Sea is planned for the initiation of the Black Sea submarine cable project. Conducting the above-mentioned research, processing the received information will help future researchers, especially for scientists interested in marine direction.

Conclusion

The construction of the "Anaklia deep-water port" and the Black Sea submarine cable is an important part of the long-term vision and contributes to the development of the transport cargo circulation of the Middle Corridor; therefore, a detailed study is necessary in order not to endanger the current projects. Georgia is a Black Sea country, and climate change and its accompanying events are characterized by high inertia; the erosion processes of the coast have become intense. The rise of the level of the Black Sea, as part of the world ocean It threatens the coastline, causes beach erosion. This is due to two main factors: the melting of glaciers and the thermal expansion of water as a result of global warming, which causes changes in the temperature of the world's oceans. In such conditions, it is an urgent task to study and predict the consequences of climate change in the coastal zone of Georgia, so as not to harm the population living on the coast and to implement the construction of the "Anaklia deep-water port" and the "Black Sea submarine cable", which are called the project of the century.

References

1. Tsivtsivadze N., Problems of the de facto Black Sea coast of Georgia and ways to eliminate them. (Book) Tbilisi, 2023.
2. Metreveli G., Machavariani L., Gulashvili Z., Positives and Negatives of Reservoirs. (Book) Tbilisi, 2022.
3. Anaklia Port Ecological Monitoring Group., Problems of Construction of Anaklia Deep-Sea Port. (Book) Tbilisi 2019.
4. A(A)IPE “Anaklia Port Ecological Monitoring Group.,” Expert Opinion: “Problems of Construction of Anaklia Deep-water Port.” Tbilisi 2019.
5. Tsivtsivadze N., “Project proposal on the feasibility of constructing an Anaklia common freight-transport hub.” Report 2018.
6. "Anaklia Development Consortium" Ltd., Anaklia Deep Water Harbor Environmental Impact Assessment Report (Project), 2017
7. Makalatia I., Bilashvili K., Kereselidze D., Morphodynamics of the Black Sea coastal zone of Adjara and Modern approaches. Baku, 2024.

1st International Scientific Conference "Modern problems in Geophysics", Proceedings,
ISBN 978-9941-36-434-1, ISSN 3088-4349, Tbilisi, Georgia, November 6-8, 2025

DEPENDENCIES REFLECTING QUANTITATIVE CHANGES IN PHYTO- AND ZOOPLANKTON IN THE TBILISI RESERVOIR

Tsivtsivadze N., Khatiashvili E., Makalatia I., Jorbenadze N., Ivanov G.

I. Javakhishvili Tbilisi State University, Tbilisi, Georgia
nodar.tsivtsivadze@tsu.ge

Abstract. *The presented article is focused on the methodology for calculating changes in phyto- and zooplankton in the Tbilisi reservoir, which mainly determines the change in organoleptic indicators of water. Such an approach is explained by the fact that consumers have expressed complaints about the smell and taste of drinking water.*

The advantage of the methodology is especially noticeable when conducting predictive calculations, which is explained by the fact that natural hydrochemical and bacteriological analyses, as a rule, are discrete and episodic in nature, which is why statistical processing does not allow obtaining complete and reliable results.

Key words: *Reservoir, phyto- and zooplankton, Population. Concentration of Substances.*

Introduction

In aquatic systems, and in particular for the Tbilisi Reservoir, the fundamental equations of non-conservative chemical or biological impurities and organisms transport by a continuous environment are used to describe the processes of phyto- and zooplankton mass change. The formulation of mathematical biology equations from these equations is based on the generally accepted and recognized general laws of biology and biochemistry, in particular Liebig's law and the Volterra-Lotka relations; For enzymatic reactions, on Michaelis-Menten ratios; for biological populations – on Monod's dependences, etc. [1]. The work was completely carried out using the above-mentioned mathematical apparatus.

For processes reflecting the growth (decrease) of biopopulations, it is permissible to neglect the convective and diffusion terms during the transfer of impurities due to their smallness; therefore, after several transformations and assumptions, the mentioned processes are described by the equations [2]:

$$Subscript\frac{dc_m}{dt}=\mu_m^1 C\text{-}aC_mC_a\text{-}\gamma_m C_m^2 \quad (1)$$

$$\frac{dC_a}{dt}=\mu_a\ \frac{C_mC_a}{K_m+C_m}-\gamma_a C_a^2 \quad (2)$$

where C_m- is the concentration of microorganisms of the m-type; $C_{a\_}$ is the concentration of their antagonistic microorganisms; μ_m and μ_a- maximum specific rate of growth (decrease) of microorganisms; K_m- is the so-called half-sedimentation constant, equal to $0.5\mu_m$^ (Michaels-Menten or Mono's constant); a, γ- are constants with dimensions $(mg/l)^{-1}$ After several assumptions and transformations, the solution of equations (1) and (2) gives us the dependence reflecting the change in the photo and zooplankton population:

For phytoplankton:

$$C_{fp}=\frac{\eta_{zp}C_BK\,D\,\frac{h\theta\tau}{h_0\theta^*\tau_m}\left(4\text{-}\frac{h}{h_0}\right)^3(1\text{-}\frac{\tau}{\tau_m})^2\left(1\text{-}\frac{\theta}{\theta^*}\right)}{1+K_z\ \ \frac{\eta_{fp}K_D\ h}{27\eta_{zp}h_0}\left(4\text{-}\frac{h}{h_0}\right)^3} \quad (3)$$

For zooplankton:

where η_{zp}-Liebig coefficient; K_D – coefficient reflecting the length of the day; θ* – temperature of the proteins, equal to 42^0; h_0 – maximum transparency of the reservoir; h – transparency of the reservoir; τ_m – duration of one shift of the phyto- and zooplankton population; τ – exposure time of a given phyto- and zooplankton population; θ – temperature of the reservoir; C_B – concentration of the limited biogenic substance.

The obtained relationships determine the values of phyto- and zooplankton mass for subsequent periods, which will give us an idea of the eutrophication processes taking place in the reservoir and, accordingly, the changes in the organoleptic (taste, smell, color) characteristics of the water [3]. What is eutrophication?

The increase in the content of biogenic elements in the upper water horizons leads to an increase in the number of phytoplankton and phytoplankton-feeding zooplankton in this zone. As a result, the transparency of the water rarely decreases, the depth of sunlight penetration decreases, and this leads to the death of plants in the lower layer due to a lack of light. Dead organisms sooner or later sink to the bottom of the reservoir, where they decompose. Anaerobic decomposition of dead organisms occurs in the bottom soil deprived of oxygen, with the formation of such strong poisons as phenols and hydrogen sulfide. As a result, the eutrophication process destroys most of the species of flora and fauna of the reservoir, almost destroys the sanitary and hygienic properties of the water, to the point that it is completely unsuitable for swimming and drinking water supply. But for this, it is necessary to calculate the polluting loads on the Aragvi River basin and the Tbilisi Reservoir.

Calculation of pollutant loads

To successfully address this problem, first of all, material was found that provides the characteristics of polluting objects: areas of pastures, hayfields, agricultural fields, and types of crops, the amount of fertilizers applied, livestock and poultry indicators, capacity of enterprises, data on auto farms and other mechanisms in the region, etc. In the process of finding data, a number of violations were identified, including encroachment and unauthorized activities within sanitary protection zones, as a result of which agricultural, household, and industrial runoff enter the water systems. The facts of grazing and watering a large number of livestock in prohibited areas, cases of placement and construction of houses or other objects in the prohibited zone, the absence of a sewage network, malfunctions of the Zhinvali-Tbilisi collector, etc. Based on the obtained data and the above calculation assumptions, the amounts of pollutants entering the Tbilisi Reservoir caused by the main polluting ingredients were determined for various areas of the Aragvi River drainage system, Zhinvali and Tbilisi reservoirs.

Table # 1

№	Indicators	Zhinvali Reservoir	Aragvi River Bulachauri	Aragvi River Natakhtari	Sioni Reservoir
1	Weighted average	1956	796	2921	990
2	Dry residue	1065	1083	1634	547
3	Organic matters	214974	19336	17976	107490
4	Nitrogen total	47024	30486	32792	23360
5	Phosphates	5820	937	1107	2910
6	Potassium	15820	8582	9236	77,25
7	Chlorides	140	39,7	57,7	69,1
8	Oxygen Biochemical demand (BOD)	90254	4950	3651	45127
9	Oxygen chemical demand	261064	19652	25287	130532
10	Surface-active substances	83,4	43,4	58,7	41,9
11	Iron common	7,7	3,6	5,9	3,9
12	Polutant particle number * 10^9	2,35	0,19	0,29	1,18

Note: Tbilisi seawater pollution is mainly formed at the expense of flows from the Zhinvali and Sioni reservoirs. Since the catchment area of the Tbilisi Sea is small, it is clear that the values of polluting loads coming from the environment are not large, although the additional flow of pollution with biogenic elements has a considerable impact on the development of phyto- and zooplankton and macrophytic algae.

From the analysis of the results of the calculations given in the table, it follows that the water of the Aragvi, Zhinvali, and Tbilisi reservoirs is satisfactory in terms of chemical pollutants. In particular, from an ecological point of view, they belong to the class of clean and slightly polluted waters, and are also suitable for water supply to the population.

Above the Zhinvali Reservoir, the pollution from industrial facilities on the Aragvi River, and especially the Pshavi' Aragvi River, is insignificant, which is completely understandable, since industry is practically not developed in these areas.

Pollution caused by agriculture (mainly total nitrogen, phosphates, potassium) in the lower part of the Aragvi River basin is twice as high as the same type of pollution in the Pshavi Aragvi and Aragvi River basins up to the Zhinvali Reservoir, which is explained by the small number of agricultural areas in the upper part of the Aragvi River. We also note that pollution caused by pesticides and toxic chemicals in the lower part of the Aragvi River is practically not observed in the Aragvi river system, which is explained by the episodic and very insignificant introduction of this type of pollutants into the territory of agricultural lands.

Pollution with nitrogen and phosphorus compounds should be distinguished separately, due to their importance. In this case, the following circumstance should be emphasized: although the polluting loads on water systems have decreased to some extent, due to the regulation of the water system and the continuous flow of biogenic elements over the years, favorable conditions have been created for the development of phyto- and zooplankton and macrophytic algae Charophyta, which developed in infiltration basins. Thus, the initial phase of eutrophication of the system has taken place. We note that eutrophication processes have begun for a long time, and there is a tendency for their development, moreover, under certain conditions, its revolutionary development is possible, which can cause irreparable damage to water intake and recreational facilities and the system as a whole.

Main conclusions

The main goal of the study was to improve the water quality of the Tbilisi Sea, primarily according to organoleptic (smell, taste, color) indicators, while maintaining the performance of the headwaters at the appropriate level. The data of hydrobiological observations obtained in various services are not only inadequate, but even the existing individual observations are too superficial and unprofessional in nature; they are practically useless, and it has become necessary to conduct full-fledged observations.

In addition, we believe that, based on the existing data and forecast calculations, the issues of the stability of the system of differential equations describing the water system under study should be investigated in order to prevent deviations greater than those envisaged during the evolutionary development of the system.

Based on numerous studies conducted abroad, measures and recommendations have been developed that will slow down and, with due effort, prevent the processes of eutrophication of the reservoir.

References

1. Voinich-Sianozhensky T.G., Hydrodynamics of River Mouths and Coasts of Non-Tidal Seas. Gidrometizdat, 1972, p. 204.
2. Jorgensen S.E. , Lake System Management. Agroprometizdat, 1985.
3. Henderson-Sellers B., Markland H.R., Dying Lakes. Gidrometizdat, 1990.

1st International Scientific Conference "Modern problems in Geophysics", Proceedings,
ISBN 978-9941-36-434-1, ISSN 3088-4349, Tbilisi, Georgia, November 6-8, 2025

ITALIAN UNDERGROUND GAS STORAGE ACTIVITIES: RISK MANAGEMENT AND SAFETY ASPECTS

***Marrazzo R., **Mazzini C.**

**ISPRA. Via V. Brancati n. 48 – 00144 Roma, Italia*
***ARPAE. P.zza Largo Caduti del Lavoro, 6 – 40122 Bologna*
romualdo.marrazzo@isprambiente.it

Abstract. *The underground storage of natural gas is an industrial process that consists of injecting gas into a depleted underground rock system to ensure its accumulation and subsequently deliver it in a second phase. The scope of the paper is to provide technical support in the safety analysis evaluation of underground natural gas storage establishments, aiming to achieve uniformity of evaluation throughout the national territory, under the Seveso III directive. The main issues concern: Italian law and legal requirements; information about the establishment and the company organizational structure; information on classification of substance under the Seveso directive; industrial safety of the plants, with the relative identification of the critical technical systems; methodological approach for assessing the risk analysis of plants, including the NaTech risk. Some references are finally given to identify the most "critical" parameters of the different techniques for risk analysis, which, if not adequately evaluated, can lead to an incorrect result of the analysis itself, also considering the correct safety measures to prevent or limit the consequences of an accident scenario, and about the proper implementation of the Safety Management System.*

Key words*: Seveso, Underground, Safety, Risk.*

1. Introduction

In the context of technologies aimed at supporting the national energy transition, underground natural gas storage facilities play a crucial role in addressing variable market demands or situations of energy supply shortages. The paper explains the results of technical assessments carried out by the national competent authorities working group, under the D.Lgs. 105/2015, the Italian implementation of the 2012/18/UE directive ("Seveso III"), regarding risk management and safety aspects in underground natural gas storage activities. The scope is to provide technical support in evaluating safety reports for these facilities, aiming to achieve uniformity in assessments throughout the national territory, taking into account plant and site-specific territorial aspects. The paper explains the main contents of the "Guidelines for the safety report evaluation of underground natural gas storage" [1], whose purpose was to have uniform evaluation throughout the national territory of the risk analyses produced.

Depending on the amount of dangerous substances present, establishments under the D.Lgs. 105/2015 are categorised in lower and upper tiers, with different obligations to prevent major accidents and to limit their consequences for human health and the environment. The requirements include, among others: notification of all concerned establishments; deploying a Major Accident Prevention Policy (MAPP) and a Safety Management System (SMS); producing a Safety Report (SR) for upper-tier establishments; producing an Internal Emergency Plan (IEP) for upper-tier establishments; and providing information in case of accidents. In Italy, based on the information in the inventory of establishment notifications, there are about 1.000 Seveso sites. Among these, twelve underground natural gas storage sites operate in four different regions in the central north of the country.

The operating storage sites are depleted gas production sites: natural structures in which gas was trapped and which, once the primary exploitation phase was completed, were converted into storage. These establishments are: surface plants (compressor and treatment units); reservoirs (deposits – natural storage systems); wells (connecting the reservoir with surface plants); interconnecting flow-lines. The activity consists of the storage of natural gas in underground geological structures (injection) and subsequent distribution, according to market demand and to guarantee the "strategic" energy supply in the country. The substances classified as dangerous under D.Lgs. 105/2015 present in these establishments are natural gas, diesel oil, and

methanol. The Italian establishments are upper-tier establishments for the quantities of natural gas held, considering the holdup of the reservoir and the holdup of the surface plants. For underground storage of natural gas, the following additional legal references may apply: the D.Lgs. 624/1996, concerning the safety and health of workers in extractive industries; the DM 17 April 2008, which applies to gas transport pipelines; the DM 17 January 2018, which provide the Italian regulatory indications for constructions, seismic verification and other structural checks (i.e. strong wind and flooding).

In the safety report, the site operator produces a risk assessment with the description of a risk analysis and measures for the prevention of major accident hazards. The Italian competent authority for the evaluation of the safety report carries out the technical evaluation for the safety report with a multidisciplinary approach. The technical evaluation identifies accident scenarios, damage distances and frequencies of occurrence, as well as the safety measures adopted, for External Emergency Planning (EEP) and Land Use Planning (LUP).

2. Guidelines for the safety report evaluation of underground natural gas storage

The guidelines do not introduce new developments, but it is the result of the experience gained over the years at a national level in the evaluation of the Safety Reports of this type of establishment. The specificity of these plants is that the safety of the underground storage is ensured by the production history of the field itself, as the geological covering structures have guaranteed the permanence on site of the gas for millions of years, and it is also managed by creating specific site geo-mechanical models and adopting monitoring techniques.

The main contents of the guidelines are: Information relating to establishment; Establishment classification and verification subject to Seveso directive; Safety of establishment; NaTech risk assessment; Identification of events and accident scenarios; Evaluation of events and scenarios frequency; Calculation of consequences; Safety systems.

3. Safety of Natural Gas Storage Establishments

There are two parameters for the safety assessment of gas reservoirs, considering a depth of 1000-2000 m: the geo-mechanical model for the gas reservoir provides quantitative assessments of the limit pressure with which safe storage can be performed; monitoring of pressure, micro-seismicity and deformation of the soil indicate the maintenance of the state of the gas reservoir in conditions of safety during injection and distribution activity. The well consists of “casing”, steel pipes, and a cement filling. Anomalies with gas leakage that can cause risks are: ineffective seal from the casing cementation of the well; risk of eruption (blowout) of the well, even during maintenance operations.

Flow-lines are connection pipelines, outside the fences of the plants, between the well/cluster areas and the surface plants (compressor units). In Italy, the “methane pipeline” standard establishes the minimum safety distances from residential areas: 100 m for pipelines with maximum operating pressures exceeding 24 bar. Concerning flow-lines, in the safety report, it is therefore important to describe: routes and construction features; interception – blocking – safety systems. Another aspect to be taken into consideration, to correctly evaluate the safety of flow-lines, is the formation of hydrates that could obstruct the pipeline. Hydrates are compounds of molecules of free water and/or condensation in the pipeline and natural gases that crystallize under specific conditions of pressure and temperature. To contrast the formation of hydrates, inhibitors such as methanol or glycol are used to move the stability curve. The evaluation of hydrate formation that can lead to variations in pressure or temperature must be done in all plant conditions (normal operation, shutdown, maintenance activities). It is then necessary to implement a procedure for the formation of hydrates and emergency instructions if the phenomenon occurs.

4. Risk analysis for surface plants and Safety Report evaluation

For the identification of events and consequent accident scenarios, it is possible to refer to the typical techniques as historical experience, what-if analysis, FMEA-FMECA, and HazOp. The analysis develops as: internal historical analysis, identifying causes of accidents, near-misses, anomalies that have occurred inside the plant; external historical analysis of events, which have occurred in similar establishments, through consultation of updated databases (MHIDAS, FACTS, eMARS, etc.); analysis of the historical experience of "delivery points" or "nodes" of the national natural gas distribution network. Care must be taken on reference databases and plant and/or management measures to prevent events or limit their probability and consequences.

The identification of failure rates differs according to complex systems (Fault tree analysis) or "Random" failure of a single component (equipment, systems, pipes). Failure rates are taken from reliability databases (Oreda, EIGIG, HSE, TNO Purple Book, EIGH, etc.): it is important to show that the data are representative of the specific plant and that the chosen failure rates can be considered conservative. In underground gas storage plants, the random failure of the pipes is the basis (Top-Event) of the most significant events (more extensive damage areas). In the case of above-ground pipes [2], the guidelines make a comparison between databases (HSE Failure Rate/TNO Purple Book 2005), giving general frequency values for pipe failure in a range of 10-5 – 10-7 occ/y*m [3]. For buried pipes, an important reference is the European Gas Pipeline Incident Data Group (EGIG) Report [4]. The guidelines suggest, however, that failure frequencies indicated in the EGIG Report can be taken as a reference for natural gas pipes (buried or not buried, even within establishments) [5]. Final consideration must be made on the incidence of the different failure causes in frequency. For example, the CONCAWE Report identifies the percentage of failure causes for buried pipes carrying hot or cold petroleum products (2011-2016 period) as below: corrosion (90% – hot products; 20% cold products), operational errors (10% – cold), and mechanical causes (20% – cold) [6].

The reduction of occurrence frequencies through an integrated analysis that combines risk analysis with the Safety Management System (SMS) allows the quantification of the positive effects of the system in order to prevent major accidents. If an inspection plan of equipment and pipes based on risk analysis has been prepared, its effectiveness in preparing an integrated analysis can be considered in order to reduce the frequency of accidents. The use of methodologies for the drafting of a risk-based inspection plan, such as the API 581: 2016 standard, is suggested. If this standard is used improperly and partially (e.g., considering in a generic way only SMS procedures), the results that are obtained will be wrong, because there will be a reduction by at least one order of magnitude of the general frequencies of equipment and pipe failure. These methodologies allow the reduction of the top frequencies for complex systems – Fault Tree Analysis [7], and specifically for random pipe failures [8]. Taking for example, the parameter "external corrosion", the quantification of this reduction is obtained by applying the methods indicated [9]. For the calculation of scenario frequency using the event tree [2], it is finally important to remember that the trigger probability values (immediate or delayed triggering) must be pertinent to the plant reality or cautiously estimated in favor of safety [10].

It is necessary to model the physical phenomena of methane release in high-pressure conditions. These are the release phases: Phase 1: expansion from the initial pressure to the hole pressure; Phase 2: expansion up to atmospheric pressure; Phase 3: initial dilution. The methane released is in supercritical conditions, that is, a fluid is at a temperature and pressure higher than the critical ones (no distinction between gaseous and liquid phase). The properties are intermediate between those of a gas and a liquid, and its density can be greater than that of gases under ordinary conditions. The density of methane proportionally affects the release rate, and therefore, the gas release rate must be calculated considering the gas density in supercritical conditions. The possible accident scenarios in case of methane release in the conditions stated above are: Flash Fire. Fire of a flammable gas cloud that disperses into the atmosphere as a light neutral gas; the factors that affect modelling are density, weather conditions, release duration, cloud dilution, and roughness. In case of interception systems, the duration of the release and the quantity released will be less: the frequency of the flash fire scenario could be reduced, as the smaller cloud is less likely to run to a trigger source. Therefore, the intervention times assumed must be consistent with the emergency procedures and be verified through field inspections; Jet Fire. The release of a pressurized gas with immediate ignition and fire of a cloud; the factors that affect modelling are gas density, jet direction, and release flow rate. Jet fire damage areas are normally included within the damaged areas for the corresponding flash fire scenarios: they must be considered especially for the purposes of evaluating a possible domino effect, Vapour Cloud Explosion (VCE). It occurs when a confinement of the mass of flammable vapors is mixed with air at the moment of ignition. It is necessary to assess whether the air/natural gas mixture can fall within the flammability range, calculating the amount of flammable mixture between LFL (Lower Flammability Limit) and UFL (Upper Flammability Limit). Conditions that facilitate the occurrence of a VCE are releases in areas with a high degree of confinement or in closed environments. The verification of the computational models chosen for the estimation of the consequences must be adequate to the physical phenomenon reality: some models do not consider the "supercritical conditions" of methane. Some software does not automatically consider the initial expansion and dilution of the methane jet. It is therefore necessary to apply a dilution factor to the release range (approximately 1/10): the value of the recalculated flow must be used as input data to any Gaussian dispersion model, since for this model the gas concentration is directly proportional to the release flow.

The main prevention and protection measures aimed at reducing the frequency and/or extent of the consequences of accident events are: Locking systems to make plants safe (ESD – Emergency Shut Down: closing of all the plant sectioning valves and opening of the blow down valves with the consequent depressurization of the system; PSD – Process Shut Down: production shutdown by closing the sectioning valves (SDV) and securing the unit; LSD – Local Shut Down: blocking and securing of the unit, or interception and stopping of the single equipment); Fire prevention measures and systems.

Finally, a numerical example can be useful to understand the conditions of use of commercial computational models for the study of the consequences in case of supercritical conditions of methane releases. A flash fire, caused by failure of a natural gas pipe (152 mm hole) at an operating pressure of 140 bar (top-event), was developed through geo-referencing of the consequence evaluation. The calculation was carried out under the following weather conditions in the area: atmospheric stability class of Pasquill D5 (neutral) with a wind speed of 5 m/s. The damage distances resulting are 284.91 m (corresponding to "LFL" threshold) and 435.88 m (corresponding to "1/2 LFL" threshold).

5. Conclusions

Underground natural gas storage establishments use depleted fields as a natural reservoir to store gas and therefore constitute strategic energy reserves. The purpose of the document is to provide technical support with reference to the evaluation of the Safety Reports of the underground natural gas storage establishments, to pursue greater uniformity of assessment throughout the national territory. Although each installation may present strictly site-specific plant and territorial aspects, there are nonetheless elements that unite all installations. The "Guidelines for the safety report evaluation of underground natural gas storage" provide specific indications and insights to support and direct the activities related to the assessment of the risks of a major accident. Legislative Decree 105/15 defines criteria, data, references, information for the preparation of the Safety Report and assigns the manager the task of identifying the dangers of major accidents and measures; consequently, it is up to the manager to choose the methodology to be used for the systematic identification of accidents, the evaluation of probability/frequencies and the calculation of the consequences, since this methodology must be justified and technically justified in the Safety Report. Instead, the competent Authority is responsible for "ensuring that the description of each scenario, complete with supporting evidence, is formulated in such a way as to highlight the consistency between the identified scenario and the measures taken". The approach used for drafting the guidelines initially envisaged the search for the references of technical regulations applicable to underground gas storage, including an overview of the approaches adopted in some European countries for the assessment of the risk of a major accident; subsequently, the problems relating to the reservoir and wells were examined, to finish with an in-depth study of the peculiar characteristics of the surface plants, considering the related safety aspects concerning major accidents, including the NaTech because of the extension of these establishments over large areas subject to extreme weather events.

References

1. Marrazzo R., Mazzini C., 2023, Risk Management and Safety Aspects in Italian Underground Gas Storage Activities, Chemical Engineering Transactions, 105, 475-480.
2. Uijt de Haag P., Ale B., 2005, TNO, Committee for the Prevention of Disasters, CPR, doc CPR 18 E, "Guidelines for quantitative risk assessment – Purple Book".
3. Keeley D., 2008, HSE, Research Report RR671 "Failure rates for underground gas storage".
4. Dröge M., Kenter R., 2018, EGIG, Doc. number VA 17.R.0395, European Gas Pipeline Incident Data Group, "10th Report of the European Gas Pipeline Incident Data Group (period 1970 – 2016)".
5. van Vliet A., Gooijer L., Laheij G., 2011, RIVM, Report 620550004/2011, "On-site natural gas piping – scenarios and failure frequencies".
6. Cech M., Davis P., Gambardella F., Haskamp A., 2018, CONCAWE, Report No. 6/18, "Performance of European cross-country oil pipelines – Statistical summary of reported spillages in 2016 and since 1971".
7. Bellamy L., Papazoglou l., Hale A., Aneziris O., Ale B., Morris M., Joy I., 2000, "I-RISK: A quantified integrated technical and Management risk control and monitoring methodology", EC, EUR-19320.
8. Milazzo et al., 2010, "The Influence of Risk Prevention Measures on the Frequency of Failure of Piping", International Journal of Performability Enineering, Vol.6.
9. Goodfellow et al., 2018, "UKOPA Pipeline Product Loss Incidents and Faults Report (1962 – 2016)", Report Number: UKOPA/17/002, Issue: 1.1.
10. Spencer et al., 1997, "Ignition Probability of Flammable Gases (Phase1)", HSE Contractor Report RSU8000/081, HSE Books.

1st International Scientific Conference "Modern problems in Geophysics", Proceedings,
ISBN 978-9941-36-434-1, ISSN 3088-4349, Tbilisi, Georgia, November 6-8, 2025

APPLICATION OF STABLE ISOTOPES IN THE STUDY OF WATER RESOURCES AND SEDIMENTATION PROCESSES

[*]Melikadze G., [*]Todadze M., [*]Tsutskiridze E., [*]Chikviladze E., [*]Kapanadze N.

[*]M. Nodia Institute of Geophysics of the I. Javakhishvili Tbilisi State University, Georgia,
1, Aleksidze str., 0160, Tbilisi, Georgia.
melikadze@gmail.com

Abstract. *Understanding the groundwater regime, the interaction between surface water and groundwater, and the factors that influence these processes requires a deeper knowledge of groundwater recharge to prevent overexploitation and further deterioration of resources. Nationwide isotope studies provide critical insights that were previously unavailable in the country, limiting advances in understanding the water cycle and effective water management. The method primarily focuses on stable isotopes of water molecules (^{18}O, ^{2}H, ^{3}H, etc.) as tracers of water origin and movement, offering information that cannot be obtained through conventional techniques. These include the residence time of groundwater, the elevation of recharge zones, the contribution of snowmelt to rivers and operational wells, and the identification of paleowaters formed under past climatic conditions. Isotopic analyses also help determine groundwater origin, flow pathways, and possible contamination sources, thereby contributing to the sustainable assessment and protection of groundwater resources.*

Key words: *Stable isotopes, Mean transit time.*

Introduction

Understanding the groundwater regime, the interaction between surface and groundwater, and the factors influencing their quantity and quality are crucial for ensuring a safe water supply for the population. Deepening our understanding of groundwater recharge is essential to prevent overexploitation of resources and deterioration of the current situation. The method primarily utilizes stable isotopes (^{18}O, ^{2}H) as tracers to study the origin and movement of water. These isotopes provide insights into various processes such as the movement of water in underground horizons, the source of underground water, the contribution of snowmelt water to rivers or operational wells, and the identification of ancient waters formed under past climate conditions. Isotopes also help trace the origin of groundwater and pathways of contamination, facilitating the assessment and protection of groundwater resources sedimentation process. These studies have been emphasized in recent projects conducted in central and eastern Georgia, with direct involvement from this scientific group.

The research mentioned below received significant support from the International Atomic Energy Agency (IAEA), which funded several projects (GEO7001; GEO7002). This support included the provision of equipment and training for project staff. The equipment provided by the IAEA will also be utilized in the current project.

Methods

To assess groundwater resources and sedimentation process, understand the impact of climate change on their dynamics, it's essential to observe the entire natural water cycle using stable isotopes. This includes studying glaciers and snowmelt waters, monitoring atmospheric precipitation, and examining surface and deep groundwater across the entire region.

For this purpose, monthly isotope measurements were conducted at eight meteorological stations, four river monitoring stations of the Environmental Agency of the Ministry of Agriculture and Environmental Protection. They are part of the Global Network of Isotopes in Precipitation and Rivers (GNIR) encompasses the Rioni (Ambrolauri), Mtkvari (Tbilisi), and Alazani (Telavi) stations. In parallel, the ecological monitoring network of the Geological Department includes 34 observation wells and 6 springs (Fig. 1).

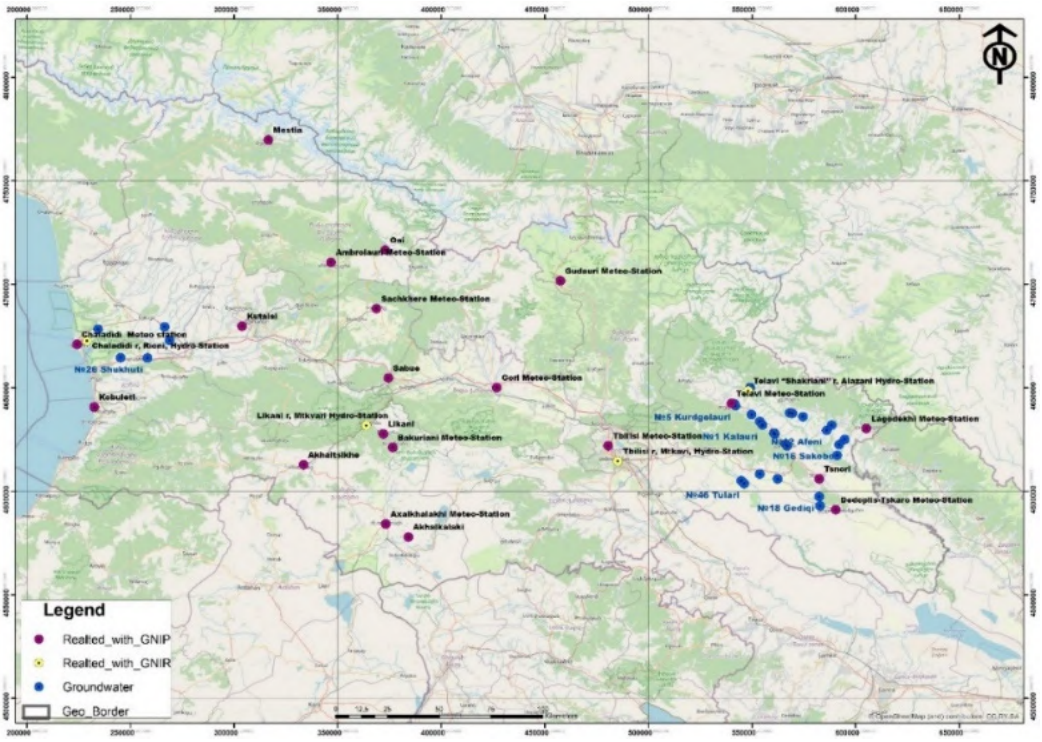

Fig. 1. Location monitoring stations.

The data collected will be utilized to analyze the temporal variation of stable isotopes and geochemical parameters, including background values, seasonality trends, etc.

As noted above, an important parameter of watershed hydrological behavior is the time lag between precipitation input and its subsequent discharge into the river. This parameter, known as the mean transit time (M T, or mean transit time), was first conceptualized in the 1980s [1–3].

A clear pattern is observed in the isotopic data: atmospheric precipitation is characterized by the lightest, or "youngest," isotopic composition. As water contributes to river discharge and moves downstream, its isotopic signature becomes progressively "heavier," reflecting mixing and flow pathways within the watershed. This shift provides valuable insight into the direction and dynamics of water flow.

Based on these indicators, it is possible to estimate the "travel time" of water flow within the catchment. This is achieved through comparative analysis of isotopic compositions. Specifically, the isotopic signature of atmospheric precipitation recorded at a meteorological station can be compared with that of river water at a gauging station or with groundwater sampled from observation wells in the study area (Fig. 2, Fig. 3).

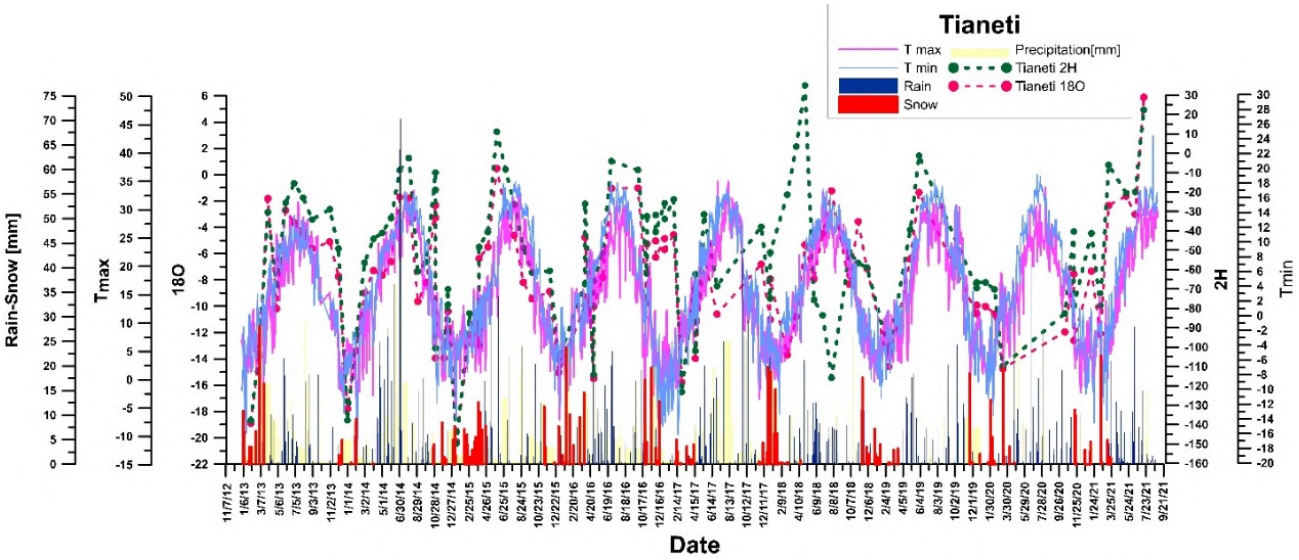

Fig. 2. Parameter variations at Tianeti Meteorological Station.

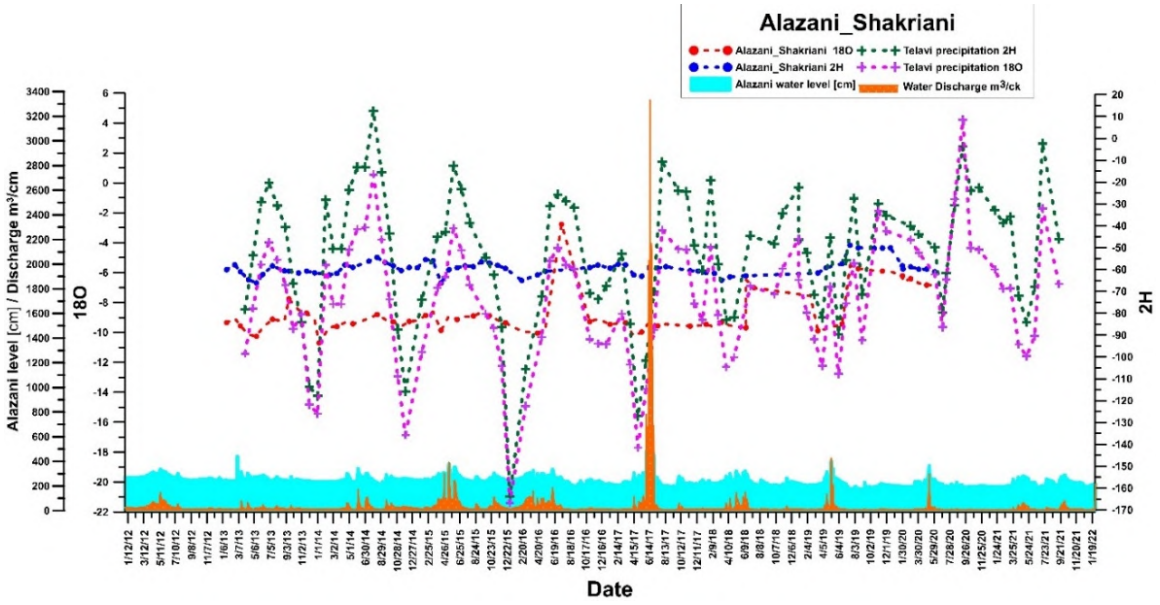

Fig. 3. Variations of parameters at Shakryani Station.

To estimate the mean transit time of groundwater, the "sinusoidal curve method" based on an exponential model was applied. Sinusoidal curves were constructed using isotopic data from individual stations, and comparative analysis was performed. Specifically, the isotopic composition of precipitation at the Tianeti station was compared with that of river water at the Shakryani station (near Telavi). The Tianeti station is located at a higher elevation within the Alazani River catchment, providing a representative input for upstream precipitation (Fig. 4).

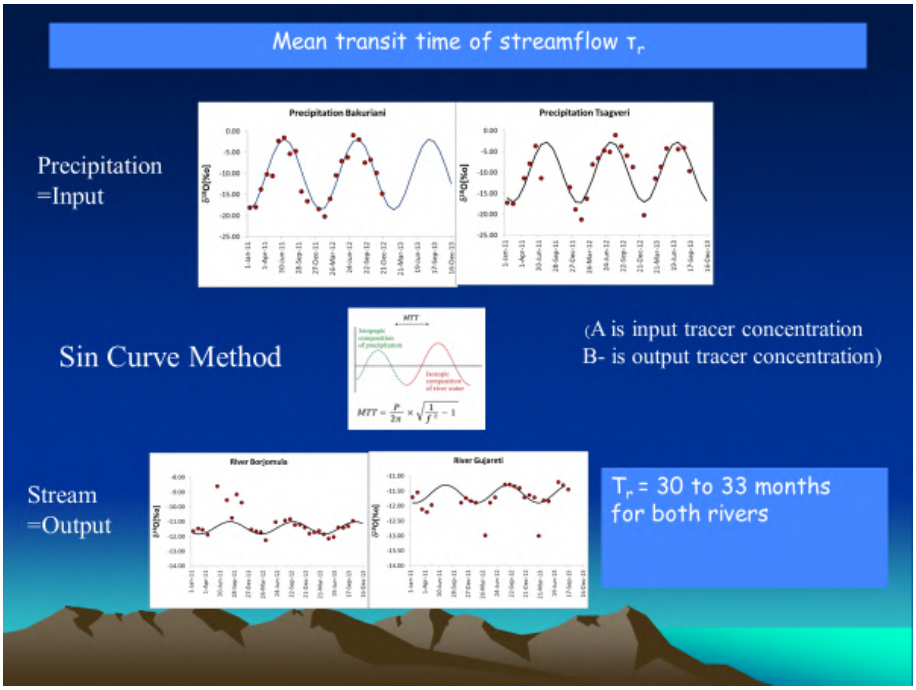

Fig. 4. Sinusoidal variation of monthly precipitation isotopes at Tianeti Station and monthly isotopes in the Alazani River.

To estimate the travel time of water, the average isotopic composition of precipitation at the Tianeti station was used as the "input" data, while the isotopic composition of the Alazani River near Shakhrani was used as the "output" data. The relationship between input and output was determined using the following diagram and formula (Fig. 4):

Where **P** is the period of the sinusoidal input (e.g., 12 months for annual variations), f = B / A, where A is – isotopic value of precipitation and B is – isotopic value of river water

Using this sinusoidal wave method, the travel time of water – from infiltration into the soil at Tianeti to its discharge into the Alazani River near Shakhrani – was estimated to be approximately one month.

Conclusion

For the first time in Georgia, this study analyzes the spatial and temporal variations of stable oxygen and hydrogen isotopes in atmospheric precipitation and river runoff. Most of the data is included in the global database. Examining these variations and their distribution patterns allows for the determination of groundwater genesis, flow direction, and intensity.

References

1. Kirchner, J., Aggregation in environmental systems -Part 1; Seasonal tracer cycles quantify young water fractions, but not mean transit times, in spatially heterogeneous catchments. // Hydrol. Earth Syst. Sci., 20, 2016, pp. 279-297. doi:10.5194/hess-20-279-2016.
2. Maloszewski, P., Zuber, A., Determining the turnover time of groundwater systems with the aid of environmental tracers, 1. Models and Their Applicability. Journal of Hydrology, 57, 1982, pp. 207–231.
3. McGuire, K. J., McDonnell, J. J., A review and evaluation of catchment transit time modeling, J. Hydrol., 330, 2006, pp. 543–563.

1st International Scientific Conference "Modern problems in Geophysics", Proceedings,
ISBN 978-9941-36-434-1, ISSN 3088-4349, Tbilisi, Georgia, November 6-8, 2025

CARBON REGULATION: EXPERIENCE IN DIFFERENT COUNTRIES AND RUSSIAN INITIATIVES

Kerimov I., Alieva Zh.

Grozny State Petroleum Technological University named after Academician M.D. Millionshchikov
ibragim_kerimov@mail.ru

Abstract: *Challenges arising from global trends in climate policy highlight the need for further development of strategies and measures to combat global climate change. This study examines the functioning of greenhouse gas emissions trading mechanisms and the development of carbon regulation in individual countries, as well as the development of national carbon regulation and legislative measures for the functioning of the carbon market in Russia. Research on this topic can contribute to understanding and addressing the challenges facing the modern world in the context of prolonged environmental instability.*

Key words: *carbon tax, greenhouse gases, carbon footprint, climate change, air pollution.*

Climate change remains one of the most serious global challenges facing the world today, causing ever-increasing climate cataclysms and threatening ecosystem destruction. A carbon tax offers a promising tool for creating incentives for environmental compliance both at the global level and at the level of individual small producers.

The relevance of this study is clear: the topic of a carbon tax intertwines with many important areas of life: from the global problem of climate change to economic justice, international trade, and national development in general.

Reducing emissions of greenhouse gases that contribute to global warming, such as carbon dioxide and methane, is crucial to addressing climate change. However, despite the barrage of climate commitments, global greenhouse gas emissions continue to rise, reaching 36.05 billion metric tons of CO_2 in 2023. By the end of 2024, emissions are projected to increase by 0.92%, reaching a record high of 37.42 billion metric tons of CO_2. Since 2000, CO_2 emissions have increased by more than 10% (Fig. 1).

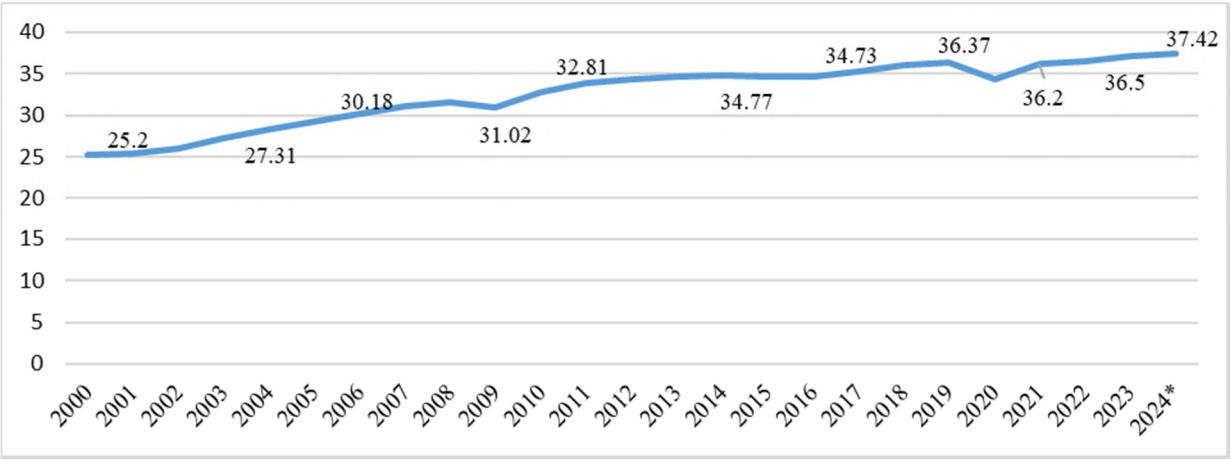

Fig. 1. Annual carbon dioxide emissions in the world from 2000-2024, billion m.t.

China is the largest contributor to greenhouse gas emissions. In 2023, China accounted for 30% of global greenhouse gas emissions, making it the world's largest emitter. It is followed by the United States and India. Together, these three countries accounted for approximately half of the greenhouse gases emitted in 2023 (Fig. 2).

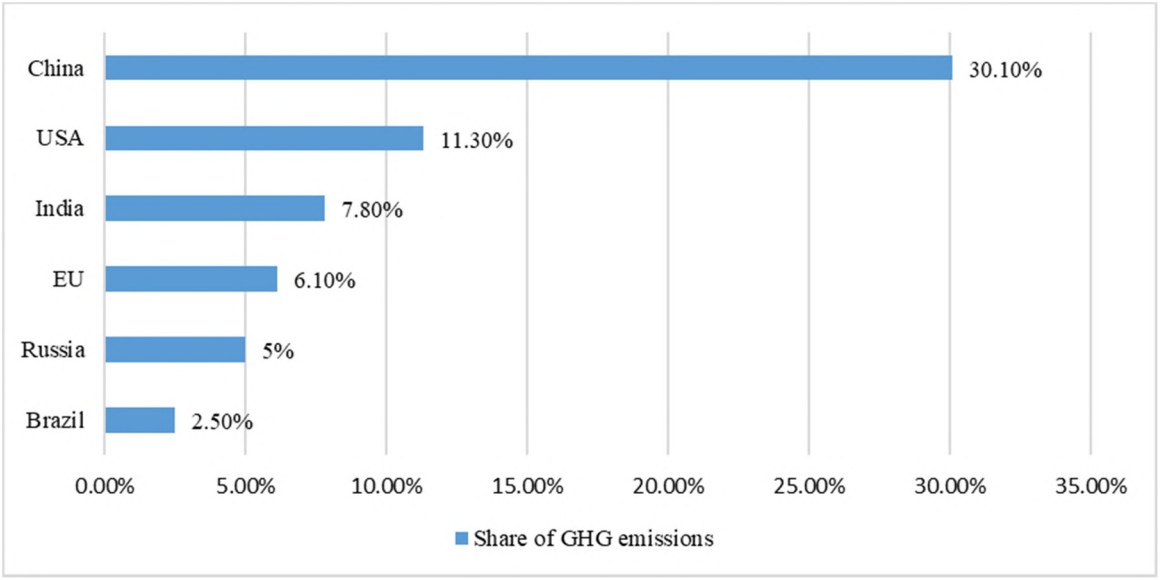

Fig. 2. Distribution of greenhouse gas emissions in the world in 2023, broken down by main emitters, %

Many countries are actively implementing new green regulatory tools. Examples include bans or phase-outs of polluting production processes, reforms to green technology subsidies, carbon taxes, new green product and fuel standards, and mandatory disclosure of information on climate change risks and corporate sustainability performance.

In 2019, the European Commission launched a new climate strategy – the European Green Deal. The core idea of this strategy is resource efficiency to mitigate climate change, halt biodiversity loss, and reduce pollution. The strategy sets the goal of achieving carbon neutrality by 2050. One component of this initiative is the European Border Carbon Tax (CBAM), which is intended not only to incentivize exporting countries to reduce the carbon intensity of their products but also to ensure that European producers do not lose their competitive advantages due to extensive climate regulation in the European Union and the lack thereof in other countries. Of course, there are many obstacles to its implementation, including whether it will actually significantly reduce carbon leakage, how other countries will respond, and whether the tax is the most effective way to reduce greenhouse gas emissions in other countries.

Discussions around carbon standards continue internationally. Since most countries have yet to fulfill their climate commitments, efforts to find a new international economic framework continue.

The COP29 climate summit, held in Baku, the capital of Azerbaijan, in November 2024, marked a significant milestone in global efforts to mitigate climate change and implement the Paris Agreement. Summit participants, including scientists, government leaders, environmentalists, and business representtatives, addressed a range of issues related to reducing greenhouse gas emissions, adapting to climate change, and securing financing for sustainable environmental projects. Key decisions at the summit included strengthening cooperation on financing climate action in developing countries. A joint decision was made to allocate $300 billion annually to developing countries for the global fight against climate change, with total climate financing expected to reach at least $1.3 trillion by 2035. The decisions and initiatives adopted at the summit will lay the foundation for countries' subsequent efforts to achieve carbon neutrality [1,2].

Currently, more than 60 countries are planning to introduce or have introduced carbon taxes.

Carbon regulation has a history of continually transforming government regulatory mechanisms, with positive effects from reducing greenhouse gas emissions being observed. The emissions trading scheme, launched in 2005 in the European Union, is the first successful example, and is currently the largest in terms of greenhouse gas emitters. Approximately 4% of global greenhouse gas emissions and almost half of all emissions from the energy, industrial, and air cargo sectors of the economies of countries within the European Economic Area are traded through the emissions trading market [3].

In addition to the EU Emissions Trading System (EU ETS), national or subnational systems are already in place or under development in Canada, China, the United Kingdom, New Zealand, South Korea and Switzerland, among others (Tab.1).

Table 1. Greenhouse gas emissions trading systems in different countries (as of the end of 2023)

No.	Countries	Emissions million CO_2- eq.	Reducing greenhouse gas emissions by 2030	Net zero emissions	Emissions trading systems million CO_2- eq.	Coverage of the emissions trading system	Price in STV, $
1.	European Union	3 400	55%	by 2050	1 500	39%	66
2.	Switzerland	45,2	50%	by 2050	5,5	12%	61
3.	United Kingdom	429,5	68%	by 2050	92,1	25%	44,5
4.	Canada	77,6	-37.5%	by 2050	51,6	80%	33
5.	Republic of Korea	676,6 .	40%	by 2050	547,9	89%	6,8
6.	New Zealand	79,8 .	50%	by 2050	27,9	48%	39,8
7.	China	12 000	–	by 2060	12 000	49%	8

Today, the need to reduce CO_2 emissions is clear to all economically developed countries. The decarbonization of industrial processes has been launched worldwide, and Russia cannot remain on the sidelines of this process.

The Russian Federation has been making significant efforts to create a hydrocarbon market for several years, but the mechanism has not yet been fully developed. In line with its announced climate commitments, Russia has declared its readiness to take measures to combat climate change and intends to become carbon neutral by 2060. To achieve this goal, Russia is developing a greenhouse gas emissions monitoring system. In the near future, it is expected that the state will participate in the creation of a trading platform, the main participants of which will be large energy consuming companies and non-residents conducting economic activity in Russia. The correct distribution of emission quotas is the greatest challenge for the carbon market. When formulating the climate agenda in the Russian Federation, it is necessary to pay attention to the country's natural resources.

In order to implement the adopted commitments, on November 4, 2020, the President of the Russian Federation signed Decree No. 666 "On the reduction of greenhouse gas emissions" [5,6]. The Government of the Russian Federation also developed a Strategy for the socio-economic development of the Russian Federation with low greenhouse gas emissions until 2050 [4].

Climate policy in Russia has gained momentum since the beginning of 2021, with discussions underway on a draft climate strategy with several scenarios for achieving carbon neutrality. Starting in 2022, many of Russia's largest enterprises with CO_2 equivalent emissions exceeding 150,000 tonnes will submit carbon reporting to the government. This year, companies with emissions of 50,000 tonnes or more have also joined this process.

The government is developing a Russian version of the EU carbon tax. The key objective is to develop national regulations, achieve international recognition, and ensure that payments for CO2 emissions in Russia are offset by the European carbon control system [1].

Russia intends to significantly reduce its carbon footprint through technological innovation, but how this will be achieved in the current environment remains unclear. Previously, Russia purchased most of its machinery, equipment, and other technological advances from the EU or China, but due to sanctions imposed in most sectors, trade has stalled, meaning its carbon management strategy will need to be reconsidered.

We can see the significant importance of carbon regulation today for all countries worldwide, and one of the key tools for reducing the negative impact on the environment is undoubtedly cross-border carbon regulation (hereinafter referred to as CBR), which includes carbon taxation mechanisms. The purpose of such taxes is to establish a price for carbon on goods and services imported from countries with less stringent environmental standards. Currently, rules for implementing the cross-border carbon regulation system during its transition phase have already been approved. This phase began on October 1, 2024, and will last until the end of 2025. Consequently, until the end of 2025, suppliers exporting to the EU will not have to pay a carbon tax on cement, steel, fertilizers, aluminum, hydrogen, and electricity. Suppliers of these goods will only be required to declare them and submit reports. It is expected that over the next two years, the information collected in this way will help improve the system and move on to the main stage of the program – paying additional taxes on the supply of “dirty” products to Europe.

The implementation of a cross-border carbon tax undoubtedly implies close international cooperation, aimed at avoiding trade conflicts and ensuring coordinated measures to combat climate change. The essence of this tax mechanism is that the more carbon emissions a company emits into the atmosphere, the more taxes it pays. This provides an economic incentive for companies to transition to more environmentally friendly solutions.

It should be remembered that the introduction of a cross-border carbon tax will have varying consequences for both importing and exporting countries. And, of course, these consequences can be both positive and negative. A cross-border carbon tax is a new reality, a new standard that all countries will have to face [5].

Based on successful examples of carbon taxes, it's clear that their effective implementation can lead to significant emissions reductions, stimulate economic growth in the green sector, and achieve climate goals. However, without considering the social and economic consequences, and without effective mechanisms to mitigate the negative impacts on the population, it can lead to negative socioeconomic consequences. Therefore, a comprehensive and differentiated approach to carbon tax implementation is needed, tailored to the specific circumstances of each country. Policymakers and governments must take into account these lessons learned and adapt their strategies to overcome challenges and achieve sustainable results.

Given the important role of the BRICS countries as major industrialized nations in global climate action, it is crucial to ensure alignment between climate policy and national socioeconomic commitments, while also taking into account the interests of developing countries and least developed countries.

The Russian Federation, taking into account its national development priorities, must develop its own approach to climate change. It is essential to take targeted measures to encourage the use of the latest developments in eco-friendly design, planning, and operation of facilities whose operations may have the greatest negative impact on the environment, including carbon dioxide emissions. The fact that some Russian enterprises and pilot regions have begun to focus on sustainable development and environmental aspects will soon become a larger and more systemic phenomenon, which will enhance the long-term competitiveness of domestic industry.

The review revealed that the planned cross-border regulatory mechanism is not without its shortcomings, but these will be adjusted as it is implemented. It is important for Russia to take a constructive stance and participate in joint final decisions, taking into account its national interests. At the same time, it is hoped that the current risks and uncertainties will be transformed into growth opportunities for Russian business and the economy as a whole.

Currently, Russia's joint efforts with other countries, including the BRICS countries, in implementing climate and environmental goals will enable it to successfully achieve its objectives of reducing greenhouse gas emissions and transitioning to sustainable development. It is important for Russia to actively participate in international initiatives and agreements aimed at combating climate change and to adapt its domestic regulatory mechanisms to international standards.

References

1. Zandraev, A. A. Introduction of a carbon tax as an instrument of transboundary carbon regulation: prospects and risks for Russia / A. A. Zandraev // Education and Science: Proceedings of the National Scientific and Practical Conference, Ulan-Ude, April 10–14, 2023. – Ulan-Ude: East Siberian State University of Technology and Management, 2023, pp. 93-95.
2. Results of the COP29 climate summit in Baku. URL: https://ecosphere.press/2024/11/25/itogi-klimaticheskogo-sammita-cop29-v-baku/
3. Review of global carbon regulation practices. URL: https://assets.ey.com/content/dam/ey-sites/ey-com/ru_kz/topics/climate-change/ey-carbon-regulation-ru.pdf
4. Order of the Government of the Russian Federation of October 29, 2021 No. 3052-r "On approval of the Strategy for the socio-economic development of the Russian Federation with low greenhouse gas emissions until 2050." URL: http://government.ru/docs/all/137358/
5. Comparative analysis of the efficiency of carbon market mechanisms and carbon tax for achieving the goals of global carbon footprint reduction / E. B. Zavyalova, C. Li // Bulletin of Peoples' Friendship University of Russia. Series: Economics. – 2023. – Vol. 31, No. 4. – P. 740-759.
6. Decree of the President of the Russian Federation of November 4, 2020 No. 666 “On the Reduction of Greenhouse Gas Emissions.” URL: http://publication.pravo.gov.ru/Document/View/0001202011040008).

1st International Scientific Conference "Modern problems in Geophysics", Proceedings,
ISBN 978-9941-36-434-1, ISSN 3088-4349, Tbilisi, Georgia, November 6-8, 2025

UNIFIED DATABASE OF GEORGIAN GLACIERS

***Kordzakhia G. I. , *Shengelia L. D., **Tvauri G. A. ***, Guliashvili G. A., ***Dzadzamia M. Sh.**

**Institute of Hydrometeorology of the Technical University (Tbilisi, Georgia),*
***I.Javakhishvili Tbilisi State University, E.Andronikashvili Institute of Physics (Tbilisi, Georgia)*
****National Environmental Agency, Tbilisi, Georgia*
Contact details of the corresponding author:
1giakordzakhia@gmail.com

Absract. *The* Georgian Glaciers *database integrates historical records from the* Catalog of Glaciers of the Former Soviet Union *(hereinafter referred to as the Catalog), topographic maps from the 1960s, and satellite remote sensing (SRS) imagery acquired in 2010 (SRS-1), 2015 (SRS-2), and 2020 (SRS-3). These datasets include imagery from Landsat 5, 7, and 8 satellites (15–30 m resolution) and the commercial Azercosmos satellite SPOT 6 (1–1.5 m resolution). All data are archived at the Institute of Hydrometeorology, Georgian Technical University.*

Key words*: Georgian Glaciers, Glacier Catalog, Satellite Remote Sensing, Topographic Maps, Glacier Database*

Introduction

Global open-access glacier databases often contain inaccuracies in preserved glacier contours. To address this, overlaying elevation data derived from satellite imagery and digital terrain models, supplemented by expert analysis, conducted contour refinement. High-resolution 3D imagery enabled precise delineation of watershed boundaries – an essential step for accurate glacier mapping.

Historical inconsistencies were identified in the original Catalog, which were corrected by comparing glacier outlines from SRS data with those depicted on classified Soviet-era topographic maps (scale 1:50,000). These maps, originally compiled for military use, were unavailable to the public during the 20th century.

As part of an international initiative aligned with the GLIMS (Global Land Ice Measurements from Space) methodology, glacier boundaries were manually digitized. For each period, key parameters were extracted from the Catalog, including glacier area, morphological type, orientation, length, minimum and maximum elevation, firn line altitude, and ablation zone extent.

Glaciers were categorized by area into: 1. **Small**: 0.1–0.5 km² (green), 2. **Medium**: 0.5–2.0 km² (gray) and 3.**Large**: >2.0 km² (blue).

Additionally, **snowfields** (**extinct glaciers** (red) were identified. Snowfields – composed of snow, firn, and ice – typically form in sheltered areas and may represent remnants of glacier degradation. Due to their limited size, snowfields were excluded from detailed analysis.

Glacier Attribute Table Structure

The *Georgian Glaciers* database is organized into structured tables that document glacier characteristics across the glacial basins of Western and Eastern Georgia. Each table is divided into **eight thematic blocks**, representing key physical attributes: 1. Area, 2. Morphological type, 3. General exposure, 4. Maximum length, 5. Minimum height, 6. Maximum height, 7. Firn line elevation, 8. Ablation area.

These blocks are preceded by **three universal identifiers**:

- **Ordinal Number**: Sequential index within the table
- **Glacier Name / Local Number**: As recorded in the Catalogue or assigned in the first glacier catalogue compiled by K.I. Podozersky (1911) [1]
- **WGI ID**: A 12-character identification code from the World Glacier Inventory

Column Structure

Each thematic block contains **10 columns**, designed for comparative analysis across multiple data sources:

No	Description
1	Glacier ID from the Catalogue Scheme
2	Glacier attribute value from the Catalogue (corrected value shown after a slanted line in the Area block)
3	Glacier ID from Topographic Map (highlighted in brown)
4	Attribute value from Topographic Map
5	Glacier ID from SRS-1 (highlighted in brown)
6	Attribute value from SRS-1
7	Glacier ID from SRS-2 (highlighted in brown)
8	Attribute value from SRS-2
9	Glacier ID from SRS-3 (highlighted in brown)
10	Attribute value from SRS-3

This tabular format provides a clear and user-friendly interface for comparing glacier characteristics across historical and satellite datasets. All satellite-derived attributes were processed using **GIS (Geographic Information Systems)** technologies.

Each block consists of 10 columns. The columns contain: 1. Glacier ”According to the Catalog Scheme No.”; 2. The value of the glacier characteristic corresponding to the block name ”According to the Catalog” (the corrected value according to the topographic map is indicated after the slanted line in the area block); 3. Glacier ”According to the Topographic Map No.” (the column is highlighted in brown); 4. The value of the glacier characteristic corresponding to the block name “According to the Topographic Map; 5. Glacier ”According to the Topographic Map No. 1” (the column is highlighted in brown); 6. The value of the glacier characteristic corresponding to the block name “According to the Topographic Map No. 1”; 7. Glacier ”According to the Topographic Map No. 2” (the column is highlighted in brown); 8. The value of the glacier characteristic corresponding to the block name ”According to SRS 2”; 9. Glacier ”According to SRS 3” (column highlighted in brown); 10. The value of the glacier characteristic corresponding to the block name ”According to SRS 3”. Such a distribution is visible and convenient for the user. Using SRS, all characteristics of the glacier are determined using GIS (Geo-Information Systems) technologies.

ID WGI consists of 12 characters. The World Catalog Identification Code consists of 12 characters. For example: SU4G09301009 and SU4G08012096. The meaning of the character according to the order (position) is discussed below:

1 and 2 – SU means that the glacier is located in the former Soviet Union;

3 – The glacier is located in Europe (4) or Asia (5). In our case, we have the symbol 4.

4 – Indicates the location of a glacier within a certain river basin. For Asia The symbols are A, B, C, D, E, F, T, V, X, and For Europe – C, E, X, Y, H, G. Let's decipher the symbols of the basins of the glacial rivers of Georgia from the symbols: from the symbols of the rivers of Asia, the symbol T means the rivers of the Black Sea basin, which flow from the southern slopes of the Caucasus, and from the symbols of the rivers of Europe, the symbol G indicates that the glacier is located in the Tergi Basin;

5 and 6 are symbols of the glacier name and correspond to the volume number of the catalog, which in turn corresponds to the volume number of the “Catalog of Surface River Resources of the USSR” (20 volumes in total). The glaciers of Georgia are presented in volumes 8 and 9.

7 – is the symbol for the name of the glacier and corresponds to the issue number of the catalog volume. Each volume has no more than 7 issues, and if the volume has only one issue, the 7th symbol is 0;

8 and 9 – are symbols of the name of the glacier and correspond to the part of the release. There can be a total of 21 parts in a release, and if the release has only 1 part, 00 is written.

10, 11 and 12 – are symbols for the glacier name and correspond to the glacier number in the catalog section. There can be from 4 to 996 glaciers in a section.

For clarity, let's decode the identification code of the SU4G09301009 glacier in WGI:

1. SU – The glacier is located in the former Soviet Union.
2. 4 – The glacier is located in Europe.
3. G − The glacier belongs to the Tergi River basin;

4. 09 – We need to find the 9th volume,
5. 3rd edition,
6. In part 1 and
7. Its serial number is 9.

Let's also decrypt SU4G08012096

1. SU – The glacier is located in the former Soviet Union;
2. 4 – The glacier is located in Europe;
3. G − The glacier belongs to the Tergi River basin;
4. 08 – We need to find the 8th volume,
5. 0 release,
6. In section 12 and
7. Its serial number is 96.

Eight blocks:

1. Area

Glacier areas in km^2 are calculated by the catalogue with an accuracy of 0.01 km^2 , and by the SRS with an accuracy of 0.000001 km^2. These values of the SRS data allow us to observe the degradation of glaciers with greater accuracy.

2. Morphological type

As a result of expert assessment, the morphological types of mountain glaciers in Georgia have been established: Corrie, Valley and Hanging glaciers, as well as transitional types − Corrie-Valley, Hanging-Corrie, Hanging-Valley, Corrie-Hanging.

3. General exposure

Using a modern method for determining glacier exposure, which is proven and accepted worldwide [2 , 3] , the following options are presented in the resulting table with the corresponding designations: West, East, South, Southwest, Southeast, North, Northwest, Northeast.

4. Maximum length

The maximum length of the glacier in meters is given in the catalog, and on the images obtained with the SRS it is determined by the length of an additional line drawn manually from the extreme upper part of the glacier contour to the tip of the glacier tongue.

5. Minimum height

The minimum height of the glacier is determined in meters using a digital terrain model (DEM).

6. Maximum height

The maximum height of the glacier is determined in meters by the digital terrain model (DEM).

7. Height of the firn line

The Geffer method was used to determine the height of the firn line, as the firn line of the glaciers of Georgia is determined by this method in the glacier catalogue.

According to Geffer, the height of the firn line is the arithmetic mean between the average height of the surrounding relief of the firn basin and the height of the end of the glacier tongue. The average height of the highest two or more peaks around the glacier basin is added to the height of the end of the glacier tongue, and the arithmetic mean of these two values is calculated [4]. It should be noted that it was possible to determine the height of the firn line by this method only for some glaciers.

8. The ablation area

The ablation area is the total number of pixels from the height of the firn line to the lowest point of the glacier multiplied by the area of one pixel gives the current area of glacier ablation.

Acknowledgement. The research was performed with the support of the Shota Rustaveli National Science Foundation project FR-21-1996 "Research on the Degradation of Georgian Glaciers in Recent Decades and the Creation of an Electronic Atlas of Georgian Glaciers".

References

1. Podozerskiy K. I., Glaciers of the Caucasus Range. Records of the Caucasian Department of the Imperial Russian Geographical Society, 1911, volume 29, 1. http://apsnyteka.org/522-podozerskiy_izbrannye_raboty.html (In Russian)
2. Shengelia L. D., Kordzakhia G. I., Tvauri G. A., Guliashvili G. N., Dzadzamia M. Sh., Results of the study of the morphology and exposure of glaciers and snowfields of the glacial basins of Western Georgia based on satellite remote sensing. // Mikheil Nodia's Number Proceedings of the Institute of Geophysics, Vol. LXXVII, 2024, pp. 43−64 (In Georgian).
3. Shengelia L., Kordzakhia G., Tvauri G., Guliashvili G., Dzadzamia M. Results of the study of the morphology and exposure of glaciers and snowfields of the glacial basins of Eastern Georgia based on satellite remote sensing. // Collection of Refereed Works of the Institute of Hydrometeorology of the Georgian Technical University, vol. №136, 2025, pp. 64-68 (In Georgian).
4. Shengelia L., Kordzakhia G., Tvauri G., TsomaiaV., Determination of the height of the firn line of a mountain glacier using satellite data using the Geffer method. “Current problems of hydrometeorology and ecology”. // Proceedings of the Institute of Hydrometeorology of the Georgian Technical University, vol. 123, 2016, pp. 77-82 (In Georgian).

1st International Scientific Conference "Modern problems in Geophysics", Proceedings,
ISBN 978-9941-36-434-1, ISSN 3088-4349, Tbilisi, Georgia, November 6-8, 2025

CHANGEABILITY OF AVERAGE VALUES OF DAILY ABSOLUTE MINIMUM, MAXIMUM, AND MEAN AIR TEMPERATURE FOR EACH MONTH OF THE YEAR IN BAKU AND TBILISI IN 2005-2024

[*]Aliyev V., [**]Amiranashvili A., [***]Kartvelishvili L., [****]Matzarakis A., [*****]Tatishvili M.

**CEO & Founder, International Event Organizer Company AMIR Technical Services, Azerbaijan, Baku, Azerbaijan*
***Mikheil Nodia Institute of Geophysics of Ivane Javakhishvili Tbilisi State University, Tbilisi, Georgia*
****Georgian National Environmental Agency, Tbilisi, Georgia*
*****Albert-Ludwigs-Universität Freiburg, Germany*
******Institute of Hydrometeorology of Georgian Technical University, Tbilisi, Georgia*
prof.vugar.aliyev@gmail.com

Abstract. *Results of statistical analysis of average values of daily absolute minimum (T_{min}), maximum (T_{max}), Daily Temperature Range (DTR) and mean (T_{mean}) air temperature for each month of the year in Baku and Tbilisi in 2005-2024 and their variability in 2020-2024 (second period) compared to 2005-2009 (first period) are presented.*

It is shown that against the background of rapid climate warming over the past two decades, in the second period of the selected temporal interval compared to the first, in both cities, increase in the specified air temperature characteristics is mainly observed (except for the average absolute maximum of T_{min} and DTR in Baku, as well as the average absolute minimum in Tbilisi). In general, in both cities, the warming effect for the average values of the absolute minimum of the specified air temperature parameters is higher than for the average values of the absolute maximum of these parameters. At the same time, the greatest warming effect is observed in Baku for the average absolute minimum for T_{min} (increase of 2.9 °C) and in Tbilisi for the average absolute minimum for T_{max} (increase of 2.4 °C).

Key Words: *Air temperature, thermal regime, regional climate, climate change, statistical analysis.*

Introduction

Global warming, especially in recent decades, and the environmental problems associated with it are well known worldwide. Therefore, in many countries, special attention is paid to climate change research and the consequences of these changes on the environment, including human health [1,2]. Similar research is also actively led in Azerbaijan [3-6] and Georgia [7-10]. Based on the results of the research, it became evident that in both countries, against the backdrop of global climate change, a significant increase in air temperature has been observed in recent years.

For example, in our latest work [11] detailed statistical analysis of daily minimum (T_{min}), maximum (T_{max}), Daily Temperature Range, and average (T_{mean}) air temperatures in Baku and Tbilisi in 2005-2024 and their variability in 2020-2024 compared to 2005-2009 against the background of climate change has been analyzed. The significant impact of rapid climate warming over the past two decades on the growth of the specified air temperature characteristics in both cities is detected. Generally, as a result of rapid climate warming in the last two decades, both in Baku and Tbilisi, an increase in thermal risks to public health is observed. In our other work [12], submitted for publication, a detailed statistical analysis of the average monthly values of the above temperature parameters in Baku and Tbilisi for the same period of time was carried out. This work is a continuation of previous joint studies on climate change in Azerbaijan and Georgia [11, 12]. Results of statistical analysis of average values of daily absolute minimum, maximum, Daily Temperature Range and mean air temperature for each month of the year in Baku and Tbilisi in 2005-2024 and their variability in 2020-2024 compared to 2005-2009 are discussed below.

Study area, material, and methods

Study area – Baku (the capital of the Republic of Azerbaijan, 40.45 °N, 50.0667 °E, -4 m above sea level) and Tbilisi on other hand (the capital of the Republic of Georgia, 41.75785 °N, 44.7552 °E, 427 m above sea level). The distance between those cities is 470 km.

In order to conduct analysis, data from the National Environment Agency of Georgia and data [http://www.pogodaiklimat.ru/] on minimum (Tmin), maximum (Tmax), and mean (Tmean) daily air temperature in Baku and Tbilisi in 2005-2024 are used.

Object of study: daily absolute minimum (T_{min}), maximum (T_{max}), Daily Temperature Range (DTR) and mean (T_{mean}) air temperatures for each month of the year.

In the proposed work, the analysis of data is carried out with the use of the standard statistical analysis methods.

The following designations, except those specified above, will be used below: Range – maximal values – minimal values; daily temperature range – DTR = $T_{max} - T_{min}$. The difference of the average values of the studied parameters was carried out using the G2 criterion for comparing the frequencies of two occasional events with a significance level of no less than 0.5. B – Baku, T – Tbilisi. I – first period: 2005-2009, II – second period: 2020-2024, F – full period: 2005-2024.

Results

Results are presented in Tables 1-3 and Fig. 1.

Table 1. Statistical characteristics of absolute minimum and maximum values of the studied temperature parameters for each month of the year in 2005-2024.

Variable	T_{min}_B	T_{min}_T	T_{mean}_B	T_{mean}_T	T_{max}_B	T_{max}_T	DTR_B	DTR_T
Parameter	Absolute minimum							
Max	11.9	13.2	20.3	17.1	22.1	20.1	1.9	3.4
Min	-9.6	-13.9	-7.4	-9.7	-5.5	-4.8	0.2	0.6
Range	21.5	27.1	27.7	26.8	27.6	24.9	1.7	2.8
Average	1.1	0.0	6.4	4.1	8.1	6.2	1.0	1.6
St Dev	8.1	9.4	9.6	9.2	9.8	8.6	0.5	0.9
Parameter	Absolute maximum							
Max	31.1	27.0	33.5	32.1	42.7	40.6	25.8	21.9
Min	8.8	9.2	12.8	11.0	20.4	16.0	13.8	15.5
Range	22.3	17.8	20.7	21.1	22.3	24.6	12.0	6.4
Average	19.6	18.2	23.4	22.4	31.6	30.6	21.0	19.2
St Dev	7.5	6.8	7.7	7.5	8.1	8.3	3.6	2.1

Table 2. Statistical characteristics of absolute minimum and maximum values of the studied temperature parameters for each month of the year in 2005-2009.

Variable	T_{min}_B	T_{min}_T	T_{mean}_B	T_{mean}_T	T_{max}_B	T_{max}_T	DTR_B	DTR_T
Parameter	Absolute minimum							
Max	13.7	13.8	20.3	17.5	22.1	21.0	2.3	3.4
Min	-9.6	-12.4	-4.4	-7.8	-2.6	-3.4	0.2	1.0
Range	23.3	26.2	24.7	25.3	24.7	24.4	2.1	2.4
Average	2.3	1.4	8.0	5.6	9.8	7.8	1.1	2.0
St Dev	7.7	8.5	8.4	8.2	8.6	7.8	0.6	0.8
Parameter	Absolute maximum							
Max	31.1	25.2	31.3	30.4	38.2	40.0	25.8	19.6
Min	7.1	5.0	8.6	7.6	15.8	15.5	13.8	14.0
Range	24.0	20.2	22.7	22.8	22.4	24.5	12.0	5.6
Average	18.8	16.5	21.7	20.9	29.0	29.0	19.3	17.4
St Dev	7.6	7.1	7.7	8.1	7.3	8.4	4.1	1.6

Table 3. Statistical characteristics of absolute minimum and maximum values of the studied temperature parameters for each month of the year in 2020-2024.

Variable	T_{min}_B	T_{min}_T	T_{mean}_B	T_{mean}_T	T_{max}_B	T_{max}_T	DTR_B	DTR_T
Parameter	Absolute minimum							
Max	17.5	14.0	23.1	20.5	25.7	24.2	3.8	4.4
Min	-4.9	-8.0	-3.9	-2.9	0.9	0.0	0.9	0.6
Range	22.4	22.0	27.0	23.4	24.8	24.2	2.9	3.8
Average	5.2	2.9	9.5	7.5	11.7	10.2	2.1	2.0
St Dev	8.1	8.0	9.0	8.9	9.1	9.0	1.0	1.2
Parameter	Absolute maximum							
Max	27.6	26.3	32.8	32.1	41.9	40.6	20.8	21.9
Min	8.3	8.7	10.7	11.0	15.7	16.0	13.4	12.5
Range	19.3	17.6	22.1	21.1	26.2	24.6	7.4	9.4
Average	18.4	17.7	22.9	22.0	30.7	30.1	17.2	17.9
St Dev	7.2	6.8	7.9	7.7	8.5	8.4	2.3	2.6

In Tables 1-3 statistical characteristics of absolute minimum and maximum values of the studied temperature parameters for each month of the year in the three periods of time are presented.

In particular, from these Tables follows that:

For all time periods, the average values of the absolute minimum and maximum T_{min}, T_{mean} and T_{max} in Baku are higher than in Tbilisi (except for the average values of the absolute maximum T_{max} in the first time period, equal to 29.0 °C).

For the full and first time periods, the average values of the absolute minimum DTR in Baku are lower than in Tbilisi, and the average values of the absolute maximum DTR in Baku are higher than in Tbilisi.

For the second time period, on the contrary, the average values of the absolute minimum DTR in Baku are higher than in Tbilisi, and the average values of the absolute maximum DTR in Baku are lower than in Tbilisi.

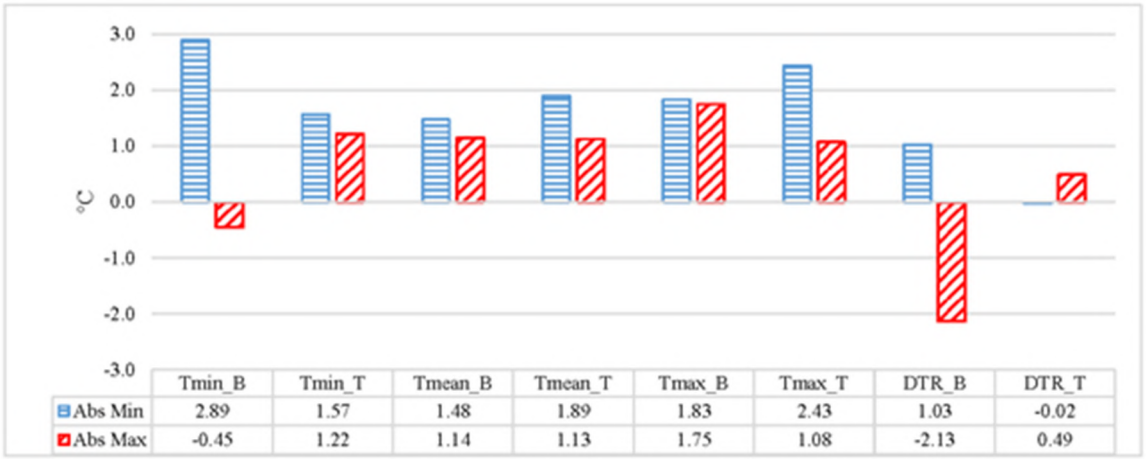

Fig. 1. Difference between mean values of the absolute minimum and maximum values of the studied temperature parameters for each month of the year in 2020-2024 and 2005-2009.

In Fig. 1 calculated difference data between the mean values of the absolute minimum and maximum values of the studied temperature parameters for each month of the year in 2020-2024 and 2005-2009 are presented.

As it follows from Fig. 1 in the second period of time, compared to the first, in both cities, an increase in the specified air temperature characteristics is mainly observed (except for the average absolute maximum of T_{min} and DTR in Baku, as well as the average absolute minimum in Tbilisi). In general, in both cities, the warming effect for the average values of the absolute minimum of the specified air temperature parameters is

higher than for the average values of the absolute maximum of these parameters. The greatest warming effect is observed in Baku for the average absolute minimum for T_{min} (an increase of 2.9 °C) and in Tbilisi for the average absolute minimum for T_{max} (an increase of 2.4 °C).

Conclusion

In the near future, it is planned to continue joint research both in terms of climate change and in terms of assessing environmental risks, including public health, associated with air temperature and various thermal indices in individual seasons and months of the year.

References

1. Rawat A., Kumar D., Khati B. S. A., Review on Climate Change Impacts, Models, and its Consequences on Different Sectors: a Systematic Approach. // Journal of Water and Climate Change, 15 (1), 2024, pp. 104–126. https://doi.org/10.2166/wcc.2023.536
2. Matzarakis A., Importance of Heat Health Warnings in Heat Management. // Atmosphere, 15, 684, 2024.
3. Nemat R. A. J., Aqa R. A. Q. B., Firuddin R. M. A., Dynamics of Climate of Azerbaijan. // Sciences review, 3(10), Vol.1. 2018, pp. 39-43.
4. Imanov F. A., Sikan A. V., Analysis of Climate Change in the Territory of Azerbaijan. // Gidrometeorologiya i Ekologiya = Journal of Hydrometeorology and Ecology, (69), 2022, pp. 607 – 619, (in Russian). doi:10.33933/2713-3001-2022-69-607-619.
5. Huseynov J. S., Tagiyev A. Sh., The Changes of the Air Temperature Characteristics in the Azerbaijan Territory During Global Climate Changes Period. // Visnyk of Taras Shevchenko National University of Kyiv, Geology. 3, 106, 2024, pp. 76-82.
6. Huseynov J. S., Huseynova T. M., Tagiyev A., Sh., Assessment of the Impact of Climate Changes on the Quality of Life of the Population in the Greater Caucasus Region of the Republic of Azerbaijan. // Journ. Geol. Geograph. Geoecology, 34(1), 2025, pp. 100-111.
7. Kartvelishvili L., Tatishvili M., Amiranashvili A., Megrelidze L., Kutaladze N., Weather, Climate and their Change Regularities for the Conditions of Georgia. // Monograph: Publishing House “Universal”, Tbilisi, 2023, 406 p.
8. Amiranashvili A., Kartvelishvili L., Kutaladze N., Megrelidze L., Tatishvili M., Comparison of the Mean Max Annual, Seasonal and Monthly Air Temperature Variability in Tbilisi and Shovi in 1956-2022. // Int. Sc. Conf. "Geophysical Processes in the Earth and its Envelopes". Proc., Publish House of Iv. Javakhishvili Tbilisi State University, November 16-17, 2023, pp. 127-132.
9. Amiranashvili A., Analysis of Variability of Mean Annual Air Temperature in Tbilisi in 1844-2023 Against the Background of Climate Change. // Int. Sc. Conf. “Complex Geophysical Monitoring in Georgia: History, Modern Problems, Promoting Sustainable Development of the Country”. Proc., Publish House of Iv. Javakhishvili Tbilisi State University, Tbilisi, Georgia, October 17-19, 2024, pp. 145 – 149.
10. Amiranashvili A. G., Japaridze N. D., Kartvelishvili L. G., Khazaradze K. R., Khazaradze R. R., Effects of Variations of the Monthly Mean Air Temperature on the Population Health of Imereti Region of Georgia. // Int. Sc. Conf. „Modern Problems of Ecology“, Proc., 6, Kutaisi, Georgia, 21-22 September, 2018, pp. 38-41.
11. Aliyev V., Amiranashvili A., Kartvelishvili L., Matzarakis A., Tatishvili M., Comparative Analysis of the Variability of Daily Minimum, Maximum and Mean Air Temperature in Baku and Tbilisi in 2005-2024. // Int. Journal of Sustainability and Rick Control, e-ISSN: 3104-8358, p-ISSN: 3104-834X, Baku, Azerbaijan, Vol. 1, No. 2 (2), September 2025, pp. 63-70. DOI: https://doi.org/10.64599/GDOF7452
12. Aliyev V., Amiranashvili A., Kartvelishvili L., Matzarakis A., Tatishvili M., Variability of Monthly Average Values of Daily Minimum, Maximum and Mean Air Temperature in Baku and Tbilisi IN 2005-2024. // Int. Journal of Sustainability and Rick Control, e-ISSN: 3104-8358, p-ISSN: 3104-834X, Baku, Azerbaijan, Vol. 1, No. 3 (3), December 2025, (in Press).

1st International Scientific Conference "Modern problems in Geophysics", Proceedings,
ISBN 978-9941-36-434-1, ISSN 3088-4349, Tbilisi, Georgia, November 6-8, 2025

DROUGHT PERIODS ASSESSMENT IN EASTERN GEORGIA USING SPI-3 INDEX IN 1936-2023

[*]Amiranashvili A., [**]Davitashvili T., [*]Kharshiladze O., [***]Samkharadze I., [*]Amilakhvari D.

[*]M. Nodia Institute of Geophysics of I. Javakhishvili Tbilisi State University, Tbilisi, Georgia
[**] Ilia Vekua Institute of Applied Mathematics of Ivane Javakhishvili Tbilisi State University, Tbilisi, Georgia
[***] Institute of Hydrometeorology of Georgian Technical University, Tbilisi, Georgia
avtandilamiranashvili@gmail.com

Abstract. *In the work detailed statistical analysis of the duration of drought periods D (months) normalized per decade for four SPI-3 categories (agriculture drought; SPI ≤ -1.0, ≤ -1.5, ≤ -2.0 and ≤ -2.5) in Eastern Georgia based on observations at 18 meteorological stations during 1936-2023 is presented. The statistical characteristics of D values in 1936-2023, 1936-1975, and 1984-2023 were compared. The variability of D values in 1984-2023 compared to 1936-1975 (ΔD) was assessed. In particular, it was found that ΔD values are different at different points. On average, for eastern Georgia, ΔD values for all SPI categories, except ≤ -2.5, are increasing (i.e., an increase in the duration of droughts is observed).*

Key Words: *SPI, atmospheric precipitation, drought categories, drought risk, climate change.*

Introduction

Drought is a gradually developing, dangerous natural phenomenon that occurs as a result of less than normal precipitation. Currently, there are many simple and complex indices for studying droughts [1]. One of the most commonly used is the so-called Standardized Precipitation Index (SPI), which is used in more than 70 countries [2]. To calculate this index, only information on precipitation is needed. A special free program is used to calculate SPI [3]. SPI was developed to quantitatively assess the precipitation deficit on various time scales or sliding averaging windows. For example, for agricultural drought, SPI for 3 months is often used [2]. In recent years, a significant number of studies of SPI variations (often in combination with other indices) have been conducted in various countries around the world, including Georgia, to analyze different types of droughts [4-8], taking into account local climate change [9].

This work is a continuation of previous studies [8]. Below is a detailed analysis of the duration of dry periods (months) normalized per decade for different SPI-3 categories in Eastern Georgia during 1936-2023.

Study area, material and methods

Study area – Eastern Georgia, 18 meteorological stations: Paravani (Par), Tsalka (Ts), Bolnisi (Bol), Gardabani (Gar), Tbilisi (Tb), Sagarejo (Sag), Gurjaani (Gur), Dedoplistskaro (Ded), Lagodekhi (Lag), Kvareli (Kv), Telavi (Tel), Tianeti (Tian), Pasanauri (Pas), Gudauri (Gud), Stepantsminda (St), Gori (Gori), Khashuri (Kh) and Shovi (Sh). The altitude range of meteorological stations is from 362 (Lag) to 2194 (Gud) m a.s.l. The study area covers 7 regions of Georgia, including its capital, Tbilisi.

Data from the Georgian National Environment Agency about the monthly sum of atmospheric precipitation in the period from 1936 to 2023 are used. SPI and SPI periods were determined using a special program [3] for 3 months (SPI-3, below – SPI). The analysis of data is carried out with the use of the standard statistical analysis methods. The SPI periods for four categories (Table 1) were determined for three time periods (1936-2023, entire period; 1936-1975, first period; 1984-2023, second period).

Table 1. SPI category [2].

SPI	Category	SPI	Category
≤ -1.0	Moderate, severe, and extreme dryness	≤ -2.0	Extreme Dryness
≤ -1.5	Severe and extreme dryness	≤ -2.5	Extreme Dryness

The work used standard methods of mathematical statistics [10]. The following designations will be used below: Mean – average values; Min – minimal values; Max – maximal values; St Dev – standard deviation, R – coefficient of linear correlation; D – duration of normalized to decade drought period (month); ΔD – difference between duration of normalized to decade drought periods in 1984-2023 and 1936-1975.

Results

Results in Fig. 1-4 and Table 2 are presented. In Fig. 1-3, data about D values in eastern Georgia in 1936-2023, 1936-1975, and 1984-2023, and in Fig. 4 – data about ΔD values are presented (for different SPI categories). Table 2 presents the statistical characteristics of D and ΔD values for different SPI categories.

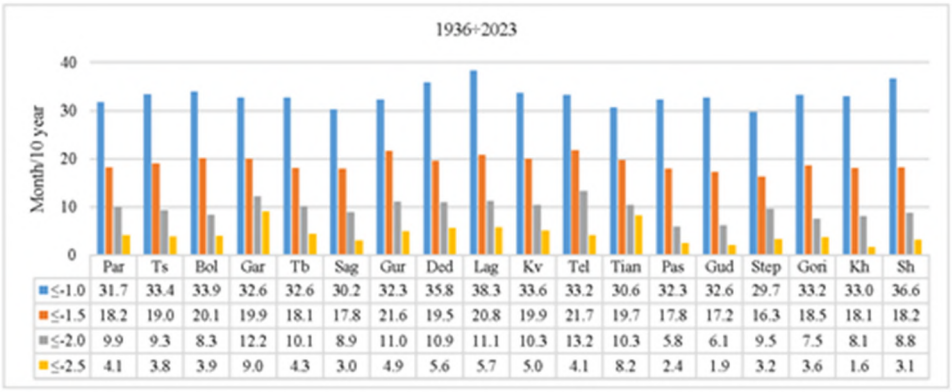

	Par	Ts	Bol	Gar	Tb	Sag	Gur	Ded	Lag	Kv	Tel	Tian	Pas	Gud	Step	Gori	Kh	Sh
≤-1.0	31.7	33.4	33.9	32.6	32.6	30.2	32.3	35.8	38.3	33.6	33.2	30.6	32.3	32.6	29.7	33.2	33.0	36.6
≤-1.5	18.2	19.0	20.1	19.9	18.1	17.8	21.6	19.5	20.8	19.9	21.7	19.7	17.8	17.2	16.3	18.5	18.1	18.2
≤-2.0	9.9	9.3	8.3	12.2	10.1	8.9	11.0	10.9	11.1	10.3	13.2	10.3	5.8	6.1	9.5	7.5	8.1	8.8
≤-2.5	4.1	3.8	3.9	9.0	4.3	3.0	4.9	5.6	5.7	5.0	4.1	8.2	2.4	1.9	3.2	3.6	1.6	3.1

Fig. 1. D values for different SPI categories in eastern Georgia in 1936-2023.

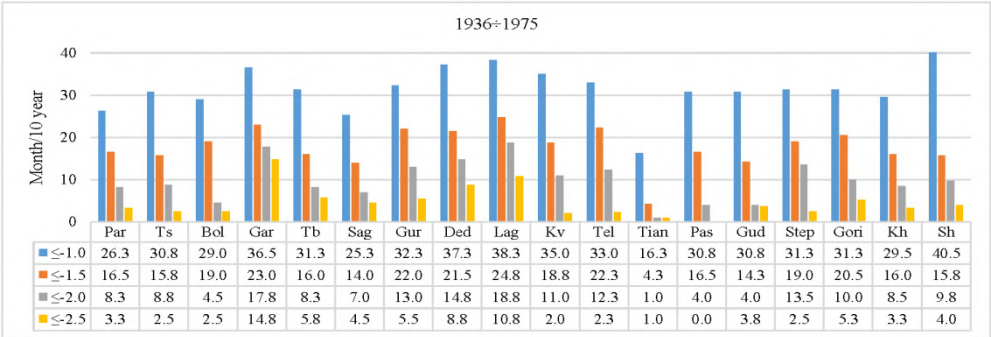

	Par	Ts	Bol	Gar	Tb	Sag	Gur	Ded	Lag	Kv	Tel	Tian	Pas	Gud	Step	Gori	Kh	Sh
≤-1.0	26.3	30.8	29.0	36.5	31.3	25.3	32.3	37.3	38.3	35.0	33.0	16.3	30.8	30.8	31.3	31.3	29.5	40.5
≤-1.5	16.5	15.8	19.0	23.0	16.0	14.0	22.0	21.5	24.8	18.8	22.3	4.3	16.5	14.3	19.0	20.5	16.0	15.8
≤-2.0	8.3	8.8	4.5	17.8	8.3	7.0	13.0	14.8	18.8	11.0	12.3	1.0	4.0	4.0	13.5	10.0	8.5	9.8
≤-2.5	3.3	2.5	2.5	14.8	5.8	4.5	5.5	8.8	10.8	2.0	2.3	1.0	0.0	3.8	2.5	5.3	3.3	4.0

Fig. 2. D values for different SPI categories in eastern Georgia in 1936-1975.

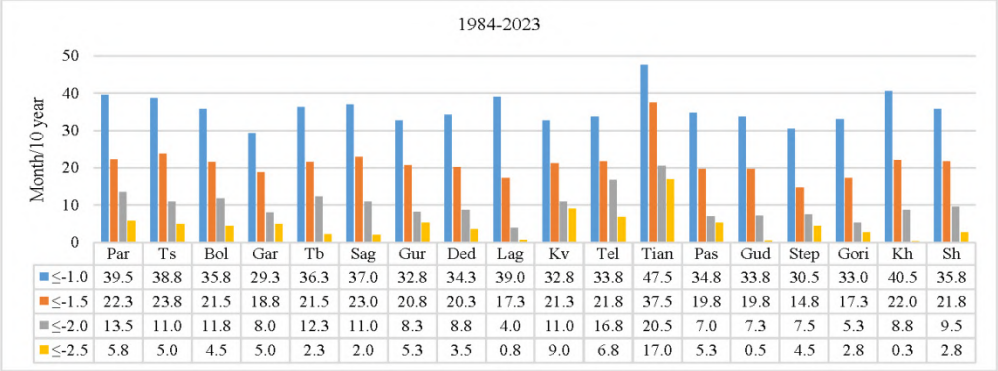

	Par	Ts	Bol	Gar	Tb	Sag	Gur	Ded	Lag	Kv	Tel	Tian	Pas	Gud	Step	Gori	Kh	Sh
≤-1.0	39.5	38.8	35.8	29.3	36.3	37.0	32.8	34.3	39.0	32.8	33.8	47.5	34.8	33.8	30.5	33.0	40.5	35.8
≤-1.5	22.3	23.8	21.5	18.8	21.5	23.0	20.8	20.3	17.3	21.3	21.8	37.5	19.8	19.8	14.8	17.3	22.0	21.8
≤-2.0	13.5	11.0	11.8	8.0	12.3	11.0	8.3	8.8	4.0	11.0	16.8	20.5	7.0	7.3	7.5	5.3	8.8	9.5
≤-2.5	5.8	5.0	4.5	5.0	2.3	2.0	5.3	3.5	0.8	9.0	6.8	17.0	5.3	0.5	4.5	2.8	0.3	2.8

Fig. 3. D values for different SPI categories in eastern Georgia in 1984-2023.

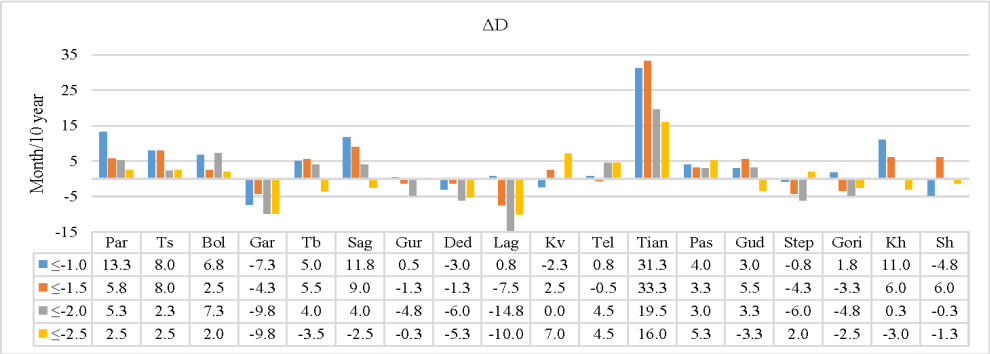

	Par	Ts	Bol	Gar	Tb	Sag	Gur	Ded	Lag	Kv	Tel	Tian	Pas	Gud	Step	Gori	Kh	Sh
≤-1.0	13.3	8.0	6.8	-7.3	5.0	11.8	0.5	-3.0	0.8	-2.3	0.8	31.3	4.0	3.0	-0.8	1.8	11.0	-4.8
≤-1.5	5.8	8.0	2.5	-4.3	5.5	9.0	-1.3	-1.3	-7.5	2.5	-0.5	33.3	3.3	5.5	-4.3	-3.3	6.0	6.0
≤-2.0	5.3	2.3	7.3	-9.8	4.0	4.0	-4.8	-6.0	-14.8	0.0	4.5	19.5	3.0	3.3	-6.0	-4.8	0.3	-0.3
≤-2.5	2.5	2.5	2.0	-9.8	-3.5	-2.5	-0.3	-5.3	-10.0	7.0	4.5	16.0	5.3	-3.3	2.0	-2.5	-3.0	-1.3

Fig. 4. ΔD values for different SPI categories in eastern Georgia.

Table 2. Statistical characteristics of D and ΔD values for different SPI categories in eastern Georgia.

Variable	≤-1.0	≤-1.5	≤-2.0	≤-2.5	≤-1.0	≤-1.5	≤-2.0	≤-2.5
Year	1936-2023				1936-1975			
Max	38.3	21.7	13.2	9	40.5	24.8	18.8	14.8
Min	29.7	16.3	5.8	1.6	16.3	4.3	1	0
Mean	33.1	19.0	9.5	4.3	31.4	17.8	9.7	4.6
St Dev	2.1	1.5	1.9	1.9	5.5	4.6	4.8	3.7
	Correlation Matrix							
≤-1.0	1	0.40	0.15	0.07	1	0.77	0.73	0.52
≤-1.5	0.40	1	0.68	0.54	0.77	1	0.83	0.57
≤-2.0	0.15	0.68	1	0.68	0.73	0.83	1	0.75
≤-2.5	0.07	0.54	0.68	1	0.52	0.57	0.75	1
Year	1984-2023				Difference: (1984-2023) – (1936-1975)			
Max	47.5	37.5	20.5	17	31.3	33.3	19.5	16
Min	29.3	14.8	4	0.3	-7.3	-7.5	-14.8	-10
Mean	35.9	21.4	10.1	4.6	4.4	3.6	0.4	0.0
St Dev	4.2	4.6	4.0	3.8	8.8	8.8	7.6	6.2
	Correlation Matrix							
≤-1.0	1	0.80	0.54	0.39	1	0.86	0.78	0.61
≤-1.5	0.80	1	0.82	0.74	0.86	1	0.87	0.70
≤-2.0	0.54	0.82	1	0.74	0.78	0.87	1	0.79
≤-2.5	0.39	0.74	0.74	1	0.61	0.70	0.79	1

In particular, from Fig. 1-4 and Table 2 it follows that the variability of D values for different SPI categories is as follows.

1936-2023. SPI ≤-1.0: D_{min} = 29.7 (Step), D_{max} = 38.3 (Lag), D_{mean} = 33.1; SPI ≤-1.5: D_{min} = 16.3 (Step), D_{max} = 21.7 (Tel), D_{mean} = 19.0; SPI ≤-2.0: D_{min} = 5.8 (Pas), D_{max} = 13.2 (Tel), D_{mean} = 9.5; SPI ≤-2.5: D_{min} = 1.6 (Kh), D_{max} = 9.0 (Gar), D_{mean} = 4.3.

Linear correlation between the parameters under study. R_{min} = 0.07 (Pair SPI: ≤-1.0÷≤-2.5, negligible correlation), R_{max} = 0.68 (Pair SPI: ≤-1.0÷≤-2.0, moderate correlation), R_{mean} = 0.42 (low correlation).

1936-1975. SPI ≤-1.0: D_{min} = 16.3 (Tian), D_{max} = 40.5 (Lag), D_{mean} = 31.4; SPI ≤-1.5: D_{min} = 4.3 (Tian), D_{max} = 24.8 (Lag), D_{mean} = 17.8; SPI ≤-2.0: D_{min} = 1.0 (Tian), D_{max} = 18.8 (Lag), D_{mean} = 9.7; SPI ≤-2.5: D_{min} = 0 (Pas), D_{max} = 14.8 (Gar), D_{mean} = 4.6.

Linear correlation between the parameters under study. R_{min} = 0.52 (Pair SPI: ≤-1.0÷≤-2.5, moderate correlation), R_{max} = 0.83 (Pair SPI: ≤-1.5÷≤-2.0, high correlation), R_{mean} = 0.69 (moderate correlation).

1984-2023. SPI ≤-1.0: D_{min} = 29.3 (Gar), D_{max} = 47.5 (Tian), D_{mean} = 35.9; SPI ≤-1.5: D_{min} = 14.8 (Step), D_{max} = 37.5 (Tian), D_{mean} = 21.4; SPI ≤-2.0: D_{min} = 4.0 (Lag), D_{max} = 20.5 (Tian), D_{mean} = 10.1; SPI ≤-2.5: D_{min} = 0.3 (Kh), D_{max} = 17.0 (Tian), D_{mean} = 4.6.

Linear correlation between the parameters under study. R_{min} = 0.39 (Pair SPI: ≤-1.0÷≤-2.5, low correlation), R_{max} = 0.82 (Pair SPI≤-1.5÷≤-2.0, high correlation), R_{mean} = 0.67 (moderate correlation).

(1984-2023) – (1936-1975). SPI ≤-1.0: ΔD_{min} = -7.3 (Gar), ΔD_{max} = 31.3 (Tian), ΔD_{mean} = 4.4; SPI ≤-1.5: ΔD_{min} = -7.5 (Lag), ΔD_{max} = 33.3 (Tian), ΔD_{mean} = 3.6; SPI ≤-2.0: ΔD_{min} = -14.8 (Lag), ΔD_{max} = 19.5 (Tian), ΔD_{mean} = 0.4; SPI ≤-2.5: ΔD_{min} = -10 (Lag), ΔD_{max} = 16.0 (Tian), ΔD_{mean} = 0.0.

Linear correlation between the parameters under study. R_{min} = 0.61 (Pair SPI: ≤-1.0÷≤-2.5, moderate correlation), R_{max} = 0.87 (Pair SPI: ≤-1.5÷≤-2.0, high correlation), R_{mean} = 0.77 (high correlation).

It should be noted that in Paravani, Tsalka, Bolnisi, Tianeti and Pasanauri, for all SPI categories, an increase in the duration of drought is observed (with a maximum in Tianeti), and in Gardabani and Dedoplistskaro, a decrease in this duration is observed (with a maximum in Gardabani). On average, for eastern Georgia, ΔD values for all SPI categories, except ≤ -2.5, are increasing (i.e., an increase in the duration of droughts is observed).

Conclusion

In the near future will be presented detailed results of SPI complex studies for 1, 3, 6, 9 and 12 months, as well as drought periods for 39 locations of Georgia in 1936-2023.

Acknowledgments. The research was funded by Shota Rustaveli National Scientific Foundation Grant No. FR-22-18445.

References

1. Handbook of Drought Indicators and Indices. // WMO-No. 1173, 2016, 52 p., https://www.droughtmanagement.info/literature/GWP_Handbook_of_Drought_Indicators_and_Indices_2016.pdf
2. Standardized Precipitation Index User Guide. // WMO, No 1090, 2012, 24 p. https://www.droughtmanagement.info/literature/WMO_standardized_precipitation_index_user_guide_en_2012.pdf
3. National Drought Mitigation Center – SPI Generator [software]. // University of Nebraska–Lincoln, 2018. https://drought.unl.edu/Monitoring/SPI/SPIProgram.aspx
4. Lloyd-Hughes B., Saunders M. A. A Drought Climatology for Europe. // International Journal of Climatology: a Journal of the Royal Meteorological Society, vol. 22, No. 13, 2002, pp. 1571-1592. https://doi.org/10.1002/joc.846
5. Yaseen Z. M., Ali M., Sharafati A., Al-Ansari N., Shahid S. Forecasting Standardized Precipitation Index using Data Intelligence Models: Regional Investigation of Bangladesh. // Scientific reports, vol. 11, 2021, e3435. https://doi.org/10.1038/s41598-021-82977-9
6. Tatishvili M., Kapadze N., Mkurnalidze I., Palavandishvili A., Drought Evaluation in Georgia using SPI and SpEI Indices. // Proceedings – Int. Sc. Conf. "Complex Geophysical Monitoring in Georgia: History, Modern Problems, Promoting Sustainable Development of the Country", Proceedings, ISBN 978-9941-36-272-9, Tbilisi, Georgia, October 17-19, 2024, pp. 96 – 100, Publish House of Iv. Javakhishvili Tbilisi State University.
7. Tsitsagi M., Gulashvili Z., Palavandishvili A., Tatishvili M., Zotikishvili N., Difficulties in Estimating the Negative Ecological and Economic Impacts of Droughts in Georgia. // Transactions IHM, GTU, vol.136, 2025, pp.109-119, (in Georgian).
8. Amiranashvili A., Davitashvili T., Kharshiladze O., Samkharadze I., Amilakhvari D., Drought Risk Assessment in Eastern Georgia Using Spi-3 Index under Regional Climate Change in 1936-2023. // Reliability: Theory and Applications, ISSN 1932-2321, Special Issue № 4 (86), Part-1, Volume 20, December 2025, (in Press).
9. Kartvelishvili L., Tatishvili M., Amiranashvili A., Megrelidze L., Kutaladze N., Weather, Climate, and their Change Regularities for the Conditions of Georgia. // Publishing House "UNIVERSAL", Tbilisi, 2023, p. 406.
10. Hinkle D. E., Wiersma W. Jurs, S. G., Applied Statistics for the Behavioral Sciences. // Boston, MA, Houghton Mifflin Company, ISBN: 0618124055; 9780618124053, 2003, p. 756.

1st International Scientific Conference "Modern problems in Geophysics", Proceedings,
ISBN 978-9941-36-434-1, ISSN 3088-4349, Tbilisi, Georgia, November 6-8, 2025

ANALYSIS OF HEAVY PRECIPITATION IN THE ADIGENI AND CHOKHATAURI MUNICIPALIITIES ON JULY 21, 2025, BASED ON SATELLITE MEASUREMENTS

[*,]Beglarashvili N., [***]Elizbarashvili I., [***]Jamrishvili N., [****]Janelidze I., [*,***]Pipia M., [***]Tavidashvili Kh.**

[*]Institute of Hydrometeorology of Georgian Technical University, Tbilisi, Georgia
[**]Samtskhe-Javakheti State University, Akhaltsikhe, Georgia
[***]Mikheil Nodia Institute of Geophysics of Ivane Javakhishvili Tbilisi State University, Tbilisi, Georgia
[****]Georgian Technical University, Tbilisi, Georgia
beglarashvilinani@yahoo.com

Abstract: *In the work some results of heavy precipitation analysis in Adigeni and Chokhatauri municipalities on July 21, 2025 based on ground-level and satellite measurements are presented. In particular, heavy rain caused damage to residents of the villages of Gomaro and Shoka in the Adigeni municipality and contributed to a landslide in the village of Zoti in the Chokhatauri municipality, which blocked the access road for eight families.*

Key Words: *atmospheric precipitation, flooding, flood, landslide.*

Introduction

Atmospheric precipitation, as one of the most important factors in climate formation, directly affects the vital functions of the environment. In this regard, in many countries of the world, including Georgia, special attention has always been paid to the study of precipitation patterns, their spatial-temporal distribution, as well as their forecasting [1-4]. Interest in these studies has increased even more in recent decades due to the process of global warming [5,6]. Both heavy precipitation (floods, landslides, mudflows, damage to vegetation, etc. [7-14]) and its deficiency (droughts, desertification, decreased crop yields, etc. [15]) hurt the environment. Thus, heavy rainfall over several days led to a landslide with casualties in Nergeeti (Imereti) on February 7, 2024 [12].

This work is a continuation of previous traditional studies [13,14]. Some results of heavy precipitation analysis in Adigeni and Chokhatauri municipalities on July 21, 2025, based on ground-level and satellite measurements are presented below.

Study area, material and methods

Study area – two municipalities of Georgia – Adigeni and Chokhatauri.

The following information is used. Satellite observation data [https://neo.gsfc.nasa.gov/view.php?datasetId=GPM_3IMERGM] about the daily sum of atmospheric precipitation. Satellite measurement resolution is 0.1˚X0.1˚ (≈90 km^2). Accordingly, for the territory of Georgia there are satellite data on precipitation for 768 points.

Lightning data – from [https://www.blitzortung.org/ru/live_lightning_maps.php?map=42].

In the proposed work the analysis of data is carried out with the use of the standard statistical analysis methods.

Results and discussion

Results in Fig. 1- Fig. 4 and Table 1 are presented.

On July 21, 2025 thunderstorms with heavy precipitation were observed over various parts of the territory of Georgia (including Adigeni and Chokhatauri municipalities).

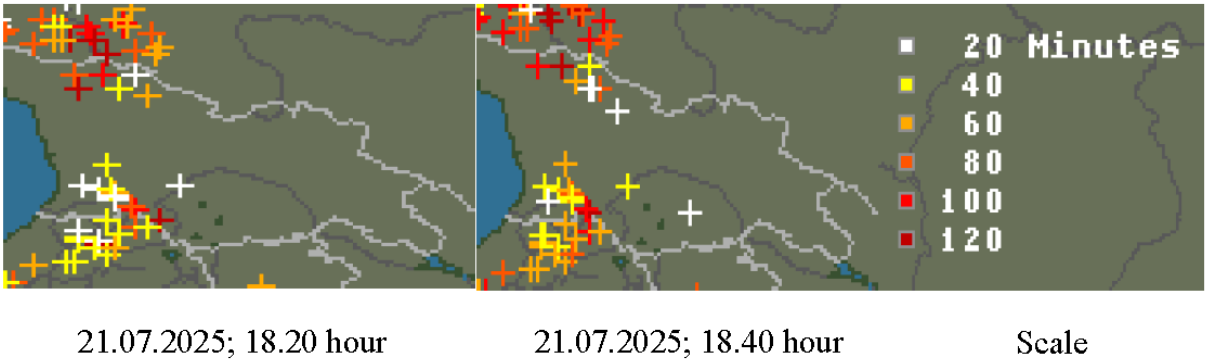

Fig. 1. An example of the distribution of lightning discharges over the territory of Georgia on July 21, 2025 at 18.20 and 18.40 hours.

In Fig. 1 an example of the distribution of lightning discharges over the territory of Georgia (including Tbilisi) on July 21, 2025, at 18.20 and 18.40 hours.

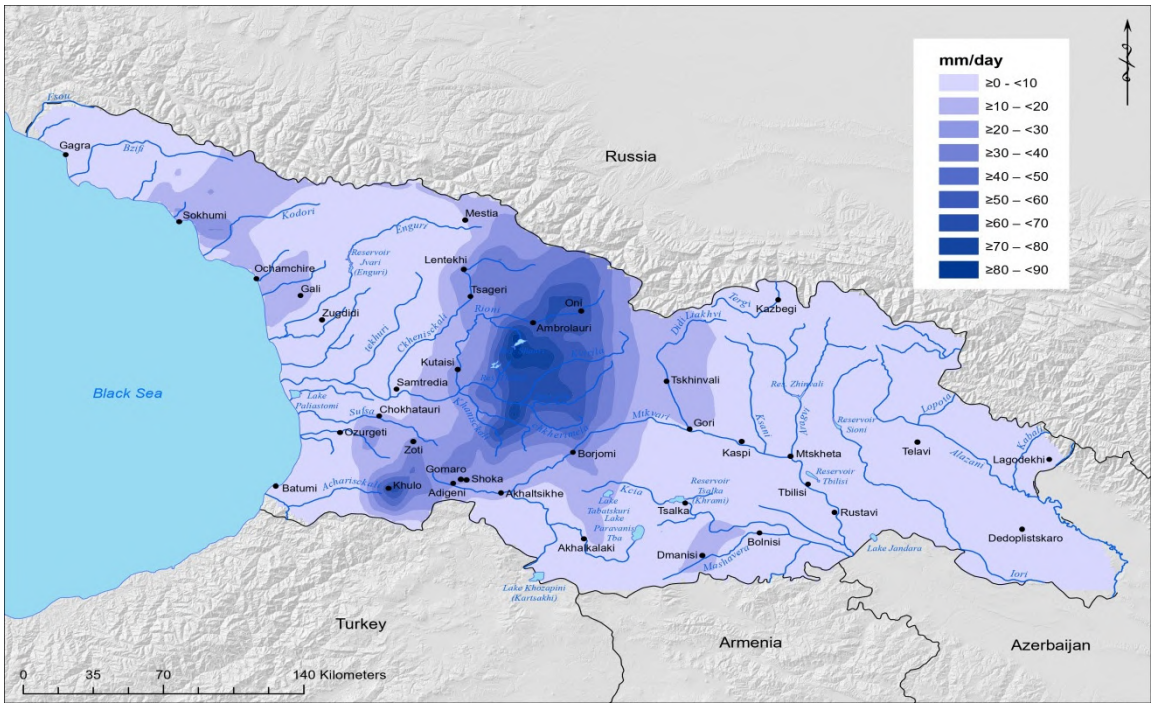

Fig. 2. Distribution of the daily sum of atmospheric precipitation on the territory of Georgia on July 21, 2025, according to satellite measurements.

In Fig. 2 and Table 1, data about the daily sum of atmospheric precipitation on the territory of Georgia on July 21, 2025, according to satellite measurements are presented. In Fig. 3 data on the repetition of the daily sum of atmospheric precipitations in Georgia are presented.

Table 1. Statistical characteristics of the daily sum of atmospheric precipitations on the territory of Georgia on July 21, 2025, according to satellite measurement (Fig. 2).

Min	Max	Average	St Dev	St Err	Count
0.00	89.5	11.7	15.6	0.56	768

As follows from Table 1, on the specified day, in accordance with satellite data, the precipitation amount varied from 0.00 mm to 89.5 mm (Ambrolauri Municipality, Racha-Lechkhumi and Kvemo Svaneti, Georgia), with an average value of 11.7 mm in the villages of Gomaro and Shoka in the Adigeni Municipality. Satellite data showed a daily rainfall of 30.2 mm. Seven families in Gomaro were affected by the disaster. Due to heavy rain, a mudflow damaged homes and yards. One house was almost completely buried by the mudflow. Furniture, appliances, and household items were damaged and destroyed. About ten cars were also damaged.

In the village of Zoti in the Chokhatauri Municipality, a daily rainfall of 36.2 mm was recorded. A landslide caused by the heavy rain blocked the access road for eight families in the village (Fig. 2).

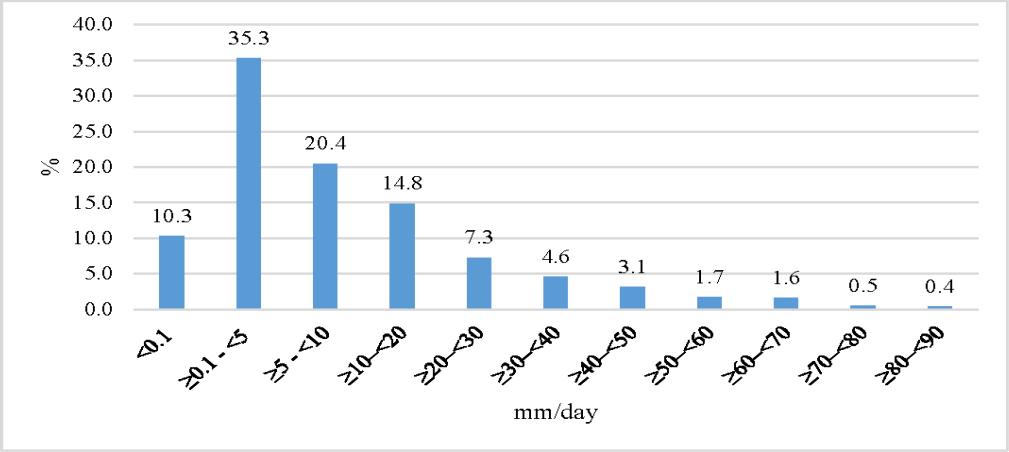

Fig. 3. Repetition of the daily sum of atmospheric precipitations in Georgia on July 21, 2025, according to satellite measurement.

Fig. 4. An example of the negative consequences of a heavy rainfall on two locations in Adigeni municipality on July 21, 2025. [https://1tv.ge/news/adigenis-municipalitetshi-ukhvma-naleqma-problemebi-sheqmna-daitbora-da-dazianda-sakhlebi-sagzao-infrastruqtura-sasoflo-sameurneo-savargulebi/].

Finally, in Fig. 4 an examples of the negative consequences of a heavy rainfall on two locations in Adigeni municipality on July 21, 2025, are presented.

Conclusion

In the future, we plan to continue similar studies for other regions of Georgia using ground-based and satellite measurement data against the backdrop of climate change.

Acknowledgement. The research is done with the support of "Shota Rustaveli National Scientist Foundation" [Grant number – FR-22-2882].The authors are grateful to the chief of the atmospheric physics department of M. Nodia Institute of Geophysics, A. Amiranashvili, for assistance in the fulfillment of this work.

References

1. Yin Xueyi, Ziyang Zhang, Zhi Lin, Jun Yin., Assessment of Rainfall Frequencies from Global Precipitation Datasets. // Atmosphere 16, no. 16 2025, 66.
2. Alibegova D., Elizbarashvili E., Statisticheskaya struktura atmosfernykh osadkov v Gornykh rayonakh. // Leningrad, 1980, 136 s
3. Amiranashvili A.G.. Special Features of Changeability of Daily Sum of Precipitation in Tbilisi in 1957-2006. // Journal of the Georgian Geophysical Society, Issue B. Physics of Atmosphere, Ocean and Space Plasma, v.18B, Tbilisi, 2015, pp.81-91.

4. Elizbarashvili M., Amiranashvili A., Elizbarashvili E., Mikuchadze G., Khuntselia T., Chikhradze N.. Comparison of RegCM4.7.1 Simulation with the Station Observation Data of Georgia,1985–2008. // Atmosphere, ISSN: 2073-4433, 15, 369, 2024, 19 pp. https://doi.org/10.3390/atmos15030369
5. Kartvelishvili L., Tatishvili M., Amiranashvili A., Megrelidze L., Kutaladze N., Weather, Climate and their Change Regularities for the Conditions of Georgia. // Monograph, Publishing House "UNIVERSAL", Tbilisi 2023, 406 p., https://doi.org/10.52340/mng.9789941334658
6. Bolashvili N., Chikhladze V., Kartvelishvili L., Tatishvili M., Variability of Atmospheric Precipitation in Tbilisi in 1844-2023. // Int. Sc. Conf. "Complex Geophysical Monitoring in Georgia: History, Modern Problems, Promoting Sustainable Development of the Country", Proceedings, ISBN 978-9941-36-272-9, Publish House of Iv. Javakhishvili Tbilisi State University, Tbilisi, Georgia, October 17-19, 2024, pp. 150 – 154. http://dspace.gela.org.ge/bitstream/123456789/10620/1/38_MM-180.pdf
7. Amiranashvili A., Basilashvili Ts., Elizbarashvili E., Varazanashvili O., Catastrophic Floods in the Vicinity of Tbilisi. // Transactions IHM, GTU, vol.133, 2023, pp. 56-61, (in Georgian), doi.org/10.36073/1512-0902-2023-133-56-61; http://openlibrary.ge/bitstream/123456789/10337/1/133-11.pdf
8. Varazanashvili O., Gaprindashvili G., Elizbarashvili E., Basilashvili Ts., Amiranashvili A., Fuchs S., The First Natural Hazard Event Database for the Republic of Georgia (GeNHs). // Catalog, 2023, 270 p. http://dspace.gela.org.ge/handle/123456789/10369
9. Chelidze T., Amiranashvili A., Svanadze D., Tsamalashvili T., Tvauri G., Terrestrial and Satellite-Based Assessment of Rainfall Triggered Landslides Activity in Georgia, Caucasus. Bull. Georg. Nat. Acad. Sci., vol. 17, no. 2, 71-77, 2023, http://science.org.ge/bnas/vol-17-2.html
10. Amiranashvili A., Kereselidze Z., Mitin M., Khvedelidze I., Chikhladze V., Alarming factors of the Microclimate of the Vere River Valley and their Influence on the Floods Intensity. // Trans. of Mikheil Nodia Institute of Geophysics, ISSN 1512-1135, v. 69, Tbilisi, 2018, pp. 204-218, (in Georgian).
11. Amiranashvili A., Chelidze T., Svanadze D., Tsamalashvili T., Tvauri G., Abnormal Precipitation Before the Landslide in Akhaldaba (A Suburb of Tbilisi, Georgia) on June 13, 2015 According to Radar Measurements. // Journal of the Georgian Geophysical Society, e-ISSN*:* 2667-9973, p-ISSN**:** 1512-1127, Physics of Solid Earth, Atmosphere, Ocean and Space Plasma, v. 26(1), 2023, pp. 30–41. https://ggs.openjournals.ge/index.php/GGS/article/view/6959; DOI: https://doi.org/10.48614/ggs2620236959
12. Amiranashvili A., Brocca L., Chelidze T., Svanadze D., Tsamalashvili T., Varamashvili N., Analysis of the Precipitation Regime that Triggered the Landslide in Nergeeti (Imereti, Georgia) on February 7, 2024. // International Scientific Conference "Complex Geophysical Monitoring in Georgia: History, Modern Problems, Promoting Sustainable Development of the Country", Proceedings, Tbilisi, Georgia, October 17-19, 2024.
13. Beglarashvili N., Jamrishvili N., Janelidze I., Pipia M., Tavidashvili Kh., Analysis of Strong Precipitation in Tbilisi on August 29, 2023. // International Scientific Conference "Geophysical Processes in the Earth and its Envelopes", Proceedings, Tbilisi, Georgia, November 16-17, 2023, pp. 154-158.
14. Beglarashvili N., Jamrishvili N., Janelidze I., Pipia M., Tavidashvili Kh., Some Results of Analysis of Heavy Precipitation in Tbilisi on July 7, 2024 Based on Ground-Level and Satellite Measurements. // Int. Sc. Conf. "Complex Geophysical Monitoring in Georgia: History, Modern Problems, Promoting Sustainable Development of the Country", Proceedings, ISBN 978-9941-36-272-9, Publish House of Iv. Javakhishvili Tbilisi State University, Tbilisi, Georgia, October 17-19, 2024, pp. 164 – 167. http://dspace.gela.org.ge/bitstream/123456789/10617/1/41_MM-180.pdf
15. Tatishvili M., Kapadze N., Mkurnalidze I., Palavandishvili A., Drought Evaluation in Georgia using SPI and SpEI Indices. // Proceedings – Int. Sc. Conf. "Complex Geophysical Monitoring in Georgia: History, Modern Problems, Promoting Sustainable Development of the Country", Proceedings, ISBN 978-9941-36-272-9, Tbilisi, Georgia, October 17-19, 2024, pp. 96 – 100.

1st International Scientific Conference "Modern problems in Geophysics", Proceedings,
ISBN 978-9941-36-434-1, ISSN 3088-4349, Tbilisi, Georgia, November 6-8, 2025

RETROSPECTIVE ANALYSIS OF THE DYNAMICS OF HAIL PROCESSES IN EASTERN GEORGIA

Elizbarashvili I.

Mikheil Nodia Institute of Geophysics of Ivane Javakhishvili Tbilisi State University, Tbilisi, Georgia
iraklielizbarashvili11@gmail.com

Abstract. *This paper presents some results of a retrospective analysis of hail processes dynamics in Eastern Georgia. Specifically, GIS technology was used to update (digitize) V. Gigineishvili's (1960) well-known map-scheme of the foci and most common trajectories of intense hail in Eastern Georgia (based on long-term data from the meteorological network and field observations). A comparison was made between the trajectories of the hail processes presented on this map-scheme and the trajectories of the hail clouds on May 28 and July 13, 2019, obtained using radar observations of them. In the future, it is planned to update other previously created maps of the distribution of hazardous hydrometeorological processes in Georgia.*

Key words: *dangerous meteorological processes, hail, radar monitoring, hail process trajectory mapping, GIS technologies.*

Introduction

Among the various types of natural disasters in Georgia, hail processes are among the most significant due to the high level of damage they cause. Therefore, over the years, a large number of works have been published on various areas of research into these processes (hail climatology [1–6], radar observations of hail clouds [7–12], etc.). Detailed information on the dynamics of hail processes is often necessary to solve various problems of scientific or practical significance [1,7,11,12]. In particular, a well-known work [1] provides a schematic map of hail process trajectories in Eastern Georgia, presented in graphical form. Later, similar studies began to be conducted using digital technologies [3,6,8,11,12]. For a more qualitative comparative analysis of modern and historical maps, it is better to convert the latter to a modern form. An example of such a comparative analysis is presented below.

Study area, material, and methods

Study area – Eastern Georgia. The following materials were used in this work.

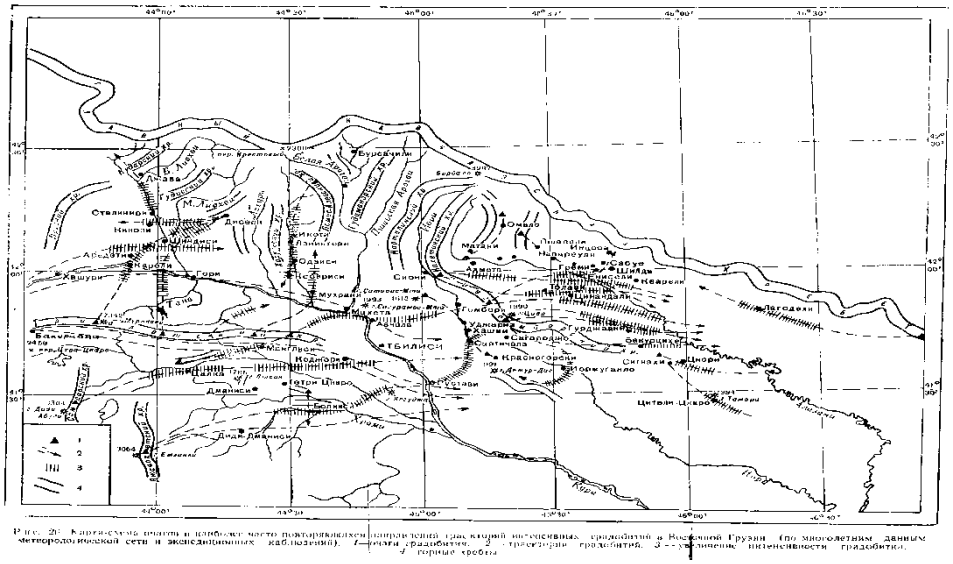

Fig. 1. Map-scheme of the foci and most frequently occurring trajectories of intense hailstorms in Eastern Georgia (based on long-term data from the meteorological network and field observations) [1].

1. Map-scheme the foci and most frequently occurring trajectories of intense hailstorms in Eastern Georgia (based on long-term data from the meteorological network and field observations) [1].
2. Radar data on hail cloud trajectories on May 28 and July 13, 2019, in Eastern Georgia [11,12]. The updating (digitization) of the map-scheme (Fig. 1) was carried out using GIS technologies.

Results and discussion

The results in Fig. 2 are presented.

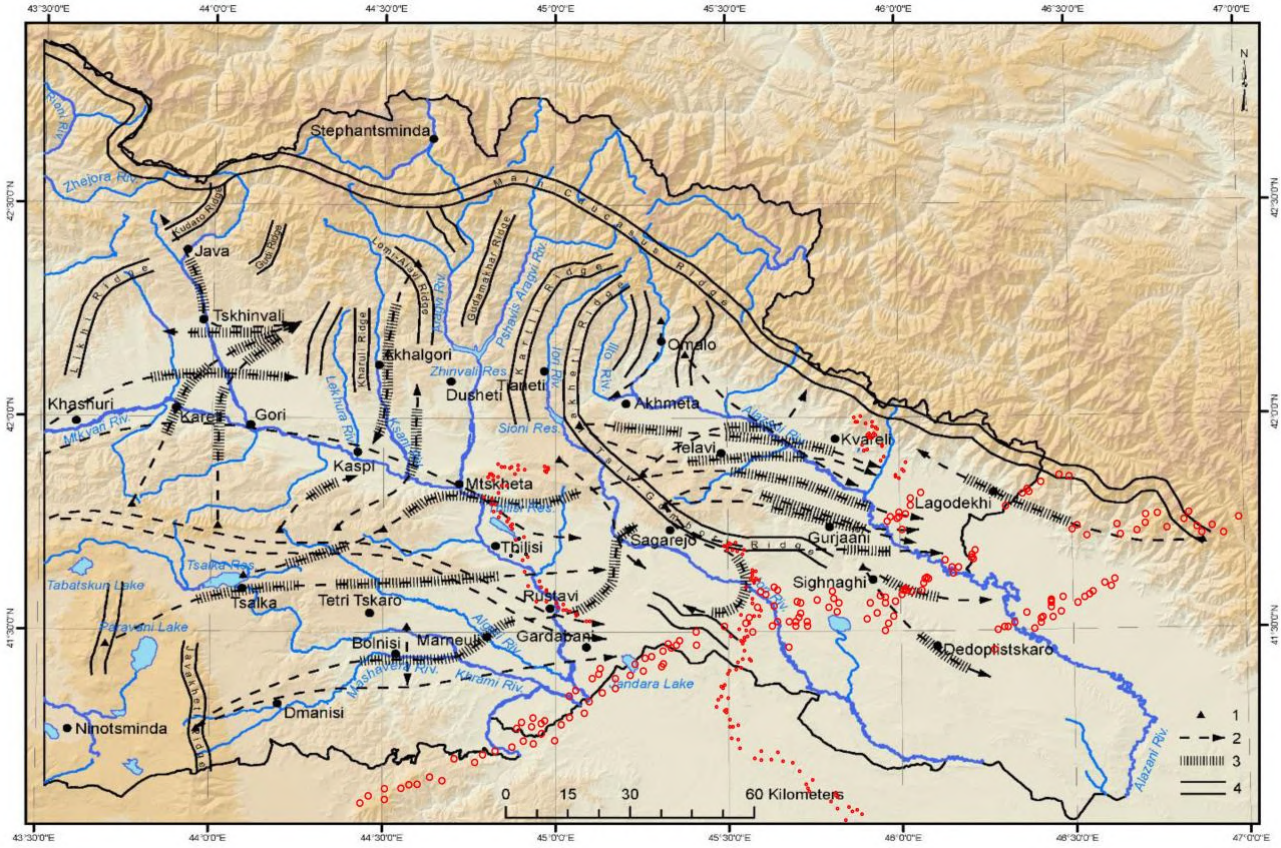

Fig. 2. Digitized map-scheme of Fig. 1.
1 – hailstorm foci. 2 – hailstorm trajectories. 3 – increasing hailstorm intensity. 4 – mountain ranges.

In Fig. 2, the digitized map-scheme of Fig. 1 is presented. Also, for example, data on the trajectories of hail clouds over the territory of Eastern Georgia on May 28 (small circles) and July 13 (large circles), 2019, obtained using radar observations of them [11,12] were superimposed on this updated map-scheme. The leading flow is Western.

As can be seen from Fig. 2, some hail cloud trajectories determined using radar observations coincide with the hail process trajectories according to [1], while others do not. For example, on May 28, 2019, some hail clouds moved from Azerbaijan to Georgia, and on July 13, 2019, from Armenia. Such trajectories are not shown on the map-scheme [1]. One explanation for this may be the lack of hail data in the specified area during the years of publication of [1]. Furthermore, radar observations are more representative for determining hail cloud trajectories than the network of meteorological stations.

It should be noted that a detailed graphic map-scheme of the trajectories of hail processes over the territory of Kakheti based on radar measurements is presented in the work [7], completed in 1982. In the future, it is planned to digitize this map, which will allow for a comparison of historical and modern radar data on the dynamics of hail processes over this territory.

As for the data from meteorological stations on hailstorms, the use of the information from the catalog [4] on them will allow a comparison of the dynamics of hail processes in Eastern Georgia in the last few decades with previous studies [1] in the context of climate change.

Conclusion

In the future, it is planned to update other previously created maps of the distribution of hazardous hydrometeorological processes in Georgia.

Acknowledgement. The author is grateful to the chief of the atmospheric physics department of M. Nodia Institute of Geophysics, A. Amiranashvili, for assistance in the fulfillment of this work.

References

1. Gigineyshvili V.M., Gradobitiya v Vostochnoy Gruzii. Leningrad, Gidrometeoizdat, 1960, 123 s., (in Russian).
2. Sulakvelidze G.K. Livnevyye osadki i grad. L., // Gidrometeoizdat, 1967, p. 412.
3. Varazanashvili O., Tsereteli N., Amiranashvili A., Tsereteli E., Elizbarashvili E., Dolidze J., Qaldani L., Saluqvadze M., Adamia Sh., Arevadze N., Gventcadze A. // Vulnerability, hazards and multiple risk assessment for Georgia. Natural Hazards, Vol. 64, Number 3 (2012), 2021-2056, DOI: 10.1007/s11069-012-0374-3, http://www.springerlink.com/content /9311p18582143662/fulltext.pdf
4. Varazanashvili O., Gaprindashvili G., Elizbarashvili E., Basilashvili, Ts., Amiranashvili A., Fuchs S. The First Natural Hazard Event Database for the Republic of Georgia (GeNHs). // Catalog, 2023, 270 p. http://dspace.gela.org.ge/handle/123456789/10369; DOI: 10.13140/RG.2.2.12474.57286
5. Kartvelishvili L., Tatishvili M., Amiranashvili A., Megrelidze L., Kutaladze N. Weat,her, Climate and their Change Regularities for the Conditions of Georgia. Monograph, Publishing House "UNIVERSAL", ISBN: 978-9941-33-465-8, Tbilisi 2023, 406 p., https://doi.org/10.52340/mng.9789941334658
6. Amiranashvili A., Beglarashvili N., Elizbarashvili E., Varazanashvili O., Pipia M., Statistical analysis of data from 30 meteorological stations of Georgia on the number of days with hail in the warm half of the year in 1941-2021. // Transactions of IHM, GTU, vol. 135, 2024, pp. 32-38 (in Georgian).
7. Doreuli R.I., Raspredeleniye srednikh skorostey peremeshcheniya i napravleniya gradoopasnykh oblakov na territorii Alazanskoy doliny i Iorskogo ploskogor'ya po dannym radiolokatsionnykh nablyudeniy. // Tr. In-ta geofiziki AN GSSR, t. 49, Tb.:, Metsniyereba, 1982, pp.. 96-102, (in Russian).
8. Amiranashvili A., Chikhladze V., Dzodzuashvili U., Ghlonti N., Sauri I., Telia Sh., Tsintsadze T., Weather Modification in Georgia: Past, Present, Prospects for Development. International Scientific Conference „Natural Disasters in Georgia: Monitoring, Prevention, Mitigation". // Proceedings, Tbilisi, Georgia, December 12-14, 2019, pp. 213-219.
9. Selex ES GmbH · Gematronik Weather Radar Systems. // Rainbow®5 User Guide, 2015, 464 p., www. gematronik.com
10. Avlokhashvili Kh., Banetashvili V., Gelovani G., Javakhishvili N., Kaishauri M., Mitin M., Samkharadze I., Tskhvediashvili G., Chargazia Kh., Khurtsidze G. Products of Meteorological Radar «METEOR 735CDP10». // Trans. of Mikheil Nodia Institute of Geophysics, ISSN 1512-1135, vol. 66, Tb., 2016, pp. 60-65, (in Russian).
11. Amiranashvili A., Bliadze T., Jamrishvili N., Kekenadze E., Tavidashvili Kh., Mitin M., Some Characteristics of Hail Process in Georgia and Azerbaijan on May 28, 2019. // Journal of the Georgian Geophysical Society, ISSN: 1512-1127, Physics of Solid Earth, Atmosphere, Ocean and Space Plasma, v. 22(2), 2019, pp. 40–54.
12. Pipia M., Amiranashvili A., Beglarashvili N., Elizbarashvili E., Varazanashvili O., Analysis and Damage Assessment of Hail Processes in Georgia and Azerbaijan Using Radar Data (On the Example of May 28 and July 13, 2019). // Reliability: Theory & Applications, ISSN: 1932-2321, vol. 18, iss. SI 5 (75), pp. 267-274, DOI: 10.24412/1932-2321-2023-575-267-274, https://cyberleninka.ru/article/n/analysis-and-damage-assessment-of-hail-processes-in-georgia-and-azerbaijan-using-radar-data-on-the-example-of-may-28-and-july-13

1st International Scientific Conference "Modern problems in Geophysics", Proceedings,
ISBN 978-9941-36-434-1, ISSN 3088-4349, Tbilisi, Georgia, November 6-8, 2025

MODELING THE DISTRIBUTION OF MEAN MAX HAIL DAMAGE TO VINEYARDS ON THE TERRITORY OF MUNICIPALITIES OF KAKHETI (GEORGIA) USING DATA OF THE ZERO ISOTHERM IN THE ATMOSPHERE AND RADAR MEASUREMENTS

[*,]Pipia M., [*]Amiranashvili A., [**,***]Beglarashvili N., [**]Elizbarashvili E., [*]Elizbarashvili I., [*]Jamrishvili N., [*]Tavidashvili Kh., [*]Varazanashvili O.**

[*]M. Nodia Institute of Geophysics of the I. Javakhishvili Tbilisi State University, Tbilisi, Georgia
[**]Institute of Hydrometeorology of the Georgian Technical University, Tbilisi, Georgia
[***] Samtskhe-Javakheti State University, Akhaltsikhe, Georgia
m.pipia@gtu.ge

Abstract. *Results of modeling the distribution of monthly mean max hail damage to vineyards (HDV) and their 99% values of the upper levels (HDV_Upp) on the territories of 8 municipalities of Kakheti (Georgia) are presented. Calculations have been carried out using data of the freezing level in the atmosphere and radar measurements of hail max sizes in clouds. The agricultural area of Kakheti (7050 km^2) was divided into 290 squares, with the range of heights – 0.21 ÷ 1.19 km. Period of investigation – from April to September. For example map of the distribution of HDV on the territory of Kakheti for April and June has been built. Data on the statistical characteristics of HDV and HDV_Upp from April to September are presented for each municipality.*

Key Words: Dangerous meteorological processes, empirical modeling, hail damage assessment, radar monitoring.

Introduction

Georgia is one of the most hail-prone countries in the world in terms of hail damage. In this regard, the problem of hail in our country is given special attention. Over many decades, including in recent years, a large number of works have been published covering a wide range of studies, including hail climatology [1-5], radar observations of hail processes [6-8], etc. To solve various problems of scientific or applied significance (the impact of climate change on hail processes, comparison of experimental data on hail processes with theoretical models of hail processes, assessment of expected damage from hail processes, planning of work on active influence on hail processes, etc.), detailed information on the spatio-temporal characteristics of hail distribution and its sizes at various points is necessary. In accordance with the above, in addition to the conducted studies, work was carried out on empirical modeling of the distribution of hailstones by average maximum diameter (D) in the territory of Kakheti (Georgia) using data on the freezing level in the atmosphere and radar measurements of the maximum sizes of hailstones in clouds [9-12]. These studies subsequently made it possible to assess the damage to some crops from hail processes in Georgia and Azerbaijan (using the example of May 28 and July 13, 2019) [13], as well as to model the distribution of mean monthly maximum values of damage to vineyards from hail in the territory of Kakheti [14].

The presented work is a continuation of the previous study [14]. Results of modeling the distribution of monthly mean max hail damage to vineyards and their 99% values of the lower and upper levels on the agricultural area of 8 municipalities of Kakheti from April to September are presented below.

Study area, material, and methods

Study area – 8 municipalities of the Kakheti region of Georgia (Akhmeta, Dedoplistskaro, Gurjaani, Kvareli, Lagodekhi, Sagarejo, Sighnaghi, Telavi).

Data of meteorological radar "METEOR 735 CDP 10 – Doppler Weather Radar" of Anti-hail service of Georgia about the max diameter of hailstones in the clouds (cm) are used (radar product HAILSZ) [15]. The

expected diameter of hailstones falling out to the earth's surface according to the Zimenkov-Ivanov model of hail melting in the atmosphere [9, 11] by taking into account the radar data about their maximum diameter in the clouds and freezing level in the atmosphere, was calculated [12]. Period of observation: April-September, 2016-2019. The degree of damage to vineyards, depending on the size of the fallen hail, was determined by compiling data on damage to these crops at different hail kinetic energy [16] and data on the average kinetic energy of hail of various sizes according to TORRO Hail Scale [https://www.torro.org.uk/research/hail/hscale].

Based on this compilation, regression equations were obtained for the relationship between the degree of damage to this crop (HDV) and the size of hailstones, which has the form of a sixth power of polynomial [13]. Calculations were carried out for the agricultural territory of Kakheti (7050 km^2), divided into 290 squares. Altitude range – 0.21 ÷ 1.19 km.

For the data analysis, the standard statistical methods are used. The following designations of statistical information are used below: Mean – average values; Min – minimal values; Max – maximal values; 99%_Upp – 99% of upper levels of the mean (below – Upp); H – altitude above sea level, km.

Results

Results in Fig. 1-2 and Table 1 are presented.

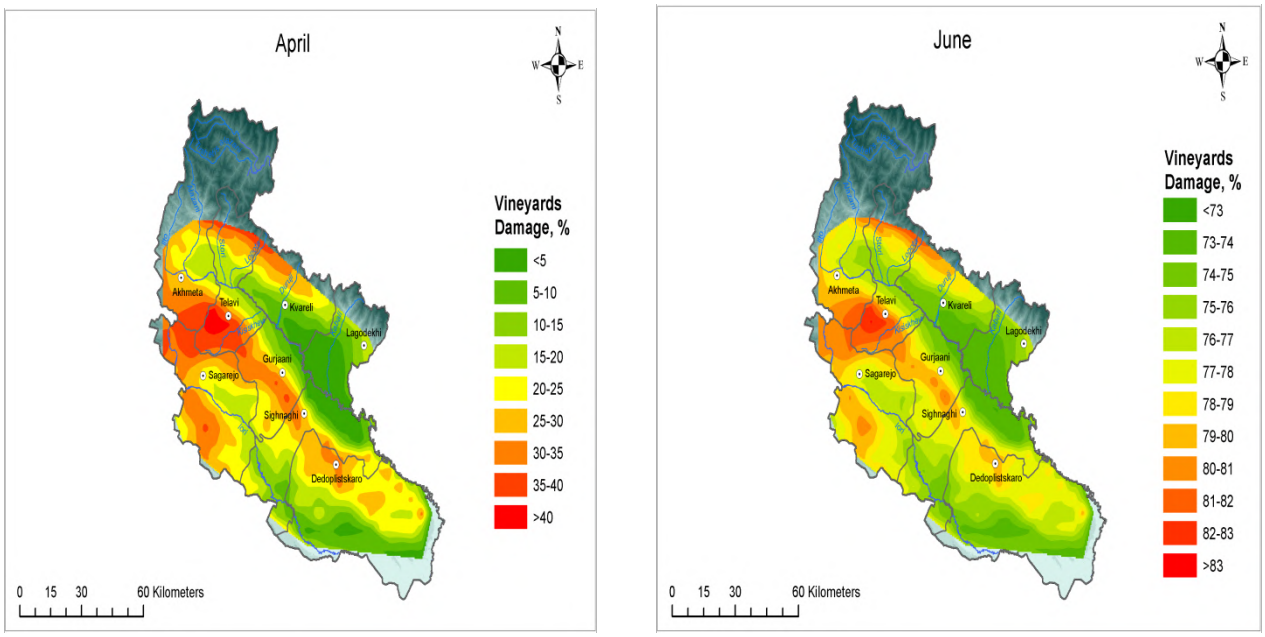

Fig. 1. Distribution of mean maximum hail damage to vineyards on the agricultural area of Kakheti in April and June.

In Fig. 1, examples of distribution of mean maximum hail damage to vineyards in the agricultural area of Kakheti in April and June are presented. In particular, as follows from these figures, the mean max of HDV in the study area is quite heterogeneous and varies from 0% to 43.3% (April) and from 73.0% to 83.1% (June). Similar pictures for other months are observed.

In Table 1 the statistical characteristics of mean maximum damage to vineyards from hail in the agricultural area of 8 municipalities of Kakheti from April to June is presented.

In particular, Table 1 shows that the variability of the mean maximum of HDV on the territory of 8 municipalities of Kakheti is as follows:

HDV_Mean. 0.0 % (August, all municipalities) ÷ 83.1% (June, Telavi municipality).

HDV_Upp. 44.3 % (August, Lagodekhi and Sighnaghi municipalities) ÷ 92.2 % (June, Telavi municipality).

The average seasonal (April – September) values of HDV_Mean and HDV_Upp for the municipalities of Kakheti are, respectively. Akhmeta: 50.5 and 74.8 %; Dedoplistskaro: 48.9 and 73.8 %; Gurjaani: 51.6 and 75.6 %; Kvareli: 47.9 and 73.1 %; Lagodekhi: 44.8 and 71.0 %; Sagarejo: 52.2 and 76.1 %; Sighnaghi: 48.2 and 73.3 %; Telavi: 52.8 and 76.8 %.

Table 1. The statistical characteristics of mean maximum damage to vineyards from hail in the agricultural area of 8 municipalities of Kakheti from April to June (%).

Month		April		May		June		July		August		September	
Variable	H	Mean	Upp	Mean	Upp	Mean	Upp	Mean	Upp	Mean	Upp	Mean	Upp
Munic.	Akhmeta												
Mean	0.58	22.9	58.6	67.2	77.7	77.3	87.5	68.0	84.5	0.0	54.5	67.7	86.2
Min	0.43	15.2	56.0	65.0	76.2	75.6	86.3	65.5	83.1	0.0	50.7	65.4	85.0
Max	0.77	30.8	61.4	69.7	79.5	79.3	88.9	70.9	86.2	0.0	58.8	70.3	87.6
Munic.	Dedoplistskaro												
Mean	0.50	18.1	57.1	65.9	76.9	76.4	86.8	66.6	83.8	0.0	52.4	66.4	85.5
Min	0.22	0.0	52.2	61.7	74.0	73.1	84.6	61.7	81.1	0.0	44.7	61.9	83.2
Max	0.83	33.0	62.3	70.4	80.0	79.8	89.3	71.8	86.7	0.0	60.0	71.1	88.0
Munic.	Gurjaani												
Mean	0.65	25.6	59.6	68.1	78.4	78.0	88.0	69.1	85.1	0.0	56.1	68.7	86.7
Min	0.36	11.2	54.9	64.0	75.6	74.9	85.7	64.3	82.5	0.0	49.0	64.3	84.4
Max	0.93	36.4	63.8	71.7	80.9	80.8	90.1	73.2	87.5	0.0	62.1	72.5	88.8
Munic.	Kvareli												
Mean	0.45	15.3	56.2	65.2	76.4	75.8	86.4	65.7	83.3	0.0	51.0	65.6	85.1
Min	0.26	3.6	52.9	62.3	74.4	73.6	84.9	62.3	81.5	0.0	45.8	62.6	83.5
Max	0.70	28.4	60.5	68.8	78.9	78.6	88.4	69.9	85.6	0.0	57.4	69.5	87.1
Munic.	Lagodekhi												
Mean	0.29	6.0	53.6	62.9	74.8	74.0	85.2	63.0	81.8	0.0	46.8	63.2	83.8
Min	0.21	0.0	52.0	61.5	73.9	73.0	84.5	61.4	81.0	0.0	44.3	61.7	83.1
Max	0.51	19.9	57.5	66.2	77.1	76.6	86.9	67.0	83.9	0.0	53.0	66.7	85.6
Munic.	Sagarejo												
Mean	0.69	27.5	60.2	68.6	78.8	78.5	88.3	69.7	85.5	0.0	57.0	69.2	87.0
Min	0.44	16.2	56.3	65.2	76.4	75.8	86.4	65.8	83.3	0.0	51.2	65.7	85.1
Max	0.95	37.0	64.1	71.9	81.1	81.0	90.3	73.5	87.7	0.0	62.5	72.7	88.9
Munic.	Sighnaghi												
Mean	0.47	16.0	56.5	65.4	76.6	76.0	86.5	66.0	83.4	0.0	51.4	65.9	85.2
Min	0.21	0.0	52.0	61.5	73.9	73.0	84.5	61.4	81.0	0.0	44.3	61.7	83.1
Max	0.97	37.5	64.3	72.1	81.2	81.2	90.4	73.7	87.9	0.0	62.8	72.9	89.1
Munic.	Telavi												
Mean	0.75	28.7	60.9	69.2	79.2	78.9	88.7	70.4	85.9	0.0	57.9	69.9	87.4
Min	0.42	14.6	55.8	64.8	76.1	75.5	86.2	65.3	83.0	0.0	50.4	65.2	84.9
Max	1.19	43.3	67.1	74.6	83.0	83.1	92.0	76.4	89.6	0.0	66.6	75.4	90.6

Conclusion

In the future, we plan to conduct modeling and build maps of the extent of hail damage to wheat and corn in Kakheti and its municipalities in different months of the year. We also plan to conduct model assessments of damage from hail and other crops. As new experimental data is obtained, we plan to further refine the results obtained.

Acknowledgments. This work was supported by Shota Rustaveli National Science Foundation of Georgia (SRNSFG), Grant number FR-22-2882.

References

1. Kartvelishvili L., Tatishvili M., Amiranashvili A., Megrelidze L., Kutaladze N., Weather, Climate and their Change Regularities for the Conditions of Georgia. // Publishing House “UNIVERSAL”, Tbilisi, 406 p., 2023.

2. Amiranashvili A., Basilashvili Ts., Elizbarashvili E., Gaprindashvili G., Varazanashvili O., Statistical Analysis of the Number of Days with Hail in Georgia According to Meteorological Stations Data in 2006-2021. //Int. Conf. of Young Scientists “Modern Problems of Earth Sciences”, proc., Tbilisi, pp. 164-168, November 21-22, 2022.
3. Pipia M., Amiranashvili A., Beglarashvili N., Elizbarashvili E., Varazanashvili O., Variability in the Number of Days with Hail in the Warm Half of the Year in Bolnisi and Tsalka in 1941-2021 and their Expected Change until 2045. // Journal of the Georgian Geophysical Society, e-ISSN: 2667-9973, p-ISSN: 1512-1127, Physics of Solid Earth, Atmosphere, Ocean and Space Plasma, v. 27(1), 2024, pp. 58–66. https://ggs.openjournals.ge/index.php/GGS/article/view/7984
4. Pipia M., Amiranashvili A., Elizbarashvili E., Varazanashvili O., Beglarashvili N., Jamrishvili N., Variability in the Number of Days with Hail in the Warm Half of the Year on the Territory of Georgia in 1941-2021. // Reliability: Theory and Applications, ISSN 1932-2321, Special Issue № 6 (81), Part-2, Vol. 19, 2024, pp. 552 – 559. https://doi.org/10.24412/1932-2321-2024-681-552-559
5. Pipia M.G., Amiranashvili A.G., Elizbarashvili E. Sh., Beglarashvili N.G., Pipia G.G., Jamrishvili N.K., Varazanashvili O. Sh., Degree and Areas of Damage Caused by Hail in the Territory of Kakheti Region (Georgia). // Journal of International Scientiíc Publications: Agriculture & Food, ISSN 1314-8591, vol. 12, 2024, pp. 54-60. https://doi.org/10.62991/AF1996546926
6. Abaiadze O., Avlokhashvili Kh., Amiranashvili A., Dzodzuashvili U., Kiria J., Lomtadze J., Osepashvili A., Sauri I., Telia Sh., Khetashvili A., Tskhvediashvili G., Chikhladze V., Radar Providing of Anti-Hail Service in Kakheti. // Trans. of Mikheil Nodia Institute of Geophysics, vol. 66, 2016, pp. 28-38. (in Russian).
7. Pipia M., Amiranashvili A., Beglarashvili N., Elizbarashvili E., Varazanashvili O. Analysis and Damage Assessment of Hail Processes in Georgia and Azerbaijan Using Radar Data (On the Example of May 28 and July 13, 2019). // Reliability: Theory & Applications, vol. 18, iss. SI 5 (75), 2023, pp. 267-274.
8. Pipia M.G., Amiranashvili A.G., Chikhladze V.A., Elizbarashvili E. Sh., Pipia G.G., Beglarashvili N.G., Varazanashvili O.Sh. Distribution of Hailstorm Areas in Kakheti Region (Georgia) According to the Diameter of Hailstones in the Clouds. // Journal of International Scientiíc Publications: Ecology & Safety, ISSN 1314-7234, vol. 18, 2024, pp.103-108. https://doi.org/10.62991/ES1996566836
9. Jamrishvili N.K., Tavidashvili Kh.Z., Estimation of the Diameter of Fallen to the Earth's Surface Hail Stones Taking Into Account Their Size in the Cloud and the Heights of Zero Isotherm Under the Conditions of Kakheti Region of Georgia. // Int. Sc. Conf. „Modern Problems of Ecology“, Proc., vol. 6, Kutaisi, Georgia, 21-22 September, 2018, pp. 130-133
10. Amiranashvili A., Bolashvili N., Gulashvili Z., Jamrishvili N., Suknidze N., Tavidashvili Kh., Distribution of Hail by Mean Max Size on the Territories of Municipalities of the Kakheti Region of Georgia. // Int. Sc. Conf. „Natural Disasters in the 21st Century: Monitoring, Prevention, Mitigation“, proc., Tbilisi, Georgia, December 20-22, 2021, pp. 84-87.
11. Zimenkov V.A., Ivanov V.V.. Raschet tayaniya gradin v estestvennykh protsessakh. // Tr. VGI. vyp. 3(5), 1966, (in Russian).
12. Amiranashvili A.G., Berianidze N.T., Jamrishvili N.K., Tavidashvili Kh.Z., Statistical Characteristics of the Monthly Average Values of the Air Temperature in the Layer of Atmosphere 0.54-27 km above the Kakheti Territory (Georgia) in 2012-2016. // Journal of the Georgian Geophysical Society, Issue B. Physics of Atmosphere, Ocean and Space Plasma, vol. 20B, pp. 24 –42, 2017.
13. Pipia M., Amiranashvili A., Beglarashvili N., Elizbarashvili E., Varazanashvili O., Analysis and Damage Assessment of Hail Processes in Georgia and Azerbaijan Using Radar Data (On the Example of May 28 and July 13, 2019) // Reliability: Theory & Applications, vol. 18, iss. SI 5 (75), 2023, pp. 267-274.
14. Pipia M.G., Amiranashvili A.G., Elizbarashvili E.Sh., Varazanashvili O.Sh., Beglarashvili N.G., Jamrishvili N.K., Modeling the Distribution of Mean Max Hail Damage to Vineyards on the Territory of Kakheti (Georgia) using Data of the Freezing Level in the Atmosphere and Radar Measurements. // Afr. J. Bio. Sc., ISSN: 2663-2187, Volume 6, Issue 14, 2024, pp. 6132-6139, https://doi.org/10.48047/AFJBS.6.14.2024.6132-6139
15. Selex E.S., GmbH Gematronik Weather Radar Systems. // Rainbow®5 User Guide, 2015, p. 464. www.gematronik.com
16. Abshaev A.M., Abshaev M.T., Barekova M.V.,Malkarova A.M., Rukovodstvo po organizacii i provedeniu protivogradovih rabot. // Pechatni dvor, Nalchik, 2014, p. 500. (in Russian).

1st International Scientific Conference "Modern problems in Geophysics", Proceedings,
ISBN 978-9941-36-434-1, ISSN 3088-4349, Tbilisi, Georgia, November 6-8, 2025

THE TURN TOWARDS GEOPHYSICS IN HISTORIC RESEARCH AND THE CHANCES IT OFFERS FOR THE STUDY OF WEATHER MODIFICATION IN GEORGIA

Schulz S.

Heidelberg University, Germany
simon.schulz@zegk.uni-heidelberg.de

Abstract: *This paper aims to inform the participants of the conference „Modern problems in Geophysics" about ongoing historic research on Geophysics and thereby enable interdisciplinary exchange. First, it is given an overview of selected scientific literature from fields such as the history of science and knowledge, environmental history and Cold War history. This literature illustrates the significantly grown interest in the history of Geophysics, in quantity and diversity alike. Then, drawing on the example of weather modification, the opportunity for such a history of Geophysics in Georgia is outlined from a historical perspective.*

Key words: *History of science, history of Geophysics, Georgia, weather modification.*

Introduction

Writing in 2003 and 2009, the historian of science Ronald Doel identified an imbalance between the historic research in biological and physical Earth sciences. Although physical Earth sciences such as oceanography, atmospheric science or hydrology have shaped the Cold War by their dramatic expansion in these decades, it was mainly the biological sciences which dominated public perception, as well as new research directions such as environmental history. Since Rachel Carson's *Silent Spring* (1962), ecological thinking has influenced the perception of the planet and the history of human interaction with it [1].

This diagnosis, however, was already accompanied by a rising interest in Geophysics among historians of various subdisciplines. Therefore, it is not surprising that, when reviewing new books in 2019, the historian Dania Achermann already finds a "New Diversity in the History of Meteorology and Climate Science" [2].

New historic literature on Geophysics

Although the reasons for such a new interest are numerous, climate change clearly stands out as the single most important influence. The ever-rising awareness for the world's changing climate, its anthropological cause and its fundamental impacts on societies resulted in an increased need for an understanding of how this today's knowledge historically arose. Closely connected to this, the concept of the *Anthropocene,* which describes humans as a force that changes the physical Earth, challenged but also stimulated research in the history of human – planetary interaction [3]. Finally, a new understanding of knowledge further drove the interest in the history of Geophysics. Knowledge, it had been highlighted, is not an absolute and ahistorical thing that simply exists, but rather historically produced and shaped by the cultural and political context in which it is developed [4].

One of the main results of the new historical interest in Geophysics were numerous studies, in which scholars such as Paul Edwards or Kristine Harper traced the genesis of numeral models in meteorology and climatology [5]. They showed how computer modelling not only transformed the disciplines itself, but has become an essential and inevitable part of today's understanding of the physical environment of the planet. Hélène Guillemot, on the other hand, underlined the flaws and uncertainties which are still part of climate models today despite enormous progress in computing and observation [6]. The historical interest, however, has not stopped there. Historians, such as James Fleming, wrote the history of meteorology in the United

States in the 19th and 20th centuries [7]. Such long-term analysis have been accompanied by regionally and thematically focused studies. Fleming himself, for example, wrote biographies of individual scholars such as Guy Stewart Callendar and Joanne Simpson [8]. In *Imperial Weather*, Fiona Williamson discussed the closely connected histories of meteorology and colonialism in Malaya [9]. By the example of meteorology in Victorian Britan, Katharine Anderson showed how the early science of weather prediction became drawn into the public discourse [10]. Deborah Coen, in turn, explored the influence of the complex structure of the Habsburg Empire on conceptional thinking in the 19th century's climatology [11] as well as the contribution of land empires such as Austria-Hungary and the Russian Empire to the early history of this discipline [12]. Jonathon Oldfield, finally, outlined the contributions to global climate science by the important Soviet climatologist Mikhail Budyko [13].

Although meteorology and climatology have attracted most of the attention, they are by far not the only geophysical disciplines studied by historians in the last years. It is oceanology that reveals one of the central objects of this historical investigation: the influence of the state, the military or economic actors on the production of geophysical knowledge. Jacob Hamblin in *Oceanographers and the Cold War* and Naomi Oreskes in *Science on a Mission: How Military Funding Shaped What We Do and Don't Know about the Ocean* [14] have shown how American oceanography gained funding and enormous new research opportunities as part of the military-industrial complex of the Cold War. Whether sea-launched nuclear missiles or vast amounts of data on the oceans, oceanography had much to offer for the scientific race between the United States and the Soviet Union.

Researchers like Julia Lajus, Sverker Sörlin, Lif Lund Jacobsen and Irina Fedorova did not only extend the historic study to further disciplines but helped as well to include the Soviet Union and the international circulation of knowledge into the history of Geophysics. Lif Lund Jacobsen, Irina Fedorova and Julia Lajus showed how seismographs became diplomatic objects as the United States and the Soviet Union exchanged these scientific instruments during the Cold War [15]. By the example of Arctic research, Julia Lajus and Sverker Sörlin examined how personal contacts enabled exchange between Scandinavia and the Soviet Union despite the East-West divide [16].

Finally, one can add that research in the Earth sciences has also reached literary studies. *Literary meteorology*, a concept introduced by Michael Gamper in 2014, understands weather in the broader context of knowledge and studies the contribution of literature to such knowledge [17].

Currently ongoing research projects in the history of Geophysics focus, for example, on the history of the Second Polar Year in the context of rising political instability, due to the Great Depression and the rise of Hitler in Germany [18], and Soviet glaciology in Central Asia, aiming to stimulate an interdisciplinary exchange between natural and social sciences [19].

My own research project deals with the history of weather modification in the Soviet Union in a regional and an international context. The most important prospects of this approach for the history of Geophysics in Georgia are outlined in the following:

Weather Modification – an opportunity for the history of Geophysics in Georgia

From the perspective of much of the literature and the projects discussed above, in particular the two aspects of international and regional context seem prosperous for future examination. As science in the 19th and 20th centuries was often embedded in transnational networks, studying these international links is vital for the understanding of a discipline's development. Even when there is no direct interaction, researchers are aware of being part of larger processes. On the other hand, however, the concrete conditions, such as the existing scientific and knowledge infrastructure, the political framework and the physical environment are determined by the concrete regional context in which research is conducted. Three approaches might be taken in order to write the history of weather modification as an example of the history of Geophysics in Georgia in an international and a regional perspective:

Firstly, the long tradition of geophysical observation and research in Georgia and the Caucasus region must be put into context. Ranging from the early 19th century and the Tsarist Empire over the Soviet Union in the 20th century to the independent Georgia in the 21st century, Geophysics in Georgia has been embedded and shaped by the various domestic and international influences. Historic research can closely analyse these

conditions and influences in order to determine their particular effect on the development of Geophysics in Georgia. The anti-hail research and activities can serve as an important case for this: having first been tried during the late Tsarist period, they were renewed and peaked in the post-war Soviet Union. While the transformation period of the 1990s led to the end of this Soviet-time work, anti-hail measures were reapplied under the now different conditions of the independent Georgia [20-22].

Secondly, including biographical elements in the study of a scientific field has proved to be highly beneficial. This is not only because individual actors and researchers developing new methods and perspectives are often vastly influential for the advancement of their fields. Rather, biographies often reveal larger processes formative for an entire generation or region, but hard to detect from a bird's-eye perspective. Moreover, they can tighten often abstract research questions and structures to personal experiences and decisions. Here, weather modification again offers numerous examples, such as the life and work of Georgi Sulakvelidze, Amiran Kartsivadze or Vasil Lominadze. Considering their professional development in Georgia, but as well their interactions with other Soviet scientists and with their Western counterparts can open a window in the complex, but formative context of Georgian Geophysics and weather modification. Sulakvelidze, for example, was also well-known and highly recognized among American researchers [23-26].

Finally, as researchers like Deborah Coen have shown, approaching the history of research in fields like meteorology, climatology or hydrology through different scales can offer important insights. Evaluating theories, experiments and findings against the background of global and local challenges and particularities sharpens awareness of the causes of success and failure. For the history of weather modification in Georgia, this especially means that the anti-hail systems developed in the Caucasus, on the one hand, can be seen as a response to local needs such as the protection of vineyards. They most importantly had to prove effective for this purpose. On the other hand, however, such specifically local conditions existed in other parts of the world, where anti-hail systems were developed as well. Nevertheless, the specific actors, interests, and goals differed from case to case and success in one case might be seen a failure in another.

Conclusion

My project aims to write the history of weather modification through such shared, but nevertheless variating local experiences and as part of a global history. It thus enables to understand the history of Geophysics in Georgia within both its global and its regional framework. Thereby, it contributes to an increasingly richer literature on the history of Geophysics.

Acknowledgement. This paper was written during a research scholarship from the Max Weber Foundation. I would like to express my gratitude to the foundation for the opportunity to conduct research in Georgia. I am very grateful to Avtandil Amiranashvili, Victor Chikhladze, Marika Tatishvili and Lado Mirianashvili for sharing their insights and experiences in weather modification in Georgia with me during this research stay.

References

1. Doel R.E., Constituting the Postwar Earth Sciences: The Military's Influence on the Environmental Sciences in the USA after 1945. // Social Studies of Science, Issue 33/5, 2003, pp. 635-666. Doel R.E. What is the Place of the Physical Environment Sciences in Environmental History? // Revue d'histoire moderne & contemporaine, Issue 56/4, 2009, pp. 137-164, (in French).
2. Achermann D., Broadening the Narrative: The New Diversity in the History of Meteorology and Climate Science. // NTM Zeitschrift für Geschichte der Wissenschaften, Technik und Medizin, Issue 27, 2019, p. 201, (in German).
3. Trischler H., The Anthropocene. A Challenge for the History of Science, Technology, and the Environment. // NTM Zeitschrift für Geschichte der Wissenschaften, Technik und Medizin, Issue 24, 2016, pp. 309–335.
4. Sarasin P., More Than Just Another Specialty: On the Prospects for the History of Knowledge. // Journal for the History of Knowledge, Issue 1/1, 2020, pp. 1–5.
5. Edwards, P.N., A Vast Machine: Computer Models, Climate Data, and the Politics of Global Warming. // Monograph, ISBN 978-0-262-01392-5, Cambridge/London, 2010, 518 pp.
6. Harper K.C., Weather by the Numbers: The Genesis of Modern Meteorology // Monograph, ISBN 978-0-262-08378-2, Cambridge, 2008, p. 308.

7. Guillemot H., How to develop climate models? The “gamble” of improving climate model parameterizations. In the book: Cultures of Prediction in Atmospheric and Climate Science. Epistemic and Cultural Shifts in Computer-based Modelling and Simulation, ISBN 9781315406282, New York, 2017, p. 272.
8. Fleming J.R. Meteorology in America, 1800-1870. // Monograph, ISBN 9780801863592, Baltimore, 1990, p. 264.
9. Fleming J.R. The Callendar Effect: The Life and Work of Guy Stewart Callendar (1898-1964), The Scientist Who Established the Carbon Dioxide Theory of Climate Change. // Monograph, ISBN 978-1878220769, Boston, 2007, p. 176.
10. Fleming J.R., First Woman: Joanne Simpson and the Tropical Atmosphere. // Monograph, ISBN 978-0198862734, New York, 2020, p. 224.
11. Williamson F. Imperial Weather. Meteorology, Science, and the Environment in Colonial Malaya. // Monograph, ISBN9780822948421,Pittsburgh, 2025, p. 320.
12. Anderson K. Predicting the Weather: Victorians and the Science of Meteorology. // Monograph, ISBN 978-0226019680, Chicago/London, 2005, 376 p=p.
13. [11] Coen D.R. Climate in Motion. Science, Empire, and the Problem of Scale // Monograph, ISBN 978-0226752334, Chicago, 2018, 425 pp.
14. [12] Coen D.R. Imperial Climatographies from Tyrol to Turkestan. // Osiris, Issue 26/1, 2011, pp. 45-65.
15. [13] Oldfield J.D. Mikhail Budyko’s (1920–2001) contributions to Global Climate Science: from heat balances to climate change and global ecology. // WIREs Climate Change, Issue 7, 2016, pp. 682–692.
16. [14] Hamblin J.D. Oceanographers and the Cold War. Disciples of Marine Science // Monograph, ISBN 9780295984827, Seattle, 2005, p. 368.
17. Oreskes N. Science on a Mission: How Military Funding Shaped What We Do and Don’t Know about the Ocean // Monograph, ISBN 9780226732381, Chicago, 2021, 744 p.
18. [15] Jacobsen L.L., Fedorova I., Lajus J. The seismograph as a diplomatic object: The Soviet–American exchange of instruments, 1958–1964 // Centaurus, Issue 63/2, 2021, pp. 277–295.
19. [16] Lajus J., Sörlin S. Melting the glacial curtain: the politics of Scandinavian-Soviet networks in the geophysical field sciences between two polar years, 1932/33-1957/58 // Journal of Historical Geography, Issue 44, 2014, pp. 44-59.
20. Gamper M. Mysteries of the atmosphere. Outlines of a 'literary meteorology'. // Zeitschrift für Germanistik, Issue 24/2, 2014, pp. 229-243 (in German).
21. See https://nias.knaw.nl/fellow/julia-lajus/ (last accessed: 28th September 2025)
22. See https://data.snf.ch/grants/grant/192203 (last accessed: 28th September 2025)
23. Amiranashvili A., Chikhladze V., Dzodzuashvili U., Ghlonti N., Sauri I., Telia Sh., Tsintsadze T., Weather Modification in Georgia: Past, Present, Prospects for Development. // International Scientific Conference „Natural Disasters in Georgia: Monitoring, Prevention, Mitigation“, Proceedings, Tbilisi, Georgia, December 12-14, 2019, pp. 213-219.
24. Amiranashvili A.G., Chikhladze V.A., Dzodzuashvili U.V., Ghlonti N.Ya., Sauri I.P. Reconstruction of Anti-Hail System in Kakheti (Georgia). // Journal of the Georgian Geophysical Society, Issue B. Physics of Atmosphere, Ocean and Space Plasma, v.18B, Tbilisi, 2015, pp. 92-106.
25. Amiranashvili A.G., History of Active Effects on Atmospheric Processes in Georgia. // In the book: Essays of the History of Weather Modification in the USSR and the Post-Soviet Territory, ISBN 978-5-86813-450-0, St. Petersburg, RSHMU, 2017, 352 pp., ill., pp. 234-254, (in Russian).
26. Battan L.J., Weather Modification in the Soviet Union – 1976. // Bulletin American Meteorological Society, Issue 58/1, 1977, p. 13.

1st International Scientific Conference "Modern problems in Geophysics", Proceedings,
ISBN 978-9941-36-434-1, ISSN 3088-4349, Tbilisi, Georgia, November 6-8, 2025

THE EFFECT OF IONIZING RADIATION ON THE STABILITY OF PHYTOCENOSIS IN CONDITIONS OF GLOBAL WARMING

***Uchaneishvili S.D.,**Avalishvili A.L,**Gunia N.A.,**Ivanishili N.I., ***Salukvadze E.D.,**Kalmakhelidze S.L,**Gogebashvili M.E**

**Laboratory of Biophysics, I.Beritashvili Center of Experimental Biomedicine. Georgia*
***Laboratory of Radiation Safety Problems, I.Beritashvili Center of Experimental Biomedicine. Georgia*
**** I.Javakhishvili State University of Tbilisi, V.Bagrationi Institute of Geography, Georgia*
sofiauchaneishvili@gmail.com

Abstact*. This study examines the role of anthropogenic load in shaping plant surface temperature under high and extreme thermal conditions. Gamma irradiation was applied as a universal damaging factor. Field experiments showed that under normal temperatures, the difference between control (non-irradiated) and irradiated plants did not exceed 2–3 °C, while under elevated and extreme temperatures, it increased to 100 °C. Laboratory analyses of transpiration intensity confirmed that radiation is a major factor reducing the transpiration potential of irradiated plants. These findings highlight the relevance of plant resistance under global warming and emphasize the need to minimize anthropogenic impacts on phytocenoses to enhance their resilience to rising temperatures associated with climate change.*

Key words*: radiation, phytocenoses, plant radioresistance, transpiration*

Global warming, more formally referred to as global climate change, is understood as fluctuations in the Earth's climate system occurring worldwide or within specific regions, expressed in statistically significant deviations of weather parameters from long-term averages over periods ranging from decades to millions of years. According to the United Nations, this phenomenon reflects long-term shifts in temperature and weather conditions, driven by both natural processes and anthropogenic influences. Among the multiple manifestations of climate change, one of the most critical consequences is the suppression of vegetation and the degradation of phytocenoses. Increasing frequency and intensity of extreme weather events subject plants to droughts, floods, hurricanes, and forest fires, resulting in physical damage, mortality, or decreased agricultural yields [1–4]. Another important factor is habitat alteration [5]; rising temperatures force plant species to migrate toward cooler regions or higher elevations, yet many cannot adapt quickly enough, leading to population decline or extinction. Regional changes in precipitation further exacerbate ecological stress. While some regions are experiencing increased rainfall, others are facing progressive aridification, often causing desiccation and large-scale mortality of plant communities. A further consequence of climate change is the disruption of phenological cycles [6]. Shifts in key processes such as flowering, fruiting, and leaf fall, when combined with anthropogenic stressors, may accelerate the degradation of entire phytocenoses. At the same time, generalizing results and interpreting model studies that employ various physicochemical factors presents certain challenges, as different mechanisms of negative impact may act simultaneously on the objects under study.

To study phytocenological stability, we used plants irradiated with gamma radiation. Ionizing radiation was selected because, according to its mechanism of action, it can be considered a *universal damaging factor* for plant communities.

The experimental material consisted of sunflower (*Helianthus annuus*) and soybean (*Glycine max*) sprouts and seeds. Radiation treatment was performed using the gamma installations GUPOS-3M and Gamma-capsula-2, with ^{137}Cs as the radiation source. The dose rate during irradiation was 1.1 Gy/min, and all procedures were carried out at a temperature of 25 ± 2 °C. A dose range of up to 150 Gy was applied. After irradiation, both experimental and control (non-irradiated) materials were planted in open ground within 3–5 days, following all standard agrobiological practices. Temperature changes in control and irradiated plants were monitored using laser surface scanning.

No significant differences in leaf surface temperature were observed between control and irradiated plants throughout most of the growing season, with differences not exceeding 2–3 °C. At atmospheric temperatures up to 30 °C, the maximum surface temperature of control plants did not exceed 27–28 °C, while plants irradiated at 100–150 Gy displayed similar values. However, under extremely high temperatures (39–43 °C), the difference became pronounced: irradiated plants exceeded the control group by up to 10–12 °C. Specifically, while the control group varied within 30–32 °C, irradiated plants at doses of 100–150 Gy reached 40–43 °C (Fig. 1).

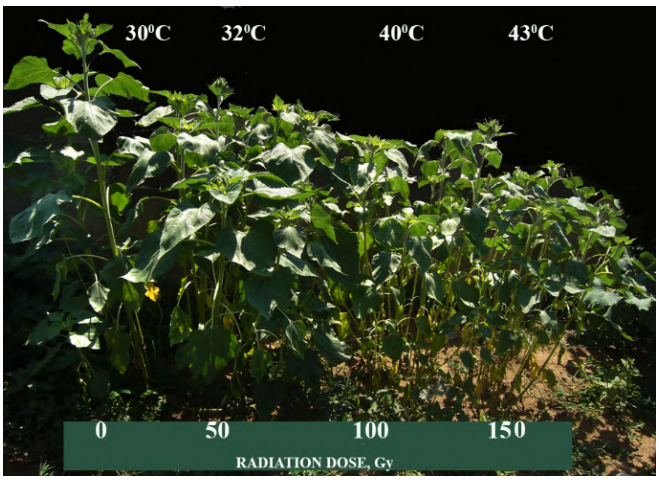

Fig. 1. Effects of radiation on growth, development, and surface heating of plants under conditions of extreme temperature increase

The observed increase in leaf surface temperature in irradiated plants can be attributed to a significant disruption of the transpiration process. This effect may result from both reduced surface evaporation and limited soil moisture availability. However, since all plants in our experiment were grown under identical field conditions, the primary cause is most likely a decrease in leaf transpiration. To investigate the dose dependence of moisture evaporation from the leaf surface, we analyzed the dynamics of the daily transpiration coefficient. In contrast to the sunflower experiment, which involved pre-sowing seed irradiation followed by open-field cultivation, transpiration activity was assessed in soybean sprouts under controlled laboratory conditions. Considering the different radioresistance of seeds and sprouts, the experiments were performed with a dose range not exceeding 20 Gy. Fig.2 presents the dose–response curve of transpiration intensity, calculated from daily surface water evaporation. As shown, the trend of the dose curve closely corresponds to the field observations of leaf surface heating under elevated temperature conditions.

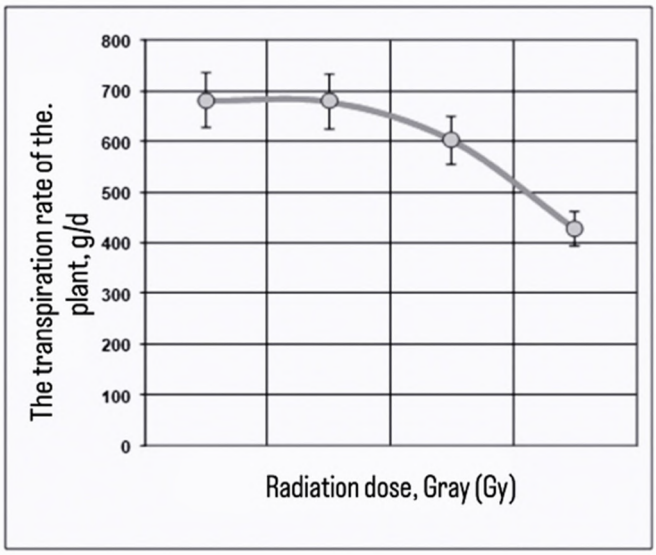

Fig. 2. Effect of gamma radiation on transpiration rate in seedlings

Summarizing the obtained data, it can be concluded that when plants are exposed to various physical and chemical stress factors under elevated or extreme temperatures, the protective system preventing leaf surface overheating is disrupted.

In general, global warming exerts a profound impact on plants and ecosystems, necessitating strategies both to mitigate its consequences and to facilitate adaptation to new conditions. Climate change and the associated temperature stress affect plants in multiple ways, one of which is the alteration of plant community composition. Shifts in interspecific competition may promote the dominance of species more resistant to high temperatures or drought, while less tolerant species are displaced. Such processes can significantly transform characteristic landscapes and, in some cases, result in irreversible ecological damage.

The reduction in transpiration levels demonstrated in our study highlights a critical mechanism of plant vulnerability, which under prolonged stress may progress to severe physiological damage or even complete plant death. Therefore, to mitigate the negative consequences of global climate change, it is essential to develop measures aimed at reducing anthropogenic pressure on phytocenoses, thereby enhancing their natural resistance to extreme thermal conditions.

References

1. William D. Fletcher Craig B. Smith., The Global Climate Crisis (Second Edition): What To Do About It. Chapter 7 – What are the effects of global warming? 2024, pp. 75-103.
2. Key assessments from the IPCC special report on global warming of 1.5 °C and the implications for the Sendai framework for disaster risk reduction. Progress in Disaster Science.Volume 1, May 2019.
3. Zdeněk Vacek, Stanislav Vacek, Jan Cukor., European forests under global climate change: Review of tree growth processes, crises and management strategies. Journal of Environmental Management. Volume 332, 2023.
4. Linchao Li and.all., Global warming increases the risk of crop yield failures driven by climate oscillations. One Earth, Том 8, Выпуск 620, 2025.
5. Sati P., Chandola V., Chandra S., Trivedi V. L, Purohit V. K., Nautiyal. M.C. , Global environmental change mediated response of wetland plants: Evidence from past decades. Science of The Total Environment. Volume 966, 25 February 2025.
6. Vázquez I. G., Valencia L. B., Galicia L., Functional attributes of seeds as indicators of germination sensitivity to global warming. Environmental Reviews. Volume 32, Issue 2, 2024, pp.173-185.

1st International Scientific Conference "Modern problems in Geophysics", Proceedings,
ISBN 978-9941-36-434-1, ISSN 3088-4349, Tbilisi, Georgia, November 6-8, 2025

CHANGES IN THE ATMOSPHERIC PRECIPITATION REGIME IN GEORGIA

Tavartkiladze K., Bolashvili N., Suknidze Nik.

Vakhushti Bagrationi Institute of Geography of the I. Javakhishvili Tbilisi State University, Tbilisi, Georgia
nana.bolashvili@tsu.ge

Abstract. *This study examines long-term changes in the atmospheric precipitation regime in Georgia from 1960 to 2019 under the impact of temperature variations and global warming. Using daily data from 14 meteorological stations, precipitation was classified into four intensity categories: light, moderate, heavy, and very heavy. Changes were evaluated with both the difference method and dynamic norm, also probability distributions and normalized analyses were conducted to evaluate regional and temporal variations. Results indicate the reduction of light precipitation days and a slight increase in very heavy precipitation events, with average annual changes across Georgia about −0.0037 mm/year for light, +0.0001 mm/year for moderate, −0.0006 mm/year for heavy, and +0.0063 mm/year for very heavy precipitation. Regional analysis shows stronger impacts in high-precipitation areas, and polynomial approximations reveal cyclic patterns of precipitation changes. These findings demonstrate that global warming is altering precipitation regimes in Georgia, increasing the frequency of extreme events while reducing the duration of light rainfall, emphasizing the need for rational water management and climate adaptation strategies.*

Keywords: *Daily precipitation, Difference Method, Dynamic Norm Method*

Introduction

Over the past century, the Earth's atmospheric energy potential has steadily increased, driving gradual changes in the climatic regime of near-surface air. The equilibrium of the so-called sublayer surface regime – established over millennia under the direct atmosphere influence – has been disrupted, causing variations across all climatic parameters. Consequently, the modern biosphere, long adapted to prevailing climate conditions, is experiencing gradual deterioration, bringing society closer to the adverse effects of climate change. Among the key climatic parameters, atmospheric precipitation is most critical.

The statistical structure of precipitation in Georgia has been studied for many decades and is relatively well understood [1–8]. However, recent changes related to global warming remain insufficiently investigated [9, 10]. This study aims to analyze the changes in the precipitation regime in Georgia under the influence of temperature field variations during 1960–2019. The period was purposefully selected: the initial phase exhibited cooling in western Georgia, despite the broader context of global warming, followed by pronounced warming in the latter half. Currently, temperature increases are more obvious in western Georgia than in eastern and southern regions.

Methodology

14 meteorological stations' daily precipitation data were compiled from 24 hourly measurements. Although more stations were operating during this period, incomplete or discontinuous records limited the study up to 14 stations with sufficiently reliable data.

Data quality was comprehensively assessed by decomposing the random function into natural orthogonal components. The study focused on the following: Duration of precipitation events; Frequency and variability across four intensity categories: light (<10 mm/day), moderate (10–40 mm/day), heavy (40–70 mm/day), and very heavy (>70 mm/day).

Changes in precipitation were assessed using: Difference Method: long-term data are divided into three equal subperiods; the difference between the third and first subperiod defines the change, excluding the middle period.

Dynamic Norm Method: applies linear approximation across all data points to estimate magnitude and direction of changes, converging to the mean under stable energy balance.

As the precipitation amount varies significantly across regions, normalized precipitation totals were calculated relative to the long-term mean (1960–2019) for each station and intensity group. This approach allows assessment of the direction and magnitude of changes rather than absolute amounts.

Results

Table 1 presents the mean annual precipitation totals across 14 stations, and their changes are calculated using both methods. Differences between methods are minor in trend direction, with discrepancies primarily in magnitude.

Table 1. Annual precipitation totals in Georgia and changes, 1960–2019

Observation Station	Elevation above Sea Level (km)	Mean Annual Precipitation (mm)	Change (mm/year)	
			Difference Method	Dynamic Norm
Poti	0.003	1963.1	+7.90	+6.21
Kobuleti	0.007	2404.4	+7.28	+6.53
Kutaisi	0.114	1389.4	+0.79	-0.28
Zugdidi	0.117	1832.2	+2.50	+0.85
Tbilisi	0.403	502.9	+0.71	+0.88
Bolnisi	0.534	513.8	-0.10	-0.20
Ambrolauri	0.544	1088.1	+2.96	+2.37
Telavi	0.568	760.4	-0.46	-0.58
Gori	0.588	513.9	-0.08	+0.06
Sagarejo	0.802	842.3	+4.58	+3.20
Akhaltsikhe	0.982	535.0	+0.18	+0.20
Pasanauri	1.070	980.4	+0.20	+0.21
Tianeti	1.099	750.1	-6.16	-5.81
Tsalka	1.457	679.1	-1.45	-1.34

The mean annual number of precipitation days was analyzed for two subperiods (1960–1989 and 1990–2019), considering intensity categories shown in Table 2.

Table 2. Changes in the number of precipitation days in Georgia, 1960–2019

Period	Annual number of precipitation days %	Annual number of precipitation days % of annual days			
		≤10 mm	10–40 mm	40–70 mm	≥70 mm
1960-1989	18.9	14.5	3.93	0.36	0.09
1990-2019	17.1	12.8	3.86	0.35	0.12

Global warming has led to a decrease in the duration of precipitation, mainly due to reduced low-intensity events. In contrast, the frequency of heavy and very heavy precipitation days increased slightly, highlighting the impact of energetic changes in the Earth–atmosphere system.

Probability distributions of precipitation days by different intensity classes were calculated using Gaussian functions. Figure 1 illustrates the probability changes between the two subperiods, showing a decline in light precipitation and a modest increase in very heavy precipitation events.

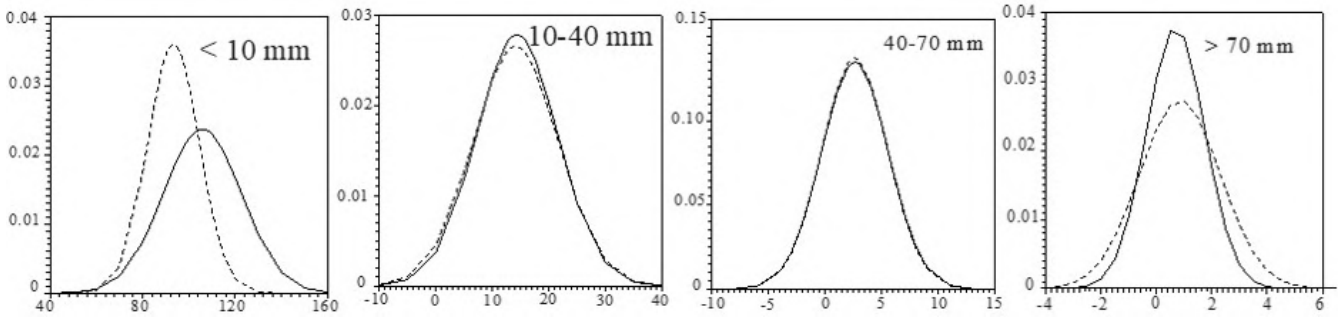

Fig. 1. Probability distribution of precipitation duration for 1960–1989 (solid curve) and 1990–2019 (dashed curve).

Normalized annual precipitation totals are shown in Fig 2. Sixth-order polynomial curves highlight cyclic variations in precipitation patterns across all intensity categories. Average annual changes (dynamic norm) were: light −0.0037 mm/year, moderate +0.0001 mm/year, heavy −0.0006 mm/year, and very heavy +0.0063 mm/year.

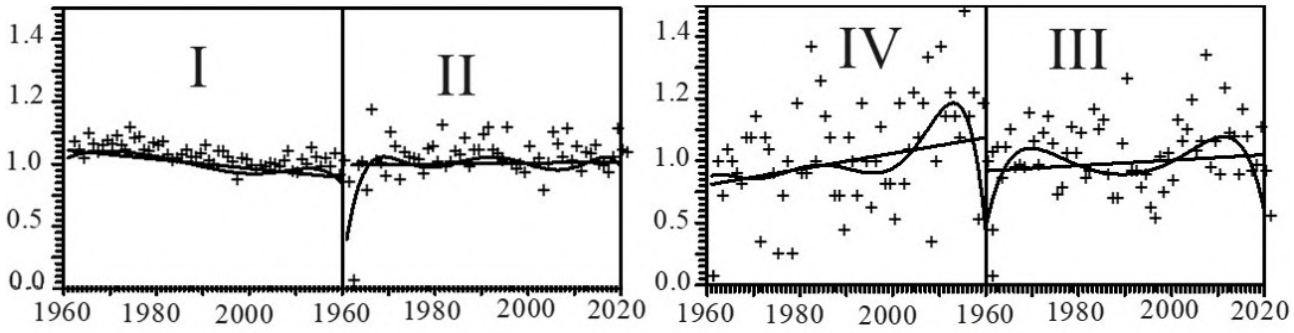

Fig. 2. Annual normalized precipitation totals in Georgia (+), dynamic norm (linear trend), and sixth-order polynomial approximation for light (I), moderate (II), heavy (III), and very heavy (IV) precipitation.

For probabilistic assessment of precipitation amounts, stations were grouped into four categories based on mean annual totals: Group 1: <600 mm (Gori, Tbilisi, Akhaltsikhe, Bolnisi), Group 2: 600–800 mm (Telavi, Tsalka, Tianeti), Group 3: 800–1100 mm (Ambrolauri, Sagarejo, Pasanauri), Group 4: >1100 mm (Kutaisi, Zugdidi, Poti, Kobuleti).

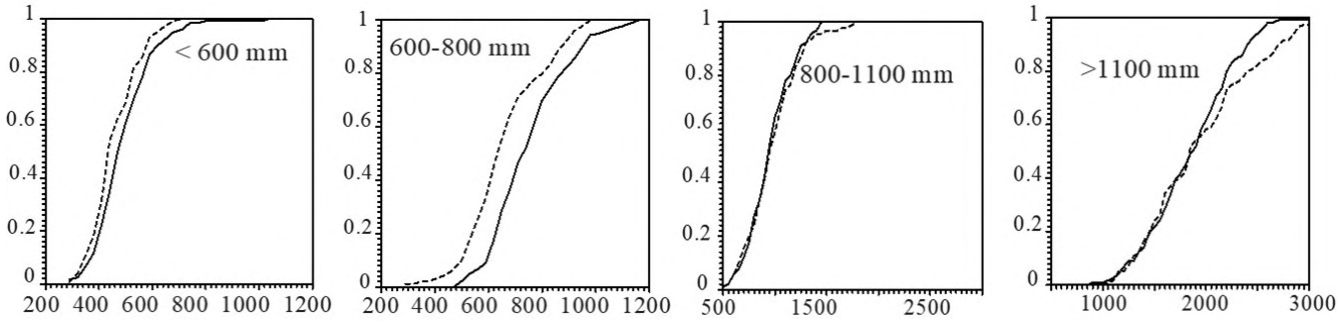

Fig. 3. Probability density distributions of annual precipitation total in Georgia for 1960–1989 (solid curve) and 1990–2019 (dashed curve), classified by annual totals.

Fig. 3 shows that Groups 1 and 2 experienced precipitation probabilities decline for all amounts, while Group 4 shows a clear shift toward higher totals.

Fig. 4 illustrates changes in the ratio of annual precipitation totals to the number of precipitation days. Linear (dynamic norm) and seventh-order polynomial approximations reveal a gradual increase of 0.027 mm per day, with cyclic variations visible in the polynomial representation.

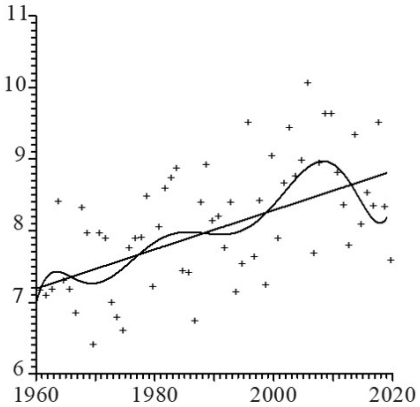

Fig. 4. Annual precipitation totals per precipitation day (+), linear (dynamic norm), and seventh-order polynomial approximation.

Conclusion

Global warming in Georgia has led to a decrease in the number of light precipitation days, whereas very heavy precipitation events have shown a slight increase. Average annual precipitation totals remain largely unchanged, in line with the physical constraint of near-constant total water content on Earth. Polynomial-based approximations highlight cyclic variations in precipitation patterns for all intensity classes. Regional analyses indicate that high-precipitation areas are most sensitive to global warming, revealing notable increases in heavy precipitation events. These results emphasize the importance of continuous monitoring of precipitation patterns to guide water resource management, agriculture, and climate adaptation strategies in Georgia.

References

1. Elizbarashvili E., Chavchanidze Z., Gvalvebi, Unaleko da Nalekiani Periodebi Sakartveloshi. // Mecniereba, 1992, p.119.
2. Gagua G., Mumladze D., Javakhishvili Sh. Klimati., Sakartvelos Geografia. // Nats.1, Mecniereba,Tb., 2000, pp. 91–103.
3. Elizbarashvili E., Papinashvili L., Atmosferuli Nalekebis Multanluri Gadmoyeneba Sakartvelos Teritoriaze. // Hidrometinstitutis Shromebi, #102, 2001 (112–116).
4. Tavartkiladze K., Sakartveloshi Nalekebis Ganasagrebis Statistikuri Struktura // Hidromet. in-tis shromebi, 105, Mecniereba, Tbilisi, 2002, pp. 117-137.
5. Kartvelishvili L., Ukleba M., Atmosferuli Nalekebis Ganatsilebis Taviseburebebi Sakartvelos Mtian Regionebshi. Vakhushti Bagrationis Geografiis Institutis Shromata Krebuli, 2(81), 2008, pp. 262-270.
6. Tavartkiladze K., Kikava A., Gvalvebisa da Gaudabnoebis Khelshemtsqobi Temperaturisa da Nalekebis Rezhimuli Struktura da Havis Tsvlilebis Gavlena Masze. Sakartvelos Soflis Meurn. // Metsn. Akad. Moambe, 28, 2010, pp. 309-317.
7. Tavartkiladze K., Kikava A., Ananidze M., Gvalvebisa da Gaudabnoebis Khelshemtskobi Nalekebis Uarkopiti Anomaliebi Sakartveloshi. Vakhushti Bagrationis Geografiis Institutis Shromata Krebuli, №6(85), 2014 pp. 128-133.
8. Tavartkiladze K., Havis Tsvlilebis Gavlenis Shesaxeb Atmosferuli Nalekebis Rezhimze. // Hidromet. In-tis Shromebi, 123, Mecniereba, Tbilisi, 2016, pp. 17-29.
9. Bolashvili N., Chikhladze V., Kartvelishvili L., Variability of Atmospheric Precipitation in Tbilisi 1844-2023, Proceedings of the International Conference “Complex geophysical monitoring in Georgia: History, Modern problems, Promoting Sustainable Development of the country”, TSU, Tbilisi, 2024, pp.150-154.
10. Tsitelashvili N. , Biggs T., Mu Y., Trapaidze V., Regional Precipitation Regimes and Evaluation of National Precipitation Datasets against Satellite-Based Precipitation Estimates, Republic of Georgia. // Journal of Hydrometeorology, American Meteorological Society, 2024. https://doi.org/10.1175/JHM-D-23-0116.1

1st International Scientific Conference "Modern problems in Geophysics", Proceedings,
ISBN 978-9941-36-434-1, ISSN 3088-4349, Tbilisi, Georgia, November 6-8, 2025

COMPARATIVE ANALYSIS OF THE CLIMATIC CHARACTERISTICS OF WIND IN THE REGIONS OF IMERETI AND KAKHETI

Davitashvili, M. D., Berdzenishvili, N. M., Zuroshvili, L. D., Margalitashvili, D. A., Tandilashvili, L. G.

Iakob Gogebashvili Telavi State University, Georgia
magda.davitashvili@tesau.edu.ge

Abstract. *The present study aims to conduct a comparative analysis of the climatic characteristics of wind in the regions of Imereti and Kakheti, based on long-term data on wind speed and direction. The study examines periodic data from 1961 to 2022 and discusses seasonal variability, spatial differences, energy potential, and natural hazards, including tornadoes. The results show that Kakheti is characterized by predominantly eastern airflows and high wind speeds, contributing to its notable energy potential. In contrast, wind directions in Imereti vary seasonally, and its energy potential is more localized. The findings of this research provide a valuable basis for the development of renewable energy, urban planning, and climate risk management.*

Key words: *wind speed, direction, Imereti, Kakheti, renewable energy, tornado, climate risks.*

Introduction

Wind is one of the key climatic factors that influences both weather formation and various sectors of human activity – including energy, urban planning, infrastructure, and agriculture. The characteristics of wind speed and direction determine local climatic conditions and participate in atmospheric circulation processes. Moreover, the efficient utilization of wind's energy potential represents an important strategic direction in the development of renewable energy [6].

In Georgia, wind climatic characteristics exhibit high geographic and seasonal variability, caused by complex topography and the influences of the Black Sea and the Caucasus Mountains. The aim of this study is to analyze long-term data on wind speed and direction in the regions of Imereti and Kakheti, to examine extreme wind events (including tornadoes), and to comparatively assess these data from the perspective of practical application – including climate risk management and the assessment of renewable energy potential [2].

Methodology

The study is based on the analysis of meteorological station data in Georgia covering the period 1961–2022. Data from the National Environment Agency of Georgia and the Hydrometeorology Institute, as well as international climate databases (e.g., MERRA-2), were utilized. Key parameters included average and extreme values of wind speed and direction, analyzed seasonally and geographically.

Statistical analysis was performed using the following methods:

- Measures of central tendency: mean, median, mode, standard deviation;
- Frequency analysis: recurrence of wind directions and distribution of wind speed ranges;
- Trend analysis: The Mann-Kendall test was utilized to identify temporal trends.
- Comparative analysis: data from Imereti and Kakheti were analyzed individually and comparatively.

For the analysis of tornadoes and other natural hazards, expeditionary research and contemporary scientific literature were used [1, 3, 4].

Results and Discussion

Analysis of wind. Directions show that in Imereti, wind directions vary seasonally. Westerly and southwesterly winds dominate in spring and summer, while easterly and northeasterly winds prevail in autumn and winter. For example, in Kutaisi, easterly winds occur up to 70% during nighttime hours [2, 8].

In Kakheti, wind directions are much more uniform. The region is dominated year-round by easterly and northeasterly air masses, due to the orographic conditions of the Alazani Valley and the influence of the Caucasus Ridge [9].

Wind speed variation and geographical distribution. In Imereti, average wind speeds in lowland areas range between 2.5 and 4.5 m/s. In mountainous zones such as Mta-Sabue, speeds reach up to 9.2 m/s. The background frequency of winds in Kutaisi is approximately 120 days per year [5, 8].

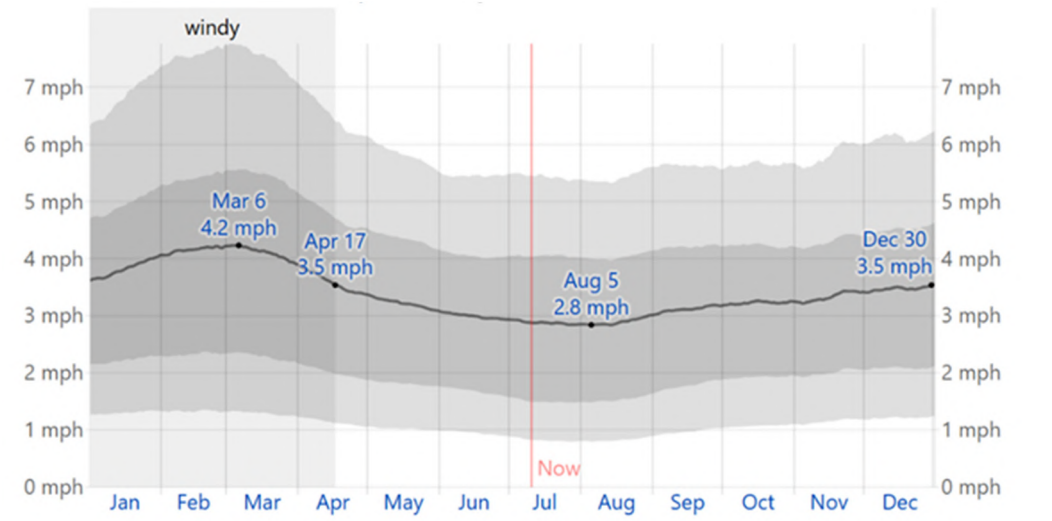

The average of mean hourly wind speeds (dark gray line), with 25th to 75th and 10th to 90th percentile bands.

	Jan	Feb	Mar	Apr	May	Jun	Jul	Aug	Sep	Oct	Nov	Dec
Wind Speed (mph)	3.8	4.2	4.1	3.6	3.2	3.0	2.9	2.9	3.1	3.2	3.3	3.5

Fig. 1. Average Wind Speed [8].

In Kakheti, average wind speeds are considerably higher. In Sagarejo, wind speeds of up to 9.5 m/s were recorded during the summer, while in Telavi, the minimum values in winter reached as low as 0.7 m/s. Eastern Kakheti is characterized by the most intense windiness [9].

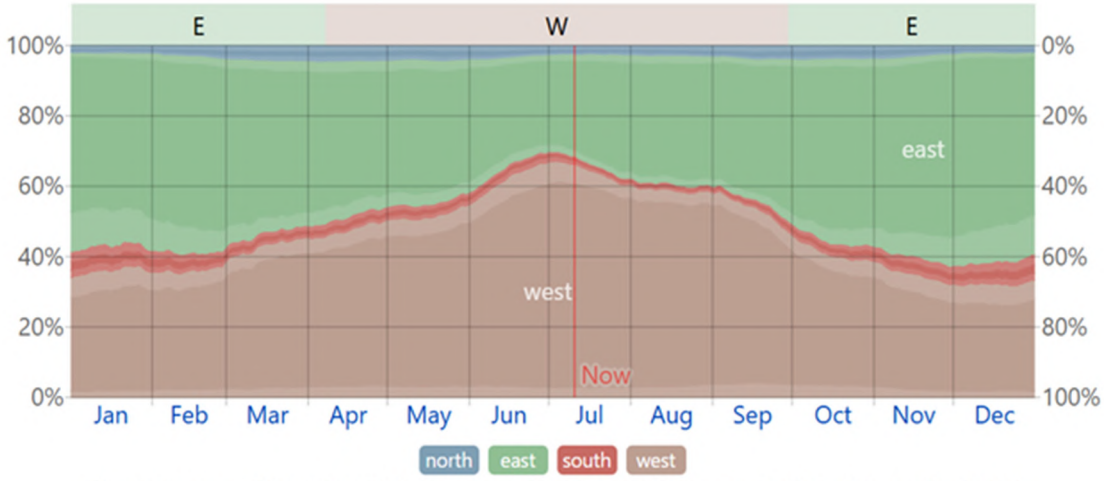

*The percentage of hours in which the mean wind direction is from each of the four cardinal wind directions, excluding hours in which the mean wind speed is less than **1.0 mph**. The lightly tinted areas at the boundaries are the percentage of hours spent in the implied intermediate directions (northeast, southeast, southwest, and northwest).*

Fig. 2. Wind Direction [8]

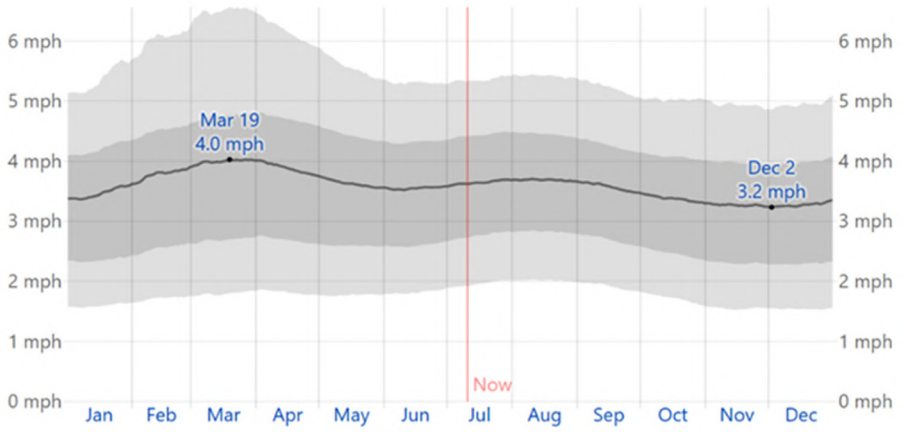

The average of mean hourly wind speeds (dark gray line), with 25th to 75th and 10th to 90th percentile bands.

	Jan	Feb	Mar	Apr	May	Jun	Jul	Aug	Sep	Oct	Nov	Dec
Wind Speed (mph)	3.5	3.8	4.0	3.9	3.6	3.6	3.6	3.7	3.6	3.4	3.3	3.3

Fig. 3. Average Wind Speed [9].

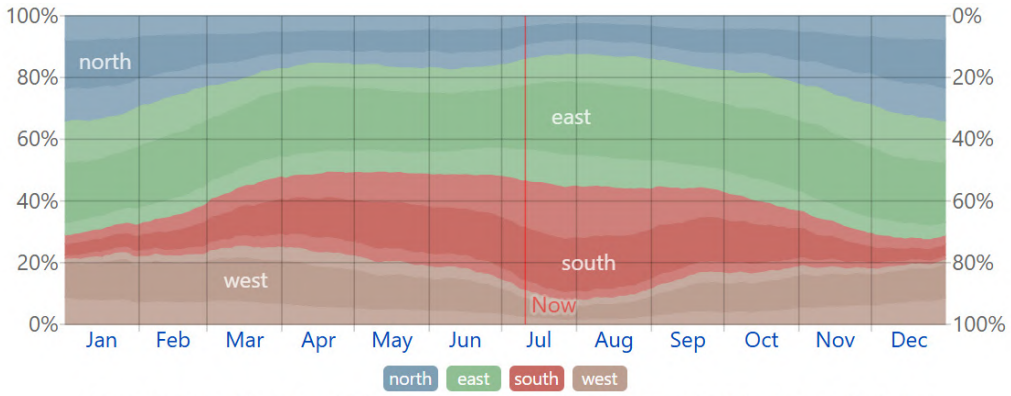

The percentage of hours in which the mean wind direction is from each of the four cardinal wind directions, excluding hours in which the mean wind speed is less than 1.0 mph. The lightly tinted areas at the boundaries are the percentage of hours spent in the implied intermediate directions (northeast, southeast, southwest, and northwest).

Fig. 4. Wind Direction [9].

Wind Energy Potential. In the mountainous zones of Imereti, the use of small-scale wind turbines is possible; however, the energy potential is localized and requires detailed zonal studies [7, 10].

In Kakheti, the technical potential for wind energy is high. There are extensive areas where the average wind speed exceeds 7–10 m/s, which is favorable for the installation of medium and large capacity turbines [7, 10].

Extreme Wind Events. Extreme wind occurrences in Imereti are rare and mostly localized. Maximum wind speeds, such as the 66 m/s event recorded in Kutaisi, are exceptions [2, 5].

In 2024, a tornado was recorded in the village of Alaverdi, Akhmeta Municipality, Kakheti. Field studies classified it as an F2 category tornado. The region has also experienced severe storms in 2012, 2021, and 2022, indicating a trend toward increasing frequency of extreme events [2].

Prospects for Use. Wind data from both regions should be integrated into spatial and urban planning. In Imereti, it is recommended to consider ventilation corridors and to implement local turbines in mountainous zones. In Kakheti, large-scale wind energy projects are feasible, requiring the development of appropriate infrastructure and refinement of risk management systems.

Conclusion:

- ❖ Wind direction in Imereti varies seasonally, while in Kakheti it remains stably easterly;
- ❖ Kakheti is characterized by higher wind speeds and greater renewable energy potential;

- ❖ Tornadoes and severe storms are primarily characteristic of Kakheti;
- ❖ Using wind data is advisable in both regions for energy and urban planning purposes.
- ❖ Zonal planning, investment research, and development of adaptation mechanisms are necessary for managing climate risks.

References

1. Amiranashvili, A. G., Chikhladze, V. A., Gvasalia, G. D., Loladze, D. A., Statistical Characteristics of the Daily Max of Wind Speed in Kakheti in 2017-2019. // Journals of Georgian Geophysical Society, 23(1), 2020.
2. Amiranashvili, A. G., Chikhladze, V. A., Pipia, M. G., Varamashvili, N. D., Some Results of an Expeditionary Study of the Tornado Distribution Area in Kakheti on June 25, 2024. // Journals of Georgian Geophysical Society, 27(N1), 2024.
3. Aryal, A., Bosch, R., & Lakshmi, V., Climate risk and vulnerability assessment of Georgian hydrology under future climate change scenarios. // Climate, 11(11), 2023, p. 222.
4. Beglarashvili, N., Pipia, M., Jamrishvili, N., Janelidze, I., Some Results of the Analysis of Number of Days with Strong Wind in Various Regions of Georgia in 2019–2022. // Georgian Geographical Journal, 3(2), 2023.
5. Berdzenishvili N., Climate resources of the Imereti region. Monograph, 2012.
6. Tatishvili, M., Khvedelidze, Z., Samkharadze, I., Zotikishvili, N., Chelidze, N., Dynamics of Atmospheric Microcirculation Processes in Certain Regions of Georgia. Georgian Geographical Journal, 4(1), 2024, pp. 57–63.
7. https://solarquarter.com/2025/05/13/powering-georgias-future-mapping-the-best-zones-for-solar-and-wind-energy-investment-irena-report/#:~:text=60.5,included%20in%20the%20final%20results
8. https://weatherspark.com/y/102441/Average-Weather-in-Kutaisi-Georgia-Year-Round
9. https://weatherspark.com/y/103846/Average-Weather-in-Telavi-Georgia-Year-Round
10. https://www.iea.org/reports/georgia-energy-profile/energy-security

1st International Scientific Conference "Modern problems in Geophysics", Proceedings,
ISBN 978-9941-36-434-1, ISSN 3088-4349, Tbilisi, Georgia, November 6-8, 2025

CLIMATIC CONDITIONS AND METEOROLOGICAL HAZARDS CHARACTERISTIC OF THE NATANEBI RIVER BASIN

[*] Elizbarashvili M., [**]Elizbarashvili E., [*]Chikhradze N.

[*] Faculty of Exact and Natural Sciences, Ivane Javakhishvili Tbilisi State University, Tbilisi, Georgia;
[**] Institute of Hydrometeorology, Georgian Technical University, Tbilisi, Georgia;
mariam.elizbarashvili@tsu.ge

Abstract. *The article examines the climatic features and characteristic meteorological hazards of the Natanebi River basin, drawing on relevant databases and field literature. It was revealed that the mountainous zone of the basin is characterized by hurricanes and hail, for which the construction of windbreaks and the use of hail protection nets are recommended. Drought is less typical for the basin. In exceptional cases, soil cultivation and irrigation are preferable.*

Keywords: *catchment basin, climate change, hazardous natural events, mitigation, and adaptation.*

1. Introduction

The article describes the climatic background and expected meteorological hazards of the Natanebi River basin.

The Natanebi River catchment is located in the humid subtropical climatic zone of western Georgia. The river originates on the northern slope of the Meskheti Range, at an altitude of 2,548 m, and flows into the Black Sea near the peak Sakornia and the village of Shekvetili; the river is 60 km long, and the basin area is 657 km² [1]. Due to a vertical layout, the distribution of climatic parameters in the basin area, despite its small size, is characterized by significant variability.

The river basin is home to settlements and agricultural fields, agricultural works are carried out, infrastructure is expanding, and companies extract inert materials in the valley. There are cases where sediment removal exceeds the permissible norm. In some villages located in the river basin, artesian wells have dried up, landslide processes are developing, and ecological problems occur. One of the reasons for the development of negative processes in the basin is the climate, which puts a detailed climatic study of the river basin and assessment of meteorological hazards on the agenda.

2. Method and material

The climatic conditions of the sediment basin and the expected meteorological hazards were analyzed using the observation data of the National Environment Agency, the Climatic Directory [2], the databases of the Institute of Hydrometeorology of the Georgian Technical University, the catalog of natural disasters created at the M. Nodia Institute of Geophysics [3] and other literary sources [4.5,6,7, 8, 9,10,11,12,13].

3. Results and discussion

The duration of sunlight in the basin area is less than 2,000 hours per year. Breeze and monsoon circulation prevail, which determines the diurnal circulation of winds and the dominance of sea winds in the warm period of the year, and the predominance of land winds in the cold period of the year (Table 3.1).

Table 3.1. Wind direction repeatability, % [7]

Station	Wind direction	Month				Year
		I	IV	VII	X	
Ureki	From the sea	23	54	83	40	49
	From land	77	46	17	60	51
Ozurgeti	From the sea	17	60	71	28	63
	From land	83	40	29	72	37

As can be seen from Table 3.1, in the basin area, as in the Kolkheti Plain in general, winds from the sea prevail in spring and summer, and from the land towards the sea in autumn and winter. At the same time, land winds are more pronounced in the cold season of the year in Ozurgeti, which is far from the sea. The average annual wind speed in the basin area is 4 m/sec or less. The number of days with strong winds, when the speed is greater than or equal to 15 m/sec, is 10-20 days per year.

The average annual air temperature in the mouth of the Natanebi River basin and the Kolkheti Plain exceeds 14 degrees, and in the upper reaches it is approximately 4-6°, the average maximum temperature in most of the basin is 36-38°, in the upper reaches it drops to 30°, the average absolute minimum temperature is -4°, -8°, and in the mountains it drops to -10°, -16° [6].

Relative air humidity is high throughout the year and averages 70-80% in January and 75-85% in July [6].

The annual total atmospheric precipitation in the basin area, also, according to the maps of the "Climatic and Agroclimatic Atlas of Georgia" [6], averages 1,800-2,400 mm. During the cold and warm periods of the year, approximately equal precipitation falls within the range of 1,000-1,600 mm. The annual duration of precipitation is more than 1,200 h [6].

The daily maximum of precipitation within the basin is 150-300 mm. During the year, there are more than 160 rainy days on average in the basin [6].

On the Meskheti range, a stable snow cover forms from November 10, which is broken in late March or early April. The snow cover lasts for approximately 100-150 days. Its decadal maximum height in the mountains reaches 200 cm. There is a medium and strong avalanche danger here [6].

Table 3.2 presents the special atmospheric events characteristic of the basin.

Table 3.2. Special atmospheric events characteristic of the Natanebi River basin [3,13]

Settlement	Atmospheric event, number of days				
	Thunderstorm	Hail	Fog	Blizzard	Hurricane
Ureki	37	1,8	9	-	0,02
Nabeghlavi	26	1,0	20	-	-
Bakhmaro	41	2,8	102	30	0,6

As can be seen from Table 3.2, among the special atmospheric phenomena, **thunderstorms** are frequent in the lowlands.

The number of **foggy** days in the mountains exceeds 100 per year. Dense fog is hazardous when visibility is less than 50 m. The frequency of such fogs during the year is quite high in Bakhmaro and is 70.

Blizzards are frequent in mountainous areas. According to Bakhmaro data, the number of blizzard days during the year is 30.

In the lowland zone of the Natanebi River basin and on the sea coast, the number of **hail** days does not exceed 2 per year on average, but hail can occur 4 times. In the mountainous zone of the basin, hail is relatively frequent and occurs on average 3 times per year, although it can occur for 14 days. The hailstorms occurring here are moderate to medium in intensity, affecting mainly areas of 2 to 7 sq. km. In the mountainous zone of the basin, hailstorms can cause significant damage (Table 3.3).

Table 3.3. Different intensities of some characteristics of hailstorms in 2000-2010 [3]

Settlement	Year	Month	Number	Distribution area, sq. km	Effect	Damage, thousands US $
Anaseuli	2002	09	08	2	Moderate	246
	2005	11	11	2	Moderate	246
Bakhmaro	2000	06	04	7	Average	984
	2002	07	10	2	Moderate	246
	2009	04	30	3	Average	492

The strong impact of hail, when agricultural harvests, crops, and pastures are destroyed, buildings, airplanes, and car bodies are seriously damaged, domestic animals are killed, and the number of human casualties is high, is practically excluded.

A dangerous weather phenomenon is **hurricane winds** when their speed exceeds 32 m/sec. Its recurrence, as can be seen from the table, is not expressed in large numbers, but it can bring catastrophic consequences.

Table 3.4. Some characteristics of hurricanes developed within the Natanebi River basin in recent years (2000-2022) [3]

Settlement	Year	Month	Number	Speed, m/sec	Distribution area, sq. km	Damage, thousands US $
Anaseuli	2002	06	12	30	900	25
	2002	09	06	35	1,200	25
Bakhmaro	2000	01	18	35	900	28
	2006	03	09	35	1,200	-

One of the dangerous weather phenomena is **drought**, the reliable indicator of which is the sum of the precipitation during the vegetation period. A drought is considered a period when the sum of precipitation during the veget

ation period does not exceed 150 mm. However, such small precipitations are not observed in the basin during the vegetation period, which also confirms that drought is not characteristic of the Natanebi basin [7].

4. Conclusion

It was found that the mountainous zone of the Natanebi River basin is characterized by hurricanes. Hurricanes are expected once every 2.5 years, and their speed reaches 40 m/s. Such hurricanes can cause medium and strong impacts.

In the lowland zone of the Natanebi River basin and on the sea coast, the number of hail days does not exceed 2 on average per year, but hail can occur 4 times. Hail mainly has a moderate and medium impact. A strong impact of hail, when agricultural harvests, crops, and pastures are destroyed, buildings, airplanes, and car bodies are seriously damaged, domestic animals are killed, and the number of human casualties is high, is practically excluded.

Recommendations:

1. To protect against weather disasters, it is desirable to create a special early warning service in the region, which will notify the population about the expected disaster, including hurricane winds and hail.

In addition, it is advisable to build impenetrable windbreaks in the upper and middle reaches of the river basin, consisting of two tiers. Details should be clarified on site in consultation with foresters and environmental protection specialists.

In the mountainous zone of the Natanebi River basin, where hail is relatively common, it is possible to use a hail protection net for agricultural crops. The net should be selected based on the type of culture in consultation with specialists.

2. Drought is not typical for the Natanebi River basin, although it is possible that during the active summer vegetation period, the relatively small amount and uneven distribution of atmospheric precipitation may sometimes not provide the amount of moisture necessary for plants in the soil, without which normal plant development is excluded. In such cases, to preserve the crop, it is preferable to loosen the soil (cultivate) or irrigate, where possible.

References

1. Apkhazava, I., Georgian Soviet Encyclopedia, Tbilisi, vol. 7, 1984, p. 327.
2. Georgian Scientific-Applied Climatic Reference Book. Tbilisi, 2020.
3. Varazanashvili O., Gaprindashvili G., Elizbarashvili E., Basilashvili Ts., Amiranashvili A., Fuchs S., The First Natural Hazard Event Database for the Republic of Georgia (GeNHs). Catalog, http://dspace.gela.org.ge/handle/123456789/10369; 2023, 270 p. DOI: 10.13140/RG.2.2.12474.57286.
4. Elizbarashvili E., Climatic Resources of Georgia. Tb. 2007.
5. Elizbarashvili E. Climate of Georgia. Tbilisi, 2017.

6. Climatic and Agroclimatic Atlas of Georgia. Tbilisi, 2011.
7. Climate of Georgia. Vol. 4, Guria. (Ed. by E. Elizbarashvili, R. Samukashvili, and J. Vachnadze). Proceedings of the Institute of Hydrometeorology, vol. 118, 2011.
8. Elizbarashvili E.S., Meskhia R.S., Elizbarashvili M.E. et al., Climate dynamics of glaciers of the Greater Caucasus for the 20th century. Russ. Meteorol. Hydrol. 34, 2009, 838–842, https://doi.org/10.3103/S1068373909120103
9. Blanutsa S., Elizbarashvili E., Kartsivadze N., Resort Ureki. Tbilisi, 1982.
10. Elizbarashvili M., Amiranashvili A., Elizbarashvili E., Mikuchadze G., Khuntselia T., Chikhradze N., Comparison of RegCM4.7.1 Simulation with the Station Observation Data of Georgia, 1985–2008. Atmosphere 15, 2024, p. 369. https://doi.org/10.3390/atmos15030369.
11. Elizbarashvili E.S., Elizbarashvili M.E., Maghlakelidze R.V., Sulkhanishvili N.G., Elizbarashvili S.E., Specific features of soil temperature regimes in Georgia. Eurasian Soil Sci. 40, 2007, pp. 761–765. https://doi.org/10.1134/S1064229307070083.
12. Varazanashvili O., Tsereteli N., Amiranashvili A., Tsereteli E., Elizbarashvili E., Dolidze J., Qaldani L., Saluqvadze M., Adamia S., Arevadze N., Gventcadze A., Vulnerability, hazards, and multiple risk assessment for Georgia. Natural Hazards Journal of the International Society for the Prevention and Mitigation of Natural Hazards. Volume 64, 2012, pp. 2021–2056. DOI 10.1007/s11069-012-0374-3.
13. Elizbarashvili E.Sh., Varazanashvili O.Sh., Tsereteli N.S., Elizbarashvili M.E., Hurricane winds on the territory of Georgia. Russian Meteorology and Hydrology volume 38, Issue 3, 2013, pp. 168–170. DOI: 10.3103/S1068373911060069.

1st International Scientific Conference "Modern problems in Geophysics", Proceedings,
ISBN 978-9941-36-434-1, ISSN 3088-4349, Tbilisi, Georgia, November 6-8, 2025

THE CYCLE OF FLOODS AND THEIR NEGATIVE CONSEQUENCES IN THE KHARAGAULI DISTRICT

***Gorgijanidze S., ****Kapanadze N., **Jincharadze G., *Pipia G., *Kobakhidze N., ***Chitadze T.**

**Institute of Hydrometeorology, Georgian Technical University,*
***Ministry of Defense of Georgia,*
****National Environmental Agency*
*****Tbilisi State University*
sophiogorgijanidze@gmail.com

Abstract. *Natural disasters pose a problem for many countries of the world, preceded by global climate warming, the result of which is landslides, avalanches, rock avalanches, glacial activities, mudslides, and flash floods. Here, we should single out the Kharaguli region, where floods and flash floods have occurred for years. Currently, tectonic processes are activated in the region, as a result of which landslides and rock avalanches are activated. As a result, the Karneba River was blocked by a landslide. In order to prevent the danger of a landslide, a channel was built, as a result of which unlimited flash floods were avoided. Therefore, constant observation and monitoring are needed to prevent catastrophic flash floods.*

Key words*. Landslide, rock avalanches, flash flood, mudslide.*

Introduction

Catastrophic events have become more frequent in the modern world. They mostly occur in mountainous regions. They cause great damage to the country's economy and population. Unfortunately, these events are also accompanied by human casualties.

Currently, natural disasters are a problem for almost every country, and their management and implementation of necessary measures are important. It is necessary to mention global climate warming, the result of which is landslides, avalanches, rock avalanches, glacial activities, and floods.

It should also be noted that Georgia is located in a zone of tectonic activity; its complex relief structure, deeply dissected steep slopes, and gravitational processes, which are facilitated by meteorological events, activate natural disasters. Such disasters are also accompanied by floods. In addition, we should not forget about the human factor, whose activities hurt nature.

By the beginning of the 21st century, 2000 landslides and rock avalanches had been mapped in Georgia. They became active over the years as a result of abundant precipitation and intensive snowmelt. Their results have been recorded in many places in Upper Adjara, Mountainous Gura, Upper Imereti, Racha, and Svaneti regions. [1, 3, 4]. In addition, Georgia is located in a 9-magnitude seismic zone.

The 1991 earthquake was special for Upper Imereti. 270 people died during the earthquake. At that time, up to 35 dammed lakes appeared in the river valleys. Of these, the largest were the lakes of Patsa, Khakhieti, and Jruchula. [3,5]. During the same period, cracks appeared in many places where surface water accumulated. It is worth noting that as a result of the breakthrough of dammed lakes, a flash flood occurs, the stream passes through the river itself, where it was dammed, and then covers the entire territory. An example of this is the breakthrough of the Khakhietistskali dammed lake. As a result, the flood flow passed the Khakhietistskali River, and the Kvirila and Rioni rivers in its continuation. The levels and passage times of the flash flood flow were recorded at all operating hydrological stations. [3,5]

Unfortunately, human casualties are also common during natural disasters, as was the case in Racha and Nergeeti. [6,7,8]

In fact, in mountainous Imereti, landslide-prone regions have been experiencing natural processes for years. An example of this is the basins of the rivers Kvirila, Dzirula, Chkherimela, Lukhuta, and Khansitskali, tributaries of the Rioni River.

In 1999, 2001, and 2003, torrential rains in the Baghdati district caused floods, which caused significant damage to the district. In 2001, floods occurred in the Baghdati district on both the Khanistskali River and its tributary, the Kershaveti River. In May of the same year, there was also a flood on the Lukhuta River, which is reflected in the works of Sofio Gorgijanidze. The river destroyed the agricultural fields of the first and second obcha of the villages. [9,2]

The basins of the Chkherimela and Dzriula rivers stand out, where there were cases of valley blockage after landslides: in 1957, 1959, 1987, 1994, 1998, 2004, and 2019. Floods, in fact, still occur locally everywhere against the backdrop of climate change. [3, 9].

Study area

Here we will highlight the Kharagauli district, where in 2001 a flood occurred on the Karneba River. The river washed away the entire erosion slopes and caused flooding in the lower reaches. With the help of expedition materials, which were conducted in December 2001 by Sofio Gorgijanidze and Vasil Tsomaia, as well as Tamila Kopadze, the river valley in the Kharagauli district was investigated. It was established that the entire river valley is landslide-prone, where creeping landslides also acquire a catastrophic character. (Fig. 2) Unfortunately, at that time, the damage and the area of flooding in the territory were not determined.

Fig. 1. Karneba River landslide, left slope (photo by S. Gorgijanidze 2001) [2].

If we follow the chronology. After that, in August 2019, scalable floods occurred again in the Kharagauli district. The flood damaged the Leghvanuri River bridge, which connected the village with the Didvake district. It also affected the population and destroyed agricultural fields. In February 2020, again in the Kharagauli district, the Chkherimela River destroyed the protective wall and the road. In January 2021, already on the Dzrula River, in the Boriti section, floods washed away bridges and damaged the road. In addition, landslides were activated in some places. In some places, mudslides developed. [2,3,5]

It is noteworthy that all of these events were preceded by excessive atmospheric precipitation. Here, climatic conditions are the primary factor, although human influence on nature is also significant.

As for the events of 2025 in the villages of Khemaghali and Ghverki in the Kharagauli district, it is associated with the activation of landslide and rock avalanche bodies in terms of tectonics, which is still the subject of research. The process began around May and intensified gradually. This was followed by the blocking of the Karneba River at the end of August. The landslide that descended on the territory of the village of Lashe blocked the river and blocked it in several places. The landslide area is actually 72.5 ha. The largest blockage was the second-dammed lake, which posed a threat to both the village of Lashi and the central railway. (Fig. 2).

It should be noted that flooding was prevented as a result of the involvement of local authorities. A channel was made on the blocked mass, from which the dammed water began to flow. The river here restored its

initial water flow, and the next day, a channel was made on the second-dammed lake. As a result, the risk of flooding was eliminated. There was also no precipitation during this period.

Fig. 2. The landslide and the dammed lake Karneba. (Photo by N. Kapanadze) 2025.

The distance between the existing points is 37 meters, and the depth of the lake itself was about 8 meters. (Fig. 3)As for the height of the blocking, it is 2.1 meters according to the research and observations of Nikoloz Kapanadze. We also have a longitudinal profile of the river (Fig. 4) and the approximate parameters of the dammed lake in its section. River length (m) is 527.6 and peromile 46.20244503. Name Z Difference, First Congestion 232.801622 2.055104 and First Congestion 230.746518. This is the first data that is still under research.

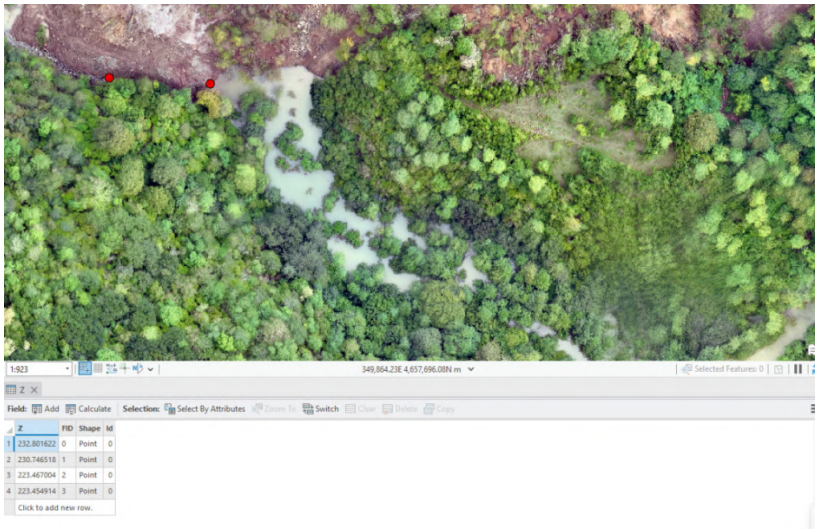

Fig. 3. Sections between the Karneba River's steep slopes.
The difference in elevation between the points is 37 meters. (N. Kapanadze) 2025.

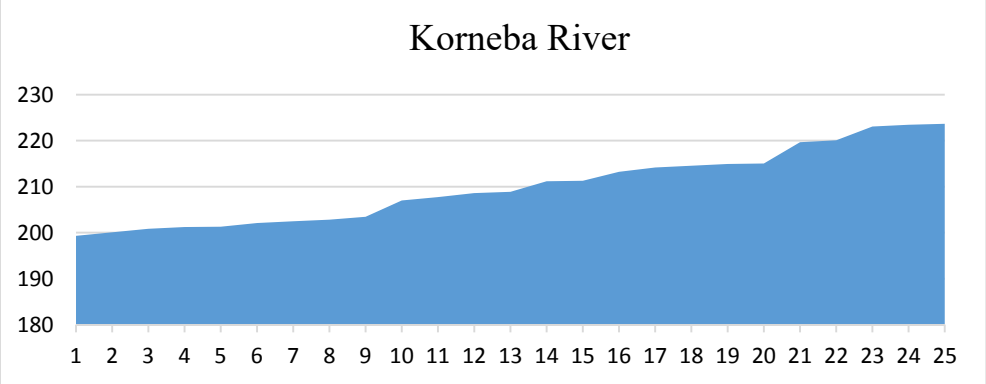

Fig. 4. Longitudinal profile of the Karneba River.

Conclusions

Based on all of the above, it is necessary not only to get acquainted with such objects, but also to constantly observe and monitor them. The fact is that against the background of modern global warming, many natural disasters have become more frequent and more severe. This requires constant attention.

As for the Kharagauli district, at the first stage, it is important to study the relief map of the region, and it is also necessary to study the hydrographic situation. It is important to record the scale of the natural disaster with geo-information maps. It is important to install early warning systems in all critical areas. Channels and drainage should be made taking into account the mechanism of a natural phenomenon. As well as early warning systems, which ensure a quick response in the event of a natural phenomenon. It is necessary to study it not as a geographical object, but as a dangerous object, the breakthrough of which will be accompanied by catastrophic flooding. In fact, these processes are still underway. [7,9]

To sum up this crucial topic, all these instruments will help us avoid the expected floods and floods.

References

1. Natural Disasters and Sustainable Development Issues in Georgia and Bordering Territories. TSU Publishing House, Tbilisi, 2003, pp. 48-58.
2. Gorgijanidze S., Flooding caused by river blockages and dangerous hydrological events related to their breaches (on the example of Georgia). 2005 p. 141. (Thesis)
3. Gorgijanidze S. THE BRIEF ANALYSIS Of GEOGRAPHY Of MOUNTAIN RIVER FLOODING IN GEORGIA /S.Gorgijanidze/ Scientific Reviewed Proceedings of the IHM, GTU, vol.132. 2022, pp. 14-18.
4. Basilashvili Ts. Floods on mountain rivers and their prediction under conditions of information deficiency. Shifr # IHM-13-12- GTU-2429. Tbilisi. 2015, pp. 78.
5. Gorgijanidze, S., Gorgodze, T., Tsintsadze Catalog of Glacially Inundated Lakes, Tbilisi: Publishing House “Samshlobo”, 2024.
6. [6] Gorgijanidze, S. M., Jincharadze, G. A., Silagadze, M. M., & Tchintcharauli, I. R., The geography of risks of the breakthrough of glacial lakes and valleys. Journals of Georgian Geophysical Society, 26(2), 2023. https://doi.org/10.60131/ggs.2.2023.7442
7. Gorgijandze S.N., Gorgodze T.Z., Jincharadze G.A., Kobakhidze N.SH., Gulashvili Z.M., Dvalashvili G.B., Silagadze M. Crucial Moment of Topographic Map for Effective Management of Natural Disasters. International Scientific Conference “Complex Geophysical Monitoring in Georgia: History, Modern Problems, Promoting Sustainable Development of the Country”, Tbilisi, Georgia. Publish House of Iv. Javakhishvili Tbilisi State University, Tbilisi, Georgia. 2024/10/17. ISBN 978-9941-36-272-9. http://openlibrary.ge/handle/123456789/10647
8. Gorgijanidze, T. Gorgodze, G. Dvalashvilic, G. Jincharadze, M. Silagadzed., Abstracts of the International Cartographic Association, 9, 39, 2025. RIMMA2025 – International Conference on Forecasting, Preparedness, Warning, and Response, University of Bern, Switzerland. https://doi.org/10.5194/ica-abs-9-39-2025
9. Gorgijanidze S., RIVER COLLAPSE, POOLS, AND FLOODS WERE CAUSED BY OUTSIDE FACTORS. Transactions of the Institute of Hydrometeorology, Georgian Technical University, vol.121, 2015, pp. 34-37.

1st International Scientific Conference "Modern problems in Geophysics", Proceedings,
ISBN 978-9941-36-434-1, ISSN 3088-4349, Tbilisi, Georgia, November 6-8, 2025

REGIONAL FEATURES OF ATMOSPHERIC CIRCULATION IN GEORGIA AND THEIR RESPONSE ASYMMETRY

Kapanadze N., Tatishvili M., Mkurnalidze I., Khutsishvili E.

Institute of Hydrometeorology, Georgian Technical University, Tbilisi, Georgia
knaili1990@gmail.com

Abstract. *The paper discusses the features of global and regional processes of atmospheric circulation in the conditions of Georgia. The main synoptic formations affecting the climate of Georgia are presented, and their seasonal repeatability and the asymmetric nature of the impact on the western and eastern regions of the country are shown. The natural hydrometeorological events that developed in Georgia as a result of circulation processes and their socio-economic consequences are given. Attention is focused on measures to mitigate climate risks. The study is based on long-term synoptic materials and literary sources, which makes it possible to reveal the complex and diverse nature of atmospheric processes in the country.*

Key words*: Circulatory processes, regional features, response asymmetry.*

Introduction

Georgia is geographically located in the temperate zone of the Eastern Hemisphere and is a region where atmospheric circulation processes manifest themselves in a complex and diverse manner. The compact territory of the country is distinguished by sharp geographical and climatic contrasts, which are due to its complex relief, as well as the proximity of the Black Sea and the barrier role of the Caucasus Range. It is against the background of this multifactorial natural environment that circulation processes in the region acquire local features, which creates a sharply expressed asymmetry in response, both at the climatic, ecosystem, and social levels.

The present work aims to analyze the regional characteristics of circulation processes in the space of Georgia and to focus on the asymmetry that is manifested in the climatic response. The analysis presented in the article is based on both modern climatological studies, as well as long-term meteorological data and literary sources, which makes it possible to identify the asymmetric response in the space of Georgia.

Main part

Atmospheric circulation is the large-scale movement of air masses over the Earth's surface, which is caused by the uneven distribution of solar energy between the equator and the poles and forms various types of winds and pressure systems, which play an important role in the distribution of energy between climatic zones.

Scientists working in Georgia: K. Papinashvili, E. Napetvaridze, V. Gigigneishvili, I. Chogovadze, E. Studies by Elizbarashvili and others have shown that the atmospheric circulation of Georgia is a multifactorial and complex system, which is simultaneously affected by global-scale synoptic processes – the Mediterranean depression, the Azores anticyclone, the Icelandic depression, the Siberian and Arctic anticyclones and the Asian depression, as well as regional and local modifications (Fig. 1), which determine sharply different meteorological conditions in different regions of the country and in different seasons [1-2]. Against this background, an asymmetric climatic response is created between Western and Eastern Georgia, which is especially noticeable in the distribution of precipitation and temperature regimes [3].

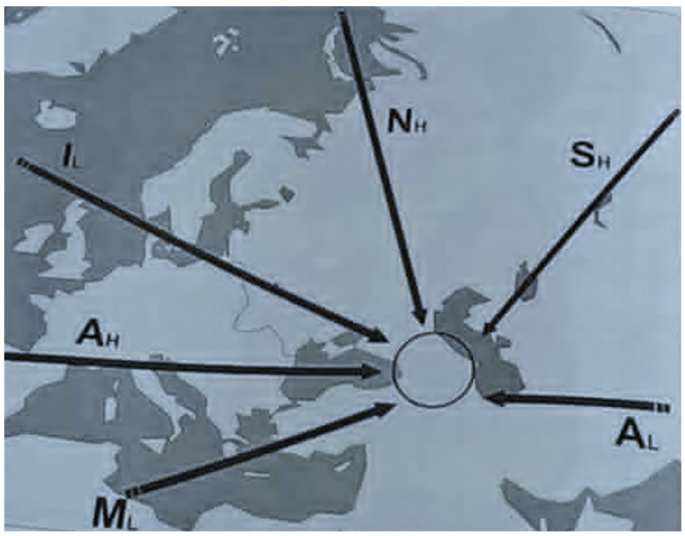

Fig. 1. Influence of circulation processes on Transcaucasia [4].

Georgia is located in the temperate zone and is affected by both air masses coming from the west (Atlantic fronts) and tropical or continental air masses coming from the east and south (Fig. 1). During the year, there is an alternation of the western circulation and bordering anticyclones (Azores or Siberian anticyclones), which have certain seasonal characteristics. For example, the Siberian anticyclone causes the influx of cold, dry air to eastern Georgia in winter, while in the west it flows with humid air through the Black Sea, which is why winters are relatively mild in the western regions. In summer, warm continental air masses often dominate, which is often accompanied by drought in eastern Georgia, while in western Georgia, humid sea air causes relatively frequent precipitation. In summer, the movement of air masses often occurs from north to south or from west to east.

Based on synoptic data published in literary sources [4national], a seasonal distribution table of the frequency of impacts of the mentioned circulation processes on Georgia was compiled.

Table 1. Frequency of impacts of circulation processes on Georgia by season (%)

Process	Spring	Summer	Autumn	Winter
Mediterranean Depression, M_L	26.7	6.1	26.2	41.0
Azores Anticyclone – A_H	17.8	49.3	23.5	9.4
Icelandic Depression – I_L	25.5	25.8	28.2	20.5
Arctic Anticyclone – N_H	30.7	30.6	26.1	12.6
Siberian Anticyclone – S_H	24	-	27.4	48.7
Asian Depression – A_L	19.4	68.4	12.2	-

Table 1 clearly shows that different circulation processes are distinguished by different activity depending on the seasons. For example, in summer, the Asian depression and the Azores anticyclone are observed with the highest frequency, with recurrences of 68.4% and 49.3%, respectively, and in winter, the Siberian anticyclone (48.7%) and the Mediterranean depression (41%). In spring and autumn, all processes affect the territory of Georgia with almost equal recurrence. It should be noted that cyclones from the Black Sea region cause heavy precipitation, often floods, while anticyclones, especially in summer, cause droughts and periods of high temperatures. In addition to the global circulation, regional and local circulation processes also have a significant impact on the climate of Georgia. For example, Georgia is characterized by orographic circulation, which is formed by the influence of local relief – especially the Caucasus and the Lesser Caucasus. These processes are complemented by the microclimatic effects of the Black Sea, which determine the high humidity in Western Georgia. It is also worth noting the presence of such phenomena as warm and cold advection, frontal systems, wave disturbances, microcirculation processes (local breezes and thermal circulations, mountain and plain circulations), etc.

The seasonal dynamics of circulation processes largely determine the occurrence and spread of natural hydrometeorological events – hail, floods and flash floods, strong winds, avalanches, and droughts. These events often cause significant economic damage, pose a threat to infrastructure, agriculture, and the population [5-6].

Table 2 provides a small list of natural events caused by various synoptic processes in the territory of Georgia, with the damage and casualties caused by them.

Table 2. Natural hydrometeorological events that occurred in Georgia

Synoptic Processes	**Natural event**	**Date**	**Spreading area**	**Losses in million GEL**	**Victims**
High Pressure Area	Drought	03-07 2000	All of Georgia	450.0	
Frontal Process	Flood -waterfall	20-30.04, 05-10.05, 27-30.05, 14-16.06. 2002	All of Georgia	78.7	
Frontal Process	now avalanche	01-05, 11-12.2005	Georgian Military Road	3.0	
Southern Wave, Intramassive, Westerly Fronts	Hail	08-10.05, 29 -31.05, 03.06, 12.06, 02.07, 09.07, 23-24.07, 21.08, 16.09, 18.09, 25.09 2005	Imereti, Racha-Lechkhumi, and all of Eastern Georgia	69.0	
Westerly and Eastward Process	Strong wind	23-25.01, 11.02, 05.06, 07.06, 19-20.06,20.08, 16.12 2009	All of Georgia	8.0	8
Heavy Rain	Flood	13.06.2015	Tbilisi, Vere River Gorge	50	22

As can be seen from Table 2, drought is mainly caused by a high-pressure field, floods and flash floods by frontal processes, hail by a southern wave, internal massive processes, and western cold fronts. Strong winds are observed during bilateral invasions, western and eastern processes.

Against the background of modern climate change, the fact that the frequency and intensity of circulation processes may change is of particular importance, which will further increase risks in the future. Studies indicate that more frequent and prolonged impacts of the Asian depression are expected in the summer, which will exacerbate the problem of droughts in Eastern Georgia, while in winter, an increase in the intensity of the Mediterranean depressions and the Siberian anticyclone may increase the risks associated with heavy precipitation and cold [7,8].

Under these conditions, it is particularly necessary to:

- Improve systems for monitoring circulation processes and increase the accuracy of synoptic forecasts;
- Timely identification of hydrometeorological hazards and development of early warning mechanisms;
- Implement measures to adapt ecosystems and agriculture (e.g., anti-hail technologies, optimization of water supply);
- Continue long-term research taking into account climate change scenarios.

Conclusion

The results of the study showed that the atmospheric circulation of Georgia is closely related to global climate systems, although its regional characteristics differ markedly due to the relief, the barrier role of the Black Sea, and the Caucasus Range. The seasonal dynamics of circulation processes determine both the spatial asymmetry of precipitation and temperature distribution, as well as the frequent occurrence of hydrometeorological natural events (drought, hail, floods, avalanches, strong winds, etc.). These events cause signifi-

cant damage to both ecosystems and socio-economic systems. Accordingly, a detailed study of the regional characteristics of atmospheric circulation is necessary for assessing climate risks and planning effective measures to prevent natural events.

References

1. Papinashvili K., Regional features of the climate of Georgia. Tbl.: “Universal”, 2002.
2. Napetvaridze E., Modification of atmospheric circulation in the Caucasus. Tbl.: “Science”, 2015.
3. Beritashvili B., Kapanadze N., Chogovadze I., Features of atmospheric processes dynamics during the extreme weather conditions development in Georgia. /./ Transactions of the Georgian Institute of Hydrometeorology of Georgia, V, 2009, p.116.
4. Gigineishvili V., Elizbarashvili, E., Kutaladze, N., Climate change impact on precipitation regimes in Georgia. Climate Research, 78(3), 2019, pp. 231–245.
5. Elizbarashvili, E., Climate of Georgia. Tbilisi State University Press., 2007.
6. Chogovadze I., Elizbarashvili E., Extreme hydrometeorological events in Georgia and their relation to atmospheric circulation. Georgian Geographical Journal, 3(2), 2011, pp. 45–56.
7. National Environmental Agency of Georgia Assessment of climate risks in Georgia. Tbilisi, 2021.
8. UNDP Climate Change Adaptation in the South Caucasus: Country Report – Georgia. UNDP Regional Bureau for Europe and CIS, 2022.

1st International Scientific Conference "Modern problems in Geophysics", Proceedings,
ISBN 978-9941-36-434-1, ISSN 3088-4349, Tbilisi, Georgia, November 6-8, 2025

SCENARIO OF CHANGES OF THE VEGETATION PERIOD AND ACTIVE TEMPERATURES IN EASTERN GEORGIA UNDER GLOBAL WARMING

Meladze M., Meladze G., Pipia M., Kapanadze N.

Institute of Hydrometeorology, Georgian Technical University, Tbilisi, Georgia
m.meladze@gtu.ge

Abstract. *Forecasts of the duration of the vegetation period (days) and the sum of active temperatures (>10°C) under global warming conditions significantly determine the growth and development of crops and their productivity. For each municipality of the regions of Eastern Georgia, a future scenario of the duration of the vegetation period (days) and the sum of active temperatures (>10°C) has been compiled, with the corresponding forecast regression equations, when the temperature increases by 2°C (2020-2049). With the above equations, the duration of the vegetation period and active temperatures for the future are determined by the municipalities.*

Key Words: *vegetation period, active temperature, crops, forecast*

Forecasts of the duration vegetation period and the sum of active temperatures (>10°C) are important for agricultural workers, farmers, and those employed in the private agricultural sector. For example, if this year, the forecasted sum of active temperatures, under optimal conditions of other factors (atmospheric precipitation, air humidity, etc.), will be higher than the sum of the average active temperatures of a given territory (by 300-400°C), we should assume that the growth and development of crops and their productivity will be ensured, and vice versa, i.e. the harvest and its quality will be lower by 20-30% or more. Also, a duration vegetation period is favorable for normal plant growth and development and high productivity, and vice versa. Therefore, in connection with global climate change, a climate change scenario has been developed for Georgia. In particular, the regional RegCM-4 and the socio-economic development future scenario A_1B_1 (temperature increase by 2°C, 2020-2049) have been used to forecast local climate change [1]. This model calculates meteorological observation data (in this case, daily average air temperatures) for the forecast period of 2020-2049. From the future forecast climate parameters, the average temperatures of each year from the meteorological observations of the National Environmental Agency have been used, and the dates of the transition of temperatures above 10°C in spring and below 10°C in autumn have been determined. Which is calculated by the following equations:

$$y = -2.4x + 79 \text{ (in spring)},$$
$$y = 3.2x - 33 \text{ (in autumn)}$$

In the equations, y is the dates of the temperature transitions up >10°C and down <10°C in spring and autumn; x – the sum of the average temperatures of two months in spring and autumn, or each month (February-March or March-April in spring, September-October or October-November in autumn), the average temperature of the first month must be less than 10°C, the second month – more than 10°C [2, 3].

The sums of active temperatures (>10°C) during the vegetation period were calculated between the received dates. The duration of the vegetation period (days) was also calculated. High correlations were identified from the mentioned characteristics. Specifically, during the vegetation period in spring, the earlier the date of the average daily air temperature exceeding >10°C is observed, the greater the sum of active temperatures accumulates, and vice versa. The duration of the vegetation period (days) is of a similar nature. In this regard, Acad. Davitaia noted that late spring is a sign of a general heat deficit. Because the low temperature in spring is generally not compensated for by the temperatures in summer and autumn.

Based on the above-mentioned regularities, we have compiled a future scenario for the duration of the vegetation period (days) and the sum of active temperatures (>10°C) for each municipality of the regions, with a temperature increase of 2°C (2020-2049), with the corresponding forecast regression equations (Table 1).

Table 1. Forecast equations for the duration of the vegetation period (days) and the sum of active temperatures (>10°C) (future scenario, with a temperature increase by 2°C, 2020-2049)

Region, Municipality	Regression equation of the vegetation period		
	Regression equation (Σn)	correlation coefficient (r)	admissible error $S_u\pm$ (day)
Kakheti, Sagarejo	Σn=-0.9624*x+268.16	r=0.86	7
Mtskheta-Mtianeti, Mtskheta	Σn=-0.9429*x+269.77	r=0.93	6
Samtskhe-Javakheti, Akhaltsikhe	Σn=-1.3175*x+286.62	r=0.89	7
Kvemo Kartli, Bolnisi	Σn=-1.0329*x+291.86	r=0.71	10
Shida Kartli, Gori	Σn=-0.9842*x+273.02	r=0.94	5
Municipality	Regression equation of the sum of active temperature (>10°C) (ΣT)		
Sagarejo	ΣT=-11.996*x+4253.14	0.75	193°C
Mtskheta	ΣT=-12.0165*x+4377.13	0.77	131°C
Akhaltsikhe	ΣT= -20.46*x+4900.01	0.75	143°C
Bolnisi	ΣT=-18.387*x+5554.21	0.74	173°C
Gori	ΣT=-12.272*x+4363.03	0.77	122°C

The reliability of the forecast equations given in Table 1 can be assessed by the admissible error of the equation, which, for the forecast of the duration of the vegetation period, depending on the region, ranges from ±5 days to ±10 days, and for the forecast of the sum of active temperatures, from 122°C to 193°C. Forecasts can be made in the spring, in the first pentad of May, in the mountainous zone (Sagarejo, Akhaltsikhe), and in the first pentad of June. When we have information on the temperatures of the two months preceding the mentioned months from the meteorological stations of the respective municipalities of the region. The forecast advance is quite long and amounts to 5-6 months [4].

Fig.1 shows the projections for the duration vegetation period (days) and the sum of active temperatures (>10°C) for the municipality of eastern Georgia regions under a 2°C temperature increase (future scenario, 2026-2049).

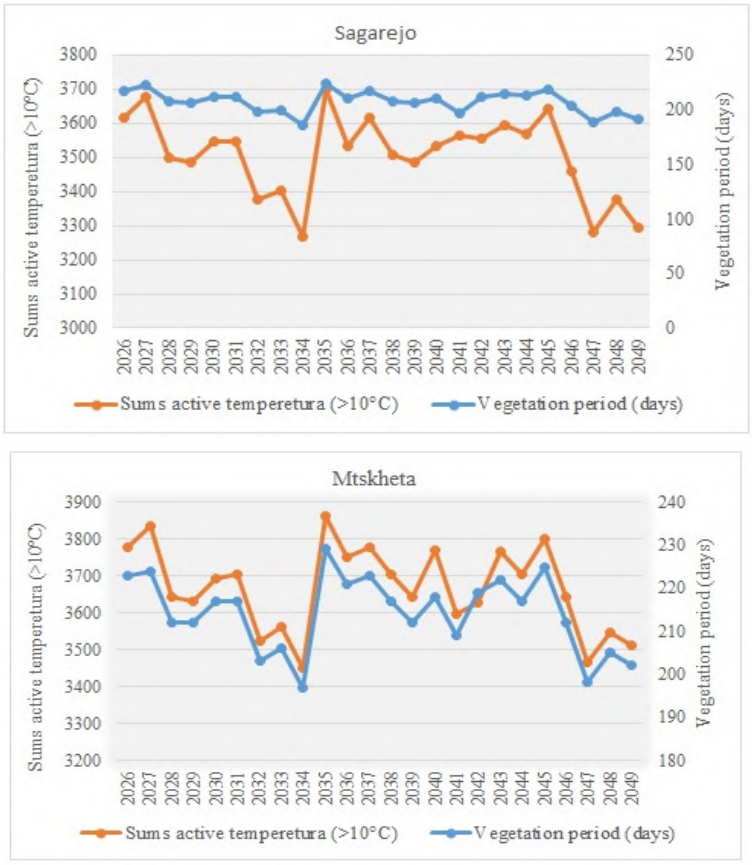

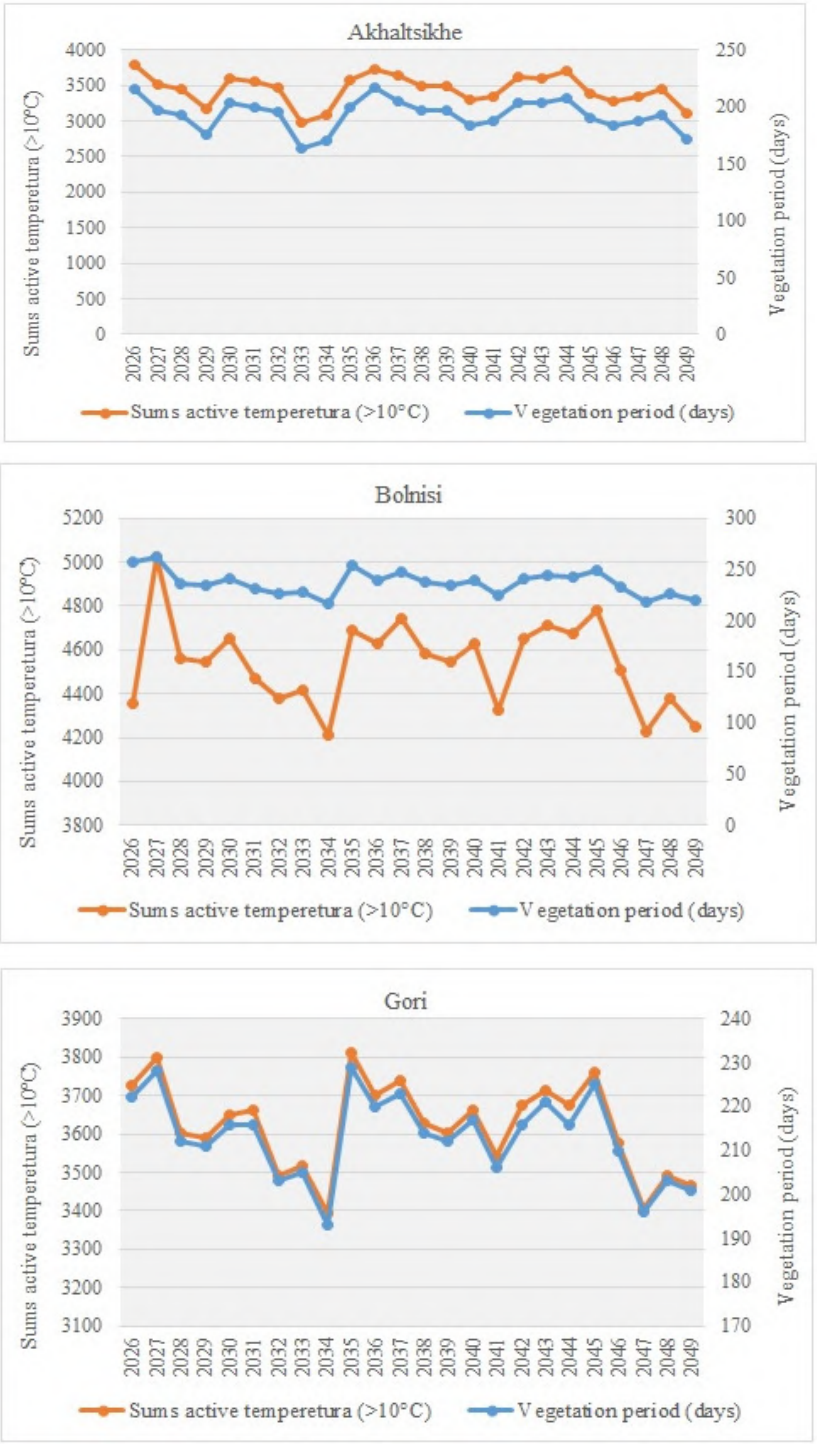

Fig. 1. The duration vegetation period (days) and the sum of active temperatures (>10°C) for the municipality of eastern Georgia regions under a 2°C temperature increase (future scenario, 2026-2049).

According to the analysis of Figure 1, the forecasts of the duration of the vegetation period by region and the sum of active temperatures (>10°C) for the entire vegetation period are noteworthy and should be taken into account. In this regard, we note that according to the forecasts made in the regions under the scenario, when the temperature increases by 2°C, the sum of active temperatures is high everywhere. Therefore, for the normal productivity of plants, it is necessary to carry out irrigation measures for crops, especially during the June-August vegetation period.

According to Figure 1, based on local climatic conditions, the Kvemo Kartli region (Bolnisi, Gardabani, Marneuli) is characterized by the highest increase in the sum of active temperatures. However, this increase in temperature will not hinder the normal development of crops if the temperature does not increase more than that envisaged by the scenario.

It is not difficult to make a forecast for the future. Agricultural workers, specialists, farmers, and those interested in drawing up a forecast for the regions for 2026-2049 can determine the dates of the temperature exceeding 10°C. To do this, data are needed to determine the date of the average temperature exceeding 10°C in the spring, in March-April. For example, let's assume that the average temperatures for March and April for the Gori municipality of the Shida Kartli region in 2026 are determined by the following equation:

$$y = -2.4*x + 79$$

The date of the temperature exceeding 10°C will be 24.III, or 1 – the number of days counted from February is – 52. By inserting the latter instead of n in the corresponding equation for the region ($\Sigma T=12.272*n+4363.03$) and performing mathematical operations, the forecast of the active temperature sum for the current year (2026) will be 3725°C. Similarly, the duration of the vegetation period for the given region from the same date is determined by the corresponding equation, where 222 days are obtained.

Based on the analysis of the above-mentioned studies, global warming during the vegetation period affects the agroclimatic characteristics of the study area. In particular, the growing season is extended, the sum of active temperatures is also increased (>10°C), and atmospheric precipitation is mainly reduced. According to these characteristics, hydrothermal coefficients are reduced, which is an indicator of the frequency and recurrence of various types of droughts. Therefore, it is necessary to develop mitigation measures in this regard. In dry subtropical and slightly elevated mountainous zones, the production of selected perennial and annual crops that are resistant to relatively high temperatures and drought resistance should be especially considered. In mountain and highland zones, it is recommended to arrange terraces on steep slopes (10° and more), which significantly reduces water runoff and intensive evaporation of water from the soil. Cultivation-loosening of the soil surface is effective, as well as the cultivation of windbreaks of plants against the prevailing winds, which creates a favorable microclimate for crops. In addition, in connection with modern climate change, varieties resistant to diseases and pests should be bred for wheat production. It is also important to widely introduce and use irrigation water by sprinkling and drip irrigation methods. Given the current global climate change, it is necessary to consider the practical use of agrometeorological forecasting methods for the occurrence of harvest and phenological phases in the scenario of a 2°C increase in temperature. It is also necessary to raise public awareness in terms of vulnerability assessment, adaptation, and the development of mitigation measures.

References

1. The Third National Communication Climate Change of Georgia, Tbilisi, 2015, p. 288.
2. Meladze G., Meladze M., Elizbarashvili N., Meladze G., Global Warming: changes of Agroclimatic Zones in Humid Subtropical, Mountainous and High Mountainous Regions of Georgia. // International Journal of Current Research, 8(7), India, 2016, pp. 35403-35409.
3. Meladze M., Meladze G. Impact of Global Warming on the Vegetation Durable and Distribution Area of Crops in the Humid Subtropical and Mountainous Regions of Georgia. // American Journal of Environmental Protection, vol.4. No.3-1, 2015, pp.162-167.
4. Meladze G., Meladze M., Climate Change: Agroclimatic Challenges and Prospects in Eastern Georgia. // Publ. House „UNIVERSAL'', Tbilisi, 2020, p. 200.

1st International Scientific Conference "Modern problems in Geophysics", Proceedings,
ISBN 978-9941-36-434-1, ISSN 3088-4349, Tbilisi, Georgia, November 6-8, 2025

MICROCIRCULATION AND HEAT UNIQUENESS OF TBILISI

***,**Tatishvili M., ***Amiranashvili A., *,**Tsitsagi M.,**
***,**Palavandishvili A., *Zotikishvili N.**

** Institute of Hydrometeorology of Georgian Technical University, Tbilisi, Georgia*
***Vakhushti Bagrationi Institute of Geography of the Ivane Javakhishvili Tbilisi State University, Tbilisi, Georgia*
****Mikheil Nodia Institute of Geophysics of Ivane Javakhishvili Tbilisi State University, Tbilisi, Georgia*
m.tatishvili@gtu.ge

Abstract*. Atmospheric processes are highly heterogeneous and anisotropic in space and time. This study examines the climate adaptation strategies. These processes are irregular everywhere, especially in such difficult physical terrain as the TransCaucasus and Georgia in particular. One of such areas is the well-known Tbilisi hollow, which is characterized by a long-standing thermal inversion layer that keeps warm air close to the relief and strengthens heat waves. Extreme heat is a hazard that is capable of causing economic problems and potentially high mortality rates. In order to investigate heat waves, NEA 1991-2020 hydrometeorological observation and ERA5 reanalysis data are used. The results are important for the early warning system and stakeholders.*

Key words*: Daily temperature, heat wave, microcirculation process, Discomfort index*

1. Introduction

Atmospheric processes are highly heterogeneous and anisotropic in space and time. The main reason for this is Solar energy uneven distribution to the Earth's surface. In the lower layers of the atmosphere, the heat regime is provided by the long-wave radiation reflected from the Earth's surface. The heterogeneous surface causes the rays to be reflected at different angles, which in turn causes an uneven distribution of the heat field. Uneven heat field causes an uneven distribution of atmospheric pressure and the formation of permanent "barrier centers". These centers provide air masses motion mainly from west to east ("leading" flow) with approximately 8-12 m/sec velocity and other zonal flows. These processes are irregular everywhere, especially in such difficult physical terrain as the Trans Caucasus and Georgia in particular [1]. There are several microregions in the territory of Georgia whose climatic conditions sharply differ from the climate, with changes in climatic parameters and impacts on weather conditions in the outer region [13]. Change in the microrelief of the Earth's surface, even on a small scale, causes local circulation of the air flow [1,2]. One such area is the well-known Tbilisi hollow [3], which is characterized by long long-standing thermal inversion layer that keeps warm air close to the relief and strengthens heat waves. This traps heat near the Earth's surface. It is usually possible to forecast heat waves, thus allowing the authorities to issue a warning in advance.

In the *Glossary of Meteorology* heat wave is defined as "A period of abnormally and uncomfortably hot and usually humid weather [4]. Typically, HW lasts two or more days. Heat waves have become more frequent and more intense over land, across almost every area on Earth, since the 1950s, with the increase in frequency and duration being caused by climate change. Heat waves form when a high-pressure area in the upper atmosphere strengthens and remains over a region for several days up to several weeks. Heat waves have an impact on the economy. They can reduce labor productivity, disrupt agricultural and industrial processes, and damage infrastructure. Severe heat waves have caused catastrophic crop failures and thousands of deaths from hyperthermia. They have increased the risk of wildfires in areas with drought. They can lead to widespread electricity outages because more air conditioning is used. A heat wave counts as extreme weather. It poses a danger to human health because heat and sunlight overwhelm the thermoregulation in humans.

2. Methodology

There is no universally accepted definition for heatwaves; they are generally considered to be periods of unusually hot weather, lasting for at least several days, and having a negative impact on human health. Also, in Georgia, no formal definition of a heatwave exists. Instead, historical data have been used to develop a heat index, which takes both temperature and relative humidity into consideration, and is an indicator of thermal comfort of the population. Heatwaves are known to be especially problematic in cities, partly due to the positive relationship between population density and perceived heat stress, and partly due to the urban heat island effect, which is prevalent in areas with high settlement density and sparse vegetation. This effect is amplified during extremely warm days. In order to investigate heat waves, NEA 1991-2020 hydrometeorological observation and ERA5 reanalysis data are used.

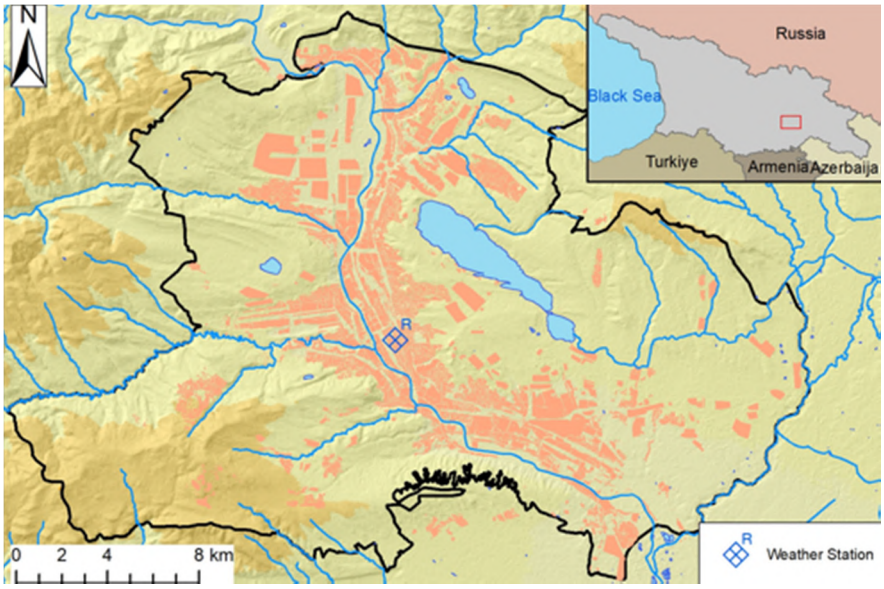

Fig.1. Location of Tbilisi meteorological station.

3. Discussion

The Caucasus Region has been affected by an increasing number of heat waves during the last decades, which have had negative impacts on human health, agriculture, and natural ecosystems. In Tbilisi during the 1991-2020-year period, 2018 was especially hot. The amount mounted 144 days, and reached its highest value of 41^0 in July 2018. Consecutive hot days reached up to 70 °C in 2018 and 120 °C in 2019, accompanied by low humidity [8,9]. July is on average the warmest month of the year, and the average high temperature is 29.9 °C. The city broke its all-time temperature record on July 4th, 2017, by 0.1°C [10,11]. The previous record had been achieved on August 1st, 2000 on when Tbilisi recorded a temperature of 40.4°C. The days with different heat wave thresholds are shown in Figure 2. This helps to identify most warmest year in the selected period.

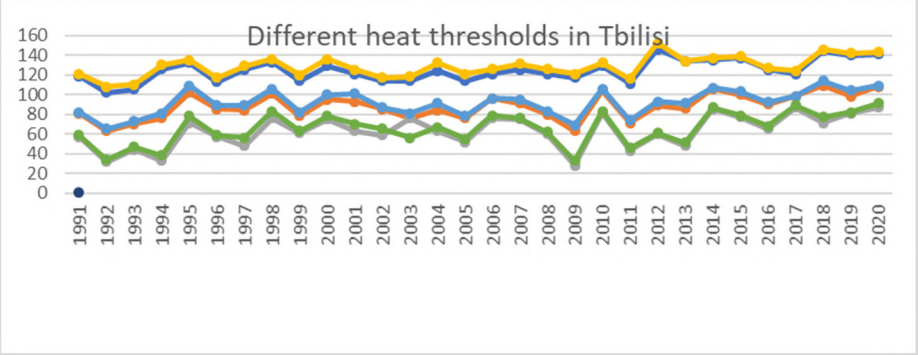

Fig. 2. Heat waves with different thresholds for the 1991-2020 period in Tbilisi

Another important index is the consecutive heat wave day number, which shows the total number of hot and dry days.

For selected years, such exceptional was 22010, 2020 years 115 and 120 days correspondingly.

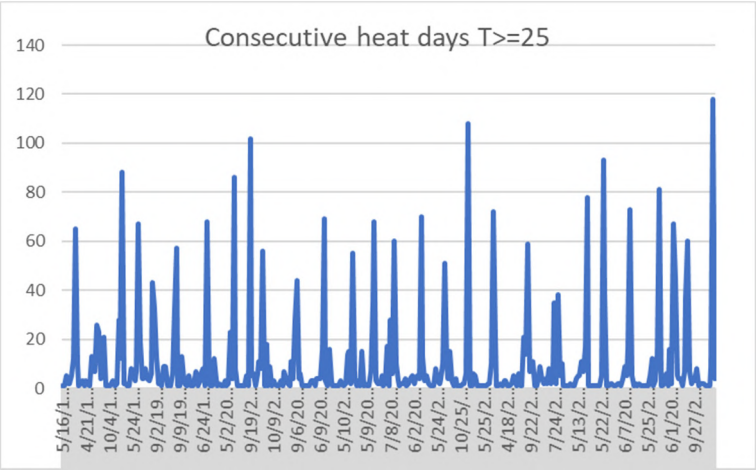

Fig. 3. Consecutive days when T_{max} was equal to/more than 250 °C

The Discomfort Index (DI) method is a method used to identify the level of thermal comfort in an area. It measures how much discomfort a person feels with a given air temperature and relative humidity. The higher the relative humidity and the air temperature, the greater the discomfort index. Conversely, the lower the temperature and humidity, the lower the discomfort index. To calculate the DI hourly temperature and relative humidity, ERA5 reanalysis 2018 26 June-09 July data are used. The calculated values are too high.

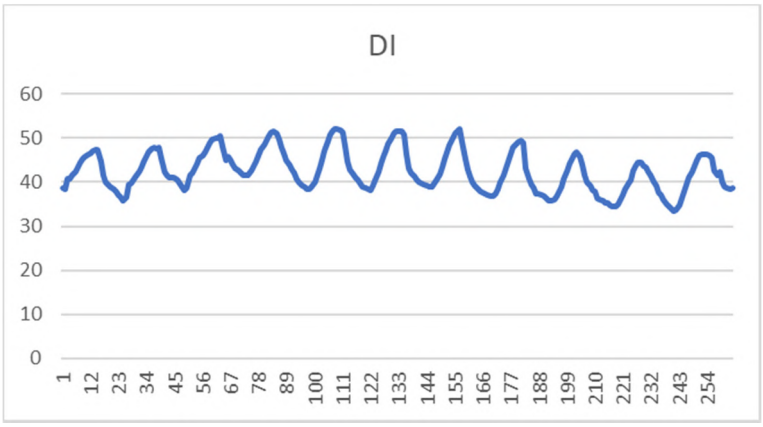

Fig.4. Discomfort Index for Tbilisi during 2018, 26 June-09 July.

While the Discomfort Index is a useful tool for gauging comfort levels, it is not directly designed to predict health risks. High values on the index can indicate conditions that might lead to heat-related illnesses if proper precautions are not taken, such as staying hydrated and avoiding excessive exposure to heat.

The environmental problems faced by the city of Tbilisi are the increase in air temperature and humidity, and the problem of air pollution. It became essential to carry out environmental engineering to solve these problems. The environmental engineering recommendations include intensifying Green Open Space, planting road shade trees, implementing green facades (vertical gardens), implementing a roof garden, and improving people's behavior.

4. Conclusions

The existence of hollows over terrain significantly complicates weather prediction [5,6]. The latent heating in a large complex of deep moist convection often produces a cyclonic vortex. These vortices can then initiate additional convection the next day. When steady wind flows around an isolated obstacle, such as a mountain

or a mountainous island, atmospheric vortex streets (AVSs) can be generated on the leeward side of the obstacle under favorable meteorological conditions. The AVS pattern exhibits a double row of counterrotating vortex pairs shedding alternately and resembles the classic von Karman vortex street; these types of vortex streets have significant weather and climate implications. Atmospheric vortex streets may modulate cloud and wind patterns over downstream regions and are an additional reason for forecasting uncertainty. To avoid all these complications together with numerical weather predictions, another model must be run: the microscale model, which depicts local atmospheric disturbance [10,6,13]. This coupling became essential, as Georgia is a country with great tourism potential, including winter sports tourism. Detailed information on the wind stream velocity can aid in safe paragliding sport and rescue missions. Additionally, research outcomes may be important for early warning systems and implementing Nature-Based Solutions (NBS).

References

1. Khvedelidze Z., Tatishvili M., Zotikishvili N., Samkharadze I., The role of mountainous relief in the investigation of air masses' local circulations. // GESJ: Physics. #1(18), 2018, pp.21-32,
2. Z. Khvedelidze Z, I. Samkharadze I, Tatishvili M, Zotikishvili., „Dynamics of microcirculation movement of air flow and climatic peculiarities in Samegrelo-Zemo Svaneti region". Scientific Reviewed Proceedings of IHM of GTU. 2020, vol.129, pp.113-115
3. Tatishvili M., Khvedelidze Z., Samkharadze I., Palavandishvili A., Atmosphere processes and climate parameters variation in the River Mtkvari basin. Int. Sc. Conf. Natural Disasters in Georgia: Monitoring, Prevention, Mitigation. Tbilisi, 2019, pp. 117-121. http://dspace.gela.org.ge/handle/123456789/8648
4. Glickman, Todd S., Glossary of Meteorology. American Meteorological Society, 2000. ISBN 9781878220493.
5. Tatishvili M. R., Khvedelidze Z. V., Demetrashvili D. I., On some weather forecasting models in Georgia. // Journal of the Georgian Geophysical Society, Physics of Solid Earth, Atmosphere, Ocean and Space Plasma, v. 23(2), 2020. ISSN: 1512-1127.
6. Tatishvili M., Developing a Weather Forecasting System in Georgia. Ecology & Environmental Sciences 2 (7), 2017. DOI:10.15406/mojes. 2017.02.00046.
7. Khvedelidze Z, Tatishvili M, Samkharadze I, Zotikishvili N., "Assessment of the role of local orography in the dynamics of the turbulent air flow of the atmosphere surface layer for certain regions of Georgia. // Proceedings of IHM of GTU, vol.133, 2023, pp.112-116.
8. Aliyev V., Amiranashvili A., Kartvelishvili L., Matzarakis A., Tatishvili M., Comparative Analysis of the Variability of Daily Minimum, Maximum, and Mean Air Temperature in Baku and Tbilisi in 2005-2024. // Int. Journal of Sustainability and Rick Control, e-ISSN: 3104 8358, p-ISSN: 3104-834X, Baku, Azerbaijan, Vol. 1, No. 2 (2), September 2025, pp. 63-70. DOI: https://doi.org/10.64599/GDOF7452
9. Aliyev V., Amiranashvili A., Kartvelishvili L., Matzarakis A., Tatishvili M. Variability of Monthly Average Values of Daily Minimum, Maximum, and Mean Air Temperature in Baku and Tbilisi IN 2005-2024. // Int. Journal of Sustainability and Rick Control, e-ISSN: 3104-8358, p-ISSN: 3104-834X, Baku, Azerbaijan, Vol. 1, No. 3 (3), December 2025, (in Press).
10. Kartvelishvili L., Tatishvili M., Amiranashvili A., Megrelidze L., Kutaladze N., Weather, Climate, and their Change Regularities for the Conditions of Georgia. // Monograph: Publishing House "Universal", Tbilisi, 2023, p. 406.
11. Amiranashvili A., Kartvelishvili L., Kutaladze N., Megrelidze L., Tatishvili M. Comparison of the Mean Max Annual, Seasonal, and Monthly Air Temperature Variability in Tbilisi and Shovi in 1956-2022. // Int. Sc. Conf. "Geophysical Processes in the Earth and its Envelopes". Proc., Publish House of Iv. Javakhishvili Tbilisi State University, November 16-17, 2023, pp. 127-132.
12. Amiranashvili A., Analysis of Variability of Mean Annual Air Temperature in Tbilisi in 1844-2023 Against the Background of Climate Change. // Int. Sc. Conf. "Complex Geophysical Monitoring in Georgia: History, Modern Problems, Promoting Sustainable Development of the Country". Proc., Publish House of Iv. Javakhishvili Tbilisi State University, Tbilisi, Georgia, October 17-19, 2024, pp. 145 – 149.
13. Tatishvili M., Khvedelidze Z. Samkharadze I., Zotikishvili N., Chelidze N., Dynamics of Atmospheric Microcirculation Processes in Certain Regions of Georgia. // Georgian Geographical Journal 4(1) 2024. https://doi.org/10.52340/ggj.2024.04.01.07.

1st International Scientific Conference "Modern problems in Geophysics", Proceedings,
ISBN 978-9941-36-434-1, ISSN 3088-4349, Tbilisi, Georgia, November 6-8, 2025

COMPARISON OF ANGSTROM FIRE INDEX FOR BAKU (AZERBAIJAN) AND TBILISI (GEORGIA)

[*]Aliyev V., [**]Bliadze T., [**]Chikhladze V., [***]Davitashvili M., [****]Tatishvili M.

[*]CEO & Founder, International Event Organizer Company AMIR Technical Services Azerbaijan, Baku, Azerbaijan
[**]Mikheil Nodia Institute of Geophysics of Ivane Javakhishvili Tbilisi State University, Tbilisi, Georgia
[***]I. Gogebashvili Telavi State University, Telavi, Georgia
[****]Institute of Hydrometeorology of Georgian Technical University, Tbilisi, Georgia
prof.vugar.aliyev@gmail.com

Abstract. *The results of a statistical analysis of the daily and mean monthly values of Angstrom Fire Index (AFI) for Baku (Azerbaijan) and Tbilisi (Georgia) in the period 2005-2024 are presented. AFI = (R/20) + (27-T)/10, where R is the minimum relative humidity, T is the maximum air temperature. The gradations of the values of I are as follows: I. AFI ≥ 4.1 – Low, II. AFI = 4.0 ÷ 3.0 – Moderate, III. AFI = 2.9 ÷ 2.5 – High, IY. AFI = 2.4 ÷ 2.0 – Very High, Y. AFI = <2.0 – Extreme. In particular, it was found that an extreme fire hazard in Baku and Tbilisi are observed on average within 75 days a year, but in general, the level of forest fire danger in Tbilisi is higher than in Baku. Between the daily and monthly mean values of AFI in Baku and Tbilisi direct linear correlation is observed.*

Key Words: *Angstrom Fire Index, temperature, fire.*

Introduction

The problem of fires, including forest fires, is relevant for many countries worldwide [http://www.sasquatchstation.com/Fire_Weather.php; http://www.forestservice.gr/meteo/fwi1.html], including Georgia [1].

This problem has become even more pressing in recent decades due to rapid global and local warming [2-4], which is increasing the fire danger [5].

Different countries use different indicators of forest fire danger [5-8]. These indices are mathematical formulas that formalize the influence of air temperature and humidity, precipitation, moisture content of forest combustible materials, thunderstorm activity, etc. In many cases, the simple Swedish Angstrom index [6,7] with a four-range [http://www.forestservice.gr/meteo/fwi1.html] or five-range [http://www.sasquatchstation.com/Fire_Weather.php] scale is used. Along with climatological and operational information on forest fire danger levels, a forecast is produced [https://www.weather.gov/fire].

In Georgia, work on assessing the fire danger of an area using the Angstrom Fire Index [6,7] began in 2019, using Tbilisi as an example [9]. Similar studies were continued for the cities of Telavi and Kutaisi, as well as the Russian cities of Nalchik and Kislovodsk [10-15].

This work is a continuation of previous studies. Below are the results of a statistical analysis of daily Angstrom Fire Danger Index (AFI) values for Baku (the capital of Azerbaijan) and Tbilisi (the capital of Georgia) using a five-range scale for the period 2005–2024.

Study area, material and methods

The study area is Baku (the capital of Azerbaijan) and Tbilisi (the capital of Georgia) cities. Data of the daily maximum of air temperature T and minimum relative humidity R in the period 2005-2024 are used [http://www.pogodaiklimat.ru/archive.php?id=ru&region=07]. The Swedish Angstrom Index calculated from the formula: AFI = (R/20) + (27-T)/10 [6,7]. The gradations of the values of AFI are as follows [http://www.sasquatchstation.com/Fire_Weather.php]: I. AFI ≥ 4.1 – Low, II. AFI = 4.0 ÷ 3.0 – Moderate, III. AFI = 2.9 ÷ 2.5 – High, IY. AFI = 2.4 ÷ 2.0 – Very High, Y. AFI = <2.0 – Extreme.

The standard statistical methods are used. The following designations will be used below: Min – minimal values; Max – maximal values; St Dev – standard deviation; C_v – coefficient of variation (%); R – coefficient

of linear correlation; AFI_Max_B and AFI_Max_T – Angstrom Fire Index with daily maximum temperatures in Baku and Tbilisi, respectively.

Results and discussion

Results in Table 1, 2 and Fig. 1,2 are presented.

Table 1. Statistical characteristics of daily values of Angstrom Fire Index in Baku and Tbilisi for different months in 2005-2024.

Month	Jan	Feb	Mar	Apr	May	Jun	Jul	Aug	Sep	Oct	Nov	Dec
Param	**Baku**											
Min	2.0	1.6	1.4	0.7	-0.1	-0.7	-1.0	-0.8	-0.5	0.9	1.8	1.7
Max	7.9	7.8	7.0	6.8	6.1	5.4	5.4	4.7	5.5	6.1	7.0	7.6
Mean	5.6	5.5	5.0	3.9	2.9	1.8	1.7	1.5	2.6	3.9	4.7	5.3
St Dev	0.94	0.99	0.97	1.16	1.15	1.01	1.03	0.98	0.96	0.92	0.78	0.82
Cv,%	16.9	18.0	19.5	29.9	40.1	56.0	61.7	64.4	37.5	23.8	16.4	15.5
	Tbilisi											
Min	2.6	1.5	1.0	0.6	0.6	-0.4	-0.2	-0.3	0.0	0.9	1.4	1.6
Max	7.3	7.6	7.3	7.2	6.2	5.5	4.4	4.8	6.0	7.0	7.2	7.3
Mean	4.9	4.6	4.0	3.3	2.8	2.1	1.8	1.6	2.5	3.5	4.3	4.9
St Dev	0.90	1.09	1.01	1.10	0.98	0.88	0.80	0.91	0.92	1.02	0.99	0.82
Cv,%	18.5	23.9	25.6	33.4	34.7	42.0	45.2	57.2	37.2	29.2	23.1	16.7
	The values of the correlation coefficient (**R**) between the AFI values in Baku and Tbilisi											
R	0.40	0.35	0.22	0.47	0.45	0.58	0.49	0.49	0.41	0.44	0.37	0.23

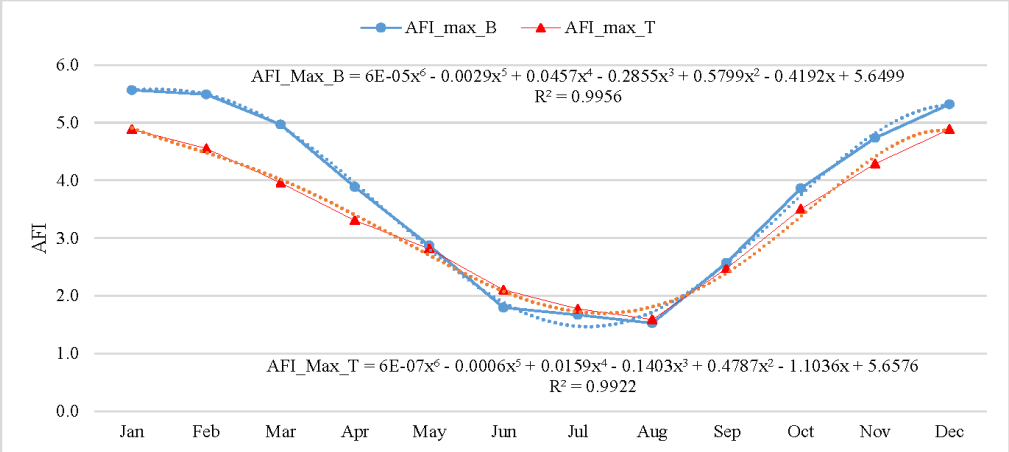

Fig. 1. The intra-annual distributions of mean monthly values of AFI in Baku and Tbilisi in 2005-2024.

In Table 1 and Fig. 1 the statistical characteristics of daily and mean monthly values of AFI in Baku and Tbilisi for different months in 2005-2024 are presented.

In particular, as follows from Table 1 in Baku values of AFI changes from -0.8 (August, fire occurrence is extreme) to 7.9 (January, fire occurrence is low). The mean monthly values of AFI) changes from 1.5 (August, fire occurrence is extreme) to 5.6 (January, fire occurrence is low).

In Tbilisi values of AFI changes from -0.4 (June, fire occurrence is extreme) to 7.6 (February, fire occurrence is low). The mean monthly values of AFI changes from 1.6 (August, fire occurrence is extreme) to 4.9 (January, December, fire occurrence is low).

The coefficient of linear correlation between daily values of AIF in Baku and Tbilisi changes from 0.22 (March, negligible correlation) to 0.58 (June, moderate correlation). Note that the coefficient of linear correlation between daily values of AIF in Baku and Tbilisi is ≈ 1.0 (very high correlation).

The intra-annual distributions of mean monthly values of AFI in Baku and Tbilisi have the form of a sixth-degree polynomial (Fig. 1).

Table 2. Repetition of AFI in Baku and Tbilisi in different months for five gradations in 2005-2024.

Location	Baku					Tbilisi				
AFI	**≥ 4.1**	**4.0 – 3.0**	**2.9 – 2.5**	**2.4 – 2.0**	**< 2.0**	**≥ 4.1**	**4.0 – 3.0**	**2.9 – 2.5**	**2.4 – 2.0**	**< 2.0**
Jan	93.7	5.3	0.2	0.6	0.2	81.9	16.6	1.5	0.0	0.0
Feb	92.0	5.3	1.4	0.5	0.7	65.1	27.6	5.1	1.8	0.4
Mar	84.7	10.5	2.6	1.5	0.8	44.0	39.2	9.2	5.3	2.3
Apr	43.3	33.3	9.5	8.0	5.8	22.7	35.5	17.2	14.2	10.5
May	12.9	31.3	20.0	13.9	21.9	10.3	27.4	22.1	19.5	20.6
Jun	2.2	9.2	10.0	17.3	61.3	1.7	14.2	15.0	25.3	43.8
Jul	2.1	6.5	12.1	17.9	61.5	0.6	6.6	9.7	19.7	63.4
Aug	1.1	4.8	9.4	18.7	66.0	0.5	6.6	9.2	14.5	69.2
Sep	6.0	25.2	20.8	22.5	25.5	5.5	20.0	21.5	23.7	29.3
Oct	38.2	45.8	9.7	3.7	2.6	26.0	41.1	18.2	10.6	4.0
Nov	80.8	17.2	1.3	0.5	0.2	54.2	38.3	5.7	1.5	0.3
Dec	92.7	5.6	0.5	0.8	0.3	86.3	12.3	1.0	0.3	0.2

In Table 2 data about repetition of AFI in Baku and Tbilisi for different months is presented. Specifically, as Table 2 shows, on average, for most days of the month extreme fire danger in Baku is observed from June to August (repetition are 61.3, 61.5, and 66.0%, respectively), while in Tbilisi it is observed in July and August (repetition are 63.4 and 69.2%, respectively).

In Baku, for most days of the month low fire danger is observed from January to March, in November and in December (repetition is over 80%), while in Tbilisi it is observed in January, February, November, and December (repetition is over 54%).

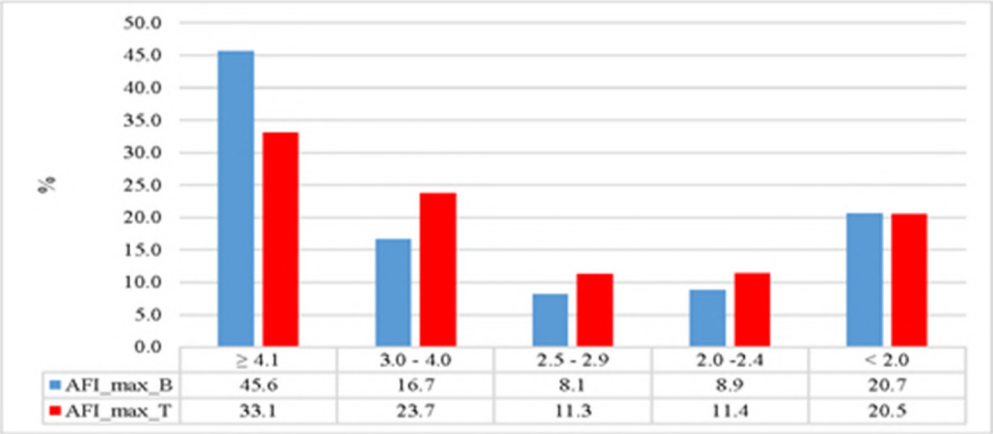

Fig. 2. Repetition of AFI in Baku and Tbilisi (full data).

A low fire hazard in Baku and Tbilisi (Fig. 2) are observed on average within 166 and 121 days a year (repetition – 45.6 and 33.1 % respectively), moderate – within 61 and 87 days a year (repetition – 16.7 and 23.7 % respectively), high – within 30 and 41 days a year (repetition – 8.1 and 11.3 % respectively), very high – within 32 and 42 days a year (repetition – 8.9 and 11.4 % respectively) and extreme – 75 days a year

in both cities (repetition – 20.5 and 20.5%, respectively). Thus, in general, the level of forest fire danger in Tbilisi is higher than in Baku.

Conclusion

It is planned to continue this research in the near future, taking into account the rapid warming of the climate in recent years.

References

1. Bliadze T., Statistical Analysis of the Weekly Fire Alerts Count in Georgia and its Regions in 2012-2023.// Int. Sc. Conf. “Complex Geophysical Monitoring in Georgia: History, Modern Problems, Promoting Sustainable Development of the Country”, Proceedings, ISBN 978-9941-36-272-9, Publish House of Iv. Javakhishvili Tbilisi State University, Tbilisi, Georgia, October 17-19, 2024, pp. 101 – 104. http://109.205.44.60/bitstream/123456789/10632/1/26_MM-180.pdf
2. Kartvelishvili L., Tatishvili M., Amiranashvili A., Megrelidze L., Kutaladze N., Weather, Climate and their Change Regularities for the Conditions of Georgia. // Monograph, Publishing House “UNIVERSAL”, ISBN: 978-9941-33-465-8, Tbilisi 2023, p. 406. https://doi.org/10.52340/mng.9789941334658
3. Aliyev V., Amiranashvili A., Kartvelishvili L., Matzarakis A., Tatishvili M., Comparative Analysis of the Variability of Daily Minimum, Maximum and Mean Air Temperature in Baku and Tbilisi in 2005-2024. // Int. Journal of Sustainability and Rick Control, e-ISSN: 3104-8358, p-ISSN: 3104-834X, Baku, Azerbaijan, Vol. 1, No. 2 (2), September 2025, pp. 63-70. DOI: https://doi.org/10.64599/GDOF7452
4. Aliyev V., Amiranashvili A., Kartvelishvili L., Matzarakis A., Tatishvili M., Variability of Monthly Average Values of Daily Minimum, Maximum and Mean Air Temperature in Baku and Tbilisi IN 2005-2024. // Int. Journal of Sustainability and Rick Control, e-ISSN: 3104-8358, p-ISSN: 3104-834X, Baku, Azerbaijan, Vol. 1, No. 3 (3), December 2025, (in Press).
5. Ullah M.R., Liu X.D., Al-Amin M., Spatial-Temporal Distribution of Forest Fires and Fire Weather Index Calculation from 2000 to 2009 in China. // Journal of Forest Science, 59, 7, 2013, pp. 279–287.
6. Skvarenina J., Mindas J., Holecy J., Tucek J., Analysis of the Natural and Meteorological Conditions During Two Largest Forest Fire Events in the Slovak Paradise National Park. // Forest fire in the wildland-urban interface and rural areas in Europe: an integral planning and management challenge. Athens. 2003.
7. Lukić T., Marić P., Hrnjak I., Gavrilov M.B., Mladjan D., Zorn M., Komac B., Milošević Z., Marković S.B., Sakulski D., Jordaan A., Đorđević J., Pavić D., Stojsavljević R., Forest Fire Analysis and Classification Based on a Serbian Case Study. // Acta Geographica Slovenica, 57-1, 2017, pp. 51–63.
8. Klassifikatsiya prirodnoy pozharnoy opasnosti lesov. // Prikaz Rosleskhoza ot 5 iyulya 2011 g. № 287, 6 s., dokument s sayta aviales.ru
9. Bliadze T., Kirkitadze D., Samkharadze I., Tsiklauri Kh., Statistical Characteristics of Angstrom Fire Index for Tbilisi. // Int. Sc. Conf. “Natural Disasters in Georgia: Monitoring, Prevention, Mitigation”. Proc., ISBN 978-9941-13-899-7, Publish House of Iv. Javakhishvili Tbilisi State University, December 12-14, Tbilisi, 2019, pp.86-90.
10. Bliadze T., Kirkitadze D., Samkharadze I., Tsiklauri Kh., Statistical Characteristics of Angstrom Fire Index for Telavi (Georgia). // International Scientific Conference „Modern Problems of Ecology“,Proceedings, ISSN 1512-1976, v. 7, Tbilisi-Telavi, Georgia, 26-28 September, 2020, pp.64-67.
11. Bliadze T., Gekkieva S., Kirkitadze D., Comparison of Angstrom Fire Index for Nalchik (Kabardino-Balkaria, Russian Federation) and Telavi (Georgia). // International Scientific Conference „Modern Problems of Ecology“,Proceedings, ISSN 1512-1976, v. 7, Tbilisi-Telavi, Georgia, 26-28 September, 2020, pp.68-72.
12. Bliadze T., Povolotskaya N., Senik I., Comparison of Angstrom Fire Index for Tbilisi (Georgia) and Kislovodsk (Russia). // Int. Sc. Conf. „Natural Disasters in the 21st Century: Monitoring, Prevention, Mitigation“. Proceedings, ISBN 978-9941-491-52-8, Tbilisi, Georgia, December 20-22, 2021. Publish House of Iv. Javakhishvili Tbilisi State University, Tbilisi, 2021, pp. 158 – 162.
13. Bliadze T., Amiranashvili A., Chkhitunidze M., Laghidze L.ნ Statistical Analysis of Angstrom Fire Index for Kutaisi, Georgia. // II International Scientific Conference “Landscape Dimensions of Sustainable Development Science – Carto/GIS – Planning – Governance”, Dedicated to the 75th Anniversary of Professor Nikoloz (Niko) Beruchashvili, Proceedings, 12-16 September 2022, Tbilisi, Georgia, Ivane Javakhishvili Tbilisi State University Press, 2022, ISBN 978-9941-36-030-5, pp. 270-274. http://www.dspace.gela.org.ge/handle/123456789/10119
14. Amiranashvili A., Bliadze T., Japaridze N., Khazaradze K., Revishvili A., Angstrom Fire Index as a Bioclimatic Indicator (Using the Example of the Impact on the Spread of Covid-19 in Tbilisi). // Int. Sc. Conf. "Geophysical Processes in the Earth and its Envelopes". Proceedings, ISBN 978-9941-36-147-0, Publish House of Iv. Javakhishvili Tbilisi State University, November 16-17, 2023, pp. 328-331. http://openlibrary.ge/handle/123456789/10467
15. Amiranashvili A., Bliadze T., Davitashvili M., Khakhiashvili M., Variability of the Angstrom Fire Index in Kakheti due to Climate Change. // Transactions of Mikheil Nodia Institute of Geophysics, ISSN 1512-1135, vol. LXXV, 2022, pp. 117-136, (in Georgian). http://openlibrary.ge/handle/123456789/10298

1st International Scientific Conference "Modern problems in Geophysics", Proceedings,
ISBN 978-9941-36-434-1, ISSN 3088-4349, Tbilisi, Georgia, November 6-8, 2025

DISTRIBUTION THE DAILY NUMBER OF AIR EFFECTIVE TEMPERATURE ACCORDING TO MISSENARD IN BATUMI BY MONTH

[*,]Japaridze N., [***,****]Kartvelishvili L., [**,*****]Khazaradze K., [******]Chkhitunidze M., [******]Nikolaishvili M., [*****]Revishvili A.**

[*]*Tbilisi State Medical University, Tbilisi, Georgia*
[**]*Ministry of Internally Displaced Persons from Occupied Territories, Labour, Health and Social Affair of Georgia, Tbilisi, Georgia*
[****]*Institute of Hydrometeorology of the Georgian Technical University, Tbilisi, Georgia*
[****]*Georgian National Environmental Agency, Tbilisi, Georgia*
[*****]*Georgian State Teaching University of Physical Education and Sport, Tbilisi, Georgia*
[******]*Mikheil Nodia Institute of Geophysics of Ivane Javakhishvili Tbilisi State University, Tbilisi, Georgia*
n.japaridze@tsmu.edu

Abstract: *The paper presents data on distribution of the number of daily mean and maximum values of air effective temperature according to Missenard in Batumi by month in 2018-2023. In particular, on average, for the mean daily values of effective air temperature with the category "Comfortable", the largest number of days are observed from June to September (15, 18, 17 and 13, respectively). For the maximum daily values of effective temperature – in June, September and October (14, 13 and 12, respectively).*

Key words: *Effective temperature, bioclimate, human health, ecology.*

Introduction

Information on the bioclimatic characteristics of the territory is important both in terms of determining the degree of their impact on public health and promoting the development of the resort and tourism industry [1–7], etc. There are many simple and complex bioclimatic indices (a combination of temperature and relative humidity, wind speed and other meteorological parameters) [1,4-13], one of which is the frequently used effective air temperature according to Missenard ET [6,11,13,14,15].

For example, in [13], the results of a statistical analysis of average monthly data on ET values in the Autonomous Republic of Adjara and the Kakheti region are presented. The intra-annual distribution of ET values was studied, their repeatability by ET categories, etc. was obtained.

In the work [15] the results of statistical analysis of the daily mean and maximum values of effective air temperature (ET_mean and ET_Max respectively) in Batumi in 2018-2023 are presented. In particular, it was found that in cold periods the highest repeatability of ET_Mean values is in the "Cold" category (50.0%), and the lowest is in the "Comfortable" category (0.8 %). The highest repeatability of ET_Max values is in the "Cold" category (41.1 %), and the lowest is in the "Hot" category (0.2%).

In warm season the highest repeatability of ET_Mean values is in the "Comfortable" category (34.3%), and the lowest is in the "Very cold" category (1.4 %). The highest repeatability of ET_Max values is in the "Hot" category (25.1 %), and the lowest is in the "Very cold" category (0.3%).

This work is part of the investigation [15]. Below are the results of a study on distribution of the number of daily mean and maximum values of air effective temperature according to Missenard in Batumi by month in 2018-2023.

Study area, material and methods

Study area – Batumi (the capital of the autonomous republic of Adjara, Georgia).

The work uses data from the Georgian National Environment Agency on average daily and urgent (at 4 p.m. local time) values of temperature (T), relative humidity (RH) and wind speed (V) for the period from 2018 to 2023.

The air effective temperature according to Missenard was calculated using the formula [14]:

$$ET = 37-(37-T)/(0.68-0.0014\cdot RH+1/(1.76+1.4\cdot V^{0.75})) -0.29\cdot T\cdot (1-0.01\cdot RH)$$

The categories of ET are presented in Table 1.

Table 1. The degree of human thermal sensation (category) depending on the values of air effective temperature.

ET	<1°C	1-9°	9-17°	17-21°	21-23°	23-27°	>27°
ET Category	Very cold	Cold	Cool	Comfortable	Warm	Hot	Very hot

In the proposed work the analysis of data is carried out with the use of the standard statistical analysis methods. The following designations will be used below: ET_Mean – daily average air effective temperature; ET_Max – daily maximum air effective temperature.

Results and discussion

Results in Fig. 1 and 2 are presented.

In Fig. 1 data about the number of days with different categories of ET_Mean in Batumi from January to December are presented.

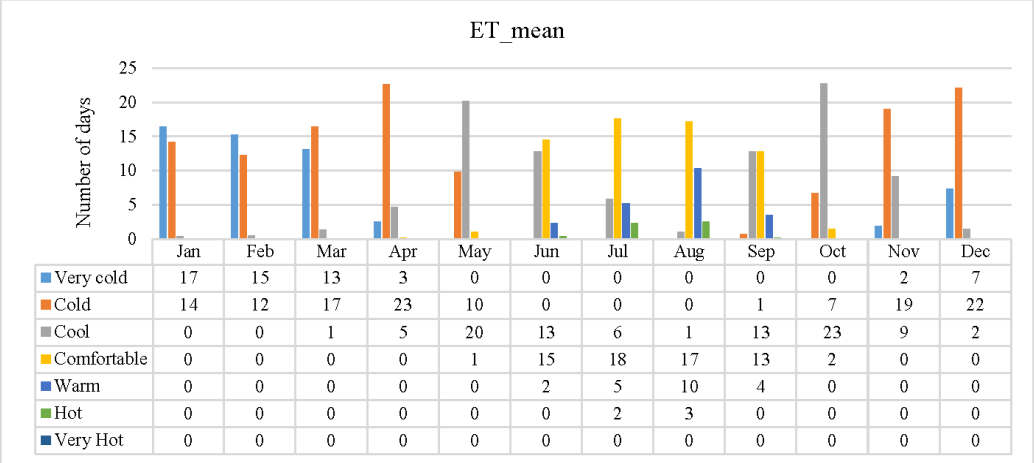

	Jan	Feb	Mar	Apr	May	Jun	Jul	Aug	Sep	Oct	Nov	Dec
Very cold	17	15	13	3	0	0	0	0	0	0	2	7
Cold	14	12	17	23	10	0	0	0	1	7	19	22
Cool	0	0	1	5	20	13	6	1	13	23	9	2
Comfortable	0	0	0	0	1	15	18	17	13	2	0	0
Warm	0	0	0	0	0	2	5	10	4	0	0	0
Hot	0	0	0	0	0	0	2	3	0	0	0	0
Very Hot	0	0	0	0	0	0	0	0	0	0	0	0

Fig. 1. Number of days with different categories of ET_Mean in Batumi from January to December.

In particular, as follows from Fig. 1, on average during the year for mean daily values of effective air temperature with the "Comfortable" category, the greatest number of days are observed from June to September (15, 18, 17 and 13, respectively), etc.

In Fig. 2 data about the number of days with different categories of ET_Max in Batumi from January to December are presented.

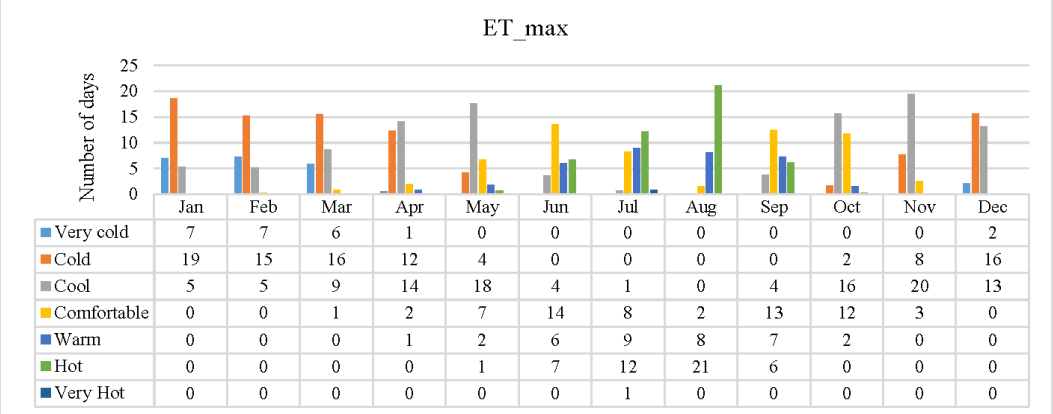

	Jan	Feb	Mar	Apr	May	Jun	Jul	Aug	Sep	Oct	Nov	Dec
Very cold	7	7	6	1	0	0	0	0	0	0	0	2
Cold	19	15	16	12	4	0	0	0	0	2	8	16
Cool	5	5	9	14	18	4	1	0	4	16	20	13
Comfortable	0	0	1	2	7	14	8	2	13	12	3	0
Warm	0	0	0	1	2	6	9	8	7	2	0	0
Hot	0	0	0	0	1	7	12	21	6	0	0	0
Very Hot	0	0	0	0	0	0	1	0	0	0	0	0

Fig. 2. Number of days with different categories of ET_Max in Batumi from January to December.

In particular, as follows from Fig. 2, on average during the year for max daily values of effective air temperature with the “Comfortable” category, the greatest number of days are observed from June, September and October (14, 13, and 12, respectively). The highest number of days of ET_Max with the “Hot” category is observed in August (21 days), etc.

Conclusion

The paper presents data on the number of daily mean and maximum values of air effective temperature according to Missenard in Batumi for each month of year, which, in addition to scientific interest, may also have practical significance for planning resort and tourist activities depending on the seasons of the year. In the future, we plan to continue similar studies for different regions of Georgia.

Acknowledgement. The authors are grateful to the chief of the atmospheric physics department of M. Nodia Institute of Geophysics A. Amiranashvili for assistance in the fulfillment of this work.

References

1. Kartvelishvili L., Tatishvili M., Amiranashvili A., Megrelidze L., Kutaladze N., Weather, Climate and their Change Regularities for the Conditions of Georgia. // Monograph, Publishing House “UNIVERSAL”, Tbilisi 2023, 406 p., https://doi.org/10.52340/mng.9789941334658
2. Japaridze N., Khazaradze K., Studies in the Field of the Influence of Natural and Anthropogenic Environmental Factors on Human Health in Georgia: Current Status and Planned Works. // Int. Sc. Conf. “Natural Disasters in Georgia: Monitoring, Prevention, Mitigation”. Proc., ISBN 978-9941-13-899-7, Publish House of Iv. Javakhishvili Tbilisi State University, December 12-14, Tbilisi, 2019, pp. 201-204. http://109.205.44.60/bitstream/123456789/8671/1/47_Conf_NDG_2019.pdf
3. Japaridze N., Khazaradze K., Chkhitunidze M., Revishvili A., A Brief Overview of Research Conducted by M. Nodia Institute of Geophysics, TSU Together with Medical Organizations in the Field of “Health of the Population of Georgia and Environment” Over the Past 10 Years. // Int. Sc. Conf. "Geophysical Processes in the Earth and its Envelopes", Proceedings, Publish House of Iv. Javakhishvili Tbilisi State University, November 16-17, Tbilisi, 2023, pp. 337-343. http://dspace.gela.org.ge/handle/123456789/10469
4. Amiranashvili A., Bolashvili N., Kartvelishvili L., Liparteliani G. , Tsirgvava G., Holiday Climate Index in Kvemo Kartli (Georgia). // Georgian Geographical Journal, E-ISSN: 2667-9701, 24(1), 2024, pp. 35-46. https://doi.org/10.52340/ggj.2024.04.01.05
5. Amiranashvili A., Kartvelishvili L., Matzarakis A., Variability of the Holiday Climate Index in Tsalka (Georgia). // Journal of the Georgian Geophysical Society, e-ISSN: 2667-9973, p-ISSN: 1512-1127, Physics of Solid Earth, Atmosphere, Ocean and Space Plasma, v. 27(1), 2024, pp. 77–90. https://ggs.openjournals.ge/index.php/GGS/article/view/7986
6. Amiranashvili A.G., Japaridze N.D., Khazaradze K.R., On the Connection of Monthly Mean of Some Simple Thermal Indices and Tourism Climate Index with the Mortality of the Population of Tbilisi City Apropos of Cardiovascular Diseases. Journal of the Georgian Geophysical Society, ISSN: 1512-1127, Physics of Solid Earth, Atmosphere, Ocean and Space Plasma, v. 21(1), Tbilisi, 2018, pp.48 -62. http://www.jl.tsu.ge/index.php/GGS/article/view/2489
7. Khazaradze K.R., Chkhitunidze M.S., Japaridze N.D., Effects of Variations of the Monthly Mean Max Air Temperature on the Population Health of Kakheti Region of Georgia. // Int. Sc. Conf. „Modern Problems of Ecology“ Proceedings, ISSN 1512-1976, v. 7, Tbilisi-Telavi, Georgia, 26-28 September, 2020, pp. 356-359. http://www.dspace.gela.org.ge/handle/123456789/8836
8. Aliyev V., Amiranashvili A., Kartvelishvili L., Matzarakis A, Tatishvili M., Comparative Analysis of the Variability of Daily Minimum, Maximum and Mean Air Temperature in Baku and Tbilisi in 2005-2024. // Int. Journal of Sustainability and Rick Control, e-ISSN: 3104-8358, p-ISSN: 3104-834X, Baku, Azerbaijan, Vol. 1, No. 2 (2), September 2025, pp. 63-70. DOI: https://doi.org/10.64599/GDOF7452
9. Aliyev V., Amiranashvili A., Kartvelishvili L., Matzarakis A., Tatishvili M., Variability of Monthly Average Values of Daily Minimum, Maximum and Mean Air Temperature in Baku and Tbilisi IN 2005-2024. // Int. Journal of Sustainability and Rick Control, e-ISSN: 3104-8358, p-ISSN: 3104-834X, Baku, Azerbaijan, Vol. 1, No. 3 (3), December 2025, (in Press).
10. Amiranashvili A.G., Revishvili A.A., Khazaradze K.R., Japaridze N.D., Connection of Holiday Climate Index with Public Health (on Example of Tbilisi and Kakheti Region, Georgia). Journal of the Georgian Geophysical Society, e-ISSN: 2667-9973, p-ISSN: 1512-1127, Physics of Solid Earth, Atmosphere, Ocean and Space Plasma, v. 24 (1), 2021, pp. 63-76. DOI: https://doi.org/10.48614/ggs2420212884

11. Amiranashvili A., Japaridze N., Kartvelishvili L., Khazaradze K., Revishvili A., Preliminary Results of a Study on the Impact of Some Simple Thermal Indices on the Spread of COVID-19 in Tbilisi. // Journal of the Georgian Geophysical Society, e-ISSN: 2667-9973, p-ISSN: 1512-1127, Physics of Solid Earth, Atmosphere, Ocean and Space Plasma, v. 25(2), 2022, pp. 59–68. DOI: https://doi.org/10.48614/ggs2520225961
12. Amiranashvili A., Bliadze T., Japaridze N., Khazaradze K., Revishvili A., Angstrom Fire Index as a Bioclimatic Indicator (Using the Example of the Impact on the Spread of Covid-19 in Tbilisi). // Int. Sc. Conf. "Geophysical Processes in the Earth and its Envelopes", Proceedings, Publish House of Iv. Javakhishvili Tbilisi State University, November 16-17, Tbilisi, 2023, pp. 328-331. http://openlibrary.ge/handle/123456789/10467
13. Amiranashvili A., Japaridze N., Kartvelishvili L., Megrelidze L., Khazaradze K., Statistical characteristics of the monthly mean values of air effective temperature on Missenard in the Autonomous Republic of Adjara and Kakheti (Georgia). // Trans. of Mikheil Nodia institute of Geophysics, ISSN 1512-1135, vol. 69, Tb., 2018, pp. 118 – 138, (in Russian). http://dspace.gela.org.ge/bitstream/123456789/7509/1/IG_T_69_2018_Red_13.pdf
14. Missenard F.A., Température effective d'une Atmosphere Généralisation Températurerés ultante d'un Milieu. // Encyclopédie in dustrielleet Commerciale, Etude physiologique et technique de la ventilation. Librerie de l'Enseignement Technique, Paris, 1933, 131-18.
15. Japaridze N., Kartvelishvili L., Khazaradze K., Chkhitunidze M., Nikolaishvili M., Revishvili A., Statistical Characteristics of the Daily Values of Air Effective Temperature According to Missenard in Batumi. // Int. Sc. Conf. "Complex Geophysical Monitoring in Georgia: History, Modern Problems, Promoting Sustainable Development of the Country", Proceedings, ISBN 978-9941-36-272-9, Publish House of Iv. Javakhishvili Tbilisi State University, Tbilisi, Georgia, October 17-19, 2024, pp. 133 – 136.
http://dspace.gela.org.ge/bitstream/123456789/10624/1/34_MM-180.pdf

1st International Scientific Conference "Modern problems in Geophysics", Proceedings,
ISBN 978-9941-36-434-1, ISSN 3088-4349, Tbilisi, Georgia, November 6-8, 2025

MODERN FEATURES OF THE SETTLEMENT OF THE TERRITORY OF THE CHECHEN REPUBLIC DEPENDING ON NATURAL CONDITIONS

Bekmurzaeva L.R., Bratkov V.V., Kerimov I.A.

Millionshchikov Grozny State Oil Technical University, Grozny, Chechen Republic
Eip-eco2017@yandex.ru

Abstract. *The analysis of residential development is a primary task in assessing the anthropogenic load on the territory. The Chechen Republic has been experiencing a construction boom in the last decade. The load on landscapes is increasing. In this regard, it is very important to assess the degree of modern residential development of landscapes. For comparison, data from remote sensing of the Earth were used, namely Landsat and Sentinel-2 images for 1985 and 2024. The material was processed using the ArcGIS and MapInfo programs. A quantitative assessment of the residential load showed that the increase in residential areas in 2024 compared to 1985 was 192%. The maximum increase in residential areas in 2024 is in steppe landscapes (by 233%). Large settlements such as Grozny and Gudermes are located in the steppe landscapes. Infrastructure development and recreational attractiveness have led to an increase in the share of residential areas in the lower montane forest (226%) and in the high-altitude subalpine forest-shrub-meadow landscapes (177%).*

Keywords: *Earth remote sensing data, landscapes, residential areas.*

Introduction

When assessing the anthropogenic load on a territory, first of all, its residential development is studied. Residential load (sometimes synonymous or similar terms are "demographic", "settlement", etc.) is defined as a type of impact on the ecological state of landscapes due to the location of settlements and the number of people living in them [5]. Natural conditions play a key role in the settlement of the territory. In this regard, the landscape approach is the most convenient way to assess the residential development of the territory [3]. There has been a construction boom in the republic in the last decade, and in this regard, the assessment of the modern residential development of the landscapes of the Chechen Republic is of great practical interest.

Materials and Methods

The landscape map of the Chechen Republic, published by a team of authors [1], was used as a landscape basis. For a comparative assessment of the residential development of the landscapes of the Chechen Republic, data from remote sensing of the Earth were used, namely Landsat and Sentinel-2 images for 1985 and 2024. Their processing was carried out by such software tools as ArcGIS and MapInfo. When calculating the territories occupied by settlements, we relied primarily on the concept of residential landscapes, i.e. landscapes of settlements (rural and urban) [4]. The calculations did not take into account the territories occupied by dacha-type settlements, since their area is insignificant.

Results

The results of satellite image processing are presented in Table 1.

Table 1. Changes in the area of settlements within the landscapes on the territory of the Chechen Republic

Landscapes	Landshafts Square, km²	Area of settlements, km²		Quantity of settlements, km²		Area gain, %
		1985г.	2024 г.	1985 г.	2024 г.	
Semi-desert and desert	4348	36,1	47,5	45	44	132
Steppe	3579	262,1	633,8	122	122	242
Delta and floodplain areas	1579	87,6	130,2	79	84	149
Low-mountain forest-shrub-meadow-steppe	863	8,1	9,5	12	16	117
Lower Mountain forests	607	9,8	14,2	32	31	145
Mid-mountain forests	2320	61,4	77,4	119	114	126
Mountain-hollow shrub-meadow-steppe	237	3,4	7,0	20	15	206
Mountain-shrub -steppe	162	4,7	3,9	17	17	83
Upper montane forest and post-forest	1051	1,9	2,0	10	9	105
High-altitude subalpine shrub-meadow	1021	2,2	2,4	9	7	109
High-altitude Alpine shrub-meadow	291	-	-	-	-	-
Highland subnival	71	-	-	-	-	-
Glacial-nival	32	-	-	-	-	-
Total	16160	477,2	927,9	465	459	450,7

As can be seen from the data presented, despite the reduction in the number of settlements in 2024, the area of residential territories has almost doubled. If in 1985 the area of residential territories was 477.2 km^2, then in 2024 it amounted to 927.9 km^2. The total increase in the area occupied by settlements amounted to 450.7 km^2. However, as noted by Bratkov and Taimaskhanov [2], "The growth of the land area of settlements is associated not so much with an increase in the area of the settlements themselves, as with a change in the status of lands within or adjacent to them." The increase in residential areas in different subtypes of landscapes occurred unevenly. Natural conditions have a significant impact on this process.

The steppe landscapes of the Chechen Republic are the most comfortable for living and conducting economic activities, primarily agricultural ones. These landscapes occupy the territory between the Tersk and Sunzha advanced ranges on the one hand and the Forested Ridge of the Greater Caucasus, occupying the territory of the Chechen inclined Plain. Here, the area of settlements has grown 2.4 times: from 262.1 to 633.8 km^2. A significant increase in the area of settlements is also associated with the addition of new territories to large cities. For example, in 2021, the villages of Gikalo and Prigorodnoye were annexed to Grozny.

Despite the small area occupied, residential territories in mountain-hollow shrub-meadow-steppe landscapes have more than doubled: from 3.4 to 7.0 km2. The increase in residential areas in mountainous landscapes is generally associated with recreational attractiveness, the desire to return to historical lands, and improved infrastructure. For example, the mountainous regions of the Chechen Republic have been gasified, roads have been laid, and resorts have been built.

Delta and floodplain and lower montane forest landscapes are being actively developed (an increase in the area of settlements occurred by 49 and 45%, respectively). If in the first case the flat terrain, convenient for development, plays a more significant role, then in the second it can be explained by the fact that they occupy adjacent territory with flat and hilly landscapes, in close proximity to the largest cities – Grozny and Gudermes.

For other landscapes, the increase in the area of settlements is not so significant, and in mountain-shrub-steppe landscapes, on the contrary, there is a decrease in residential areas, which is associated with the inaccessibility of these areas.

As for the population of the Chechen Republic, it has been steadily growing every year since 2001 (Fig. 2). The proportion of the urban population is also increasing. If in 2002 the share of the urban population was 33.8%, then in 2024 it was 401% [6].

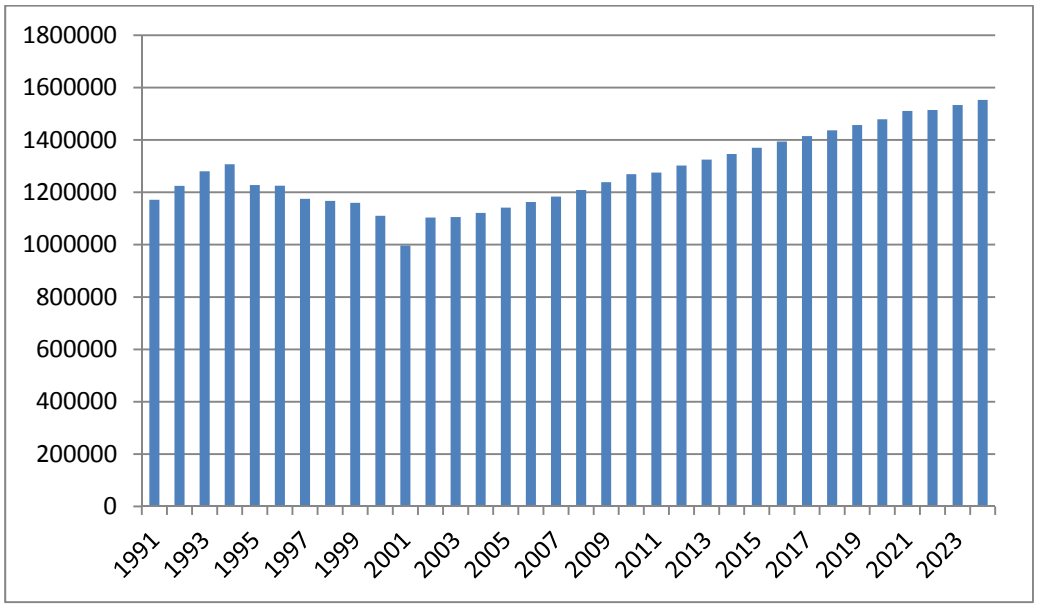

Fig. 2. Population of the Chechen Republic by year

Based on the data from Chechenstat, we calculated the population of the Chechen Republic within each subtype of the landscape (Table 2).

Table 2. The population of the Chechen Republic as of 01.01.2024 by landscape

Landscapes	**Landshafts Square, km²**	**Population**	**Quantity of settlements, km²**	**Population density, people per km²**
Semi-desert and desert	4348	69364	44	16,0
Steppe	3579	987989	122	276,1
Delta and floodplain areas	1579	218377	84	138,3
Low-mountain forest-shrub-meadow-steppe	863	10044	16	11,6
Lower Mountain forests	607	21175	31	34,9
Mid-mountain forests	2320	86125	114	37,1
Mountain-hollow shrub-meadow-steppe	237	4606	15	19,4
Mountain-shrub -steppe	162	4987	17	30,9
Upper montane forest and post-forest	1051	1373	9	1,3
High-altitude subalpine shrub-meadow	1021	2237	7	2,2
High-altitude Alpine shrub-meadow	291	-	-	-
Highland subnival	71	-	-	-
Glacial-nival	32	-	-	-
Total	16160	1406277	459	87,0

The main population of the Chechen Republic is concentrated in the steppe landscapes. The population density in steppe landscapes is 276.1 people per km^2. The delta and floodplain landscapes of the Chechen Republic are also quite densely populated, with a density of 138.3 people per km^2. In the mountainous landscapes of the Chechen Republic, population density decreases with increasing altitude. The density of semi-desert and desert landscapes is relatively low (16.0 people per km^2), which is due to the small population and large area of the landscape.

Conclusions

The natural conditions play a primary role in the settlement and development of the territory of the Chechen Republic. The steppe landscapes are the most populated, as they are the most comfortable for living and conducting economic activities. In 2024, there is a 2.4-fold increase in the area of residential territories in steppe landscapes compared to 1985, and the population density here is also the highest at 276.1 people per km^2. In the mountainous landscapes of the Chechen Republic, population density decreases with increasing altitude. However, a comparative analysis of residential areas has shown that in comparison with 1985, there is an increase in the area of settlements in the mountains. This is primarily due to the recreational appeal, the improvement of infrastructure and the desire to return to historical lands.

Acknowledgments. The work was carried out within the framework of the state assignment of Millionshchikov Grozny State Oil Technical University FZNU-2024-0001 «Assessment of the impact of modern climate change on natural and natural-anthropogenic complexes (using the example of the Chechen Republic).

References

1. Bratkov V.V., Idrisova R.A., Alsabekova A.A., Landscape diversity of the Chechen Republic. // Bulletin of the North Caucasus State Technical University. No. 1, 2009, pp. 34-39. (in Russian)
2. Bratkov V.V., Taimaskhanov Kh.E., Changing the areas of settlements in the Chechen Republic and the possible consequences of this process. Monitoring. // Science and technology. No. 1(55), 2023, pp.67-73. (in Russian)
3. Zaurbekov Sh.Sh., Bratkov V.V., Bekmurzayeva L.R., Geoecological assessment of anthropogenic modification of landscapes of the Chechen Republic // Izvestiya Dagestan State Pedagogical University. Natural and exact sciences. No. 1 (10), 2010, pp. 86-91. (in Russian)
4. Milkov F.N., Man and landscapes. – M.: Mysl, 1973. P. 224. (in Russian)
5. Sennaya E.I., Molodan Ya.E., Assessment of residential load on landscapes in the process of regional landscape and ecological research // Scientific notes of the Russian State State Medical University. Issue 28, 2013, pp. 88-92. (in Russian)
6. The Chechen Republic in numbers. 2024: A short statistical collection / Chechenstat – Grozny 2024. p. 148. (in Russian)

1st International Scientific Conference "Modern problems in Geophysics", Proceedings,
ISBN 978-9941-36-434-1, ISSN 3088-4349, Tbilisi, Georgia, November 6-8, 2025

UNCONVENTIONAL ENERGY SOURCES AS A WAY TO DECARBONIZE THE CONSTRUCTION INDUSTRY (USING THE EXAMPLE OF THE CHECHEN REPUBLIC)

Bekmurzaeva L.R., Saidumov M.S.

Millionshchikov Grozny State Oil Technical University, Grozny, Chechen Republic
Eip-eco2017@yandex.ru

Annotation. *The article considers the possibility of using unconventional energy sources in the construction industry of the Chechen Republic as a way to decarbonize the industry. The initial conditions of the Chechen Republic make it possible, without large monetary injections, to provide the districts of Grozny with heat due to geothermal deposits located in the city district. In addition, the republic has a great solar energy potential, which allows it to be used by solar installations of any type.*

Keywords: *non-traditional energy sources, geothermal energy, solar energy potential*

Introduction

The electric power industry is the largest source of greenhouse gas emissions, accounting for about 35% of global emissions. At the same time, the construction industry is one of the largest consumers of electricity (up to 38%) [4], therefore, decarbonization of the construction industry is a priority. Despite the fact that many environmental strategies encourage the introduction of energy-saving technologies in construction, the pace of their implementation is still low. This is due to the fact that the main benefit from the introduction of innovative technologies in construction falls to the end user of the building, while for the developer, the introduction of innovative technologies only increases the cost of the construction process. In this regard, the use of non-traditional energy sources, in our opinion, is promising.

Results

The Chechen Republic today is a dynamically developing region of the Russian Federation, which is experiencing a construction boom. Over the past decade, many new modern buildings and high-rise apartment buildings have been erected in the capital of the Republic of Grozny.

The most promising in the Chechen Republic is the use of solar and geothermal energy.

The Chechen Republic has a good solar energy potential. The values of solar energy resources in the Chechen Republic are approaching the maximum values in the Russian Federation. The annual amount of total (direct plus diffuse) radiation on a horizontal surface is 4,900 MJ/m^2, with a maximum in Russia of 5,019 MJ/m^2. The annual amount of direct radiation also has high values – 2,800 MJ/m^2, with a maximum in Russia of 2,859 MJ/m^2 [1].

Solar energy can be used by various types of solar installations (thermodynamic and photovoltaic). The use of solar power plants is advisable for such large facilities under construction as, for example, the Akhmat Tower, the international terminal of the Severny Airport, or facilities already in operation, for example, the Grozny Mall shopping center. The use of solar installations will significantly save energy resources during the operation of buildings, especially in the summer, when indoor air conditioning is required.

Providing heat to residents of Grozny through the use of geothermal resources is very promising and does not require huge costs. There are four thermal water deposits around the city of Grozny: Khankalskoye, Petropavlovsk (Grozny), Goytinskoye and Gunushki. The largest is the Khankalskoye field. The Khankalskoye thermal water deposit is the largest thermal energy water deposit in the Chechen Republic, located 10 km southeast of Grozny. It is multi-layered with a water-pressure regime, 22 aquifers are allocated. The

strata are composed mainly of quartz sandstone and contain poorly mineralized thermal waters with a total mineralization of 0.6 to 3.5 g/l and a temperature of 65 to 110 °C. The area of the deposit is estimated at about 15-20 km2.

From 1976 to 1994, the field was exploited, and then, like the entire industry of the republic, it fell into disrepair. In 2013-2015, a pilot geothermal plant was built on the basis of the Khankalskoye field based on the implementation of a circulation scheme for the use of deep Earth heat. The resulting thermal energy is used to heat nearby greenhouses (Fig. 1).

In addition to thermal energy, the waters of the Khankalskoye field, according to the conclusion of the Pyatigorsk Research Institute of Balneology and Physiotherapy, the waters of the XIII reservoir of well 4t belong to therapeutic mineral siliceous nitrogen therms. They can be used for balneological purposes for external and internal use [2].

Fig. 3. Pilot industrial geothermal plant based on the implementation of a circulation scheme for the use of deep Earth heat. Khankalskoye thermal water deposit.

According to estimates by Farkhutdinov A.M. et al. [3], with the sustainable use of the Khankalskoye field, a decrease in temperature in the well should not occur within 30 to 40 years.

Conclusions

The use of unconventional energy sources contributes to the decarbonization of the construction industry. Due to its geographical and geological features, the most promising in the Chechen Republic is the use of solar and geothermal energy, as their use is the most affordable and does not require large investments for their implementation.

Acknowledgments: The work was performed within the framework of the state assignment of the GGNTU named after Academician M.D. Millionshchikov FZNU-2024-0003 "Development of a complex of low-carbon technologies for increasing productivity and sequestration potential of ecosystems in urbanized territories with the production of secondary composite materials for multifunctional purposes."

References

1. Kobysheva N.V., Akentyeva E.M., Ilyina O.B., Karpenko V.N., Klyueva M.V., Lyulkovich I.N., Pigoltsina G.B., Razova E.N., Semenov Yu.A., Khairullin K.Sh., Encyclopedia of Climate Resources. St. Petersburg: Gidrometeoizdat. 2005, p. 319. EDN: QQXMOD. (in Russian)
2. Machigova F.I., Shaipov A.A., Bekmurzaeva L.R., Cherkasov S.V., Geochemical studies of thermal waters of the Khankala deposit in the Chechen Republic. // Sustainable development of mountain territories. No 2 (20), 2014, pp. 61-64. EDN: SILFIT. (in Russian)
3. Farkhutdinov A.M., Ismagilov R.A., Farkhutdinov I.M., Cherkasov S.V., Mintsaev M.Sh., Prospects for the use of thermal power waters of the Chechen Republic based on the experience of similar works in France (Paris basin). // Bulletin of Tomsk State University, No. 398, 2015, pp. 257–264. DOI: 10.17223/15617793/398/40. EDN: VHTIXB (in Russian)
4. Umberto Berardi Stakeholders' influence on the adoption of energy-saving technologies in Italian homes. // Energy Policy. Vol. 60, 2013, pp. 520-530. (in English)

1st International Scientific Conference "Modern problems in Geophysics", Proceedings,
ISBN 978-9941-36-434-1, ISSN 3088-4349, Tbilisi, Georgia, November 6-8, 2025

AGRICULTURAL BY-PRODUCTS: ECOLOGICAL, ECONOMIC, AND SOCIAL DIMENSIONS AND PATHWAYS TOWARD SUSTAINABLE TECHNOLOGIES

Papunidze G.R. , Chkhartishvili I.N. , S.G. Papunidze, N.R. Seidishvili, D.A. Abuladze

Shota Rustaveli State University, Institute of Agrarian and Membrane Technologies, 6000 Batumi, Georgia
guram.papunidze@bsu.edu.ge

Abstract. *By-products arising from the industrial processing of agricultural raw materials impose considerable ecological, economic, and social challenges. The uncontrolled disposal of organic matter in landfills leads to methane emissions, which account for nearly 20% of global greenhouse gas outputs and represent a major driver of climate change and global warming. Environmental pollution further threatens human health and biodiversity while exacerbating ecosystem and soil degradation. Economically, the underutilization of agricultural by-products results in estimated annual global losses ranging from USD 780 billion to 1 trillion. Socially, approximately 1.3 billion tons of food are lost worldwide each year, even as 690–829 million people experience chronic hunger, 3 billion lack access to nutritious diets, and thousands of children die annually due to food scarcity. Within the framework of the circular economy, the valorization of agricultural by-products offers a sustainable pathway for their safe conversion into value-added food products, thereby promoting integrated economic growth, social well-being, and environmental protection. In this study, we examine the recovery of dietary fiber from by-products derived from the industrial processing of mandarin (Citrus reticulata) flowers and assess the biosorption capacity of the extracted fiber.*

Keywords: *mandarin flower by-products; waste management; biosorption; dietary fiber; circular economy*

Introduction

Globally, more than 2.1 billion tons of waste are generated each year, a figure projected to increase by 70% by 2050, thereby intensifying social, economic, health, and environmental pressures. Considerable research has focused on the valorization of agro-industrial by-products, particularly those derived from fruits and vegetables, for the production of novel, value-added products that are already being successfully implemented across multiple sectors. In contrast, the valorization of floral by-products, originating from both ornamental and edible flowers, remains a critical global challenge.

Edible flowers are experiencing growing consumer interest due to their proven safety for human consumption, high nutritional value, and long-standing culinary use, which dates back to antiquity. They are further distinguished by their medicinal properties and richness in biologically active compounds, attributes that enhance their attractiveness within the food industry. Edible flowers can be incorporated into a wide range of products, including beverages, confectionery, and savory dishes, and are consumed in diverse forms. Market trends highlight the urgent need for a systematic and comprehensive analysis of edible flowers, encompassing their taxonomy, origin, bioactive constituents, nutritional characteristics, and potential applications in the food sector [1,2].

The Netherlands is responsible for approximately 52% of global flower production, whereas in India an estimated 700 million tons of floral waste are generated annually. Each year, more than 80 million tons of these wastes are discarded into rivers and landfills, negatively impacting soil quality, water resources, and aquatic ecosystems. Comparable conditions are observed in other countries, where the degradation of floral waste occurs at a considerably slower rate than that of other organic residues

Studies on temple-derived floral waste have shown that the application of tailored microbial consortia can accelerate decomposition processes and produce high-quality biofertilizers without inflicting environmental harm. In parallel, contemporary research has increasingly emphasized the valorization of floral waste into value-added products, including compost, bioethanol, natural dyes, food ingredients, incense sticks, biofuels, organic acids, surface-active biomolecules, and handmade paper [3].

Concurrently, the problem of environmental contamination by heavy metals is becoming more acute. To mitigate these impacts, a variety of biosorption-based strategies have been developed, for instance, biomass derived from discarded flowers of *Rosa gruss* and *Canna indica* has been successfully employed for the biosorption of Pb(II) and Co(II) ions from aqueous solutions [4].

[5] reported that floral waste from *Hibiscus rosa-sinensis* (Chinese hibiscus), an environmentally friendly and low-cost raw material, can be effectively employed for the biosorption of heavy metals from water and soil. Similarly, [6] investigated the biosorption capacity of biomass derived from red rose petals for the removal of Pb(II) and Co(II) ions from aqueous solutions. Their study evaluated the impact of multiple process parameters, including pH, biosorbent dosage, particle size, temperature, contact time, initial metal concentration, and biomass pretreatment, on biosorption efficiency.

Edible flowers are increasingly recognized for their functional and nutritional properties and are widely incorporated into beverages, confectionery, and culinary preparations. Recent studies have examined the chemical composition of mandarin flowers and highlighted their potential applications in the food industry as a non-traditional raw material. Industrial processing of mandarin (*Citrus reticulata*) flowers produces extracts that serve as precursors for a wide range of products, including non-alcoholic and alcoholic beverages (e.g., liqueurs, vodka), low-alcohol drinks, tinctures, syrups, and artificial honey. The residual floral by-products generated after extract production, traditionally discarded through linear processing systems, represent an underutilized but valuable raw material for the recovery of high-quality dietary fiber.

Objective of the Study

This study aimed to evaluate the physicochemical characteristics and sorption capacity of dietary fiber obtained from industrial by-products of mandarin (*Citrus unshiu*) flowers.

Materials

The experimental material consisted of dietary fiber isolated from the by-products generated during the industrial processing of mandarin (*Citrus unshiu*) flowers.

Reagents and Methods

All reagents used were of analytical grade. Activated carbon and $Pb(NO_3)_2$ were procured from Sigma-Aldrich (Taufkirchen, Germany). Physicochemical properties were assessed using the following standard procedures: determination of dry matter (AOAC Official Method); measurement of active acidity (pH) (AOAC Official Method); and phytochemical analysis by spectrophotometry (Shimadzu, Japan). Sorption parameters were evaluated using titrimetric methods [8],

Technological Scheme for By-product Processing

Dietary fiber was extracted from floral by-products following a standardized technological process. The floral waste was dried at 40–45 °C for 40–60 minutes, milled to a uniform particle size, and packaged under oxygen-free conditions. The packaged material was then stored at +4 °C until subsequent analyses.

Sorption properties of dietary fiber

Water Retention Capacity (WRC) and Fat Absorption Capacity (FAC) were determined using the gravity method described by Núñez-Gómez et al. [7]. WRC – 1 g of sample was mixed with 20 mL of distilled water and maintained at 25°C for 24 hours, then centrifuged at 3000×g for 15 minutes. The supernatants were removed, the mass of the residue after hydration was measured and WRC was determined.

$$WRC\ (g/g) = m_2 - m_1 / m_1$$

where m_1 – the mass of the dry sample (g) before hydration, m_2 – the mass of the sample (g) after hydration.
FAC – 0.5 g of sample was mixed with 20 mL of sunflower oil in the centrifuge tube and incubated at 37 °C for 1 hour. After incubation, the sample was centrifuged at 3000 rpm for 15 minutes. The supernatant was removed, and the residue was weighed.

Fat Absorption Capacity (FAC) is measured by the amount of absorbed oil (in grams) using the following formula:

$$FAC\ (g/g) = m_2 - m_1 / m_1$$

where m_1 – weight of the sample (g) before incubation with oil, m_2 – weight of the sample (g) after incubation with oil. [7].

Sorption capacity of dietary fibers toward lead ions – Lead ions were used in the form of analytical grade Pb $(NO_3)_2$ solution (0.025 mol/L). One gram of dietary fiber was mixed with 50 mL of the metal salt solution. Six flasks were incubated for 5, 10, 15, 20, 25, and 30 minutes, respectively, to obtain the sorption kinetics. The quantitative analysis of lead cations in the solution was carried out by titrimetric method [8]. From each flask, 2 mL of the test solution was transferred into a titration vessel using a volumetric pipette. Then, 0.1–0.2 g of dry hexamethylenetetramine (urotropine) was added to adjust the pH to 5.0, followed by three drops of Xylenol Orange indicator. The solution was then titrated with a standard EDTA solution (0.025 M) until the color changed from violet to lemon yellow.

To obtain sorption kinetic curves, 1 g of sorbent (m) was placed in a series of test tubes and treated with 50 mL (V) of aqueous metal salt solution. Contact time varies from 5 minutes to 1 hour. At specified time intervals, the solution was separated from the sorbent, and the concentration of metal ions (C□) in the filtrate was determined using titration. The sorption capacity (At) of the sorbents at each time point was calculated using the following formula:

$$At = (C_0 - C_t) \times V / m$$

The removal efficiency (α) of lead ions was calculated using the equation:

$$\alpha = (C_0 - C_\tau) / C_0 \times 100\%$$

Statistical Analysis. All measurements were performed in triplicate. Data was processed using R Studio (version 4.0.5) supported by the R Foundation for Statistical Computing. Mean values and standard deviations were calculated. Differences among means were evaluated using Stewart's t-test at a significance level of $p < 0.05$. Pearson correlation coefficients were used to assess relationships between functional and phytochemical properties.

Results and Discussion

The chemical composition of mandarin flowers and their corresponding by-products (dietary fiber) is summarized in **Table 1**.

Table 1. Chemical composition of mandarin flowers (fresh weight basis) and floral by-products/dietary fiber (dry weight basis) (%).

№	Parameter	Mandarin flower (fresh weight)	Floral by-product / dietary fiber (dry weight)
1	Dry matter (%)	18.3 ± 0.21	6.8 ± 0.23
2	Acidity (%)	0.45 ± 0.08	0.08 ± 0.06
3	Total sugars (%)	14.7 ± 0.12	1.5 ± 0.10
4	Total pectin (%)	2.2 ± 0.21	11.5 ± 0.18
5	Hemicellulose (%)	0.9 ± 0.15	4.6 ± 0.16
6	Cellulose (%)	1.7 ± 0.08	8.5 ± 0.08
7	Lignin (%)	3.2 ± 0.20	17.4 ± 0.20
8	Total nitrogen (%)	0.3 ± 0.01	1.1 ± 0.01
9	Essential oil (%)	0.05 ± 0.03	0.008 ± 0.03
10	Vitamin C (mg/%)	366.7 ± 4.0	8.1 ± 3.0
11	Vitamin P (mg/%)	3.5 ± 0.14	18.0 ± 0.14
12	Vitamin B1 (thiamine, mg/kg)	2.3 ± 3.8	13.8 ± 4.1
13	Vitamin B2 (riboflavin, mg/kg)	2.8 ± 3.2	14.1 ± 3.2
14	Vitamin B6 (pyridoxine, mg/kg)	18.5 ± 3.3	88.6 ± 3.2

Different letters within rows indicate statistically significant differences between groups ($p < 0.05$).

The results demonstrate that, in comparison with mandarin flowers, mandarin floral by-products contain significantly higher levels of key constituents, including pectin, hemicellulose, cellulose, dietary fiber, vitamin P, and B-complex vitamins. The dietary fiber extracted from these by-products exhibited a low content of simple sugars (1.5±0.02%) and a correspondingly high proportion of structural polysaccharides (89.3±0.1%). A lower proportion of low-molecular-weight compounds (simple sugars) is generally associated with improved dietary fiber quality, enhanced sorption capacity, and greater physiological functionality [9].

Table 2. The content of fibrous polysaccharides (raw mass)

A way to get dietary fiber	Dry matter%	Simple sugars %	Fibrous Polysaccharide %
Mandarin flower	90.4±0.1	1.2±0.02	89.3±0.1

The sorption characteristics of the dietary fiber, namely water retention capacity (WRC), fat absorption capacity (FAC), and Pb(II) adsorption capacity are presented in Table 3.

The assessment of sorption properties demonstrated that dietary fiber derived from mandarin flowers exhibits a high capacity for binding water, fat, bile acids, and lead. Comparative data reported by [9] indicated that the functional parameters of dietary fiber obtained from black currant, cranberry, and sea buckthorn press residues (powders) were as follows: WRC (g/g) – 2.78 ± 0.02, 3.87 ± 0.18, and 4.24 ± 0.02, respectively; and FAC (g/g) – 1.14 ± 0.01, 1.57 ± 0.05, and 1.09 ± 0.02, respectively.

Table 3. Sorption properties of floral dietary fiber

Sorption properties	WRC (g/g)	FAC (g)	Lead Sorption Capacity (mg/g)
Mandarin flower by-product fiber	13.3±0.02	2.1±0.05	20.1±0.4

(Different letters among columns indicate significant differences ($p < 0.05$).

For dietary fiber obtained from mandarin flowers, the measured values were WRC – 13.3 ± 0.42 g/g, FAC – 2.1 ± 0.05 g/g, and Pb(II) adsorption capacity – 9.2 ± 0.02 mg/g. These results indicate that mandarin flower dietary fiber possesses substantially higher water- and fat-binding capacities compared with berry-derived fibers [9].

The functional properties of dietary fiber are strongly influenced by its hydration and lipid-binding capacities. Consequently, its incorporation into food formulations as a bioactive additive is of considerable importance, as it can confer beneficial physiological effects, including hypoglycemic and hypolipidemic activities.

Contamination by toxic heavy metals represents a critical global environmental challenge. Lead [Pb(II)] is among the most hazardous metals, with major anthropogenic sources including automobile exhaust and lead-based paints. Elevated Pb(II) concentrations in the human body can cause anemia, hypertension, and neurological damage, Furthermore, Pb(II) exposure has been linked to neurotoxicity and genotoxicity, while chronic accumulation may contribute to carcinogenesis [6].

Adsorption is one of the most widely adopted techniques for heavy metal remediation, owing to its operational simplicity, cost-effectiveness, and high efficiency in removing toxic compounds. It has been extensively applied in wastewater treatment through biosorption. The adsorption performance of sorbents is influenced by multiple parameters, including adsorbent dosage, contact time, solution pH, initial adsorbate concentration, particle size, and temperature, with pH generally considered the most critical factor [10].

The experiment was carried out following the methodology described in [8] under conditions of pH = 5, employing floral by-product fiber and activated carbon as sorbents. The adsorption capacity (AT) of the sorbents at each time interval is presented in **Fig. 1**, which depicts the relationship between adsorption efficiency and contact time with Pb(II) ions. From these data, the adsorption activity-defined as the degree of Pb(II) ion removal-was calculated (**Fig. 2**).

The kinetic analysis demonstrated that Pb(II) ion binding occurred considerably faster with floral by-product fiber than with activated carbon. After 5 minutes, floral fiber adsorbed 20% of Pb(II) ions, whereas activated carbon adsorbed only 4.54%. Thus, within the first 5 minutes, the binding efficiency of floral fiber was approximately four times greater.

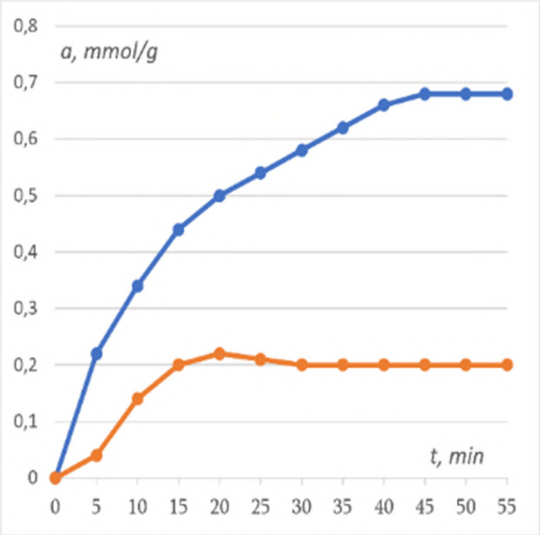

Fig. 1. Kinetics of Pb(II) ion adsorption by enterosorbents: ● – floral by-product fiber; ● – activated carbon.

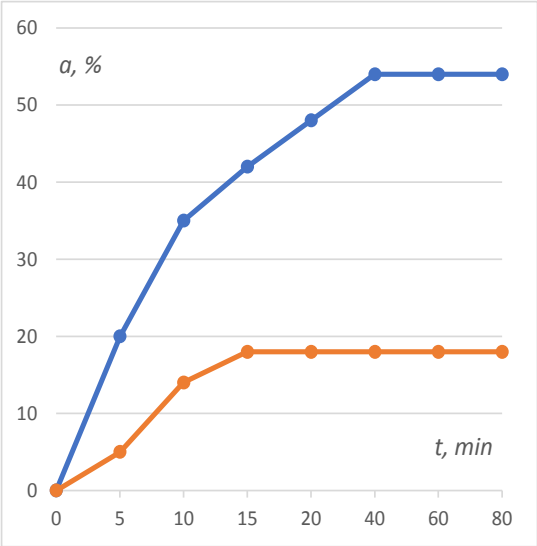

Fig. 2. Adsorption efficiency of Pb(II) ions by enterosorbents: ● – floral by-product fiber; ● – activated carbon.

The maximum adsorption capacity of Pb(II) ions was determined to be 51.8 mg/g for activated carbon and 140 mg/g for floral by-product fiber. These results indicate that floral by-product fiber exhibits superior sorption performance and may be considered a promising candidate for application as a natural detoxifying agent for Pb(II) ions.

Conclusion

The article considers a global problem in the world, which is created using the linear economy model. Processing of agricultural raw materials in a circular economy contributes to the transformation of waste into safe and attractive food products and sustainable development. According to the studies, highly purified dietary fibers with a high content of fibrous polysaccharides (89.3 ± 0.1) and a low content of low-molecular compounds (1.2 ± 0.2), with a high water-binding capacity (WRC) and fat (FAC) were obtained from the waste of industrial processing of mandarin flowers (Citrus Unshiu), which can be used as a prebiotic additive in bread, cookies, confectionery, dairy and meat products, improving the rheological, organoleptic and functional properties of products, promoting health and disease prevention. Cheap and high-value biomass of flower waste as a biosorbent of lead ions can be recommended for the development of a dosage form, as a detoxifier, as well as for wastewater purification from Pb (II) ions. The amount of waste discharged into the environment will be reduced and the negative environmental impact on it will be reduced.

Acknowledgments. This research was financed by Shota Rustaveli National Science Foundation of Georgia, Project FR-23-1945 „Multifunctional bio supplements for functional products from waste remaining after processing subtropical raw material following the model of circular economy“.

References

1. Kaza S., Yao L.C., Bhada-Tata P., Van Woerden F., What a Waste //2.0: A Global Snapshot of Solid Waste Management to 2050;World Bank Publications:Washington, DC,USA,2018. https://doi.org/10.1596/978-1-4648-1329-0
2. Duggirala K., Mummaleti G., Kong F., Roy A. and Mohan A. Edible flowers: a sustainable source of natural food ingredient. // J. Food Bioact. 2024;000:000–000 **DOI:** https://doi.org/10.26599/JFB.2024.95027383
3. Jadhav A.R., Flower Waste Degradation Using Microbial Consortium. J. Agric. Vet. Sci. 2013, 3, 1–4 www.iosrjournals.org
4. Bhatti H., Khadim R., Hanif M., Biosorption of Pb (II) and Co (II) on red rose waste biomass. // Iranian J. Chem. Chem Eng. 30, 2011, pp. 81–88 . www.iosrjournals.org
5. Venkata K., Srivani M., Health benefits of Hibiscus rosa sinensis and its role in removing heavy metals- Review. //International Journal of Botany. India. 2021. Volume 6, Issue 3, 2021, pp. .592-595 www.botanyjournals.com
6. Haq Nawaz B., Khadim R., Hanif M., Biosorption of Pb (II) and Co(II) on Red Rose Waste Biomass. // Iran. J. Chem. Chem. Eng. Vol. 30, No. 4, 2011. 10.30492/ijcce.2011.6093
7. Núñez-Gómez V., San Mateo M, González-Barrio R and Periago M.J., Chemical Composition, Functional and Antioxidant Properties of Dietary Fiber Extracted from Lemon Peel after Enzymatic Treatment// Molecules, 29, 2024, p. 269. https://doi.org/10.3390/
8. Ryabinina E.I., Zotova E.E., Ponomareva N.I., Timashova A.A., Andreeva N.A., Sorption activity of sugar beet pulp towards lead ions. // Young scientist. 19(99), 2015, pp. 71-74. https://moluch.ru/archive/99/22218/
9. Jureviciute I., Keršiene M., Bašinskiene L., Leskauskaite D. An Jasutiene d. Characterization of Berry Pomace Powders as Dietary Fiber-Rich Food Ingredients with Functional Properties. // Foods 11, 2022, p. 716. https://doi.org/10.3390/foods11050716
10. Pathak P.D., Mandavgane S.A., Kulkarni B.D., Fruit peel waste as a novel low-cost bio adsorbent. // Rev. Chem. Eng. 31(4), 2015, pp. 361–381. https://doi.org/10.1515/revce-2014-0041

1st International Scientific Conference "Modern problems in Geophysics", Proceedings,
ISBN 978-9941-36-434-1, ISSN 3088-4349, Tbilisi, Georgia, November 6-8, 2025

STUDYING SOME FOREST CHARACTERISTICS USING A DRONE

Kerimov I.A., Elzhaev A.S.

Grozny State Oil Technological University named after Academician M.D. Millionshchikov, Grozny, Chechen Republic
ibragim_kerimov@mail.ru

Abstract. *The article presents some results of the study of the Roshni-Chu forest area using the Geoscan 401 unmanned aerial vehicle. The research methods include multispectral and lidar imaging. The equipment used includes a digital camera, a multispectral camera, and a laser scanner.*

Key words: *research area, multispectral survey, lidar survey, NDVI, height of trees, crown volume.*

Introduction

There is a steady trend towards the development of the unmanned aerial systems market and the active use of unmanned technologies in the economy for solving various tasks (geological exploration and mining, construction, agriculture, forestry, etc.). As part of this area, we are conducting work using aerial photogrammetry, multispectral, and laser data collection tools to further process the obtained data, create thematic maps, and conduct analysis.

In the current year, in order to obtain information about the heights of trees and the volumes of their crowns, we conducted multispectral and lidar surveys using the *Geoscan 401* unmanned aerial vehicle.

The surveys were conducted in the forest area in the village of Roshni-Chu in the Chechen Republic [2, 6].

Methods and techniques

We conducted remote measurements (multispectral and lidar surveys) on the study site using the Geoscan 401 drone, which was equipped with a high-performance *Geoscan Pollux* multispectral camera, an *AGM MS 1.2* laser scanner, and a *Sony ZV-e10* digital camera [5].

The Geoscan Pollux multispectral camera allows you to capture images simultaneously in five narrow (12-40 nm) bands. In addition to the main visible spectrum channels (blue, red, and green), the camera captures far-red and infrared wavelengths, enabling the calculation of various vegetation indices.

A laser scanner (lidar) provides rapid acquisition of accurate and detailed digital terrain models for subsequent mapping of vegetation cover and measurement of tree height, biomass volume, and other measurements.

Using an aerial camera simultaneously with a laser scanner allows you to create the most accurate orthophotos. Thanks to the camera's swivel mechanism, all details of objects are recorded, and a detailed three-dimensional model can be created based on the obtained materials.

Aerial, multispectral and lidar data were processed using *Agisoft Metashape* and *LiDAR 360* software.

Multispectral survey. The survey was conducted at an altitude of 250 m. at a speed of 10 m/s. The coverage area was 3.43 km^2. To avoid gaps in the terrain, the survey was conducted with a 60% overlap. A total of 12210 images were captured. After uploading the images to the Agisoft Metashape software and aligning them, a dense point cloud was created for better terrain detail and model construction.

Different indices are used for visualization and practical application of multispectral imaging materials. The vegetation condition is determined using vegetation indices, the most common of which is the Normalized Difference Vegetation Index (NDVI) [1, 3, 4].

Lidar survey. The survey was conducted in order to obtain accurate and detailed digital models of the studied area and to construct cartograms of tree heights and crown volumes for the subsequent determination of quantitative values of these parameters. The survey was performed at a height of 110 m with the relief

skirting. The density of points on the studied surface at the specified height was about 300 points/m^2. The total area of the scanned forest area is 240 ha. The data obtained allowed us to obtain the desired taxation indicators (tree height and crown volume) and construct the corresponding cartograms.

Results and conclusions

Based on the multispectral data we calculated the NDVI index and created maps to assess the vegetation activity of the plants (Fig. 1). Figure 1 (a) shows the NDVI map based on the multispectral data collected in May 2023. Fig. 1 (b) shows the NDVI map based on the multispectral data collected in October 2023 on the same site.

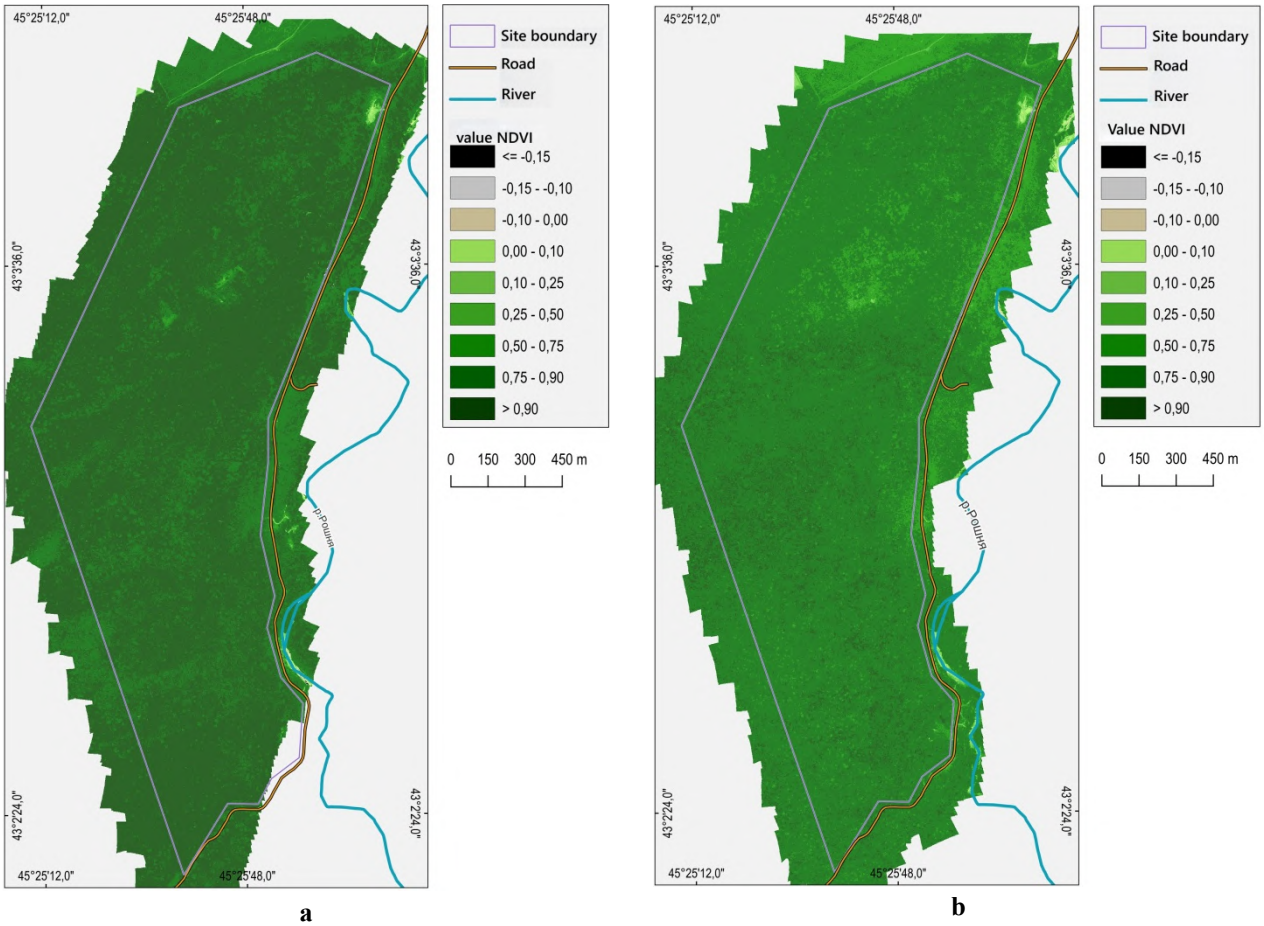

Fig. 1. NDVI maps constructed during the period of maximum vegetation (a) and during the period of reduced vegetation activity (b)

From fig. 1 (a) it can be seen that the "Roshni-chu" site is dominated by high values of the NDVI index, which are characteristic of physiologically healthy green foliage and fall within the range of 0.75-0.90. These values were obtained at the beginning of the maximum vegetation period.

Fig. 1 (b) shows a decrease in the NDVI index values, which is consistent with the autumn decline in plant vegetation activity. The values are predominantly within the range of 0.25-0.50.

Processing of lidar survey data allowed to obtain a three-dimensional point model (point cloud), consisting of an array of laser reflection points (LRPs) with a density of up to several hundred points per 1 m^2 and an accuracy of determining their coordinates of up to 5 cm. in plan and in height. Further processing included automatic classification of LRPs using such modules of the LiDAR360 program as *Forestry* and *Terrain*. Three-dimensional digital elevation models were obtained. Fig. 2 (a) shows a 3D terrain model processed in the Forestry module, and figure 2 (b) shows a 3D terrain model processed in the Terrain module.

The heights of the trees and the volume of their crowns were calculated. The maps of the heights of the trees and the volumes of their crowns were created using the *QGIS* GIS system. To create these maps, the original data was converted to the GPKG format and represented as a vector point layer, where each point

was interpreted as a single tree. The file containing the data on the trees contained 119,000 objects. The study area was divided into 50x50 m cells, and the maximum and average values for «tree height» and «crown volume» were recorded for each cell. As an example, the average values of crown height and volume are shown in Fig. 3.

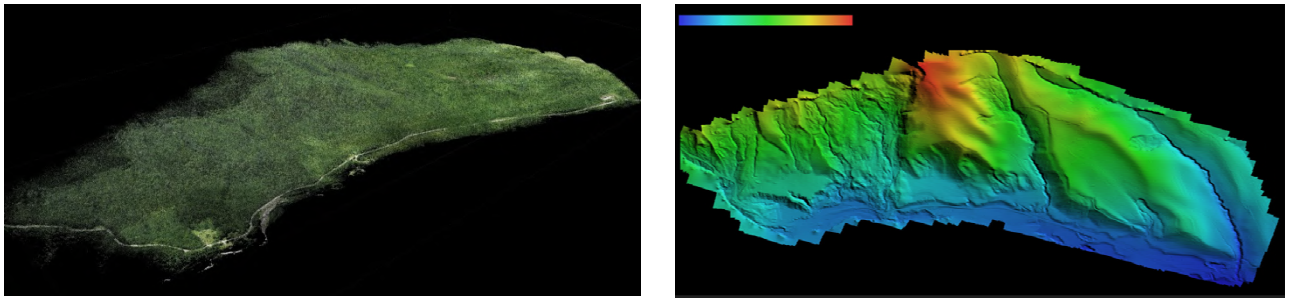

a **b**

Fig. 2. Digital elevation model built in modules Forestry (a) и Terrain (b)

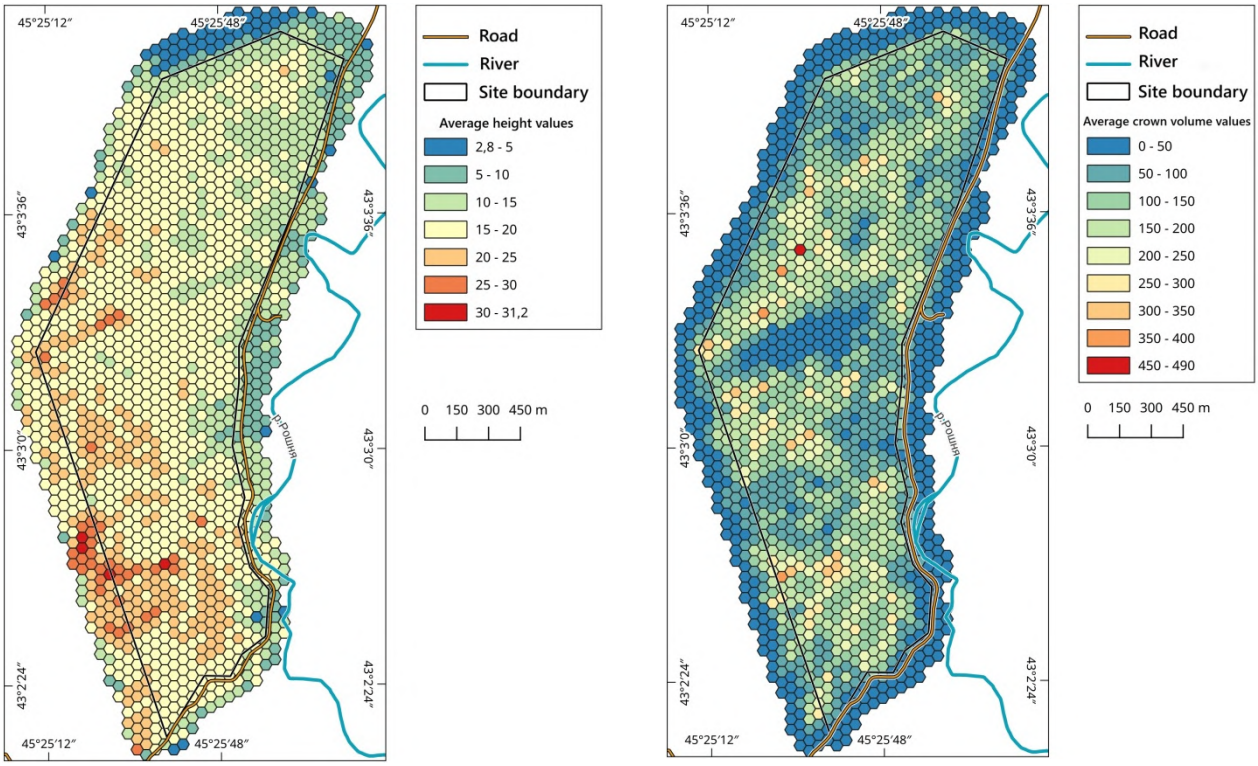

a **b**

Fig. 3. Maps of average tree height (a) and crown volume (b)

The analysis of the results obtained allowed us to draw the following conclusions:

1. The materials obtained from multispectral and lidar surveys are of high quality and can be used to solve a wide range of problems in various fields of human activity.
2. The NDVI map constructed from the multispectral survey data confirms the conclusion that the forest area under study consists of healthy trees.
3. Detailed topographic models were constructed based on the results of the lidar survey, and quantitative indicators of tree heights and crown volumes were calculated. The data on tree heights and crown volumes are representative. The area is dominated by trees with heights of 20-30 m.

Acknowledgment. The article was prepared within the framework of the state assignment for scientific research work No. FZNU-2024-0002

References

1. Druz' R.A., Protasova A.V., Okhunov Sh.R., Kshanovskaya A.V., Comparative assessment of airborne laser scanning and aerial photography from unmanned aerial vehicles. // Mining information and analytical bulletin, No. 5, 2023, pp. 130-141. (in Russian)
2. Kerimov I.A., Gayrabekov U.T., Makhmudova L.Sh., Carbon polygon of the Chechen Republic: I. Landscape features and structure. // Grozny natural science bulletin, Vol. 6. No. 3(25), 2021, pp. 35-47. (in Russian)
3. Kerimov I.A., Batukaev A.A., Vegetation indices of vegetation: a literature review. // Current trends in low-carbon development: global and regional aspects. // Proceedings of the international scientific conference. Grozny, 2023, pp. 36-49. (in Russian)
4. Kerimov I.A., Ezirbaev T.B., Using multispectral imaging in monitoring the state of forest cover. // Geology and Geophysics of Southern Russia. Vol. 12. No. 3, 2022, pp. 182-194. (in Russian)
5. Kurkov M.V., Klestov D.A., Brusilo V.A., Kurkov V.M., Kiseleva A.S., Experience of using the Geoscan 401 lidar complex as an unmanned topographic system for airborne laser scanning and aerial photography. Geoprofi. No. 4., 2021, pp. 17-23. (in Russian)
6. Olchev A.V., Mukhartova Yu.V., Kerimov I.A., Gibadullin R.R., 3D hydrodynamic modeling of CO2 and CH4 fluxes in the atmospheric surface layer (Based on the example of the Roshni-Chu forest area). // Sustainable development of mountain territories, Vol. 15, No. 2, 2023, pp. 408-418. (in Russian)

1st International Scientific Conference "Modern problems in Geophysics", Proceedings,
ISBN 978-9941-36-434-1, ISSN 3088-4349, Tbilisi, Georgia, November 6-8, 2025

SEASONAL VARIABILITY OF AIR INFILTRATION RATES IN BUILDINGS WITH DIFFERING AIRTIGHTNESS

***Kovač B., **Vaupotič J., *Dovjak M.**

**Faculty of Civil and Geodetic Engineering, University of Ljubljana, Ljubljana, Slovenia*
***Jožef Stefan Institute, Ljubljana, Slovenia*
bruno.kovac@fgg.uni-lj.si

Abstract. *This study investigates the seasonal variability of air infiltration rates (N_{inf}) in two residential buildings with differing envelope airtightness (B1: older, lower; B2: newer, higher). N_{inf} were quantified using the CO_2 decay method in February and June 2025. N_{inf} were higher and more variable (B1: 0.14–0.27 h^{-1}, avg 0.19 h^{-1}; B2: 0.04–0.21 h^{-1}, avg 0.10 h^{-1}) in winter and lower (B1: 0.06–0.25 h^{-1}, avg 0.13 h^{-1}; B2: 0.00–0.22 h^{-1}, avg 0.06 h^{-1}) in summer. N_{inf} decreased with increasing outdoor temperature, with meteorological influences more evident in the less airtight building.*

Key Words: *Air infiltration rate, CO_2 decay method, seasonal variability.*

Introduction

The construction of energy-efficient buildings relies on achieving enhanced airtightness of the building envelope, which reduces uncontrolled heat losses and supports the optimal indoor air quality (IAQ) through the integration of an efficient ventilation system. However, approximately 75% of the existing building stock comprises older buildings with lower envelope airtightness, creating ongoing challenges for improving energy performance and maintaining adequate IAQ [1].

A key indicator of building envelope airtightness is the air infiltration rate (N_{inf}), which quantifies the uncontrolled inward leakage of air into spaces through unintended openings in ceilings, floors, and walls. Driven by pressure, resulting from wind, temperature gradients (stack effect), and mechanical imbalances, air infiltration increases heating and cooling demand, leading to higher energy use, introduces outdoor pollutants, and causes drafts that reduce thermal comfort [2,3]. Its magnitude depends on the building age, materials and construction quality, with older buildings typically exhibiting 0.25–0.60 air changes per hour (ACH) under normal conditions, compared to 0.10–0.23 ACH in newly constructed buildings [4,5].

In newly constructed buildings, airtightness is typically assessed using the standardised blower door test, a static method defined by EN ISO 9972:2015 [6], which measures leakage under a pressure differential of 50 pascals between the interior and exterior of the building envelope. While helpful in benchmarking, this static test does not reflect the dynamic effects of wind, temperature fluctuations, or material ageing, all of which alter leakage pathways over time [7,8]. In contrast, the tracer gas method (i.e., CO_2, SF_6) enables long-term, non-intrusive monitoring under natural conditions, capturing seasonal variability. Comparative studies have shown that tracer gas approaches yield up to 38% greater accuracy and lower uncertainty than blower door measurements [7,8].

Given these considerations, the present study investigates seasonal variations in air infiltration rates in two residential buildings with differing levels of airtightness. The objectives are: (1) to quantify air infiltration rates in winter and summer; (2) to monitor meteorological parameters simultaneously; (3) to evaluate the influence of weather conditions on infiltration dynamics; and (4) to compare seasonal differences between buildings.

Study area, material and methods

The study was conducted in two residential buildings with differing airtightness: B1, a multi-apartment building constructed in 2000 with lower airtightness, and B2, a single-family house built in 2014 with higher airtightness. Measurements were performed in one room per building, with net volumes 64 m^3 (B1) and 33 m^3 (B2).

Air infiltration rates (N_{inf}, expressed as air changes per hour, h^{-1}) were determined using the tracer gas method, specifically the CO_2 decay technique [9]. Measurements were conducted in closed and unoccupied spaces on working days between 8:00 and 16:00 in February (winter) and June 2025 (summer), producing four datasets (B1 and B2 in winter and summer). Indoor CO_2 concentrations were monitored using a HOBO® MX Logger, while indoor air temperature and relative air humidity were recorded with an AirLink 7212 sensor. Outdoor meteorological data (air temperature, wind speed, relative air humidity, and precipitation) were obtained from the Slovenian Environment Agency (ARSO).

Data processing and statistical analysis were performed using RStudio. For each dataset, avg N_{inf} values were calculated within the measurement window. Ventilation heat losses for heating and non-heating seasons were calculated using KI Energija software. Descriptive statistics, Pearson correlation coefficients with significance levels (p-values) for N_{inf} versus monitored parameters, and ratios of seasonal and inter-buildings differences were computed. Results were visualized as (1) seasonal average hourly values to compare daily patterns across buildings and seasons, and (2) diurnal variations on selected days to illustrate short-term fluctuations.

Results

Fig. 1a shows the winter and summer variability of average hourly air infiltration rates (N_{inf}), while Fig. 1b presents outdoor air temperature ($T_{outdoor}$) for B1 (low-airtight envelope) and B2 (high-airtight envelope) during February and June 2025 (B1_Feb, B1_Jun, B2_Feb, B2_Jun). N_{inf} were consistently higher in February than in June across B1 and B2, confirming the seasonal effect. A decreasing diurnal trend was observed across all datasets, indicating reduced air infiltration during warmer afternoon hours. The distribution of N_{inf} values also varied by building and season. In B1, the range was wider in June (0.10–0.19 h^{-1}) than in February (0.16–0.22 h^{-1}), reflecting greater within-day variability during summer. This pattern aligned with the broader temperature span in June compared with February. In B2, the N_{inf} values showed a narrower distribution and weaker seasonally contrasts, with ranges of 0.09–0.11 h^{-1} in February and 0.05–0.08 h^{-1} in June. $T_{outdoor}$ showed a steady daytime increase, with June averages (24.0 °C in B1, 23.0 °C in B2) approximately 15–20 °C higher than those in February (4.0 °C in B1, 5.7 °C in B2).

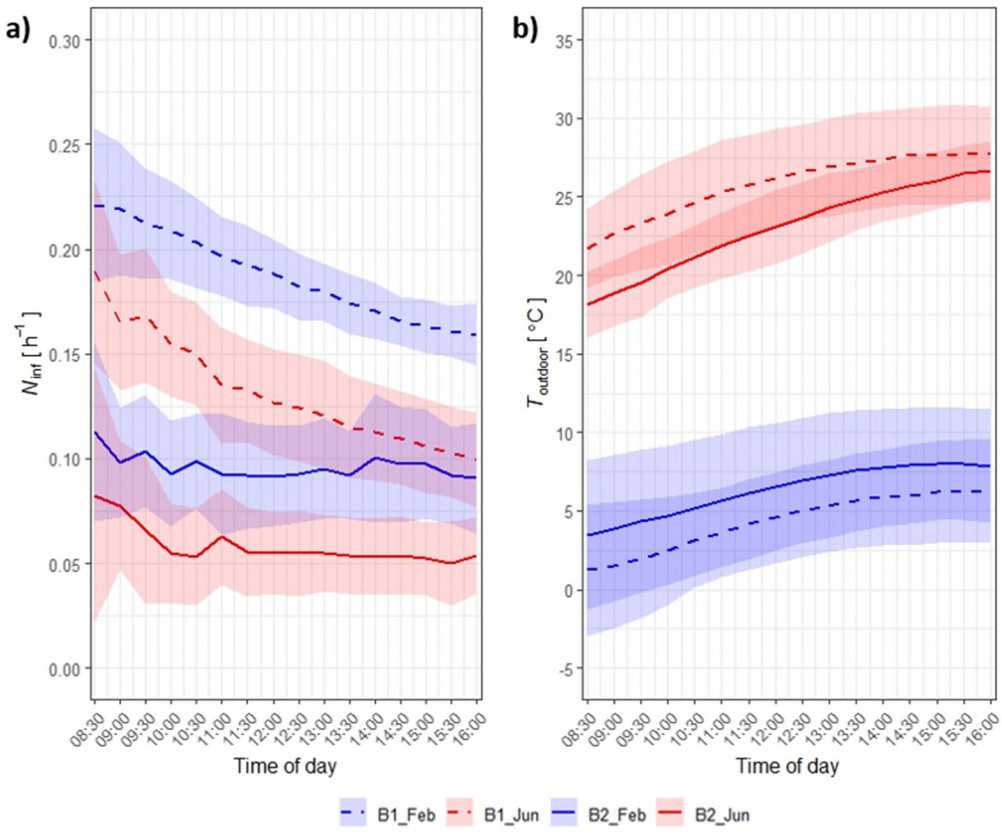

Fig. 1. Winter and summer variability of average hourly a) air infiltration rates (N_{inf}, h^{-1}) and b) outdor air temperature ($T_{outdoor}$, °C) for two buildings with differing airtightness (B1_Feb, B1_Jun, B2_Feb, B2_Jun).

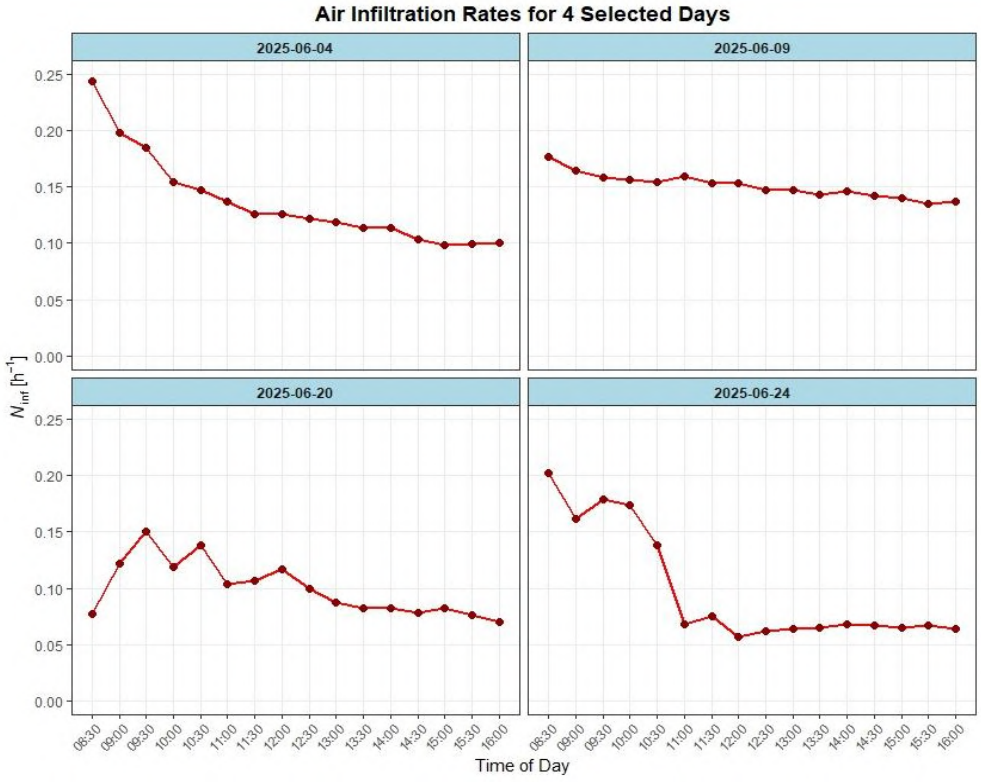

Fig. 2. Diurnal variations of air infiltration rates (N_{inf}, h^{-1}) in four selected days in B1, June 2025.

Fig. 2 illustrates the diurnal variation of N_{inf} in B1 across four representative days in June 2025 (4th, 9th, 20th, and 24th), highlighting differences in short-term fluctuations driven by meteorological conditions. On June 4th, a pronounced decrease in N_{inf}, (from 0.25 to 0.10 h^{-1}) was observed, associated with higher wind speed (> 3.0 m s^{-1}), which suppressed N_{inf}. On June 9th, N_{inf} remained relatively high and stable (0.17–0.14 h^{-1}), likely due to lower $T_{outdoor}$. June 20th exhibited moderate variability, with peak values reaching 0.15 h^{-1} and a subsequent decline to 0.07 h^{-1}. In contrast, June 24th showed the sharpest drop in N_{inf}, decreasing from 0.20 h^{-1} in the morning to 0.06 h^{-1} by noon, after which the values remained low. On both days, N_{inf} reflected the combined influence of $T_{outdoor}$ and wind speed.

Across buildings, the variability of N_{inf} was driven by different meteorological parameters. In B1, N_{inf} was primarily influenced by $T_{outdoor}$ (p= –0.69), followed by the outdoor/indoor temperature difference (T_{diff}) and air pressure in February, and by T_{diff} and relative humidity (RH) in June. In B2, $T_{outdoor}$ had a weaker effect on N_{inf} (p= –0.16 in February; –0.33 in June), while stronger drivers included RH and T_{diff} in February, and air pressure and wind speed in June. These building-specific drivers may explain the observed diurnal fluctuations.

Table 1 summarises statistics on calculated N_{inf} and measured $T_{outdoor}$ in B1 and B2 during February and June 2025, along with winter-to-summer ratio analysis.

Table 1. Statistical analysis and ratios of air infiltration rates (N_{inf}) and outdoor temperatures ($T_{outdoor}$) for different seasons and buildings.

	Basic statistics of calculated and measured data								**Seasonal N_{inf} ratio**	
	B1_Feb		B2_Feb		B1_Jun		B2_Jun		winter / summer	
	N_{inf}	$T_{outdoor}$	N_{inf}	$T_{outdoor}$	N_{inf}	$T_{outdoor}$	N_{inf}	$T_{outdoor}$	B1_Feb / B1_Jun	B2_Feb / B2_Jun
MIN	0.14	–5.4	0.04	–3.7	0.06	14.3	0.00	12.4	2.33	*
MAX	0.27	12.2	0.21	15.1	0.25	33.0	0.22	29.8	1.08	0.95
AVG	0.19	4.3	0.10	6.3	0.13	25.8	0.06	23.0	1.46	1.67
STDEV	0.03	3.6	0.03	4.3	0.04	3.5	0.03	3.4	0.75	1.00
***p* (N_{inf}, $T_{outdoor}$)**		–0.69		–0.16		–0.61		–0.33	–	–

N_{inf} values exhibited considerable variability across seasons and buildings, ranging from 0.00 h^{-1} (B2_Jun minimum) to 0.27 h^{-1} (B1_Feb maximum). In B1, February values ranged from 0.14 to 0.27 h^{-1} (avg 0.19 h^{-1}), while June values ranged from 0.06 to 0.25 h^{-1} (avg 0.13 h^{-1}). Similarly, B2 showed a February range of 0.04 to 0.21 h^{-1} (avg 0.10 h^{-1}), and a June range of 0.00 to 0.22 h^{-1} (avg 0.06 h^{-1}). The winter-to-summer ratios further highlight this pattern: in B1 it was 1.46, and in B2 1.67, indicating that winter air infiltration was approximately 1.5 to 1.7 times higher than in summer. When comparing the two buildings, B1 consistently exhibited higher infiltration rates than B2, with values being 1.9 times higher in February and 2.2 times higher in June. Correlation coefficients between N_{inf} and $T_{outdoor}$ ranged from –0.16 (B2_Feb) to –0.69 (B1_Feb), confirming a moderate to strong inverse relationships. Higher air infiltration rates in B1 during winter (avg 0.19 h^{-1}) compared to B2 (avg 0.10 h^{-1}), combined with its larger room volume of B1, resulted in significantly greater ventilation heat losses: 57 kWh in B1 versus 15 kWh in B2 during February.

Conclusion

Air infiltration rates, determined using the CO_2 decay method, exhibited seasonal and inter-building differences in two residential buildings (B1, B2) with contrasting airtightness. Winter air infiltration rates consistently exceeded summer values, with winter-to-summer ratios ranging from 1.46 (B1) to 1.67 (B2). Airtightness governed the overall magnitude of air infiltration, while outdoor air temperature emerged as the primary dynamic driver, particularly in B1 with its less airtight envelope, where the correlation coefficient reached –0.69. These findings are consistent with previous studies [4,5,10].

Tracer gas (CO_2) monitoring under natural operating conditions effectively captured temporal variations in air infiltration, thereby complementing standardised tests by reflecting real building performance. The results highlight that an airtight envelope can reduce uncontrolled air infiltration and ventilation heat losses, supporting more stable indoor environments across seasons.

References

1. European Commission. Energy Performance of Buildings Directive. // European Commission, 2024. Available at: https://energy.ec.europa.eu/topics/energy-efficiency/energy-efficient-buildings/energy-performance-buildings-directive_en [Accessed 25 September 2025].
2. ASHRAE. ANSI/ASHRAE Standard 62.1 – 2022. Ventilation and Acceptable Indoor Air Quality. // American Society of Heating, Refrigerating and Air-Conditioning Engineers, Atlanta, GA, 2022.
3. Lu, Y., Xiang, Y., Chen, G., Liu, J., & Wang, Y., On-site measurement and zonal simulation on winter indoor environment and air infiltration in an atrium in a severe cold region. // Energy and Buildings, v. 223, 2020, 110160. https://doi.org/10.1016/j.enbuild.2020.110160.
4. Ji, Y., Duanmu, L., Liu, Y., & Dong, H., Air infiltration rate of typical zones of public buildings under natural conditions. // Sustainable Cities and Society, v. 61, 2020, 102290. https://doi.org/10.1016/j.scs.2020.102290.
5. Du, Y., Ji, Y., Lin, D., & Hu, S., A case study of air infiltration for highly airtight buildings under the typical meteorological conditions of China. // Buildings, v. 14, 2024, 1585. https://doi.org/10.3390/buildings14061585.
6. EN ISO 9972:2015. Thermal performance of buildings – Determination of air permeability of buildings – Fan pressurization method. // European Committee for Standardization, Brussels, 2015.
7. Patel, T., Mitsingas, C., Miller, J., & Newell, T., Comparison of blower door and tracer gas testing methods for determination of air infiltration rates through building envelopes at normal operating conditions. // ASME Energy Sustainability Conference, 2011, pp. 1013–1019. https://doi.org/10.1115/ES2011-54373.
8. Undram, M., Song, D., & Kim, J., A review of the test methods for airtightness performance of building components using the blower door system. // Korean Journal of Air-Conditioning and Refrigeration Engineering, v. 31, 2019, p. 216. https://doi.org/10.6110/KJACR.2019.31.5.216.
9. Shi Y., Li X., A convenient method to assess air infiltration rate using particle mass balance principle. // E3S Web of Conferences, v. 111, 2019, 06039. https://doi.org/10.1051/e3sconf/201911106039.
10. Younes, C. Air infiltration through building envelopes: A review. Indoor and Built Environment, v. 21, 2012, pp. 142–157. https://doi.org/10.1177/1744259111423085.

1st International Scientific Conference "Modern problems in Geophysics", Proceedings,
ISBN 978-9941-36-434-1, ISSN 3088-4349, Tbilisi, Georgia, November 6-8, 2025

IMPLEMENTATION OF NEW TECHNOLOGIES IN THE RED SOILS OF ADJARA (WITHOUT THE USE OF MINERAL FERTILIZERS)

Kutaladze N., GogolishviliT., Abuladze D., Bolkvadze Ts., Gorgiladze T., Telia K.

Shota Rustaveli State University of Batumi, Institute of Agrarian and Membrane Technologies,
Batumi, Georgia
nunukutaladze@gmail.com

Abstract. *To prevent soil contamination and to obtain environmentally safe agricultural products, ecologically safe biopreparations – BlackJack, GeoHumate, and the insecticide Cu^{++}were purposefully introduced for the first time into stationary field experiments conducted on red soils of Adjara under mandarin (Citrus unshiu) plantations, without the application of mineral fertilizers.*

The field experiments were conducted on the Chakvi collection plots located on red soil under a mandarin (Citrus unshiu, broadleaf type) plantation. The trials were arranged in three replications, comprising a total of six model plants, while each treatment variant included nine plants. Prior to the establishment of the experiment and throughout its duration, soil samples were collected at a depth of 50 cm, along with leaf samples from the plants, to determine their biochemical parameters. During the experimental period, pest and disease monitoring was performed twice.

The experimental design consisted of three treatment variants. The biofertilizers were applied according to the scheme four times during the vegetation period (April, May, June, and July). As a background treatment, the Cu^{++} insecticide was applied both to the soil (by drenching) and to the plants (by foliar spraying), exerting a positive effect on pest and disease suppression.

Multiple monitoring activities conducted throughout the vegetation period revealed the positive influence of the applied bioformulations. Based on the data obtained from the experiments, the following results were established:

- *The biofertilizers BlackJack (soil application and foliar spraying) and GeoHumate (soil application and foliar spraying), when used in combination with Cu^{++} (2 mL per 10 L of water as foliar spray) and without the use of mineral fertilizers, demonstrated the best overall performance.*
- *Soil fertility improved significantly, and the content of essential nutrients in plant leaves increased.*
- *Throughout the vegetation period, the positive effect of the applied preparations was consistently observed.*
- *Pest- and disease-induced plant damage was eliminated, and most importantly, a high-yielding, environmentally clean, and high-quality harvest was obtained.*

According to the data presented in the tables, toxic elements such as As, Cd, Cr, Hg, and Pb were not detected in the soil, and consequently, were also absent in the plants and fruit. This outcome is attributed to the fact that the soil was enriched exclusively with ecologically clean fertilizers, thereby preventing contamination of the low-fertility red soils of Adjara.

Key words: *biofertilizer, red soil, citrus, toxic elements, ecological safety*

Introduction

Soil is the source of life, a mixture of minerals and organic matter that determines plant germination and growth. It directly influences the food consumed by humans, the water they drink, the air they breathe, as well as the flora, fauna, and human health. Consequently, soil pollution triggers chain reactions that adversely affect all other environmental components.

With the growth of industrialization, the harmful impact of industrial waste on the environment has significantly increased, particularly affecting water and soil, where heavy metals tend to accumulate. Contamination of soil and water by heavy metals has become a serious global environmental issue.

Addressing soil contamination requires considerable time, resources, and effort, as it poses both environmental and public health challenges. Over the years, various methods and technologies have been introduced to combat this problem [1].

With the growth of the human population, the demand for food is constantly increasing, yet food production is impossible without soil. Healthy soil ensures healthy food, which is why it is essential to devote particular attention to soil care and fertility management, especially today, when soil contamination has become a pressing global issue.

Plants grown on polluted soil can accumulate excessive amounts of toxic elements, including mercury (Hg), cadmium (Cd), arsenic (As), chromium (Cr), thallium (Tl), and lead (Pb). The accumulation of these elements in soil leads to soil pollution, which in turn poses a serious threat to flora, fauna, and human health [4].

Excessive accumulation of heavy metals presents significant health risks to humans. For instance, cadmium uptake can cause severe disorders such as cancer and bone demineralization, among others. Lead is particularly hazardous for children, as it damages brain cells and the central nervous system.

Excessive application of chemical fertilizers may also impair soil microbial activity, reducing the ability of bacteria to decompose organic matter and to produce vital nutrients essential for plant growth. Similarly, pesticides negatively affect beneficial soil bacteria and other important organisms [5].

Therefore, to prevent soil contamination and to produce environmentally safe agricultural products, we conducted, for the first time, stationary field experiments on the red soils of Adjara under mandarin (Citrus unshiu) plantations. The experiments involved the targeted application of ecologically safe biopreparations, BlackJack, GeoHumate, and the Cu^{++} insecticide, without the use of mineral fertilizers.

BlackJack is a 100% natural product, certified in Germany for organic agriculture. It is an innovative formulation distinguished from other preparations by its content of humic and ulmic acids – compounds that stimulate and activate plant root and vegetative systems. In addition, it reduces salt concentration, enhances the adsorption of nutrients, increases the activity of beneficial microelements, and acts as a carrier agent for micro- and macro-nutrients, facilitating their transformation into more bioavailable forms and their uniform distribution throughout the plant.

BlackJack can be applied both as a foliar spray and through drip irrigation systems. It may be used alone or in combination with other agents.

- Foliar feeding: 10 mL dissolved in 2 L of water per plant; application interval: every 10–15 days.
- Root feeding: 10 mL dissolved in 1.5 L of water per plant; application interval: every 10–15 days.

GeoHumate is an ecologically clean humic biofertilizer, rich in microelements, and often referred to as a plant growth stimulator. It helps to alleviate plant stress, promotes green mass development, bud formation, and prolonged, abundant flowering. GeoHumate is used for comprehensive nutrition of agricultural crops, beginning with seed treatment and continuing with subsequent plant applications. It is particularly effective when used via drip irrigation systems, both in open-field and greenhouse conditions.

- Foliar application: four treatments are recommended during the vegetation period; dilution rate: 5 mL per 1 L of water per plant.

Cu^{++} (Copper) is essential for the functioning of the plant immune system. It serves as a catalyst in photosynthetic reactions, promotes lignin synthesis, and supports protein metabolism and respiratory activity. Copper also enhances the plant's resistance to pests and diseases.

- Recommended dosage: 10 mL dissolved in 3.5 L of water.

The field experiments were conducted on the Chakvi collection plots located on red soils under a mandarin (Citrus unshiu, broadleaf type) plantation. The trials were arranged in three replications, comprising a total of six model plants, while each variant included nine plants. Prior to and during the experiment, soil samples were collected from a 50 cm depth, and leaf samples were taken to determine biochemical parameters. During the experimental period, pest and disease incidence was monitored twice.

The experimental design included three variants. The biofertilizers were applied four times during the vegetation period (April, May, June, and July) in accordance with the established scheme.

The experiments were established according to the following scheme:

1. BlackJack – applied both as foliar spray and soil drench (8 mL dissolved in 2 L of water per plant; application interval: every 10–15 days). Cu^{++} (10 mg dissolved in 3.5 L of water) applied as foliar spray.

2. GeoHumate – applied both as foliar spray and soil drench (5 mL dissolved in 1 L of water per plant; application interval: every 10–15 days). Cu^{++} (10 mg dissolved in 3.5 L of water) applied as foliar spray.
3. Control (without biofertilizers)

After the experimental treatments, a multi-element analysis of the soil water extract was performed to determine the macro- and microelement composition. The analytical results are presented in Table 1.

Table 1. Results of multi-element analysis in the soil water extract (red soil, Chakvi site, 08.07.2025)

Element	Concentration (mg/L)	Element	Concentration (mg/L)	Element	Concentration (mg/L)
Al	1.81	**As**	-0.0107	**B**	0.327
Ba	0.0031	**Be**	0.0012 L	**Ca**	9.98
Cd	-0.0201	**Co**	-0.0122	**Cr**	-0.0475
Cu	-0.0998	**Fe**	3.18	**Hg**	-2.43
K	3.13	**Li**	1.99	**Mg**	2.80
Mn	0.0144	**Mo**	-0.0299	**Na**	-0.364
Ni	0.0008	**P**	0.392 L	**Pb**	-0.155
Sb	-0.0862	**Se**	0.0194 L	**Si**	59.2
Ti	0.175	**Tl**	-0.0107	**V**	-0.154
Zn	-0.0341				

Emphasis was placed on determining the content of toxic elements – arsenic (As), cadmium (Cd), chromium (Cr), mercury (Hg), nickel (Ni), and lead (Pb) which are primarily responsible for soil contamination.

Specifically, the measured concentrations of these elements in the soil water extract were as follows: As – 0.011 mg/L, Cd – 0.020 mg/L, Cr – 0.046 mg/L, Hg – trace, Ni – 0.0008 mg/L, and Pb – 0.155 mg/L.

These results indicate that the concentrations of toxic heavy metals are extremely low, remaining below internationally accepted threshold limits, thereby confirming the absence of contamination and the ecological safety of the studied soils.

To further assess the effect of biofertilizer application, mandarin leaf samples were collected after treatment. The chemical composition (macro- and microelements) of the leaves was analyzed, and the results are presented in Table 2.

Chemical Composition of Mandarin Leaves (Macro- and Microelements) After Biofertilizer Application (22–28 August 2025)

Table 2. Composition of macro- and microelements in mandarin leaves following the application of biofertilizers.

Variant	Al (mg/L)	As (mg/L)	B (mg/L)	Ba (mg/L)	Be (mg/L)	Ca (mg/L)	Cd (mg/L)	Co (mg/L)	Cr (mg/L)
BlackJack (20 mL per 3 L of water, applied to soil and foliage) + Cu^{++} (20 mL per 10 L of water, foliar spray)	54.4	-0.0723	15.0	30.0	0.0020L	2043.37	-0.0216	-0.0206	-0.083
GeoHumate (15 mL per 3 L of water, applied to soil and foliage) + Cu^{++} (20 mL per 10 L of water, foliar spray)	66.3	-0.0618	17.7	40.5	0.0021 L	2174.00	-0.0238	-0.0264	-0.049
Without biofertilizers (control)	27.9	-0.102	8.4	18.4	0.0009 L	1985.40	-0.0284	-0.0284	-0.0487

Table 3. Concentration of additional macro- and microelements in mandarin leaves after biofertilizer application (22–28 August 2025)

Variant	Cu (mg/L)	Fe (mg/L)	Hg (mg/L)	K (mg/L)	Li (mg/L)	Mg (mg/L)	Mn (mg/L)	Mo (mg/L)	Na (mg/L)
BlackJack (20 mL per 3 L of water, applied to soil and foliage) + Cu^{++} (20 mL per 10 L of water, foliar spray)	17.1	31.6	-11.4	3400	-2.33	844	8.58	-0.095	311
GeoHumate (15 mL per 3 L of water, applied to soil and foliage) + Cu^{++} (20 mL per 10 L of water, foliar spray)	36.4	35.4	-11.7	3760	-1.45	951	10.7	-0.0321	427
Without biofertilizers (control)	4.32	16.9	-7.7	2590	-3.44	608	4.19	-0.0358	372

Table 4. Concentration of trace elements in mandarin leaves after biofertilizer application (22–28 August 2025)

Variant	Ni (mg/L)	P (mg/L)	Pb (mg/L)	Sb (mg/L)	Se (mg/L)	Si (mg/L)	Ti (mg/L)	Tl (mg/L)	V (mg/L)	Zn (mg/L)
BlackJack (20 mL/3 L water, soil + foliar application) + Cu^{++} (20 mL/10 L water, foliar spray)	1.28	978	-0.12	-0.452	0.227 L	198	-0.0816 L	-0.22	-0.0177	7.20
GeoHumate (15 mL/3 L water, soil + foliar application) + Cu^{++} (20 mL/10 L water, foliar spray)	1.35	1280	-0.105	-0.277	0.120 L	254	-0.0244 L	-0.299	-0.0165	9.08
Without biofertilizers (Control)	0.575	766	-0.251	-0.426	0.144 L	99.4	0.0387 L	-0.284	-0.0338	3.59

The toxic elements, As, Hg, Cd, Sb, Pb, and Ni, were not detected in the mandarin leaves. As a background treatment, the Cu^{++} insecticide was applied both to the soil (by drenching) and to the plants (by foliar spraying), which also exerted a positive effect on the suppression of pest and disease incidence. Multiple monitoring sessions conducted during the vegetation period confirmed the positive influence of the applied preparations on plant health and development.

The soil and plant analyses were performed at the Institute of Agrarian and Membrane Technologies, within the Laboratory of Agrochemistry and Soil Science, using a plasma atomic emission spectrophotometer (ICPE-9820). Analyses were carried out under both wet and dry ashing conditions [2,3].

Based on three years of experimental data, we can now provide scientifically validated recommendations and methodological guidelines. The results obtained can be effectively used by farmers, as well as by research centers and professionals in related fields, biochemists, biologists, agrochemists, soil scientists, and entomologists to prevent soil contamination. It is recommended that only the identified ecologically clean biofertilizers be used to achieve environmentally safe, high-quality yields.

Conclusions

Based on the results obtained from the experiments conducted, the following conclusions were drawn:

- The applied biofertilizers BlackJack (soil and foliar application) and GeoHumate (soil and foliar application) in combination with Cu^{++} (2 mL per 10 L of water, foliar spray), without the use of mineral fertilizers, produced the best overall results.
- Soil fertility improved significantly.
- The concentration of essential nutrient elements in mandarin leaves increased.

- During the vegetation period, a positive effect of the applied formulations was observed, and plant diseases and pest infestations were effectively suppressed.
- Most importantly, a high, ecologically clean, and high-quality yield was obtained.

According to the analytical data presented in the tables, no pesticide residues or toxic elements such as As, Cd, Cr, Hg, or Pb were detected in the soil, plants, or fruit. This confirms that the soil was enriched exclusively with environmentally safe fertilizers, thereby preventing contamination of the low-fertility red soils of Adjara.

References

1. Avqopashvili, M., Remediation of Soils Contaminated with Heavy Metals: Monograph. Tbilisi, 2022, pp. 172–178.
2. Margvelashvili, G. Chemical Analysis of Soil. Tbilisi, 2019, pp. 59–64, pp. 120–122, pp. 149–152.
3. Margvelashvili, G., Dzadzamia, T., Practices in Agrochemistry. Tbilisi, 2021. ISBN: 978-9941-8-1511-9.
4. Chanishvili, Sh. (1973). Methodology of Experimental Work. Tbilisi: Metsniereba Publishers.
5. Fikry, A. M., Radhi, K. S., Abourehab, M., Effect of Inorganic and Organic Nitrogen Sources and Biofertilizer on Murcott Mandarin Fruit Quality. // Life, 12(12), 2022. Article 2120. https://doi.org/10.3390/life12122120
6. Muhammad, H., & Hassan, S., Paradigm Shift towards Beneficial Microbes Enhancing the Efficiency of Organic and Inorganic Nitrogen Sources for a Sustainable Environment. // Land, 12(3), 2023. Article 680. https://doi.org/10.3390/land120

1st International Scientific Conference "Modern problems in Geophysics", Proceedings,
ISBN 978-9941-36-434-1, ISSN 3088-4349, Tbilisi, Georgia, November 6-8, 2025

ADHESIVE CEMENTS BASED ON HOUSEHOLD WASTE

Markarashvili E.G., Khakhutaishvili A.T., Snesar A., Shermadini Kh.Kh., Chikvaidze I.Sh, Bazgadze Z.Z.

Ivane Javakhishvili Tbilisi State University, Department of Macromolecular Chemistry, Tbilisi, Georgia
eliza.markarashvili@tsu.ge

Abstract. Protection of the environment from pollution by domestic waste, in particular, should be the concern of every member of the community of the Black Sea coastline, and to a certain extent, for all people. The work envisaged obtaining new safe materials on the basis of household plastics and rubber household waste in the Black Sea coastline, which provides the opportunity to turn harmful waste into a useful product. New construction materials are obtained on the basis of glass waste, plastics, rubber waste and adhesive cements. New environmentally safe polymer composites were obtained for the first time. These composites can be used in building materials, artistic and decorative paints and household items. For these composite materials, the following were studied: water absorption, bending and tensile strength, impact viscosity, physical-mechanical and thermal properties, supramolecular structure of the surface by SEM scanning electron microscopy, unfolding and correction time.

Key words: adhesive cement; ethylsilicate; glass.

Improvement of the ecological state of the environment is one of the most important issues of modern times. In this regard, it is essential to deepen the knowledge of those environmental problems, which are related to application of polymeric materials. Environment protection from domestic waste pollution posing a real threat to the environment has to become a main care for each member of the society. This work foresees familiarization with the second aspect of waste disposal and management – the opportunity of harmful waste transformation into useful products, which is realized through chemical and technological processes, as well. Plastic waste disintegrates into small pieces in rivers and are eaten by fish. Afterwards these wastes hit human organisms and have a harmful effect on health. Prevention of plastic pollution means salvation of water inhabitants as well and this fact is acknowledged well in the European Union. In March 2019, the European Parliament adopted the law prohibiting production of single use plastic, for example plastic plates, knives and forks, ear sticks and other similar products. At the same time, a new processing method has been instituted (collection of 90% of plastic bottles until 2029) and increased responsibility of manufacturers has been established. Plastic is one of the most stable environmental pollutants and over the last 50-60 years it has been collected in vast numbers worldwide. It should be noted that it is not a problem for humans only. Plastics remain stable for a long time, and some of them – up to 100-500 years, so it is obvious that such type of waste creates a problem for the environment and represents one of the most stable pollutants. This work is important both from ecological viewpoint and in the light of receipt of new materials, in particular, receipt of new safe, ecologically clean composite waterproofing materials on the basis of household plastics, rubbers and glass waste, which are applicable in the construction industry [1-6].

The environmental protection problem may be solved by two ways – waste destruction and disposal (recycling). The latter implies its transformation into useful products. Burial and incineration are among main methods of destruction of solid domestic waste and packing materials. Burial of solid domestic waste requires allotment of large land areas for landfills. Obviously, these lands become unfit for further useful application. Roughly 90% of solid domestic waste are disposed at landfills (garbage dumps), which occupy more than 20 000 hectares of land area. So, each of these landfills "swallows" hectares of land. In addition, valuable secondary raw materials (waste paper, plastic, glass, metals etc.), which necessarily must be involved in the beneficial industrial cycles, are brought to the landfills. Incineration may be applied both to solid and liquid waste. This method is neither rational nor cost-effective, since toxic gases (SO_2, NO_2, CO) are separated during burning. This process is accompanied by rapid wear of equipment (garbage furnaces), emission of harmful combustion products into the atmosphere and therefore its recontamination, and penetra-

tion of heavy metals, toxic salts into soil and water, and thereby into human organisms. Garbage burning equipment, as a rule, is a complex and expensive device, since it has to be equipped with effective filters and gas traps. Due to this reason, this method of solid domestic waste destruction is not frequently used. Domestic and industrial residuals, which are suitable for further processing are called secondary polymer wastes. They include unprocessed goods made of polymers and other materials, composite materials, which have lost their consumer properties due to physical wear [7-12].

Based on the household plastics, glass and rubber available in the Black Sea coastal area, as well as using renewable vegetable raw materials, new organosilicon binder and antipyrene for the first time there have been received new ecologically safe polymer composites. The mentioned composites as waterproofing materials may be used in construction materials, for manufacture of drawing and building paints and household goods. These composite materials have been studied regarding their water absorption, bending and tensile strength, impact strength (viscosity), physical-mechanical and thermal properties, and supramolecular structure of surfaces using SEM scanning electron microscope.

Sample preparation is a direct process and it includes mixing of different ingredients in an ordinary container. Selection of mixer, ingredients' blending and testing of obtained composite occurs depending on total mixture mass. Cement, sand and fillers are among typical main ingredients. New recipes are variations of old ones, with alteration of quantity of components, their mass content and change of ingredients (mainly fillers). We have prepared new samples, for which purpose we have added powdered glass in different quantities. Glass was added at the expense of sand amount reduction. 1, 3 and 5% of glass and in all cases 5% of grinded rubber tire powder were added (Table 1). In addition to waste tire powder, 1% of diethyleneglycol ethyl ether and methylcellulose were added to the mixture in different weight ratios.

In order to keep waste tire powder usability and for its safe use, we have determined the content of toxic elements established under the European Union regulations for polymeric materials.

New composite materials were tested for adhesion ability. Adhesion is mainly determined on a periodical basis, depending on which sample is tested. In our case, an experiment was held in a 7- or 28-day interval. Results are given in Table 1. In order to test adhesion to waterproofing materials, square-shaped samples were prepared, which afterwards were attached to cement tile. Preparation process starts with cutting of large tiles, which is followed by tiles' inspection. Each tile has to have specific size in order to avoid erroneous results during an experiment, and they are checked using a ruler, respectively their size has to meet relevant rules and regulations. After preparation, tiles are glued to large cement tiles. It is necessary to prepare surfaces properly, typically a surface must have two layers, after putting the second layer we glue small tiles, put weight on them and then remove it in a given time. We are waiting for it to dry. After completion of this process we glue metal plates to attached tiles using epoxide. In a few days, using an adhesiometer we measure a force needed to tile detachment. It should be noted that great attention is paid to what surface remains on a plate after detachment. As it was mentioned in the experimental part, different percentages of glass and in all cases 5% of rubber tire powder were added for receipt of new composite materials. Results of mechanical parameters' determination for new composite materials are given in Table 1, from where it is seen that a standard extension of a sample CN 68 equals to 24,5/24,5 cm after 1 minute. The best possible results close to this value are obtained when 5% of glass was added.

Table 1. Results of mechanical parameters' determination for obtained composite (waterproofing) materials

Sample	Bending, MPa	Compression, MPa	Extension (min)	Days	Storage conditions
CN68	1,74	7,2/7,2	24,5/24,5 cm	1	23°C/50% humidity
	5,17	18,1/18,6		28	23°C/50% humidity
CN68 + 5% glass + 5% rubber tire	1,7	7,6/7,5	23/23 cm	1	23°C/50% humidity
Powder	4,8	18,5/18,1		28	23°C/50% humidity
CN68 + 3% glass + 5% rubber tire	1,7	8,12/8,12	23,5/23,5	1	23°C/50% humidity
Powder	5,25	19,2/19,2		28	23°C/50% humidity
CN68+ 1% glass + 5% rubber tire	1,7	7,55/7,84	24/23,5	1	23°C/50% humidity
Powder	5,0	19,2/18,4		28	23°C/50% humidity

Results of different elements' determination in waste tire powder used for receipt of new waterproofing materials are presented in Table 2. Based on the obtained experimental data one may consider that the content of none of the toxically hazardous heavy metals in waste tire powder exceeds permissible standards established for heavy metals in polymeric materials. This fact points at the usability of waste tire powder and in addition, at its safe use as a raw material for receipt of waterproofing materials.

Table 2. Content of some metals (mg/kg) in waste tire powder

Element	mg/kg	NF EN 71-3, mg/kg
Aluminum (Al)	1 530	70 000
Antimony (Sb)	21	560
Arsenic (As)	1.4	47
Barium (Ba)	21	18 750
Cadmium (Cd)	1.0	17
Calcium (Ca)	4 710	-
Chromium (Cr total)	5.4	Chromium (III) – 460 Chromium (VI) – 0.2
Cobalt (Co)	26.3	130
Copper (Cu)	517.0	7 700
Iron (Fe)	4 909.9	-
Lead (Pb)	36.6	160
Lithium (Li)	2.0	-
Magnesium (Mg)	1 010	-
Manganese (Mn)	53.8	15 000
Molybdenum (Mo)	1.0	-
Nickel (Ni)	11.8	930
Sodium (Na)	571.4	-
Silica (Si)	53.0	-
Potassium (K)	944.6	-
Zinc (Zn)	6 417	46 000

Results of new composite (waterproofing) material tests for adhesion ability are presented in Table 3, from where it is seen that adhesion ability is the best possible in case of adding 5% of glass compared to application of 1 and 3% of glass. In addition, 5% of glass content provides the best mechanical properties of composite materials obtained by us.

Table 3. Test of new composite samples for adhesion ability

CM 11 + adhesion in standard condition after 14 D.	
Test method	EN 12004-2:2012/2018
Storage conditions	23 ^{0}C/ 50% (humidity)
Standard	1.07 MPa
1% glass	1.1 MPa
3% glass	1.1 MPa
5 % glass	1.2 MPa
Comment	Glass addition at the expense of sand

New recipes of cement glues, which are variations of old ones, have been developed. We have changed quantities of components entering cement glue and added new components, which respectively lead to percentage change of components and improvement of properties. Ethyl silicate, household plastic and rubber articles waste have been added to new samples prepared by us, which opens up the opportunity of harmful waste transformation into useful products using chemical and technological processes. None of the toxically hazardous heavy metals' content in waste tire powder exceeds permissible standards established for heavy metals' content in polymeric materials, which points at usability of waste tire waste as well as at its safe use

as a raw material for receipt of waterproofing materials. One may draw the conclusion that prepared new samples of cement glue, to which 1, 3, 5% of glass powder have been added and 5% of rubber waste have been taken in all cases, have improved their mechanical properties. The best results have been obtained when 5% of glass and 5% of powdered rubber tires have been added.

References

1. Hernandez R. J., Selke S. E. M., and Culter J. D., Plastics Packaging, Hanser, Munich, 2000.
2. Hunger H. K., Industrial Organic Pigments, VCH, Weinheim, 1993.
3. Sorokin M.F., Lyalyushko K.A., Practicum in chemistry and technology of film-forming substances. M. Chemistry, 1971, p. 246. (in Russian)
4. Puri VP., Effect of crystallinity and degree of polymerization of cellulose on enzymatic saccharification. // Biotechnol Bioeng 26, 1984, pp. 1219-22.
5. Okonko I.O., Adeola O.T., Aloysius F.E., Damilola AO, Adewale OA. Utilization of food wastes for sustainable development, electronic. // J Environ Agric Food Chem 8, 2007, pp. 263-86.
6. Torres F.G., Cubillas M.I., Study of the interfacial properties of natural fiber reinforced polyethylene, Polymer Testing, 24, 6, 2005, pp. 694-698. http://dx.doi.org/10.1016/j.polymertesting.2005.05.004.
7. Gorlovsky I.F., Bocharova A.M., Suvorova V.D., Laboratory practicum on pigment chemistry and technology. // L., Chemistry, 1978, p. 223. (in Russian).
8. Bagazhkov S.G., Sukhanova N.A., Practicum on lacquer coating technology. // M. Chemistry, 1982. p. 240. (in Russian).
9. Yakovlev A.D., Powder paint. // L., Chemistry, 1987, p. 216. (in Russian).
10. Karyakina M.I., Poptsov V.E., Polymeric coating technology. // M. Chemistry, 1983, p. 335. (in Russian).
11. Microwave plasma atomic emission spectroscopy (MP-AES), January 2021. Agilent.
12. European Standard, Supersedes EN 71-3:2013, October 2014, https://law.resource.org/pub/eu/toys/en.71.3.2015.html

1st International Scientific Conference "Modern problems in Geophysics", Proceedings,
ISBN 978-9941-36-434-1, ISSN 3088-4349, Tbilisi, Georgia, November 6-8, 2025

TECHNOGENIC LANDSCAPE – AS PARADYNAMIC SYSTEMS DETERMINING THE ECOLOGICAL CONDITION OF MINING IMPACT ZONES

Seperteladze Z., Davitaia E., Kikvadze T., Aleksidze T., Rukhadze N.

Ivane Javakhishvili Tbilisi State University, Tbilisi, Georgia
*Georgian Technical University, Tbilisi, Georgia**
seperteladze@tsu.ge

Abstract. *The present work concerns some landscape-geochemical peculiarities of Georgia. The exploitation of the fields has caused chemism modification of the environment. The dependence of the linear process of biologic recultivation on physiographic factors is obtained by means of multifactor regression analysis and the ways of effective optimization of the mining region environment, damaged under the influence of technogenesis, are distinguished. The influence of anthropogenic factors is spread even on the territories outside the field exploitation area (approximately twice exceeding its area) and causes regime changes of soil waters and migration of chemical elements, activation of erosive processes, falling of ground efficiency, etc. Besides the coefficient of every single opening roof layer (Tchiatura) i.e. Bever coefficient has been calculated and the optimum admissible parity has been determined that excludes the possibility of annual erosion.*

Theoretical and practical results of the research can be successfully applied in forecasting technogenic processes and in the field of solving environment optimization problems.

Key Words*: landscape recultivation, geochemical situation, physiographic factor, Ecological problems.*

Intoduction

Ecological problems of environment protection are mostly stipulated by geochemical functioning of geocomplexes, influenced by technogenesis, in particular, by the migration of mineral and biogenic substances in them. Resulting from the active anthropogenic influence, certain modification of landscape (technogenic) is formed, which in its turn, causes qualitatively new forms of element migration and situation formation, ecologically different from the previous one.

Peculiarities of spreading diffused elements and their areal in mining regions are, at some rate, determined by metalogenetic specificity of certain provinces and zones, distinguished by the set of typical (mining) metals, as well as by types of fields, mirroring the soil, areal and background waters, etc. on the background of metalogenetic peculiarities of the mining provinces some other air factors of the diffused metal formation are revealed: landscape-geochemical character of the region, mining formations, soil varieties and soil forming layer, their phisiochemical consistence, etc.

Landscape-geochemical conditions of Georgia, determining the region environment, where the processes of diffused metal area formation (in soil and waters) take place, are complex and miscellaneous. A wide range of mining regions is located in mountain forest and mountain meadow areas. The combination of high mountainous Alpine regions, characterized by cold and mildly continental climate, with the middle mountain ones, characterized by the mildly damp climate, creates the complexity of landscape-geochemical conditions, where the migration of the products of oxidizing mining fields takes place [3].

On the territory of quarries soil surface, natural and cultural vegetation and natural-anthropogenic complex, in general, having shaped during the centuries, are totally disappearing [1]. Quarry vicinities often appear to be the locus of erosive and sliding processes and the reason for soil, air, surface and underground water pollution [2]. Here sometimes harmful and even dangerous environments can be created, that complicates utilization of the territory from the agricultural point of view, reduces yielding ability and worsens living conditions of the population.

The main aim of the present research is the evaluation of recultivation time period of technogenic landscapes by means of mathematical statistics method and determines interdependence of natural factors influencing the process of optimal rehabilitation of the territory.

Objects and Methods

The object of the present research is the manganous mining region located in mountain forest and mountain meadow zones in western Georgia, administratively belonging to Tchiatura district. The region to be researched is known with its brown forest, humus-carbonate and mountain meadow soils. The above mentioned soils are characterized by original morphochemical and micromorphogenic parameters [4, 5].

Traditional methods of research together with the modern ones were applied for structural-dynamic research of modern, anthropogenic, particularly technogenic landscapes. The method of mathematical statistics has been used aimed at estimating recultivation time periods. With the account of the fact that technogenic landscapes are characterized by the migration of biogenic and mineral substances, specific geochemical methods of research have been applied.

Results and Their Discussion

Approximately 4000 hectares of agricultural lands have been practically made useless resulting from mineral mining in Georgia. If we take into consideration the fact that the price of 1 hectare is more than 20-25 thousand GEL (approx. 14 000-14 500 $), it will become clear, that the research of technogenic complexes and their optimization is of paramount importance.

The exploitation of the fields has caused chemism modification of the environment. River waters have been enriched with acid products, migrating from far distances from the ore body (approx. 2-2,5 km). High concentration of metals and sulfate-ions can be observed not far from the ore body (primary area). Lower to the river flow the concentration is becoming higher, accordingly pH parameter is increasing. In comparatively longer distances (2-2,5 km from the ore body) the migration of sulfate-ions, zinc and molybdenum. As for the ore elements (copper, lead and iron) the radius of their migration doesn't exceed 800 m [6]. The most considerable geochemical situation is distinguished in the soils of ore-bearing regions. Resulting from the hydrochemical research of the lead-zinc field of Georgia it has been concluded that the lead consistency is ecologically of a very dangerous ingredient, reaching up to 50 mg/l and the area of its diffusion is 100-150 m.

The influence of anthropogenic factors is spread even on the territories outside the field exploitation area (approximately twice exceeding its area) and causes regime changes of soil waters and migration of chemical elements, activation of erosive processes, falling of ground efficiency, etc. Despite the above mentioned negative influence, in view of high profitability open quarry method is widely applied in many countries of the world.

In Georgia the open quarry method of minerals is applied in all the places with the appropriate geological conditions, in particular lithologic structure of the composing and optimum capacity of roof layer. In Tchiatura manganese field only the economy made by the application of this method, constitutes a rather solid sum. The coefficient of opening roof layer i.e. Bever coefficient, calculated by the interrelation of roof layer capacity and ore-bearing layer (Fig.1), is set according to optimum capacity of layer and enables to determine the possibility of open field elaboration. The optimum admissible parity is considered to be calculated 40:1 (Fig. 2).

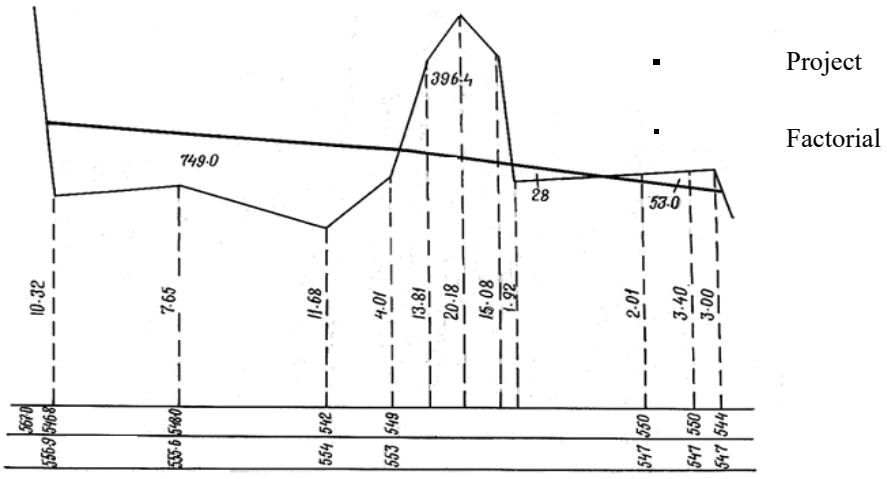

Fig. 1. Parity of project and factual level of Zodi quarry surface

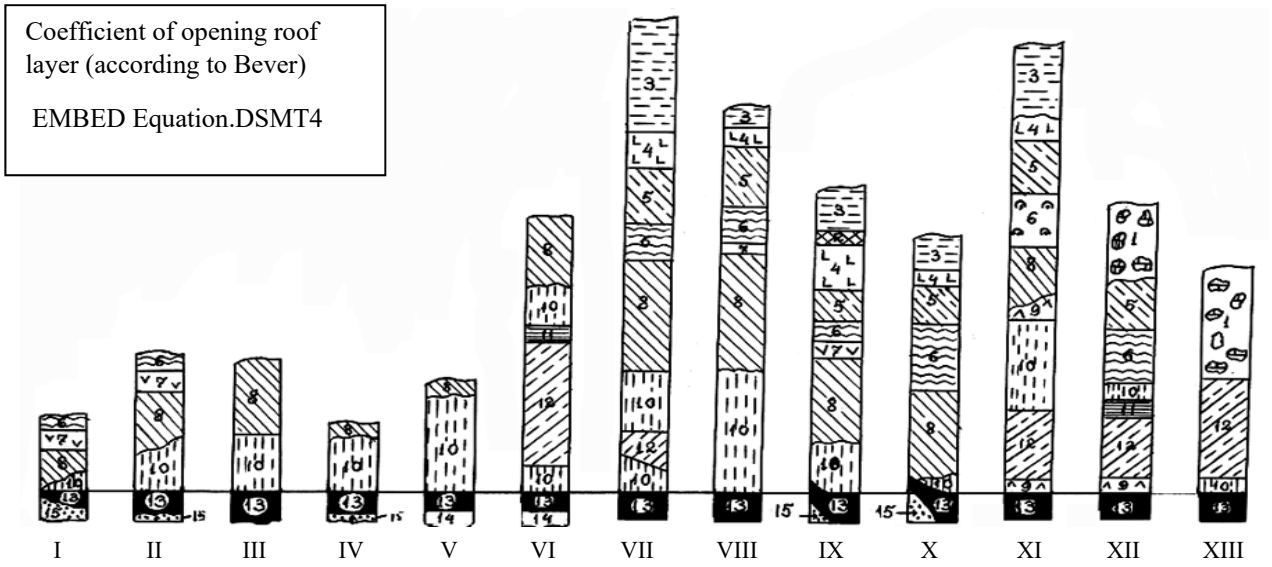

Fig. 2. Stratigraphic cut of separate plateaus manganese field of Tchiatura

I- Kveda Rgani; II-Rgani, III-Zeda Rgani, IV-Bunikauri, V-Tabagrevi, VI-Mgvimevi, VII-Itkhvisi, VIII-Shukruti, IX-Perevisa, X-Merevi, XI-Pastseti, XII-Darkveti, XIII-Sareki
1-diluvium; 2-basalt; 3-clays; 4-polite limestones; 5-sandy limestones; 6-clays, limestones; 7-limestones; 8-quartz, sands, sandstone; 9-shaly clays; 10-spongolitic sandstones; 11-manganese-bearing top horizon; 12- Maikop clays; 13- manganese-bearing bottom horizon; 14-low-ore sandstones; 15-limestones, sandstones.

First attempts to recultivate the landscapes, damaged by technogenesis in Georgia, were taken in the 60s of XX century. Despite the fact that practical works on landscape recultivation have been carried out for quite a long time, the elaboration of these issues from theoretical and scientific point of view began in Georgia only several years ago, though many scientific works by foreign authors have been dedicated to it [7, 8].

Judging from the fact that soil is one of the landscape content elements, the difference between the land recultivation and landscape recultivation can be traced in the fact, that during the landscape recultivation alongside with the soil, quasibalance and some other components (geological structure, relief, climate, flora, fauna, etc.) are taken into consideration.

Recultivation process is mostly defined by the following factors: phisiographic situation of the region, its hydrogeological character, soil and fauna and phisiochemical condition of the soil. From the social factors it is reasonable to take into account the demographic situation of the region, level of the economy development and its tendencies.

A bit more complex is the process of restoring technogenic complexes, emerged as a result of underground ore elaboration i.e. the result of quasibalance of phytocenosis through self-regulation.

In Georgia approximately 160 ha has been degraded because of the above mentioned reason and in Tchiatura only this figure reaches 91,6 ha. In the case when recultivation is carried out alongside with the works carried out through the open method, it is crucial to take into consideration the time factor, necessary for the completion of field elaboration. Besides, it must be taken into account that mineral alloys existing on the surface are represented by the masses of absolutely barren soils, consisting of ore element admixture, having a negative influence on the ecological condition of the environment. Eg.; on the territory of carboniferous fields (Tkibuli, Tkvarcheli) dumps and waste heaps consist of not only neutral admixture, but active substances (pyrite, coal, timber, etc) as well. At air penetration in the waste heap depth self-ignition takes place, what in its turn often causes flora extermination.

The aim of the research was to establish the approach of the recultivation (self-recovery) duration(y) for the following factors [9]:

where y is the reclamation time period (resultant factor). The explanatory factors are:

– the power of the roof layer (m), – x_1
– the horizontal section of the relief (km/km^2)- x_2 – the vertical section of the relief (m/km^2)-x_3
– the relief inclination (deg.) – x_4
– the soil humus layer thickness (sm)- x_5

– indicator of the soil acidity (pH) – x_6
– the maximal difference between project and surface indices of the dirt pile (m)- x_7
– the dirt pile area (m^2) and – x_8
– the dirt pile volume ($10^3 m^3$) – x_9

The table below (2) presents the respective surveillance data of the 9 recultivation objects of the research region.

For the revelation of interdependence character between various parameters, scientists often apply the method of mathematical statistics [10], mostly the method of multifactor regressional analysis. The practice of studying the parameter (factor) interdependence proves the possibility of linear model application:

1) $y = a_1x_1 + a_2x_2 + \ldots + a_nx_n + b$

By using the relevant statistical computer program have been adopted the following multiple regressive linear equation:

2) $y = 0{,}0044x_1 + 0{,}00392x_2 + 0{,}006x_3 + 0{,}0601x_4 - 0{,}2702x_5 + 0{,}5587x_6 - 0{,}1406x_7 + 0{,}0003x_8 + + 0{,}0028x_9 + 0{,}035,$

Elasticity coefficient of i-th explanatory factor is one of the important statistical characteristics that are used for the analysis of regression relationship:

$$E_i = a_i \frac{\overline{x}_i}{\overline{y}}$$

where $\overline{x}_i$ and $\overline{y}$ are average values of i-th and output factors. These factors show the amount of percent of change of the dependent factors at 1% change of i-th factor when the others may stay constant. In particular, for the physical and geographical factors that were selected by us, the following values of elasticity were obtained: E_1=0,0915, E_2=0,0034, E_3=0,1674, E_4=0,1527,
E_5=0,1351, E_6=0,8957, E_7=0,4958, E_8=0,2450, E_9=0,1170.

As one can see, the influence of x_6, x_7 and x_8 factors are important in the region under the study.

The accuracy of the obtained statistical dependence is determined by the volume and objectivity of the empiric information. Due to shortage of necessary materials and some other reasons, the maximum needed information was not obtained. So, we have no claim to high accuracy of our results, although prognosis on the mining region optimization with satisfactory correctness is feasible by means of generalization of the obtained dependence and reasonable conclusions about the ecological quality of separate reclamation zones can be made.

The practical acceptance of our method is proved by the fact that in 2006 parameters of Shukruti, one of the sites of Tchiatura manganese field was: x_1=134,0 m; x_2=3,6 sm/km^2; x_3=75,0 m/km^2; x_4=13,9°; x_5=2,4 sm; x_6=6,5; x_7=12,5 m; x_8=2700 m^3; x_9=68,5 th.m^3.

Recultivation process on this site was completed in summer, 2010. The factual reclamation time period of the process was 4,5 years. If we set the same values of regression, we'll get:

$$0{,}0044 \times 134{,}0 + 0{,}00392 \times 3{,}6 + 0{,}006 \times 75{,}0 + 0{,}0601 \times 13{,}9 - 0{,}2702 \times 2{,}4 + 0{,}5587 \times$$

$$\times 6{,}5 - 0{,}1406 \times 12{,}5 + 0{,}0003 \times 2700 + 0{,}0028 \times 68{,}5 + 0{,}035 \approx 4{,}15 \text{ (year)}.$$

The availability of the necessary amount of valid statistical information will enable the scientists to make accurate prognosis of the reclamation time period and to set the way of efficient soil optimization in mountain-ore regions.

Conclusion

1. Complexes and their components under the long technogenesis influence have become coordinated to external conditions, that's why their restoration is so complex and is practically impossible.

2. Resulting from the geochemical analysis of underground and surface waters, soil and atmosphere of the vicinities of the objects under study the conclusions have been made that separate components, as well as the natural territorial complexes in general, undergo the transformation and the landscape-ecological situa-

tion is becoming even worse. High concentration of chemical elements is traced at the zone of mineral extraction, at 2-2,5 radiuses from the ore bodies. The surrounding territories are quite impoverished from ingredients, because of abatement of active chemical elements.

3. The analytical formula of reclamation time dependency on phisiographic factors has been obtained for Tchiatura mountain ore region through the method of multifactor regression analysis.

4. indicator of the soil acidity (pH)- (x_6), the maximal difference between project and surface indices of the dirt pile (m)-x_7, the dirt pile area (m^2) and – x_8 have great influence on the reclamation time period.

5.The availability of the necessary amount of valid statistical information gives the opportunity to make accurate prognosis of the reclamation time period. The presented approach may serve to be the methodological base for the research of dependency between any factors, particularly for studying interrelations between technogenic landscapes and their separate components, representing the object of scientific research.

References

1. Gerasimov I.P., Interaction between Nature and Society // Moscow, „Nauka", 1973, P. 532.
2. Glazovskaya M.A., Technogenesis and Problems of Landscape-Geochemical Prognosis // Vestnik MSU, ser. 5, Geography, 1968, pp. 30-36.
3. Seperteladze Z, Daviaia E, Kikvadze T. Natural Antropogenic Mining Complexes and the Problems of their Optimization // Bulletin Georgian National Academy of Sciences, vol. I (= vol. 175), no. 3, 2007. pp. 64-66.
5. Urushadze T.F., Soil Map of Georgia (1: 500 000), Tbilisi. 1999.
6. World Reference Base for Soil Resources. Food and Agriculture Organization of the United Nations. Rome, 1998, P. 91.
7. Zautashvili B.C., Hydrogeochemistry of Ore Deposit // Tbilisi, „Metsniereba", 2004, p.190.
8. Bauer L., Weinitschke Y., Landsschaftsflege und Naturschutz // 2 Aufl. Iena, VEB Gustav Tischer Verlag, 1967, p. 303.
9. Franke H.G., Zu fragen der Weiserurbar machung im Erz und Steinkohlebergbau der DDR // Bergakedemie, 1, 1969. pp. 38-58.
10. Davitaia E.Ph., Estimation of Technogenic Landscape Restoration Probability and of its Ecological Validity by using the Method of Multi-factorial Regression Analysis (on the Patterns of Manganese Ore of Tchiatura) // Bulletin of the Academy of Sciences, vol. 137, #2, 1990, pp. 329-331.
11. Dreiper N. Smith G., Applied Regressive Analysis // Finances and Statistics. Moscow, 1968. p. 366.

1st International Scientific Conference "Modern problems in Geophysics", Proceedings,
ISBN 978-9941-36-434-1, ISSN 3088-4349, Tbilisi, Georgia, November 6-8, 2025

VALORIZATION OF PERSIMMON (*DIOSPYROS KAKI L.*) BY-PRODUCTS UNDER CIRCULAR ECONOMY CONDITIONS

Ardzenadze M., Chikovani D., Khakhutaishvili M., Kartsivadze I., Khamadadze E., Telia K.

Shota Rustaveli State University, Batumi, Georgia
merab.ardzenadze@bsu.edu.ge

Abstract. *Persimmon (Diospyros kaki L.) is a widely cultivated subtropical fruit rich in nutrients and bioactive compounds with demonstrated antimicrobial, anticancer, antidiabetic, antithrombotic, and anti-inflammatory activities. However, its production, processing, and commercialization generate substantial amounts of by-products that are rarely recovered or properly managed, resulting in environmentally harmful disposal practices. Owing to their high content of bioactive constituents, these by-products represent an underutilized source of high-value compounds for the food and nutraceutical industries. This study assessed the potential of industrial persimmon by-products as raw materials for the development of value-added products and examined low-waste and zero-waste processing technologies suitable for their recovery. In Georgia, persimmon by-products remain largely unexploited and are typically discarded, contributing to the contamination of water, soil, and air and posing significant ecological risks.Through experimental research, innovative technological processes were developed to ensure the efficient utilization of persimmon raw materials and by-products. These processes enable the conversion of processing residues into biologically active, nutrient-rich additives with enhanced nutritional and functional value. The outcomes of this study support the valorization of persimmon by-products, contributing to the sustainability of the agri-food sector and fostering the advancement of circular economy practices.*

Keywords: *persimmon, phytochemicals, food additives, valorization, environmental pollution.*

Ensuring the sustainability and integrity of the human environment necessitates the improvement of food quality, the provision of safe drinking water, and the prevention of atmospheric, aquatic, and soil pollution. These challenges are particularly relevant to enterprises within the food industry, which constitute one of the strategic sectors of the national economy.

Among the environmental impacts of food industry enterprises, the most significant effect is exerted on water resources. In addition, harmful influences extend to soil and air. Wastewater containing plant-derived residues is poorly filtered, undergoes decomposition, releases malodorous compounds, and negatively affects human health. When discharged into water bodies, it deteriorates water quality, and at certain concentrations, it can cause the death of fish and plankton populations.

To address this problem, it is essential to implement the ecologization of production, that is, the development of zero-waste technological processes aligned with the principles of the circular economy.

The circular economy represents a modern economic model whose core objective is the efficient use of resources through reduced consumption, extended product life cycles, elimination of primary resource depletion, and the recycling and re-utilization of products and their components.

The circular economy has the potential to become the main paradigm of sustainable development, as the linear economic model exerts harmful effects on the environment and leads to the depletion of natural resources [1].

The introduction of low-waste and zero-waste technologies allows, on the one hand, for the maximum and comprehensive extraction of valuable components from raw materials and their conversion into useful products, and on the other hand, for the elimination or reduction of environmental damage caused by industrial waste.

At present, most technological processes used in production are highly waste-intensive. A significant portion of these wastes is generated by food processing and agro-industrial enterprises. The recycling of secondary raw materials enables the production of new products without the need for additional primary resources.

Fruit by-products, as the main category of secondary raw materials, typically contain 5–15% dry matter, which makes them highly perishable. They rapidly ferment and acidify, leading to the loss of valuable bioactive components and contributing to environmental pollution. Their storage life does not exceed 2–3 days, which necessitates the intensification of raw material utilization, enhancement of processing depth, and comprehensive valorization through the application of advanced, environmentally safe technologies that ensure the maximum recovery of high-value compounds.

Scientific research has established that in the food industry, comprehensive utilization of raw materials allows for the effective recovery and reuse of nearly all waste streams and co-products. Reintroducing these by-products into production as secondary raw materials enables the creation of new, health-beneficial products through sustainable technologies, thereby generating added value within the food industry [3].

According to FAO data, approximately 50% of total food loss and waste originates from fruits and vegetables, with the majority generated during fresh fruit consumption and industrial processing [4].

In recent years, the management and valorization of solid residues remaining after food production have become a major global environmental challenge. While the industrial processing of fruit crops helps reduce post-harvest losses, it simultaneously produces large amounts of processing by-products, primarily consisting of peels, pulp membranes, juice residues, and seeds.

In our study, we conducted a chemical analysis of by-products derived from the processing of two main persimmon (*Diospyros kaki* L.) cultivars, *Hachiya* and *Hyakume*.

Hachiya: dry matter (by drying) – 18.45%, pectin – 4.5%, dietary fiber – 3.9%, cellulose – 0.8%, total carotenoids – 20.2 mg%, phenolic compounds – 2.0%, protein – 0.48%.

Hyakume: dry matter (by drying) – 20.25%, pectin – 3.9%, dietary fiber – 2.9%, total carotenoids – 18.2 mg%, phenolic compounds – 1.0%.

Unfortunately, only about 0.5% of fruit by-products are currently converted into useful value-added products [5].

The subtropical persimmon is an ancient cultivated species encompassing a large diversity of varieties. Persimmon (*Diospyros kaki* L.) is produced in many countries worldwide, including China, Japan, the United States, Italy, Israel, Brazil, and others. According to current international statistical databases, global persimmon production has reached approximately 5 million tons [6].

In Georgia, the potential exists to produce up to 45,000 tons of fresh fruit annually.

The fruit of the subtropical persimmon possesses high nutritional value, containing 14–24% extractive substances, including 17–20% total sugars, as well as polyphenols, pectic substances, proteins, minerals, vitamin C, α- and β-carotene, and lycopene – compounds that determine its dietary and therapeutic properties [7].

The concentration of nutritional and functional bioactive compounds is higher in the peel than in the pulp; however, the fruit peel is typically disregarded and not subjected to further processing. One of the reasons for this is the broad varietal diversity and pronounced seasonality of persimmon, which complicates raw material processing and the rational utilization of the harvest.

Additionally, a significant proportion of the harvested fruit is non-standard in size and consequently discarded. As a result, 35–40% of the total yield remains unutilized. Another critical issue is that current processing technologies generate 35–45% of by-products and waste, for which no utilization methods currently exist, posing a serious risk of environmental pollution.

The comprehensive and rational utilization of the harvest requires the development of scientifically substantiated technologies for industrial processing. To ensure the full exploitation of the beneficial compounds in persimmon fruits, it is necessary to design integrated processing technologies that consider the chemical and technological characteristics specific to each variety.

Since persimmon contains a significant number of extractive substances and carbohydrates, a considerable portion of these components – along with plant residues – enters the wastewater during processing, resulting in the loss of valuable compounds.

The novelty of this research lies in its focus on the development of new value-added products derived from persimmon and on the valorization of persimmon by-products.

To achieve the complete utilization of persimmon's bioactive components, considering its chemical-technological characteristics, we are developing scientifically validated innovative technologies for both the fruit and its by-products. These include the production of functional extracts and concentrates for preventive use,

as well as nutritional powders and pastes enriched with high levels of carbohydrates (glucose, fructose), phenolic compounds, pectic substances, and carotenoids.

In addition to the main product, further processing of by-products allows the production of nutrient-dense food products and additives of high nutritional value.

The proposed technologies also enable the reduction of energy consumption through the optimization of technological operations, improvement of product quality and yield, and the conversion of processing by-products into useful materials, thereby minimizing adverse environmental impacts.

The proposed methods and technologies include the following:

– Preliminary thermal and CO_2 (carbon dioxide) treatment of raw materials, which will regulate the level of astringency in both the raw material and the extracts, enabling the production of balanced phenolic profiles and high organoleptic quality products such as extracts, powders, pastes, and confitures.
– Intensification of the concentration (thickening) process of persimmon extracts will be achieved through a combination of membrane filtration (fractionation of extracts based on molecular weight) and vacuum evaporation (water removal under low-temperature conditions). This approach enhances energy efficiency while preserving thermolabile bioactive compounds.
– During the extraction of biologically active compounds rich in phenolic constituents from the fruit, the ultrasound-assisted extraction method will be employed. This is one of the recognized "green extraction" techniques, suitable for the efficient recovery of bioactive compounds, particularly polyphenols, while minimizing solvent use and thermal degradation.

Based on the conducted studies, persimmon paste enriched with carotenoids and dietary fiber will be produced from whole fruits, including overripe, transport-unsuitable, and astringent varieties.

The application of high-efficiency methods and advanced technical solutions will enhance the technological processes for by-product utilization, establishing an industrial circular system that ensures the targeted valorization of industrial by-products and promotes the development of the region's agri-food sector.

Conclusion

The implementation of low-waste and zero-waste technologies in industrial production will facilitate the manufacture of valuable food products and additives derived from persimmon raw materials and their processing by-products, while simultaneously contributing to environmental improvement and sustainability.

For the persimmon industry, the current challenge lies in developing strategies that enhance the value of discarded fruits and increase the utilization efficiency of processing by-products, thereby creating opportunities for a more sustainable production system that actively contributes to the circular economy.

Acknowledgment. This research is supported by the Shota Rustaveli National Science Foundation of Georgia (SRNSFG) and is being implemented within the framework of the grant project No. FR-24-4157.

References

1. Erkomaishvili G., Ecology and the Policy of Sustainable Environmental Development in Georgia. Universal Publishing House, October 2021. ISBN: 978-9941-33-060-5.
2. Dvalishvili L., Global Ecological Problems and Georgia. http://pgie.tsu.ge/contentimage/konferenciebi/2017_.pdf
3. Osorio L. L. D. R., Flórez-López E., Grande-Tovar C. D., The Potential of Selected Agri-Food Loss and Waste to Contribute to a Circular Economy: Applications in the Food, Cosmetic and Pharmaceutical Industries. Molecules, 26, 2021, p. 515. https://doi.org/10.3390/molecules26020515
4. Russo C., Maugeri A., Lombardo G. E., Musumeci L., Barreca D., Rapisarda, A., et al., The Second Life of Citrus Fruit Waste: A Valuable Source of Bioactive Compounds. Molecules, 26, 2021, pp. 5991–6020. https://doi.org/10.3390/molecules26195991
5. Lam S. S., Liew R. K., Lim X. Y., Ani F. N., Jusoh A., Fruit Waste as Feedstock for Recovery by Pyrolysis Technique. International Biodeterioration & Biodegradation, 113, 2016, 325–333. https://doi.org/10.1016/j.ibiod.2016.02.021
6. FAO – Food and Agriculture Organization of the United Nations. FAOSTAT Database. Available online: http://www.fao.org/faostat/en/#data (Accessed 25 January 2021), 2017.
7. Ardzenadze M., Papunidze G., Chikovani D., Papunidze S., Davitadze, R. Effect of Heat Treatment on the Physicochemical Properties of Wine and Alcohol Derived from Persimmon. Journal of the National Academy of Sciences "Moambe", Vol. 18, No. 1, 2024, pp. 130–134. http://science.org.ge/bnas/vol-18-1.html.

1st International Scientific Conference "Modern problems in Geophysics", Proceedings,
ISBN 978-9941-36-434-1, ISSN 3088-4349, Tbilisi, Georgia, November 6-8, 2025

CURRENT STATE OF VEGETATION IN THE CARBON POLYGON "WAY CARBON" (CHECHEN REPUBLIC)

***Makhmudova L.Sh, *,**Aristarkhova E.A., *Duskaev M.Z., *Mamadiev N.A.**

**M.D. Millionshchikov Grozny State Oil Technical University, Grozny, Russia*
***M.V. Lomonosov Moscow State University, Moscow, Russia*
kattariss@ya.ru

Abstract. *As part of the monitoring, route studies were conducted at the WayCarbon carbon site (Chechen Republic) in two areas (the operator – M.D. Millionshchikov Grozny State Oil Technical University) in July 2024. Area 1 is located in the Green Zone of Grozny City (nature reserve name) and its surroundings, and Area 2 (Carbon Farm) is located in the reclaimed urban landfill, which is now an experimental area. Complete geobotanical descriptions were compiled for the test sites in the forest and meadow communities. Groups of plant associations and their current state have been identified. The results are important for monitoring the dynamics of the state of the plant cover in the implementation of programs of the carbon polygon for monitoring and control of the balance within natural ecosystems.*

Key Words: *Carbon farm, Chechen Republic, vegetation, ecosystem*

Introduction

The Way Carbon carbon farm, as one of the links in the Russian carbon farm network, is a land area with representative biogeocenosis components, such as topography, vegetation, and soil cover. It is designed to develop and test technologies for controlling the balance of climate-active gases and other parameters relevant to climate change within natural ecosystems.

The Way Carbon experimental sites are used for annual monitoring of vegetation and soil cover, CO2 gas exchange, photosynthesis parameters of woody plants, and more [2, 3, 8]. An important task is to monitor the state of ecosystems in each of the carbon plot areas, primarily the dynamics of vegetation as an indicator of ecosystem health.

Study area, material and methods

In 2024, studies of vegetation cover were conducted in two areas of the carbon polygon. Route studies sites took place in early July 2024 during a period of stable temperatures from +17 to +20 (at night) and from +31 to +35 (during the day) degrees (Celsius).

Complete geobotanical descriptions of test sites in forest and meadow communities and route notes in the form of short descriptions of biotopes and notes were compiled. The coordinates of the test geobotanical sites (points of vegetation description) are presented in Tables 1 and 2.

The surveyed Area 1 is located on the territory of the natural reserve – The Green Zone of the Grozny City (Sheikh-Mansurovsky District, Grozny). The area is located on the right bank of the valley complex of the Sunzha River. The relief is quite flat and poorly dissected, with slopes of 3-5 degrees and heights of 100-200 m (above sea level). The terrace complexes of the Sunzha River are composed of Upper Quaternary deposits of loams, sands, and clays. The soils on the site are brown forest soils under forest vegetation, leached chernozems in areas with reduced lowland forests, and alluvial soils of the meadow-chernozem type in the floodplains of the Sunzha River tributaries [4, 7] (Table 1).

Table 1. GPS coordinates of vegetation descriptions (Area 1)

Point №	1	2	3	4	5	6	7
N	43,25719	43,25867	43,25475	43,2514	43,24497	43,23769	43,237
E	45,63865	45,63925	45,64096	45,63955	45,63662	45,63501	45,62355

The study Area 2 (Table 2), with an area of 24 ha, was previously a heavily disturbed area under an urban unauthorized landfill, and was given for reclamation. It is located in the northeastern part of Grozny, in the Alkhanchurt valley, in the interfluve of the Sunzha River and its left tributary, the Neftyanka River. The area has a slight elevation difference (within 10 m) and a flat terrain, and is composed of loess-like loam. It belongs genetically to the group of dry steppe landscapes, at the moment it is cultivated – here the drip irrigation system is organized and experimental plantings of woody plants with different ecological properties (linden, poplar, ash, willow, etc.) are made, their growth and vital condition are observed. Also on the site there are laid the paths from the fill soil and installed the sensors for soil and meteorological measurements, where regular observations are made within the Way Carbon program.

Table 2. GPS coordinates of vegetation descriptions (Area 2)

Point №	1	2	3	4	5
N	43,35926	43,35895	43,35924	43,35767	43,35652
E	45,74379	45,74323	45,74146	45,74135	45,74021

The descriptions were made according to the generally accepted methodology of field studies of flora and vegetation [1, 6]. Several groups of plant associations were identified.

Results

The area of plot 1 is dominated by broad-leaved valley forests. During the period of their development, these forests were affected by economic activities such as logging, grazing, haymaking, and construction. In areas where forests have been cleared, agriculture and horticulture are also practiced. These landscapes are characterized by the process of steppe formation.

In the area, as well as in other lowland and flat forests of the river valleys in the Central and Western Caucasus, the main tree species is the oak (*Quercus robur*), which grows in various combinations with ash (*Fraxinus excelsior*), maple (*Acer platanoides, A. campestre*), gray and black alder, and wild pear (*Pyrus caucasica*). Dogwood (*Cornus mas, C. sanguinea* subsp. *australis*), hazel (*Corylus avellana*), elder (*Sambucus nigra, S. racemosa*) and viburnum (*Viburnum opulus*) are the most common in the shrub layer. Ivy (*Hedera* sp.), grape-leaved clematis and grapes (*Vitis vinifera* subsp. *sylvestris*) represent extra-tiered vegetation (Table 3).

Table 3. Forest vegetation in the Area 1

Point №	Tree stand formula (tier A)	Crown closeness score	Average height (m) (tier A)	Tree trunks, average diameter(cm)	Projective coverage and average height (tier B)	Average height (cm) (tier C)	Projective coverage (%) (tier C)
1	**5Q.r.4Al.n.1Pr.c. +Ac.p, Ac.c** (*Quercus robur-Alnus nigra-Pyrus caucasica-Acer platanoides-A. campestre*)	0.9	25-28 (max 32)	40-50	35%, 3 m (*Corylus avellana*, *Crataegus* spp.)	10-20	15-20%

2	**8R.ps.2F.ex.+Ac.c.** (*Robinia pseudo-acacia-Fraxinus excelsior-Acer campestre*)	0.7	10-12 (max 15)	20-30	25%, 2-5 m (*Sambucus nigra, S. racemosa, Cornus mas*)	60 (150)	80%
3	**5Ac.p.5Q.r.+Sb.t.** (*Acer platanoides-Quercus robur-Sorbus torminalis*)	0.9	25-30	35-40	30%, 2-3 m (*Sambucus nigra, Swida australis, Corylus avellana*)	25	20%
4	**4C3F.ex.3Ac.p. +P.al.** *Carpinus caucasica-Fraxinus excelsior-Acer platanoides-Populus alba*)	0.9	30	40 (60)	20-25%, (*Corylus avellana*, *Sambucus nigra*)	25-30	35-40%
5	**8F.ex.1Sb.t.1Q.r.** *Fraxinus excelsior-Sorbus torminalis-Quercus robur*)	0.7	16-18 (max 22)	25-35	15-20%, 2-4 m (*Sambucus nigra, S. racemosa, Cornus mas, Crataegus* spp.)	100-150	90%
6	**5F.ex.3C1Ac.p.1Ac.c.** *Fraxinus excelsior-Carpinus caucasica-Acer platanoides-Acer campestre*)	0.8	25 (max 30)	30	10%, 2-3 m (*Corylus avellana, Cornus mas*)	10-25	70%
7	**9F.ex.2Q.r.** (*Fraxinus excelsior-Quercus robur*)	0.8-0.9	30	25-30 (40)	25%, 3 m (*Cornus mas, Corylus avellana*)	20	80%

The classification of tiers (A, B, C) is based on plant life forms [5]

Low forest permeability with the greatest amount of fallen trees and dense shrubs is observed in places along watercourses and tributaries of the Sunzha River. Throughout the area, there is a renewal of forests, with young trees consisting of ash, oak, and maple. In some areas, young trees (ash and maple) reach a height of 1.5-3 m with a coverage of 10-15%. The area is relatively clean.

The study area 2 includes sectors occupied by artificial plantations (crops). The vegetation does not have the high diversity typical of steppe communities. It is mainly composed of weeds and grasses, including fodder and wild representatives of grain crops. The grass cover is low in some areas, and the communities are sparse, with bare soil patches and typical ruderal species of overgrown fields. The vertical structure of some areas is characterized by contrast: there are low-growing and ground-covering species (5-10 cm) such as knotweed, rostraria, stork, and the highest species (150-180 cm) such as sweet clover, coltsfoot, and thistle, while the phytomass of the middle layer (*Ambrosia artemisiifolia, Cynodon dactylon*, *Linaria vulgaris*) is insignificant.

Conclusion

Area 1 is occupied by forest vegetation of oak-ash and oak poly-dominant forests. The current state of the forest vegetation is normal, the forest is not heavily littered with deadwood, and deadwood is present in some areas. It is necessary to preserve these plant communities as unique ecosystems of the broad-leaved forests of the valley landscapes of the Sunzha River and its tributaries.

The studied Area 2 includes sectors occupied by artificial plantations (cultures). The vegetation does not have the high diversity typical of steppe communities. The main communities are represented by weeds and grasses. In the future, it is proposed to establish a recreational cluster on site 2, similar to an eco-park.

Acknowledgements: The work was carried out as part of the state assignment of the M.D. Millionshchikov Grozny State Oil Technical University, № FZNU 2024-0004 “Comprehensive study of greenhouse gas flows in natural and anthropogenically disturbed landscapes of the Chechen Republic and development of scientifically grounded recommendations for restoring the bioresources potential of disturbed lands”.

References

1. Conservation and Restoration of Biodiversity. V.E. Flint, O.V. Smirnova, L.B. Zaugolnova, L.G. Khanina, M.V. Bobrovsky, N.A. Toropova, O.P., Melekhova, and A.G. Sorokin. Edited by M.V. Gusev et al. // Moscow: Scientific and Educational Center Publishing House, 2002, p. 286, (in Russian).
2. Busch F.A., Photosynthetic gas exchange in land plants at the leaf level. In: Covshoff, S. (eds) Photosynthesis. Methods in molecular biology. Vol. 1770. Humana Press, New York, NY, 2018. DOI: 10.1007/978-1-4939-7786-4_2.
3. Farquhar G.D., von Caemmerer, S., Berry, J.A., A biochemical model of photosynthetic CO2 assimilation in leaves of C3 plants. // Planta, Vol. 149, 1980, pp. 78-90.
4. Gulisashvili V., Makhatadze L., Prilipko L., Rastitelnost Kavkaza. // Academ. Academy of Sciences in the Georgian Soviet. Soc. Resp., Tbilisi Forest Institute. Moscow.: Nauka, 1975, p. 236. (in Russian).
5. Korchagin A. Polevaja geobotanika. // Leningrad.: Nauka, Vol. 5, 1976, p. 313. (in Russian).
6. Methods of Field Geobotanical Research. // Botanical Institute of the USSR Academy of Sciences. Moscow-Leningrad: USSR Academy of Sciences, 1938, p. 214. (in Russian).
7. National atlas of soils of the Russian Federation. Moscow, Astrel, 2011, p. 632. (in Russian).
8. Pridacha V.B., Makhmudova L.Sh., Aristarkhova, E.A, Duskaev Kh., Shamkhanov M. Ch., Study of CO2 gas exchange and photosynthesis parameters of woody plants at the experimental site «Chernorechye». Grozny Natural Science Bulletin, Vol. 8, №4 (34), 2024, pp. 89–95. DOI: 10.25744/genb.2023.62.4.015, (in Russian).

1st International Scientific Conference "Modern problems in Geophysics", Proceedings,
ISBN 978-9941-36-434-1, ISSN 3088-4349, Tbilisi, Georgia, November 6-8, 2025

PROSPECTS FOR RECYCLING OF GARBAGE WASTE USING W2E TECHNOLOGY

Kerimov I.A., Debiev M.V.

M.D. Millionshchikov Grozny State Oil Technical University, Grozny, Chechen Republic
ibragim_kerimov@mail.ru

Abstract. *The article provides an overview of the world's methods of energy recycling of waste recycling (W2E technology). Data on the accumulation of municipal solid waste and its processing by the construction of waste processing plants in the Chechen Republic are presented. For the possibility of comparison, information has been collected on the volume of municipal solid waste generated and processed, recycling technologies, and the efficiency of enterprises both in Russia and abroad. Some analysis of the degree of impact of incinerators on the environment is carried out. Attention is drawn to the trends, political and social aspects of the construction of such facilities. The possibility and levers of bringing into effect the widespread introduction of the principle of waste-free production and the role of the architectural appearance of buildings in this matter are being considered. The conclusion is made about the prospects of building a plant based on W2E technology on the territory of the Chechen Republic.*

Key Words: *MSW, energy from waste, incinerator, W2E technologies*

In the European Union, energy waste disposal is considered as part of measures to achieve the goals set by the European Commission in the Waste Disposal Directive. According to CEWEP data for 2017, Finland is the European leader in incineration, sending 58% of garbage for energy disposal, followed by Denmark, Sweden and Norway with 53%, as well as Switzerland with 47%. In Germany, Austria, France and Italy, this figure is about 20-40%. The average for the 28 EU countries was 28% [3, 5, 8]. In the USA in 2017, 12.7% of all solid household waste (MSW) was burned to generate energy, 52.1% of MSW ended up in landfills. In 2018, 68 American plants generated about 14 billion US dollars. kWh of electricity due to the combustion of 29.5 million tons of combustible solid waste.

In Asian countries, against the backdrop of rapid urbanization and annual population and solid waste growth, governments are promoting various energy recycling programs. China's government targets include the processing of half of MSW at W2E plants in the 2020s. The deployment of W2E enterprises in India is slow: just under 300 MW of capacity was installed at the end of 2017, and the country's largest plant (24 MW) was commissioned in New Delhi only in 2017. In Thailand, as part of the Alternative Energy Development Plan, a long–term goal has been set – to increase the installed capacity of waste recycling plants to 550 MW by 2036. Pakistan, Vietnam and Indonesia are encouraging the creation of new enterprises through a guaranteed tariff for electricity [4].

According to the general contractor Octopus Renewables, in the Oldhall industrial area in Erwin (Ayrshire, Scotland), the planned complex will be able to produce 17 MW of electricity. This will allow it to supply energy to 30,000 homes, as well as provide heat and steam to industrial enterprises adjacent to the territory. Meanwhile, construction of the world's largest Waste Energy plant continues in Dubai (United Arab Emirates), which is currently about 45% ready. The plant's capacity will be 1.9 million tons of waste per year, which is about 45% of Dubai's total waste. The company will generate 200 MWh of energy, most of which will be supplied to the local grid, supplying electricity to more than 135 thousand homes annually. The plant, which was first announced in 2018, will allow Sharjah to increase its current waste disposal rate from 76% to 100%. The launch of the enterprise will allow Sharjah to become the first city in the Middle East with zero waste, turning tailings into renewable energy. The company in Sharjah is capable of disposing of 300,000 tons of non-recyclable waste annually, producing 30 MW of electricity for 28,000 homes. At the same time, it will also reduce CO2 emissions in the amount of 450 thousand tons annually [6, 7, 9].

In the capital of the Danish Kingdom (Denmark) The Amager Bakke plant operates in Kopenganen, capable of processing up to 440 thousand tons. garbage per year. Another landmark Danish project in the city of Roskilde, which has a capacity of up to 350 thousand tons of waste per year.

In Sweden in 2017, 34 incinerators accepted 2.4 million tons of Swedish household waste and 1.5 million tons of imported waste. The plant in Poland is capable of incinerating 220 thousand tons of household waste annually. In 2007, the Isseane Syctom plant with a capacity of 460 thousand tons of MSW per year was built in France on the banks of the Seine. In 2011, the largest Riverside plant for the thermal processing of MSW with a capacity of 670 thousand tons of waste per year was commissioned in London. The Gross Green plant in Leeds, England, opened in April 2016, incinerates more than 200,000 tons of waste. A large thermal waste recycling plant in the Netherlands (AEB Amsterdam) is located in Amsterdam and supplies electricity and heat to 75% of all residents and offices in Amsterdam, recycling 300,000 tons of waste per year. In China, about 200 million tons of waste are incinerated per year, which is about 40% of all Chinese garbage. This figure is planned to be raised to 60%. One of the most famous projects today is the Shenzhen East waste–to-Energy Plant, which is capable of processing more than 5,000 tons of garbage per day (182 million tons per year). In Japan, 5% of MSW is subject to burial. 70% is burned by plasma gasification. The capacity of one of the plants here is about 300 thousand tons per year, which is a quarter of the city's garbage. The West Palm Beach waste-to-energy processing plant operates in Florida, the largest city in the United States. Its capacity allows to burn 3 thousand tons of MSW per day, which is 1 million tons per year and is a high-tech plant of the W2E type [10, 11, 12].

The volume of landfills in Russia has reached 4 million hectares, which is comparable to the territory of the Netherlands. Energy recycling should be implemented only within the broader hierarchy of waste management in the areas of prevention, preparation for reuse, recycling, recovery and disposal. W2E plants cause less air pollution than coal-fired thermal power plants, but more than those powered by natural gas.

In the Russian Federation, household waste has only recently been treated as an energy carrier. For example, the current RT-Invest energy waste disposal plant (part of Rostec State Corporation) has confirmed the status of a facility operating on the basis of renewable energy sources, completed the certification procedure for generating equipment and began supplying power to the wholesale electricity market. Since commissioning, the plant has generated almost 70 million kWh, disposed of 150 thousand tons of municipal waste unsuitable for recycling [1, 3].

The RT-Invest energy recycling plant, located in the Urban district of Voskresensk, Moscow region, processes about 2 thousand tons of waste daily. Annually, the plant is able to dispose of 700 thousand tons of waste unsuitable for recycling, generating about 500 million kWh of electric energy. RT-Invest is building three more energy recycling plants in the Moscow Region: in Solnechnogorsk, Naro-Fominsk and Bogorodsky districts. And another factory in the Republic of Tatarstan. In total, five green power plants will produce more than 2.2 billion tons. kWh of energy per year.

In the Krasnodar Territory, it is planned to build two waste incineration plants in the region (using W2E technology). RT-Invest of Rostec State Corporation will be engaged in the construction. During the peak summer period, over 1 million people can be present at the same time on the territory of the city of Sochi, located in the Krasnodar Territory. These are residents and guests of the resort. According to the Sochi city administration, in 2021, the amount of waste from the Belorechensk landfill exceeded 320 thousand tons. Waste recycling issues, as well as problems related to reducing existing landfills around Russian cities, are an important socio-economic task. A significant number of waste incineration plant projects are regularly proposed for consideration by regional leaders and other high-ranking civil servants, and the vast majority of such proposals are rejected [1, 2, 7].

For example, the highest 100% value of electricity consumption in the Chechen Republic in 2024 reached 3615 million kWh, which means that electricity generation from the existing four waste sorting complexes of the republic with a total capacity of 270 thousand tons per year may amount to about 170 million kW.hours per year. This value of electricity generation will provide the republic with up to 5%. In order to reduce the volume of MSW sent for burial in the Chechen Republic, thanks to the financial support of the Ministry of Natural Resources of the Russian Federation in the amount of 725198.6 thousand tons. In 2022, four waste sorting complexes with a total capacity of 270 thousand tons per year were commissioned, including: in Gudermes, with a capacity of 100 thousand tons per year; in Shali, with a capacity of 100 thousand tons per year; in Achkhoy–Martanovsky

municipal district, Samashki village, with a capacity of 50 thousand tons per year; in the Nadterechny municipal district, Znamenskoye village, with a capacity of 20 thousand tons per year.

Thanks to the support of the Ministry of Natural Resources of Russia, in 2022, the Ministry of Construction of the Chechen Republic purchased containers for the separate accumulation of municipal solid waste in the amount of 6927 units. in the amount of 131.062 million rubles. The Government of the Russian Federation has signed an order on the allocation of funds for the construction of a waste recycling plant in Grozny, Chechen Republic, in 2025 for the production of products with the selection of useful fractions at the waste sorting ecotechnopark. Thus, the Chechen Republic has significant potential and prospects for the creation of a modern waste incinerator with electricity generation based on technology.

Conclusions

- It is necessary to carry out systematic explanatory work among the population about the rules of waste management, the need for separate garbage collection.
- As part of the "garbage" reform in Russia, it is useful to adopt the Japanese practice of developing environmental requirements for emissions of harmful substances at MSZ, including in the field of drawing up their own, more stringent than state, environmental standards for individual enterprises.
- The development of enterprises' own environmental standards and their implementation will contribute to improving the environmental performance of individual plants, as well as improving public opinion on thermal waste disposal.
- The development of MSW energy utilization in the Chechen Republic will contribute to improving the environmental situation and create new jobs.

References

1. Alexandrova E.V., Medvedeva N.V., Prospects and directions of development of solid household waste recycling in Moscow. // Scientific potential. No. 4-1 (47), 2024, pp. 60-64.
2. Debiev M.V., Analysis of the effectiveness of the development of the regional energy industry (on the example of the Chechen Republic): PhD Candidate of Technical Sciences: 13.05.01. Volgograd State Technical University. un-T. Volgograd, 2014, p. 212.
3. Kozlovskiy V.A. Kolyasnikov S.A., Construction and use of thermal waste treatment plants as a stage in the development of green economy technologies. // Economics and Management: theory and practice. Vol. 8. No. 1, 2022, pp. 31-36.
4. Mochalova L.A. Grinenko D.A., Yurak V.V., Municipal solid waste management system: foreign and domestic experience // Proceedings of the Ural State Mining University, No. 3. 2017, pp. 97-101.
5. Neumolotova D.O. Modern waste recycling methods: world experience in the development of the industry / Naukosphere. 2021. No. 8-1. pp. 31-41.
6. Osipov V.I., Sustainable development. The ecological aspect / V.I. Osipov. / Bulletin of the Russian Academy of Sciences, 2019, No. 7, pp. 718-727.
7. Pavlovsky A.A., On the issue of the placement of waste-processing facilities in the largest cities of Russia /Astrakhan. // Bulletin of Environmental Education, No. 4 (58), 2020, pp. 44-56.
8. Abraham, A., Park, H., Choi, O., Sang, B.I., Anaerobic co-digestion of bioplastics as a sustainable mode of waste management with improved energy production – a review. // Bioresour. Technol., 322, 2021, 124537. DOI: 10.1016/j.biortech.2020.124537 EDN: EUIMMO.
9. Adaramola, M.S., Quansah, D.A., Agelin-Chaab, M., Paul, S.S., Multipurpose renewable energy resources based hybrid energy system for remote community in northern Ghana. Sustain. Energy Technol. Assessments 22, 2017, pp. 161–170. DOI: 10.1016/j.seta.2017.02.011.
10. Ghimire M., Pandey S., Woo J., Assessing stakeholders' risk perception in public-private partnerships for waste-to-energy projects: a case study of Nepal Energy for Sustainable Development. 2024. T. 79. C. 101414.
11. Hoang A.T., Varbanov P.S., Nižetić S., Sirohi R., Pandey A., Luque R., Ng K.H., Pham V.V., Perspective review on municipal solid waste-to-energy route: characteristics, management strategy, and role in circular economy. // Journal of Cleaner Production. 2022. T. 359. C. 131897.
12. Zhou Y., Zheng S., Lei J., Zi Y., A cross-scale modelling and decarbonisation quantification approach for navigating Carbon Neutrality Pathways in China. Energy Conversion and Management 297, 2023, 117733. DOI: 10.1016/j.enconman.2023.117733.

1st International Scientific Conference "Modern problems in Geophysics", Proceedings,
ISBN 978-9941-36-434-1, ISSN 3088-4349, Tbilisi, Georgia, November 6-8, 2025

TRANSDERMAL DELIVERY OF ENDOGENOUS GROWTH INHIBITING PROTEINS USING POLYVINYL ALCOHOL BASED FILMS

Khvedelidze N.Sh., Markarashvili E.G., Esatia I.GH., Otiashvili D.B., Dzidziguri D.V.

Ivane Javakhishvili Tbilisi State University, Tbilisi, Georgia
Nodar.khvedelidze106@ens.tsu.edu.ge

Abstract: *To evaluate the feasibility of non-invasive, specifically transdermal, delivery of a thermostable growth – inhibiting protein complex (TPC) isolated from adult rat liver, we investigated its effects on cell proliferation in the tissues of juvenile rats when immobilized in polyvinyl alcohol (PVA)-based films of different compositions. It was found that immobilization of TPC in films composed of polyvinyl alcohol and vinyltriethoxysilane (VTES) led to a significant reduction in the mitotic index of liver and kidney cells in experimental animals compared with controls (by 46% and 30%, respectively). In contrast, immobilization of TPC in films composed solely of polyvinyl alcohol did not produce an inhibitory effect in any tissue. In parallel, we examined whether the incorporation of starch as a third component could enhance film solubility and the release of proteins. The results showed that starch addition did not increase film solubility, nor did it alter the antiproliferative activity of the immobilized TPC.*

Key words: *transdermal delivery, polyvinyl alcohol, vinyltriethoxysilane, thermostable protein complex (TPC).*

Introduction

It is well known that various routes of drug administration exist, including oral, intravenous, intramuscular, and subcutaneous delivery; however, each of these routes is associated with specific limitations. These include the low stability of the drug in the gastrointestinal tract and its susceptibility to first-pass metabolism. In addition, drugs may undergo degradation due to enzymatic activity or the acidic environment of the stomach [1]. These and other limitations are particularly pronounced when administering peptide- or protein-based drugs [2]. Therefore, the search for alternative routes for delivering protein compounds into the body is highly relevant. One such route is the transdermal delivery of bioactive substances.

Transdermal drug delivery (TDD) is a noninvasive or minimally invasive method that allows a certain amount of drug to pass through the epidermal layer of the skin by free diffusion or other means and continues to enter the systemic circulation at a controlled rate [3]. When substances are delivered via this route, the aforementioned limitations are largely avoided.

Among transdermal delivery systems, films are the most common and widely used form. The film-forming polymers can be applied alone or in combination with other polymers to produce films with the desired properties [4]. Accordingly, the aim of the present study was to evaluate the feasibility of delivering a thermostable protein complex (TPC), which inhibits cell growth, immobilized in polyvinyl alcohol-based films of varying composition, into the body.

Materials and Methods

Experiments were carried out on non-linear white juvenile rats (7 days old). Animals were housed under controlled conditions at a temperature of 25 ± 2^0C, relative humidity of 60±10%, with room air changes 12-18 times/hour, and a 14/10 h light/dark cycle.

The experimental material consisted of a thermostable protein complex (TPC) isolated from the liver tissue of adult rats using alcohol extraction method [5]. Protein concentration was determined using the Lowry method [6]. Components of the protein complex were identified via native polyacrylamide gel electrophoresis (current: 7 mA; voltage: 100 V), and gels were stained with silver nitrate [7].

Following characterization, the protein complex was immobilized in polyvinyl alcohol (PVA)-based films of varying composition. Films were prepared using a 7% PVA solution (Mw 85,000–124,000). Experimental films included vinyltriethoxysilane (VTES) and 3 mg of lyophilized TPC. For starch-containing films, 5% starch

was incorporated. In a second series, films were prepared similarly but without VTES. Films (50 μm thick) were cut into 15 equal squares (1.5 cm²), each containing approximately 130 μg of immobilized TPC.

To evaluate the effect of TPC immobilized in the films on cell proliferation, liver and kidney tissues were collected from juvenile rats. Two hours prior to tissue collection, control and experimental animals received colchicine injections (1 mg/kg). Tissues were fixed in 4% formaldehyde prepared in phosphate buffer (pH 7.4). Following standard processing, 5 μm-thick sections were prepared and stained with hematoxylin-eosin for microscopic analysis. At least 5000 cells were counted per sample, and the mitotic index was calculated per 1000 cells and expressed in per mille (‰). Each experimental group included a minimum of 12 animals.

In parallel, proliferative activity was also evaluated by Ki-67 immunohistochemistry. After deparaffinization, sections underwent antigen retrieval in citrate buffer, blocking with goat serum, and incubation with Ki-67 antibody (Abcam, 1:100). Detection was performed with biotinylated secondary antibody, DAB, and Mayer's hematoxylin counterstain. Ki-67-positive cells were quantified per 1000 cells (‰).

Data were analyzed using IBM SPSS software. One-way ANOVA was applied to assess differences in mitotic activity across tissue types. Post hoc comparisons were performed using Tukey's HSD test. Results are expressed as mean ± SEM. Differences were considered statistically significant at $P < 0.05$, with confidence levels ranging from 95% to 99%.

Results

At the initial stage of the study, native electrophoretic analysis of the growth-inhibitory thermostable protein complex (TPC) isolated from adult white rat liver was performed. The protein complex was found to contain high-molecular-weight (25–100 kDa) and low-molecular-weight (10–20 kDa) subfractions (Figure 1A). Notably, the low-molecular-weight component (14–17 kDa) has been shown to suppress cellular mitotic activity through transcriptional inhibition [8].

Initially, we assessed whether PVA/VTES films without immobilized protein affected mitotic activity in the liver and kidney tissues of juvenile rats. The analysis indicated no statistically significant differences compared to intact controls, with mitotic indices of 5.56 ± 0.15‰ versus 5.22 ± 0.15‰ in the liver ($p = 0.631$) and 5.52 ± 0.37‰ versus 5.55 ± 0.31‰ in the kidney ($p = 0.999$) (Fig. 1B). In contrast, in the experimental group treated with PVA/VTES films containing the thermostable protein complex (TPC), mitotic activity significantly decreased in both liver (3.02 ± 0.25‰, $p < 0.00005$) and kidney (3.92 ± 0.20‰, $p < 0.005$) tissues (Fig. 1B). Compared to intact controls, the mitotic index was reduced by 46% in the liver and by 30% in the kidney.

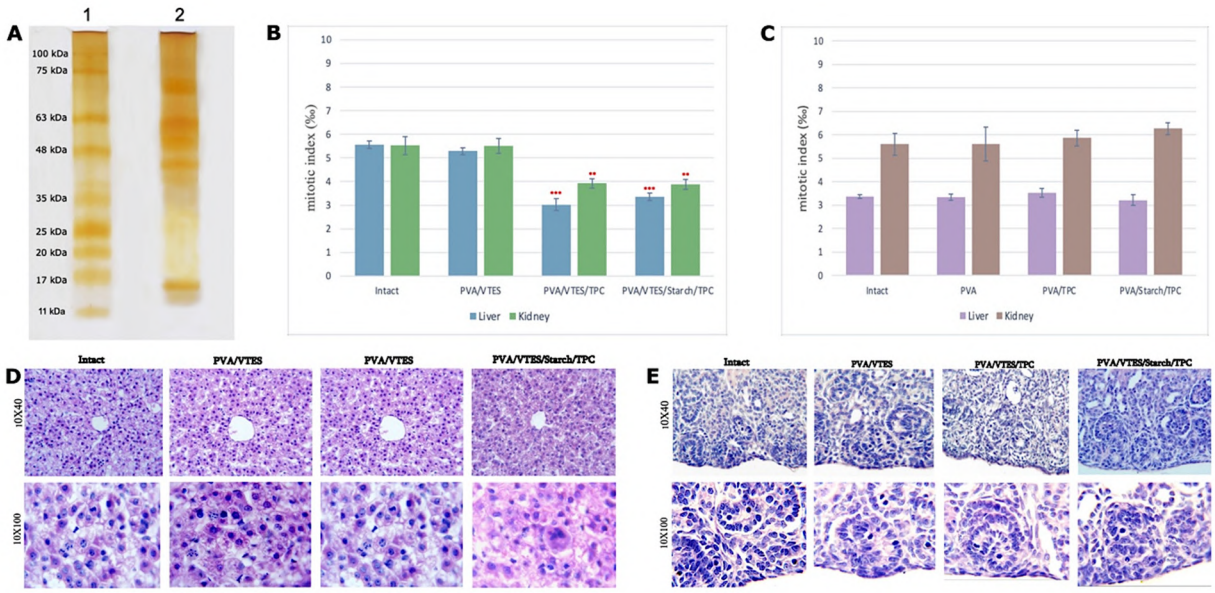

Fig. 1. (A) Native electrophoresis of proteins in a polyacrylamide gradient gel (10–25%): 1 – protein markers; 2 – thermostable protein complex (TPC) from adult white rat liver. (B) Effect of TPC immobilized in PVA/VTES films on mitotic activity in liver and kidney. (C) Effect of TPC immobilized in PVA films on mitotic activity in liver and kidney. (D) Liver histoarchitecture in control and experimental groups. (E) Kidney histoarchitecture in control and experimental groups.

To further evaluate the effect of TPC immobilized in the film on proliferative activity, we performed immunohistochemical analysis using antibodies against Ki-67, a marker of proliferating cells (Fig. 2). Analysis showed that in intact animals, the number of Ki-67-positive cells was 4.06 ± 0.16‰ in the liver (Fig. 2A) and 6.56 ± 0.47‰ in the kidney (Fig. 2B). After treatment with TPC-immobilized films, Ki-67-positive cells increased to 8.02 ± 0.21‰ in the liver and 11.54 ± 0.25‰ in the kidney.

To exclude any potential adverse effects of the polymer and TPC on the morpho-functional activity of cells, we evaluated the impact of the polyvinyl alcohol polymer on the histoarchitecture of liver and kidney tissues of white rats.

Histological examination showed that in both control and experimental animals, hepatocytes in the centrilobular region exhibited cytoplasmic vacuolization, reflecting normal physiological development and glycogen accumulation. The liver parenchyma contained numerous hematopoietic foci, which are characteristic of normal liver up to postnatal day 10 (PND10) [9]. No structural alterations were observed in the portal triads or hepatic sinusoids. Furthermore, no excessive infiltration of circulating cells was detected, indicating the absence of inflammation or other pathological processes (Fig. 1D).

In kidney sections, the cortical regions adjacent to the subcapsular zone exhibited an active nephrogenic area containing proliferating cells, including immature glomeruli and other developing nephron structures. Centrally located glomeruli appeared more mature, reflecting the normal gradient of nephron development. In both control and experimental groups, no evidence of inflammation, necrosis, or fibrosis was observed in the kidney tissue (Fig. 1E).

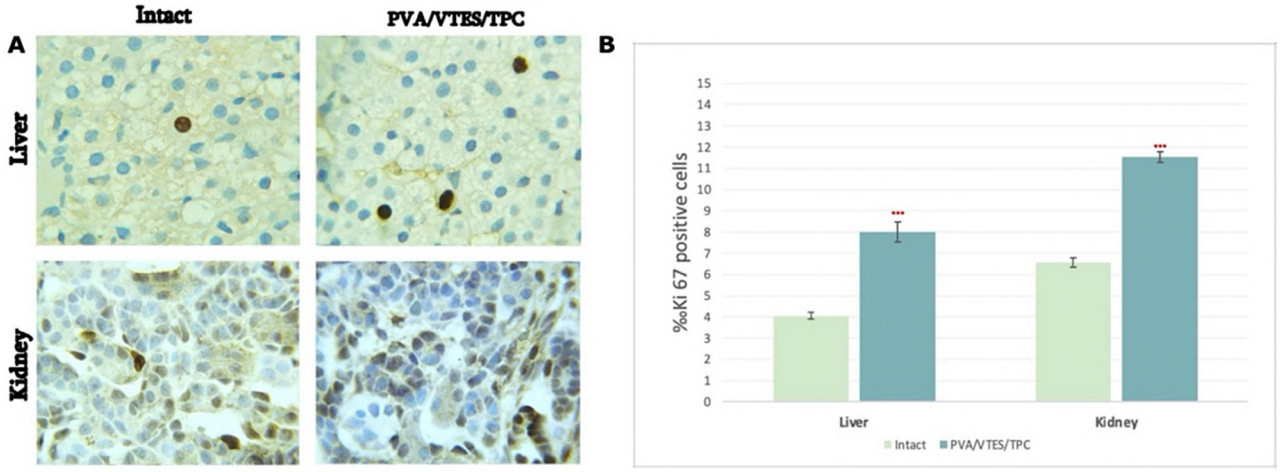

Fig. 2. Immunohistochemical staining using Ki-67 antibodies. (A) Histological sections of liver and kidney from control and experimental animals (10×100). (B) Effect of TPC immobilized in PVA/VTES films on the number of Ki-67-positive cells in liver and kidney.

Additionally, to evaluate the influence of the components used in film preparation on film solubility, a second series of experiments was conducted using TPC immobilized in PVA films without VTES.

In intact animals, the mitotic index was 3.37 ± 0.08‰ in the liver and 5.6 ± 0.46‰ in the kidney. After treatment with TPC immobilized in PVA-only films, mitotic activity in the experimental group was not significantly altered: liver 3.53 ± 0.17‰ ($p > 0.05$) and kidney 5.87 ± 0.33‰ ($p > 0.05$) (Figs. 1C, 2B).

At the next stage of the study, we aimed to improve the properties of PVA-based films of different compositions. To achieve this, starch was used, as it is known from the literature to increase PVA film solubility, water retention, and environmental biodegradability [10], which could enhance the release of immobilized proteins from the film and, consequently, their biological effect.

The study showed that in PVA-only films, the addition of starch did not confer any antiproliferative effect of the immobilized TPC on liver or kidney tissues. In contrast, in PVA/VTES films, the addition of starch did not alter the antiproliferative effect of the immobilized TPC in these tissues.

Discussion

We have previously demonstrated that TPC inhibits cell proliferation through transcriptional suppression [8]. In the present study, we sought to determine whether this endogenous protein complex retains its biological activity in vivo when administered noninvasively via the transdermal route. For this purpose, PVA-based films were used.

To exclude any potential negative (toxic) effects of the polymer films on the morpho-functional activity of cells, we evaluated their impact on liver histoarchitecture in white rats. The results demonstrated that film application did not induce any histoarchitectural changes in the liver or kidney tissues of experimental animals, indicating that the observed reduction in mitotic activity was due to the specific biological action of the protein complex rather than polymer toxicity.

Compared to intact controls, treatment with TPC immobilized in PVA/VTES films resulted in a significant decrease in mitotic activity in both liver and kidney, suggesting that TPC is absorbed through the skin and reaches these organs, retaining its ability to suppress mitotic activity in juvenile rat tissues. In contrast, TPC immobilized in PVA-only films showed no effect on proliferative activity in liver or kidney, indicating that the presence of a crosslinker, in this case VTES, is essential for protein release from the film.

Furthermore, the addition of starch to PVA-only films did not confer antiproliferative activity of immobilized TPC, confirming that VTES is necessary for protein release. In PVA/VTES films, starch addition did not increase the antiproliferative effect of immobilized TPC, which may be due to the limited absorption rate through the skin despite enhanced release from the film.

Interestingly, in tissues of experimental animals, while the mitotic index decreased under TPC treatment, the number of Ki-67-positive cells increased, likely reflecting compensatory accelerated entry of cells into the cell cycle in the juvenile organism.

Conclusion

Based on the results of the present study, we can conclude that the feasibility of using a polyvinyl alcohol/vinyltriethoxysilane (PVA/VTES) film for non-invasive delivery of biologically active substances is directly dependent on the presence of vinyltriethoxysilane. Moreover, the use of starch as an additional component in a film based on polyvinyl alcohol cannot ensure an increase in the penetration rate of the thermostable protein complex through the film, and consequently, does not enhance its inhibitory effect.

References

1. Dahan A, Miller JM, Amidon GL., Prediction of solubility and permeability class membership: provisional BCS classification of the world's top oral drugs. // AAPS J. 11, 2009, 740–6.
2. Wen N.X., Venkatraman S. Protein delivery options: how well have we succeeded? Ther Deliv., 6, 2015, pp. 537–539. doi: 10.4155/tde.15.11.
3. Long L., Zhang J., Yang Z., Guo Y., Hu X., Wang Y., Transdermal delivery of peptide and protein drugs: Strategies, advantages and disadvantages. Journal of Drug Delivery Science and Technology, 60, 2020, 102007.
4. Pünnel L.C., Lunter D.J., Film-Forming Systems for Dermal Drug Delivery. Pharmaceutics. 2021 Jun 23;13(7), 2021, p. 932. doi: 10.3390/pharmaceutics13070932. PMID: 34201668; PMCID: PMC8308977.
5. Balazs A, Blazsek I., Control of cell proliferation by endogenous inhibitors. Akademia Kiado (Budapest) 1979;302
6. Lowry D.H., Rosenbrough N.J., Farr A.L., Randell R.J., Protein measurement with the folin phenol reagent. // J. Biol. Chem. , vol. 193, 1951, pp. 265-275.
7. Davis B., J. Ann. New York Acad. Sei 121, 1964, p. 404.
8. Dzidziguri D, Modebadze I, Bakuradze E, Mosidze G, Berulava M. Determination of The Properties of Rat Brain Thermostable Protein Complex which Inhibit Cell Proliferation. Cell J. 2018 Jan;19(4), 2018, pp. 552-558. doi: 10.22074/cellj.2018.4835. Epub 2017 Nov 4. PMID: 29105389; PMCID: PMC5672093
9. Parker, G. A., Picut, C. A., Hofbauer, C. S. (Eds.). Atlas of histology of the juvenile rat. Academic Press, 2016.
10. Negim, EL-Sayed & Urkimbaeva, P.I. & Rakhmetullayeva, Raikhan & S.T., Primzharova & Yeligbayeva, Gulzhakhan & Kaldybekov, Daulet & Khatib, Jamal & Mun, Grigoriy & Williams, Craig. Improving Biodegradability of Polyvinyl alcohol/Starch Blend films for Packaging Applications. International Journal of Basic and Applied Sciences, 3, 2014 pp. 263-273. doi:10.14419/ijbas.v3i3.2842.

1st International Scientific Conference "Modern problems in Geophysics", Proceedings,
ISBN 978-9941-36-434-1, ISSN 3088-4349, Tbilisi, Georgia, November 6-8, 2025

RESEARCH AND EVALUATION OF THE MAIN QUALITATIVE INDICATORS OF MEDICINAL ROSEMARY SPREAD IN ADJARA-GURIA REGION

Kiknadze, N., Chikovani, D., Gogitidze, A., Kochalidze, J., Tavdgiridze, G.

Batumi Shota Rustaveli State University, Batumi, Georgia
nino.kiknadze@bsu.edu.ge

Abstract. *Analysis of the main qualitative indicators of rosemary (Salvia Rosmarinus) leaves spread in western Georgia is carried out. For the evaluation of the medicinal properties of rosemary of this species, a number of qualitative indicators and elemental composition of plant leaves are carried out.The research objects were rosemary green biomass taken from the Black Sea areas of Batumi, Kobuleti and Ureki. According to the analysis, the titer acidity is low in all three locations, the overall acidity increases simultaneously with the decrease in altitude and increase in humidity. The amount of dry matter in the leaves correlates with relative air humidity.The amount of essential oils, vitamin C and polyphenols is maximum in the raw material taken at Kobuleti location. The content of K, Ca, Mg and P is maximum, while the content of Na is minimal in rosemary leaves taken at Kobuleti location. From micro – and ultramicroelements in rosemary leaves were not observed: Cd, Co, V, as, Li, Ba, Ti, Be, Hg, Sb. Rosemary leaves taken in Kobuleti contain more trace elements-Fe, B, Zn.*

Key words: *Rosemary; Qualitative indicators; Analysis; Morphology; Elements.*

Actuality

Rosemary-a fragrant plant and evergreen shrub, decorated with delicate lilac flowers during the flowering period. "Sea health" – this is how rosmarinus is translated, which is found in the Wild on the Mediterranean coast. The plant is still known from ancient Rome, in the Empire it was called Sea dew. It was believed that it is the sea waves that give rosemary flowers such a beautiful color [1, 13]. The healing properties of rosemary are due to the content in its chemical composition of a number of valuable compounds: rosmarinic acid (it has antioxidant properties that protect cells from damage); carnosic acid, which is also an antioxidant and has an anti-inflammatory effect; ursolic acid, which has antimicrobial and anti-inflammatory effects; Essential oils (cineol, camphor, limonene), flavonoids, Phytoncides, which provide the aroma characteristic of rosemary and a number of therapeutic effects. The complex of the above compounds conditions the healing and other therapeutic effects of rosemary (calming effect, memory improvement) [11, 14]. Studies are underway on the potential of rosemary to treat severe diseases such as Alzheimer's, cancer and diabetes. Essential oil obtained from rosemary leaves and twigs is used in perfumery and medicine. Medicinal Rosemary (Salvia rosmarinus) is an ornamental, fragrant and medicinal plant, has a calming effect, and helps to improve memory. All of the above determined the relevance of the research [3, 11].

Methods Used: Gravimetric [6, 7]; Titrimetric [4, 5]; Plasma Atomic Emission Spectrometry [11, 12].

Research Results

I. Botanical-morphological characterization of rosemary

The Latin name for Rosemary is Rosmarinus L., Kingdom: plants; division: scaly seeds (Angiospermae); class: dicotyledonous; family:Lamiaceae; genus: rosemary [1]. The homeland of the plant is the coastal regions of the Mediterranean Sea. Salvia Rosmarinus is an evergreen shrub 0.5 to 2 meters high with frequent branching, which is due to its ability to make numerous root sprouts. The bushes are grouped, the branches are not branched, they are linear and crowded with sessile abundant leaves, which have a very small stalk.Rosemary is characterized by abundant shearing. The Leaf is elongated, lanceolate-shaped , with a short stalk, the tip is

slightly taper, the edges on the underside of the Leaf seem to be cocked. The upper side of the leaf plate is dark bright green, and the underside is grayish and slightly pubescent. The upper part of the leaf plate is smooth. The grayish-bluish flowers of rosemary are characteristic ortucha of the typical Lamiaceae family, which are collected in a sagebrush inflorescence and are located at the ends of short shoots [2]. The upper lip of the flower is much larger than the lower lip, they sit almost at the ends of the stems in groups, have long stamens and small nut-shaped fruits. Rosemary thrives well in sunny, well-drained soil and is drought tolerant. The evergreen low shrub loves dry and hot places, but if necessary, it can also withstand severe frosts: Mediterranean varieties with frost up to -20°C cannot do anything with it [3].

II. Study of Physico-Chemical indicators of rosemary.

The pH of the aqueous extract of rosemary leaves was: 5.8 in Kobuleti sample; 5.46 in Ureki sample; 5.6 in Batumi sample. The reaction of the aqueous extract of rosemary leaves at all three locations was weak acid. Titer acidity was low in all three locations: 0.040%-Kobuleti; 0.028%-Ureki; 0.02% – Batumi. The overall acidity in the rosemary leaves increased, along with a decrease in height and an increase in tannin. Dry matter content was maximum in Batumi location, minimum – in Kobuleti (Table 1). This indicator was correlated with relative humidity in the study locations. In particular: in Kobuleti, where Leaf humidity was 49.75%, the amount of dry matter was 50.25%; in Batumi, relative humidity was 53.87% and dry matter was 46.13%; in Ureki, leaf humidity was 56.66% and dry matter was 43.34%. The ash content was highest in rosemary leaves taken from Kobuleti location and less-in Ureki and Batumi locations.

Table 1. Dry matter, moisture and ash content in the leaves

№	*Location*	*Dry Matter (%)*	*Humidity, %*	*Ash content*
1	Kobuleti	50,25	49,75	12,85
2	Ureki	43,34	56,66	12,68
3	Batumi	46,13	53,87	11,47

Determination of essential oils in rosemary leaves [8] revealed that their amount was maximum in green biomass taken at Kobuleti location (0.41%). The content of essential oils decreased simultaneously with the decrease in humidity: in Ureki town, their content was 0.37%; in Batumi-0.37%. The content of polyphenols in the raw mass of leaves taken at Kobuleti location was 2.42% [9]. The content of tannins in Ureki and Batumi locations was approximately the same (in Ureki-2.34%; in Batumi-2.32%). The content of vitamin C [10] was high in all three locations, but rosemary leaves taken from Kobuleti location were distinguished in this regard (Table 2).

Table 2. The content of the main qualitative indicators in rosemary leaves

№	**Location**	**Essential Oil Content (%)**		**Polyphenolic Compounds (%)**		**Vitamin C Content, mg%**	
		raw	***in terms of dry matter***	***raw***	***in terms of dry matter***	***raw***	***in terms of dry matter***
1	Kobuleti	0,41	0,82	2,42	5,58	87,47	201,82
2	Ureki	0,37	0,85	2,34	5,07	85,53	185,41
3	Batumi	0,35	0,76	2,32	4,62	86,71	172,56

III. Multi-Element Analysis.

The dominant macroelements in the rosemary leaves were potassium (K) and calcium (Ca)**.** The richest in these elements were the leaves of plants taken from the Kobuleti location, in which the content of the sodium (Na) was minimal (Table 3). They were also distinguished by magnesium (Mg) and phosphorus (P) content, unlike Batumi and Ureki locations. Micro – and ultramicroelements in rosemary leaves were not observed: cadmium (Cd), cobalt (Co), vanadium (V), arsenic (As), lithium (Li), barium (Ba), titanium (Ti), beryllium (Be), mercury (Hg), and antimony (Sb)**.** At all three locations, plant leaves contained negligible

amounts of selenium (Se), chromium (Cr), and nickel (Ni). Rosemary leaves in Kobuleti contain such important microelements as iron (Fe), boron (B), and zinc (Zn).

Table 3. Concentration of Micro- and Ultra-Microelements in Rosemary Leaves

Location	*Fe*	*Si*	*B*	*Al*	*Cu*	*Mn*	*Mo*	*Zn*	*Se*	*Cr*	*Ni*
Batumi	19.7	59.2	1.67	51.4	2.87	5.29	<0.025	5.48	<0.102	<0.279	0.073
Ureki	12.1	51.8	2.46	45.2	2.24	4.05	<0.066	4.21	<0.120	<0.266	<0.058
Kobuleti	30.5	47.0	2.83	28.4	2.42	3.9	0.089	10.2	<0.063	<0.121	0.024

Conclusion

Studies have established that the green biomass of rosemary taken at Kobuleti location was the best in the content of dry matter, essential oils, polyphenols, vitamin C. The dominant macronutrients in rosemary leaves are K, Ca. The leaves of the plant taken at Kobuleti location were distinguished by more Mg and P content, unlike Batumi and Ureki locations, they are also rich in Fe, B, Zn. The green biomass of rosemary taken from Kobuleti seaside was distinguished by the content of dry matter, moisture, essential oils, polyphenols, vitamin C, macro-and microelements. The obtained results show that Rosemary Green biomass inhabiting the Black Sea coast of Adjara-Guria can be successfully used in Pharmacognosy as an excellent antimicrobial, antibacterial, antioxidant, cognitive, anti-inflammatory, digestive system, and perfumery. It can be used as a spice, as well as a decoction and ready-made tea.

References

1. Georgian Soviet Encyclopedia. Tbilisi, Georgia. Volume 8, 1984, p. 422.
2. Gaprindashvili I., Kalandia A., Chikovani D., Standardization and certification of food products, Batumi: Publishing House of Batumi Shota Rustaveli State University, 2024, pp. 99–119.
3. Mwvane Aftiaqi. (n.d.). Rosemary, herbal supplements made from it, and beneficial products for the body. Retrieved August 28, 2025, from https://mwvane-aftiaqi.com/categoriebi.php?id=215
4. Studfile.net. (n.d.). Determination of titratable acidity. Retrieved August 28, 2025, from https://studfile.net/preview/16716105/page:9/
5. Studfile.net. (n.d.). Determination of active acidity. Retrieved August 28, 2025, from https://studfile.net/preview/16716105/page:9/
6. International Organization for Standardization. (2013). ISO 1572:2013 – Tea – Method for preparation of ground sample and determination of dry matter content. Retrieved August 28, 2025, from https://meganorm.ru/Index2/1/4293775/4293775983.htm
7. International Organization for Standardization. (2013). ISO 1575:2013 – Tea – Methods for determining total, water-insoluble and water-soluble ash. Retrieved August 28, 2025, from https://meganorm.ru/Data2/1/4294826/4294826205.pdf
8. International Organization for Standardization. (2014). ISO 875:2014 – Essential oil raw materials – Flower-herbal – Methods of sampling, determination of moisture, impurities and essential oil. Retrieved August 28, 2025, from https://files.stroyinf.ru/Data/661/66103.pdf
9. International Organization for Standardization. ISO 14502-1:2005 – Determination of substances characteristic of green and black tea – Part 1: Content of total polyphenols in tea – Colorimetric method using Folin-Ciocalteu reagent. Retrieved August 28, 2025, from https://www.iso.org/standard/31356.html
10. International Organization for Standardization. ISO 6557-2:1984 – Determination of ascorbic acid (vitamin C) and its compounds, 1984. [PDF file]. (Local access: file:///C:/Users/ICP/Downloads/AB-098_5.pdf)
11. Kiknadze, N., Comparative characteristic of some qualitative indicators of black and green bay tea based on expertise research and evaluation. In Proceedings of the International Scientific-Practical Conference "Functional Destination Foods Production Innovative Technologies", 2015, April 17, pp. 266–269. Kutaisi: Akaki Tsereteli State University.
12. Shimadzu Corporation. (n.d.). Simultaneous ICP Atomic Emission Spectrometers. ICPE-9820 series. Retrieved August 28, 2025, from https://www.shimadzu.com/an/products/elemental-analysis/inductively-coupled-plasma-emission-spectroscopy/icpe-9800-series/index.html
13. Nieto G., Ros G., Castillo, J., Antioxidant and antimicrobial properties of rosemary (Rosmarinus officinalis L.): A review. Medicines, 5(3), 2018, p. 98. https://pubmed.ncbi.nlm.nih.gov/30181448/
14. Ghasemzadeh Rahbardar M., Hosseinzadeh H., Therapeutic effects of rosemary (Rosmarinus officinalis L.) and its active constituents on nervous system disorders. Iranian Journal of Basic Medical Sciences, 23(9), 2020, pp. 1100–1112. https://doi.org/10.22038/ijbms.2020.45269.10541

1st International Scientific Conference "Modern problems in Geophysics", Proceedings,
ISBN 978-9941-36-434-1, ISSN 3088-4349, Tbilisi, Georgia, November 6-8, 2025

MODELING AS A TOOL FOR PREDICTING URBAN DEVELOPMENT: THE CASE OF BREST, REPUBLIC OF BELARUS

***Shchasnaya I., **Krupskaya M.**

**Belarusian state University, Belarus, Minsk*
***UE "BELNIIPGRADOSTROITELSTVA", Belarus, Minsk*
irina.schastnaya@gmail.com

Abstract. *The work considers the application of a two-layer SD-ANN-CA model for exploring trends in land use and land cover (LULC) and making LULC prediction for 2030 and 2035 for the city of Brest as a case study. Within the framework of the study a set of input data is identified, the features of the used model are emphasised and a workflow for its use is defined.*

Key Words: *modelling, prediction, land use, planning constraints, urban planning*

Introduction

The land use and land cover (LULC) prediction is of great importance for urban planning, especially in multifunctional cities, where planners must not only consider a wide range of factors – most notably spatial, temporal, and socio-economic influences on urban development – but also place emphasis on maintaining the quality of the environment. In today's context, modeling provides the most reliable approach for producing such comprehensive predictions [1].

In recent years, LULC models have advanced significantly – from the earliest quantitative approaches, which merely projected land-use demand and broad LULC trends, to modern spatial methods that simulate and reconstruct the spatial structure of land use [2]. Commonly used quantitative approaches include system dynamics (SD), grey models (GMs), Markov models, and artificial neural networks (ANN). Common spatial approaches include the Conversion of Land Use and its Effects model (CLUE), the Dynamic Land System model (DLS), cellular automata (CA), and multi-agent systems (MAS). Among these, CA models stand out for their dynamic evolution mechanisms and their capacity for fine-scale, high-resolution analysis, which has been extensively applied over the past decades [3, 4].

Unlike many studies that focus only on individual districts or a single type of land use, the approach discussed here adopts a more comprehensive perspective. The modeling is conducted at the scale of a major regional city and incorporates an extensive set of land-use categories. Although the model is not fully exhaustive, its elaboration is sufficient for city-level analysis, as it treats the entire urban area as a single system and integrates dynamic indicators of its development over the period 2015–2025.

Study area, material and methods

The city of Brest, which is one of the regional centres of the Republic of Belarus (population ~340 thousand people, area 146 km^2), was chosen as the object of the study as a representative example of a large city with a complex and multifunctional land use structure. Its territory is marked by sharp zoning contrasts: industrial and residential districts are concentrated in the east and northeast, while the western and southern parts preserve the natural landscapes of the Polesian Lowland, including forests and wetlands. Of particular importance for modeling is the extensive network of green spaces and the riparian ecosystems of the Mukhavets and Bug rivers, which form the city's ecological framework and serve as one of the key limiting factors for spatial development. This combination of urbanized areas and valuable natural complexes makes Brest a suitable case for applying LULC prediction methods at the city scale.

This study requires two types of data: spatial and numerical (Table 1). To ensure proper model operation, spatial data must be standardized, and vector data converted into raster format. The coordinate system is

unified using Pulkovo 1942/CS63 zone C1 (EPSG:3351) through the raster projection tool. The pixel size for all spatial data is set to 30 m using the resampling tool. The number of rows and columns in the raster data is standardized using the "Clip" tool. To ensure compatibility between QGIS and MATLAB, the raster format is additionally converted to ASCII-GRID format.

The data for the study are from open sources: raster images of Sentinel-2 mission, vector data of OpenStreetMap and official statistical indicators published by the National Statistical Committee of the Republic of Belarus.

Table 1. Set and specification of the input data.

Data type	Data	Time period	Description	Format / Resolution
Spatial Data	Remote sensing imagery	2015 2020 2025	Three input datasets representing land-use conditions (processed remote sensing data)	Raster, 10 m
	Digital Elevation Model (DEM)	2025	Surface elevation data obtained from DEM analysis; used as a model constraint	Raster, 30 m
	Road network	2025	Constraint for the model	Shapefile (lines)
	Water bodies	2025	Constraint for the model	Shapefile (polygons)
	Residential areas	2025	Constraint for the model	Shapefile (polygons)
	Administrative boundaries	2025	Delimitation of the modeling area	Shapefile (polygons)
	Protected areas	2025	Constraint set for the model (protected areas, green spaces, riparian buffers)	Shapefile (polygons)
Numerical Data	Demographic data	2015-2025	Input for the SD model: urban and rural population, population growth rates	PDF
	Industrial output	2015-2025	SD model: value added of primary, secondary, and tertiary sectors, along with their growth rates	PDF
	Agricultural output	2015-2025	SD model: production volumes, per capita consumption levels	PDF
	Urban development data	2015-2025	SD model: urbanization level, residential area, housing demand, land allocation by categories	PDF

The acquisition of land-use data involves image mosaicking, clipping, calibration, and supervised classification in QGIS. For the purposes of this study, the territory of Brest is categorized into six land-use types: cropland, forest, grassland, water bodies, built-up areas, and other land. Processing of DEM data for slope and elevation is conducted using 3D analysis tools, while Euclidean distances for road networks, water bodies, and settlements are calculated through spatial analysis tools.

To examine land-use change across the six categories – cropland, forest, grassland, water bodies, built-up areas, and other land – a two-layer model is employed, integrating system dynamics (SD) and an artificial neural network–cellular automata (ANN-CA) framework [5].

The upper layer of the model defines constraints. These include meso-level drivers influencing land-use change and macro-level projections of demand for each land-use category. This component, developed through system dynamics, captures general principles: it identifies factors affecting land-use change, their key interrelations, and overall demand for each category. In effect, the upper layer communicates to the lower one how much land of each type will be required in the future.

The lower layer is designed to forecast and spatially allocate all six land-use categories under the imposed constraints. Within the ANN stage of the ANN-CA model, the neural network is trained on the factor relationships and feedbacks identified in the SD layer to establish transition rules for subsequent simulation

by cellular automata. These rules parameterize the CA, which operates with consideration of micro-spatial constraints – namely, centers of land-use gravity, or areas around which changes are most likely to occur, derived using a gravity-transfer method. In this way, the lower layer determines the precise spatial distribution of land-use categories on the map.

Furthermore, the ANN-CA outputs are validated against the macro-level constraints: a forecast map is accepted only if the deviation between the areas of the four key categories (arable land, built-up land, forest, and grassland) as projected by the SD model and as simulated by ANN-CA does not exceed ±5%. The overall structure of the model is presented in Fig. 1.

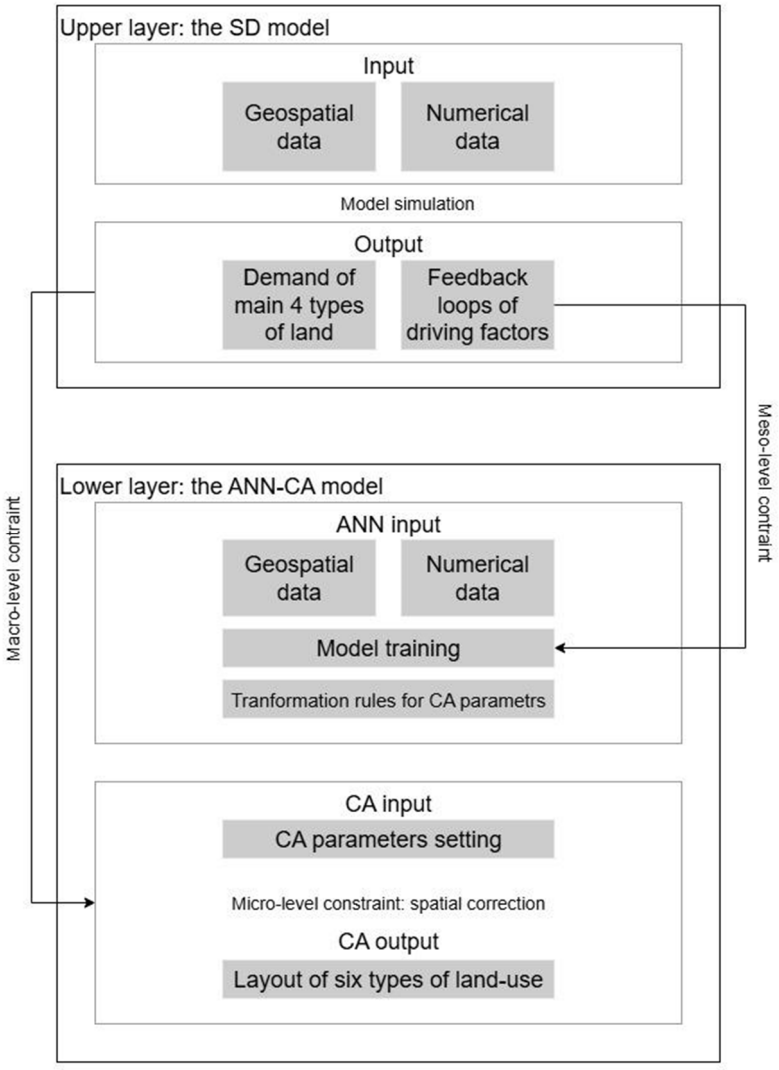

Fig. 1. Two-layer SD-ANN-CA model execution procedure.

To compare forecast results with the actual state of land use and land cover, the following equations were employed to assess model accuracy:

$$OA = N_{inc}/N_{tot}\ OA = N_{inc}/N_{tot} \tag{1}$$

$$k = (P_a - P_e)/(P_i - P_e)\ k = (P_a - P_e)/(P_i - P_e) \tag{2}$$

Equation (1) calculates the proportion of misclassified pixels relative to the total number of pixels in the samples, where N_{inc} N_{inc} denotes the number of pixels incorrectly predicted by the model and N_{tot} N_{tot} the total number of pixels. Equation (2) is applied in evaluating CA simulations, where kk represents the kappa coefficient; Pa indicates actual accuracy; Pe the expected accuracy; Pi and the ideal accuracy (100%).

Moving to the next stage – specifying model constraints – it is important to note that LULC outcomes result from the interplay between anthropogenic and natural factors, which include political, institutional, economic, cultural, technological, and environmental drivers. In existing studies, two principal categories are generally considered: geographical (including natural) and socio-economic factors.

Spatial (geographical) drivers of land-use change are typically consistent across studies and include elevation, slope, distance to main roads, distance to water bodies, and distance to administrative centers. These factors are also incorporated in the considered model. Because spatial variables vary widely in scale and range (e.g., slopes from 0° to over 30°, road distances from 0 to 5,000 m), they are normalized to a 0–1 range. Normalization accelerates neural network training while preserving the original probability distribution.

In contrast, the proposed set of socio-economic drivers is broader and more diverse. In the model, the upper SD layer captures socio-economic trends for the period 2015–2025. When combined with spatial drivers, this enables the transfer of significant socio-economic dynamics into the ANN-CA learning process, thereby improving the capacity to identify land-use change patterns. Selected socio-economic indicators include demographic data, measures of industrial and agricultural output, and information on urban development.

Furthermore, the study extends traditional LULC analysis by incorporating constraint layers representing protected areas: protected areas, green spaces, and riparian buffers. A defining feature of this approach is the assignment of land-use categories within these zones as fixed and unchangeable, thereby safeguarding their ecological potential throughout the predicting horizon.

Conclusion

The study considered a method for predicting land use and land cover (LULC) change based on an integrated two-layer model that combines system dynamics for the quantitative assessment of land demand with an artificial neural network–cellular automata (ANN-CA) framework for spatial simulation.

Considered method encompasses the full research cycle: from data collection and preprocessing of spatial and statistical information, specification of constraints, and construction of a transition matrix, to calibration, presicting, and the evaluation of both predictive and spatial accuracy. A key feature of the approach is the integration of macro-level constraints derived from the system dynamics model, which ensures quantitative consistency of land allocation, as well as the application of ANN-CA, which captures local trends and spatial configurations of change.

The implementation of this method enables the generation of reproducible scenarios of land use development for 2030 and 2035, while also providing insights into the respective contributions of macro- and micro-level factors to territorial transformation. The study outcomes will have practical relevance for spatial planning, environmental management and sustainable regional development strategies.

References

1. Laurini R., Promises of Artificial Intelligence for Urban and Regional Planning and Policymaking. // In: Laurini R., Nijkamp P., Kourtit K., Bouzouina L. (eds). Knowledge Management for Regional Policymaking. Springer, Cham, 2022, pp. 3–20. https://doi.org/10.1007/978-3-031-15648-9_1
2. Li X., Gong P., Urban growth models: progress and perspective. // Science Bulletin, 61, 2016, pp. 1637–1650. https://doi.org/10.1007/s11434-016-1111-1
3. Wang R., Derdouri A., Murayama Y., Spatiotemporal Simulation of Future Land Use/Cover Change Scenarios in the Tokyo Metropolitan Area. // Sustainability, 10, 2018, 2056, pp. 1–18. https://doi.org/10.3390/su10062056
4. Liu X., Liang X., Li X., Xu X., Ou J., Chen Y., Li S., Wang S., Pei F., A future land use simulation model (FLUS) for simulating multiple land use scenarios by coupling human and natural effects. // Landscape and Urban Planning, 168, 2017, pp. 94–116.
5. Zhao J., Zhu X., Zhang F., Gao L., A Two-Layer SD-ANN-CA Model Framework for Multi-Typed Land Use and Land Cover Change Prediction under Constraints: Case Study of Ya'an City Area, Western China. // Land, 13, 2024, 714, pp. 1–20. https:/doi.org/10.3390/land13050714

1st International Scientific Conference "Modern problems in Geophysics", Proceedings,
ISBN 978-9941-36-434-1, ISSN 3088-4349, Tbilisi, Georgia, November 6-8, 2025

DATA ANALYSIS ON MEAN MONTHLY AND ANNUAL CONCENTRATIONS OF PARTICULATE MATTER PM2.5 AND PM10 IN TBILISI IN 2017-2024

[*]Bliadze T., [**]Berdzenishvili N., [*]Chikhladze V., [*]Chkhitunidze M., [*]Kirkitadze D.

[*]Mikheil Nodia Institute of Geophysics of Ivane Javakhishvili Tbilisi State University, Tbilisi, Georgia
[**]I. Gogebashvili Telavi State University, Telavi, Georgia
teimuraz.bliadze@gmail.com

Abstract. *The article presents the results of statistical analysis of mean monthly and annual concentrations of particulate matter PM2.5 and PM10 at three points in Tbilisi (Kazbegi av., Tsereteli av. and Varketili) for 2017-2024. An analysis of correlations between the specified characteristics of air pollution was carried out. The variability of mean annual values of PM2.5 and PM10 during the observation period under study was studied. In particular, it was found that in 2022-2024, compared to 2017-2019, an average decrease in the concentration of PM2.5 and PM10 was recorded for all observation points. As before, in general, over the entire observation period, the mean annual concentration of PM2.5 and PM10 were above the permissible limit.*

Key words: *Atmospheric aerosols, particulate matter, PM2.5, PM10.*

Introduction

Over the past sixty years, various studies of atmospheric aerosols have been conducted at the M. Nodia Institute of Geophysics, TSU, including systematic measurements, field work, laboratory experiments, statistical analysis of official data, and theoretical modeling [1–13].

In particular, the results of studies of photochemical smog formation processes in Tbilisi are presented in [1]. The works [4,5] compare the level of aerosol air pollution with PM2.5 and PM10 particles in four populated areas of Georgia – Tbilisi, Batumi, Kutaisi, and Rustavi. The work [10] numerically simulated the change in time and space of the concentration of PM10 scattered in the atmosphere of the city of Kutaisi during the calm period, etc.

Particular attention was paid to studies of the dynamics of aerosol air pollution in Tbilisi, the results of which were constantly updated as new data became available [11–13].

This work is a continuation of previous studies. Below are the results of statistical analysis of mean monthly and annual concentrations of PM2.5 and PM10 particles in Tbilisi for 2017–2024.

Study area, material and methods

Study area – three locations of Tbilisi (A. Kazbegi av. – KZBG, A. Tsereteli av. – TSRT, Varketili – VRKT). Coordinates of these locations of air pollution measurements points in [11] are presented.

The data of the Georgian National Environmental Agency about the daily mean values of dust concentration (atmospheric particulate matter – PM2.5 and PM10) [http://air.gov.ge/reports_page] that averaged on three indicated stations are used. Period of observation: January 2017 – December 2024.

In the proposed work the analysis of data is carried out with the use of the standard statistical analysis methods [14]. Missed data of time-series of observations were restored in the correspondence with the standard methods.

The following designations will be used below: Min – minimal values; Max – maximal values; St Dev – standard deviation; C_v = 100·St Dev/Average, coefficient of variation (%); R coefficient of linear correlation. KZBG(PM2.5), KZBG(PM10) …etc. – concentrations of particulate matter PM2.5 and PM10 on the Kazbegi av. measurement point, etc.; Av(PM2.5) and Av(PM10) – averaged over all three stations PM2.5 and PM10.

In correspondence with the standards of the World Health Organization maximum permissible concentration (MPC) composes: annual mean for PM2.5 – 10 mcg/m³ and for PM10 – 20 mcg/m³ [15]. In the text below, the dimension of aerosol concentration (mcg/m³) is mostly omitted.

Results and discussion

Results in Table 1 and Fig. 1,2 are presented.

In Table 1 statistical characteristics of mean monthly values of PM2.5 and PM10 in Tbilisi in 2017-2024 are presented. In Fig. 1 time-series of mean annual values of PM2.5 and PM10 at three points in Tbilisi and their averaged values for all measurement points in 2017-2024 are presented. In Fig. 2 data about mean annual values of PM2.5 and PM10 in three points in Tbilisi in 2017-2019 and 2022-2024 are presented.

Table 1. Statistical characteristics of mean monthly values of PM2.5 and PM10 in Tbilisi in 2017-2024.

Variable	KZBG (PM2.5)	KZBG (PM10)	TSRT (PM2.5)	TSRT (PM10)	VRKT (PM2.5)	VRKT (PM10)	Av (PM2.5)	Av (PM10)
Max	32.7	61.2	43.6	88.1	39.3	60.1	34.4	58.6
Min	0.3	11.3	0.8	5.4	0.5	9.3	0.5	8.6
Average	14.8	34.1	19.6	45.3	16.1	32.6	16.8	37.3
St Dev	5.6	8.9	7.7	15.8	7.2	9.3	6.6	9.6
C_v, %	37.6	26.2	39.2	34.9	44.8	28.6	39.4	25.8
	Correlation Matrix							
KZBG(PM2.5)	1	0.74	0.90	0.52	0.96	0.83	0.98	0.78
KZBG(PM10)	0.74	1	0.67	0.50	0.65	0.83	0.70	0.85
TSRT(PM2.5)	0.90	0.67	1	0.73	0.90	0.74	0.96	0.85
TSRT(PM10)	0.52	0.50	0.73	1	0.48	0.47	0.60	0.85
VRKT(PM2.5)	0.96	0.65	0.90	0.48	1	0.84	0.98	0.73
VRKT(PM10)	0.83	0.83	0.74	0.47	0.84	1	0.82	0.84
Av(PM2.5)	0.98	0.70	0.96	0.60	0.98	0.82	1	0.81
Av(PM10)	0.78	0.85	0.85	0.85	0.73	0.84	0.81	1

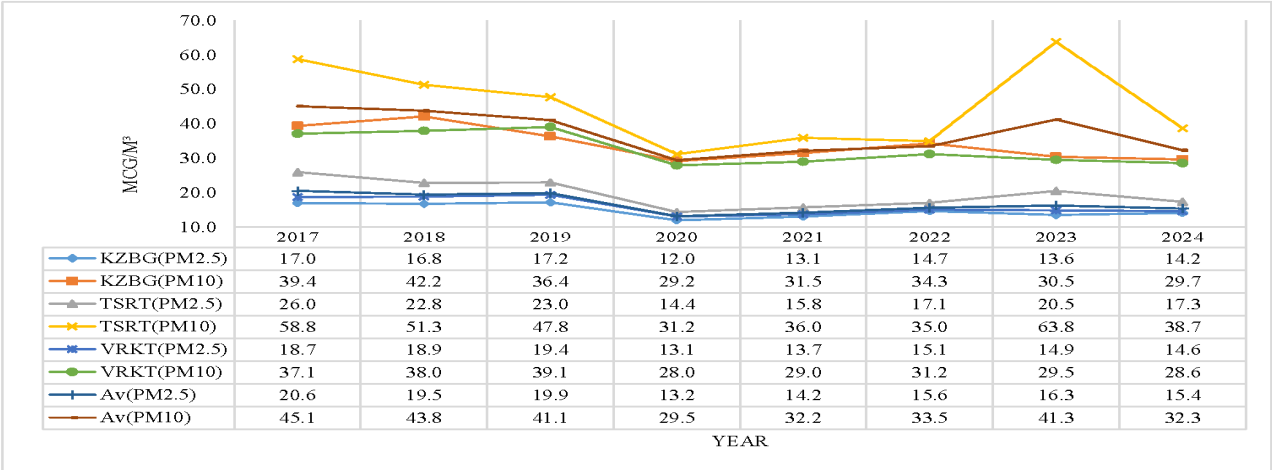

	2017	2018	2019	2020	2021	2022	2023	2024
KZBG(PM2.5)	17.0	16.8	17.2	12.0	13.1	14.7	13.6	14.2
KZBG(PM10)	39.4	42.2	36.4	29.2	31.5	34.3	30.5	29.7
TSRT(PM2.5)	26.0	22.8	23.0	14.4	15.8	17.1	20.5	17.3
TSRT(PM10)	58.8	51.3	47.8	31.2	36.0	35.0	63.8	38.7
VRKT(PM2.5)	18.7	18.9	19.4	13.1	13.7	15.1	14.9	14.6
VRKT(PM10)	37.1	38.0	39.1	28.0	29.0	31.2	29.5	28.6
Av(PM2.5)	20.6	19.5	19.9	13.2	14.2	15.6	16.3	15.4
Av(PM10)	45.1	43.8	41.1	29.5	32.2	33.5	41.3	32.3

Fig. 1. Time series of mean annual values of PM2.5 and PM10 at three points in Tbilisi and their averaged values for all measurement points in 2017-2024.

In particular, as follows from Table 1 and Fig. 1, in 2017-2024 the range of variability of the average values of PM2.5 for the specified period of time is from 14.8 (KZBG) to 19.6 (TSRT), and PM10 – from 32.6 (VRKT) to 45.3 (TSRT). The smallest variations in PM2.5 values is observed at KZBG (C_v = 37.6%), the largest ones at

VRKT (C_v = 44.8%). The smallest variations in PM10 values is observed at KZBG (C_v = 26.2%), the largest ones at TSRT (C_v = 34.9%). In general, the variations in PM2.5 values are higher than those of PM10.

The R value for PM2.5 varies from 0.90 (high correlation, pair TSRT (PM2.5) -VRKT (PM2.5) and pair KZBG(PM2.5) – TSRT (PM2.5)) to 0.98 (very high correlation, pair Av(PM2.5) – KZBG(PM2.5)).

The R value for PM10 varies from 0.47 (low correlation, pair VRKT(PM10) – TSRT(PM10)) to 0.85 (high correlation, pair Av(PM10) – KZBG(PM2.5) and pair Av(PM10) – TSRT(PM10)).

The R value between PM2.5 and PM10 for individual stations varied from 0.73 (high correlation, TSRT) to 0.84 (high correlation, VRKT). Between Av(PM2.5) and Av(PM10) the R value is 0.78 (high correlation).

The average maximum values of PM2.5 and PM10 for all points (Fig. 2) were observed in 2017 (20.6 and 45.1, respectively), the minimum – in 2020 (13.2 and 29.5, respectively, the period with COVID-19). At the same time, the maximum excess of annual concentrations of PM2.5 and PM10 over their maximum permissible limits was 106 and 126%, respectively, and the minimum was 32 and 47%, respectively.

The PM10/ PM2.5 ratio for KZBG and TSRT is on average 2.3, and for VRKT – 2.0.

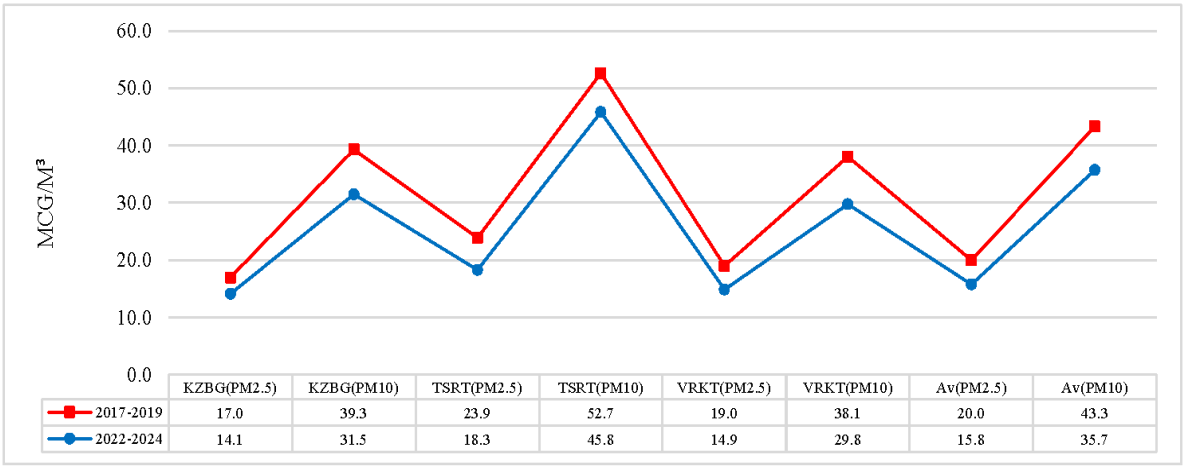

	KZBG(PM2.5)	KZBG(PM10)	TSRT(PM2.5)	TSRT(PM10)	VRKT(PM2.5)	VRKT(PM10)	Av(PM2.5)	Av(PM10)
2017-2019	17.0	39.3	23.9	52.7	19.0	38.1	20.0	43.3
2022-2024	14.1	31.5	18.3	45.8	14.9	29.8	15.8	35.7

Fig. 2. Mean annual values of PM2.5 and PM10 in three points in Tbilisi and their averaged values for all measurement points in 2017-2019 and 2022-2024.

In Fig. 2 data about mean annual values of PM2.5 and PM10 in three points in Tbilisi and their averaged values for all measurement points in 2017-2019 and 2022-2024 are presented. As follows from this Figure, in the last three years, compared to 2017-2019, there has been a noticeable decrease in PM2.5 and PM10 concentrations. The greatest decrease in these concentrations is observed in VRKT (by 6.8 and 8.3, respectively), the smallest – in TSRT (by 2.8 and 6.8, respectively).

Conclusion

In the future, as new data accumulates, it is planned to continue similar studies for Tbilisi and other regions of Georgia.

Acknowledgement. The authors are grateful to the chief of the atmospheric physics department of M. Nodia Institute of Geophysics A. Amiranashvili for assistance in the fulfillment of this work.

References

1. Amiranashvili A., Bliadze T., Chikhladze V., Photochemical smog in Tbilisi. // Monograph, Trans. of Mikheil Nodia institute of Geophysics, ISSN 1512-1135, vol. 63, Tb., 2012, p. 160. (in Georgian).
2. Kirkitadze D., Nikiforov G., Chankvetadze A., Chkhaidze G., Some Results of Studies of Atmospheric Aerosols in M. Nodia Institute of Geophysics in the Recent Three Decades. // Trans. of Mikheil Nodia Institute of Geophysics, ISSN 1512-1135, vol. 66, Tbilisi, 2016, pp. 178-185, (in Russian).
3. Amiranashvili A., Chargazia Kh., Intra-Annual and Seasonal Variations of Sub-Micron Aerosols Concentration and their Connection with Radon Content in Surface Boundary Layer of Tbilisi City. // Bulletin of the Georgian National Academy of Sciences, vol. 10, N 2, 2016, pp. 72-78.

4. Bliadze T.G., Kirkitadze D.D., Tchankvetadze A. Sh., Chikhladze V.A., Comparative Analysis of Air Pollution in Tbilisi and Kutaisi. // Int. Sc. Conf. „Modern Problems of Ecology“, Proceedings, ISSN 1512-1976, v. 6, Kutaisi, Georgia, 21-22 September, 2018, pp. 157-160.
5. Bliadze T., Chikhladze V., Chkhitunidze M., Kirkitadze D., Comparative Analysis of Mean Monthly and Annual Concentrations of Particulate Matter PM2.5 and PM10 in Tbilisi, Batumi, Kutaisi and Rustavi in 2019-2022. // Int. Sc. Conf. "Geophysical Processes in the Earth and its Envelopes". Proceedings, ISBN 978-9941-36-147-0, Publish House of Iv. Javakhishvili Tbilisi State University, November 16-17, 2023, pp. 292-296. http://openlibrary.ge/handle/123456789/10459.
6. Amiranashvili A.G., Kirkitadze D.D., Kekenadze E.N., Pandemic of Coronavirus COVID-19 and Air Pollution in Tbilisi in Spring 2020. // Journal of the Georgian Geophysical Society, ISSN: 1512-1127, Physics of Solid Earth, Atmosphere, Ocean and Space Plasma, v. 23(1), 2020, pp. 57-72.
7. Kirkitadze D., Changeability of Monthly Mean Values of PM2.5 and PM10 in Three Points of Tbilisi from January 2017 to October 2021. Pandemic of Coronavirus Covid-19 and PM2.5/10 in Tbilisi from March 2020 to August 2021. // Int. Sc. Conf. „Natural Disasters in the 21st Century: Monitoring, Prevention, Mitigation“, Proc., ISBN 978-9941-491-52-8, Tbilisi, Georgia, December 20-22, 2021. Publish House of Iv. Javakhishvili Tbilisi State University, Tbilisi, 2021, pp. 101 – 105.
8. Kirkitadze D., Variability of Monthly Mean Values of PM2.5 and PM10 in Three Points of Tbilisi from January 2017 to May 2020. Pandemic of Coronavirus COVID-19 and PM2.5/10 in Spring 2020 in Tbilisi. // Int. Sc. Conf. „Modern Problems of Ecology“, Proc., ISSN 1512-1976, v. 7, Tbilisi-Telavi, Georgia, 26-28 September, 2020, pp. 268-272.
9. Kukhalashvili V., Pipia M., Gigauri N., Surmava A., Intskirveli L., Study of Tbilisi City Atmosphere Pollution with PM2.5 and PM10-Microparticles During COVID-19 Pandemic Period. // Journal of the Georgian Geophysical Society, e-*I*SSN*:* 2667-9973*,* p-ISSN*:* 1512-1127, Physics of Solid Earth, Atmosphere, Ocean and Space Plasma, v. 25(2), 2022, pp. 29–37. DOI**:** https://doi.org/10.48614/ggs2520225958
10. Surmava A., Kukhalashvili V., Gigauri N., Intskirveli L., Numerical Modeling of Changes in Time and Space of the Concentration of PM10 Dispersed in the Atmosphere of Kutaisi City During Calm. // Int. Sc. Conf. “Complex Geophysical Monitoring in Georgia: History, Modern Problems, Promoting Sustainable Development of the Country”, Proceedings, ISBN 978-9941-36-272-9, Publish House of Iv. Javakhishvili Tbilisi State University, Tbilisi, Georgia, October 17-19, 2024, pp. 109 – 112, (in Georgian). http://openlibrary.ge/bitstream/123456789/10630/1/28_MM-180.pdf
11. Kirkitadze D.D., Statistical Characteristics of Aerosol Pollution of Atmosphere in Three Points of Tbilisi in 2017-2018. // Journal of the Georgian Geophysical Society, ISSN: 1512-1127, Physics of Solid Earth, Atmosphere, Ocean and Space Plasma, v. 22(2), 2019, pp. 55–62.
12. Kirkitadze D.D., Statistical Characteristics of Monthly Mean and Annual Concentrations of Particulate Matter PM2.5 and PM10 in Three Points of Tbilisi in 2017-2022. // Journal of the Georgian Geophysical Society, e-ISSN: 2667-9973, p-ISSN*:* 1512-1127, Physics of Solid Earth, Atmosphere, Ocean and Space Plasma, v. 26(1***)***, 2023, pp. 67-82.
13. Bliadze T., Chkhitunidze M., Kirkitadze D., Statistical Characteristics of Mean Monthly and Annual Concentrations of Particulate Matter PM2.5 and PM10 in Tbilisi in 2017-2023. // Int. Sc. Conf. “Complex Geophysical Monitoring in Georgia: History, Modern Problems, Promoting Sustainable Development of the Country”, Proceedings, ISBN 978-9941-36-272-9, Publish House of Iv. Javakhishvili Tbilisi State University, Tbilisi, Georgia, October 17-19, 2024, pp. 105 – 108. http://109.205.44.60/bitstream/123456789/10631/1/27_MM-180.pdf
14. Hinkle D. E., Wiersma W., Jurs S. G., Applied Statistics for the Behavioral Sciences. // Boston, MA, Houghton Mifflin Company, ISBN: 0618124055; 9780618124053, 2003, p. 756.
15. WHO Air quality guidelines for particulate matter, ozone, nitrogen dioxide and sulfur dioxide. Global update 2005 Summary of risk assessment. World Health Organization, 2006, p. 22. http://apps.who.int/iris/bitstream/handle/10665/69477/WHO_SDE_PHE_OEH_06.02_eng.pdf;jsessionid=48F380E7090ADBB4A166AC7A8610624A?sequence=1

1st International Scientific Conference "Modern problems in Geophysics", Proceedings,
ISBN 978-9941-36-434-1, ISSN 3088-4349, Tbilisi, Georgia, November 6-8, 2025

NUMERICAL MODELING OF KUTAISI CITY ATMOSPHERIC AIR POLLUTION WITH PM2.5 PARTICLES IN WINTER DURING CALM

***Surmava A., *Gigauri N., **Kukhalashvili V., *Intskirveli L.**

** Georgian Technical University, Institute of Hydrometeorology, Georgia, Tbilisi*
*** Ivane Javakhishvili Tbilisi State University, Mikheil Nodia Institute of Geophysics, Georgia, Tbilisi*
aasurmava@yahoo.com

Abstract. *Propagation of PM2,5 particles discharged by the motor transport in Kutaisi city air in winter under background calm meteorological conditions has been numerically simulated through combined integration of 3D model of meso-scale atmospheric processes in Caucasus and equation of atmospheric propagation of passive polluting admixtures. It has been shown that ground-level concentrations reach high figures twice a day – at 7-9 h in the morning (7-9AM) and 20-21 h in the evening (8-9PM). It has been obtained that the process of aerosol propagation depends on orography of dynamic fields, territory and thermal regime of underlying surface.*

Key words. *PM2.5, atmospheric pollution, numerical modeling, concentration, calm.*

Introduction

Numerical modeling of atmospheric propagation of PM2.5 particles is of great relevance nowadays for industrial centers, megapolices and separate small cities, where their air concentration frequently exceeds maximum permissible levels [1-3]. According to observation point data [air.nea.gov.ge] Kutaisi is not ranked among heavily polluted cities of the world [4], however, in separate cases air concentration of PM2.5 particles surpasses maximum permissible values [5]. Patterns of propagation and time change of PM2.5 particles discharged in the atmosphere of Kutaisi and its adjacent territories due to motor transport traffic have been simulated and analyzed in the presented article by means of computer modeling of atmospheric propagation of admixtures.

Research method

Propagation of PM2,5 particles discharged by the motor transport in the atmosphere of Kutaisi city has been numerically simulated through combined integration of 3D model of meso-scale atmospheric processes development in Caucasus and equation of atmospheric propagation of passive polluting admixtures [6, 7].

Numerical modeling results

PM2.5 aerosol propagation has been modeled in the spatial domain with an area of $13.4\times13.4\times9$ km^3, with Kutaisi in its center. Orography height in the modeling area varies from 80 to 400 m. Numerical integration of equations of mathematical model [8, 9] has been made using respective initial and boundary conditions. Numerical grid steps in horizontal direction are 200 m, and in vertical direction of free atmosphere – 300 m. Vertical steps in the 100 m thick surface layer of the atmosphere vary from 0.3 to 15 m. The time step is 1 sec. Calculations have been made for a 3-day period. A case of Kutaisi atmospheric pollution with PM2.5 has been modeled in December. At 100 m height of the atmosphere surface layer a situation of calm – background wind with velocity 0 m/sec takes place. There is a western wind above the surface layer, its velocity linearly increases with height and reaches 20 m/sec at 9 km height. Relative humidity of the atmosphere is 50%.

It has been assumed that the atmosphere is polluted with PM2.5 as a result of motor transport traffic in Kutaisi and its adjacent territory. Aerosol is discharged from the earth ground to 0.3 m height in areas of 5 types: at highways, central streets of the city, residential, industrial zones and unpopulated territories of adjacent villages. Emission rate is different depending on the area, is periodical with 24-hour period and proportional to motor transport traffic intensity. It is minimal within the 0-4 h time interval, then linearly increases

from 4 to 10h, and is constant within the time interval from 10 to 18 h. From 18 to 24 h, emission rate linearly decreases and becomes equal to that existing at 0h.

Fig. 1 shows fields of wind velocity and PM2.5 during concentration increase at 2, 100 and 600 m heights from the Earth surface obtained via modeling. It is seen from this Figure that during background calm the effect of Kutaisi terrain forms local cyclonic vortex of wind velocity. This vortex is quasi-stationary. Its center is located in the north-east part of Kutaisi at the territories of administrative units of City-Museum, Ukimerioni and Dzelkviani having complex terrain.

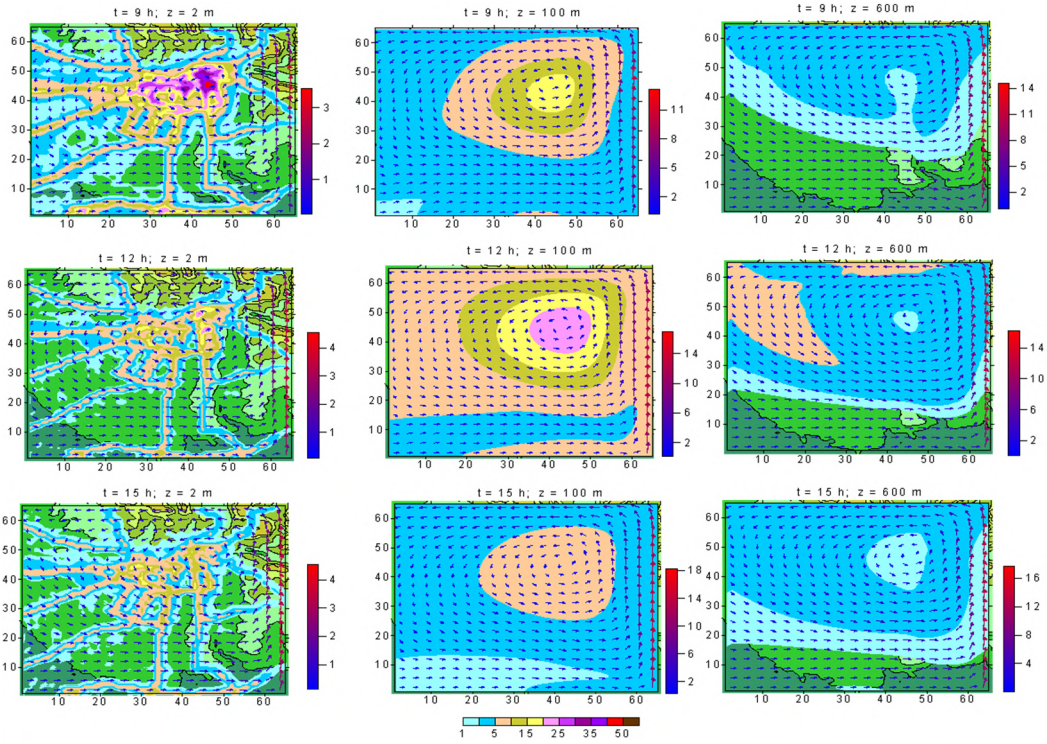

Fig. 1. Distribution of PM2.5 concentration ($\mu g/m^3$) and wind velocity (m/s) fields at 2, 100 and 600 m height from the earth surface, when t = 9, 12 and 15 h

Fig. 2 shows vertical distribution of PM2.5 concentration in the surface layer of the atmosphere obtained via modeling, in the zonal section passing the central part of the city. It is seen from Fig. 2, that atmospheric propagation of PM2,5 particles occurs at the expense of turbulent diffusion and advective and convective processes. The role of these processes is of different importance at different points of time. By 9 h in the morning (9AM) the effect of a convective process on aerosol propagation in the central part of vertical section is more substantial, while at 12 and 18 h (6PM) turbulent and advective processes play active role in aerosol propagation in the lower 40-50 m thick band of surface layer of the atmosphere.

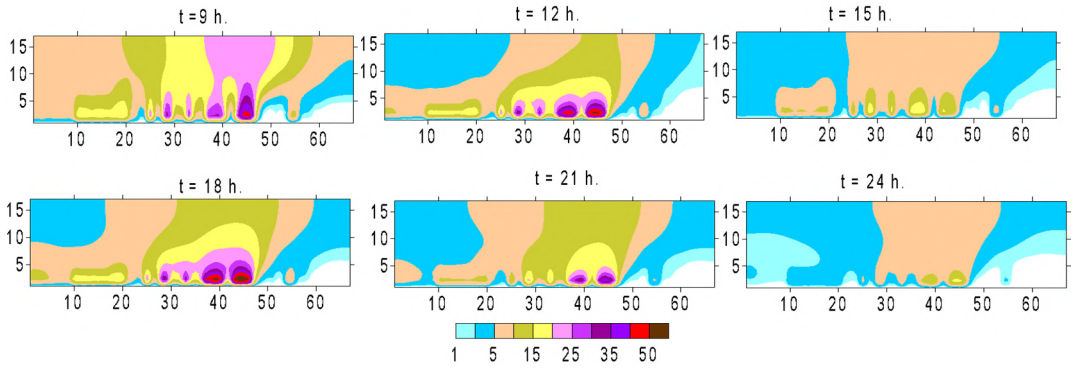

Fig. 2. Distribution of PM2.5 concentrations ($\mu g/m^3$) in surface layer of the atmosphere in the vertical section along a parallel passing the city center

Conclusions

Peculiarities of spatial distribution and time change of PM2,5 particles generated by the motor transport at the territory of Kutaisi has been investigated via numerical modeling in winter season during ground-level calm and background western wind in the free atmosphere. It has been obtained via calculations that in the winter season, interaction of meso-scale regional terrain with background western wind forms a cyclonic vortex of wind velocity. Formed dynamic and thermobaric fields have an effect on spatial distribution of aerosols discharged into the atmosphere due to motor transport traffic. Resulting from modeling, patterns of spatial distribution of PM2.5 concentration have been obtained, time behavior of concentration has been established both in surface and boundary layers of the atmosphere. It has been shown that vertical distribution and time change of concentration depend on both aerosol emission rate and motor transport traffic intensity, and on kinematics of surface layer of the atmosphere and local circulation systems formed due to diurnal variation of thermal regime at underlying surface. High and average pollution levels at the territory of the city and its surrounding and change in their location during a day have been determined.

Acknowledgment. The scientific research has been funded and performed within the framework of grant project FR-22-4765 the Shota Rustaveli National Science Foundation**.**

References

1. Mortality and burden of disease from ambient air pollution-WHO. 2020. https://www.who.int/gho/phe/outdoor_air_pollution/burden/en/.
2. Udristioiu M., Mghouchi Y., Yildizhan H., Prediction, modelling, and forecasting of PM and AQI using hybrid machine learning. // Journal of Cleaner Production,Volume 421, 2023. https://doi.org/10.1016/j.jclepro.2023.138496Get rights and content.
3. Draper J. E., Taylor W. R., Metcalfe S., Estimating background concentrations of $PM_{2.5}$ for urban air quality modelling in a data poor environment. Atmospheric Environment, Volume 314, 2023, 120107. https://doi.org/10.1016/j.atmosenv.2023.120107Get rights and content. https://www.nature.com/articles/s41598-021-91253-9
4. World's most polluted cities (historical data 2017-2022) https://www.iqair.com/world-most-polluted-cities.
5. Gigauri N., Surmava A., Kukhalashvili V., Intskirveli L., Beglarashvili N., Investigation of the distribution of PM2.5 and PM10 in the atmosphere of c. Kutaisi through experimental observations. Collection of Scientific Refereed Works of the Institute of Hydrometeorology of the Tbilisi Georgian Tecnical University, v.135, 2024, pp. 82-87. Doi.org/10.36073/1512-0902-2024-135-82-87, (Geo).
6. Surmava A., Intskirveli L., Kordzakhia G., Numerical modeling of dust propagation in the atmosphere of a city with complex terrain. The case of background eastern light air. Journal of Applied Mathematics and Physics, 8.7, 2020, pp. 1222-1228. https://doi.org/10.4236/jamp.2020.87092.
7. Surmava A., IntskirveliL., Kukhalashvili V., Numerical Modeling of the Transborder, Regional and Local Diffusion of the Dust in Georgian Atmosphere, Publishing House, Technical University",Tbilisi, Georgia, 2021, p.139. ISBN 978-9941-28-810-4, http//www.gtu.ge (in Georgian).
8. Surmava A., Intskirveli L., Gigauri N., PM2.5 and PM10 microaerosols in the atmosphere of city Tbilisi. // Publishing House of the Hydrometeorology Institute of the Tbilisi Georgian Technical University, Tbilisi, 2021, p. 94. (in Georgian).
9. Gigauri N., Intskirveli L., Surmava A., Kukhalashvili V., The Results of Kutaisi City Atmospheric Air Pollution with PM Particles. Bulletin of the Georgian National Academy of Sciences, vol.18,no3, 2024, pp .90-96.

1st International Scientific Conference "Modern problems in Geophysics", Proceedings,
ISBN 978-9941-36-434-1, ISSN 3088-4349, Tbilisi, Georgia, November 6-8, 2025

VARIABILITY OF MORTALITY IN GEORGIA AND ITS REGIONS IN 1994-2024

[*,]Japaridze N., [**,***]Khazaradze K.,**
[****]Chkhitunidze M., [***]Revishvili A.

[*]Tbilisi State Medical University, Tbilisi, Georgia
[**]Ministry of Internally Displaced Persons from Occupied Territories, Labour, Health and Social Affair of Georgia, Tbilisi, Georgia
[***]Georgian State Teaching University of Physical Education and Sport, Tbilisi, Georgia
[****]Mikheil Nodia Institute of Geophysics of Ivane Javakhishvili Tbilisi State University, Tbilisi, Georgia
n.japaridze@tsmu.edu

Abstract: *The paper presents the results of statistical analysis of variability mortality rate (annual mortality per 1000 population) in the regions of Georgia in 1994-2024. It was shown that in Guria and Kakheti, in the post-COVID-19 period (2022-2024), compared to the pre-COVID-19 period (2017-2019), the mortality rate decreased by 1.0 and 1.1, respectively. In all other regions, this rate did not change significantly during these time periods. In 2024, compared to 2023, a slight increase in mortality was observed in all regions except Tbilisi (unchanged) and Racha-Lechkhumi Kvemo Svaneti. Correlations between regions of Georgia by the mortality rates were studied.*

Key words: *Human health, mortality, environment, statistical analysis.*

Introduction

M. Nodia Institute of Geophysics of TSU, together with various medical organizations, has been conducting a systematic analysis of various demographic indicators (birth rate, mortality, population growth) in Georgia, as well as their vulnerability to the impact of various natural and anthropogenic factors (astro-meteo-geophysical factors, air pollution, photochemical smog, radon, ozone, viral diseases, etc.) [1-8].

In particular, during the COVID-19 pandemic, a series of works were carried out on the statistical analysis of various components of the pandemic (infection cases, infection rate, deaths), including ten-day, two-week and monthly interval forecasting of these components [9,10].

Research on the influence of various bioclimatic indicators on the spread of this infection has been conducted [11-13]. It studied the impact of the COVID-19 pandemic on the demographic indicators of Georgia during and after the pandemic [14,15].

For example, paper [15] presents the results of statistical analysis of variability of birth (B), death (D) and population growth (PG) in Georgia in 1994-2023. The role of the COVID-19 pandemic in the deterioration of the demographic situation during its existence (2020-2021) and in the post-COVID-19 period (2022-2023) is shown. It was revealed that throughout the entire thirty-year period, Georgia had the worst demographic indicators in 2019-2023: B = 12.0, D = 13.4, PG = -1.4 (out of 1000 population).

This work is a continuation of previous studies, taking into account new data on the demographic situation in Georgia. The results of statistical analysis of variability of mortality in Georgia and its regions in 1994-2024 are presented below.

Study area, material and methods

Study area – Georgia and its regions: Georgia (GEO); Tbilisi (Tb); Adjara (Adj); Guria (Gur); Imereti (Im); Kakheti (Kakh); Mtskheta-Mtianeti (M-M); Racha-Lechkhumi and Kvemo Svaneti (R-L KS); Samegrelo-Zemo Svaneti (S-ZS); Samtskhe-Javakheti (S-J); Kvemo Kartli (KK); Shida Kartli (Sh K).

Data from the National Statistics Office of Georgia [https://www.geostat.ge/en] on annual mortality to 1000 population (M) from 1994 to 2024 is used. In the proposed work the analysis of data is carried out with the use of the standard statistical analysis methods [16].

The following designations will be used below: Mean – average values; Min – minimal values; Max – maximal values; St Dev – standard deviation; C_v – coefficient of variations ($C_v = 100 \cdot$ St Dev/ Mean, %); R – coefficient of linear correlation. Difference between mean annual values of M was produced with the use of Student's criterion with the level of significance α not worse than 0.25.

Results and discussion

Results in Fig. 1 and Table 1 are presented.

In Fig. 1 the time series of population death rate in Georgia and its regions from 1994 to 2024, and in Table 1 the statistical characteristics of this parameter are presented.

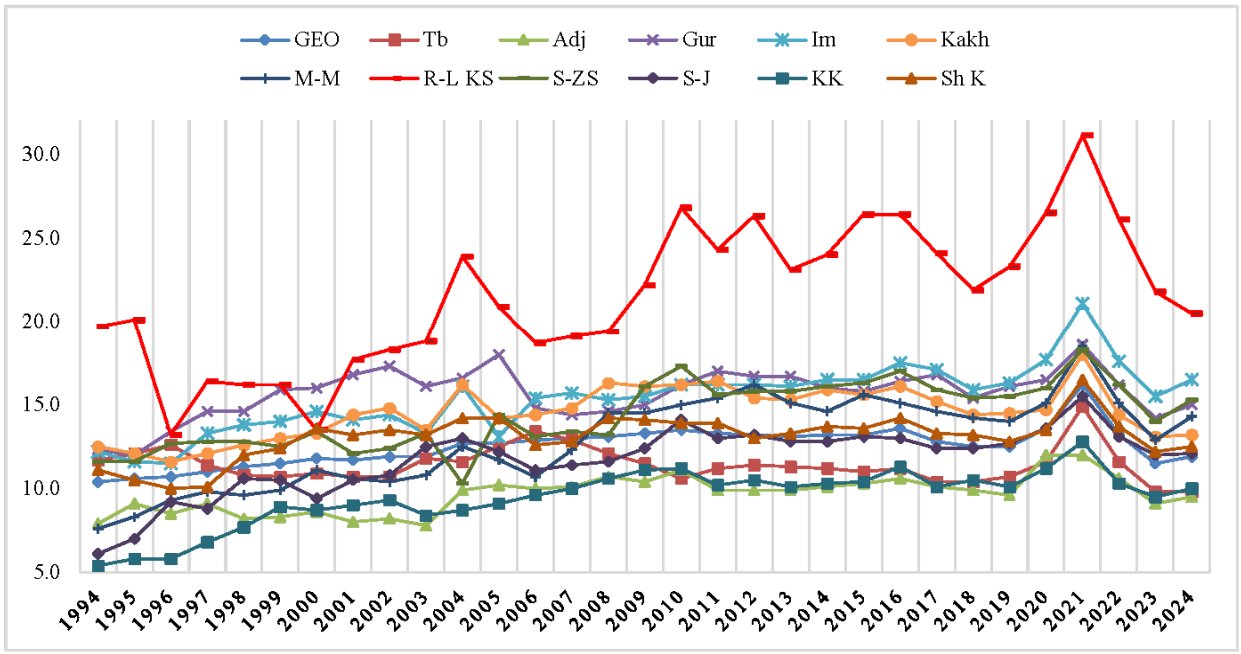

Fig. 1. Changeability of population death rates in regions of Georgia in 1994-2024.

In particular, as follows from Fig. 1 and Table 1, the values of M in different regions of Georgia in 1994-2024 change from 5.4 (Kvemo Kartli, 1994) to 31.1 (Racha-Lechkhumi and Kvemo Svaneti, 2021, COVID-19 period). The average values of M for these regions change from 9.5 to 21.5 respectively. The average value of M for Georgia is 12.5 and change from 10.4 (1994) to 16.2 (2021). In Tbilisi the average value of M is 11.4 and change from 9.8 (2023, 2024) to 14.9 (2021).

In Guria and Kakheti, in the post-COVID-19 period (2022-2024), compared to the pre-COVID-19 period (2017-2019), the mortality rate decreased by 1.0 and 1.1, respectively. In all other regions, this rate did not change significantly during these time periods. In 2024, compared to 2023, a slight increase in mortality was observed in all regions except Tbilisi (unchanged) and Racha-Lechkhumi Kvemo Svaneti.

The analysis of correlations between regions of Georgia in terms of mortality rates shows the following (Table 1).

Regions of Georgia. Values of R change from 0.01 (pair: Tb÷S-ZS, negligible correlation) to 0.90 (pair: KK÷M-M, very high correlation), average – 0.63 (moderate correlation).

Regions of Georgia without Tbilisi. Values of R change from 0.39 (pair: Adj÷Gur, low correlation) to 0.90 (pair: KK÷M-M, very high correlation), average – 0.74 (high correlation).

Table 1. Statistical characteristics of population death rates in regions of Georgia in 1994-2024 (R_{min} = 0.24, α = 0.2).

Variable	GEO	Tb	Adj	Gur	Im	Kakh	M-M	R-L KS	S-ZS	S-J	KK	Sh K
Max	16.2	14.9	12	18.6	21.1	18	18.5	31.1	18.3	15.5	12.8	16.5
Min	10.4	9.8	7.8	12	11.5	11.6	7.6	13.2	10.3	6.1	5.4	10
Mean	12.5	11.4	9.7	15.7	15.4	14.5	12.9	21.5	14.4	11.7	9.5	13.1
St Dev	1.2	1.1	1.1	1.5	2.0	1.5	2.7	4.3	2.0	2.0	1.7	1.3
Cv,%	9.3	9.2	11.5	9.4	13.0	10.6	20.7	19.8	13.7	17.1	18.1	10.2
	Correlation Matrix											
GEO	1	0.40	0.85	0.68	0.89	0.90	0.88	0.79	0.76	0.86	0.90	0.87
Tb	0.40	1	0.34	0.05	0.11	0.23	0.04	0.12	0.01	0.05	0.03	0.20
Adj	0.85	0.34	1	0.39	0.77	0.71	0.81	0.78	0.72	0.71	0.76	0.61
Gur	0.68	0.05	0.39	1	0.61	0.65	0.60	0.49	0.49	0.75	0.68	0.78
Im	0.89	0.11	0.77	0.61	1	0.78	0.90	0.80	0.76	0.83	0.89	0.76
Kakh	0.90	0.23	0.71	0.65	0.78	1	0.81	0.75	0.60	0.78	0.84	0.88
M-M	0.88	0.04	0.81	0.60	0.90	0.81	1	0.83	0.87	0.89	0.90	0.74
R-L KS	0.79	0.12	0.78	0.49	0.80	0.75	0.83	1	0.75	0.75	0.71	0.64
S-ZS	0.76	0.01	0.72	0.49	0.76	0.60	0.87	0.75	1	0.75	0.79	0.57
S-J	0.86	0.05	0.71	0.75	0.83	0.78	0.89	0.75	0.75	1	0.90	0.79
KK	0.90	0.03	0.76	0.68	0.89	0.84	0.90	0.71	0.79	0.90	1	0.84
Sh K	0.87	0.20	0.61	0.78	0.76	0.88	0.74	0.64	0.57	0.79	0.84	1

Georgia and regions of Georgia. Values of R change from 0.40 (pair: Tb÷Geo, low correlation) to 0.90 (pairs: Kakh÷Geo and KK÷Geo, very high correlation), average – 0.80 (high correlation).

Georgia and regions of Georgia without Tbilisi. Values of R change from 0.68 (pair: Gur÷Geo, moderate correlation) to 0.90 (pairs: Kakh÷Geo and KK÷Geo, very high correlation), average – 0.84 (high correlation).

Conclusion

A detailed statistical analysis of mortality variability in Georgia and its regions from 1994 to 2024 was conducted. Specifically, it was found that there is a complete lack of correlation in mortality rates between Tbilisi and the rest of Georgia's regions (except Adjara). The correlation coefficient for the Tbilisi ÷ Adjara pair is 0.34 (low correlation). Further research will analyze the reasons for this.

Acknowledgement. The authors are grateful to the chief of the atmospheric physics department of M. Nodia Institute of Geophysics A. Amiranashvili for assistance in the fulfillment of this work.

References

1. Japaridze N., Khazaradze K. Changeability of Mortality in Georgia in Different Seasons and Periods of Year into 1993-2017. // Int. Sc. Conf. “Natural Disasters in Georgia: Monitoring, Prevention, Mitigation”. Proc., ISBN 978-9941-13-899-7, Publish House of Iv. Javakhishvili Tbilisi State University, December 12-14, Tbilisi, 2019, pp. 205-208. http://www.dspace.gela.org.ge/bitstream/123456789/8672/1/48_Conf_NDG_2019.pdf
2. Khazaradze K.R., Chkhitunidze M.S., Japaridze N.D., Changeability of Annual Values of Mortality as Whole in Georgia and Kakheti Region from 1993 to 2018. // Int. Sc. Conf. „Modern Problems of Ecology“ Proceedings, ISSN 1512-1976, v. 7, Tbilisi-Telavi, Georgia, 26-28 September, 2020, pp. 360-363. http://dspace.gela.org.ge/handle/123456789/8837
3. Japaridze N., Khazaradze K., Studies in the Field of the Influence of Natural and Anthropogenic Environmental Factors on Human Health in Georgia: Current Status and Planned Works. // Int. Sc. Conf. “Natural Disasters in Georgia: Monitoring, Prevention, Mitigation”. Proc., ISBN 978-9941-13-899-7, Publish House of Iv. Javakhishvili Tbilisi State University, December 12-14, Tbilisi, 2019, pp. 201-204. http://109.205.44.60/bitstream/123456789/8671/1/47_Conf_NDG_2019.pdf
4. Japaridze N., Khazaradze K., Chkhitunidze M., Revishvili A. A Brief Overview of Research Conducted by M. Nodia Institute of Geophysics, TSU Together with Medical Organizations in the Field of “Health of the Population of Georgia and Environment” Over the Past 10 Years. // Int. Sc. Conf. "Geophysical Processes in the Earth and its

Envelopes", Proceedings, Publish House of Iv. Javakhishvili Tbilisi State University, November 16-17, Tbilisi, 2023, pp. 337-343. http://dspace.gela.org.ge/handle/123456789/10469

5. Amiranashvili A.G., Japaridze N.D., Khazaradze K.R., On the Connection of Monthly Mean of Some Simple Thermal Indices and Tourism Climate Index with the Mortality of the Population of Tbilisi City Apropos of Cardiovascular Diseases. // Journal of the Georgian Geophysical Society, ISSN: 1512-1127, Physics of Solid Earth, Atmosphere, Ocean and Space Plasma, v. 21(1), Tbilisi, 2018, pp. 48 -62. http://www.jl.tsu.ge/index.php/GGS/article/view/2489
6. Amiranashvili A., Bliadze T., Chikhladze V., Photochemical smog in Tbilisi. // Monograph, Trans. of Mikheil Nodia institute of Geophysics, ISSN 1512-1135, vol. 63, Tb., 2012, p. 160. (in Georgian).
7. Amiranashvili A., Bakradze T., Ghlonti N., Khazaradze K., Japaridze N., Revishvili A., Influence of Variations of the Annual Intensity of Galactic Cosmic Rays on the Mortality of the Population of Georgia. Int. Sc. Conf. „Natural Disasters in the 21st Century: Monitoring, Prevention, Mitigation“. Proceedings, ISBN 978-9941-491-52-8, Tbilisi, Georgia, December 20-22, 2021. Publish House of Iv. Javakhishvili Tbilisi State University, Tbilisi, 2021, pp. 163 – 166.
8. Amiranashvili A.G., Revishvili A.A., Khazaradze K.R., Japaridze N.D., Connection of Holiday Climate Index with Public Health (on Example of Tbilisi and Kakheti Region, Georgia). Journal of the Georgian Geophysical Society, e-ISSN: 2667-9973, p-ISSN: 1512-1127, // Physics of Solid Earth, Atmosphere, Ocean and Space Plasma, v. 24 (1), 2021, pp. 63-76. DOI: https://doi.org/10.48614/ggs2420212884
9. Amiranashvili A.G., Khazaradze K.R., Japaridze N.D., The statistical analysis of daily data associated with different parameters of the New Coronavirus COVID-19 pandemic in Georgia and their monthly interval prediction from January 1, 2022 to March 31, 2022. 20 p. // Preprint from medRxiv, 21Apr 2022, medRxiv 2022.04.19.22274044; doi: https://doi.org/10.1101/2022.04.19.22274044
10. Amiranashvili A.G., Khazaradze K.R., Japaridze N.D., Comparative Analysis of Reported Deaths Cases Associated with the New Coronavirus COVID-19 Pandemic in the South Caucasus Countries (Armenia, Azerbaijan, Georgia) from March 2020 to May 2022. // medRxiv 2022.04.19.22274044; doi: https://doi.org/10.1101/2022.04.19.22274044
11. Amiranashvili A., Japaridze N., Kartvelishvili L., Khazaradze K., Revishvili A., Preliminary Results of a Study on the Impact of Some Simple Thermal Indices on the Spread of COVID-19 in Tbilisi. // Journal of the Georgian Geophysical Society, e-ISSN: 2667-9973, p-ISSN*:* 1512-1127, Physics of Solid Earth, Atmosphere, Ocean and Space Plasma, v. 25(2), 2022, pp. 59–68. DOI**:** https://doi.org/10.48614/ggs2520225961
12. Amiranashvili A., Bliadze T., Japaridze N., Khazaradze K., Revishvili A., Angstrom Fire Index as a Bioclimatic Indicator (Using the Example of the Impact on the Spread of Covid-19 in Tbilisi). // Int. Sc. Conf. "Geophysical Processes in the Earth and its Envelopes", Proceedings, Publish House of Iv. Javakhishvili Tbilisi State University, November 16-17, Tbilisi, 2023, pp. 328-331. http://openlibrary.ge/handle/123456789/10467
13. Amiranashvili A., Japaridze N., Kharchilava J., Khazaradze K., Revishvili A., Results of a Study on the Impact of Surface Ozone Concentration on the Spread of COVID-19 in Tbilisi. // Journal of the Georgian Geophysical Society, e-ISSN: 2667-9973*,* p-ISSN*:* 1512-1127, Physics of Solid Earth, Atmosphere, Ocean and Space Plasma, v. 26(2), 2023, pp. 57–64.
14. Japaridze N., Khazaradze K., Chkhitunidze M., Revishvili A. Mortality Variability in Georgia in 1994-2022. // Int. Sc. Conf. "Geophysical Processes in the Earth and its Envelopes", // Proceedings, Publish House of Iv. Javakhishvili Tbilisi State University, November 16-17, Tbilisi, 2023, pp. 332-336. http://openlibrary.ge/handle/123456789/10468
15. Japaridze N., Khazaradze K., Chkhitunidze M., Revishvili A., Variability of the Birth, Death and Population Growth Rates in Georgia in 1994-2023. // Int. Sc. Conf. “Complex Geophysical Monitoring in Georgia: History, Modern Problems, Promoting Sustainable Development of the Country”, Proceedings, ISBN 978-9941-36-272-9, Publish House of Iv. Javakhishvili Tbilisi State University, Tbilisi, Georgia, October 17-19, 2024, pp. 129 – 132. http://109.205.44.60/bitstream/123456789/10625/1/33_MM-180.pdf
16. Hinkle D. E., Wiersma W., Jurs S. G., Applied Statistics for the Behavioral Sciences. // Boston, MA, Houghton Mifflin Company, ISBN: 0618124055; 9780618124053, 2003, p. 756.

1st International Scientific Conference "Modern problems in Geophysics", Proceedings,
ISBN 978-9941-36-434-1, ISSN 3088-4349, Tbilisi, Georgia, November 6-8, 2025

GEOPHYSICS AND MENTAL HEALTH: PREPARING FOR EFFECTIVE PUBLIC COMMUNICATION

Okribelashvili N., Pirtskhalava E.

Ivane Javakhishvili Tbilisi State University, Tbilisi, Georgia
nino.okribelashvili@tsu.ge

Abstract. *Natural disasters, particularly earthquakes, are not merely geological phenomena but complex psychological events with lasting impacts. This paper examines the 2002 Tbilisi earthquake case of a 26-year-old mother, highlighting early trauma, cultural narratives, and stress responses. The discussion emphasizes cumulative trauma, intergenerational effects, and survival behavior. Recommendations include integrating trauma-informed care, psychological first aid, and long-term monitoring.*

Key words*: Earthquakes, Trauma, Mental Health, Disaster Preparedness*

Introduction

Earthquakes are typically understood through seismic parameters such as magnitude, depth, and structural damage. However, they represent one of the most complex and psychologically traumatic events, combining elements of immediate threat, unpredictability, loss of control, and long-term consequences [3]. As a form of collective trauma, earthquakes share similarities with war, yet unlike war, they have no identifiable "enemy." This often complicates survivors' ability to direct anger, intensifying feelings of guilt or helplessness (Goenjian et al., 2000). Earthquakes and other natural disasters leave enduring impacts on individuals, influencing behavior, emotional regulation, and decision-making under stress.

Study Area, Material and Methods: The study area is Tbilisi, Georgia, which experienced an earthquake on April 25, 2002 (magnitude 4.5–5.0 Mw). The material for this report is based on the psychiatric evaluation of a 26-year-old woman in August 2002, whose depressive symptoms were temporally associated with the earthquake. Diagnostic assessment was carried out using standard psychiatric evaluation and clinical interview, with reference to ICD-10 criteria. Literature sources on disaster-related trauma and depression were used to contextualize the case.

Historical Context – Accounts of the patient's earlier exposure to the 1988 Spitak and 1991 Racha earthquakes, which provide insight into cumulative trauma.

Secondary Sources – Peer-reviewed literature on disaster psychiatry, post-traumatic stress disorder (PTSD), and cultural narratives surrounding survival behaviors. [4, 5, 6]

Qualitative Content Analysis. Narratives related to family influence (e.g., emphasis on salvaging valuables), symbolic behaviors (e.g., rescuing jewelry), and emotional responses were coded thematically. This allowed for identification of cultural scripts and intergenerational messages that guided behavior under stress.

Comparative Historical Analysis. The patient's reactions were compared across three seismic events (Spitak 1988, Racha 1991, Tbilisi 2002) to demonstrate the concept of cumulative trauma.

Interdisciplinary Integration. Clinical insights were combined with geophysical context, emphasizing the importance of cross-disciplinary frameworks that consider both physical hazards and psychological vulnerability.

The methodological design highlights the limitations of relying solely on structural or epidemiological data in disaster studies. Instead, it underscores the necessity of incorporating psychosocial and cultural dimensions when assessing the full impact of earthquakes in seismically active regions.

Case Description

In August 2002, a 26-year-old woman – a mother of two young children – was assessed by a psychiatrist. She presented severe depressive symptoms, including suicidal ideation, anhedonia, significant weight loss, insomnia, and emotional numbing [1]. Although her clinical presentation met criteria for postpartum depression, the onset of symptoms coincided with the Tbilisi earthquake. During the event, she rapidly evacuated her home carrying a box of jewelry, only realizing 30 minutes later that her children had been left inside. This incident triggered profound maternal guilt and persistent depressive symptoms.

Historical Context of Trauma: Her response was shaped by early-life exposure to seismic events. At age 10, she experienced the 1988 Spitak earthquake (Mw 6.8–6.9), recalling her mother's panic and cultural messages emphasizing salvaging valuables. At age 13, she was at the epicenter of the 1991 Racha earthquake (Mw 7.0), where her family's house was damaged and two neighbors perished. Her parents' absence reinforced helplessness and abandonment. These experiences highlight how prior trauma shapes responses to future crises, illustrating the principle of cumulative trauma.

Relevance in the Era of Global Crises: This case highlights that disasters are not solely geological events; they are deeply personal, psychological, and intergenerational phenomena. Survivors often carry invisible burdens such as trauma, guilt, and silence. Mental health systems remain underprepared to address PTSD, survivor guilt, and other sequelae, particularly in hazard-prone regions. Viewing disasters through this broader lens is increasingly urgent in the context of climate change, armed conflicts, and recurrent seismic activity.

Discussion

Trauma Mechanisms. Natural disasters disrupt the basic sense of safety. The unpredictability and uncontrollability of earthquakes activate survival mechanisms such as "freeze," "fight," or "flight." Behaviors that appear irrational (e.g., carrying valuables instead of saving children) may represent dissociative responses or unconscious survival patterns rather than deliberate choices.

Accumulated Childhood Trauma. Previous exposure to disasters leaves lasting "emotional imprints." Early traumatic experiences (Spitak, Racha) sensitized the patient's nervous system, lowering her threshold for stress tolerance. Each new catastrophe reactivated earlier wounds, producing more intense reactions – a phenomenon known as cumulative trauma.

Cultural Narratives and Family Influence. Social and cultural messages significantly shape survival behavior. In this case, repeated family remarks that "those who saved gold could start anew" became an internalized script. Under stress, the patient acted according to this narrative, showing how collective beliefs can override individual instincts.

Guilt and Identity Breakdown. The survivor's guilt was amplified by maternal identity. Leaving her children behind, even briefly, created a rupture between the ideal of the "protective mother" and the reality of the traumatic moment. This dissonance often fuels depression, self-blame, and suicidal ideation after disasters.

Symbolic Meaning of Material Objects.Saving jewelry went beyond materialism, symbolizing an unconscious effort to maintain stability, control, and hope amid chaos. Material possessions can anchor identity and represent survival or the possibility of rebuilding.

Intergenerational Transmission. The patient's story illustrates how trauma is not confined to one generation. Unprocessed fear, cultural scripts, and silence can be passed down to children, shaping their psychological resilience or vulnerability in future disasters.

Limitations and Future Directions

While this case provides valuable insights into the interplay of cultural narratives, cumulative trauma, and seismic hazards, it remains a single-case study and therefore cannot be generalized to the wider population. Further research should incorporate longitudinal studies and larger samples to assess how psychological vulnerability and resilience evolve in communities repeatedly exposed to earthquakes. Moreover, future investigations should examine gender differences, children's adaptation, and the role of social support systems in mitigating post-disaster psychological impacts. Integrating mental health considerations into geophysical risk communication strategies remains an essential goal for sustainable disaster preparedness.

Implications for Contemporary Practice

Modern disaster response necessitates a broader and more integrative perspective. Trauma-informed care should be embedded within disaster preparedness plans, not only in hazard-prone areas but also across clinics, schools, and community centers where vulnerable groups are likely to seek support. In addition, geophysicists and emergency response personnel would benefit from basic training in psychological first aid, enabling them to recognize acute distress and provide immediate, supportive interventions. Equally important is the implementation of long-term mental health monitoring systems, with particular attention to children and mothers living in disaster-prone regions, as these groups are especially susceptible to enduring psychological consequences.

Bridging Psychiatry and Geophysics: The University's Third Mission

The intersection of psychiatry and geophysics illustrates how science transforms when it crosses disciplinary boundaries to engage society directly. While geophysics offers vital knowledge on earthquake prediction, risk assessment, and infrastructure safety, psychiatry addresses the human dimension – trauma, PTSD, social support, and long-term psychological effects that may persist across generations. In this context, the university's third mission of public engagement becomes essential, shifting scientific communication from "What was the earthquake's magnitude?" to "How did people endure psychologically?" [2] Such integration not only advances scholarship but also embodies civic responsibility, positioning universities as centers for understanding and managing collective trauma.

References

1. Can H., Gürsoy S., Göktaş S., Investigation of post-traumatic stress disorder and depression in postpartum women after the earthquake in Turkey. // Current Psychology, 2025. https://doi.org/10.1007/s12144-025-08133-y
2. Goenjian A. K., Steinberg A. M., Najarian L. M., Fairbanks L. A., Tashjian M., Pynoos, R. S., Prospective study of posttraumatic stress, anxiety, and depressive reactions after earthquake and political violence. // American Journal of Psychiatry, 157(6), 2000, pp. 911–916.
3. North C. S., Pfefferbaum B., Mental health response to community disasters: A systematic review. // Disaster and Military Medicine, 1, 2015, p. 17.
4. Qiao D., Liu X., Wang W., The mediating role of intrusive rumination in the relationship between earthquake exposure and PTSD: A gender perspective. // BMC Public Health, 24(1), 2024, p. 456.
5. Xiong X., Harville E. W., Mattison D. R., Elkind-Hirsch K., Pridjian G., Buekens P., Exposure to Hurricane Katrina, post-traumatic stress disorder and depression among pregnant women. American Journal of Disaster Medicine, 5(3), 2010, pp.181–187.
6. Norris F. H., Friedman M. J., Watson P. J., Byrne C. M., Diaz E., Kaniasty K. 60,000 disaster victims speak: Part I. An empirical review of the empirical literature, 1981–2001. // Psychiatry, 65(3), 2002, pp.207–239.
7. Galea S., Nandi A., Vlahov D. The epidemiology of post-traumatic stress disorder after disasters. Epidemiologic Reviews, 27(1), 2005, pp. 78–91.

1st International Scientific Conference "Modern problems in Geophysics", Proceedings,
ISBN 978-9941-36-434-1, ISSN 3088-4349, Tbilisi, Georgia, November 6-8, 2025

THE IMPACT OF SCHUMANN RESONANCE ON THE HUMAN BODY

Mkurnalidze I., Kapanadze N.

Institute of Hydrometeorology, Georgian Technical University, Tbilisi, Georgia
knaili1990@gmail.com

Abstract. *This paper provides an informative review of studies on the Earth's natural electromagnetic resonance, the so-called Schumann resonance. It discusses the potential applications of this phenomenon in various fields, with particular emphasis on its role in the sensing and monitoring of catastrophic events. Special attention is given to its interaction with living organisms, especially the human body, due to its proximity to brainwave frequencies (delta, theta, alpha, beta, gamma). Research findings indicate that the fundamental Schumann frequency of 7.83 Hz may reduce stress, improve sleep quality, enhance cognitive functions, and contribute to emotional stability.*

Key words: *Schumann resonance, harmonic oscillations, synchronization, vibration.*

Introduction

Schumann resonance is a natural electromagnetic wave that occurs in the cavity between the Earth and the ionosphere at extremely low frequencies, primarily at 7.83 Hz and its higher harmonics (14.07, 20.25, 26.41, 35.42 Hz). It is generated mainly by global lightning activity and propagates in the form of standing waves within the Earth–ionosphere cavity.

For resonance to occur, the wavelength must be a multiple of the Earth's circumference. Under these conditions, peaks in the extremely low frequency (ELF) range emerge – about 100,000 times smaller than radio wave frequencies. As these waves encircle the planet, constructive interference occurs, producing standing oscillations (Fig. 1).

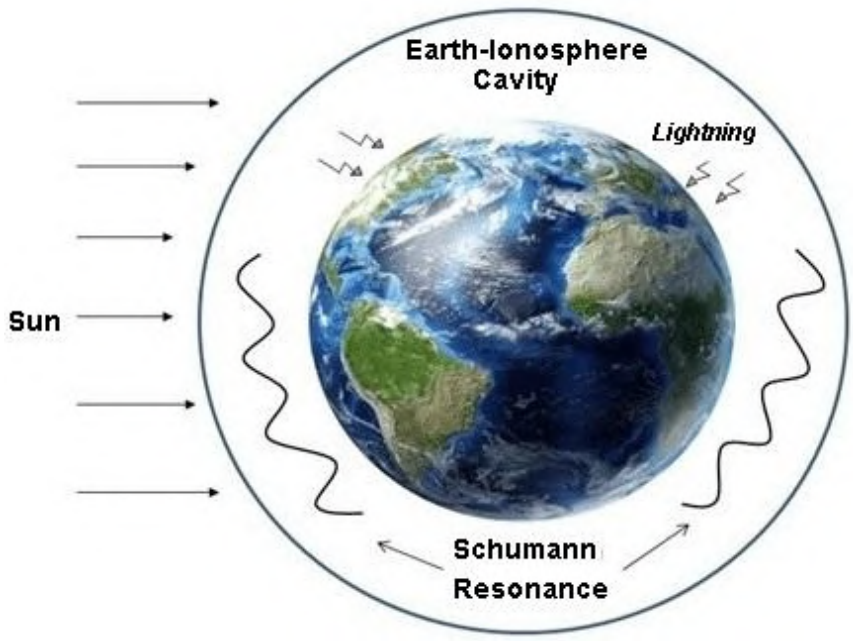

Fig. 1. Schumann resonance.

This unique global electromagnetic phenomenon has been linked to various catastrophic events on Earth. Observations suggest that the frequency and intensity of Schumann resonances may vary during lightning

storms, volcanic eruptions, and possibly earthquakes and climate-related changes [1–5]. Additionally, studies highlight its interaction with biological systems, as Schumann frequencies closely correspond to human brain rhythms, potentially influencing both physiological and psychological processes.

Main part

Schumann resonance is often referred to as the "pulse of the Earth," analogous to a planetary heartbeat. Numerous studies emphasize its direct impact not only on physical health but also on emotional and psychological well-being. The fundamental frequency (7.83 Hz) is particularly associated with positive effects on cognition, stress reduction, and sleep regulation.

Human brain activity is commonly categorized into frequency ranges:

- **Delta waves (0–4 Hz):** deep sleep, subconscious activity, emotions, endocrine regulation;
- **Theta waves (4–8 Hz):** REM sleep, relaxation, creativity, learning processes;
- **Alpha waves (8–12 Hz):** relaxation with closed eyes, mental calmness, focus, visualization;
- **Beta waves (12–30 Hz):** active wakefulness, concentration, alertness, heightened anxiety;
- **Gamma waves (30+ Hz):** higher cognitive functions, problem solving, creativity, meditation, global neural synchronization.

When alpha and theta brainwaves synchronize with Schumann frequencies, the human body enters states of relaxation and restorative resonance. Research suggests that such synchronization contributes to cellular regeneration, stress relief, and overall healing.

Fig. 2 shows the spectrogram showing changes in the Earth's vibrational level.

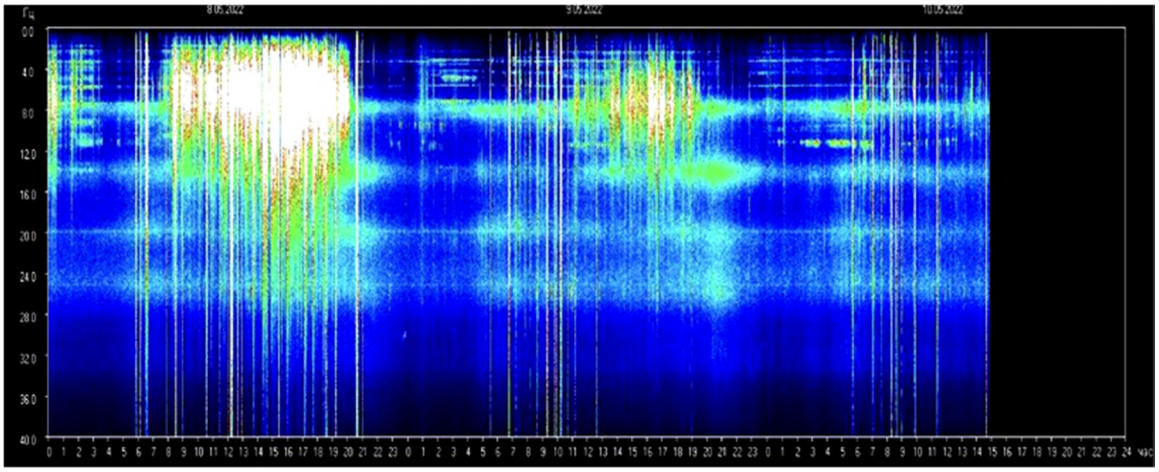

Fig. 2. Spectrogram showing changes in the Earth's vibrational level.

Spectrogram analysis shows that:

- **Blue areas** indicate the basic Schumann resonance level, associated with homeostasis and adaptation;
- **Green areas** reflect processes of "energy purification," often linked with irritability or emotional instability at the individual level;
- **White vertical lines** (40–100 Hz) correspond to high-frequency "energy charges" from space, often associated with heightened excitability, fatigue, or unusual physical sensations;
- **Red areas** mark dense energetic blockages, often correlated with exacerbation of health symptoms during intense energetic "loads."

Synchronization with Schumann frequencies can occur naturally through direct contact with nature – such as walking in forests, being near the sea, stargazing, meditation, or listening to resonant sound frequencies. Additionally, medical technologies such as **PEMF devices** (e.g., Helper ML) have been developed to artificially generate 7.83 Hz oscillations for therapeutic purposes [6–10].

It is important to note that the 7.83 Hz frequency can act both as a sedative and as a stimulator, supporting overall physiological harmony.

Conclusion

Schumann resonance, often described as the Earth's natural "pulse," represents a global synchronization mechanism between the planet and living organisms. Its fundamental and harmonic frequencies contribute to homeostasis, cellular repair, and the optimization of neurocognitive functions. Exposure to Schumann resonance is associated with improved physical health, emotional stability, and adaptive capacity. Although the phenomenon remains insufficiently studied, existing research strongly suggests its importance for human well-being and its potential role in monitoring global geophysical processes.

References

1. Liu J., Huang J., Li Z., Zhao Z., Zeren Z., Shen X., Wang Q., Recent advances and challenges in Schumann resonance observations and research. Remote Sensing, 15(14), 2023, 3557. https://doi.org/10.3390/rs15143557
2. Nikolenko A. P., Hoyokowo M., Resonances in the Earth–Ionosphere cavity. // Journal of Earthquake Research, London: Kluwer Academic Publishers, 13(2), 2024,
3. Bennett J., Harrison R. G., Surface measurement system for atmospheric vertical conductivity current density with bias current density correction. Journal of Atmospheric and Solar-Terrestrial Physics, 20, 2008, pp. 1373–1377.

a. Wikipedia contributors. (n.d.). Schumann resonance. In Wikipedia. Retrieved June 18, 2025, from https://en.wikipedia.org/wiki/Schumann_resonance Nikolenko A. P., Shvets A. V., Goluk Yu., Schekotov A. Yu., Hoyokowo M., Mezentsev A., Romero R., De Rosa R., Kudintseva L. G. (n.d.).

4. Mkurnalidze I., Kapanadze N., Schumann resonance and catastrophic events on Earth. Transactions of the Institute of Hydrometeorology, Georgian Technical University, vol.136, 2025.
5. Altimed. (n.d.)., Rezonans Shumana: osnovy i meditsinskaya znachimost. Retrieved June 18, 2025, from https://www.altimed.net/rezonans-shumana-osnovy-i-medicinskaya-znachimost/
6. Persinger M., ELF and VLF electromagnetic field effects. New York: Plenum Press. 1974. https://doi.org/10.1007/978-1-4684-2814-3
7. Persinger M., Dadsetan P., Jahangiri H., Encyclopedia of psychological testing, evaluation and treatment: (AL). Riga, Latvia: Scholar's Press, Volume 1, 2020. ISBN 978-613-8-94244-3
8. Persinger M., Dadsetan P., Jahangiri H., Encyclopedia of psychological testing, assessment and treatment: (M–Z). Riga, Latvia: Scholar's, Press, Volume 2, 2020. ISBN 978-613-8-93134-8

1st International Scientific Conference "Modern problems in Geophysics", Proceedings,
ISBN 978-9941-36-434-1, ISSN 3088-4349, Tbilisi, Georgia, November 6-8, 2025

ANALYSIS OF THE FORBUSH EFFECT OF COSMIC RAY VARIATIONS BASED ON DATA FROM THE PERIOD MAY 30-JUNE 10 REGISTERED AT THE TBILISI COSMOPHYSICAL OBSERVATORY

[*]Bakradze T., [*]Glonti N., [*]Erkomaishvili T., [*]Demurishvili Z., [*]Takadze G., [*]Barbakadze P., [*]Alania E., [**]Vanishvili G.

[*]Ivane Javakhishvili Tbilisi State University, Mikheil Nodia Institute of Geophysics, Cosmophysical Observatory, Tbilisi, Georgia
[**]Sokhumi State University, Tbilisi, Georgia
temuribakradze@yahoo.com

***Abstract**. Cosmic rays, reaching from the depths of the galaxy and the Sun, bring information to Earth about the space where they are formed, accelerated, and propagated. The method of studying variations in cosmic rays allows us to use this information channel to study the processes that occur in interplanetary space, on the Sun, and in the Earth's atmosphere. The article discusses the analysis of data on the neutron component of cosmic rays observed at the Cosmophysical Observatory of the Institute of Geophysics for the period from May 30 to June 10, 2025 in relation to the parameters of the Earth's magnetic field.*

***Key words**: cosmic rays, Forbush effects, magnetosphere, solar wind.*

Cosmic rays, which are high-energy charged particles, reaching the Earth from the depths of the galaxy and the Sun, carry information about the space where they are generated, accelerated, and propagated. The method of studying the variation of cosmic rays allows us to use this information channel to study the processes that take place in interplanetary space, on the Sun, around the Earth, and in the Earth's atmosphere. Observations of cosmic rays are being conducted in interplanetary space, in the Earth's atmosphere, on the Earth's surface, and underground in various energy ranges. These observations complement each other in terms of informativeness, among which the variations of cosmic rays observed on the Earth's surface are important. One such object is the Cosmophysical Observatory of the Institute of Geophysics, where the neutron components of cosmic rays and atmospheric pressure have been continuously recorded since 1972. [1]

The intensity of cosmic rays recorded on Earth reveals time-varying features called cosmic ray intensity variations. The study of cosmic ray variations is one of the methods that provides information for studying physical processes occurring in interplanetary and near-Earth spaces. Cosmic ray emission data are important for studies such as magnetic storms, auroras, geomagnetic and ionospheric phenomena, and others. [2]

Cosmic ray variations during strong geomagnetic storms are the result of magnetodynamic interactions with interplanetary shock waves during solar chromospheric flares and significant changes in the magnetospheric space. Cosmic ray variations caused by changes in the magnetosphere provide unique information about the processes taking place in the Earth's magnetosphere. The study of these effects and their physical interpretation is a very complex problem that is still not fully understood.

During strong magnetic storms, the magnetospheric structure changes significantly, since the magnetospheric state changes, namely, the "closed" magnetosphere turns into an "open" magnetosphere, the size of the magnetosphere decreases, and its induced current system increases. The state of the magnetospheric structure depends on the shock wave and magnetic clouds. The magnetohydrodynamic parameters of high-speed plasma clouds can change from case to case, which occurs during chromospheric flares on the Sun. Therefore, magnetospheric structures are subject to qualitatively different changes. The change in the magnetosphere has a qualitative effect on the trajectory of cosmic ray particles in the geomagnetic field and the location of the impact zone from which cosmic rays reach the Earth. [3]

The article discusses the analysis of data on the neutrino component of cosmic rays observed at the Cosmophysical Observatory of the Institute of Geophysics during the period from March 30 to June 10, 2025.

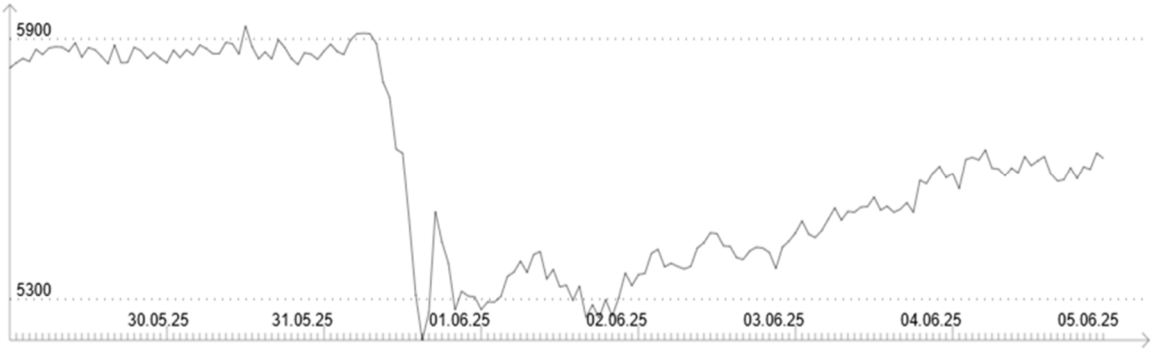

Fig.1

Fig. 1 shows the Forbush effect of cosmic ray variations observed at the Cosmophysical Observatory, with its three main phases: 1) the decay phase, 2) the main phase, and 3) the recovery phase. The graphical representations of the data clearly show pronounced anomalous fluctuations. A rather strong Forbush decay effect is observed for this period. Fig. 2 shows a diagram of the geomagnetic data from the Tbilisi station. As is known and generally accepted, geomagnetic storms and Forbush effects of cosmic rays have common causes. These are high-speed flows of solar plasma clouds resembling flares or flares. When discussing these two effects, one should always keep in mind which parameters of the solar wind are responsible for the formation of geomagnetic storms and which effects cause Forbush effects in cosmic rays. [4]

Solar flares are associated with a geophysical phenomenon – the fall of galactic cosmic rays. They are called solar Forbush effects (falls). This phenomenon is explained by the fact that the stream emitted during solar chromospheric flares brings with it a fairly significant magnetic field and cosmic rays, which are partially scattered and partially reflected from the Earth back into space. Such a stream for a certain time (several days) acts as a screen protecting the Earth from galactic cosmic rays, which leads to the fall of galactic cosmic rays (Forbush effect). About a day after the explosions on the Sun, magnetic storms begin on Earth. At first, a short-term increase in the Earth's magnetic field from its normal state by about 0.1% is observed, then a decrease in the magnetic field strength by several percent occurs and lasts for several hours (the main phase). Finally, after a few days, the magnetic field gradually recovers and returns to its original state [5].

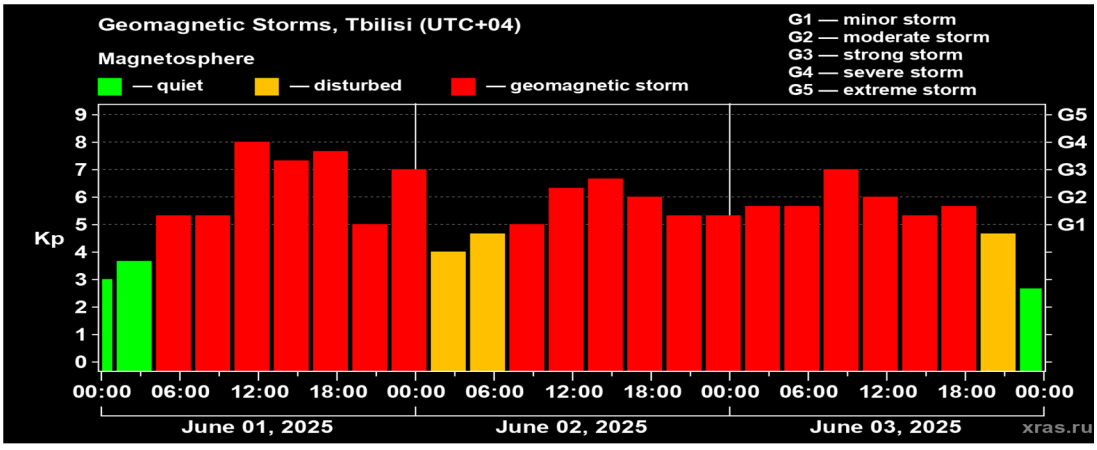

Fig. 2

Fig. 2 shows a diagram depicting a very strong G4 type magnetic storm that occurred in Tbilisi from May 31 to July 10, 2025. Fig. 1 shows the intensity data of the neutron component of cosmic rays, where the Forbush effect with an 8% decrease is observed [6].

Our conclusion is that both of these effects are caused by chromospheric flares on the Sun. The flares on the Sun occur mainly in the solar corona. A significant part of the energy is released as additional kinetic energy from the relatively dense plasma. As a result, a plasma cloud is ejected from the solar corona into

interplanetary space. This cloud creates a downdraft wave because it interferes with the interplanetary plasma (solar wind), which also comes from the Sun, but at a lower speed. By penetrating the Earth's magnetic field, it causes the field lines to compress, which temporarily increases the Earth's magnetic field. The main phase begins when the plasma caused by the shock wave enters the magnetosphere, where the wave causes the energy of the plasma particles that already existed in the magnetosphere to increase. In either case, the magnetic lines of force are released and the magnetic field strength decreases.

References

1. Dorman L.I., "Variations in Cosmic Rays and Space Exploration". // Nauka Publishing House, Moscow, 1963.
2. Egeland A., Holter O., Omholm A., "Space Geophysics". // Mir Publishing House, Moscow, 1976.
3. Toptygin I.N. “Cosmic Rays in Interplanetary Magnetic Fields”, // Nauka Publishing House, Moscow, 1983
4. Chkhetia A. M., “Results of the Study of the Main Geophysical Phenomena of the Complex Problem of Solar-Terrestrial Relations”, Tbilisi, 1992.
5. Ginzburg V. A., “Astrophysics of Cosmic Rays”, // Nauka Publishing House, Moscow, 1984.
6. Bakradze T., Glonti N., Erkomaishvili T., Demurishvili Z., Takadze G., Barbakadze P., Gogua R., Alania E., “Modulation Effects of Cosmic Rays in Connection with Solar Activities”, // International Scientific Conference, Tbilisi, 2024.

1st International Scientific Conference "Modern problems in Geophysics", Proceedings,
ISBN 978-9941-36-434-1, ISSN 3088-4349, Tbilisi, Georgia, November 6-8, 2025

INVESTIGATION OF THE CONNECTION BETWEEN THE SPACE WEATHER AND EARTH ATMOSPHERIC INSTABILITIES USING AI

*******Elbakidze K., *Kharshiladze O., ***,****Sorriso-Valvo L.,**
****Tatishvili M., *Tsulukidze L., **Palavandishvili A.**

**M. Nodia Institute of Geophysics of the I. Javakhishvili Tbilisi State University, Tbilisi, Georgia*
***Institute of Hydrometeorology of the Georgian Technical University, Tbilisi, Georgia*
****CNR – Istituto per la Scienza e la Tecnologia dei Plasmi, Bari, Italy*
***** KTH – Space and Plasma Physics, Stockholm, Sweden*
******Alte University, Tbilisi, Georgia*
khatuna.chargazia@gmail.com

Abstract. *The study of space weather, particularly its influence on Earth's atmospheric dynamics, has gained attention due to its potential impact on various technological systems, communication networks, and even global climate. Recent advancements in Artificial Intelligence (AI) have opened new pathways to investigate and understand the connections between space weather phenomena and atmospheric instabilities on Earth. This paper explores the application of AI models, particularly machine learning (ML) techniques, to examine the interplay between space weather events – such as solar flares, geomagnetic storms, and cosmic rays – and atmospheric disturbances like thunderstorms, turbulence, and jet stream anomalies. By analyzing large datasets from both space weather satellites and ground-based atmospheric sensors, AI-driven algorithms aim to identify correlations and predict how space weather can trigger or exacerbate atmospheric instability.*

Key Words: *Climate change, solar wind – magnetic field interaction, artificial intelligence.*

Introduction

Space weather refers to the changing conditions in space driven primarily by solar activity, including solar flares, CMEs, high-speed solar wind streams, and variations in the interplanetary magnetic field (IMF). When these disturbances interact with Earth's magnetosphere and ionosphere, they can trigger geomagnetic storms, ionospheric scintillations, and even influence tropospheric circulation patterns.

Understanding the connection between solar space weather and Earth's atmospheric instabilities is a complex problem due to: the multi-scale nature of interactions, the nonlinear coupling between solar drivers and atmospheric responses, and the rarity of extreme events such as Carrington-class storms.

Traditional models based on magnetohydrodynamics (MHD) and atmospheric circulation provide insights but are limited in forecasting skill. AI and machine learning (ML) offer complementary capabilities: the ability to process massive datasets, identify hidden structures, and improve predictive power.

Prikryl et al. [2], for example, found a connection between SW activity and extratropical cyclones in the northern hemisphere. They hypothesized that high-speed SWs generate atmospheric gravity waves that can reach the troposphere, transferring energy from the aurora region to the troposphere, initiating convection and altering the distribution of clouds and precipitation. Earlier, Elsner and Jagger [3] found a similar connection between intense tropical cyclones occurred during stronger solar activity, finding that their results were in accordance with the heat-engine theory of hurricanes: an active sun warms the lower stratosphere and upper troposphere due to the ozone's absorption of UV radiation, which reduces the temperature difference between the surface and the top of hurricanes.

More recently, working on even smaller timescales, Todorović and Vujović [4] researched the link between geomagnetic activity and the passage of atmospheric cold fronts. They proposed a mechanism for which when less solar UV radiation reaches the stratosphere, less ozone is created, less warming happens in the stratosphere, and the temperature gradient is weaker, ultimately leading to a weakening of the stratospheric jet stream.

Earth's atmosphere and its ionized part, the ionosphere, are influenced by several processes of external origin, i.e., solar and magnetospheric processes [5]. Solar electromagnetic radiation and solar wind (SW) particle flux deeply affect the circumterrestrial environment. In particular, solar wind energy is transmitted to the different layers of the atmosphere through magnetospheric processes. For example, energetic particle precipitation at auroral latitudes from the radiation belts and magnetic Field-Aligned Currents closing in the high-latitude ionosphere are very important in producing changes in the structure of the atmosphere. The electron precipitation during magnetospheric storms and substorms plays a role, by ionization, in the atmospheric chemical composition and conductivity variations.

This study aims to investigate the potential links between space weather events and atmospheric instabilities using AI-based models. By leveraging deep learning algorithms and advanced statistical techniques, we seek to identify patterns, causal relationships, and predictive indicators that could improve our understanding of how space-originated disturbances affect atmospheric behavior [1]. The ultimate goal is to enhance predictive meteorological models and contribute to a more resilient understanding of Earth's coupled space-atmosphere system. Research in recent decades has particularly focused on finding links between the changing activity of the sun and processes in Earth's atmosphere lasting not less than several days or years. Only relatively recently have scientists put efforts into understanding how geomagnetic activity can affect the weather over timescales of less than a week. Most of them suggested that there is an important downward impact from the SW to the middle and then lower atmosphere that influences weather development.

Study area, material and methods

In this study, using monthly resolution data to understand more broadly the conditions that lead to geomagnetic storms is analysed. By incorporating the interplanetary magnetic field and other heliophysical variables like solar wind speed and interplanetary magnetic field the effect of the latter with geomagnetic field fluctuations is revealed.

The data used in this study are from the OMNI2 dataset, which is available in the https://omniweb.gsfc.nasa.gov/ directory of the NASA OMNIWEB website. These data comprise hourly mean values of the interplanetary magnetic field (IMF), solar wind plasma parameters, and various geomagnetic and solar activity indices, as well as energetic proton fluxes [1].

OMNI2 was developed at the NSSDC (National Space Science Data and Services Center) in 2003 as an evolution of the OMNI data set, initially created in the mid-1970s. These data are collected from various NASA space missions, including: IMP 1, 3, 4, 5, 6, 7, 8 these space probes [6], also known as Explorers, have contributed significantly to the collection of data on the interplanetary environment near Earth orbit; WIND [7], is a space mission equipped with a magnetometer, has provided detailed measurements of the solar wind and the interplanetary magnetic field; ACE (Advanced Composition Explorer) [8] which is a space probe that has collected precise measurements of solar wind and energetic particles from its orbit around the L1 Lagrange point; and Geotail [9], a joint mission between JAXA (Japan Aerospace Exploration Agency) and NASA; among others.

Also, data from the Dusheti Observatory is used to study the properties of global geomagnetic storms as measured in the territory of Georgia. This analysis is crucial due to the impacts of the storms on technology and human activities, for example causing power outages and disturbing communication, making it important to understand their local effects [10], whose extent in Georgia is currently unknown.

The Dusheti geomagnetic data have been used only in a very limited number of studies [11, 12], and are therefore currently strongly under-exploited. Being the only geomagnetic 159 field measurement station in Georgia, this database represents a unique, precious asset 160 for the study of geomagnetism and space weather in the Caucasus area. This study focuses on data collected from January to August, 2024. We will use measurements of the horizontal component of the geomagnetic field, H, with 1-minute resolution, allowing for a detailed temporal analysis and still ensuring sufficient coverage. A few data gaps, which amounted to roughly 0.7% of the entire geomagnetic data, were filled using linear interpolation. The data used in this study are available in a Zenodo repository 1 [11]. As an initial assessment of data quality, we compare the Dusheti measurements of H with the SYM-H index obtained from OMNIWeb. The comparison shows excellent agreement between the two measurements, visually validating the accuracy of the Dusheti Observatory data. This enables further analysis of Dusheti Observatory measurements of the geomagnetic field perturba-

tions. During storm commencements (SCs), abrupt increases in the geomagnetic field H component are systematically recorded by magnetometers worldwide, with amplitudes as large as 69.2 nT being well documented for the May 2024 storm [14]. The Dusheti Observatory measurements showed a similar increase, with the H component reaching -307 nT.

The approach involves robust statistical models, including multiple linear and nonlinear regressions and machine learning models, to capture the non-linear dynamics between the number of Geomagnetic storms and predictor variables. This offers a more comprehensive understanding of the factors influencing them and enhances predictive accuracy beyond traditional correlational analyses.

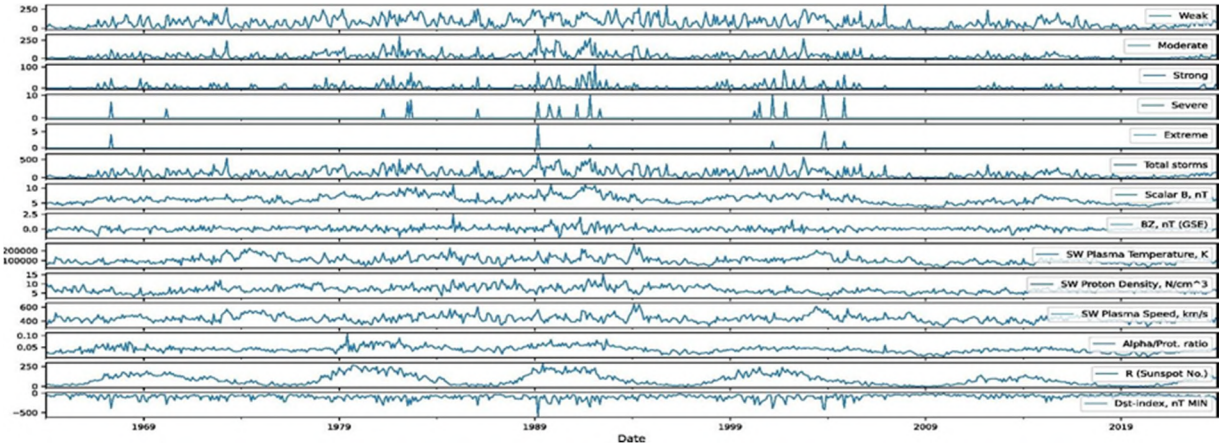

Fig. 1. Temporal distribution and evolution of geomagnetic storms.

Fig. 1. shows the temporal distribution and evolution of geomagnetic storms according to Dst index, for cycles 20 to 25 (still in progress) from the data collected and processed. Additionally, the temporal distribution of the heliospheric dynamics supporting variables is shown. The figure shows a clear correlative trend between the number of geomagnetic storms and some solar indices, particularly sunspots and interplanetary magnetic fields.

In order to detail a methodology, HSIC-Lasso nonlinear regression analysis is used to detect nonlinear Granger-causal relationships from solar-wind and interplanetary magnetic field (IMF) variables onto geomagnetic indices (e.g., Dst, SYM-H, AE, Kp). The results are results with linear Granger causality and information-theoretic methods (transfer entropy / conditional mutual information), validated via permutation tests and storm case studies, and assess robustness across solar-cycle phases.

Geomagnetic indices respond nonlinearly to drivers such as IMF Bz, solar wind speed/density and dynamic pressure; linear Granger tests miss nonlinear couplings. HSIC (Hilbert–Schmidt Independence Criterion) measures nonlinear dependence in RKHS; HSIC-Lasso blends HSIC dependency scoring with Lasso-style sparse selection, making it suitable to discover a sparse set of nonlinear predictors from many lagged candidate variables.

Fig. 2. shows which lagged solar wind features (like Bz lag 5 or V lag 10) are most strongly selected as causal predictors of the geomagnetic index (Dst).

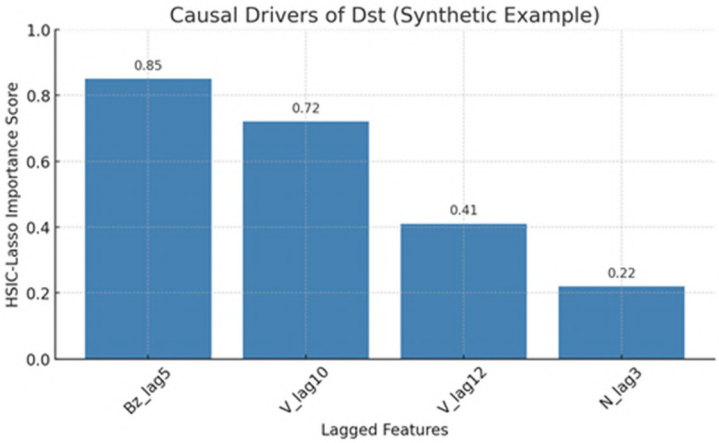

Fig. 2. the HSIC-Lasso causal importance plot.

Conclusion

The study of solar wind–geomagnetic interactions remains a central challenge in space weather research, as nonlinear coupling processes govern how interplanetary conditions drive magnetospheric and ionospheric responses. Traditional approaches such as linear Granger causality provide valuable insights into time-lagged dependencies, but they often fail to capture the nonlinear and high-dimensional nature of solar wind–magnetosphere coupling.

In this work, the integration of HSIC-Lasso with causality analysis demonstrates a powerful framework for identifying the most relevant solar wind drivers of geomagnetic activity. By combining nonlinear dependence measures with sparse feature selection, HSIC-Lasso is capable of isolating meaningful lagged predictors – such as southward IMF Bz and solar wind speed at 20–60 minute delays – while suppressing spurious correlations. This ability to extract causal structures directly from complex, multivariate time series offers a more physically consistent representation of the solar wind–geomagnetic system compared with purely linear methods.

The results underscore that nonlinear causality models are better suited than linear Granger causality for space weather studies, particularly during intense geomagnetic storms where interactions are highly nonlinear. Moreover, this methodology provides a foundation for operational forecasting systems, in which causal drivers identified by HSIC-Lasso can be integrated into hybrid AI models for real-time storm prediction.

Future work should extend this framework to include multi-scale analysis (e.g., wavelet-based decomposition), cross-index coupling (Dst, SYM-H, AE, Kp), and validation across multiple storm events to test robustness. In addition, integrating this causality-based feature selection with deep learning architectures could further enhance both interpretability and predictive performance.

In summary, HSIC-Lasso–based Granger causality analysis offers a promising pathway to uncovering the nonlinear causal mechanisms that connect solar wind dynamics to Earth's magnetospheric response, strengthening both scientific understanding and the practical forecasting of space weather hazards.

References

1. Sierra-Porta D., Petro-Ramos J.D., Ruiz-Morales D.J., Herrera-Acevedo D.D., García A.F., Teheran, M. Tarazona Alvarado., Machine learning models for predicting geomagnetic storms across five solar cycles u sing Dst index and heliospheric variables. // Advances in Space Research. V. 74, Issue 8, 2024, pp. 3483-3495.
2. Prikryl P., Iwao K. Muldrew D.B., Rušin V., Rybanský M., Bruntz R., A link between high-speed solar wind streams and explosive extratropical cyclones. // J. Atmos. Sol.-Terr. Phys. 149, 2016, pp. 219–231.
3. Elsner J.B., Jagger T.H., United States and Caribbean tropical cyclone activity related to the solar cycle. // Geophys. Res. Lett. 2008, 35, L18705.
4. Todorović N., Vujović D., Links between geomagnetic activity and atmospheric cold fronts passage over the Belgrade region, Serbia. Meteorol. Appl. 29, 2022, e2107.
5. Yiğit E., Knížová P.K., Georgieva K., Ward W., A review of vertical coupling in the Atmosphere-Ionosphere system: Effects of waves, sudden stratospheric warmings, space weather, and of solar activity. // J. Atmos. Sol.-Terr. Phys. 141, 2016, pp. 1–12.
6. Fairfield D., Lepping R., Hones Jr. E. , et al., Simultaneous measurements of magnetotail dynamics by imp spacecraft. J. Geophys. Res.: Space Phys., 86 (A3), 1981, pp. 1396-1414, 10.1029/JA086iA03p01396
7. Ogilvie K.,Desch M., The wind spacecraft and its early scientific results. Adv. Space Res., 20 (4–5), 1997, pp. 559-568, 10.1016/S0273-1177(97)00439-0
8. Garrard T., Davis A., Hammond J. et al., The ace science center. The Advanced Composition Explorer Mission,1998, pp. 649–663. doi: 10.1007/978-94-011-4762-0_23.
9. Frank L.A., Comprehensive Plasma Instrumentation (CPU) for the Geotail spacecraft. Technical Report., 1994. URL:https://ntrs.nasa.gov/api/citations/19960041496/downloads/19960041496.pdf
10. Breus T., Halberg G., Cornelissen G., Effect of solar activity on the physiological rhythms of biological systems. Biofizika, 40 (4), 1995, pp. 737–748.
11. Tsulukidze L., Geomagnetic data from dusheti geophysical observatory, 2023-07-25 to 2024-10-12. (2025, March). https://doi.org/10750.5281/zenodo.14973514. doi: 10.5281/zenodo.14973514751
12. Tsulukidze L. K., Kharshiladze O. A., Ghurchumelia A. P., Sorriso-Valvo L., Elbakidze K. Z., Matiashvili, T. G., Coherent analysis of intense geomagnetic disturbances using Dusheti observatory data and the dst index. Journals of Georgian Geophysical Society, 27 (2), 2024.
13. Diaz J., Monitoring may 2024 solar and geomagnetic storm using broadband seismometers. Scientific Reports, 14 (1), 2024, pp. 1–13.

1st International Scientific Conference "Modern problems in Geophysics", Proceedings,
ISBN 978-9941-36-434-1, ISSN 3088-4349, Tbilisi, Georgia, November 6-8, 2025

MODELING SOLAR WIND ACTIVITY USING A PHYSICAL SECOND-ORDER OSCILLATOR APPROACH

Kiria T., Nikolaishvili M., Chkhaidze T.

Mikheil Nodia Institute of Geophysics of IvaneJavakhishvili Tbilisi State University, Tbilisi, Georgia
kiria8@gmail.com

Abstract. *This paper presents a second-order differential equation model describing the dynamics of solar wind activity. The model captures the system's oscillatory nature by incorporating lunar illumination and daily periodic forcing as external drivers. Parameter calibration shows the model's capacity to forecast activity trends with physical interpretability.*

Key words*: geomagnetism, geophysics, modeling*

1. Introduction

Solar wind represents a continuous flow of charged particles ejected from the upper atmosphere of the Sun. These particles carry with them magnetic fields and energy that interact with Earth's magnetosphere, producing a variety of geophysical effects such as auroras, geomagnetic storms, and disruptions to satellite communications and GPS systems. The ability to model and predict variations in solar wind activity is critical for space weather forecasting and for understanding broader Sun-Earth interactions.

Traditional models often rely on statistical correlations or machine learning approaches that lack physical interpretability. In contrast, this work proposes a second-order differential equation model based on physical principles, treating solar wind activity as an oscillating system influenced by both the Earth's diurnal cycle and lunar gravitational modulation.

2. Model Description

We consider the solar wind intensity S(t) to be governed by a forced damped oscillator model, described by the equation:

$$d^2S/dt^2 + \gamma \cdot dS/dt + \omega_0^2 \cdot S = A \cdot \cos(\omega \cdot t + \varphi) + B \cdot M(t)$$

This equation models the dynamics of solar wind as a system responding to two primary external influences:

1. The periodic effect of Earth's rotation, approximated by a cosine function with frequency ω and amplitude A.
2. The modulating effect of the Moon, modeled using lunar illumination percentage M(t), scaled by coefficient B.

The left-hand side represents the internal dynamics of the system, including acceleration (second derivative), damping (first derivative), and restoring force (proportional to S). This model framework reflects the dynamics of many naturally oscillating systems such as pendulums, circuits, and planetary orbits. [1]

3. Calibration and Results

To make the model applicable to real-world data, we performed parameter optimization using historical solar wind records and corresponding lunar data. The optimization aimed to minimize the mean squared error between modeled and observed daily average solar wind activity.

Calibrated parameters:

- **γ (damping): 0.150**
- **ω_0 (natural frequency): 0.600**

– **A (forcing amplitude): 2.000**
– **ω (daily cycle frequency): 0.262**
– **φ (phase shift): ~0**
– **B (lunar coefficient): 0.030**

Simulation results indicate that the model captures the general wave-like pattern in solar wind variations. The periodic response aligns with known geomagnetic modulations, although rapid transitions and anomalies remain outside the scope of this simplified physical model. [2,3]

4. Discussion

This oscillator-based approach provides several scientific advantages:

– It offers a mechanistic understanding of solar wind dynamics grounded in physical laws.
– The model is interpretable and extendable, allowing integration of additional forces (e.g., solar flares).
– Unlike black-box methods, this formulation can explain not just when a change occurs, but why.

The use of lunar illumination as a modulating factor is an innovative element, representing the gravitational or tidal effect on solar-terrestrial coupling. While small in magnitude, its inclusion slightly improves model accuracy and reflects a realistic celestial interaction.

We acknowledge limitations: the current model assumes linearity and does not account for stochastic effects or multi-scale turbulence. Further improvements may include introducing nonlinear restoring terms or stochastic forcing to represent solar flare randomness.

In future work, the model may be expanded by incorporating a cubic nonlinearity in the restoring force, enabling the system to exhibit asymmetrical oscillations or potential bifurcations. Such modifications can simulate threshold-based behavior commonly seen in space weather events, especially during geomagnetic storm triggers. [4]

Additionally, a hybrid approach can be explored where the physical model provides the foundational trend, and a residual machine learning model (such as a recurrent neural network) predicts rapid fluctuations. This combination of physical interpretability and data-driven precision could provide a robust framework for operational forecasting systems in heliophysics.

This work represents a step toward blending physical intuition with predictive precision in geophysical modeling (Fig.1, Fig. 2).

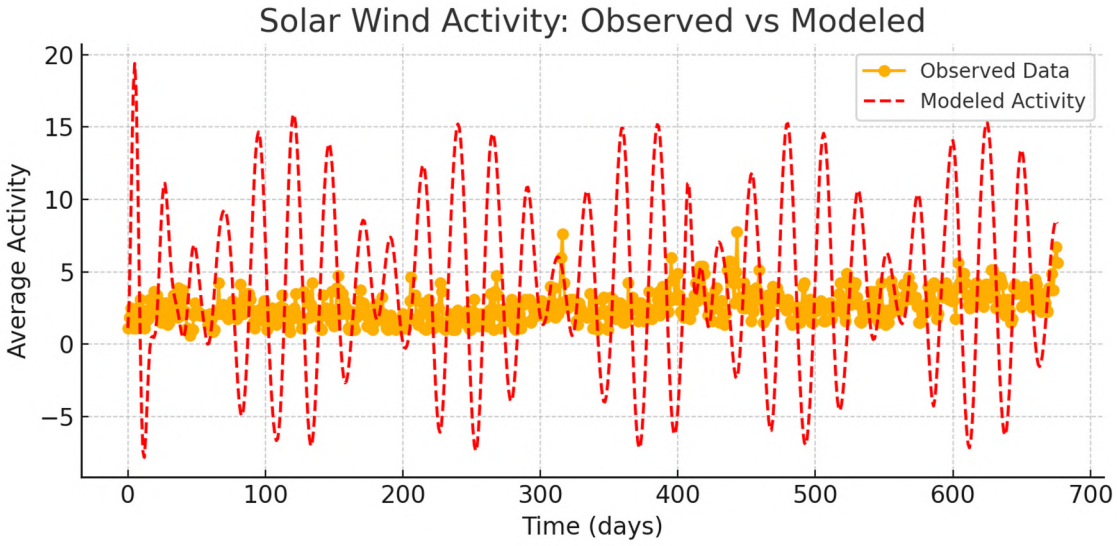

Fig. 1. Solar Wind Activity: Observed vs Modeled.

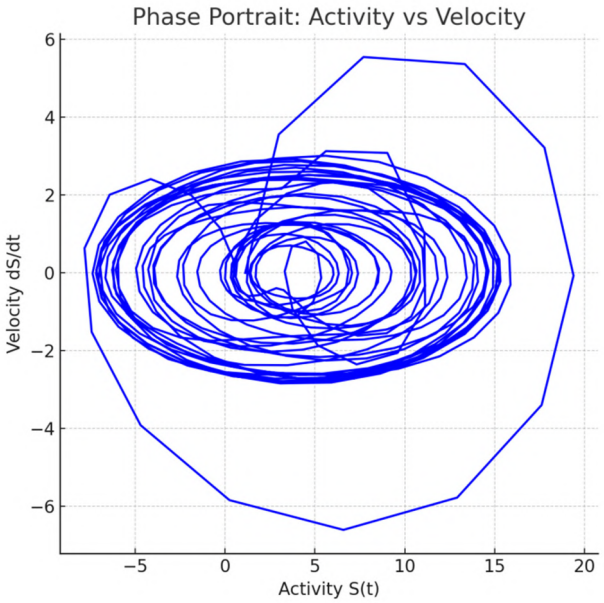

Fig. 2. Phase Portrait: Activity vs Velocity

5. Conclusion

The proposed second-order physical model demonstrates that solar wind activity can be effectively represented using a damped harmonic oscillator framework. This model, with calibrated coefficients, serves not only as a forecasting tool but also as a foundation for theoretical exploration of space weather systems. The results encourage the incorporation of both celestial mechanics and physical dynamics into future predictive models.

Potential expansions include:

– Coupling this model with magnetospheric response simulations
– Embedding stochastic terms to reflect flare unpredictability
– Hybrid modeling with machine learning to improve short-term accuracy

This work represents a step toward blending physical intuition with predictive precision in geophysical modeling.

References

1. Hargreaves J.K., The Solar-Terrestrial Environment, Cambridge University Press, 1992, pp. 1–420.
2. Schwenn R., Space Weather: The Solar Perspective, Living Reviews in Solar Physics, 2006, pp. 1–72.
3. Zhang J. et al., Solar Wind Sources and Heliospheric Impacts // Journal of Geophysical Research, 2015, pp. 6005–6024.
4. Kiria T., et al., On the Oscillatory Modelling of Geomagnetic Parameters // Georgian Geophysical Journal, v. 2023, pp. 22–30.

1st International Scientific Conference "Modern problems in Geophysics", Proceedings,
ISBN 978-9941-36-434-1, ISSN 3088-4349, Tbilisi, Georgia, November 6-8, 2025

FORBUSH EFFECT AND THE MAY 2024 AURORA IN GEORGIA: APPLICATION OF THE HAVOK METHOD IN COSMIC RAY ANALYSIS

Takadze G., Lary D., Bakradze T., Glonti N., Erkomaiashvili T., Demurishvili Z.

Ivane Javakhishvili Tbilisi State University, Mikheil Nodia Institute of Geophysics, Tbilisi, Georgia
Cosmic Ray Observatory, Tbilisi, Georgia
gtakadze95@gmail.com

Abstract*. The Forbush decrease – a sudden and temporary reduction in the intensity of galactic cosmic rays – is one of the key physical processes driven by solar coronal mass ejections (CMEs) and dynamic variations of the interplanetary magnetic field. These phenomena are closely linked to space weather and can cause both technological disruptions (e.g., satellite communication failures) and spectacular optical effects such as auroras. In May 2024, Georgia experienced a rare event – the naked-eye observation of aurora – associated with an extreme geomagnetic storm and a concurrent Forbush decrease. Such manifestations are extremely uncommon at Georgia's latitude and provide a unique opportunity to study how global solar activity is reflected in regional cosmic ray variations. This paper describes the mechanism of the Forbush effect, examines the May 2024 event, applies the HAVOK method for the analysis of cosmic ray data, and incorporates both local observations (from the Tbilisi Neutron Monitor) and global datasets.*

Key words: *cosmic rays, Forbush decreases, magnetosphere, solar wind*

The Forbush effect was first described by Scott Forbush in 1937. It is based on the influence of magnetic clouds ejected after solar eruptions, which, upon reaching Earth, temporarily "block" high-energy galactic particles, i.e., cosmic rays. As a result, the intensity of cosmic rays recorded by neutron monitors drops sharply within a few hours and then gradually returns to its normal level. The magnitude of this decrease can range from 2% to 30%, depending on the storm. Forbush effects occur most frequently during the years of maximum solar activity. The year 2024, marking the peak of Solar Cycle 25, corresponds precisely to such a period [1-5].

The May 2024 Event and the Aurora in Georgia

At the beginning of May, specifically between May 10–12, an X-class solar flare occurred – a sudden and powerful energy release on the solar surface caused by the reconnection and abrupt release of magnetic field lines. Such flares emit large amounts of electromagnetic radiation, including X-rays and ultraviolet radiation, which can affect Earth's ionosphere and lead to radio communication disturbances.

The solar active region AR3664, highly dynamic during May 2024, stood out due to its size and complex magnetic structure, making it one of the most active and powerful regions of Solar Cycle 25.

On May 10, 2024, AR3664 produced an X3.98-class solar flare, which caused temporary radio communication disruptions across Asia and Eastern Europe. Later, on May 14, the same region generated an X8.7-class flare – the strongest recorded flare of Solar Cycle 25. These events were also associated with coronal mass ejections (CMEs) directed toward Earth, which triggered severe geomagnetic storms, reaching G5 level – the highest on the geomagnetic storm scale.

When the CME impacted Earth's magnetosphere a few days later, a G5 geomagnetic storm was registered, with a Dst index of −412 nT, indicating a major distortion of Earth's magnetic field. As a result of this storm, solar energetic particles penetrated into the lower layers of the ionosphere, producing:

- **Forbush decrease** (with neutron monitor data showing an intensity reduction of approximately 12–15%);
- **Expansion of the auroral zone** toward lower geographic latitudes (documented by photographs from Georgia, Turkey, and Greece);
- **Temporary disruptions of radio communication** in the HF spectrum.

The Georgian Cosmic Ray Laboratory (affiliated with Tbilisi State University) recorded a significant drop in cosmic ray intensity on May 11–12, 2024. A change of this magnitude had last been observed in 2003, during the so-called "Halloween storms."

Application of the HAVOK Method

Method Description HAVOK (Hankel Alternative View of Koopman) is a modern technique for analyzing nonlinear dynamical systems. It is based on the following principles:

1. **Construction of the Hankel matrix**: from the observed time series, a Hankel matrix is built, where the rows represent lagged snapshots.
2. **SVD (Singular Value Decomposition)**: applied to the matrix to separate the dominant components.
3. **Reconstruction of the Koopman operator**: the underlying time dynamics are recovered through a linear oscillatory system.

$$\frac{d\mathbf{v}}{dt} = \mathbf{A}\mathbf{v} + Br(t)$$

where **v** represents the SVD-projected dimension, and **r(t)** denotes the unmodeled (chaotic) component.

Application in the Analysis of the Forbush Effect

The HAVOK model was built using data from the Tbilisi Neutron Monitor (5-minute averaged intensity) for the period of May 5–15, 2024.

- Main finding: the second SVD component clearly shows the drop in high-energy cosmic ray intensity during May 11–12, corresponding to the Forbush decrease.
- Koopman system reconstruction: a differential model was obtained that describes the dynamics of neutron activity and recovers structural resonances.
- The residual HAVOK forcing term r(t) reached its peak during the night of May 11, indicating external physical forcing from a solar origin.

Beyond the impact on the geomagnetic environment, variations in cosmic ray intensity are also expected to influence the chemical composition of Earth's lower atmosphere. In particular, cosmic-ray-induced ionization may affect concentrations of reactive species such as NO_2, ozone (O_3), and even particulate matter (PM2.5), which are key indicators of air quality (AQI).

The application of the HAVOK method allows us to evaluate whether nonlinear or time-lagged relationships exist between cosmic rays and air quality. For this purpose, data from spring 2024 were analyzed:

- Five-minute cosmic ray intensity records from the Tbilisi Neutron Monitor;
- Hourly PM2.5, PM10, and NO_2 measurements from air quality sensors in Tbilisi (stations: Tsereteli, Varketili, Dighomi).

HAVOK models were constructed separately for both datasets, yielding several important observations:

- SVD components revealed simultaneous or slightly time-shifted variations on May 11–12, coinciding with the Forbush event;
- Koopman system analysis showed that peaks in the hidden chaotic forcing of neutron activity matched negative changes in air quality, particularly for NO_2;
- The relationship was not strictly linear or correlational, but the HAVOK residual (forcing term) indicated that atmospheric conditions responded to external cosmic influences with a time delay of 3–6 hours.

These results suggest that HAVOK can serve as an intermediate analysis tool capable of identifying possible links between different physical processes even when conventional statistical methods fail. Future work includes expanding the dataset to cover the full years 2023–2024 and performing simultaneous analyses with additional environmental parameters such as temperature and humidity. The hypothesis that cosmic rays influence atmospheric ion balance, thereby creating conditions for transformations of reactive atmospheric components, requires further confirmation through laboratory and satellite observations.

Global and Regional Parallels The geomagnetic storm of May 11–12, 2024, exceeded even the intensity of the famous 2003 events. During the same days:

- In the Barents Sea, auroras were observed accompanied by disruptions in the navigation systems of nuclear submarines.
- In Japan, HF radio communication was interrupted for about five hours.
- In Australia, neutron monitor data showed a Forbush decrease of ≥20%.

By comparison, the Tbilisi Neutron Monitor recorded an intensity drop of about ~13% – a significant value for Georgia's latitude – confirming that the event was truly global in scale and extended into mid-latitudes.

Conclusion

The Forbush decrease is a key manifestation of solar activity that impacts both the global and local environment. The May 2024 storm and the appearance of aurora in Georgia represented rare and scientifically valuable events. The application of the HAVOK method made it possible to achieve a disciplined interpretation of the data, separating external solar forcing from intrinsic system dynamics. Looking ahead, the use of this method may become part of space weather forecasting, especially as high-resolution time series data continue to become rapidly available.

References

1. Abunina M. A., On the features of great Forbush effect during May 2024 extreme geomagnetic storm.
2. Mavromichalaki H., et al., Unusual Forbush Decreases and Geomagnetic Storms on 24 March, 2024 and 11 May, 2024.
3. Hayakawa H., et al., The Solar and Geomagnetic Storms in May 2024: A Flash Data Report.
4. Global Survey Method (GSM) and Ring of Stations Method (RSM). Holt–Winters Method for Time Series Analysis.
5. Bakradze T., Glonti N., Erkomaiashvili T., Demurishvili Z., Takadze G., Barbakadze P., Gogua R., Alania E., Cosmic ray modulation effects related to solar activity. International Scientific Conference, Tbilisi, 2024.

1st International Scientific Conference "Modern problems in Geophysics", Proceedings,
ISBN 978-9941-36-434-1, ISSN 3088-4349, Tbilisi, Georgia, November 6-8, 2025

WAVELET-COHERENCE AND MULTIFRACTAL ANALYSIS OF GEOMAGNETIC DISTURBANCES

[*]Kharshiladze O., [*]Tsulukidze L., *Zilpimiani D.,*Ghurchumelia A., [,***]Sorriso-Valvo L., [***]Elbakidze K., [*****]Yordanova E., [*]Matiashvili T.,**

[*]M. Nodia Institute of Geophysics of the I. Javakhishvili Tbilisi State University, Tbilisi, Georgia
[**]Space and Plasma Physics, KTH Royal Institute of Technology, Stockholm, Sweden
[***]CNR, Istituto per la Scienza e Tecnologia dei Plasmi, Bari, Italy
[****]Business and Technology University, Tbilisi, Georgia
[*****]Swedish Institute of Space Physics (IRF), Uppsala, Sweden
oleg.kharshiladze@tsu.ge

Abstract*. This work explores the solar wind–magnetosphere interaction during the major geomagnetic disturbances of 2024, with particular focus on the May 11 storm. We examined how variations in the interplanetary magnetic field's B_z B_z component and solar wind dynamic pressure (P_d P_d) translate into magnetic perturbations on Earth. The response of the terrestrial system was evaluated using horizontal field measurements from mid-latitude observatories together with the global SYM-H and auroral AL indices. Time–frequency analysis with wavelet coherence exposed the highly scale-dependent and non-stationary character of the coupling process. In addition, multifractal detrended fluctuation analysis revealed a marked reduction in the Hurst exponent during the May 11 event. This feature was present in both mid-latitude and auroral electrojet records but absent in SYM-H, highlighting distinct regional responses. The absence of this feature in the ring current index, coupled with its presence in mid-latitude and auroral records, indicates that the auroral oval expanded equatorward, leaving a clear imprint at lower latitudes. Our findings highlight that combining localized and global perspectives is essential to fully capture the diverse impacts of severe geomagnetic storms on the near-Earth environment.*

Key Words: *Space weather, Geomagnetic activity, Coherence analysis, Multifractal analysis.*

Introduction

The dynamics of the solar wind and magnetosphere interaction form a fundamental domain of space physics, giving rise to a number of space weather phenomena [1]. The biggest consequence of this interaction is the geomagnetic storm [2], a severe global perturbation of the Earth's magnetic field. These events are not solely of theoretical interest; they have significant practical implications, including the induction of geomagnetically induced currents (GICs) that can damage power grids [3], the disruption of satellite-based communications and navigation systems, and the creation of radiation hazards for both aviation and human spaceflight. Consequently, a comprehensive understanding of the dynamics of these events is essential. This study examines the magnetospheric response to solar wind drivers during the geomagnetic storms of early 2024, integrating both local, ground-based measurements and global geomagnetic indices to provide a multi-scale analysis of the system's complex behavior.

Study area, material, and methods

The primary material for this investigation is the intense space weather events of 2024, most importantly the geomagnetic storm of May 11. Our analysis is based on a multi-source dataset designed to capture both global and local magnetospheric responses.

High-resolution (1-minute) data were utilized from a mid-latitude geomagnetic observatory (like Dusheti, Georgia) to provide a localized perspective on the magnetic field variations. To place these local measurements in a global context, we employed two widely used geomagnetic indices. The Symmetric disturbance index (SYM-H) was used to characterize the evolution of the globally symmetric ring current,

which is a primary driver of magnetic field disturbance during storms [4]. To capture high-latitude activity, we used the Auroral Low (AL) index, which measures the maximum westward auroral electrojet and serves as a key indicator of magnetospheric substorm activity [5].

The external drivers of these magnetospheric changes were characterized using solar wind parameters obtained from the OMNIweb database, time-shifted to the Earth's bow shock nose [6]. We applied Wavelet Coherence Analysis to resolve time–frequency correlations between solar wind drivers and geomagnetic responses, and Multifractal Detrended Fluctuation Analysis (MFDFA) to characterize long-range memory and scaling complexity of the time series.

Results

Wavelet-Coherence analysis.

To explore time-dependent correlations between two signals, we applied wavelet coherence, which maps the correlation of the series across both time and frequency scales. This approach has become a standard tool in space physics and geophysics applications [7,8]. Our analysis reveals that during the intense geomagnetic storms, the coherence between the interplanetary magnetic field. Coherence between B_z B_z and the geomagnetic field's H component covers a wider range of frequencies than during the quiet times. It is noteworthy that the coherence picture between solar wind drivers and the geomagnetic response was different for the AL and SYM-H indices, suggesting that the auroral and ring current systems respond with different frequency-dependent characteristics to the same solar wind drivers. The same analysis was used for pressure (P_d P_d) and the horizontal component of the geomagnetic field, which showcased generally the same but slightly different coherent picture. These results are presented in Fig. 1.

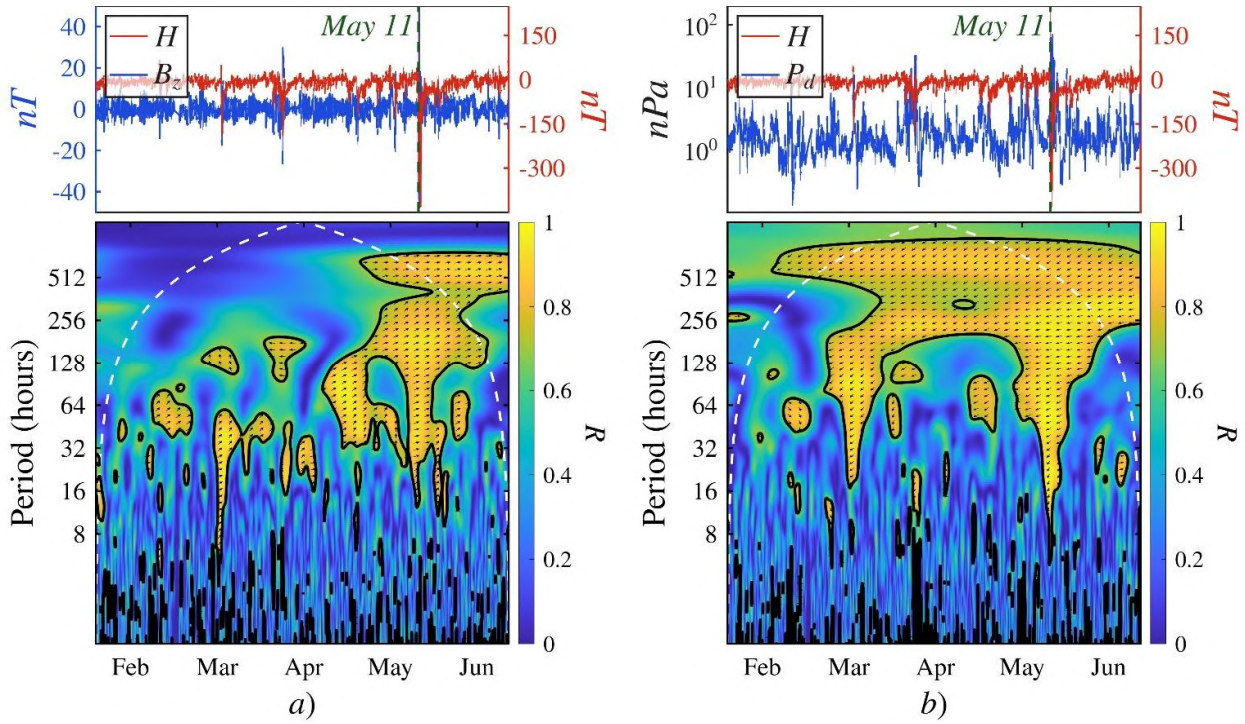

Fig. 1. Wavelet coherence analysis illustrating the coupling between the local horizontal geomagnetic field component (H) and key solar wind drivers. Panel (a) displays the coherence with the z component of the Interplanetary Magnetic Field (B_z B_z), while panel (b) shows the coherence with the solar wind dynamic pressure (P_d P_d).

Multifractal Detrended Fluctuation Analysis.

Detrended fluctuation analysis (DFA) was used to investigate the geomagnetic data, in this case horizontal component of the Earth's magnetic field, recorded at the mid-latitude stations and geomagnetic indices like AL and SYM-H. Through DFA we derived the Hurst exponent, an indicator of whether the fluctuations in the signal are random, persistent, or anti-persistent across scales.

Our analysis showcases the sharp changes in the Hurst exponent associated with the major geomagnetic storms. A particularly interesting result was observed during the intense storm of May 11, 2024. We found a simultaneous sharp drop in the Hurst exponent for both mid-latitude station data and the AL index (Results are shown in Fig. 2). Crucially, this drop was not present in the SYM-H index. This synchronicity suggests a significant expansion of the auroral oval, causing auroral-driven dynamics to directly influence the geomagnetic field at mid-latitudes – a phenomenon not captured by the globally averaged ring current index.

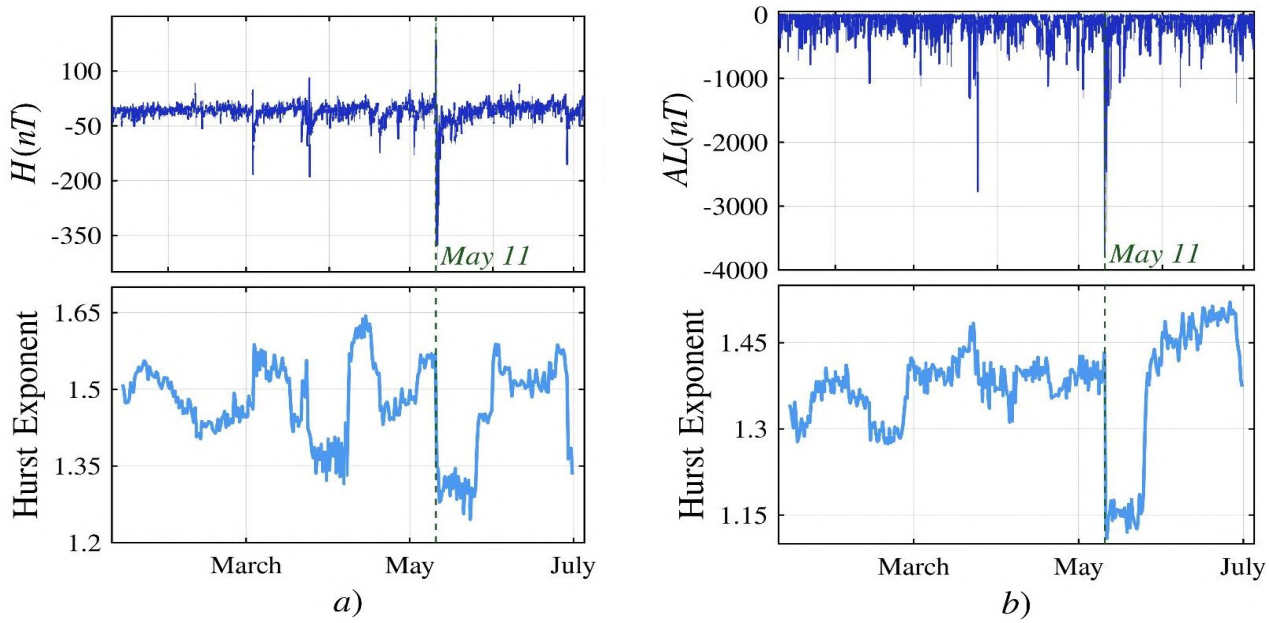

Fig. 2. Panel (a) – Windowed DFA results of the Horizontal component of the Earth's magnetic field and Panel (b) – Windowed DFA results of the AL index

Furthermore, we conducted preliminary multifractal analysis using multifractal detrended fluctuation analysis (MFDFA) [9] to quantify the complexity of these time series. The results indicate a difference in the multifractal nature:

- The AL index, representing the highly turbulent and intermittent auroral electrojet, is the most multifractal
- The mid-latitude ground station data exhibits a lesser degree of multifractality
- The SYM-H index, which represents the smoother, globally averaged ring current, is the least multifractal of all.

Conclusion

This study analyzed the intense geomagnetic storms of 2024 by comparing local mid-latitude data with global auroral (AL) and ring current (SYM-H) indices. Wavelet coherence analysis revealed the frequency-dependent nature of solar wind-magnetosphere coupling, which differs for the ring current and auroral regions. Most significantly, Detrended Fluctuation Analysis demonstrated that during the May 11 superstorm, the auroral zone expanded to mid-latitudes. This dynamic was captured by the simultaneous change in complexity in local data and the AL index, but was absent in the SYM-H index. The observed hierarchy of multifractality (AL being the most multifractal and followed by mid-latitude H and SYM-H) further quantifies the different levels of complexity in these magnetospheric regions. This work underscores the critical value of combining local and global datasets to build a comprehensive picture of geomagnetic storm dynamics.

References

1. Dungey J. W., Interplanetary magnetic field and the auroral zones. // Physical Review Letters, 6(2), 1961, pp. 47-48.
2. Chernogor L. F., What are a geospace storm and a pan-planetary storm? Advances in Space Research, 2025.

3. Kappenman J. G., Geomagnetic storms and the electric power grid. In Space weather: The physics behind the science, 2010, pp. 257-285.
4. Iyemori T., Storm-time magnetospheric currents inferred from mid-latitude geomagnetic field variations. // Journal of geomagnetism and geoelectricity, 42(11), 1990, pp. 1249-1265.
5. Davis T. N., Sugiura M., Auroral electrojet activity index AE and its universal time variations. // Journal of Geophysical Research, 71(3), 1966, pp. 785-801.
6. King J. H., Papitashvili N. E., OMNI 1-min data set, 2020.
7. Tsulukidze L. K., Kharshiladze O. A., Ghurchumelia A. P., Sorriso-Valvo L., Elbakidze K. Z., Matiashvili T. G. Coherent Analysis of Intense Geomagnetic Disturbances Using Dusheti Observatory Data and the DST Index. // Journals of Georgian Geophysical Society, 27(2), 2024.
8. Kharshiladze O. A., Tsulukidze L. K., Martiashvili M. J., Wavelet Coherence Analysis of Magnetic Declination During Quiet and Disturbed Geomagnetic Activity. // Journals of Georgian Geophysical Society, 28(1), 2025.
9. Ihlen E. A., Introduction to multifractal detrended fluctuation analysis in Matlab. // Frontiers in physiology, 3, 2012, p. 141.

1st International Scientific Conference "Modern problems in Geophysics", Proceedings,
ISBN 978-9941-36-434-1, ISSN 3088-4349, Tbilisi, Georgia, November 6-8, 2025

ENERGY SPECTRUM OF THE JUNE 2025 FORBUSH DECREASE

[*]Alania E., [*]Bochorishvili T., [*]Aslamazashvili R., [*]Bakradze T., [*]Glonti N., [*]Kiria J., [*]Erkomaishvili T., [**]Vanishvili G.

**Michael. Nodia Institute of Geophysics, Ivane Javakhishvili Tbilisi State University, Georgia.*
***Sokhumi State University, Georgia.*
g.vanishvili@sou.edu.ge

Abstract. *The article presents the determination of the energy spectrum of the intensity variations of cosmic rays, using the method developed by M. Alania and co-authors. but using a new theoretical method for determining the coupling coefficients, based on quantum field theory, which was presented by the staff of the Athens Neutron Monitor Station. Based on these assumptions, Coupling Coefficients and Energy Spectrum calculated.*

Key Words: *Coupling Coefficient, Energy Spectrum, Cut Off Rigidity, Primary Variations, Secondary Cosmic Rays Variations.*

Elementary particles moving with acceleration from the centers of galaxies and the cores of stars into interstellar and interplanetary space are called primary cosmic rays. In the process of penetrating the Earth's magnetosphere and atmosphere, as a result of interaction with matter, they lose energy and transform into secondary cosmic rays. They are registered on Earth by a worldwide network of cosmic ray stations.

The intensity $N^i_{\lambda,f}(h_0)$ of secondary cosmic rays, of any *i* type, hard (μ-mesons) or soft (neutrons), component, penetrating the Earth's Magnetosphere and Atmosphere, primary cosmic rays, recorded at a geographic λ latitude and a f longitude, with h_0 atmospheric pressure, can be represented as follows [1]:

$$N^i_{\lambda,f} = \int_{\varepsilon^{min}_{\lambda,f}}^{\infty} D(\varepsilon)\, m^i(\varepsilon, h_0)\, d\varepsilon \tag{1}$$

where $D(\varepsilon)$ is the differential energy spectrum of the primary cosmic rays; $m^i(\varepsilon, h_0)$ is a quantity that can be called "multiplicity", and represents the number of secondary elementary particles produced as a result of mutual collisions of leptons, nuclei and nucleons, with a total energy ε, which is registered by the instrument at the level of observation at atmospheric pressure h_0; $\varepsilon^{min}_{\lambda,f}$ – the effective value of minimal (critical) energy, permitted by the Magnetic Field of the Earth (Geomagnetic Cut Off Rigidity). By varying this equation, we shall obtain:

$$\delta N^i_{\lambda,f} = -\delta\varepsilon^{min}_{\lambda,f} D(\varepsilon^{min}_{\lambda,f}) m^i(\varepsilon^{min}_{\lambda,f}, h_0) + \int_{\varepsilon^{min}_{\lambda,f}}^{\infty} \delta D(\varepsilon) m^i(\varepsilon, h_0)\, d\varepsilon + \int_{\varepsilon^{min}_{\lambda,f}}^{\infty} D(\varepsilon)\, \delta m^i(\varepsilon, h_0)\, d\varepsilon \tag{2}$$

By dividing (1) on ((2), we obtain:

$$\frac{\delta N^i_{\lambda,f}(h_0)}{N^i_{\lambda,f}(h_0)} = -\delta\varepsilon^{min}_{\lambda,f} W^i_{\lambda,f}(\varepsilon, h_0)\, d\varepsilon + \int_{\varepsilon^{min}_{\lambda,f}}^{\infty} \frac{\delta D(\varepsilon)}{D(\varepsilon)} W^i_{\lambda,f}(\varepsilon, h_0)\, d\varepsilon + \int_{\varepsilon^{min}_{\lambda,f}}^{\infty} \frac{\delta m^i(\varepsilon, h_0)}{m^i(\varepsilon, h_0)} W^i_{\lambda,f}(\varepsilon, h_0)\, d\varepsilon \tag{3}$$

where $W^i_{\lambda,f}(\varepsilon, h_0) = \dfrac{D(\varepsilon) m^i(\varepsilon, h_0)}{N^i_{\lambda,f}(h_0)}$ is the coupling coefficient between primary and secondary cosmic rays.

Alania et al. have developed a method for determining the energy spectrum of secondary variations of cosmic rays based on the ratio of the intensities of secondary variations of cosmic rays at two or more stations [2,3,4,5,6].

Xaplanteris at al. developed a theoretical method for determining coupling coefficients, based on quantum field theory [7].

The article presents the determination of the energy spectrum of the intensity variations of cosmic rays, using the method developed by M. Alania and co-authors [2,3,4,5,6]. but using a new theoretical method for determining the coupling coefficients, based on quantum field theory, which was presented by the staff of the Athens Neutron Monitor Station [7].

On the first stage the Coupling Coefficients were calculated according to assumption done and formula presented, in the article of Xaplanteris at al. The following results have been obtained W = 5.1062, 5.1761, and 6.32, for Tbilisi, Athens, and Rome, with Rigidities: R= 6,91, 8.72, and 6.32 GV, respectively.

On the next stage, we found the relationship between power spectrum index γ and the functions A_1 A_2 and their ratios $A_1 A_2$, for any two stations, with just calculated Coupling Coefficient values (Rome, Tbilisi, Athens).

After determining the range of power spectrum index γ, corresponding profiles of their variations were calculated and drawn based on the average profile of intensity variations of real A_1 and A_2.

Fig.1., Fig2., Fig. 3 presents the power spectrum index γ variations, for the following pair of stations: Tbilisi/Rome, Rome/Athens, Athens/Tbilisi.

These stations are located at lower latitudes, where the Cut off Rigidity is high, and therefore, the corresponding power spectrum index γ is hard.

Using the same approach, the coupling coefficients were calculated according to assumption done and formula presented, in the article of Xaplanteris at al., for the stations located at high latitudes, with lower Cut Off Rigidity. The following results have been obtained W = -3.4124, -99.525, -9.0306, -4.9884, -714.22, -35.902, -68.374, and -32.867, for Moscow, Apatity, Newark, Kiel, Inuvik, Kergelen, Oulu, and Yakutsk, with Rigidities 2.46, 0.65, 1.97, 2.29, 0.18, 1.14, 0.81, and 1.19 GV, respectively.

Fig. 4 – Fig. 10 presents the power spectrum index γ variations, for the following pair of stations: Tbilisi/Rome, Rome/Athens, Athens/Tbilisi. Moscow/Apatity, Moscow/Newark, Moscow/Kiel, Moscow/Inuvik, Moscow/Kergelen, Moscow/Oulu, Moscow/Yakutsk.

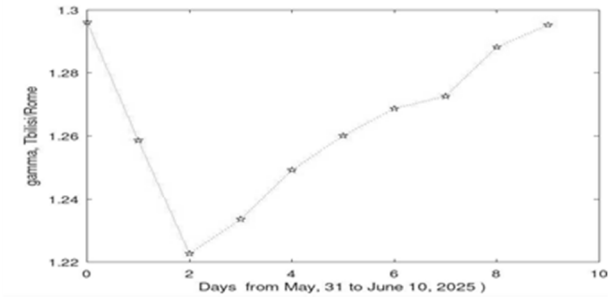

Fig. 1

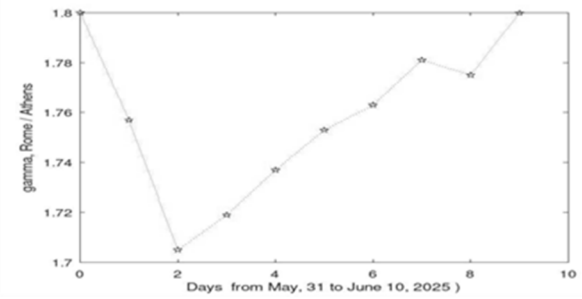

Fig.2.

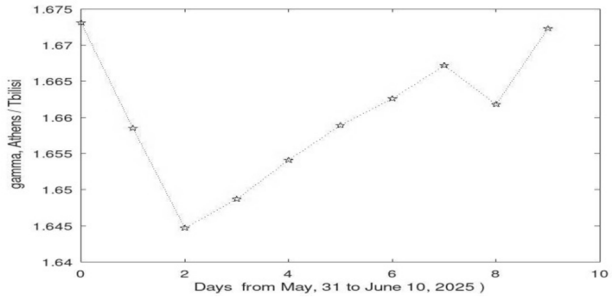

Fig 3.

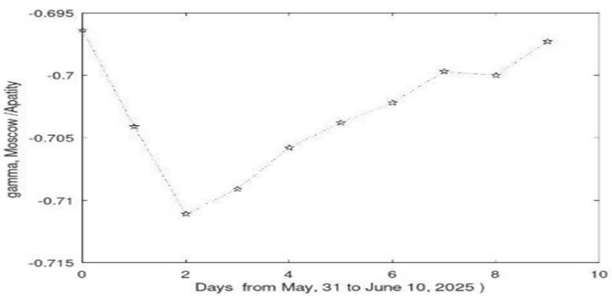

Fig. 4

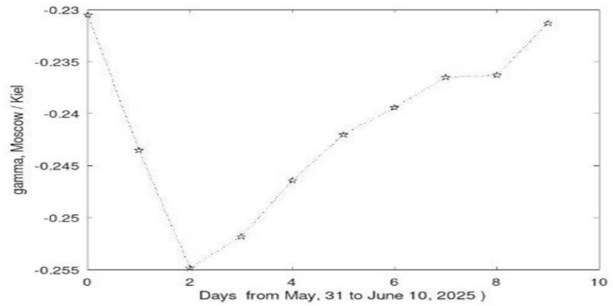

Fig 5.

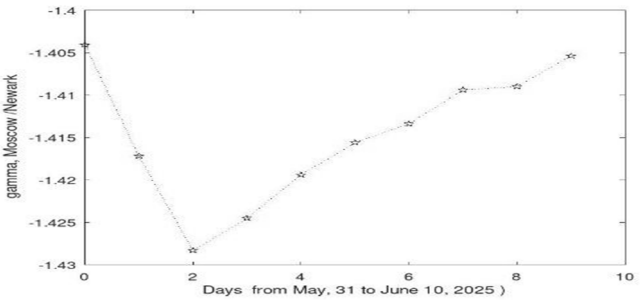

Fig. 6

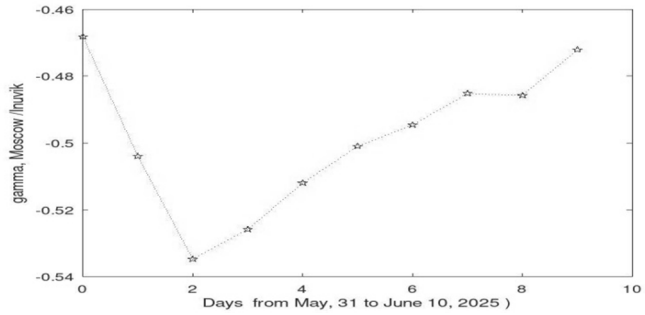

Fig 7.

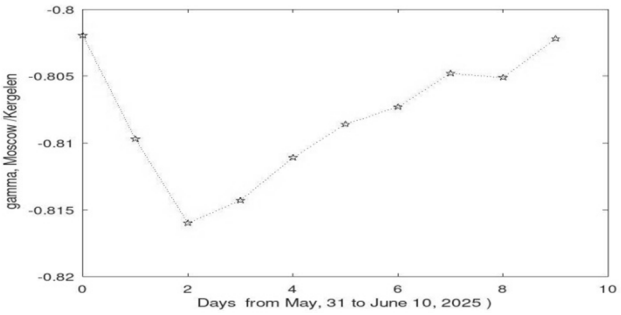

Fig. 8

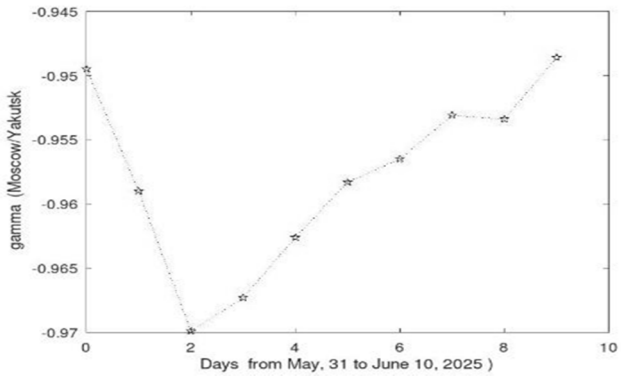

Fig 9.

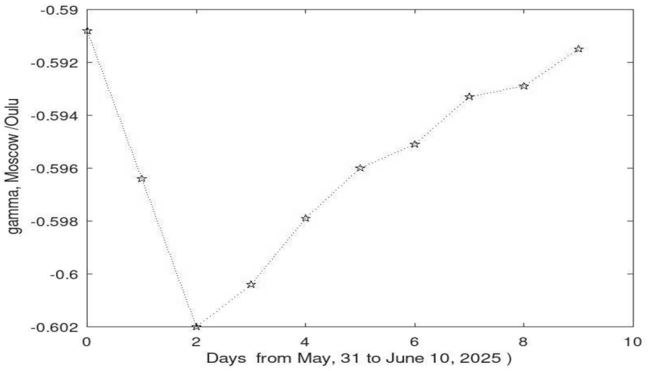

Fig. 10

These stations located at higher latitudes, where the Cut off Rigidity is low, and therefore, the corresponding power spectrum index γ is soft.

Conclusion

The energy spectrum of the Forbush effects of cosmic rays according to the data of the Neutron Monitor data with the lower CutOff Rigidity is softer than that of the second group Neutron Monitor Data with the higher CutOff Rigidity.

References

1. Dorman L. I., "Variations of Cosmic Rays". Moscow, "Main Publishing House of Technical Literature," 1957.
2. Alania M. V., Dorman L. I., Aslamazashvili R. G., Gushchina R. T., Dzhapiashvili T. V., "Modulation of Galactic Physics by the Solar Wind." Tbilisi, "Metsniereba," 1987.
3. Bochorishvili T. B., "Experimental and Model Studies of the Energy Spectrum of Long-Period Variations of Cosmic Rays." Tbilisi, 1990.
4. Alania M. V. and Wawrzynczak A., "On the Relationship of the Interplanetary Magnetic Field Turbulence and the Energy Spectrum of The Forbush Effects" – 29th International Cosmic Rays Conference Pune 1, 2005, pp. 371-374.
5. Siluszyk M., Alania M.V., Iskra K. andpMiernicki S., "Interplanetary Magnetic Field Turbulence and Rigidity Spectrum of the Galactic Cosmic Rays Variations (1969 – 2011) – Journal of Geophysical research: Space physics, pp. 30-38.
6. Alania M.V., Iskra K., Siluszyk M., "New index of The galactic cosmic ray intensity variations".
7. L. Xaplanteris, M. Livada, H. Mavromichalak "Cosmic ray spectral index by two coupling functions using data from the neutron monitor network".
https://register-as.oma.be/esww16/contributions/public/S3-P1/S3-P1-20-KsaplanterisLoukas/ESWW16S3P20XAPLANTERISetal.pdf

1st International Scientific Conference "Modern problems in Geophysics", Proceedings,
ISBN 978-9941-36-434-1, ISSN 3088-4349, Tbilisi, Georgia, November 6-8, 2025

THE EFFECTS OF LEAD RADIOISOTOPES FORMED DURING THE DECAY OF RADON ON THE HUMAN BODY AND ASSOCIATED HEALTH RISKS

[*]Gogebashvili M.E., [*]Grebenchuk H.S.,
[*]Ivanishili N.I., [*]Kalmakhelidze S.L,[**]Tulashvili E.V.

[*]Laboratory of Radiation Safety Problems, I.Beritashvili Center of Experimental Biomedicine. Georgia
[**]Material Research Institute, Iv.Javakhishvili Tbilisi State University. Georgia
gogebashvili@gmail.com

Abstract*. The work shows the pattern of formation of radiation load on red bone marrow under the influence of radon. The study is based on the process of radiation decay of radon with the formation of a lead radioisotope (210Pb). The calculation of the dose load was carried out in the following sequence: inhaled radon, radon entering the blood, distribution of the formed lead isotope, localization of lead-210 in the bones and irradiation of the red bone marrow with this radioisotope as the main hematopoietic system. The issue of the significance of the accumulation of radioactive lead in flat bones as a factor in chronic irradiation of the hematopoietic system and the associated health risks is considered.*

Key word*: radon, Lead-210, red bone marrow.*

Radon is a radioactive gas that forms as a result of the decay of uranium and radium present in rocks and soil. Being a gas of geophysical origin, it is one of the most common factors of radiation exposure in urban areas. According to the World Health Organization, it, along with tobacco smoking, is considered one of the main causes of lung cancer [1]. Based on numerous scientific studies, it has been established that the landscapes of Georgia are characterized by a high content of this gas [2]. Urban buildings are no exception [3]. Studies conducted in various residential and office premises have shown significant variations in radon content and the associated different levels of risk for the urban population [4,5]. As is known, radon is an alpha emitter. Alpha particles have high energy, but relatively low penetration ability. Therefore, radon is most dangerous when inhaled, when it enters the lungs. Moreover, the risk increases with an increase in radon concentration and duration of exposure. This is the reason why the main focus of researchers in the field of biomedicine is directed to evaluate the damaging radiobiological effect on the lungs [6,7].

However, the chain of radiation transformation of radon does not stop there. In particular, when radon enters the blood through the pulmonary alveolar mechanism, and therefore into other internal organs. However, in the scientific literature less attention is paid to the secondary effects of radon after it enters the body. In our study, we analyzed and calculated the radiation dose of critical organs, in particular, the hematopoietic system. In this regard, one of the key processes is associated with a long-lived product of radon decay – radioactive lead (^{210}Pb), which tends to accumulate in bone tissue. During the decay of ^{210}Pb, polonium-210 (^{210}Po) is formed, emitting alpha particles with an energy of 5.3 MeV. And if we take into account the fact that the main hematopoietic organ, the bone marrow, is concentrated in flat bones, and then the radiation impact on this system can be of great importance in predicting risks for the population in the case of high doses of radon exposure.

Calculating the effect of radon on critical human organs is complicated by the fact that radon itself is practically not involved in the formation of the radiobiological effect. The main radiation threat to the body is its decay products. Thus, it is precisely the calculation of the level of radiation exposure to decay products that is the main task in predicting health risks caused by elevated radon levels in urban areas. Unfortunately, today it is not completely clear with which specific types of radon decay (as well as its progens) can be adequately associated with indicators in becquerels. Therefore, the calculation was performed under the assumption that the above activity values (e.g., 100 Bq/m3) really belong to radon, although it is not possible to veri-

fy this experimentally, since counting the number of decays is not an a priori targeted process indicating their origin. In our opinion, to resolve this problem, it would be necessary to switch to an energy (spectral) analysis of radon decay products or to proceed from the well-known process of its decay. At the same time, it seems more rational to experimentally (hardware) determine the number of lead nuclei ^{210}Pb in a biological object exposed to radon and, based on this, determine the amount of radon, as well as the dose of radiation absorbed by this object.

The main objective of our study was to calculate the level of radiation exposure to the hematopoietic system of the body under conditions of the alveolar mechanism of radon intake. For this purpose, we compared the received radiation doses and the amount of ^{210}Pb arising during the decay of radon with a given activity. The calculations were carried out, on the one hand, by calculating them by estimating the decay of radon atoms based on their number, and on the other hand, based on their specific activity. The calculations were carried out for the initial specific volumetric activity of 100 Bq/m3, while it is assumed that the radon concentration remains unchanged due to its balancing from external sources. A radon dose of 100 Bq/m3 is the maximum permissible level for household conditions.

As a result of the calculations presented in Tables 1 and 2, it can be concluded that at a dose of 100 Bq/m3 (the average human weight is 70 kg blood with its volume of 5 liters), up to 6.9 x 1010 radon nuclei will enter. Later, during its decay and distribution of the formed radioactive lead in the organs (table 2), approximately 5.7% of this isotope in the flat bones (4-5 kg) (2.37), as a result the red bone marrow located in the flat bones is chronically irradiated with a dose of 2.36 nGy. However, in reality, based on the conditions of the urbanized environment, the values of radon exposure can vary widely [4,8]. And under these conditions, when determining the proportion of radioactive lead entering the body, it naturally increases in proportion to the level of inhaled radon. In this case, the most important factor is the degree of cumulativeness of a particular radioisotope mostly in bone tissue.

Table 1. Calculation of the amount of radon entering the blood
(with an activity in the air of 100 Bq/m3)

Concentration of radon nuclei in the air, N/м^3	$N_o = \varphi/\lambda$ $N_o = 100/(2{,}1 \times 10^{-6} c^{-1}) = 47.619047619 \times 10^8 =$ $= 4.7619047619 \times 10^9$
Activity in blood, Bq/м^3 (conversion factor 0.23)	0,23 x 100=23
The number of radon nuclei and an equal number of lead nuclei ^{210}Pb that entered the blood (5 liter), exposure-1 year	$1.89257142857 \times 10^8 \times 365 = 690.788571428 \times 10^8$
Decay energy of radon ^{222}Ra to lead ^{210}Pb, MeV	$22.18 \times 690.788571428 \times 10^8 = 15321.6905143 \times 10^8$
Decay energy of ^{222}Rn to lead ^{210}Pb, Joule	$15321.6905143 \times 10^8 \times 1{,}602\ 176\ 634 \times 10^{-19} =$ $= 2{,}45480545353 \times 10^{-7}$
Specific dose absorbed by blood Joule/L (Gy)	$2{,}45480545353 \times 10^{-7}/5 = 0.4909610907 \times 10^{-7}$Gy= $= 4{,}909610907 \times 10^{-8}$Gy =49,09610907 x 10^{-9}Gy = = 49,09610907 nGy
The decay energy of one nucleus ^{210}Pb to ^{206}Pb, MeV	7.404MeV

Table 2. Calculation of the amount of radioactive lead (210Pb) formed as a result of radon decay, as well as the dose load on the red bone marrow of flat bones.

Total lead atoms in blood	$690.788571428 \times 10^8$
Total, lead atoms in hard tissues ^{210}Pb-14,58 %	$690.788571428 \times 10^8 \times 0{,}1458 = 100.716973714 \times 10^8$
In skeletal tissues -8,3%	$690.788571428 \times 10^8 \times 0{,}083 = 57.3354514285 \times 10^8$
Absorbed dose, Ev	$57.3354514285 \times 10^8 \times 7.404 \times 10^6 = 424.511682377 \times 10^{14}$
Specific Absorbed Dose J/кg (Gy)	$680.142993824 \times 10^{-5}/10 = 6.80142993824 \times 10^{-4} =$ $= 0.680142993824$ mGr
Flat bones 5.7% ^{210}Pb	$100.716973714 \times 10^8 \times 0{,}057 = 5.7408675017 \times 10^8$
Absorbed dose, Ev	$5.7408675017 \times 7.404 \times 10^{14}$
Absorbed dose, joule	$425.053829826 \times 10^{-6}$

Specific absorbed dose J/kg (Gy)	42.5053829826 x 10^{-5}/4,5=94.456406628 μGy
Soft tissues. 3.27% lead atoms ^{210}Pb	22.5887862857 x 10^{12}x 690.788571428 x 10^{8}x 0,0327 = =22.5887862857x 10^{8}
Absorbed dose, Ev	22.5887862857 x 10^{8}x 7,404 x 10^{6}=167.247373659 x 10^{14}
Absorbed dose, joule (J)	104.387554691x 10^{14}x10^{-19}= 104.387554691x10^{-5}
Specific absorbed dose J/kg (Gy)	1043.87554691x 10^{-6}/mass
Including bone marrow 0.1308 %Ev	22.5887862857 x 10^{12}x 0,001308 = 2,954613246 x 10^{10}
Absorbed dose, joule (J)	2,954613246 x 10^{10}x1,602 176 634·10^{-19} = = 4.73381436166 x 10^{-9}
Specific absorbed dose J/kg (Gy)	4.73381436166x10^{-9}/2= 2.36690718083 x 10^{-9}= = 2.36690718083 nGy

According to a number of authors [9], in addition to the tendency to accumulate and fix lead ions, partial clearing occurs in parallel, as a result of which some of the lead ions leave the bone tissue. However, with high activity of inhaled radon, an imbalance occurs between the level of radioactive lead clearance and its accumulation in bone tissue. Thus, conditions are created for an increased level of radioactive lead accumulation in flat bones, which in turn causes an increased level of radiation exposure to the hematopoietic system. Indirectly, this position is confirmed by other studies of this process. In particular, it has been shown that with inhalation of increased concentrations of radon in the blood, the level of chromosomal abnormalities increases [10]. It can be concluded that with an increased level of radon in the environment, a high radiation risk is not only irradiation of the lungs, but also the hematopoietic system, leading to chronic irradiation from radioactive lead localized in the flat bones of the body.

References

1. WHO handbook on indoor radon: a public health perspective / edited by Hajo Zeeb, and Ferid Shannoun. World Health Organization 2009, p. 95.
2. Melikadze G. I., Kapanadze N.A., Chankvetadze A.S, Kotetishvili K.V., Chelidze L.T., Giorgadze I.S., Radon Distribution on the Territory of West Georgia. // Journals of Georgian Geophysical Society, 23(2), 2020, pp. 10-13.
3. Amiranashvili A., Particularity of Tbilisi City Air Pollution, or Norm for the Urbanized Locality?, XIV International Conference on Atmospheric Electricity, August 08-12, 2011, Rio de Janeiro, Brazil.
4. Metskhvarishvili M.R., Pagava S.V., Gorgadze K.M., Dekanosidze S.V., Kalandadze I.G1, Beridze M.G., Beriashvili N.Z. Determination of radon concentrations in Mtatsminda districts of Tbilisi. // Journal of Radiobiology and Radiation Safety Vol.2, №3, 2022, pp.74-77.
5. Iaoxiang Miao, Yinping Su, Changsong Hou, Yanchao Song, Bowei Ding, Hongxing Cui,Yunyun Wu, and Quanfu Sun. Indoor Radon Survey in 31 Provincial Capital Cities and Estimation of Lung Cancer Risk in Urban Areas of China. Biomed Environ Sci, 37(11), 2024, pp. 1294-1302.
6. Lucía Martín-Gisbert, Alberto Ruano-Ravina, Guadalupe García, María Pineiro-Lamas, Marta García-Talavera, Ana Teijeiro, Cristina Candal-Pedreira. Duration versus intensity of exposure on the risk of lung cancer due to radon exposure in the general population. Science of The Total Environment**.** Volume 981, 2025.
7. Yan Liu, Yanqing Xu, Wei Xu, Zhengzhong He, Cong Fu, Fen Du. Radon and lung cancer: Current status and future prospects. Critical Reviews in Oncology/Hematology. Volume 198, June 2024, 104363.
8. Kekelidze N., Jakhutashvili T., Tulashvili E., Berishvili Z., Chkhaidze M., Mtsariashvili L, Kajaia G., Material of conference, Daily and seasonal dependence of "indoor" radon in Tbilisi. pp. 243-250.
9. Rabinowitz M. B., Wetherill G. W. and Kopple J. D., Kinetic analysis of lead metabolism in healthy humans. Journal of clinical investigation Vol.58, #1, 1976, pp.260-270.
10. Abo-Elmagd M., Manal M., Daif, H.M. Eissa, Cytogenetic effects of radon inhalation. Radiation Measurements**,** Volume 43, Issue 7, 2008, pp. 1265-1269.

1st International Scientific Conference "Modern problems in Geophysics", Proceedings,
ISBN 978-9941-36-434-1, ISSN 3088-4349, Tbilisi, Georgia, November 6-8, 2025

ABOUT SOME ISSUES OF RADON MEASUREMENT TECHNIQUES

Grebenchuk H.S.

Iv. Beritashvili Center of Experimental Biomedicine, Tbilisi, Georgia
h.grebenchuk@lifescience.org.ge

Abstact. *The article examines the validity of measuring radon in units of activity – becquerels, and shows that such an approach in the methodology, recommended by the International Commission on Radiation Protection (ICRP) and currently widely used, leads to a false fourfold increase of radon concentration estimations.*

Key words*: Radon concentration measurement, Becquerel, Radon decay.*

The noble radioactive gas radon, which is a product of the decay of radium, is quite widespread and has a significant impact on living nature. High concentrations of radon are observed in mine workings and groundwater outlets, and are often used for medical purposes.

According to the currently accepted and recommended by International Commission of Radiation Protection (ISRP) methodology, radon is quantified through its activity in becquerels.

Becquerel is a measure (unit) of the number of decays of the corresponding substance per 1 second. Usually, we are talking about the number of decays per second (or rate) in a specific volume, for example, a cubic meter or a liter. Moreover, when measuring radon activity, it is usually assumed and declared that all decays belong specifically to radon, although control of this aspect is not provided, and is hardly possible due to the fact that the number of decays itself does not provide information about their genetic origin or nature, since it does not document the source, but although it is assumed that it is radon itself. Such a statement can be confirmed or refuted solely by spectral (energy) analysis of subatomic particles, generated in decay, which goes too far beyond the scope of simply calculating the rate of decay, in other words, its activity.

On the other hand, it is well known that the decay of the radon atomic nucleus is a cascade process, involving the sequential generation of four alpha particles, four electrons and four gamma quanta (see Table).

Table1. Cascade decay of radon ^{222}Rn

Element	Type of decay	Energy, MeV	Half-life
222Rn	α	5,49	3,9235 days
218Po	α	6,0	3,11 min
214 Pb	β	0,67, 0,73	26,8 min
	γ	0,352, 0,30, 0,24	
214Bi	β	1,54, 1,51, 3,27	19,9 min
	γ	0,61, 1,76, 1.12	
214Po	α	7,69	164,3 mks
210Pb	β	0,06, 0,02	22,3 years
	γ	0,044	
210 Bi	β	1,16	5,012 days
	γ	0,27, 0,30	
210 Po	α	5,3	138,376 days
206Pb	Stab.		

If we assume that the main, most energy-intensive processes of the cascade decay of radon, associated with the generation of alpha particles, are the ones that generate the above mentioned becquerels, then it turns out that only one of the decays, the very first of them, belongs to radon itself, and the other three belongs to its progenies, namely polonium Po218, polonium Po214 and polonium Po210, that is, not all alpha particles that create impulses in activity registration devices genetically belongs to the decay of radon itself.

Moreover, if we abandon the calculation of becquerels and switch to methods of deposition of alpha particles on activated carbon, the result will also be identical – only one out of every four alpha particles will be responsible for the activity of radon itself and, accordingly, for its concentration in the environment.

So, in principle, it is impossible to talk about the activity of radon in becquerels, since this falsely quadruples the radon concentration as a result.

If, in addition to this, the decays associated with the emission of β and γ will be also taken into account in becquerels, this will cause an even greater increase in the Radon activity index. This circumstance can cause serious errors in estimates of the number of radon decayed nucleus and, accordingly, the energy of radiation exposure on biological objects and the accumulation of decay products in them.

Meanwhile, it seems that correct calculation of both the absorbed dose and the amount of decay products accumulated (incorporated) by the body is possible only on the basis of solving the well-known radioactive decay equation.

The radiation decay equation is

$$dN/dt = -\lambda N \,(1),$$
$$N(t) = Noexp(-\lambda t)\,(2),$$

where $d\big(N(t)\big) = d(No(exp\ exp\ (-\lambda t)\ ) = \ -\lambda No(exp\ exp\ (\lambda t)\ dt$ (3),

where N_0 is the number of radioactive nuclei at time t=0, and λ is the decay constant (probability) for radon 222Rn, determined from the expression $T_{1/2}$=ln2/λ, or λ= ln2/$T_{1/2}$, and all calculations in these expressions should be conducted in SI units for avoid of obtaining incorrect values:

ln2=0,69314718056, (dimensionless quantity),
$T_{1/2}$ = 3,8235 (half-life in days),
$T_{1/2}$ = (3,8235 x24 x60 x 60) = 330350.4 (half-life in seconds).
Then λ=0,69314718056 / (3,8235 x24 x60 x 60) = 0,69314718056/330350,4 = 0,00000209821
or λ ≈ 2,1 x $10^{-6}c^{-1}$.

In addition, from the same equation shall be obtained an estimation of the decay rate or, in other words, the activity at radon constant concentration N_{oconst}:

$$\mu = \frac{dN}{dt} = \lambda Noconst \qquad (4).$$

Thus, the connection between the two most important constants of radiation decay is established – the probability of decay λ and its activity μ at a known concentration of radioactive nuclei N_0, or, vice versa, the concentration of radon nuclei

$$No = \mu/\lambda \qquad (5).$$

From the above mentioned it follows that the currently used method for assessing the radon concentration by becquerels is incorrect and unable to provide an adequate representation of its prevalence in the natural environment and, accordingly, the danger for living organisms.

The simplest approximate way to avoid this situation during determining the radon concentration is to divide the recorded radon activity in becquerels by 4, i.e. on the number of α-particles, generated by the cascade decay of 1 radon nucleus, but this is only possible in case of energy discrimination of becquerels, associated with other types of decays – β and γ.

Another, more realistic method for estimating radon concentration may be the well-known method of accumulation of α-particles on activated carbon, of course, modified to take into account the cascade decay of radon with the generation of four (4) α-particles and dividing the result by 4.

References

1. Grebenchuk H., About Radon measurement techniques – Researchgate.net, July 8, 2025.
2. Grebenchuk H., Gogebashvili M., Ivanishvili N., Nadareishvili D.– Patent of Georgia P 2020 7206 B, Method for determining the radiation dose absorbed by a biological object under the influence of radon, priority 09-10-2019, registration 21-12-2020.
3. Grebenchuk H., Gogebashvili M., Ivanishvili N., Nadareishvili D.- Patent of Georgia P 2021 7304 B – Method for assessing and predicting the complex biological effects of radon, priority 16-07-2020, registration 05-10-2021.
4. Grebenchuk H., Gogebashvili M., Ivanishvili N., Long-term effects of the cumulative impact of low concentrations of radon on the body and mechanisms of their implementation. Researchgate.net, July 2021, DOI: 10.13140/RG.2.2.15656.08960,122 Reads, Research Interest Score 2.1.
5. Grebenchuk H., Gogebashvili M., Nadareishvili D., Ivanishvili N., The role of Lead 210Pb in the manifestation of the effects of radon exposure on living organism: a conceptual analysis. – Radiobiology and Radiation Safety, Vol.1, 2021, pp. 26-33, ISSN 2667-9787.
6. Gogebashvili M., Ivanishvili N., Grebenchuk H., Modern approaches to radiation risk management in urban areas (systems) – International Scientific-Practical Conference, Tbilisi, Georgia, "Biomedical aspects of dangers, caused by the methodological shortcomings of radiobiological studies, conducted in Georgia." November 16-17, 2021.
7. Grebenchuk H., Gogebashvili M., Nadareishvili D., Ivanishvili N., The problem of Lead 210Pb in the manifestation of the effects of the radon exposure on living organism: a conceptual analysis. – In the book "Systemic, Cellular and Molecular Mechanisms of Physiological Functions and Their Disorders. // Proceedings of Iv.Beritashvili Center for Experimental Biomedicine, Edd. – N.Nachkebia and N.Mitagvaria, Nova Medicine and Health, New York, Charter 3, pp. 23-33, 2021.
8. Gogebashvili M., Grebenchuk G., Tulashvili E., Ivanishvili N., Kalmakhelidze S., Shubitidze M., Safety study of the use of Tskaltubo mineral-radon waters, "Experimental and clinical medicine". // Journal of Experimental and clinical medicine, Georgia, 4. N3, 2023, (In Georgian).

1st International Scientific Conference "Modern problems in Geophysics", Proceedings,
ISBN 978-9941-36-434-1, ISSN 3088-4349, Tbilisi, Georgia, November 6-8, 2025

CARBON BALANCE IN GEORGIA'S INDUSTRIAL SOILS AND ECO-PHYTOREMEDIATION-BASED REGENERATION

[*]Matiashvili S., [**]Chanqseliani Z.

[*]M. Nodia Institute of Geophysics of the I. Javakhishvili Tbilisi State University, Tbilisi, Georgia
***Soil Fertility Research Service of the Agricultural Scientific Research Center, Georgia*
sophiko.matiashvili@tsu.ge

Abstract. *Industrial soils are experiencing severe degradation and a sharp decrease in organic carbon content as a result of anthropogenic impacts. This study analyzes the main mechanisms of soil carbon balance disturbance in industrial zones and discusses possible restoration strategies based on ecophytoremediation approaches. The study pays special attention to the possibility of using industrial hemp (Cannabis sativa) as one of the most effective means for carbon dioxide sequestration. The methodology is based on the analysis of literary sources, the summary of soil data and the evaluation of practical reclamation models. The results show that the selection of the right plant cover and enrichment with biocarbon contribute to the partial restoration of the carbon balance in industrial soils.*

Key words*: industrial soils, carbon balance, ecophytoremediation, biocarbon, industrial hemp.*

Introduction

Soil carbon storage is a vital ecosystem function driven by the interaction of ecological processes. Soil is a key element in the global carbon cycle. Soil stores a large amount of carbon originating from aboveground and belowground organic matter. However, in industrial areas – where the land surface is subjected to massive human intervention – organic carbon content is sharply reduced. This affects both microbial activity and the physical and chemical structure of the soil. [1,2.] The relevance of the issue is particularly emphasized in the context of climate change, where the soil carbon function is considered a potential means of reducing atmospheric CO_2. The majority of Georgia's economic activities are related to industrial processes, including factories, the distribution of industrial soils, the use of modern technologies, and urban development. These factors affect soil quality, the biosphere, and carbon exchange. [3]

The carbon balance of soils located in industrial zones is significantly disrupted as a result of intensive anthropogenic impact. Such soils are characterized by low organic carbon content, reduced biological activity and structural degradation, which leads to a weakening of the ability to retain carbon. As a result of industrial activities, numerous hectares of soil are contaminated in Georgia, which require restoration and reclassification. The main causes of carbon loss are industrial activities. [4] The process of carbon reduction in unincorporated areas is determined by a number of factors:

- Mechanical disturbance of the land surface as a result of construction, mining or infrastructure works, which leads to the disruption and decomposition of stable organic matter;
- Pollution with heavy metals and chemical compounds, which hinders the functioning of soil microflora and slows down the process of humus formation;
- Soil compaction and disruption of the hydrological balance, which reduces oxygen exchange and slows down microbial destruction, but at the same time contributes to the constant release of carbon;
- Insufficient ecological management – soils are largely left to natural regeneration and are not being recultivated or rehabilitated.

As a result of these processes, soils in industrial areas often completely lose their ability to store and store carbon, which poses a long-term ecological challenge.

Despite their extremely degraded state, industrial soils have the potential to store carbon with the right environmental and agronomic approaches. The main contributing factors are:

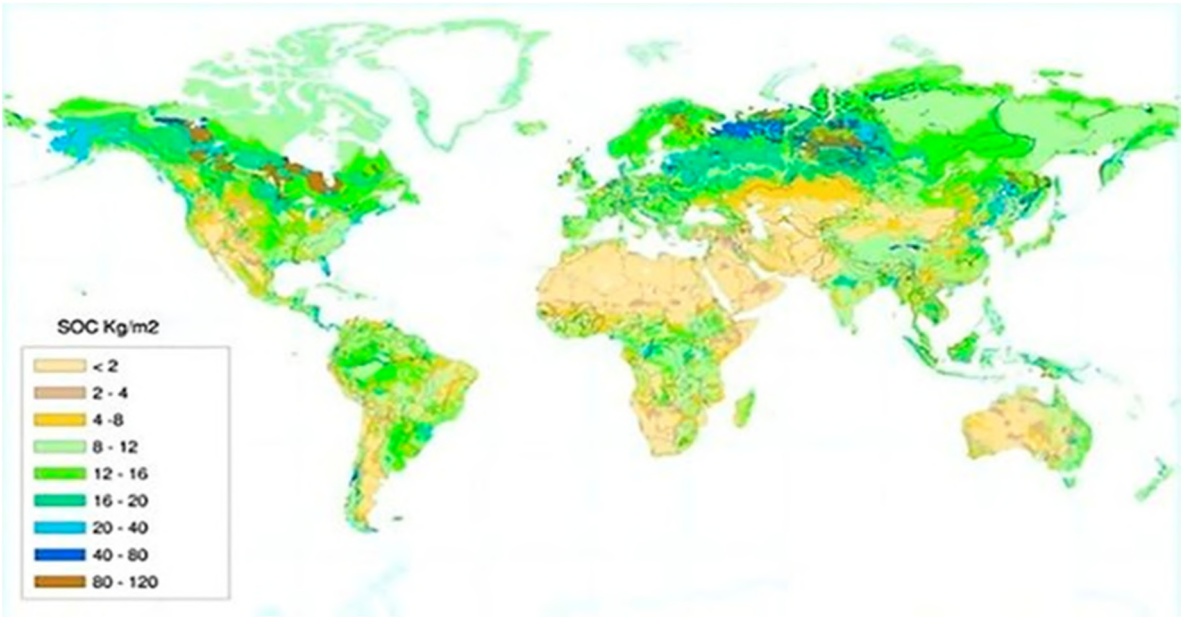

Fig. 1. Soil organic carbon content in kg/m².

Phytoremediation – the integration of plant species that have a high tolerance to heavy metals and pollution and can slowly enrich the soil with organic waste; Phytoremediation of industrial soils is an ecological and innovative process aimed at rehabilitating the soil using the natural abilities of plants. Recognized as a sustainable and environmentally friendly approach, it is attracting significant attention as a promising strategy for reducing the environmental impact of heavy metals and organic compounds. [5,6.]

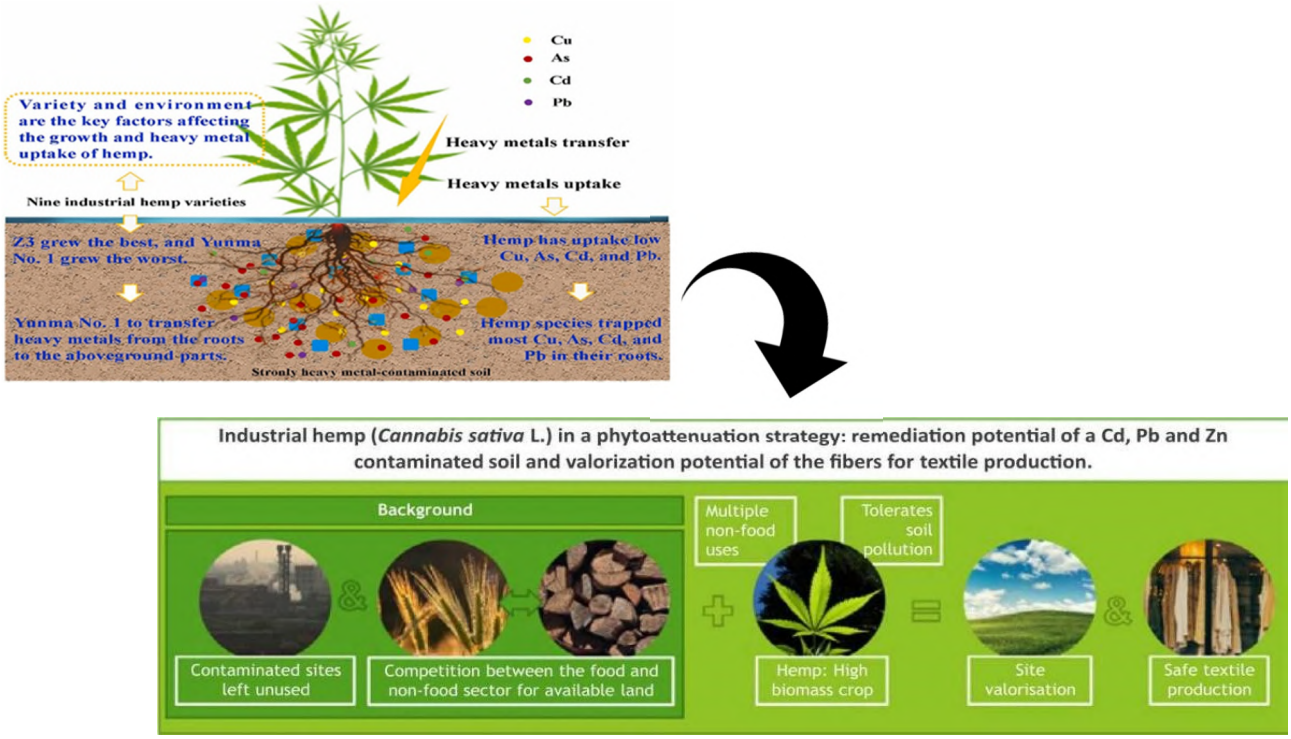

Fig. 2 and Fig. 3. Use of industrial hemp (Cannabis sativa) as a phytoremediator.

One interesting example is the use of industrial hemp (Cannabis sativa) as a phytoremediator. [Fig.2] Its rapid growth, deep root system, and high biomass production contribute to CO_2 sequestration rates of 8–15 tons per hectare per year – significantly higher than those observed in some forest ecosystems (2–6 tons/ha/year). Industrial hemp has great potential for use in soils contaminated with heavy metals for its safe, non-food uses. We focus on the following cultivar, Wanma. This plant has the ability to accumulate Cu, As, Cd, and Pb in its

roots from contaminated soil and to absorb them from the soil. [7] We will focus on one of the technologies for removing heavy metals – phytoremediation. This is the cheapest and most promising technology.

Georgia has great potential for the introduction of eco-phytoremediation and regeneration, especially in the industrial belt, as industrial areas on the territory of Georgia suffer from soil contamination with radionuclides and heavy metals. Inorganic pollutants such as heavy metals, radionuclides, phosphates, and nitrates are widespread. While some heavy metals are essential for plant growth, excessive levels of lead, cadmium, mercury, and arsenic pose a serious threat to both humans and wildlife. Plants can absorb nonessential inorganic compounds, requiring mechanisms to retain essential nutrients such as Cu, Zn, and Mn, which can be toxic at high concentrations. [8,9.] This method is particularly effective for remediating industrial soils contaminated with heavy metals, petroleum products, or other toxic chemicals.

Fig. 4. Carbon transformation in soil from plant root residues and

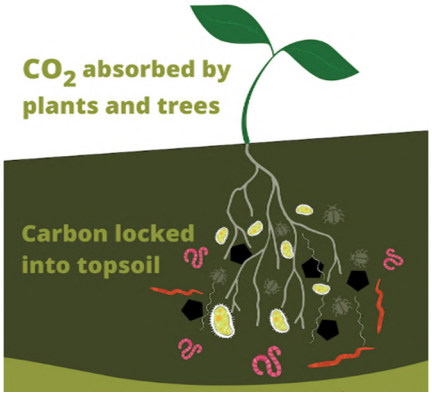

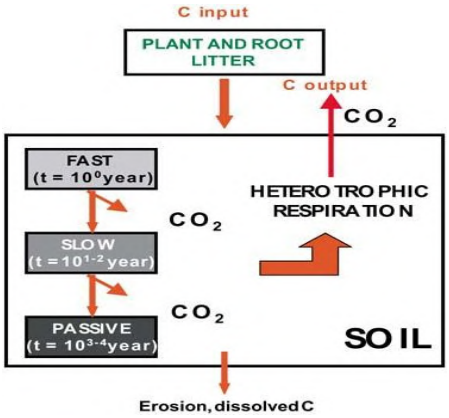

Fig. 5 Carbon uptake, storage, and circulation in the atmosphere

In terms of environmental safety, phytoremediation is less harmful to the environment than chemical and mechanical methods. The technology is more effective in cases of surface contamination. [10]

Results and Discussion

The results showed that industrial hemp biomass absorbs 8–15 tons of CO_2/ha annually, which is higher than the average forest ecosystem (2–6 tons/ha) (Cambridge Institute of Natural Materials, 2022). The use of biochar increases the water retention capacity of the soil and prevents carbon loss through mineralization (Lehmann et al., 2015). An effective phytoremediation model involves treating contaminated soil with a combination of organic amendments, re-vegetation, and continuous monitoring of microbial analysis. Phytoremediation is influenced by environmental factors such as soil type, pH, moisture, and climate. Comprehensive site assessments are essential to identify suitable plants and ensure their sustainability, integrating them into the local ecosystem []. Laboratory and field experiments, along with small-scale pilot studies, are crucial to assess plant tolerance and accumulation capacity, and to validate the feasibility of large-scale projects. To examine the impact of regenerative agriculture on soil carbon sequestration, we searched for studies that measured changes in SOC stock or content or other similar soil carbon parameters (such as total soil carbon or labile carbon). For greenhouse gases, we considered emissions of carbon dioxide (CO2), methane (CH4), and nitrous oxide (N2O). These three gases are the most common greenhouse gases associated with agricultural land use (USDA, 2022). We selected search terms relevant to regenerative agriculture practices from previous analyses of key regenerative agriculture practices related to climate change mitigation (Bossio et al., 2020, Lal, 2004a, Lal, 2004b, Mikolajczyk, 2021, Smith et al., 2008). These terms were also derived from interviews with farmers in Southeast Asia who use sustainable or regenerative soil-based agricultural methods.

Conclusion

The carbon balance of industrial soils can be improved through complex and integrated approaches. Ecophytoremediation strategies, especially the use of industrial hemp and the integration of biochar, repre-

sent a promising path for carbon sequestration. According to current projections, if Georgia activates the implementation of regenerative projects, its carbon levels will be properly controlled, and the country's combined climate goals will be achieved. Important steps are:

- Investing in the development of new technologies and innovations.
- Raising public awareness.
- Supporting the government and international organizations with projects.
- Tightening regulations and supporting environmental activities.

Improving the carbon balance of industrial soils is both an ecological and climate priority. Developing the right management strategies and implementing phytoremediation technologies will allow for the gradual restoration of carbon cycling and the creation of a solid foundation for the regeneration of soil ecosystem services.

References

1. Lal, R., Soil health and carbon management. Food and Energy Security, 5(4), 2016, pp. 212–222. https://doi.org/10.1002/fes3.96
2. Plants (Basel). 2022 Feb 23;11(5):595. doi: 10.3390/plants11050595. PMID: 35270065; PMCID: PMC8912475. https://pmc.ncbi.nlm.nih.gov/articles/PMC8912475/
3. Băbău A.M.C., Micle V., Damian G.E., Sur I.M., Sustainable ecological restoration of sterile dumps using Robinia pseudoacacia. Sustainability.13, 2021, 14021. doi: 10.3390/su132414021. [DOI] [Google Scholar]
4. Sumiahadi A., Acar R., A review of phytoremediation technology: Heavy metals uptake by plants. IOP Conf. Ser. Earth Environ. Sci. 142, 2018, 012023. doi: 10.1088/1755-1315/142/1/012023. [DOI] [Google Scholar]
5. Udawat P., Singh J., Phytoremediation: A way towards sustainable Agriculture. Int. J. Environ. Agric. Biotechnol. 5, 2020, pp. 1167–1173. doi: 10.22161/ijeab.54.37. [DOI] [Google Scholar]
6. Avkopashvili G., Avkopashvili M., Gongadze A., Gakhokidze R., Eco-monitoring of Georgia's Contaminated Soil and Water with Heavy Metals. Carpathian J. Earth & Env. Sci., 12(2), 2017, pp. 595-604.
7. Avkopashvili M., Gongadze A., Avkopashvili G., Matchavariani L., Asanidze L., Lagidze L. Metals distribution in soil contaminated by gold and copper mining in Georgia. Journal of Environmental Biology, SI “Environment, Biodiversity, Geography”, Vol.41(2), 2020, pp. 310-317.
8. Avkopashvili M., Avkopashvili G., Avkopashvili I., Asanidze L., Matchavariani L., Gongadze A., Gakhokidze R., Mining-Related Metal Pollution and Ecological Risk Factors in South-Eastern Georgia. Sustainability, Switzerland, vol.14, issue 9, 2022, 5621.
9. Matiashvili S., Chankseliani Z., Mepharidze, E. Comparison of radionuclides and heavy metals distribution in Georgian soils. Journal of the Georgian Geophysical Society, 25(1), 2022, pp. 95-102.
10. Gventsadze G., Ghambashidze G., Chankseliani Z., Sarjveladze I., Blum W.E.H. Impacts of crop-specific agricultural practices on the accumulation of heavy metals in soil in Kvemo Kartli region (Georgia): A preliminary assessment. Sustainability, 16(10), 2024, 4244.

Content

Ivane Javakhishvili Tbilisi State University
Mikheil Nodia Institute of Geophysics

Technical University of Georgia
Institute of Hydrometeorology
Georgian Geophysical Association

1st INTERNATIONAL SCIENTIFIC CONFERENCE

"Modern problems in Geophysics"

Tbilisi, Georgia, November 6-8, 2025

PROCEEDINGS

Circulation 60 copy.

ISBN 978-9941-36-434-1

ISSN 3088-4349ISSN

E-mail: geophysics@tsu.ge
http://dspace.gela.org.ge/handle/123456789/254

2025 – Tbilisi

Typesetter Lali Kurdghelashvili
Cover Designer Mariam Ebralidze

1, Ilia Tchavtchavadze Ave., Tbilisi 0128
Tel 995(32) 225 04 84, 6284/6279
https://www.tsu.ge/ka/publishing-house